Synthetic, Reactivity, and Mechanistic Studies Relevant to Olefin Oligomerization and Polymerization

Thesis by
Theodor Agapie

In Partial Fulfillment of the Requirements for the Degree of
Doctor of Philosophy

Division of Chemistry and Chemical Engineering

California Institute of Technology
Pasadena, California
2007

(Defended January 22, 2007)

To my father and my sister
and the memory of my mother.

Multumesc.

Acknowledgments

Looking back, almost at the end of my graduate career, I can definitely say I enjoyed these years. There were ups and downs, but overall I had a great time at Caltech. I believe this was the case because of the amazing environment this chemistry department provides. The people I had the opportunity to overlap and interact with are amazing and helped me make the most of my graduate career. I would like to take the chance and briefly thank them here.

First and foremost I would like to thank John Bercaw. His enthusiasm for science and his inclination to ask and try to answer difficult questions about how chemical transformations work will always be a source of inspiration for me. His door has always been open to talk science or anything else. I would also like to thank John for igniting in me the passion of high mountain hiking. I have not had the time to do it as often as I would have liked, but I thoroughly enjoyed it every time. Thank you, John!

I would like to acknowledge some faculty members for the contribution they had to my development as a chemist. The members of my committee, Bob Grubbs, Harry Gray, Dave MacMillan, and Jonas Peters have all had insightful and much appreciated suggestions for my projects. Their excitement about chemistry has been a treat. Thank you, Bob, for climbing advice too and belaying me on my first 5.9 climb at Joshua Tree. Jonas, thank you for taking the time to chat and giving good advice. Harry, thank you for hosting drinks at the Ath after the organometallics seminars; it was great to continue the discussions over a beer. Thanks, Harry, for sponsoring the burger eating contest – I got my fill of McDonalds hamburgers for years to come. I would like to thank Jay Labinger for stimulating discussions regarding labeling experiments. Brian Stoltz, thank you for the great class in organic synthesis; I very much enjoyed it.

I would also like to thank the people who had an important contribution in my earlier development as a chemist. My elementary school teacher, Georgeta Enescu, infused in me the enthusiasm for running chemical reactions when she gave me access to her chemical stockroom full of wonders. My high school teacher, Lia Chiru, helped me add breath to my chemical knowledge. With her support, I participated in many chemistry competitions; in that context, my

interactions with peers and instructors (too many to name here) nourished my passion for chemistry. My undergraduate years, at MIT, were amazing. Again, there are too many people I would need to thank for what they taught me there. My undergraduate research advisor, Kit Cummins, had a great role in my development as a synthetic chemist and as a scientist in general. His enthusiasm for chemistry is simply contagious. Thank you for initiating me into the wonders of chemical bonding and for giving me the opportunity to be part of your group.

Being part of the Bercaw group, at Caltech, has been a very fulfilling experience. A good part of what I learned during my graduate years came from my fellow group members. I am also glad that our interaction extended beyond science, to hiking, rock-climbing, cooking, dancing, visits to Lucky Baldwin's... I would like to thank Lily Ackerman, whose hood-mate I became when I started in the group, for introducing me to high vacuum line techniques. Thank you also for the driving lessons. Upon Lily graduating, Steve Baldwin joined me on the South side of 209. Steve, I appreciate your scientific scrutiny. I would like to thank you for being a great baymate and for your help with accommodating the undergraduates I mentored. I would like to thank Susan Schofer, Sara Kalmo, and Paul Elowe (the chromium team); and Jeff Byers, Endy Min, and Cliff Baar (the kinetic resolution team) for insightful discussions. Susan, I enjoyed our rock-climbing and hiking trips; I am glad I was able to provide entertainment (with my rock-climbing wimpyness). Sara thanks for inspiring me to start running – I had a great time at the LA Marathon; I learned a great deal from your efforts on the kinetics for propylene polymerization. Paul, I appreciate your knowledge about films; great job with making 1-octene and good luck on the hydroformylation project! Jeff, my classmate, I would like to thank for patience on coaching the Romanian on the basketball court. We learned a great deal teaching John's class together. Good luck at MIT! Endy, thank you for teaching me a few salsa and swing steps! Cliff, I much appreciated your cynical manner. I started at Caltech at about the same time with Dave Weinberg and I am happy we quickly became friends. I much enjoyed our discussions about chemical bonding. Our mountaineering adventures are unforgettable; I am glad we survived that lightning storm on top of Langley, a 14,000 ft peak. Thank you for

the surfing lesson, too! I am looking forward to more outdoor adventures; good luck with finishing up! Jon Owen, it was great to extend our discussions about science over drinks at Lucky's. I also enjoyed our rock-climbing trips. Bolin Lin, thanks for helping me to get started with Jaguar; I also enjoyed our discussions about history and China. George Chen, you can definitely show a different perspective! Good luck with training for the marathon. I also wish good luck to the newer members of the group, Suzanne Golisz, Ian Tonks, and Edward (Ted) Weintrob. Suzanne, you are off to great start – I am sure you all will take the tridentate frameworks a long way. Here, I would also like to thank Pat Andersen for organizing the Bercaw group business.

During my time in the Bercaw group, I was lucky to overlap with a number of postdoctoral associates and visiting scientists that have provided good experimental advice and different view-points – Christoph Balzarek, Reto Dorta, Xingwei Li, Adam Johnson, Gerry Niccolai, John Moss, Parisa Mehrkhodavandi, Alan Heyduk, Tom Driver, Travis Williams, Aaron Wilson, and Nilay Hazari. In particular I would like to thank Parisa for our discussions about polymerization catalysis, opera, and philosophy. Quite crazy of you to join Dave and me for a sick, one day 14-er trip; but two of them?!

Mentoring undergraduate researchers was an important part of my graduate career. I was fortunate to work with two very talented Caltech undergraduates. Smaranda Marinescu, I very much enjoyed seeing you grow as a chemist! I hope you enjoyed working on the group 3 chemistry as much as I did. Great job with understanding the group 3 exchange processes! I also enjoyed our trip with Parisa, Dave, and Yen to the top of White Montain Peak (without sleeping from Pasadena). I am glad we became good, friends and I look forward to seeing your career unfold. Best of luck! Daniel, I hope you enjoyed exploring group 4 anilide chemistry; great start at developing the coordination chemistry of this new ligand! I am sure you will keep up the great work!

The interaction with other groups at Caltech has been an important avenue to both learn about other areas in chemistry and receive ideas related to my projects. Discussions with people in the Peters, Grubbs, Stoltz, Gray, and MacMillan groups have been invaluable. In particular I would like to thank

Paula Diaconescu, Andy Hejl, Tobias Ritter and Raissa Trend. Paula, thank you for your friendship over the years. I was lucky to have you close by both in Boston and in Los Angeles; I have appreciated your scientific critique very much and I have enjoyed your cynical optimism. Andy, I much enjoyed our bridge sessions and discussions about mechanism and kinetics. Tobias, I appreciate your creative synthetic ideas and excitement about chemistry. Our trip to the Palisade Basin was memorable, even though we did not manage to reach the summit. Raissa, I enjoyed our discussions about chemistry, at Lucky's, and your desire to explore new scientific areas. Good luck with your biochemical postdoc!

Many thanks go to the people that run the facilities and the administrative staff at Caltech. Larry Henling and Mike Day, I relied heavily on you for my crystallographic studies. Thanks a lot for your help. Larry, I know that at least one or two of the crystals I brought to you were not as bad as you always complained. However, I think your making fun about my crystal growing skills had a beneficial effect overall. I enjoyed our discussions about crystallography. Thank you! Scott Ross, thank you for spending endless hours teaching me how to deal with hg1 problems. Tom Dunn, thank you for your help with maintaining the NMR facility; thanks also for your supportive words! Mona Shahgholi, I appreciate your help with MS samples. Rick Gerhart, thanks for the glass-blowing wonders. Dian Buchness, thanks for the welcoming words and for taking care of a lot of paperwork for us.

I would also like to acknowledge a number of good friends that have provided support over the years. Florin Albeanu, I have much enjoyed our philosophical discussions. Our trip to Venezuela with Michel, Simona, Vasi, and Claudiu was memorable; hopefully we will get to travel again soon to other interesting places. Stefan Carp, I am looking forward to grilling some more tasty skewers like the ones we had in Death Valley – I can still taste that awesome garlic sauce. Daniel Preda (Pylot), somehow, our climbing trips often turn into "epics", which makes them unforgettable; I hope we will climb more in the future. Daniel Nedelcu, your tripe soup is just unbelievable, sign me up next time you cook some more! The Romanians at Caltech (ARCA) have provided a Romanian home away from Romania, through occasional parties, dinners, and

outings. I know we will keep in touch and I am looking forward to seeing where we will all end up.

My deepest gratitude goes to my father, Toader, my late mother, Maria, and my sister, Elena, for their unconditioned support and love. None of my chemical adventures would have been possible without them.

Abstract

Chapters 2 and 3 present synthetic, structural, and mechanistic studies relevant to the selective trimerization of ethylene to 1-hexene using a chromium diphosphine catalyst system. The studied diphosphines, PNP^{L}=(*o*-L-$C_6H_4)_2PN(Me)P(o$-L-$C_6H_4)_2$, display a PNP backbone with phosphine-aryl groups ortho-substituted with ethers, amines, or thioethers (L=OMe, NMe_2, or SMe). Chromium(0) and chromium(III) complexes have been prepared, characterized structurally, and tested for catalytic activity, highlighting the importance of the pendant ether groups. A chromacyclopentane model complex, (PNP^{O4})Cr(*o*,*o*-biphenyldiyl)Br, has been isolated using the parent phosphine system (PNP^{O4}, L=OMe). Starting with this model system, the olefin trimerization reaction has been investigated using *trans*-, *cis*-, and *gem*-d_2-ethylene as well as mixtures of C_2D_4 and C_2H_4. The selectivity of α-olefin insertion into the chromacyclopentane mimic and that of β-H elimination from chromacycloheptanes have been studied. The relative rates of insertion of terminal and internal olefins into the chromacyclopentane moiety have been measured.

Chapters 4, 5, and 6 present synthetic studies of tantalum, titanium, and zirconium complexes supported by a new tridentate bisphenolate framework, along with applications to olefin polymerization and mechanistic studies of organometallic transformations based on these architectures. The utilized ligand framework involves a bisphenol connected at the *ortho* positions via semirigid, ring-ring (sp^2-sp^2) linkages to a flat ring (pyridine, thiophene, furan, or benzene). These ligands were found to coordinate to metals in a mer fashion to give a variety of binding geometries. A tantalum system supported by the benzene

bridged bisphenolate was found to undergo intramolecular CH activation faster than metal-alkyl protonolysis by a pendant phenol, un unprecedented process for early metals. An α-H abstraction reaction has afforded access to a tantalum benzylidene supported by the pyridine linked bisphenolate. Isotope labeling studies and variable temperature kinetics measurements were used to investigate the mechanisms of these transformations. Group 4 complexes supported by the present bisphenolates were found to have interesting catalytic behavior for the propylene polymerization and oligomerization, upon activation with excess MAO. The propylene polymerization activity of present zirconium complexes is excellent, exceeding 10^6 g polypropylene / (mol Zr • h), in some cases.

Chapter 7 presents the synthesis and study of group 3 dialkyl complexes supported by tetradentate L_2N-phenolates (L = S, N, O). These complexes were found to undergo a non-dissociative ligand exchange process in solution. The mechanism of this process was studied by using variable temperature NMR spectroscopy.

Table of Contents

Chapter 1

General Introduction

This dissertation describes various aspects of organometallic chemistry with a focus on early transition metals. Mechanistic studies of olefin oligomerization reactions and the design, synthesis, and characterization of novel metal-ligand frameworks for supporting chemical transformations of interest represent the main thrust of the present work. The quest for developing and understanding organometallic, catalytic, and coordination chemistry has led the author to the exploration of systems based on group 3, 4, 5, and 6 transition metals. Pertinent background information, with references, for each of the topics discussed is presented at the beginning of each chapter; this note represents a general introduction of the development of our interests in the problems described in this dissertation.

The study and application of olefin oligomerization and polymerization have been the starting points for the projects described here. These processes are very important for today's technological society. They are used to generate very high volume chemicals and materials with applications ranging from the automotive and construction industries to food packaging and information age technologies. These applications stem from the versatile properties of the polymers. Developments over the last sixty years have illustrated the fact that materials of desirable properties can be accessed by the rational design of metal catalysts. In this context, current challenges include the design of catalysts capable of more versatile control of polymer microstructure, of improved product selectivity, of higher productivity, under more environmentally friendly, more energetically inexpensive conditions.

The catalytic trimerization of ethylene to 1-hexene is one example of an unusually selective organometallic transformation leading to a valuable product (in this case, a comonomer in the synthesis of linear low density polyethylene). This presents a very interesting fundamental problem with important industrial applications. A great opportunity to study this process came with a report by scientists at bp. An *in situ* generated chromium/diphosphine/MAO system was found to generate 1-hexene from ethylene with excellent selectivity and productivity. The bp team invited us to collaborate and study the fundamental aspects of this transformation. We prepared the first well-defined chromium complexes supported by the catalytically competent ligand framework (Chapter 2); this structural information allowed an investigation into the important features of the ligand with respect to catalyst productivity and selectivity. Access to well-defined complexes capable of catalysis upon stoichimetric activation allowed an entry into mechanistic studies. Experiments with labeled ethylene and other olefins afforded great insight into the mechanism of this transformation (Chapter 3). Experiments designed and reported by us have been used by other scientists, in industry and academia, for investigating and better understanding processes leading to other useful products. In fact, a team of scientists at Sasol has reported systems based on related ligands able to perform the selective tetramerization of ethylene leading to 1-octene, another valuable olefin. In the opinion of the author, the development of this project represents an immediate and instructive example of symbiotic interaction (both direct and

indirect, as well as collaborative and competitive) between scientists in both academia and industry, leading to scientific advancement.

Related to olefin oligomerization by mechanism and industrial application, the polymerization of α-olefins presents a number of interesting and challenging problems. The development of non-metallocene polymerization catalysts represents a topic of broad recent interest due to potential applications in areas such as living polymerization, generation of block-copolymers, control of polymer microstructure, etc. The author's work in this area began with the exploration of the kinetic resolution of racemic, 3-substituted α-olefins by selective polymerization of one of the olefin enantiomers. Given that 3-substituted α-olefins are bulkier and more difficult to polymerize, the catalysts chosen for study were based on very active, zirconium tetradentate bisphenolate systems. These frameworks were modified for elaborate, enantiopure zirconium complexes; these were found to lack enatioselectivity for the polymerization of 3-methyl-1-pentene (Appendix 1). The experience gained with tetradentate bisphenolate ligand frameworks was used to enter an area relatively unexplored, but of interest to olefin polymerization catalysis – group 3 dialkyl species. These complexes were supported by tetradentate monoanionic phenolate ligands. This project provided the opportunity for a great collaborative effort with undergraduate Smaranda C. Marinescu who completed the author's initial studies on yttrium and explored scandium analogs (Chapter 7). This work uncovered an interesting ligand exchange process. The ethylene polymerization

activity was found to be very low, possibly due to a reduced stability of these relatively flexible ligands frameworks.

Reasoning that the lack of selectivity in the kinetic resolution above was also due to the inherent flexibility in this ligand framework, new architectures of higher rigidity were targeted. Tridentate bisphenolate frameworks connected at the *ortho* positions via semi-rigid, ring-ring (sp^2-sp^2) linkages to a flat ring (pyridine, thiophene, furan, or benzene) were designed. The coordination chemistry of these ligands and their ability to support organometallic transformation was first explored using tantalum centers (Chapters 4 and 5). These studies allowed for a comparison with the more studied metallocene systems. Investigations of the tantalum species supported by these architectures led to mechanistic studies of fundamental organometallic transformations – σ-bond metathesis and α-H abstraction. Notably, a process very unusual for an early metal center was uncovered – CH bond activation was found to be faster than protonolysis of a Ta-Me moiety. Encouraged by the promising results in tantalum chemistry, a study of group 4 chemistry supported by the present semirigid, tridentate bisphenolate ligands was undertaken (Chapter 6). This study led to the discovery of very active propylene polymerization catalysts. A collaboration with undergraduate Daniel Tofan led to the development of related bisanilide frameworks that are currently under study for polymerization activity (not presented here). Graduate student Suzanne Golisz has shown that a steric variant of the pyridine bisphenolate ligands introduced here displays interesting control of polymer microstructure, lending promise to further exploration.

Diverse topics in early metal organometallic chemistry are explored in this work. Some of the studied problems are of fundamental nature, while some of them have direct applications in catalysis. Significant progress has been made toward better understanding the fundamental reasons behind the observed selectivity for ethylene trimerization to generate 1-hexene, a compound with important industrial applications. Basic experiments to generally study this type of transformation have been developed. The exploration of new ligand architectures for early metals has led to the development of new chemical reactivity of fundamental interest. From an application viewpoint, very active olefin polymerization catalysts have been discovered. The promising initial findings based on the introduced ligand framework augurs for exciting further development.

Chapter 2

A Chromium Diphosphine System for Catalytic Ethylene Trimerization: Synthetic and Structural Studies of Chromium Complexes with a Nitrogen-Bridged Diphosphine Ligand

The text for this chapter was taken in part from:

Agapie, T.; Day, M. W.; Henling, L. M.; Labinger, J. A.; Bercaw, J. E. *Organometallics* **2004**, *25*, 2733-2742.

Abstract

To gain molecular-level insight into the important features of a chromium-diphosphine catalytic system for ethylene trimerization, the coordination chemistry of chromium with "PNP" ligands ($PNP^{L3L'}$=(*o*-L-$C_6H_4)_2PN(Me)P$(*o*-L-C_6H_4)(*o*-L'-C_6H_4), L=L'=OMe; L=L'=NMe_2; L=OMe, L'=NMe_2 or SMe; $P^{t\text{-}Bu}N^{i\text{-}amyl}P^{O4}$ = (2-MeO-4-*t*-$BuC_6H_3)_2PN$(*i*-amyl)P(2-MeO-4-*t*-$BuC_6H_3)_2$) has been explored. Chromium(0) carbonyl complexes have been synthesized by CO displacement with diphosphine. Oxidation of $Cr(CO)_4[\kappa^2$-(P,P)-$(PNP^{O4})]$ with I_2, Br_2, and $PhICl_2$ generates the corresponding chromium(III) halide complexes. Chromium(III) complexes, $CrCl_3[(\kappa^3$-(P,P,O)-$(PNP^{O4})]$, $CrCl_3$ $[\kappa^3$-(P,P,O)-$(P^{t\text{-}Bu}N^{i\text{-}amyl}P^{O4})]$, and $CrCl_2(CH_3)[\kappa^3$-(P,P,O)-$(PNP^{O4})]$ can be synthesized by metallation with $CrCl_3(THF)_3$ or $CrCl_2(CH_3)(THF)_3$. Reaction of $CrCl_3[\kappa^3$-(P,P,O)-$(PNP^{O4})]$ with *o,o'*-biphenyldiyl diGrignard affords CrBr(*o,o'*-biphenyldiyl)$[\kappa^3$-(P,P,O)-$(PNP^{O4})]$. Single-crystal X-ray diffraction studies show that the Cr-O and Cr-P distances can vary significantly as a function of metal oxidation state and the other ligands bound to chromium. Variable temperature ^2H NMR spectroscopy studies of chromium(III) complexes supported by PNP^{O4} ligands indicate fluxional behavior with the ether groups interchanging at higher temperatures. Low temperature ^2H NMR spectra are consistent with solution structures similar to the ones determined in the solid state. Chromium(III) complexes supported by PNP ligands with N and S donors show preferential binding to N and S rather than O and P, in the solid state. Trimerization trials with well-defined $Cr(PNP^{O4})$ precursors give competent

catalytic systems. Systems based on the PNP ligands displaying pendant donors other than oxygen show limited or no catalytic trimerization activity.

Introduction

The oligomerization of ethylene typically leads to a broad range of α-olefins, requiring fractional distillation to isolate individual α-olefins.[1] There is increasing interest in developing catalytic systems that give better selectivity toward desirable alkenes. One of the most commercially useful olefins is 1-hexene, a comonomer for the synthesis of linear low-density polyethylene (LLDPE). Several recent reports describe catalytic systems that trimerize ethylene to 1-hexene with high selectivity.[2-24] Some ethylene trimerization catalysts are based on titanium[13,15] and tantalum,[19] but the most numerous and successful systems are based on chromium.

A catalyst generated from $CrCl_3(THF)_3$, a diphosphine ligand (**1**) and methaluminoxane (MAO) (eq 1) trimerizes ethylene to 1-hexene with unprecedented selectivity (99.9% 1-hexene in the hexenes fraction) and productivity (~2 x 10^6 turnovers/h).[17] The effect of changing the diphosphine on trimerization activity was investigated (Figure 1); key features appear to be the *ortho*-methoxy substituted aryl groups and the PNP backbone. Changing the amide in the PNP backbone to a methylene group (**6**) or replacing the *ortho*-methoxy groups with ethyl groups (**2**) greatly diminishes the catalytic activity. Recent studies involving a variety of related PNP ligands have shown that trimerization and tetramerization of ethylene can be achieved in the absence

of *ortho*-donors, but these catalysts operate at higher pressures of ethylene and with lower selectivity for the terminal olefin in the corresponding C_n (n = 6 or 8) fraction.[6,18,25]

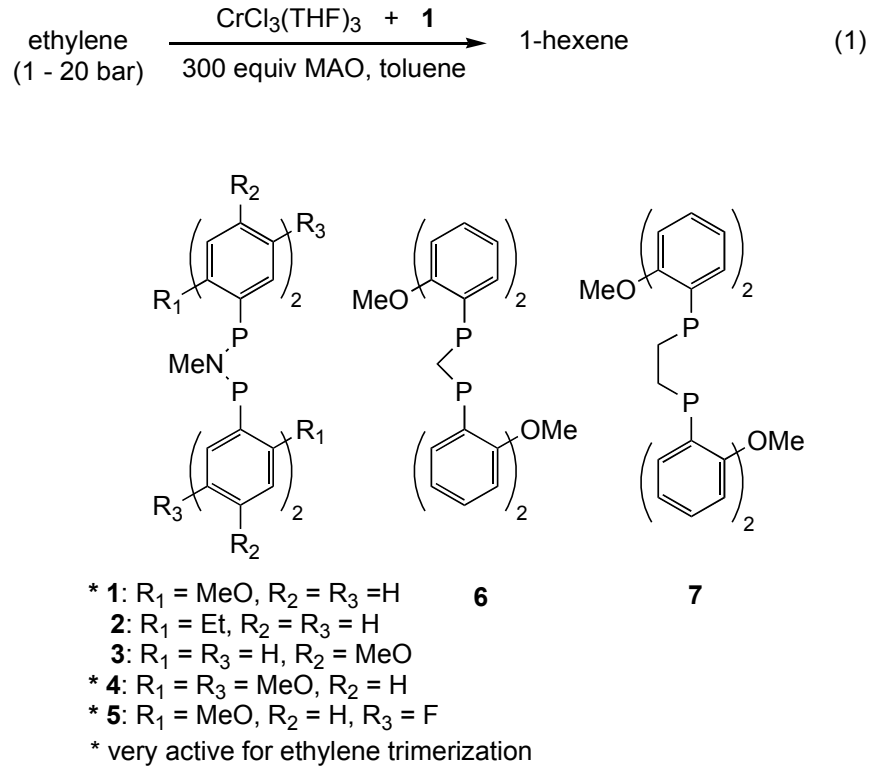

Figure 1. Diphosphines tested for supporting catalytic chromium ethylene trimerization activity.

The mechanism of the trimerization reaction will be discussed in detail Chapter 3, along with relevant background information. The present chapter is focused on the development of synthetic tools to access well defined chromium complexes displaying PNP ligands and on the study the structural features relevant to catalysis. We report herein the synthesis, characterization, and reactivity of chromium carbonyl, halide, alkyl, and aryl complexes supported by

PNP ligands with *ortho*-methoxyaryl substituents. The effects of varying the nature of the *ortho*-substituents on the coordination chemistry of the diphosphine to chromium and their effects on the catalytic system are presented as well.

Results and Discussion

Synthesis of PNP ligands

^{2}H NMR spectroscopy provides a valuable handle for the study of paramagnetic compounds.[26] Deuterium labeling can be achieved readily at the *ortho*-methoxyaryl position by methylating the appropriate phenol with CD_3I (Scheme 1). Two routes have been used for the synthesis of the diphosphine ligands (Schemes 1 and 2). For both routes ^{31}P NMR spectroscopy is a useful tool for monitoring the progress of the reaction. Scheme 1 outlines a linear protocol, involving reaction of the Grignard reagent from deuterated 2-bromomethylphenylether (**8**) with PBr_3 to give bromodiarylphosphine.[27] Condensation with $(CH_3)NH_3Cl$ in the presence of excess tertiary amine provides the desired product. Even though this route could provide clean product in 60% - 70% yields, it was found that the last step was difficult to reproduce.

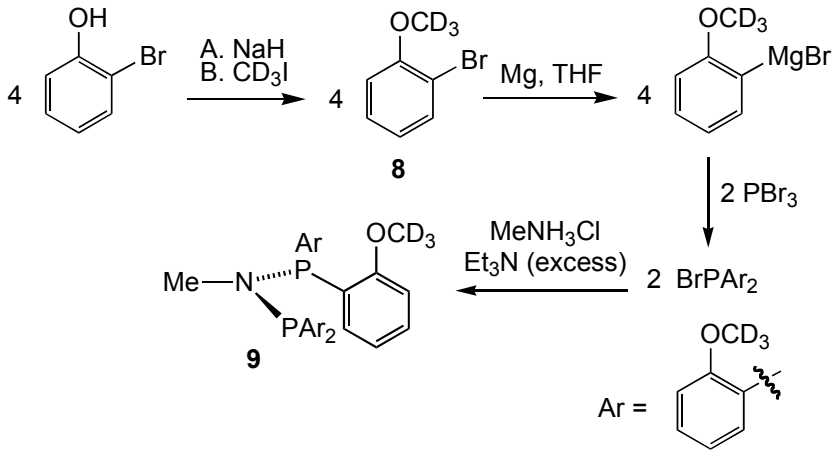

Scheme 1. Linear protocol for the synthesis of PNP ligands.

A convergent route was found to work well for the synthesis of a variety of PNP ligands (Scheme 2). This synthetic protocol takes advantage of the facile preparation of the PNP backbone unit (**12** or **13**),[28,29] which can be subsequently treated with a Grignard of choice (prepared from bromides such as **8**, **10**, or **11**) to give the desired diphosphines. Compound **14** was targeted as a more hydrocarbon-soluble version of **9**, as well as a system for comparison. During the last step in the preparation of **14**, intermediates such as the partially arylated species ($Ar_2PN(R^2)PArCl$ and $ArClPN(R^2)PArCl$) were observed by ^{31}P NMR spectroscopy. These results inspired a strategy to prepare diphosphine with mixed pendant donor sets. A Grignard reagent (**12** or **18**) displaying a pendant donor was treated with excess $(Cl_2P)_2NMe$ to generate $Cl_2PN(Me)PAr^LCl$ (Scheme 3). Upon removing excess $(Cl_2P)_2NMe$, the methoxy-substituted Grignard reagent (**8**) was added. This procedure allows access to PNP diphosphines (**21** and **22**) with mixed aryl sets in a ratio of 3:1. Initial experiments provided just impure samples of **21** and **22**; no optimization attempts were made

since this area of study was not developed beyond the crystallographic characterization of two chromium complexes and the related catalytic trimerization trials.

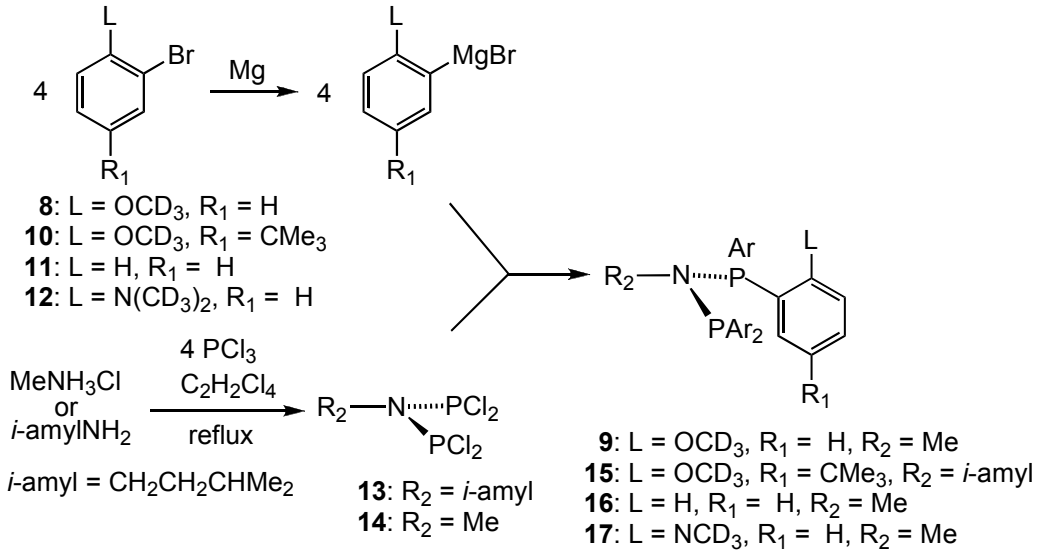

Scheme 2. Synthesis of PNP ligands with four identical aryl groups.

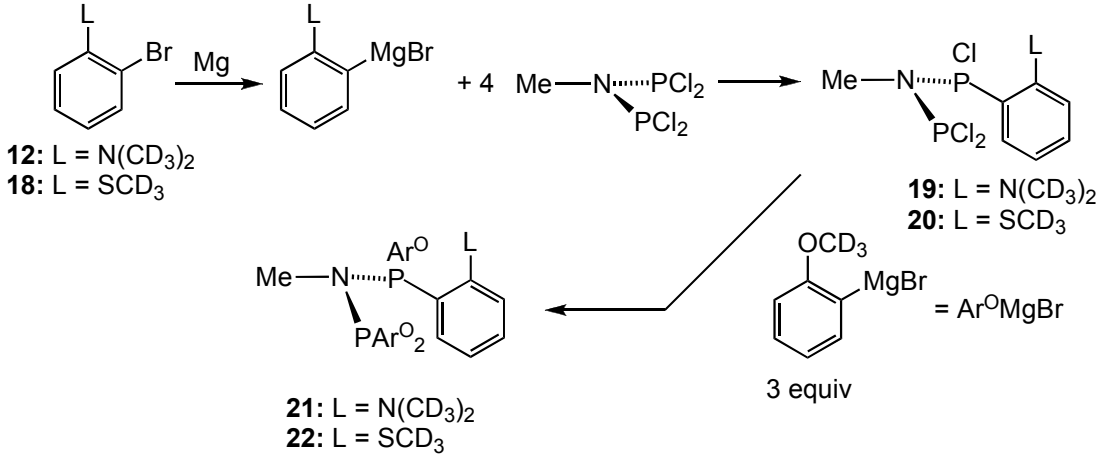

Scheme 3. Synthesis of PNP ligands with mixed aryl groups.

Synthesis of $Cr(CO)_4[(P,P)\text{-}\kappa^2\text{-}(PNP^{O4})]$ (23)

Chromium(0) carbonyls provide a possible entry into chromium-diphosphine chemistry, and indeed, a chromium tetracarbonyl complex (**23**) supported by diphosphine **9** can be prepared readily starting from $Cr(CO)_6$ (eq 2). Spectroscopic data are consistent with a (P,P)- κ^2 coordination mode, without involvement of the ether groups. The average stretching frequency for the four CO normal modes is 1916 cm^{-1} (CH_2Cl_2) in **23**, about 10 cm^{-1} lower than those reported for $Cr(CO)_4[(C_6H_5)_2PCH_2P(C_6H_5)_2]$ or $Cr(CO)_4[(C_6H_5)_2PCH_2CH_2P(C_6H_5)_2]$ (~1927 cm^{-1}) (Table 1).[30] On the other hand, the average CO stretching frequency for the tetracarbonyl complex (**24**) supported by the PNP phosphine without ether substituents (**16**) is 1925 cm^{-1}, very similar to the values for $(C_6H_5)_2PCH_2P(C_6H_5)_2$ and $(C_6H_5)_2PCH_2CH_2P(C_6H_5)_2$. This suggests that the presence of more electron-rich aryl groups bearing ethers in **9** is the main reason for the greater electron density at the metal center in **23**.[31] The amide in the ligand backbone has a smaller effect.

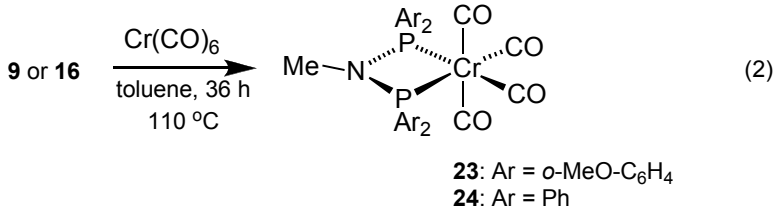

(2)

23: Ar = *o*-MeO-C_6H_4
24: Ar = Ph

Table 1. Carbonyl stretching frequencies for selected complexes.

	ν(CO) (CH_2Cl_2, cm^{-1})	$\nu(CO)_{ave}$ (CH_2Cl_2, cm^{-1})
$Cr(CO)_4[MeN(P(o\text{-}MeOC_6H_4)_2)_2]$	2003, 1906, 1886, 1867	1916
$Cr(CO)_4[MeN(PPh_2)_2]$	2008, 1917, 1895, ~1881	1925
$Cr(CO)_4[CH_2(PPh_2)_2]$	2011, 1918, 1903, 1878	1927
$Cr(CO)_4[C_2H_4(PPh_2)_2]$	2011, 1917, 1903, 1878	1927

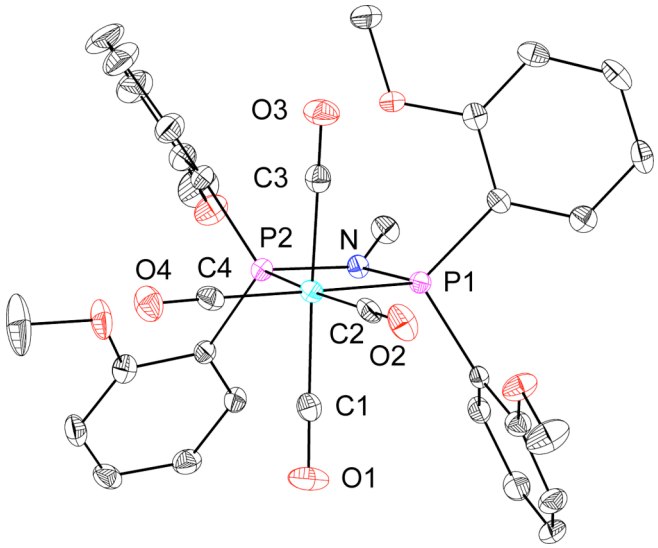

Figure 2. Structural drawing of **23** with displacement ellipsoids at the 50% probability level. Selected bond lengths (Å) and angles (°): Cr-P_1 2.3557(6); Cr-P_2 2.3712(5); Cr-C_2,C_4 (ave) 1.841; Cr-C_1,C_3 (ave) 1.875; C_2-O_2,C_4-O_4 (ave) 1.164; C_1-O_1,C_3-O_3 (ave) 1.152; N-P_1 1.6946(14); N-P_2 1.7046(14); P_1-N-P_2 101.24(7); P_1-Cr-P_2 67.536(18).

A single-crystal X-ray diffraction study confirmed the spectroscopic assignment of **23** (Figure 1). The Cr-P bond lengths are similar to the ones reported for analogous compounds.[32,33] Compared to $Cr(CO)_4(Me_2PCH_2PMe_2)$, **23** has a smaller P-Cr-P angle (67.54(2)° vs. 70.78(3)°) and a larger P-N-P angle (101.24(7)° vs. 95.74°) for P-C-P.[33]

Oxidation of $Cr(CO)_4[(P,P)\text{-}\kappa^2\text{-}(PNP^{O4})]$ – Accessing (PNP)chromium(III) complexes

Considering that chromium(I)/chromium(III) is one of the possible redox couples performing the trimerization reaction (see Chapter 3), chromium(III) or chromium(I) – PNP complexes could furnish useful information regarding the relevant coordination chemistry of the catalyst and could provide good synthetic entries for mechanistic studies. The oxidation of **23** with $C_6H_5ICl_2$, Br_2, or I_2 affords $CrX_3(PNP^{O4})$ (eq 3). The products with X = Cl (**25**) and I (**27**) were structurally characterized (Figures 2 and 3), confirming the structures shown with the PNP ligand bound in a κ^3-(P,P,O) fashion. While all the above products are paramagnetic (^{2}H NMR), diamagnetic byproducts are present as well in the crude reaction mixture. Recrystallization from CH_2Cl_2/petroleum ether mixture affords the desired chromium(III) products cleanly.

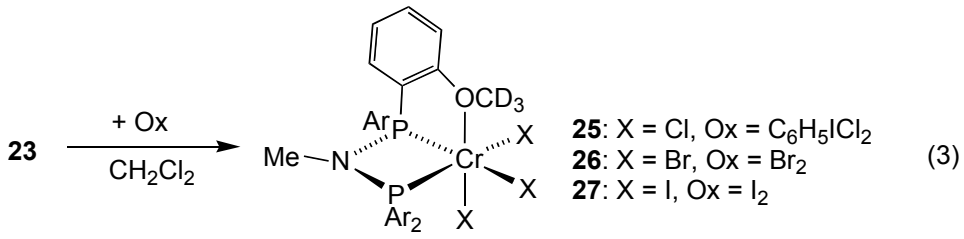

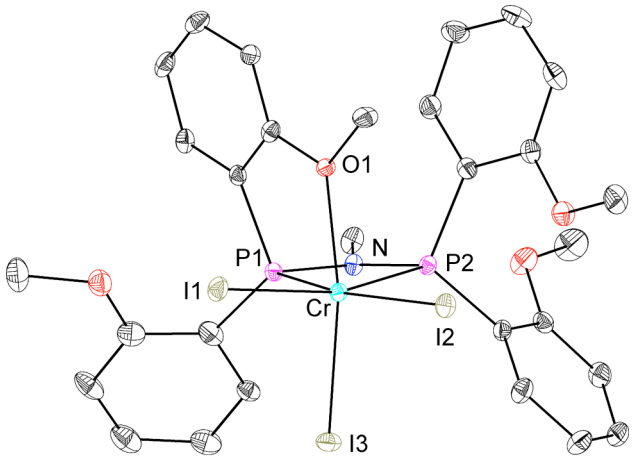

Figure 3. Structural drawing of **27** with displacement ellipsoids at the 50% probability level. Selected bond lengths (Å) and angles (°): Cr-P_1 2.3891(6); Cr-P_2 2.5205(6); Cr-O_1 2.1820(14); Cr-I_1 2.6604(3); Cr-I_2 2.6765(3); Cr-I_3 2.6481(3); N-P_1 1.6990(16); N-P_2 1.7020(16); P_2-Cr-P_1 66.825(18); O_1-Cr-C_{30} 163.77(4); P_1-N-P_2 105.42(9).

Synthesis of $CrCl_3[\kappa^3$-(P,P,O)-$(PNP^{O4})]$ (25), $CrCl_3[\kappa^3$-(P,P,O)-$(P^{t\text{-}Bu}N^{i\text{-}amyl}P^{O4})]$ (28), and $CrCl_2(CH_3)[\kappa^3$-(P,P,O)-$(PNP^{O4})]$ (29) from chromium(III) starting materials

Direct metallation with chromium(III) precursors provides an alternative pathway for the synthesis of PNP supported chromium(III) complexes.

Chromium(III) starting materials are commercially available ($CrCl_3(THF)_3$) or easy to prepare ($CrCl_2(CH_3)(THF)_3$),[34] facilitating the access to the complexes and their characterization (eq 4). Compounds **25**, **28**, and **29** were prepared by displacement of THF with the diphosphine ligand in CH_2Cl_2. Because coordinating solvents, such as THF, compete with the diphosphine for coordination to chromium(III), their use has been avoided or minimized. ^2H NMR spectroscopy is very useful in the characterization of the paramagnetic reaction products. Broad peaks downfield from the diamagnetic region indicate the formation of paramagnetic species.

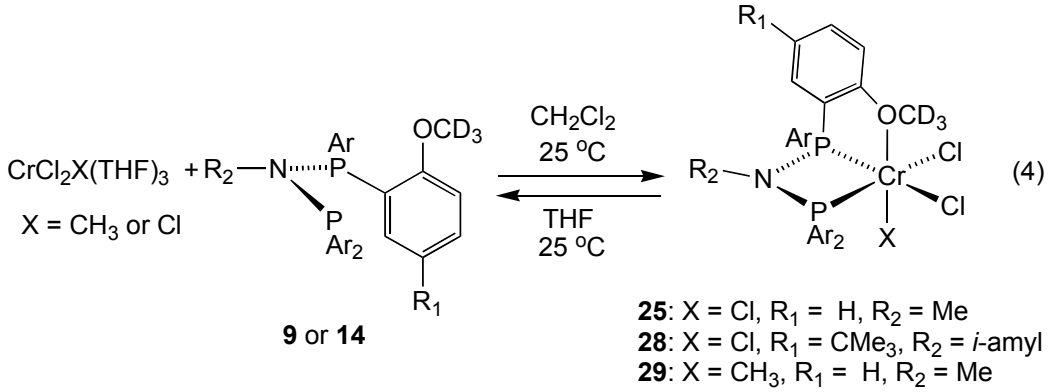

Solution magnetic susceptibility measurements obtained by the method of Evans[35,36] for the isolated compounds are consistent with a quartet ground state (μ_{eff} = 3.8 μ_B for **25**, 3.9 μ_B for **28**, and 3.7 μ_B for **29**). Compounds **25** (Figure 4), **28** (Figure 5), and **29** (Figure 6) were structurally characterized by single crystal X-ray diffraction; all display κ^3-**(P,P,O)** coordination of the diphosphine to yield a coordination number of six around the metal center. In **29**, the methyl group coordinates *trans* to the oxygen, rather than to the phosphorus, presumably due to a smaller *trans* influence for the ether donor. Due to the presence of a few

disordered solvent molecules in the crystal, reliable structural parameters were not obtained for **28**; however, connectivity similar to **25** was observed (Figure 5). The fact that **25** and **28** have similar molecular structures may indicate that making changes at the periphery of the ligand (*i.e.*, replacing a distal aryl-H with CMe_3 or replacing the N-methyl with N-*i*-amyl), while keeping the basic ligand framework constant (*i.e.*, preserving the PNP backbone and *o*-ether substituted aryls), does not substantially alter the binding mode of the methoxy substituted diphosphine ligands. Comparisons among the structures of **25**, **28**, and **29** are presented in a later section.

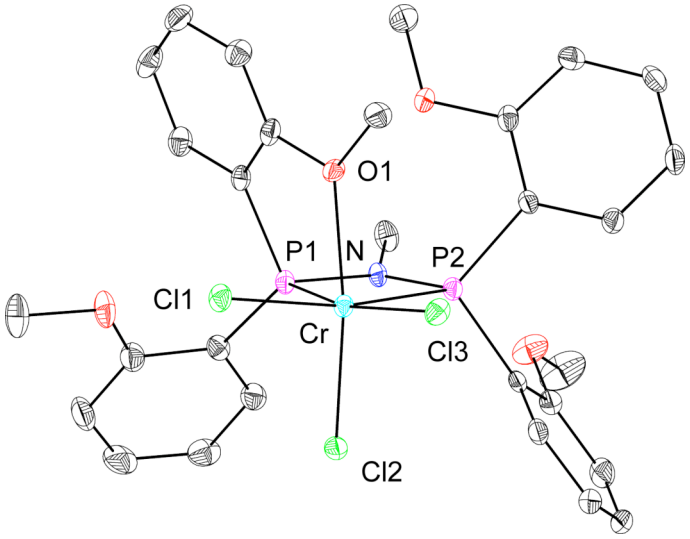

Figure 4. Structural drawing of **25** with displacement ellipsoids at the 50% probability level. Selected bond lengths (Å) and angles (°): Cr-P_1 2.3855(7); Cr-P_2 2.5098(7); Cr-O_1 2.1562(15); Cr-Cl_1 2.2937(6); Cr-Cl_2 2.2776(6); Cr-Cl_3 2.3210(7); N-P_1 1.6920(18); N-P_2 1.6978(18); P_2-Cr-P_1 66.56(2); O_1-Cr-Cl_2 165.62(4); P_2-N-P_1 104.95(10).

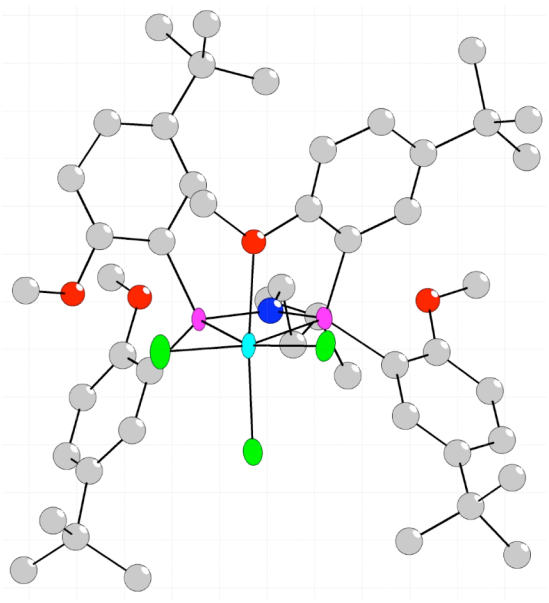

Figure 5. Structural drawing of **28**. The quality of the dataset precluded reliable determination of structural parameters.

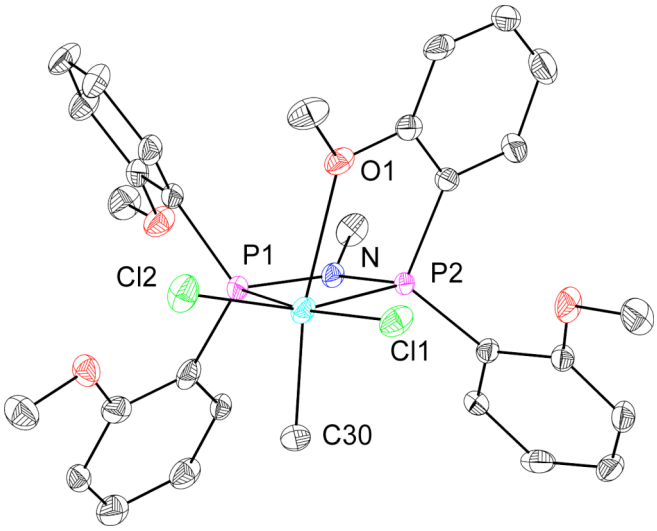

Figure 6. Structural drawing of **29** with displacement ellipsoids at the 50% probability level. Selected bond lengths (Å) and angles (°): Cr-P_1 2.4010(10); Cr-P_2 2.5204(10); Cr-O_1 2.435(2); Cr-C_{30} 2.061(4); Cr-Cl_1 2.2939(10); Cr-Cl_2 2.3011(9); N-P_1 1.701(2); N-P_2 1.691(3); P_2-Cr-P_1 66.54(3); O_1-Cr-C_{30} 166.44(15); P_1-N-P_2 105.58(14).

Chromium chlorides supported by PNP ligands with amine pendant groups

In order to study the effect of changing the nature of pendant donors, the coordination chemistry of diphosphine **17** has been investigated. Reaction of **17** with $CrCl_3(THF)_3$ in CH_2Cl_2 generates **30** (Eq 5) cleanly according to ^2H NMR spectroscopy. Compound **30** has been structurally characterized by single crystal X-ray diffraction (Figure 7). In contrast to the diphosphine ligands substituted with methoxy groups (**9** and **15**), **16** binds to chromium in a *mer*-(P,N,N)-κ^3 fashion. This coordination mode indicates that the amine chelates to chromium better than the ether, by displacing one of the phosphine arms. Displacement of the phosphine is probably due to a combination of better binding ability for the amine and more favorable ring size for the chelate in **30**. The Cr-N bond lengths are slightly longer than the ones for reported chromium(III) trichlorides supported by trialkyl amines.[37,38] This difference could be due to a better donating ability of trialkyl amines vs. dialkylaryl amines, or to strain in the chelate. It is interesting to note that the P-N-P angle can reach a value as large as 122°, in contrast to the significantly smaller angles (< 107°) observed in compounds with both phosphines coordinated.

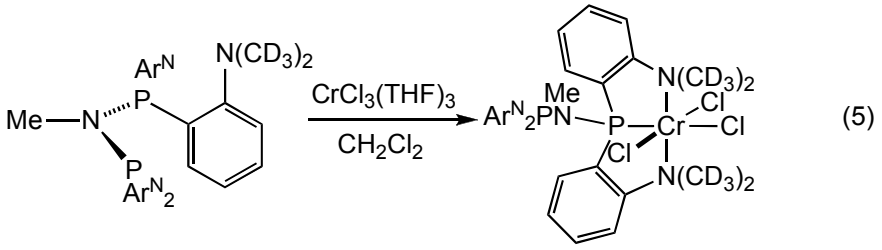

(5)

17 **30**

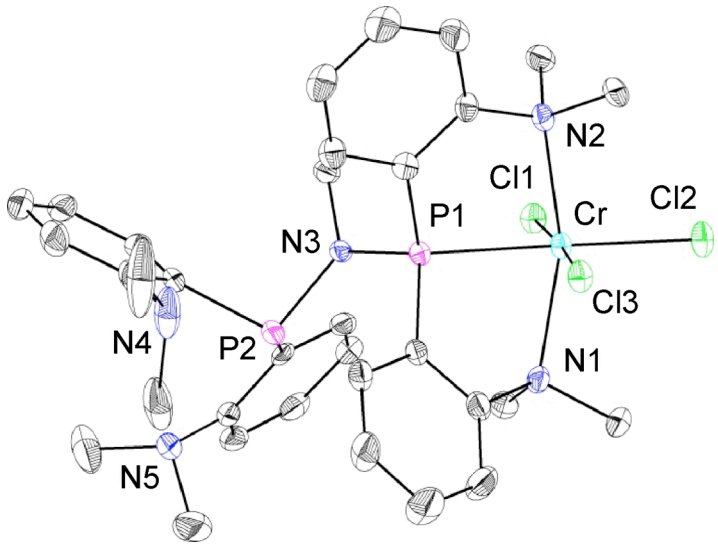

Figure 7. Structural drawing of **30** with thermal ellipsoids at the 50% probability level. Selected bond lengths (Å) and angles (°): Cr-P_1 2.3485(7); Cr-N_2 2.2269(19); Cr-N_1 2.2319(19); Cr-Cl_1 2.3123(7); Cr-Cl_2 2.3488(7); Cr-Cl_3 2.3186(7); N_3-P_1 1.6798(18); N_1-P_2 1.7396(18); N_2-Cr-P_1 82.23(5); P_1-N_1-P_2 122.8(1).

Reaction of diphosphine **21**, displaying one amine and three ether pendant donors, with $CrCl_3(THF)_3$ was investigated. This provided access to X-ray quality single crystals of **31** (Figure 8). The dimeric structure, with bridging chlorides, is surprising given that a phosphine and three ether pendant donors are available for chelation to the metal center. Notably, coordination to nitrogen is observed rather than oxygen or the other phosphine. This suggests that the PNP phosphines with various pendant donors display a subtle balance between different binding modes, possible controlled by ring strain of different chelates and the donating ability of different donors. Crystallization of this particular structure could be due to lower solubility and does not give information about the ligand binding modes that may occur in solution. This ligand system was not further explored.

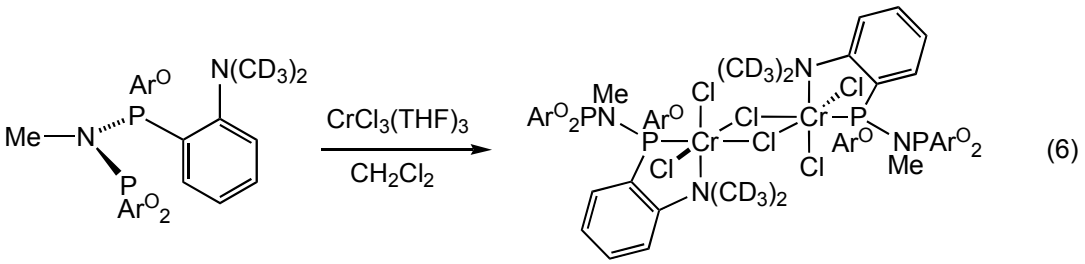

21 **31** (6)

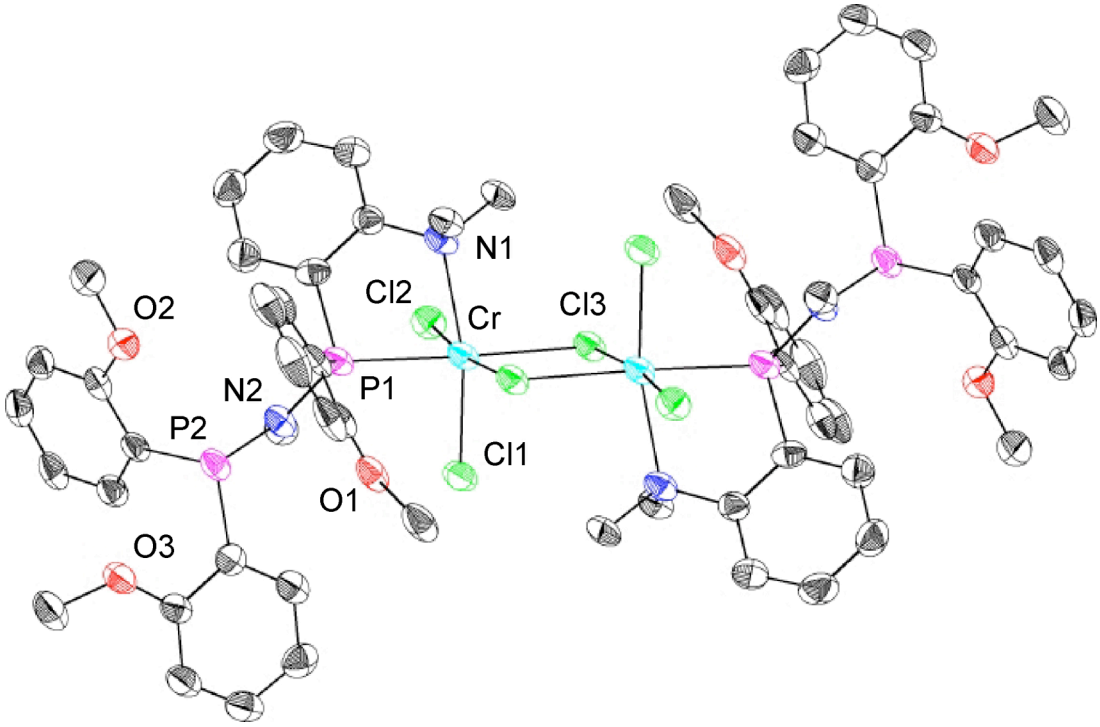

Figure 8. Structural drawing of **31** with thermal ellipsoids at the 50% probability level. Selected bond lengths (Å) and angles (°): Cr-P_1 2.4319(9); Cr-N_1 2.244(2); Cr-Cl_1 2.2931(9); Cr-Cl_2 2.2777(9); Cr-Cl_3 2.4415(8); Cr-Cl_{3A} 2.3536(9); N_2-P_1 1.677(2); N_2-P_2 1.742(2); N_2-Cr-P_1 78.43(6); P_1-N_1-P_2 121.38(14).

Chromium alkyls and metallacyclopentanes as entry points for mechanistic studies – Synthesis of CrBr(*o,o′*-biphenyldiyl)[κ^3-(P,P,O)-(PNP^{O4})] (32)

The proposed mechanism involves a chromacyclopentane intermediate;[29,39-42] isolation of such a complex could provide, upon activation, direct access to models of the species in the proposed catalytic cycle. Attempts to prepare analogs of metallacyclopentane have been successful, probably because chelation makes the products stable to side reactions. Compound **32** has been prepared from *o,o′*-biphenyldiyl Grignard reagent and chromium trichloride **25** (eq 5). The solid-state structure of **32** (Figure 9) shows distorted octahedral coordination with the biphenyldiyl group *trans* to the weakly bound donors – the ether and the outside phosphine. The structure of **32** will be discussed in further detail in the next section. Bromide abstraction from **32** may be effected with Na[B(3,5-$(CF_3)_2$-$C_6H_3)_4$] in order to access a cationic chromium *o,o′*-biphenyldiyl complex. Although reaction occurred readily, giving one major product as assessed by ^{2}H NMR spectroscopy, its structure has not yet been fully characterized.

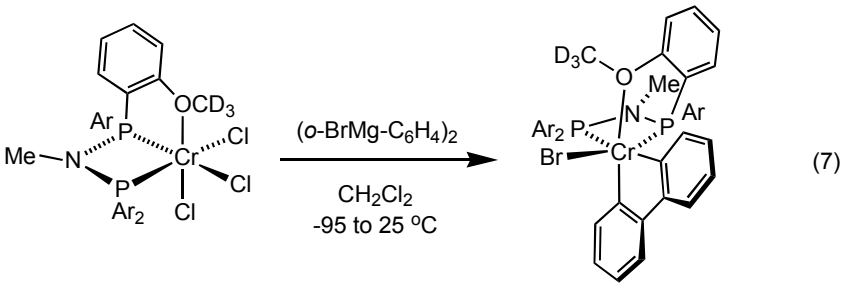

25 **32** (7)

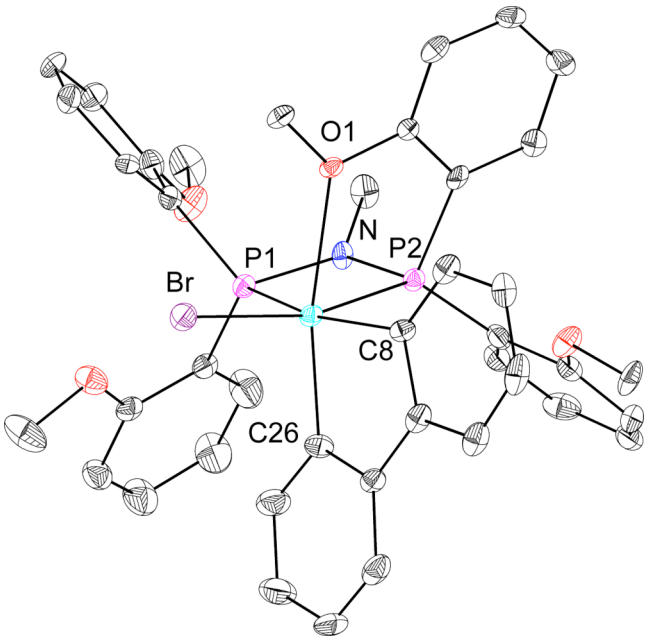

Figure 9. Structural drawing of **32** with displacement ellipsoids at the 50% probability level. Selected bond lengths (Å) and angles (°): Cr-P_1 2.6606(14); Cr-P_2 2.4287(14); Cr-O_1 2.3331(33); Cr-C_{26} 2.0361(51); Cr-C_8 2.0611(49); Cr-Br 2.4811(9); N-P_1 1.7055(40); N-P_2 1.7049(38); P_2-Cr-P_1 64.97(4); C_{26}-Cr-C_8 82.04(21); P_1-N-P_2 106.93(19).

The structures of **25**, **28**, and **29** show κ^3 coordination mode of the ligand. Since MAO is commonly used to generate a cationic transition metal alkyl from halide precursors, the active species in the proposed catalytic cycle (Scheme 2) may be a cationic chromium(III) dialkyl complex with one or more additional ether groups coordinated. Halide abstraction reactions from **25** and **29** occurs readily, even with mild reagents like Na[B(3,5-$(CF_3)_2$-$C_6H_3)_4$], but the resulting species have not been structurally characterized. Preparations of alkyl complexes, starting from **25**, **28**, and **29** and alkylating agents such as Grignard

reagents and lithium, aluminum, and zinc alkyls, have been attempted, but have been unsuccessful thus far.

Following an alternative route to (PNP)Cr-phenyl complexes reported by Bercaw *et al.*, diphosphine **22** was treated with $CrPh_3(THF)_3$ in CH_2Cl_2.[5] Complex **33** was obtained as green crystals from a petroleum ether / CH_2Cl_2 solution. It is not clear if this complex is formed by halide abstraction from the solvent or if the halide is derived from an impurity in the chromium precursor. The solid-state structure of **33** shows coordination of the two phosphines along with the thioether (Figure 10). The chromium coordinated phenyl groups are *trans* to a phosphine and to a thioether, similar to the structure of **32**. Coordination of the thioether in preference to one of the three ethers suggests that the sulfur-based ligand is a better donor for chromium center in this case. This system was not further explored.

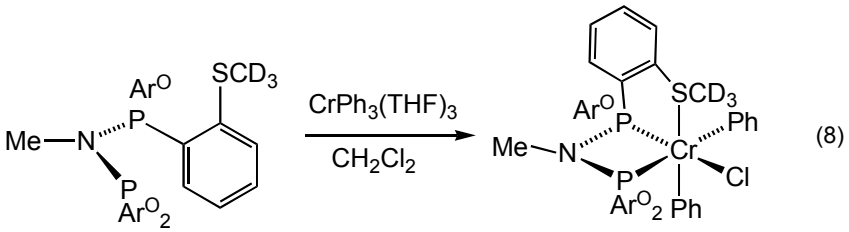

(8)

22 **33**

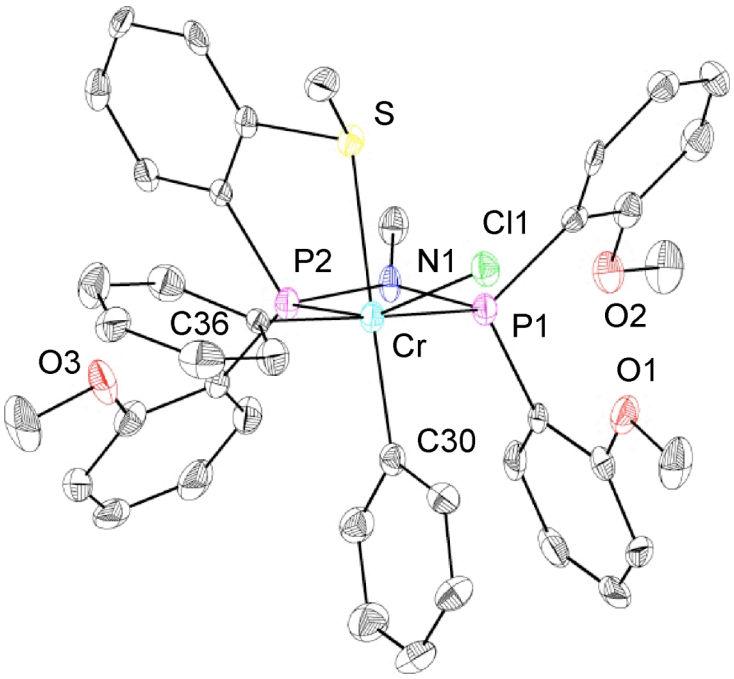

Figure 10. Structural drawing of **33** with displacement ellipsoids at the 50% probability level. Selected bond lengths (Å) and angles (°): Cr-P_1 2.5755(9); Cr-P_2 2.5235(9); Cr-S_1 2.5450(9); Cr-C_{36} 2.078(3); Cr-C_{30} 2.042(3); Cr-Cl_1 2.3117(9); N-P_1 1.717(2); N-P_2 1.702(2); P_2-Cr-P_1 65.36(3); S_1-Cr-C_{30} 174.90(9); P_1-N-P_2 107.30(11).

Ether exchange processes in complexes supported by PNP^{O4} ligands

^{2}H NMR spectroscopy proved to be instrumental in understanding the solution behavior of the (PNP)chromium(III) complexes. The number of peaks observed in the ^{2}H NMR spectra of all reported compounds is smaller than expected for the static solid state structure. This suggests a dynamic process that allows the exchange of ether groups, and a variable-temperature ^{2}H NMR study was therefore undertaken (Figure 6).

Compounds **25**-**29** and **32** display one peak in the ^{2}H NMR spectra at the fast exchange limit (temperatures higher than 40 °C). Upon cooling, two decoalescence processes are apparent (Table 2). At the lowest temperatures one broad, presumably paramagnetically shifted peak corresponding to one ether and one (or two for **32**) sharper peak(s) are observed (Figure 11). At intermediate temperatures two peaks in a one to one ratio of intensities are observed, one broader and more paramagnetically downfield shifted (Figure 11, -25 °C spectrum, and Figure 12).

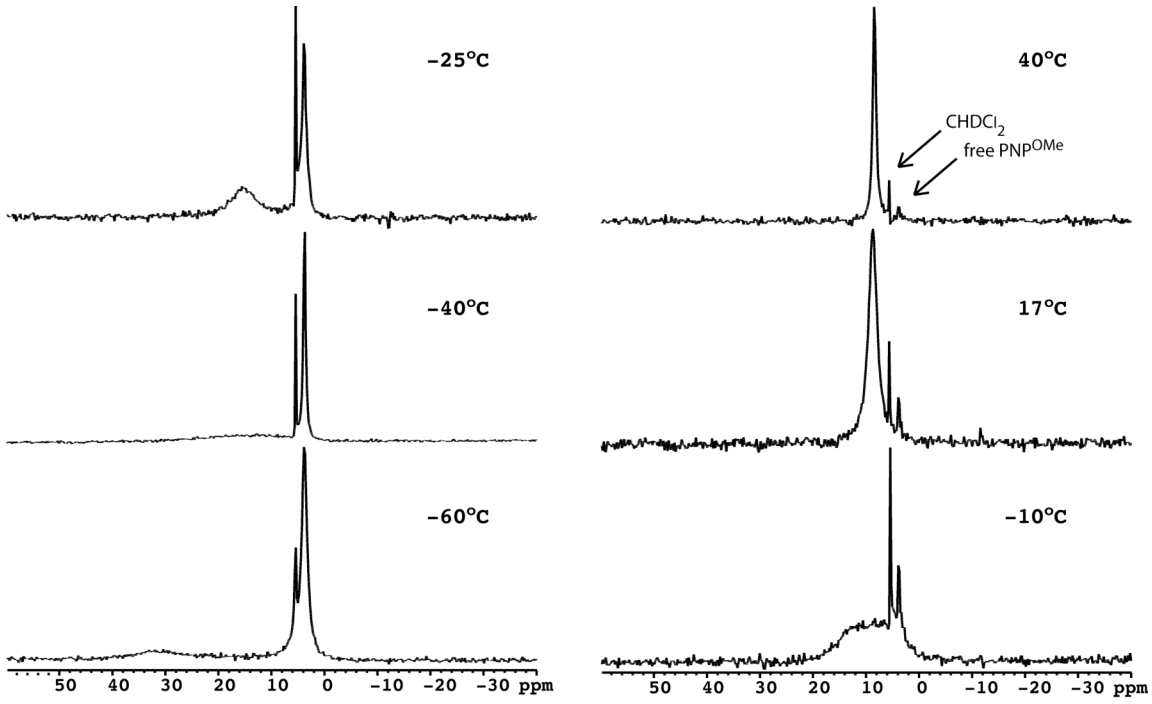

Figure 11. Variable temperature ^{2}H NMR (CH_2Cl_2) spectroscopic study of **25**.

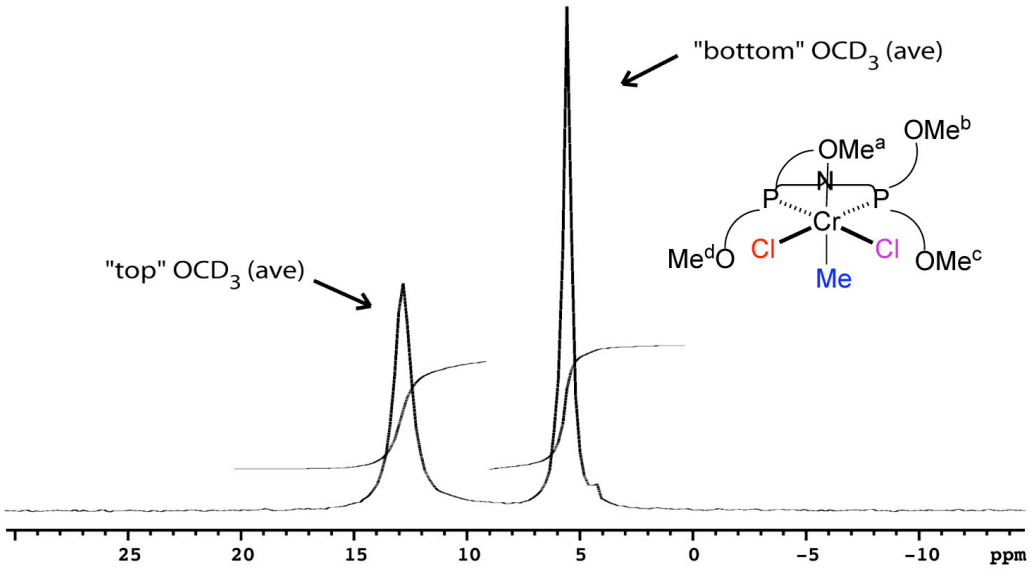

Figure 12. Room temperature ^{2}H NMR (CH_2Cl_2) spectrum of **29**.

Table 2. Coalescence temperatures for compounds **25**, **28**, **29**, and **32** in CH_2Cl_2.

	1st Coalescence (°C)	2nd Coalescence (°C)
25	-50	-10
28	-5	18
29	<-80	40[a]
32	-10	15

[a] in chlorobenzene

The proposed processes that allow the stepwise, dynamic exchange of the ether groups are shown in Schemes 4 and 5 for compounds **25** and **29**. The lower barrier corresponds to uncoordination of the ether group allowing two sets of two ether groups to interchange. The higher barrier corresponds to Berry pseudorotations that exchange the "top" and "bottom" of the molecule. In the case of complex **25**, only one Berry pseudorotation is necessary for this exchange (Scheme 4), while complex **29** requires three such processes (Scheme 5). Thus, at the highest temperatures, where this barrier is overcome, the ^{2}H NMR spectra display only one peak corresponding to fast interchange of the ether groups (Figure 11 – 17 °C and 40 °C spectra). Similar variable temperature behavior was observed for compounds **21** and **23**, indicating that ether exchange occurs in a variety of related complexes displaying different anionic ligands and peripheral ligand framework. The overlap of the noncoordinated ether signals even at low temperature (Figure 11, – 60 °C spectrum) is probably due to smaller paramagnetic shifts and, hence, a smaller difference in their chemical shifts along with a broadening of the peaks due to the sample paramagnetism and increased viscosity.

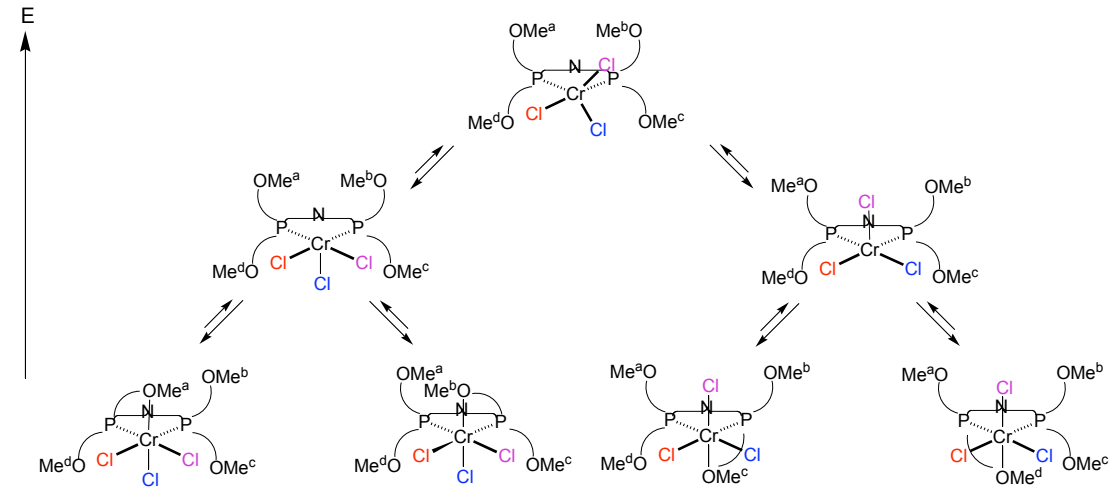

Scheme 4. Proposed mechanism for the exchange of ether groups in **25**.

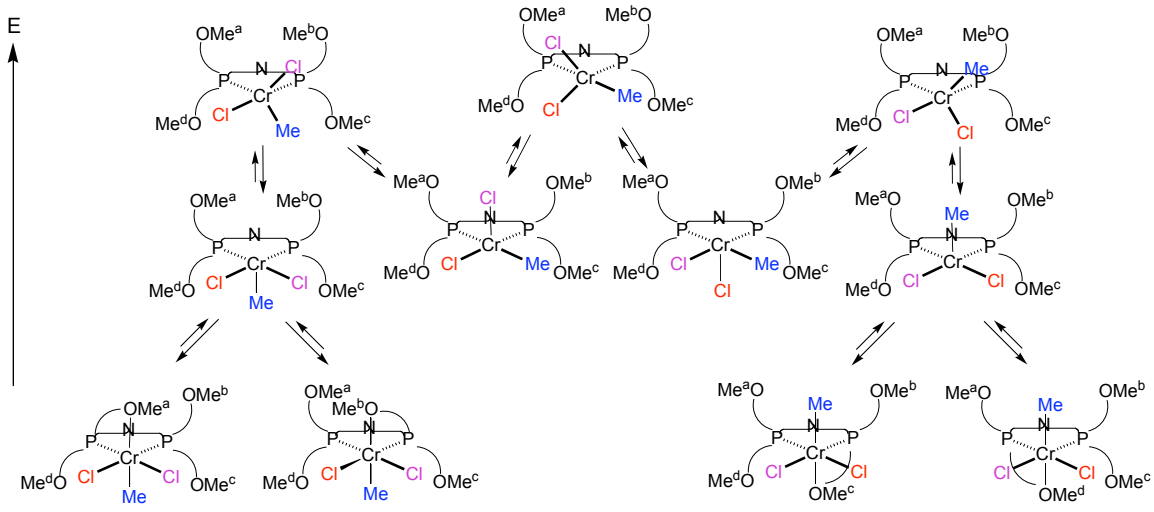

Scheme 5. Proposed mechanism for the exchange of ether groups in **29**.

Quantifying the thermodynamic barriers, for example by fitting the chemical shifts and line widths to predicted values, was not attempted, due to paramagnetic contributions in broadening and chemical shift. However, a qualitative analysis of some of the factors that could influence those energies suggests that the relative size of the barriers may correlate with the differences in

the coalescence temperatures. For instance, comparing **25** and **29**, the first barrier is expected to be lower in **29** because of the stronger *trans* influence of the methyl group (ground state destabilized). The second barrier is expected to be higher in **29** because that process involves placing a methyl rather than a chloride *trans* to a phosphine (intermediate destabilized – more than the ground state).

Fluxional process in complex 30, supported by the PNP^{N4} ligand

Complex **30**, with ^{2}H–labeled amine groups, was investigated by variable temperature ^{2}H NMR spectroscopy (CH_2Cl_2). At low temperature, four very broad paramagnetically shifted peaks are observed along with two sharper peaks in the diamagnetic region (Figure 13). At higher temperatures, two broad, paramagnetically shifted peaks and one sharp peak in the diamagnetic region are observed. The low temperature spectrum is consistent with a C_1-symmetric structure like the solid-state one (Figure 7). At high temperature, rotation around the N3-P1 bond allows exchange of the methyl groups related by a pseudo-mirror plane containing P1 and Cr and bisecting the N1-N2 vector. However, the methyl groups found on the same nitrogen (N1 or N2) cannot exchange by this process and hence, give rise to two paramagnetically shifted peaks. Importantly, at these temperatures the coordinated amines do not exchange with the noncoordinated amines, in contrast to the behavior observed for the systems with ether pendant groups. This indicates that the amines are tighter bound compared to the ether groups.

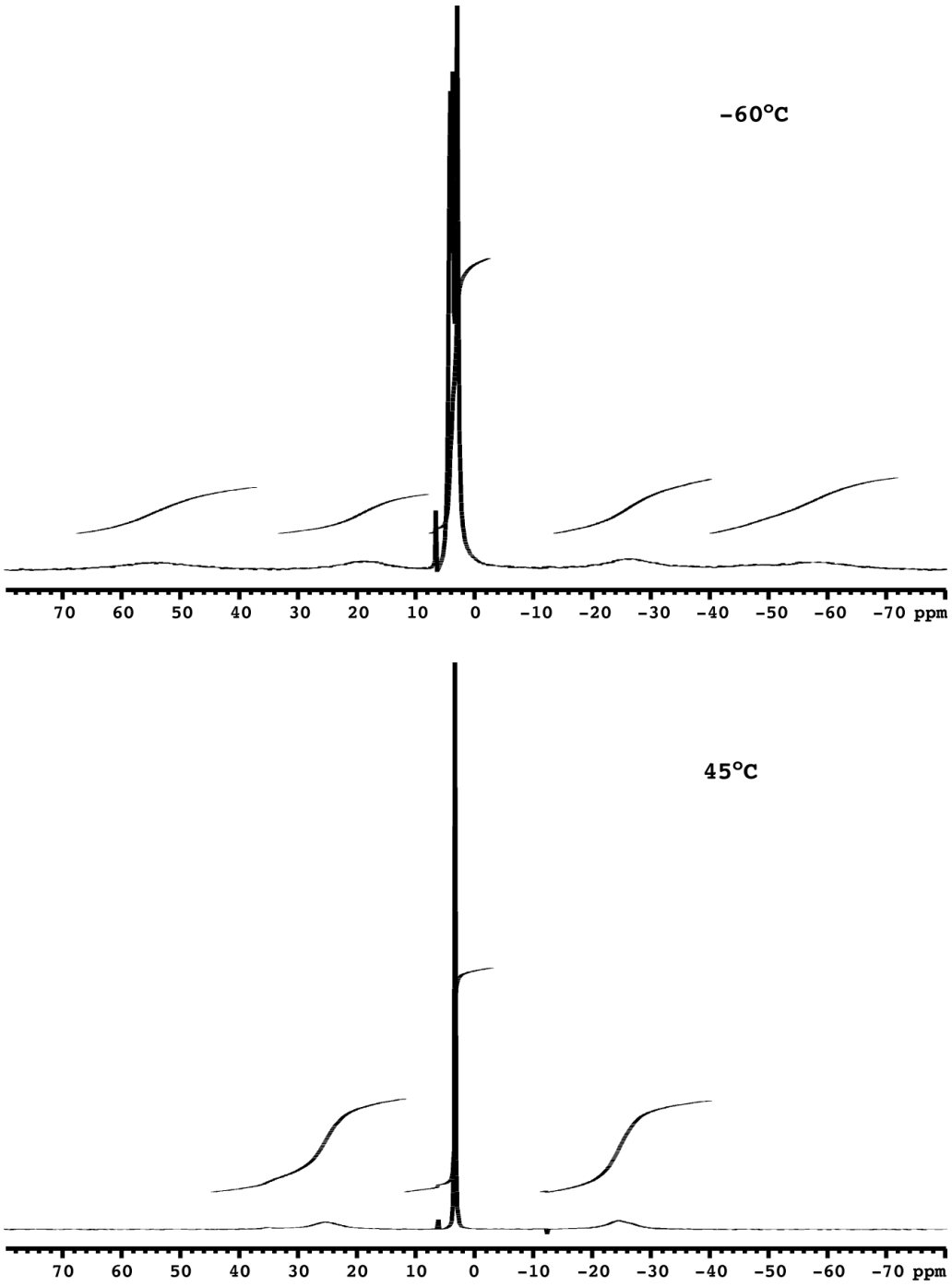

Figure 13. Variable temperature ^{2}H NMR (CH_2Cl_2) spectroscopic study of **30**.

Structural comparisons between Cr/PNP^{O4} complexes

In all the characterized compounds, the metal center is six-coordinate. Moving from chromium(0) to chromium(III) the Cr-P bond lengths increase significantly (Table 3). The same general trend was found for other reported chromium(0) and chromium(III) complexes.[32,33,43-45] This may be due to a mismatch between the hard chromium(III) center and the soft phosphines, which counterbalances the contraction of the metal in the higher oxidation state. The P-Cr-P and P-N-P angles are each quite similar for the reported compounds; the most notable difference is in the P-N-P angle for chromium(0) vs chromium(III).

Table 3. Selected structural parameters for **23**, **25**, **27**, Cr(PNP^{O4})Ph$_3$, **29**, and **32**. P$_a$ corresponds to the outside phosphine (not chelated through an ether).

	Cr-P$_a$ (Å)	Cr-P$_b$ (Å)	Cr-O (Å)	P-N-P (°)	P-Cr-P (°)
23	2.3712(5)	2.3557(6)	---	101.24(7)	67.54(2)
25	2.5098(7)	2.3855(7)	2.1562(15)	104.95(10)	66.56(2)
27	2.5205(6)	2.3891(6)	2.1820(14)	105.42(9)	66.83(2)
CrPh$_3$(PNP^{O4}) [a]	2.6381	2.4971	2.286	105.72	64.02
29	2.5204(10)	2.4010(10)	2.435(2)	105.58(14)	66.54(3)
32	2.6606(14)	2.4287(14)	2.3331(33)	106.93(19)	64.97(4)

[a] Average for the two molecules in the asymmetric unit

The two Cr-P bond lengths in all the chromium(III) compounds are significantly different, with Cr-P_b (P_b corresponds to the phosphine whose pendant ether coordinates to the metal) being shorter due to oxygen chelation. In the compounds containing homoleptic anionic ligand sets, the difference between the two Cr-P bond lengths is quite constant – between 0.12 (in **25**) and 0.14 Å (in $CrPh_3(PNP^{O4})$)[5]. The halide complexes show similar Cr-P as well as Cr-O bond lengths. Compared to the halide complexes, $CrPh_3(PNP^{O4})$ shows elongation of all the Cr-PNP^{O4} contacts, probably due to an increased *trans* influence from the phenyl groups.

When the anionic ligand sets are heteroleptic, the differences in structural parameters are more substantial. For instance, replacement of a chloride (in **18**) with a methyl (in **29**) leads to Cr-O bond elongation by almost 0.3 Å, likely due to a strong *trans* influence from the methyl group. The effect on the Cr-P bond lengths is small (< 0.02 Å), suggesting that the PPO framework is quite flexible, so that each donor is able to adjust its distance to chromium without affecting the others significantly. In **32**, the presence of two different ligands (halide and aryl) in the P-Cr-P plane causes a larger difference between the two Cr-P bond lengths (~0.23 Å). The Cr-P_b bond *trans* to the aryl groups elongated to 2.6606(14) Å, the longest Cr-P bond length to our knowledge.[46] The relatively small increase of the P-N-P angle and decrease of the P-Cr-P angle from **25** to **32** correlate with the increase in the Cr-P bond lengths, probably to minimize the overall ring deformation. Since the species involved in the catalytic cycle are presumably chromium alkyls, it is important to note that the methyl in **29** prefers to ligate

trans to the ether, not to the phosphine, and that the *o,o'*-biphenyldiyl in **32** prefers to ligate *trans* to a phosphine and an ether rather than two phosphines.

Trimerization trials with well defined (PNP)chromium(III) precursors

With (PNP)chromium(III) complexes in hand, ethylene trimerization tests were performed. Chromium complexes **25**, **28**, and **32** were activated with excess methyl aluminoxane (MAO, 300 equiv) in toluene under ethylene to generate systems active for catalytic ethylene trimerization. The catalysts generated under these conditions are not stable catalyst systems, however, and ethylene trimerization activity decreases to ~10% the initial value within 30 minutes. Considering that the large excess of MAO hinders the utilization of ^{1}H NMR spectroscopy for mechanistic studies, stoichiometric activators have been investigated as well. It has been found that compound **32** can trimerize ethylene catalytically upon activation with Na[B(3,5-$(CF_3)_2$-$C_6H_3)_4$]. When **32** is exposed to ethylene without halide abstraction, no 1-hexene formation is observed (^{1}H NMR). This may be due to various factors including decreased electrophilicity or a smaller number of coordination sites available to an incoming olefin in the neutral complex.

Trimerization trials with PNP^{N4} (16), PNP^{O3N} (21), and PNP^{O3S} (22)

To investigate the effect of the pendant donors on the catalytic trimerization activity, diphosphines with various numbers of non-oxygen pendant donors were studied. Either diphosphine in combination with $CrCl_3(THF)_3$ or an isolated chromium complex in toluene were used as precursors for activation with MAO, under ethylene. Limited (for **21**) or practically no catalytic activity (for **16** and **21**) is observed for these systems. It is important to note that the preparation of mixed systems **21** and **22** may lead to a small impurity of PNP^{O4} to be present if excess $MeN(PCl_2)_2$ is not completely removed (Scheme 3). This could lead to some 1-hexene generation. However, the observed decrease in catalytic activity suggest that sulfur and nitrogen based donors are detrimental to 1-hexene formation under these conditions. This could be due to their better binding ability compared to the ethers (as suggested by solid-state structures and exchange studies) which may block a coordination site necessary during catalysis.

Conclusions

A series of chromium(0) and chromium(III) complexes supported by PNP ligands has been synthesized and characterized. It has been found that the PNP^{O4} ligand can display κ^2-(P,P) and *fac*-κ^3-(P,P,O) coordination modes. In all the cases investigated, a coordination number of six is observed for the chromium(III) center. The Cr-O bond length is very dependent (2.16 to 2.44 Å)

on the nature of the ligand *trans* to the ether. Coordination of the pendant ether draws the corresponding phosphorus donor ca. 0.12 - 0.23 Å closer to Cr. One of the halide ligands is found to be labile in chromium(III)(PNP^{O4}) complexes, facilitating the generation of cationic species. This has allowed the generation of a catalytic system for ethylene trimerization based on a chromium(III)(PNP^{O4}) biphenyldiyl complex upon activation with stoichiometric amounts of $Na[B(3,5\text{-}(CF_3)_2\text{-}C_6H_3)_4]$. Activation of well-defined precursors with excess MAO also generates systems active for catalytic trimerization of ethylene. ^2H NMR spectroscopy has been very useful for the characterization of paramagnetic compounds. Variable temperature ^2H NMR spectroscopy studies show that, in solution, the ether groups are involved in a dynamic exchange process. This indicates that, while binding to the ether groups is possible, the interaction is not very strong. PNP ligands with thioethers and amine ortho substituents show a preference of binding to sulfur or nitrogen vs phosphorous or ether. Trimerization trials with diphosphines displaying nitrogen and sulfur based donors (PNP^{N4}, PNP^{O3N}, PNP^{O3S}) show limited or no catalytic activity under the investigated conditions. This indicates that donors that bind better than the pendant ethers decrease the catalytic activity. Hence, lability of pendant donors is required for catalytic activity in these systems.

Experimental Section

General Considerations. All air- and moisture-sensitive compounds were manipulated using standard vacuum line, Schlenk, or cannula techniques or in a

drybox under a nitrogen atmosphere. Solvents for air- and moisture-sensitive reactions were dried over sodium benzophenone ketyl, calcium hydride, or by the method of Grubbs.[47] Compound **13**[29,34] and $CrCl_2(CH_3)(THF)_3$[34] were prepared as described previously. Dichloromethane-d_2 was purchased from Cambridge Isotopes and distilled from calcium hydride. Other materials were used as received. Methylaluminumoxane was purchased from Aldrich. UV-Vis measurements were taken on a Hewlett-Packard 8452A diode array spectrometer using a quartz crystal cell. Elemental analyses were performed by Desert Analytics, Tucson, AZ and by Midwest Microlab, Indianapolis, IN. ^{1}H and ^{13}C NMR spectra were recorded on Varian Mercury 300 or Varian INOVA-500 spectrometers at room temperature, unless indicated otherwise. Chemical shifts are reported with respect to internal solvent: 5.32 (t) ppm, and 54.00 (t) ppm (CD_2Cl_2); 7.27 ppm (s) and 77.23 ppm (t) ($CDCl_3$) for ^{1}H and ^{13}C data. ^{2}H NMR spectra were recorded on a Varian INOVA-500 spectrometer; the chemical shifts are reported with respect to an external D_2O reference (4.8 ppm). ^{31}P chemical shifts are reported with respect to an external H_3PO_4 85% reference (0 ppm).

Diphosphine synthesis: Procedure 1.[48] Compound **8** (8.36 g, 44 mmol, 4 equiv) in tetrahydrofuran (THF, 100 mL) was added to magnesium turnings (1.32 g, 55 mmol, 5 equiv) using a pressure-equalizing funnel. The reaction mixture was stirred at 40 °C for ~12 h. After cooling to room temperature, excess Mg was removed by filtration and the filtrate was added to a cold (-78° C) solution of PBr_3 (2.09 mL, 22 mmol, 2 equiv) in THF (total volume ~300 mL). After stirring for 1 h at low temperature, the mixture was allowed to reach room temperature and stir for 6 h (^{31}P NMR (121 MHz) of PAr_2Br δ: 63.2). NEt_3 (17 mL) was vacuum

transferred to the reaction mixture followed by solid $MeNH_3Cl$ (0.743 g, 11 mmol, 1 equiv). The resulting mixture was stirred at room temperature overnight. Volatiles were removed under vacuum and MeOH (70 mL) was added. The resulting slurry was cannula transferred to a sintered glass funnel and the desired product **9** was collected by filtration (3.7 g, 7 mmol, 63% yield). ^{1}H NMR (300 MHz, $CDCl_3$) δ: 2.43 (t, $^3J_{HP}$=3.3 Hz, 3H, NC*H*$_3$), 3.61 (s, 12H, OC*H*$_3$ – unlabeled version), 6.86 (app t, 8H, aryl-*H*), 7.07-7.11 (m, 4H, aryl-*H*), 7.31 (td, 4H, aryl-*H*). ^{13}C NMR (75 MHz, $CDCl_3$) δ: 33.9 (t, $^2J_{CP}$=5.7 Hz, NCH_3), 55.2 (OCH_3), 110, 120.1, 127.0 (t), 130, 133 (t), 160.7 (t). ^{31}P NMR (121 MHz, $CDCl_3$) δ: 52.2.

Diphosphine synthesis: Procedure 2. Compound **8** (7.14 g, 37.6 mmol, 4 equiv) was added via syringe to a mixture of magnesium turnings (1.21 g, 50 mmol, 5.2 equiv) and tetrahydrofuran (40 mL). The reaction mixture was stirred at 50°C for ~12 h. After cooling to room temperature, excess Mg was removed by filtration. The filtrate was added to a THF solution of **14** (2.19 g, 9.4 mmol, 1 equiv). The transfer was completed with the aid of some THF (total solution volume ~250 mL). The reaction mixture was stirred at 60°C for ~18 h. The reaction mixture was quenched with water and extracted with CH_2Cl_2. The combined organic fractions were dried over $MgSO_4$, and then filtered. Volatile materials were removed via rotary evaporation. The residue was dissolved in CH_2Cl_2 and half a volume of methanol was added. Upon concentration under vacuum, a white solid precipitated out and was collected by filtration. This procedure afforded 4.26 g (8 mmol, 85% yield) of spectroscopically pure desired product **9**.

(*i*-amyl)$NPCl_2$ (13). Compound **13** was synthesized using the published procedure used for **13**.[28,29] A mixture of *i*-amylamine (5 mL, 43 mmol, 1 equiv), PCl_3 (15 mL, 172 mmol, 4 equiv) and $C_2H_2Cl_4$ (30 mL) was refluxed, under argon, in an oil bath maintained at 150 °C. After 21 h the temperature was increased to 165 °C and the mixture was refluxed for an additional 48 h. Then, the reaction mixture was allowed to cool and the desired product was collected by low-pressure distillation (60 ºC, 0.03 torr) as a colorless liquid, analytically pure by NMR spectroscopy (6.12 g, 51% yield). ^{1}H NMR (300 MHz, C_6D_6) δ: 0.73 (d, 6H, C*H*$_3$), 1.31 (nonet, 1H, $(CH_3)_2CHCH_2$), 1.64 (m, 2H, CHC*H*$_2$), 3.56 (m, 2H, NC*H*$_2$). ^{13}C NMR (75 MHz, C_6D_6) δ: 22.7, 27.3, 41, 47.7 (t, $^2J_{CP}$=4.9 Hz, NCH_2). ^{31}P NMR (121 MHz, $CDCl_3$) δ: 166.25.

(2-MeO-4-*t*-BuC_6H_3)$_2$PN(*i*-amyl)P(2-MeO-4-*t*-BuC_6H_3)$_2$, $P^{t\text{-Bu}}N^{i\text{-amyl}}P^{O4}$ (15). Procedure 2 was employed: 38% isolated yield. ^{1}H NMR (300 MHz, C_6D_6) δ: 0.59 (d, 6H, CH(C*H*$_3$)$_2$), 1.75 (br m, 2H, CHC*H*$_2$), 1.23 (s, 36H, C(C*H*$_3$)$_3$), 3.75 (br m, 2H, NC*H*$_2$), 6.58 and 7.23 (app d, 8H, aryl-*H*), 7.76 (app s, aryl-*H*). ^{13}C NMR (75 MHz, C_6D_6) δ: 23.4, 27.8, 32.1, 34.7, 41.2 (t, $^3J_{CP}$=3.9 Hz, NCH_2CH_2), 53.9 (t, $^2J_{CP}$=11.1 Hz, NCH_2), 110.7, 126.8, 129.5 (t), 132.1 (t), 142.9, 159.9 (t). ^{31}P NMR (121 MHz, C_6D_6) δ: 44.7. If the last step in the preparation of **14** is performed at room temperature, intermediates are observed by ^{31}P NMR spectroscopy (121 MHz, $CDCl_3$) δ: 138 (s, ArCl*P*N(*i*-amyl)*P*ArCl); 54 (d, $^2J_{PP}$=330 Hz, Ar$_2$*P*N(*i*-amyl)PArCl), 141 (d, Ar$_2$PN(*i*-amyl)*P*ArCl).

(2-Me_2N-C_6H_4)$_2$PN(Me)P(2-Me_2N-C_6H_4)$_2$, PNP^{N4} (17). Procedure 2 was employed: 44% isolated yield. ^{1}H NMR (300 MHz, $CDCl_3$) δ: 2.31 (t, $^3J_{HP}$=3.3 Hz,

3H, PNCH_3), 2.57 (s, 24H, N(CH_3)$_3$ – unlabeled version), 6.91 and 7.24 (triplets, 8H, 4- and 5-aryl-*H*), 7.04-7.11 (m, 8H, 3- and 6-aryl-*H*). ^{1}H NMR (500 MHz, CD_2Cl_2) δ: 2.26 (t, $^3J_{HP}$=3.3 Hz, 3H, PNCH_3), 2.56 (s, 24H, N(CH_3)$_3$ – unlabeled version), 6.92 and 7.24 (triplets, 8H, 4- and 5-aryl-*H*), 6.99 and 7.13 (doublets, 8H, 3- and 6-aryl-*H*). ^{13}C NMR (125 MHz, CD_2Cl_2) δ: 34.0 (NCH_3), 45.5 (t, N(CH_3)$_2$), 120.3, 123.5, 129.4, 134.0, 137.9, 157.0 (t) (aryl). ^{31}P NMR (121 MHz, CD_2Cl_2) δ: 55.3. HRMS $C_{33}H_{42}N_5P_2$: Calcd mass: 570.2915. Measured mass: 570.2916.

(2-MeO-C$_6$H$_4$)$_2$PN(Me)P(2-MeO-C$_6$H$_4$)(2-Me$_2$N-C$_6$H$_4$), **PNP^{O3N}** (**21**).

Compound **12** (0.813 g, 3.9 mmol, 1 equiv) was added via syringe to a mixture of magnesium turnings (0.284 g, 11.3 mmol, 2.9 equiv) and THF (5 mL). The reaction mixture was stirred at 50°C for ~12 h. After cooling to room temperature, excess Mg was removed by filtration. The filtrate was added to a THF (5 mL) solution of **14** (3.7 g, 15.9 mmol, 4 equiv). The progress of the reaction was monitored by ^{13}P NMR spectroscopy – appearance of two doublets was observed at δ: 115.6 and 169.2 ppm, J_{PP}=491 Hz. Volatiles were removed under vacuum and unreacted **14** was distilled off under vacuum. THF was added to the residue via syringe followed by a solution of previously prepared ortho-methoxy-phenyl Grignard reagent. The reaction mixture was stirred at 60 °C. ^{31}P NMR spectrum of the crude mixture shows the formation of a major species (δ: 54.3 and 54.8 ppm), but not cleanly. Aqueous work up was performed as described in procedure 2 to give a white foamy solid. The resulting solid (0.775 g) contains the desired product according to HRMS, but only in about 80% purity according to ^{1}H NMR spectroscopy. No optimization was attempted as

the chemistry of this ligand was not developed in depth. ^{1}H NMR (500 MHz, C_6D_6) δ: 2.64 (t, 3H, PNCH_3). ^{31}P NMR (121 MHz, CD_2Cl_2) δ: 54.5. HRMS $C_{30}H_{20}N_2O_3P_2{}^2H_{15}$: Calcd mass: 548.3065. Measured mass: 548.3038.

(2-MeO-C_6H_4)$_2$PN(Me)P(2-MeO-C_6H_4)(2-MeS-C_6H_4), PNP^{O3S} (22). The procedure described for the synthesis of **21** was used. Starting from **18** (1 g) led to the isolation of 0.858 g of **22**. Material of 95% purity was obtained and used for further experiments. No optimization was attempted as the chemistry of this ligand was not developed in depth. ^{1}H NMR (500 MHz, CD_2Cl_2) δ: 2.39 (t, $^{3}J_{HP}$=2.8 Hz, 3H, NCH_3), 6.82-6.92 (m, 6H, aryl-*H*), 6.96-7.00 (m, 2H, aryl-*H*), 7.07-7.12 (m, 2H, aryl-*H*), 7.19 (app d, 1H aryl-*H*), 7.32-7.37 (m, 5H aryl-*H*). ^{13}C NMR (125 MHz, CD_2Cl_2) δ: 33.8 (t, $^{2}J_{CP}$=5.7 Hz, NCH_3), 110.5, 110.6, 110.8, 120.5, 120.6, 120.7, 125.0, 127.6, 129.4, 130.5, 130.6, 130.9, 132.4, 133.1, 133.6, 134.0, 160.9-161.2 (m) (aryl). ^{31}P NMR (121 MHz, CD_2Cl_2) δ: 50.4 and 54.4 (d, $^{3}J_{PP}$ = 312 Hz). HRMS $C_{29}H_{20}NSO_3P_2{}^2H_{12}$: Calcd mass: 548.2331. Measured mass: 548.2343.

Cr(CO)$_4$(PNP^{O4}) (23). A toluene solution (30 mL) of $Cr(CO)_6$ (0.468 g, 2.12 mmol, 1 equiv) and PNP^{O4} (1.13 g, 2.12 mmol, 1 equiv) was stirred at 110° C in a sealed Schlenk tube for 36 h. The color of the solution gradually changed from colorless to bright yellow. Volatile materials were removed *in vacuo*. The yellow residue was dissolved in CH_2Cl_2 and filtered to remove a brown impurity. Upon cooling to -35° C crystallization occurred. The mother liquor was decanted and the residue was dried *in vacuo* to provide 1.166 g (1.68 mmol, 80% yield) of crystalline yellow product in two crops. ^{1}H NMR (300 MHz, $CDCl_3$) δ: 2.86 (t, $^{3}J_{HP}$=8.7 Hz, 3H, NCH_3), 3.47 (s, 12H, OCH_3), 6.85 and 7.65 (app dd, 8H, 3- and 6-

aryl-*H*), 7.02 and 7.40 (app td, 8H, 4- and 5-aryl-*H*). ^{13}C NMR (75 MHz, $CDCl_3$) δ: 37.1 (t, $^2J_{CP}$=6.8 Hz, N*C*H$_3$), 55.1 (s, O*C*H$_3$), 110, (s, aryl), 120.5 (app t, aryl), 125.8 (app t, aryl), 131.8 (s, aryl), 133.2 (app t, aryl), 160.0 (s, aryl), 222.4 (t, $^2J_{CP}$=13.4 Hz, *C*O), 229.8 (app t, $^2J_{CP}$=9.1 Hz, *C*O). ^{31}P NMR (121 MHz, $CDCl_3$) δ: 102.6. ν_{CO} (cm^{-1}, KBr plates, CH_2Cl_2 solution): 1867, 1886, 1906, 2002. Anal. calcd. for $C_{33}H_{31}NO_8P_2Cr{\cdot}CH_2Cl_2$ (%): C, 53.14; H, 4.29; N, 1.82. Found: C, 53.64; H, 4.65; N, 1.74.

Cr(CO)$_4$[NMe(PPh$_2$)$_2$] (24). A procedure similar to the one used for the preparation of **23** was employed. Yield: 54%. ^{1}H NMR (300 MHz, CD_6C_6) δ: 2.32 (t, $^3J_{HP}$=8.4 Hz, 3H, NC*H*$_3$), 7.02 and 7.47 (m, 20H, aryl-*H*). ^{13}C NMR (75 MHz, C_6D_6) δ: 33.8 (t, $^2J_{CP}$=6.1 Hz, N*C*H$_3$), 129.2 (t, aryl), 131.1 (s, aryl), 132.4 (t, aryl), 137.3 (app t, aryl), 223.1 (t, $^2J_{CP}$=12.9 Hz, *C*O), 229.1 (t, $^2J_{CP}$=9.5 Hz, *C*O). ^{31}P NMR (121 MHz, C_6D_6) δ: 114. ν_{CO} (cm^{-1}, KBr plates, CH_2Cl_2 solution): ~1881 (shoulder), 1895, 1917, 2008. Anal. calcd. for $C_{29}H_{25}NO_4P_2Cr$ (%): C, 61.82; H, 4.11; N, 2.49. Found: C, 62.79; H, 4.30; N, 2.39.

Oxidation of 23 – General procedure. Dichloromethane solutions of oxidant (I_2, Br_2, or $C_6H_5ICl_2$, 1-1.6 equiv) were added dropwise to dichloromethane solutions of yellow **23** (1 equiv) and stirred from 15 min to 6 h. The color of the reaction mixture changes upon addition to bright green (for Br_2) or dark blue ($PhICl_2$). When the oxidation was performed with I_2 (red), the color of the mixture changes slightly, to red-brown. In some cases gas evolution was observed. Generally, the ^{2}H NMR spectra of the reaction mixtures display a broad peak downfield from the diamagnetic region and some diamagnetic peaks. Recrystalization from

CH_2Cl_2 at -35° C followed by collection on a sintered glass funnel provided pure products according to ^2H NMR spectroscopy.

Compound **26**: 50% yield. ^2H NMR (76 MHz, CH_2Cl_2) δ: 9.6 (br s, OCD_3). μ_{eff} = 3.6 μ_B. λ_{max} (CH_2Cl_2, nm): ~550 (br shoulder, ε = 361 $M^{-1}cm^{-1}$), 665 (ε = 681 $M^{-1}cm^{-1}$). Anal. calcd. for $C_{29}H_{19}D_{12}Br_3NO_4P_2Cr{\cdot}CH_2Cl_2$ (%): C, 39.67; H, 3.63; N, 1.54. Found: C, 40.11; H, 3.82; N, 2.21.

Compound **27**: 37% yield. ^2H NMR (76 MHz, CH_2Cl_2) δ: 9.0 (br s, OCD_3). μ_{eff} = 3.6 μ_B. λ_{max} (CH_2Cl_2, nm): 381 (shoulder, ε = 8100 $M^{-1}cm^{-1}$), 679 (ε = 953 $M^{-1}cm^{-1}$). Anal. calcd. for $C_{29}H_{19}D_{12}I_3NO_4P_2Cr{\cdot}CH_2Cl_2$ (%): C, 34.34; H, 3.14; N, 1.33. Found: C, 34.57; H, 3.42; N, 1.33.

$CrCl_3(PNP^{O4})$ (25). A dichloromethane solution (20 mL) of $CrCl_3(THF)_3$ (1.513 g, 2.9 mmol, 1 equiv) was added to a solution of **1** (1.098 g, 2.9 mmol, 1 equiv) in dichloromethane (30 mL). The color of the reaction mixture turned from purple to blue within 5 min of stirring. The reaction mixture was stirred for 1 h. Volatile materials were removed *in vacuo* and the blue residue was triturated three times with dichloromethane. The resulting solid was suspended in dichloromethane and stored at –35° C overnight. The desired product was collected as a bright blue powder by filtration through a sintered glass frit, washed with dichloromethane, and dried under vacuum. The filtrate contained one or two unidentified paramagnetic species, displaying peaks at 4.85 and 9.5 ppm in the ^2H NMR spectrum. Compound **23** obtained in this manner amounted to 1.188 g (53% yield). ^2H NMR (76 MHz, CH_2Cl_2) δ: 8.8 (br s, OCD_3); at 40 °C: 8.4 (br s); at -60 °C: 3.8 (br s), 32 (v br s). Coalescence temperatures (°C): -50, -10. μ_{eff} =

3.8 μ_B. λ_{max} (CH_2Cl_2, nm): 536 (ε = 269 $M^{-1}cm^{-1}$), 661 (ε = 484 $M^{-1}cm^{-1}$). Anal. calcd. for $C_{29}H_{31}Cl_3NO_4P_2Cr{\cdot}CH_2Cl_2$ (%): C, 47.23; H, 4.32; N, 1.84. Found: C, 46.24; H, 4.29; N, 1.77.

$CrCl_3(P^{t\text{-}Bu}N^{i\text{-}amyl}P^{O4})$ (28). A procedure similar to the one used for the preparation of **25** was employed. Recrystallization from a CH_2Cl_2 solution layered with petroleum ether afforded the desired product as a purple powder in 75% yield. ^{2}H NMR (76 MHz, CH_2Cl_2) δ: 7 (v br, OCD_3); at 40 °C: 7.1 (br s); at -90 °C: 4.4 (br s), 28 (v br s). Coalescence temperatures (°C): -5, 18. μ_{eff} = 3.9 μ_B. λ_{max} (CH_2Cl_2, nm): 517 (ε = 250 $M^{-1}cm^{-1}$), 663 (ε = 498 $M^{-1}cm^{-1}$). Anal. calcd. for $C_{49}H_{59}D_{12}Cl_3NO_4P_2Cr{\cdot}CH_2Cl_2$ (%): C, 59.35; H, 7.21; N, 1.38. Found: C, 59.76; H, 7.63; N, 1.34.

$CrCl_2(CH_3)(PNP^{O4})$ (29). A dichloromethane solution of PNP^{O4} (105 mg, 0.20 mmol, 1 equiv) was added to a dichloromethane solution of $CrCl_2(CH_3)(THF)_3$ (70 mg, 0.20 mmol, 1 equiv) to generate a brown-green solution. The reaction mixture was stirred for 10 min, and then the volatiles were removed under vacuum. Upon concentration, the color of the solution turned olive green. The residue was dissolved in CH_2Cl_2 and layered with petroleum ether. Storing at –35° C, caused product crystallization as dark brown needles. The mother liquor was decanted and the crystals were washed with a cold CH_2Cl_2 / petroleum ether mixture. This procedure afforded 109 mg (82% yield) desired product. ^{2}H NMR (76 MHz, CH_2Cl_2) δ: 6.3 (br s, 6D, OCD_3), 13.6 (br s, 6D, OCD_3); at -90 °C: 6.9 (br s), ~25 (v br s); at 71° C (PhCl): 7.3 (br s). Coalescence temperatures (°C): <-80, 40. μ_{eff} = 3.7 m_B. λ_{max} (CH_2Cl_2, nm): 462 (ε = 495 $M^{-1}cm^{-1}$), 495 ((ε = 379 $M^{-1}cm^{-1}$)

shoulder), 700 (ε = 261 $M^{-1}cm^{-1}$). Anal. calcd. for $C_{30}H_{22}D_{12}Cl_2NO_4P_2Cr \cdot CH_2Cl_2$ (%): C, 49.37; H, 4.77; N, 1.85. Found: C, 48.98; H, 5.13; N, 1.76.

$CrCl_3(PNP^{N4})$ (30). A procedure similar to the one used for the preparation of **25** was employed. Recrystallization from a CH_2Cl_2 solution layered with petroleum ether afforded green X-ray quality single crystals. ^2H NMR (76 MHz, CH_2Cl_2) δ: -30.2 (v br s, 6D, CrNCD_3), 3.27 (s, 12D, NCD_3), 25.2 (v br s, 6D, CrNCD_3). ^2H NMR (76 MHz, CH_2Cl_2, -60°C) δ: -58.6 (v br s, 3D, CrNCD_3), -26.7 (v br s, 3D, CrNCD_3), 3.65 (s, 6D, NCD_3), 4.03 (s, 6D, NCD_3), 19.1 (v br s, 3D, CrNCD_3), 54.6 (v br s, 3D, CrNCD_3).

$CrCl_3(PNP^{O3N})$ (31). A procedure similar to the one used for the preparation of **25** was employed. ^2H NMR spectroscopy analysis of the crude reaction mixture shows broad peaks at -33.5, -16.4, -5.7, 27.9, 41.4, and sharp peaks at 4.0-7.0 ppm. Recrystallization from a CH_2Cl_2 solution layered with petroleum ether afforded X-ray quality single crystals or **31**. This system was not explored further.

$CrCl_3(PNP^{O3S})$ (33). A procedure similar to the one used for the preparation of **25** was employed. The reaction mixture turns brown initially but then slowly changes to green brown. ^2H NMR spectroscopy analysis of the crude reaction mixture shows broad peaks at -3.6 and 2.9-4.6 ppm. Recrystallization from a CH_2Cl_2 solution afforded green X-ray quality single crystals of **33**. This system was not explored further.

CrBr(*o,o′*-biphenyldiyl)(PNP^{O4}) (32). Magnesium turnings (12.3 mg, 1.4 mmol, 8 equiv) were added to a diethylether solution (10 mL) of *o,o′*-dibromobiphenyl (53.5 mg, 0.17 mmol, 1 equiv) and stirred overnight at room temperature or with

heating. The solution was decanted and concentrated to approximately 5 mL to cause precipitation of a white solid, which was dissolved by addition of dichloromethane. The resulting solution was cooled to almost freezing then added to a thawing dichloromethane solution (20 mL) of **25** (0.1183 mg, 0.17 mmol, 1 equiv). The color of the reaction mixture gradually changed from dark blue to forest green upon warming. The reaction mixture was stirred for 2 h, then volatile materials were removed *in vacuo*. Dichloromethane was added to the green residue and the mixture filtered through Celite to remove a brown solid. The green filtrate was concentrated, layered with petroleum ether, and cooled to –35° C to cause crystallization of **32** as a green material. The green solid was collected on a sintered glass frit, washed with cold dichloromethane and dried under vacuum to provide 104.2 mg of desired product (0.12 mmol, 75% yield). In cases when a white powder (probably magnesium salts) precipitated out along with the desired product, an additional recrystallization provided clean product. ^{2}H NMR (76 MHz, CH_2Cl_2) δ: 5.8 (br s, OCD_3), 9 (v br s, OCD_3); at 45 °C: 7.3 (br s); at -87 °C: 2.7 (br s), 5.7 (br s), 29.2 (v br s). Coalescence temperatures (°C): -10, 15. μ_{eff} = 3.8 μ_B. λ_{max} (CH_2Cl_2, nm): 382 (ε=1937 $M^{-1}cm^{-1}$), 449 (ε=809 $M^{-1}cm^{-1}$), 598 (ε =364 $M^{-1}cm^{-1}$). Anal. calcd. for $C_{41}H_{39}NO_4P_2BrCr$ (%): C, 61.28; H, 4.89; N, 1.74. Found: C, 61.38; H, 4.93; N, 2.10.

Trimerization trials with MAO activation. A toluene solution (30 mL, $4x10^{-4}$ *M*) of a well defined chromium(III)(PNP) complex or a stoichiometric mixture of diphosphine and $CrCl_3(THF)_3$ was prepared. The mixture was cooled to –78° C in a dry ice/acetone bath and degassed, then allowed to warm to room temperature. The solution was magnetically stirred under ethylene and MAO

(10% in toluene, 300 equiv) was added via syringe. Ethylene consumption was monitored by noting the decrease in pressure in the system over time (the pressure was kept between 771 and 655 Torr) and 1-hexene formation was documented by GC and GC-MS. For one hour runs, the reaction produces 1-hexene with a range of 1900 - 2800 turnovers in greater than 80% overall selectivity for **25**; 300-600 turnovers in greater than 90% overall selectivity for **32**; and 1300-2000 turnovers in greater than 70% overall selectivity for **28**. The C10 fraction is the major impurity detectable. For **21**/$CrCl_3(THF)_3$, 280 turnovers were observed in 13 h while **17** and **22** gave essentially inactive catalyst systems.

Trimerization of ethylene with 23 upon halide abstraction. D_2-dichloromethane was vacuum transferred to a J-Young tube or Schlenk flask charged with **23** (8 - 34 mg, 10 - 42 μmol, 1 equiv) and $NaB[C_6H_3(CF_3)_2]_4$ (10.5-45 mg, 12-51 μmol, 1.2 equiv). The mixture was warmed to room temperature using a water bath followed by mixing (via mechanical rotation for NMR tubes or magnetic stirring for flasks) for 10 min. The mixture turned brown as the starting materials dissolved. Ethylene (128.2 mL at 30-125 Torr, 200 - 860 μmol, 17.5 - 23 equiv) was condensed in (~2.3 - 3.8 atm in the vessel at room temperature). The reaction mixture was mixed for 1 - 1.5 h at room temperature during which the mixture turned brown-green. *O*-vinyl-biphenyl and 1-hexene were detected by ^{1}H NMR spectroscopy. Relative to the amount of *o*-vinyl-biphenyl observed, about 3.5 equiv of 1-hexene is formed (ca 60%).

Reaction of 23 with ethylene. D_2-dichloromethane was vacuum transferred to a J-Young tube charged with **23** (8.1 mg, 10.1 mmol, 1 equiv). Ethylene (43.48 mL at 87 Torr, 200 mmol, 20 equiv) was condensed in (~ 2 atm in the tube at room

temperature). The mixture was warmed to room temperature using a water bath then mixed by mechanical rotation for 1 h. During this time the mixture achieved a brown-green color. *O*-vinyl-biphenyl was detected by ^{1}H NMR spectroscopy, but no 1-hexene was observed. After an additional 1 h of mixing the mixture turned brown-red, but no 1-hexene was formed according to ^{1}H NMR spectroscopy.

X-ray Crystal Data: General Procedure. Crystals grown from THF (**23**), CH_2Cl_2 / petroleum ether (**25**, **27**, **29**, **30**, **31** and **32**), or CH_2Cl_2 (**33**) at -35°C were removed quickly from a scintillation vial to a microscope slide coated with Paratone N oil. Samples were selected and mounted on a glass fiber with Paratone N oil. Data collection was carried out on a Bruker Smart 1000 CCD diffractometer. The structures were solved by direct (**23**, **25**, **29**, **30**, **31**, **32**, and **33**) or Patterson methods (**27**) (SHELXTL-97, Sheldrick, 1990) in conjunction with standard difference Fourier techniques. All non-hydrogen atoms were refined anisotropically. Some details regarding refined data and cell parameters are available in Tables 4 and 5. Selected bond distances and angles are supplied in Table 3 and in the captions of Figures 2, 3, 4, 5, 6, 7, 8 and 9.

Table 4. Crystal and refinement data for complexes **23**, **25**, **27**, and **29**.

	23	**25**	**27**	**29**
Empirical formula	$C_{33}H_{31}NO_8P_2Cr \cdot C_4H_8O$	$C_{29}H_{31}Cl_3NO_4P_2Cr \cdot CH_2Cl_2$	$C_{29}H_{31}NO_4P_2I_3Cr \cdot CH_2Cl_2$	$C_{30}H_{34}Cl_2NO_4P_2Cr \cdot CH_2Cl_2$
Formula weight	755.63	762.76	1037.11	742.35

T (K)	98(2)	98(2)	98(2)	100(2)
a, Å	11.7105(5)	10.6977(7)	13.5277(3)	9.7683(6)
b, Å	16.3059(8)	15.0041(10)	13.5151(3)	16.6273(10)
c, Å	19.3321(9)	21.4755(14)	20.3801(5)	20.9934(13)
α, deg				
β, deg	102.333(1)	96.172(1)	107.892(1)	94.990(1)
γ, deg				
Volume, $Å^3$	3606.3(3)	3427.0(4)	3545.85(14)	3396.8(4)
Z	4	4	4	4
Crystal system	Monoclinic	Monoclinic	Monoclinic	Monoclinic
Space group	$P2_1/n$ (# 14)	$P2_1/n$ (# 14)	$P2_1/n$ (# 14)	$P2_1/c$ (# 14)
d_{calc}, g/cm^3	1.392	1.478	1.943	1.452
θ range, deg	1.65 to 28.43	1.66 to 28.17	1.61 to 35.00	1.56 to 28.33
μ, mm^{-1}	0.462	0.853	3.211	0.782
Abs. correction	None	None	None	None
GOF	1.755	1.579	1.405	2.760
R_1,[a] wR_2[b] [I>2σ(I)]	0.0394, 0.0620	0.0370, 0.0621	0.0335, 0.0499	0.0618, 0.0988

[a] $R_1 = \sum | |F_o| - |F_c| | / \sum |F_o|$. [b] $wR_2 = [\sum[w(F_o^2-F_c^2)^2] / \sum[w(F_o^2)^2]]^{1/2}$.

Table 5. Crystal and refinement data for complexes **30**, **31**, **32**, and **33**.

	30	**31**	**32**	**33**
Empirical formula	$C_{33}H_{43}N_5P_2Cl_3Cr \cdot CH_2Cl_2$	$C_{60}H_{68}Cl_6N_4O_6P_4Cr_2$	$C_{41}H_{39}NO_4P_2BrCr \cdot CH_2Cl_2$	$C_{41}H_{41}NO_3P_2SClCr \cdot CH_2Cl_2$
Formula weight	814.94	1381.76	888.51	862.12
T (K)	100(2)	100(2)	98(2)	100(2)
a, Å	14.791(1)	12.405(1)	9.9167(6)	10.9007(15)
b, Å	16.152(1)	14.884(1)	11.9935(8)	11.2020(15)
c, Å	16.244(1)	22.544(2)	17.9725(11)	18.034(2)
α, deg			77.371(1)	92.419(3)
β, deg	104.516(1)	104.558(1)	76.328(1)	96.426(3)
γ, deg			70.670(1)	114.021(3)
Volume, Å^3	3756.8(4)	4028.9(6)	1936.8(2)	1989.4(5)
Z	4	2	2	2
Crystal system	Monoclinic	Monoclinic	Triclinic	Triclinic
Space group	$P2_1/c$	$P2_1/n$	$P\bar{1}$ (# 2)	$P\bar{1}$ (# 2)
d_{calc}, g/cm^3	1.441	1.139	1.524	1.439

θ range, deg	1.81 to 28.31	1.66 to 28.43	1.82 to 28.29	2.00 to 28.78
μ, mm^{-1}	0.778	0.589	1.592	0.663
Abs. correction	None	None	None	TWINABS
GOF	1.645	1.508	1.731	1.253
R_1,[a] wR_2[b] [I>2σ(I)]	0.0411, 0.0651	0.0565, 0.0769	0.0416, 0.0744	0.0527, 0.1012

[a] $R_1 = \sum | |F_o| - |F_c| | / \sum |F_o|$. [b] $wR_2 = [\sum[w(F_o^2-F_c^2)^2] / \sum[w(F_o^2)^2]]^{1/2}$.

References

(1) Skupinska, J. *Chem. Rev.* **1991**, *91*, 613-648.

(2) Dixon, J. T.; Green, M. J.; Hess, F. M.; Morgan, D. H. *J. Organomet. Chem.* **2004**, *689*, 3641-3668.

(3) Wang, C.; Huang, J. L. *Chin. J. Chem.* **2006**, *24*, 1397-1401.

(4) Walsh, R.; Morgan, D. H.; Bollmann, A.; Dixon, J. T. *Appl. Catal. A-Gen.* **2006**, *306*, 184-191.

(5) Schofer, S. J.; Day, M. W.; Henling, L. M.; Labinger, J. A.; Bercaw, J. E. *Organometallics* **2006**, *25*, 2743-2749.

(6) Overett, M. J.; Blann, K.; Bollmann, A.; Dixon, J. T.; Hess, F.; Killian, E.; Maumela, H.; Morgan, D. H.; Neveling, A.; Otto, S. *Chem. Commun.* **2005**, 622-624.

(7) Overett, M. J.; Blann, K.; Bollmann, A.; Dixon, J. T.; Haasbroek, D.; Killian, E.; Maumela, H.; McGuinness, D. S.; Morgan, D. H. *J. Am. Chem. Soc.* **2005**, *127*, 10723-10730.

(8) McGuinness, D. S.; Wasserscheid, P.; Morgan, D. H.; Dixon, J. T. *Organometallics* **2005**, *24*, 552-556.

(9) McGuinness, D. S.; Wasserscheid, P.; Keim, W.; Morgan, D.; Dixon, J. T.; Bollmann, A.; Maumela, H.; Hess, F.; Englert, U. *J. Am. Chem. Soc.* **2003**, *125*, 5272-5273.

(10) McGuinness, D. S.; Wasserscheid, P.; Keim, W.; Hu, C. H.; Englert, U.; Dixon, J. T.; Grove, C. *Chem. Commun.* **2003**, 334-335.

(11) McGuinness, D. S.; Brown, D. B.; Tooze, R. P.; Hess, F. M.; Dixon, J. T.; Slawin, A. M. Z. *Organometallics* **2006**, *25*, 3605-3610.

(12) Mahomed, H.; Bollmann, A.; Dixon, J. T.; Gokul, V.; Griesel, L.; Grove, C.; Hess, F.; Maumela, H.; Pepler, L. *Appl. Catal. A-Gen.* **2003**, *255*, 355-359.

(13) Hessen, B. *J. Mol. Catal. A-Chem.* **2004**, *213*, 129-135.

(14) Deckers, P. J. W.; Hessen, B.; Teuben, J. H. *Angew. Chem.-Int. Edit. Engl.* **2001**, *40*, 2516-2519.

(15) Deckers, P. J. W.; Hessen, B.; Teuben, J. H. *Organometallics* **2002**, *21*, 5122-5135.

(16) Crewdson, P.; Gambarotta, S.; Djoman, M. C.; Korobkov, I.; Duchateau, R. *Organometallics* **2005**, *24*, 5214-5216.

(17) Carter, A.; Cohen, S. A.; Cooley, N. A.; Murphy, A.; Scutt, J.; Wass, D. F. *Chem. Commun.* **2002**, 858-859.

(18) Bollmann, A.; Blann, K.; Dixon, J. T.; Hess, F. M.; Killian, E.; Maumela, H.; McGuinness, D. S.; Morgan, D. H.; Neveling, A.; Otto, S.; Overett, M.; Slawin, A. M. Z.; Wasserscheid, P.; Kuhlmann, S. *J. Am. Chem. Soc.* **2004**, *126*, 14712-14713.

(19) Andes, C.; Harkins, S. B.; Murtuza, S.; Oyler, K.; Sen, A. *J. Am. Chem. Soc.* **2001**, *123*, 7423-4.

(20) Reagen, W. K.; Conroy, B. K.; Phillips Petroleum Co.: CA 2020509, 1991.

(21) Wu, F.-j.; Amoco Corp.: US 5,744,677, 1998.

(22) Elowe, P. R.; McCann, C.; Pringle, P. G.; Spitzmesser, S. K.; Bercaw, J. E. *Organometallics* **2006**, *25*, 5255-5260.

(23) Agapie, T.; Day, M. W.; Henling, L. M.; Labinger, J. A.; Bercaw, J. E. *Organometallics* **2006**, *25*, 2733-2742.

(24) Bluhm, M. E.; Walter, O.; Doring, M. *J. Organomet. Chem.* **2005**, *690*, 713-721.

(25) Blann, K.; Bollmann, A.; Dixon, J. T.; Hess, F. M.; Killian, E.; Maumela, H.; Morgan, D. H.; Neveling, A.; Otto, S.; Overett, M. J. *Chem. Commun.* **2005**, 620-621.

(26) La Mar, G. N.; Horrocks, W. D., Jr.; Holm, R. H. *NMR of Paramagnetic Molecules*; Academic Press: New York, 1973.

(27) Dossett, S. J.; Wass, D. F.; Jones, M. D.; Gillon, A.; Orpen, A. G.; Fleming, J. S.; Pringle, P. G. *Chem. Commun.* **2001**, 699-700.

(28) King, R. B.; Gimeno, J. *Inor. Chem.* **1978**, *17*, 2390-5.

(29) Nixon, J. F. *J. Chem. Soc. A* **1968**, 2689-92.

(30) Gabelein, H.; Ellermann, J. *J. Organomet. Chem.* **1978**, *156*, 389.

(31) Tolman, C. A. *Chem. Rev.* **1977**, *77*, 313-48.

(32) Bennett, M. J.; Cotton, F. A.; LaPrade, M. D. *Acta Cryst.* **1971**, *B27*, 1899.

(33) Jones, P. G.; Jager, S. *Z. Kristallogr.* **1997**, *212*, 85.

(34) Nishimura, K.; Kuribayashi, H.; Yamamoto, A.; Ikeda, S. *J. Organomet. Chem.* **1972**, *37*, 317-29.

(35) Evans, D. F. *J. Chem. Soc.* **1959**, 2003-5.

(36) Sur, S. K. *J. Mag. Res.* **1989**, *82*, 169-73.

(37) Wu, F.-J.; Stahly, G. P.; Fronczek, F. R.; Watkins, S. F. *Acta Cryst., Sect. C* **1995**, *51*, 18.

(38) Kohn, R. D.; Haufe, M.; Kociok-Kohn, G.; Grimm, S.; Wasserscheid, P.; Keim, W. *Angew. Chem. Int. Ed.* **2000**, *39*, 4337.

(39) Agapie, T.; Schofer, S. J.; Labinger, J. A.; Bercaw, J. E. *J. Am. Chem. Soc.* **2004**, *126*, 1304-1305.

(40) Briggs, J. R. *Chem. Commun.* **1989**, 674-5.

(41) Emrich, R.; Heinemann, O.; Jolly, P. W.; Krueger, C.; Verhovnik, G. P. J. *Organometallics* **1997**, *16*, 1511-1513.

(42) Theopold, K. H. *Eur. J. Inor. Chem.* **1998**, 15-24.

(43) Arif, A. M.; Jones, R. A.; Hefner, J. G. *J. Crystallogr. Spectrosc. Res.* **1986**, *16*, 673-9.

(44) Gardner, T. G.; Girolami, G. S. *Chem. Commun.* **1987**, 1758-60.

(45) Gray, L. R.; Hale, A. L.; Levason, W.; McCullough, F. P.; Webster, M. *Dalton Trans.* **1984**, 47-53.

(46) Cotton, F. A.; Duraj, S. A.; Powell, G. L.; Roth, W. J. *Inor. Chim. Acta* **1986**, *113*, 81-5.

(47) Pangborn, A. B.; Giardello, M. A.; Grubbs, R. H.; Rosen, R. K.; Timmers, F. J. *Organometallics* **1996**, *15*, 1518-20.

(48) Cooley, N. A.; Green, S. M.; Wass, D. F.; Heslop, K.; Orpen, A. G.; Pringle, P. G. *Organometallics* **2001**, *20*, 4769-4771.

Chapter 3

Mechanistic Studies of Olefin and Alkyne Trimerization with Chromium Catalysts – Deuterium Labeling and Studies of Regiochemistry Using a Model Cromacyclopentane Complex

Part of this chapter was published previously in:

Agapie, T.; Schofer, S. J.; Labinger, J. A.; Bercaw, J. E. *J. Am. Chem. Soc.* **2004**, *126*, 1304-1305.

Abstract

A system for catalytic trimerization of ethylene utilizing chromium(III) precursors supported by diphosphine ligand PNP^{O4} = (*o*-MeO-$C_6H_4)_2PN(Me)P$(*o*-MeO-$C_6H_4)_2$ has been investigated. The mechanism of the olefin trimerization reaction was detailed using deuterium labeling and studies of reactions with α-olefins and internal olefins. A well defined chromium precursor utilized in this studies is Cr(PNP^{O4})(*o*,*o'*-biphenyldiyl)Br (**1**). A cationic species, obtained by halide abstraction with $NaB[C_6H_3(CF_3)_2]_4$, is required for catalytic turnover to generate 1-hexene from ethylene. The initiation byproduct is vinylbiphenyl; this is formed even without activation by halide abstraction. Trimerization of 2-butyne is accomplished by the same cationic system but not by the neutral species. Catalytic trimerization, with various (PNP^{O4})Cr precursors, of a 1:1 mixture of C_2D_4 and C_2H_4 gives isotopologs of 1-hexene without H/D scrambling (C_6D_{12}, $C_6D_8H_4$, $C_6D_4H_8$, and C_6H_{12} in a 1:3:3:1 ratio). The lack of crossover supports a mechanism involving metallacyclic intermediates. Using a SHOP catalyst to perform the oligomerization of a 1:1 mixture of C_2D_4 and C_2H_4 leads to the generation of a broader distribution of 1-hexene isotopologs. This is consistent with the mechanim a Cossee-type mechanims for 1-hexene formation. The mechanism of the ethylene trimerization reaction was studied the reaction of *trans*-, *cis*-, and *gem*-ethylene-d_2 with **4** upon activation with $NaB[C_6H_3(CF_3)_2]_4$. The trimerization of *cis*- and *trans*- ethylene-d_2 generates 1-hexene isotopomers having terminal CDH groups, with an isotope effect of 3.1(1) and 4.1(1),

respectively. These results are consistent with reductive elimination of 1-hexene from a putative $Cr(H)[(CH_2)_4CH=CH_2]$ occurring much faster than a hydride 2,1-insertion or with concerted 1-hexene formation from a chromacycloheptane via a 3,7-H shift. The trimerization of *gem*- ethylene-d_2 has an isotope effect of 1.3(1), consistent with irreversible formation of a chromacycloheptane intermediate on route to 1-hexene formation. The reaction of olefins with a model of a chromacyclopentane was investigated starting from complex **1**. α-Olefins react with cationic chromabiphenyldiyl species to generate products from 1,2-insertion. A study of the reaction of 2-butenes indicated that b-H elimination occurs preferentially from the ring CH rather than *exo*-CH bond in the metallacycloheptane intermediate. A study of cotrimerization of ethylene with propylene correlates with these regioselectivity findings. Competition experiments with mixtures of two olefins indicate that the relative insertion rates generally decrease with increasing size of the olefins.

Introduction

α-Olefins: applications and synthesis

α-Olefins are important commodity chemicals with uses in a variety of applications including the copolymerization with ethylene and the generation of plasticizers, detergents, surfactants, and lubricants.[1] A significant part of the light fraction (C_4-C_8) is utilized as comonomer for the copolymerization with ethylene to generate Linear Low Density PolyEthylene (LLDPE). In this context, 1-hexene

and 1-octene are particularly valuable, imparting polymers good tear resistance and other desirable properties.[2] The C_6-C_{10} fractions are mostly used for plasticizers in polyvinylchloride. Higher fractions are used for the generation of lubricants and detergents. For the later applications, the α-olefins are chemically modified by hydroformilation (the Oxo process), sulfonation, arylation, isomerization–disproportionation, etc.[1]

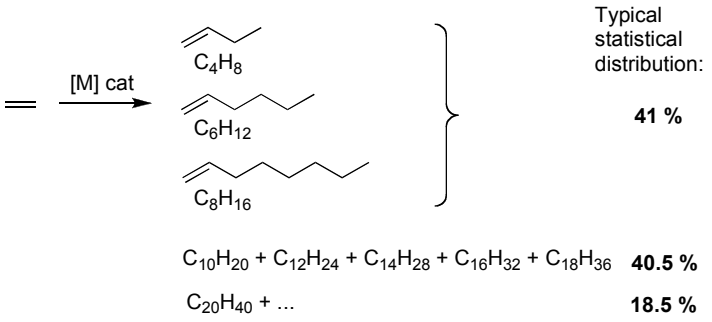

Scheme 1. Non-selective, industrial preparation of α-olefins.

Even carbon number α-olefins are generated industrially mostly via non-selective oligomerization of ethylene.[1] Non-selective oligomerization of ethylene with nickel (Shell Higher Olefin Process), aluminum (Albermarle and Chevron Processes), or aluminum / zirconium catalysts (Idemitsu Process) leads to a statistical distribution of α-olefins (Scheme 1).[3] This mixture is separated and processed as a function of the final application of the products. However, each component olefin is obtained in minor fraction and its isolation requires purification by distillation. Given the broad uses of α-olefins, there is increasing interest in developing catalytic systems that give better selectivity toward desirable alkenes. Two of the most commercially useful olefins are 1-hexene and

1-octene, comonomers for the synthesis of LLDPE. For this application, very good purity of α-olefin is essential, as internal olefins are undesirable impurities in polymerization. Furthermore, separation of α-olefin from an internal olefin with the same number of carbons is more challenging and expensive that separation of α-olefin homologs. Several recent reports describe the non-statistical oligomerization of ethylene to 1-hexene or mixtures of 1-hexene and 1-octene with good selectivities for the α-olefin.[4-25] Ethylene trimerization has been reported for titanium,[15,17,22] tantalum,[21] and chromium systems. The chromium systems however, are the most numerous, selective, and productive. In fact, a chromium system based on mixtures of chromium salts, aluminum alkyls, and pyrol bases is currently used for the commercial production of 1-hexene by Chevron-Philllips Chemical Company.[23]

The chromium systems for the trimerization or tetramerization of ethylene are generally based on multidentate supporting ligands. Chromium systems based on phosphine, amine, ether, and thioether multidentate donor frameworks have been reported (Figure 1). Systems capable of trimerizing α-olefins, based on 1,3,5-triazacyclohexane ligands, have been reported as well; with ethylene these systems lead to the formation of polyethylene with some trimerization activity.[26-28] Typically, multidentate ligand precursors are allowed to react *in situ* with a chromium precursor followed by activation with an aluminum reagent leading to systems competent for the selective oligomerization of ethylene. Well-defined chromium complexes have been characterized and utilized as precursors to catalytic ethylene oligomerization systems upon activation with excess

aluminum reagents. Only few examples of well-defined precursors, reported by Bercaw *et al.*, have allowed for stoichiometric activation of chromium precursors to lead to catalytically active species.[7,29] Direct characterization of the catalytically active species remains a challenge, mainly stemming from the fact that the initial catalytic activity of the reported systems decreases quickly indicating catalyst decomposition, as well as from the paramagnetic nature of the chromium complexes involved in catalysis.[7,26,29,30]

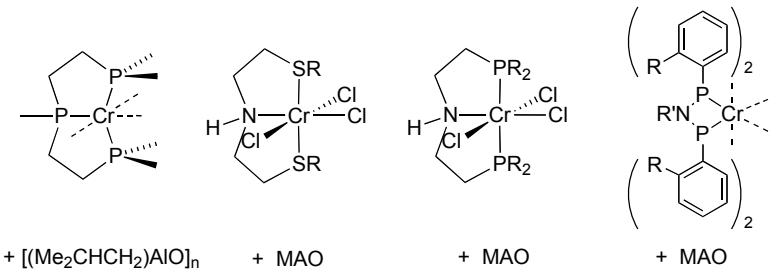

Figure 1. Chromium ethylene trimerization systems based on multidentate ligand frameworks.

Mechanism of selective ethylene oligomerization

Many of the details of the mechanisms of the trimerization and tetramerization of ethylene are not clear. The formation of 1-hexene in a non-selective fashion is proposed to occur via a Cossee type mechanism involving intermediate liniar alkyl chains which, upon β-H elimination lead to the formation of α-olefins (Scheme 2). It is difficult to account for selective 1-hexene formation based on this mechanism instead of a Shultz-Flory distribution with formation of higher homologs. However, only recently was this mechanism shown experimentally, by Bercaw *et al.*, to be inconsistent with the selective

formation of 1-hexene, under catalytic conditions.[31] The most popular proposed mechanism to account for the high selectivity involves metallacyclic intermediates (Scheme 3). Initial coordination of two equivalents of ethylene to a ligated Cr^n species followed by oxidative coupling forms a chromacyclopentane of oxidation state Cr^{n+2}. The transition state for β-hydrogen elimination from the chromacyclopentane leading to 1-butene is expected to be rather strained; hence ring expansion by ethylene insertion dominates. The resulting chromacycloheptane is flexible enough to undergo rapid β-hydrogen elimination, giving a chromium-alkenyl-hydride species that reductively eliminates 1-hexene to regenerate Cr^n and closes the catalytic cycle. In agreement, Jolly and coworkers have reported well characterized chromacyclopentane and chromacycloheptane complexes; the latter decomposes more readily and yields 1-hexene.[32] More recently, it has been suggested that the release of 1-hexene from the metallacycloheptane intermediate proceeds via a concerted 3,7-hydrogen shift with formal 2-electron reduction of the metal (purple dashed arrow).[33-40]

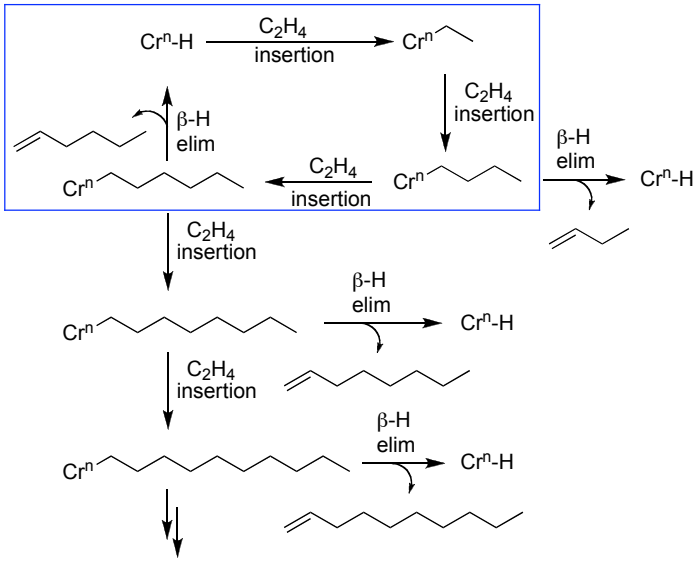

Scheme 2. Formation of 1-hexene via Cossee-type mechanism (blue section); generation of α-olefin homologs possible.

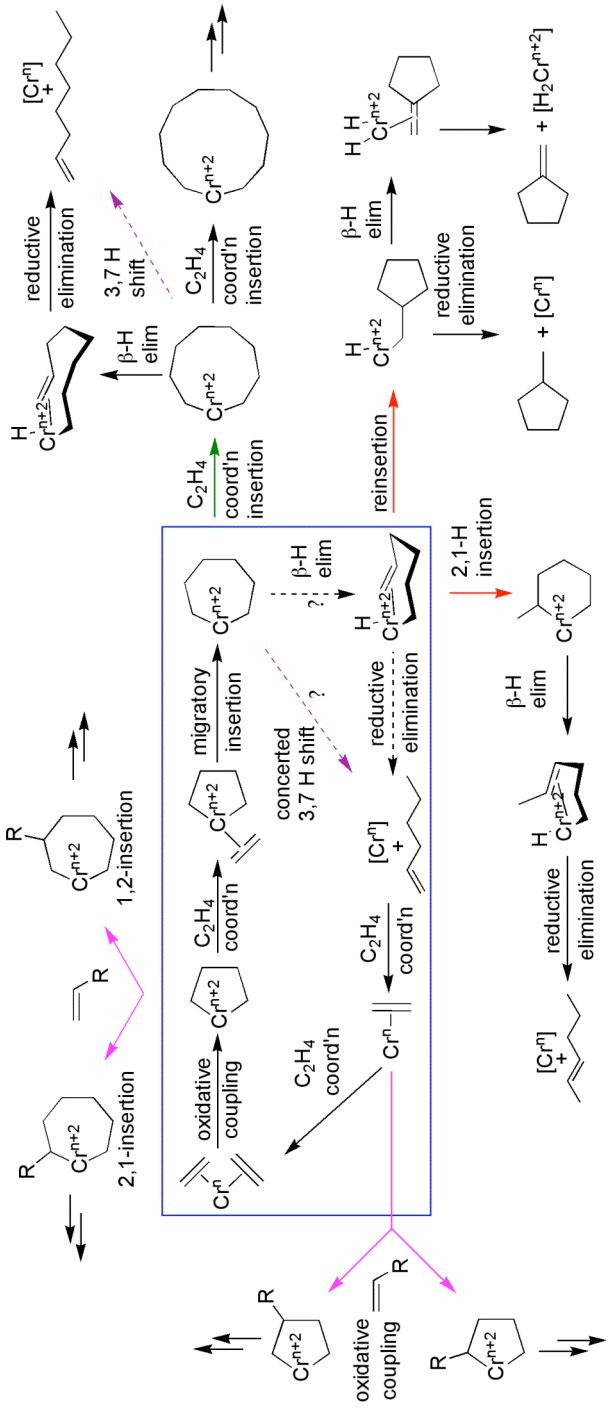

Scheme 3. Formation of 1-hexene via metallacyclic mechanism (blue section); generation of α-olefin homologs, isomers, and incorporation of product α-olefins possible.

While the metallacyclic mechanism could explain the selective formation of 1-hexene, there are many mechanistic pathways that would lead to a diverse selection of products (Scheme 3). Examples of side reactions include A) additional ethylene insertions (green arrow), B) hydride or alkyl reinsertion into intermediate pendant olefins (red arrows), and C) incorporation of the product α-olefin into the metallacyclic intermediates (magenta arrow). A) The chromacycloheptane intermediate could further insert ethylene to generate large metallacycles. This would occur if ethylene insertion could compete with β-H elimination. In this regime, ring expansion would be favored by higher concentrations (pressures) of ethylene.[20,30] Futhermore, if the preference for β-H elimination from each of the resulting metallacycles is similar, then a Shultz-Flory distribution is expected. In fact, a recent report by Gibson *et al.* indicates that a chromium system is capable of non-selective ethylene oligomerization via the metallacyclic mechanism.[41,42] B) If β-H elimination is faster than ethylene insertion in the chromacycloheptane intermediate, then a chromium hydride alkyl complex forms. Given the presence of a pendant olefin, hydride reinsertion could occur to generate a chromacyclohexane which in turn could β-H eliminate from the ring to lead to the chain walked product, with an internal double bond (2-hexene). The alternative mechanism involving a 3,7-H shift bypasses the formation of a chromium hydride and hence does not allow isomerization. It is important to note, however, that evidence for the formation of intermediate chromium-alkenyl-hydride complexes has been presented for the system competent for both ethylene trimerization and tetramerization.[9,20,30] In that case, the observation of methylcyclopentane and methylenecyclopentane as major side

products is an indication of pendant olefin insertion into intermediate alkyl species followed by either reductive elimination (methylcyclopentane) or β-H elimination (methylenecyclopentane). C) The cotrimerization of α-olefin product with ethylene is a minor side reaction in particular at high conversions when the concentration of α-olefin product is increased.[19] The incorporation styrene into trimers with ethylene has been reported recently.[43]

The nature of the intermediates involved in the mechanism of selective ethylene oligomerization, in particular the metal oxidation states, remains uncertain. It is clear that the metallacyclic mechanism requires two-electron redox cycles (Cr^{n}-Cr^{n+2}). Currently the redox couple favored in the literature is chromium(I)-chromium(III), however, given the propensity for decomposition in this system it is hard to obtain clean data in this regard and allow for definitive conclusions. The large majority of the reported systems involve chromium(III) precursors, but catalytic activity can be attained with chromium(II) starting materials as well. Solution measurement of the magnetic susceptibility under catalytic conditions has been used to indicate the presence of chromium(III) species.[26] Notably, it has been reported that alkyl aluminum species have the ability to induce oxidation state changes in the chromium complexes, possibly by disproportionation.[44-46]

Ligand effects on the nature of the products in PNP diphosphine-chromium systems for the selective trimerization and tetramerization of ethylene

One of the most intriguing chromium systems for the selective oligomerization of ethylene is based on the "PNP" diphosphines (Figure 1).[19,29,31]

Variants of these ligands have been shown to lead to competent catalysts for the trimerization of ethylene to generate 1-hexene, 1-octene, or a mixture of the two, with variable degrees of selectivity in the corresponding Cn fraction and catalyst lifetime. The initial report of the PNP system, by bp, involved *in situ* preparation of the catalytic species by mixing the phosphine with a chromium precursor, in toluene and activating with MAO.[19] Ethylene trimerization trials were performed at relatively low pressures of ethylene (1 atm at room temperature, 4-20 atm at 80 °C). Under those conditions very good 1-hexene selectivity and productivity was observed for the diphosphines that display *ortho*-MeO substitution on the phenyl groups. In contrast, diphosphines lacking *ortho*-MeO substitution or with a PCP backbone instead of PNP have been reported to give negligible 1-hexene formation at 1 atm of ethylene.

Later reports from Sasol described the oligomerization of ethylene with related diphosphine systems at higher pressures (30-45 atm) and different temperatures (45 and 65 °C).[8,20,47] They found that the nature of the products (1-hexene and 1-octene) depended greatly on the nature of the *ortho*-substituent. In the absence of *ortho*-substituents, the greatest selectivity for C8 vs. C6 is observed (best ratio at 71.6 to 17.8). Interestingly, the C6 fraction shows decreased selectivity for 1-hexene (at most 70%). *Ortho*-substitution with one bulky alkyl groups on each P-bound phenyl leads to catalysts competent for the generation of 1-hexene (> 86 to 10 ratio of C6 to C8, 45 atm and 45 °C). Removal of only one of these *ortho*-substituents leads to significant increase in the generation of 1-octene and a decrease in selectivity for 1-hexene (82%) in the C6 fraction (41 to 42 ratio of C6 to C8). Further removal of *ortho*-subtituents lead to increased formation of 1-octene vs. 1-hexene. If the *ortho*-substituents are ether groups, then the oligomerization behaviour is slightly different. Again, the phosphine with

four *ortho*-substituents is the most selective for 1-hexene. Decrease in the number of *ortho* donors, even down to a single one, does decrease the selectivity for C6 (63%) but less significantly than for the alkyl substitution and without a significant effect on the selectivity of 1-hexene (98%) in the C6 fraction. Under these conditions, smaller amounts of 1-octene are formed (17%). A significant increase in the ratio of C8 to C6 (68 to 17) occurs only upon complete removal of *ortho*-donors. These results have been rationalized as an indication of two effects of *ortho* substituents. A) Overall steric bulk favors the formation of 1-hexene, possibly facilitating the geometry of β-H elimination from the chromacycloheptane. B) Pendant donor ligands favor formation of 1-hexene even in the absence of overall steric bulk, possibly by binding to the metal center and competing with further ethylene coordination and insertion. In addition the more open systems, besides facilitating further ethylene insertion, also allow for more isomerization by reinsertion mechanisms (methylcyclohexane and methylenecyclohexane) to erode the 1-hexene selectivity in the C6 fraction.

Reports by Bercaw et al., indeed confirm the ability of the pendant ligands to coordinate to the metal center.[7,29,31] All chromium(III) systems supported by PNP^{O4} show coordination of two phosphines and one ether group. However, fluxional processes have been observed in solution indicating that the ether groups are labile. The effect of the nature of the pendant donors was investigated by preparing phophines bearing thioether (PNP^{S4}), amine (PNP^{N4}), and mixed donor groups (PNP^{SO3} and PNP^{NO3}). In the solid-state, all these new systems show a preference for coordinating sulfur and nitrogen donors rather than oxygen and phosphorous donors. Furthermore, little or no catalytic activity was observed for the systems bearing sulfur and nitrogen donors (under 1 atm ethylene). This suggests that while a labile pendant donor is beneficial for

oligomerization activity, strong pendant donors deactivate the catalyst. A possible explanation for this behavior could involve ether coordination to compete with additional ethylene insertion, but facile ether decoordination to make orbitals available on the metal center for the β-H elimination process (or 3,7-H shift). It is important to note that ethylene coordination to the first chromacycloalkane (metallacyclopentane) is required for catalytic turnover. If this process is completely shut down by pendant group coordination, then no oligomerization should be observed. These features underscore the importance of having a well balanced system in order to achieve good selectivity and productivity for the desired oligomer.

We present herein studies aiming to detail the mechanism of the formation of 1-hexene from ethylene with the chromium/PNP^{O4} system. Part of this work was published previously.[31] Here we discuss in detail labeling experiments that distinguish between metallacyclic and Cossee-type mechanisms. Presented experiments with partially labeled ethylene explain the observed selectivity for 1-hexene in the C6 fraction. Studies of olefin reaction with a model chromabiphenyldiyl complex address questions of regioselectivity of insertion into a metallacyclopentane and β-H elimination from metallacycloheptane. Relative rates of olefin insertion into chromabiphenyldiyl are discussed.

Results and Discussion

Neutral vs. cationic species in the trimerization of ethylene and 2-butyne

Most of the systems reported to perform selective trimerization of ethylene to 1-hexene involve the use of large excess of activators, mainly alkylaluminumoxanes. Alkylaluminumoxanes act both as alkylating agents to swap metal halides for metal alkyls as well as halide or alkide abstracting agents to generate cationic metal complexes. Given the large excess normally employed for these reagents it is not clear what is nature of the *in situ* generated species capable of performing ethylene trimerization. The chromium biphenyldiyl species (**1**) synthesized as communicated before (Chapter 2) provides a useful starting material to answer the question of whether a cationic or neutral species is required for catalytic activity (Scheme 4). Halide abstraction from this complex occurs readily with $Na[B(C_6H_3(CF_3)_2)_4]$. In this context, a solution of complex **1** was placed under ethylene, in a J-Young tube. Within one hour, the formation of vinylbiphenyl was observed by ^1H NMR spectroscopy and GC-MS. No formation of 1-hexene was observed under these conditions. In a different experiment, a cationic species was generated by halide extraction and then was placed under ethylene. Under these conditions, the formation of vinylbiphenyl as well as of 1-hexene was observed by spectroscopy. These experiments indicate that a cationic species is required for the catalytic generation of 1-hexene.

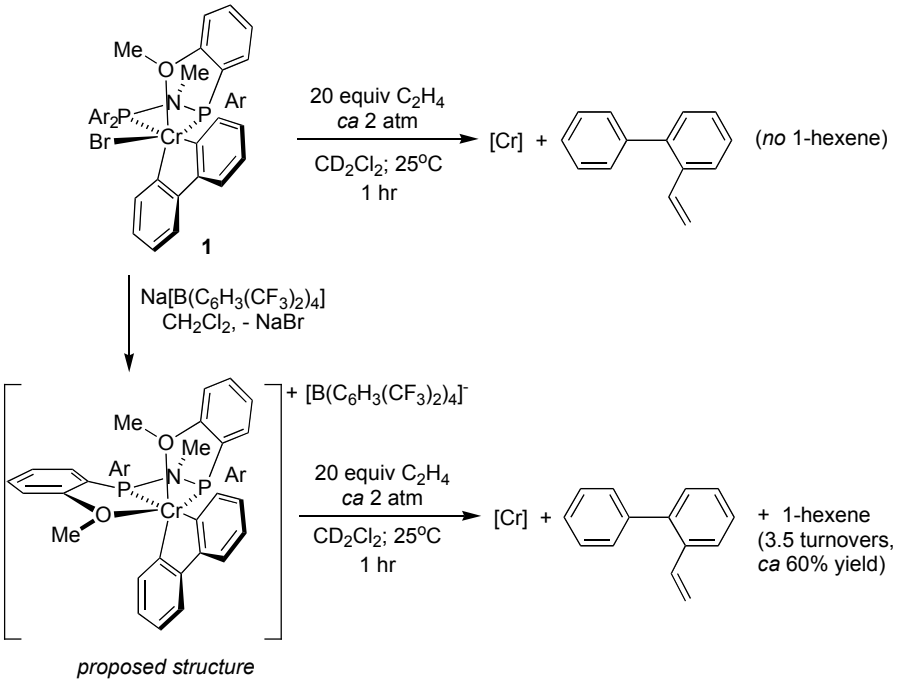

Scheme 4. Reaction of neutral and cationic chromabiphenyldiyl species with ethylene.

The formation of vinylbiphenyl suggests a likely mechanism for the initiation reaction (Scheme 5). The starting chromium biphenyldiyl species coordinates ethylene followed by insertion to generate a chromabiphenyldiylcycloheptane species. β-H elimination can occur to generate a chromium-alkenyl-hydride which, upon reductive elimination, leads to the formation of vinylbiphenyl. It is interesting that vinylbiphenyl is formed from both neutral and cationic chromium precursors. This indicates that the chromium center can coordinate ethylene, presumably by displacing the labile ether donor, insert, β-H eliminate, and reductively eliminate in the neutral form. The generated metal byproduct should be a chromium(I) species. If this byproduct is neutral, then ethylene trimerization does not occur. Multiple reasons could reside behind the ability of the cationic species to turnover

are multiple – a more electrophilic metal center may be necessary for ethylene coordination and oxidative coupling to generate a new metallacyclopentane, an additional coordination site may be needed for this process, or, the low-coordinate neutral chromium(I) species is more likely to deactivate by forming dimeric species via halide bridges.

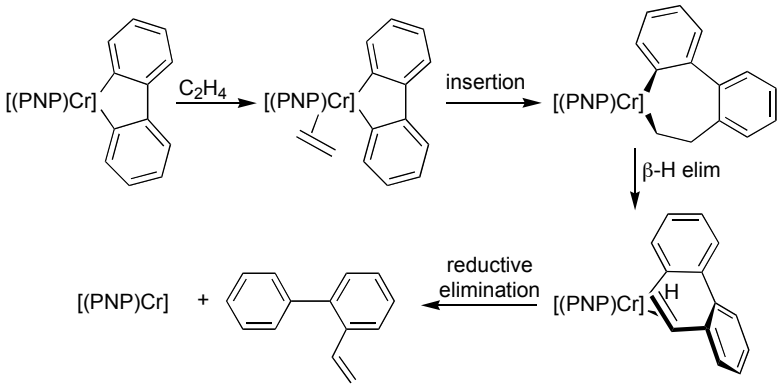

Scheme 5. Initiation mechanism of chromabiphenyldiyl species with ethylene.

To further test the role of neutral vs cationic chromium species in trimerization catalysis, the reaction with 2-butyne was investigated (Scheme 6). We envisioned that alkynes would be more reactive toward oxidative coupling and allow catalytic turnover even with neutral chromium species. A solution of the neutral species **1** was exposed to 2-butyne – formation of 9,10-dimethyl phenantrene was observed, but no hexamethyl benzene. If halide abstraction is performed first, however, the formation of 9,10-dimethyl phenantrene as well as the catalytic formation of hexamethyl benzene is observed. Hence, mirroring the reactivity behavior of ethylene in this system, 2-butyne is trimerized only by the cationic species, possibly due to related reasons. With respect to the mechanism of initiation and catalytic trimerization, two pathways are possible (Scheme 7).

The chromabiphenyldiyl species could react with the alkyne by an insertion or a Diels-Alder mechanism.[48] The Diels-Alder mechanism is less likely in this case since it disrupts the aromaticity of two arenes. In either case, reductive elimination generates a cationic chromium(I) species. This intermediate coordinates two molecules of alkyne and, upon oxidative coupling, generates a chromacyclopentadienyl species. Another alkyne molecule can react with the chromacyclopentadienyl intermediate via the insertion or the Diels-Alder patways to form the alkyne trimer, upon reductive elimination.

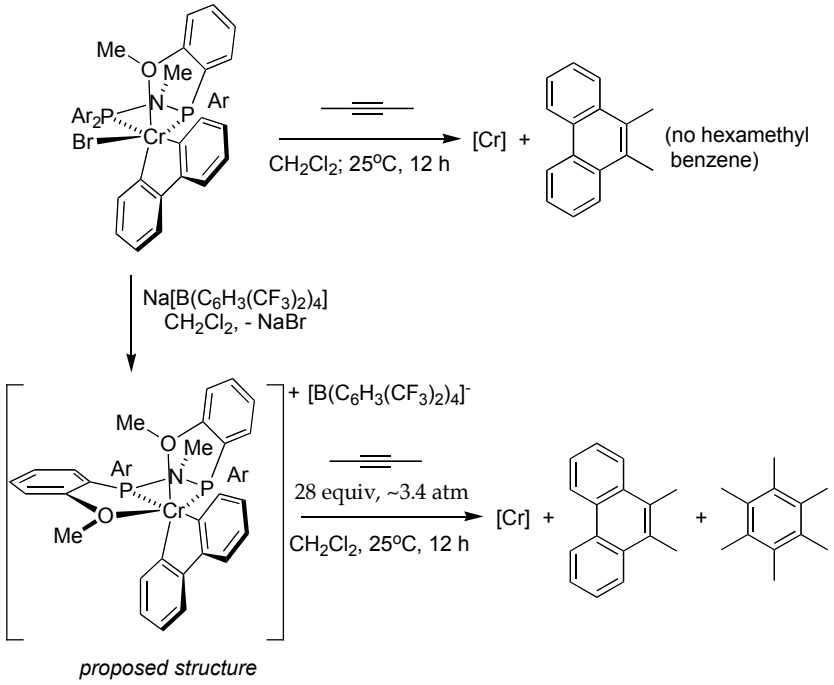

Scheme 6. Reaction of neutral and cationic chromabiphenyldiyl species with 2-butyne.

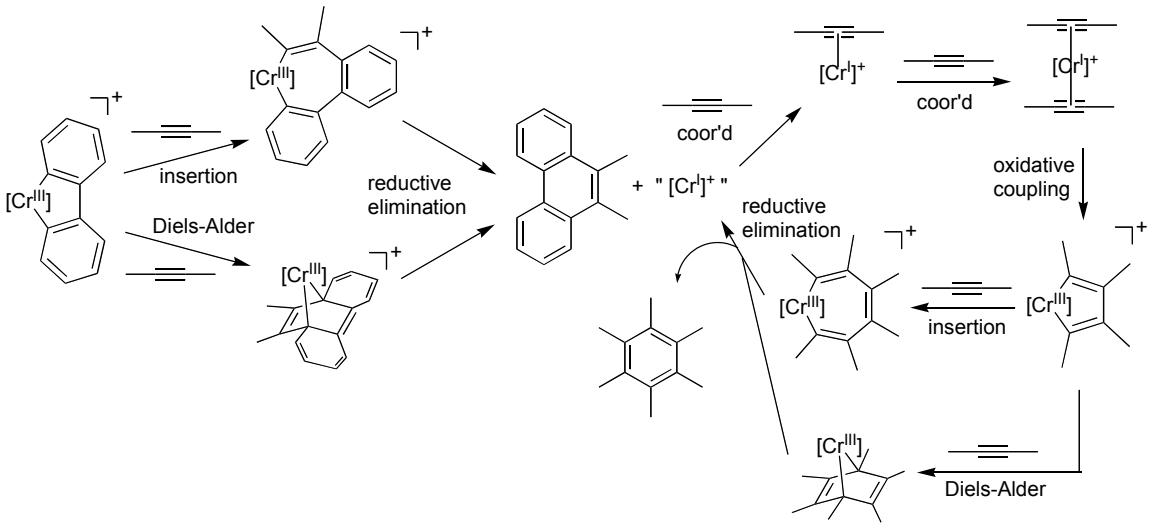

Scheme 7. Proposed mechanisms for the formation of 9,10-dimethyl phenantrene and hexamethyl benzene from 2-butyne.

The trimerization of alkynes or cotrimerization of alkynes and olefins is a transformation with applications in synthesis.[49-51] Interestingly, the potential of olefin trimerization catalysts to perform alkyne trimerization has not been reported to our knowledge. Chromium systems have been used as catalysts (but not optimized systems) and as stoichiometric variants for the study of the mechanism of alkyne trimerization.[52-54] More recently, *in situ* prepared neutral chromabiphenyldiyl species have been reported to undergo reaction with alkynes to generate the corresponding phenantrene derivatives.[55] One recent application involves a zirconium / chromium system for the cotrimerization of alkynes with nitriles and isocyanates.[56] This system is proposed to involve the formation of a neutral chromacyclopentadiene species which reacts with π-bonds to lead to the formation of cotrimers. While these systems are stoichiometric in chromium, the current results indicate that the development of catalytic applications for organic synthesis may be possible, one approach being to develop cationic chromium systems.

Crossover experiment with the Cr(PNP^{O4}) system for ethylene trimerization

The chromabiphenyldiyl species provides a system that can catalytically generate 1-hexene upon stoichiometric activation and allows for further studies of the mechanism of the trimerization of ethylene. Our first studies are directed toward designing a test to distinguish the two mechanistic proposals for 1-hexene formation: metallacyclic vs. Cossee-type mechanism. A mixture of C_2H_4 and C_2D_4 (1:1) was trimerized with the cationic chromabiphenyldiyl species. Formation of d_0 and d_4 vinylbiphenyl was observed along with the generation of four 1-hexene isotopologs, C_6H_{12}, $C_6D_4H_8$, $C_6D_8H_4$, and C_6D_{12} in a 1:3:3:1 ratio (Figure 2). Interestingly, alternative preparations of the catalytic system (complex **1** activated with excess MAO, or the *in situ* prepared bp system comprised of a toluene solution of $CrCl_3(THF)_3$, PNP^{O4}, and excess MAO, or $CrPh_3$(PNP^{O4}) activated with $[H(OEt_2)][B(C_6H_3(CF_3)_2)_4]$) led to a similar distribution of isotopologs indicating that the same mechanism occurs in all these cases.

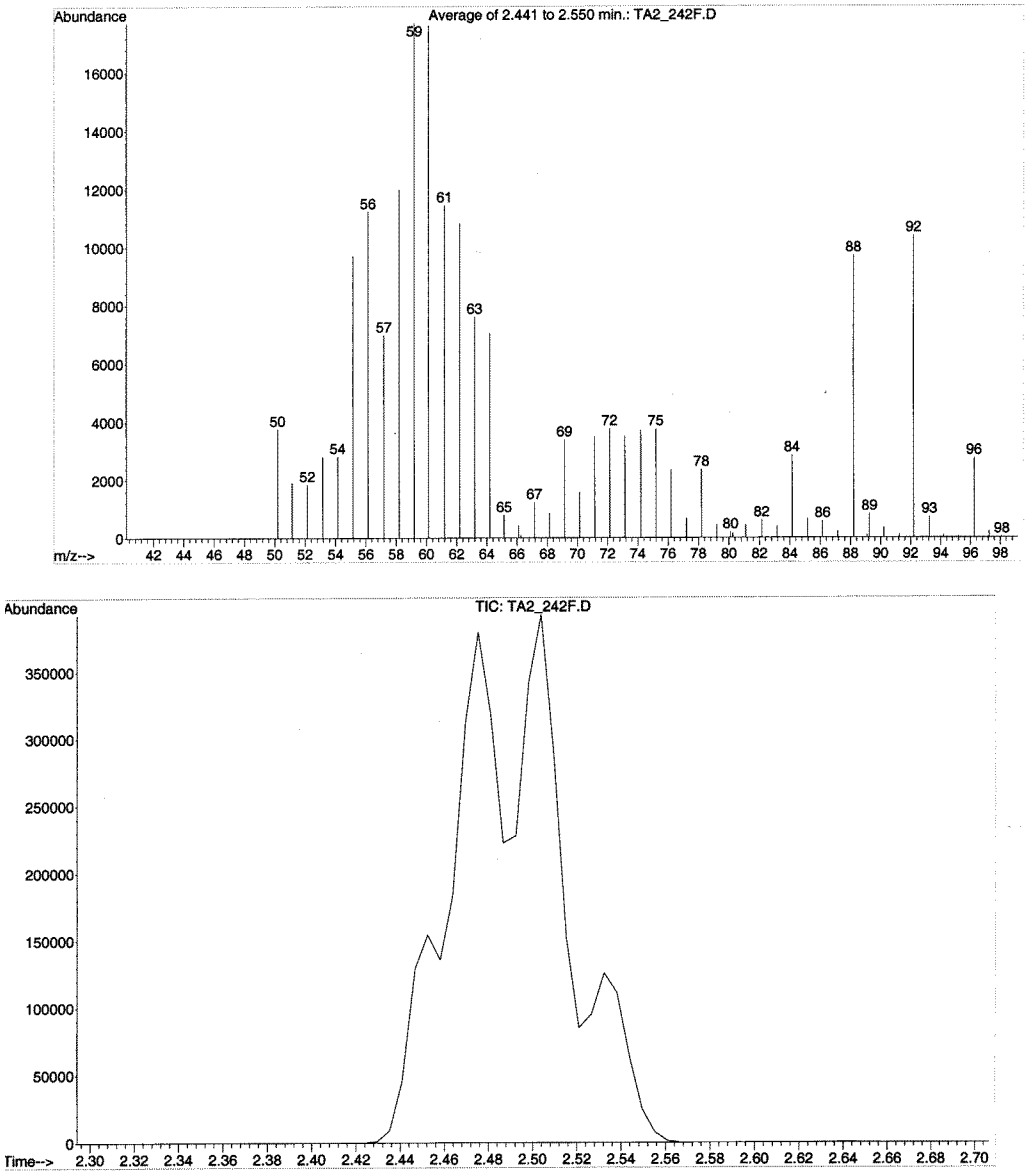

Figure 2. Typical MS (top) and GC (bottom) of the 1-hexene generated by chromium/PNP^{O4} catalysts with a C_2D_4/C_2H_4 mixture.

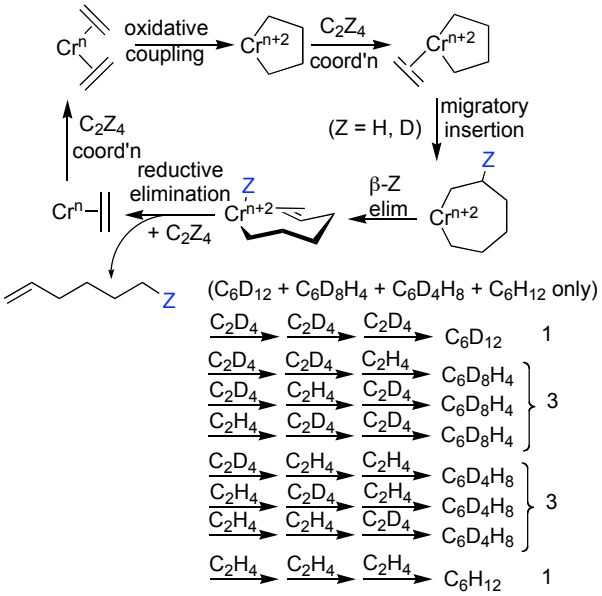

Scheme 8. Predicted isotopolog distribution for the trimerization of a C_2H_4/C_2D_4 mixture via a metallacyclic mechanism.

To account for the observed distribution of 1-hexene isotopologs the two proposed mechanisms need to be analyzed more closely. The metallacyclic mechanism can generate intermediates with both hydrogen and deuterium in the β-position (Scheme 8). Hence β-Z (Z = H or D) elimination would move either a hydrogen or a deuterium from the alkyl chain to the chromium center. However, in the subsequent reductive elimination step the transferred Z atom would be returned to the same alkyl chain. The net effect involves no hydrogen / deuterium scrambling between different molecules of 1-hexene. In consequence only isotopologs bearing even number deuteriums and hydrogens are expected from the metallacyclic mechanism. Taking into account the possible routes to access each of the isotopologs, we find that the distribution corresponds to the binomial expansion coefficients – for the trimerization reaction the calculated

ratio is 1:3:3:1. Hence, the metallacyclic mechanism is consistent with the experimental results.

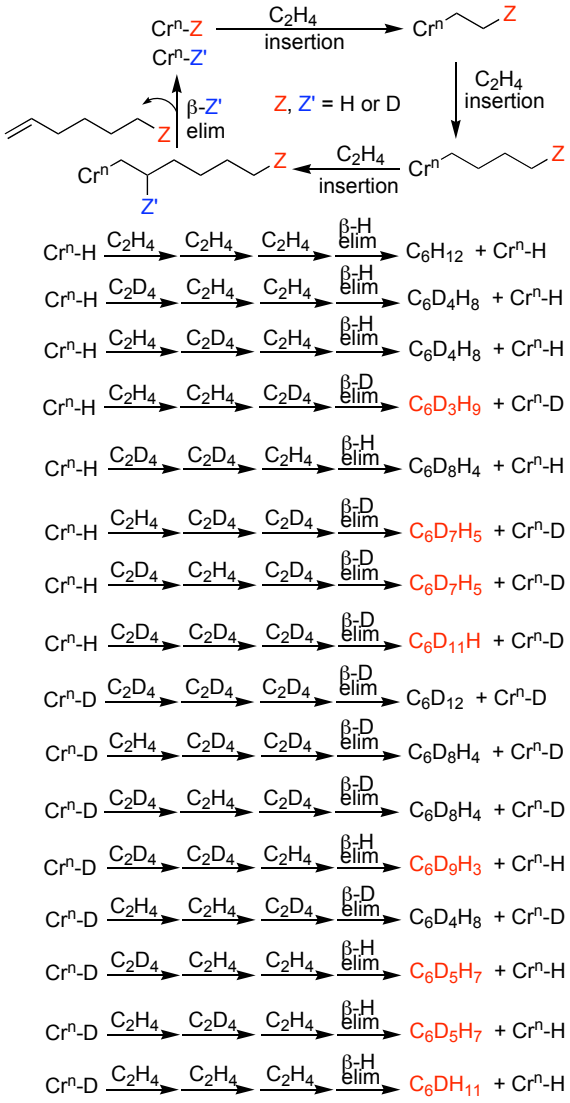

Scheme 9. Predicted isotopolog distribution for the trimerization of a C_2H_4/C_2D_4 mixture via a Cossee-type mechanism.

As described earlier, the Cossee type mechanism also involves hydride or deuteride intermediates. Upon ethylene insertion the initial Z (Z = H or D) moves away from the metals center, to the end of the linear alkyl chain (Scheme

9). Further ethylene insertions increase the distance between the metal center and the initial hydride or deuteride atom. Unlike for the metallacyclic mechanism, the atom (Z', Z' = H or D) abstracted in the metal-hexyl species to give 1-hexene is not the same with the initially metal bound one (Z). In consequence, scrambling of deuterium and hydrogen is expected between different 1-hexene molecules. Hence, isotopologs bearing odd numbers of hydrogens and deuteriums are expected for Cossee-type mechanism. The various possibilities to access 1-hexene isotopologs by this mechanism lead to a much broader distrobution – ten isotopologs can be formed theoretically, with six of them containing odd numbers of hydrogens and deuteriums. This is not observed experimentally. Hence the present experiment supports the metallacyclic mechanism and is not consistent with the Cossee-type mechanism.

Crossover experiment with the SHOP catalyst

It is important to note that the above experimental test is able to distinguish between metalacyclic and Cossee-type mechanims for any type of olefin olygomerization and is not limited to trimerizations. In fact other research groups have used this test since our initial report.[9,41,42] To document the outcome of this experiment under the conditions of a Cossee-type mechanism, the above test was performed with a nickel based non-selective ethylene oligomerization catalyst ($Ni(Ph_2PCH_2COO)(PPh_3)(Ph)$).[57] Formation of a broad distribution of α-olefins was observed (Figure 3). Analysis of the C6 fraction reveals an isotopolog distribution reflecting the predicted one. Interestingly, slightly more of the

isotopologs enriched in hydrogen are present in this fraction. This is better illustrated by a bar plot showing the expected and observed isotopolog distributions for the metallacyclic and Cossee-type mechanism (Figure 4).

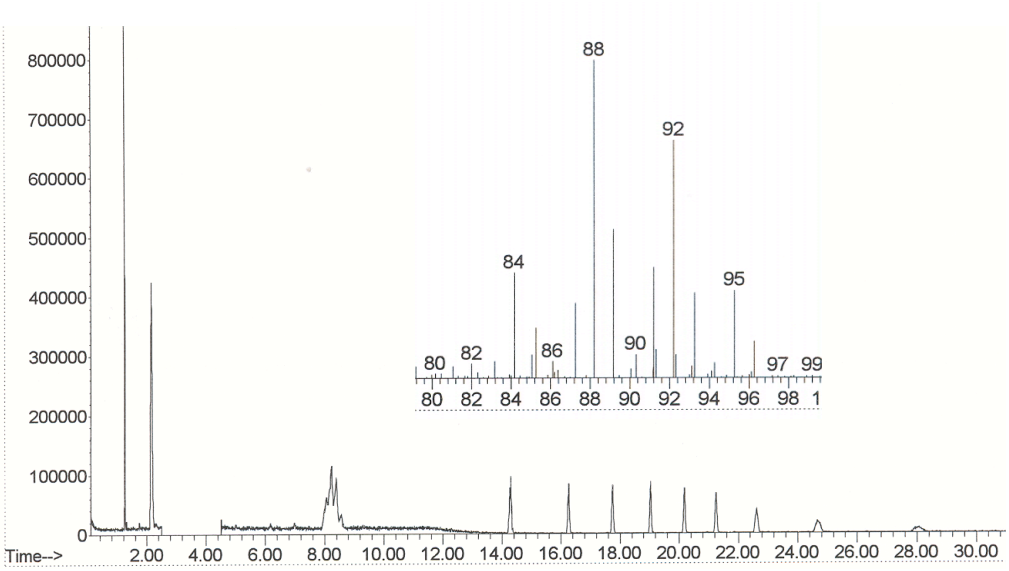

Figure 3. GC of the oligomers generated by $Ni(Ph_2PCH_2COO)(PPh_3)(Ph)$ with C_2D_4/C_2H_4 and MS (inset) of the 1-hexene fraction.

The results of this experiment are best illustrated by a bar plot showing the expected and observed isotopolog distributions for the metallacyclic and Cossee-type mechanism (Figure 4). This plot highlights the fact that the chromium trimerization reaction gives a better match between the predicted and isotopomer distributions. This is due to the fact that only trimerization is possible in this case and no "leaching" of deuterons or hydrogens to another oligomer fraction can occur. For the SHOP oligomerization however, there is a mechanistic branching point for each intermediate metal-alkyl species (Scheme 2): ethylene insertion can occur to increase the chain length or β-H elimination can occur to

generate the corresponding α-olefin. While ethylene insertion is expected to have just a small, secondary isotope effect, the β-H elimination will have a larger, primary isotope effect; the later will be the main contributor to the isotope effects on the isotopolog distributions. Every time the last inserted ethylene is C_2D_4, the metal alkyl will have a slower rate of β-Z elimination leading to a higher probability to insert another monomer and, in effect, carrying more deuterons to the higher olefins. This isotope effect on the isotopolog distribution cannot occur if only one oligomer is formed, as in the selective formation of 1-hexene, and no branching points are possible. However, a similar enrichment with hydrogens in the lower oligomers is expected even for a metallacyclic mechanism, if it is not fully selective for one of the oligomers. This effect has been reported for the metallacyclic nonselective ethylene oligomerization with chromium catalysts.[41,42] In that case, simulation of the observed distributions in the low oligomers including an isotope effect gave the best fit. For the selective trimerization and tetramerization of ethylene with a Cr(PNP) system, it was reported that more deuterium was incorporated in the C8 than in the C6 fraction.[9] This is well accounted for by the above proposal invoking primary isotope effects for β-H elimination (or 3,7-H shift) step. The rational proposed in the literature for the different isotope distributions in the C6 and C8 fractions involves a secondary isotope effect for the formation of the metallacyclopentane intermediate. This isotope effect, however, should be small and inverse, and should affect both the C6 and C8 fractions, which is not the case.

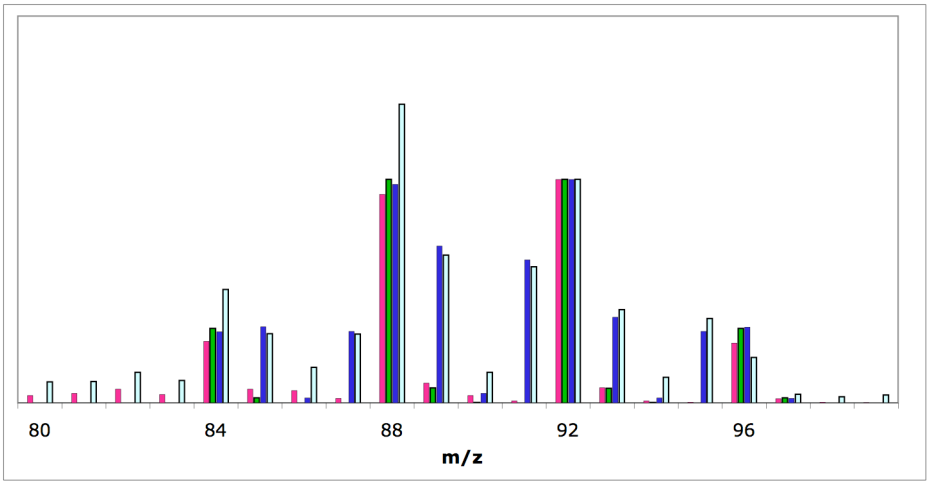

Figure 4. Red; experimental MS data for a chromium ethylene trimerization reaction. Green; simulated isotopomer distribution for a mechanism involving metallacyclic intermediates. Blue; simulated isotopomer distribution for a Cossee-type mechanism. Light blue; experimental MS data for a nickel ethylene oligomerization reaction.

Reactions with 1,2-dideuteroethylene

Trimerization of partially deuterated ethylene has provided further insight into the mechanism of formation of 1-hexene. *Cis*- and *trans*-ethylene-d_2 were trimerized using the cationic chromabiphenyldiyl precursor. The volatile materials, consisting of 1-hexenes, CD_2Cl_2, and unreacted ethylene were vacuum transferred to a J-Young tube and analyzed by NMR spectroscopy. The olefinic region of the ^{1}H NMR spectra reveals two types of isotopomers with either two hydrogens or two deuteriums bound to the double bond, and with a =CDH teminal methylene group. Upon conversion of ethylene to 1-hexene, the

geometry around the double bond is formally rotated by 180°. For example, *cis*-ethylene-d_2 leads to the formation of 1-hexene that has the two deuteriums or hydrogens trans to each other. The ratio of the two observed isotopomers for the trimerization of *cis*-ethylene-d_2 was found to be 3.1(1) at 25 °C, 3.7(4) at 0 °C, and 3.6(1) at -25 °C (reactions performed in Schlenk flasks). The values reported in the initial communication are somewhat different, due to the use of short recycling delays in the ^{1}H NMR spectroscopy experiments. Current values were measured with recycling delays of 250 s. The ratio of the two observed isotopomers for the trimerization of *trans*-ethylene-d_2 was found to be 4.1(1) at 25 °C.

Analysis of the metallacyclic mechanism in the context of the trimerization of 1,2-ethylene-d_2 indicates that the steps leading to the formation of the chromacycloheptane should not be affected significantly compared to non-deuterated ethylene – only small, secondary isotope effects are expected. The chromacycloheptane intermediate has one hydrogen and one deuterium on each carbon in the ring and it represents a branching point between β-H and β-D eliminations (Scheme 10). This two pathways are completely analogous; only one will described in detail. Upon β-H elimination, a chromium-alkenyl-hydride species is formed which can undergo reductive elimination to generate a 1-hexene isotopomer with a =CDH end group. Alternatively, the chromium-alkenyl-hydride species could perform a 2,1-H insertion to lead to the formation of a chromacyclohexane. From this intermediate, β-D elimination from the exo position generates a chromium-alkenyl-hydride species. Reductive elimination leads to a 1-hexene isotopomer with a =CH_2 end group. Experimentally, only 1-

hexene isotopomers with a =CDH end group are observed, without any detectable isotopomers with $=CH_2$ or $=CD_2$ end groups. This indicates that reductive elimination from a putative chromium-alkenyl-hydride species is much faster than 2,1-H reinsertion.

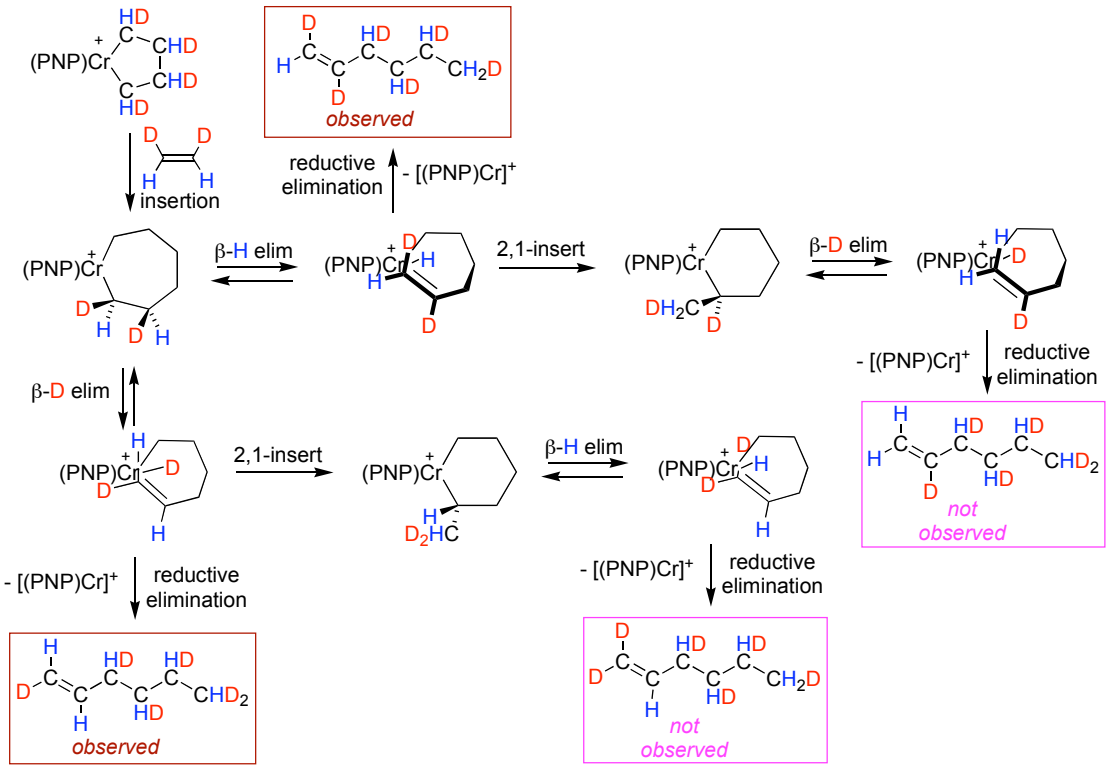

Scheme 10. Mechanism of the trimerization of *cis*-ethylene-d_2 showing routes to possible 1-hexene isotopomers.

In the context of the trimerization of 1,2-ethylene-d_2, the possibility of a 1,2-H reinsertion from chromium-alkenyl-hydride species becomes an interesting question. Analysis of the stereochemistry of the α-, β-, and γ-carbons of a metallacycloheptane presents the outcome of such process (Scheme 11). The pendant olefin raises not only issues of regioselectivity for the hydride

reinsertion (of which, 2,1-insertion was discussed above), but also of stereoselectivity with respect to the enantioface of the olefin. Simple 1,2-H reinsertion in the chromium-alkenyl-hydride intermediate using the same face of olefin leads to the initial chromacycloheptane species. The pendant olefin, however, can dissociate and coordinate via the opposite face. 1,2-H reinsertion using the opposite face of the olefin leads to inversion in configuration at the α- and β-carbons compared to the γ-carbon. From either of these diastereomers, the same olefin isotopomers are obtained, the 1,2-H reinsertion process being inconsequential to the outcome of the reaction.

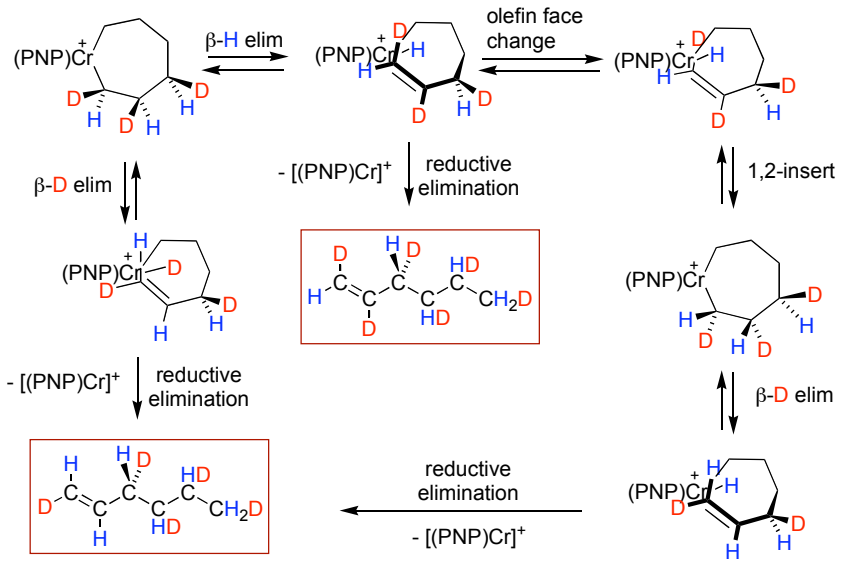

Scheme 11. Partial mechanism of the trimerization of *cis*-ethylene-d_2 showing the lack of effect of 1,2-H reinsertion on the final products.

The results the trimerization of 1,2-ethylene-d_2 indicate that the reductive elimination from chromium-alkenyl-hydride is fast compared to 2,1-H reinsertion (Scheme 12). This has important consequences on the purity of the

resulting trimerization product. If 2,1-H insertion would be a competitive process then the resulting chromacyclohexane could undergo β-H elimination from the ring CH bonds, followed by reductive elimination which would lead to the formation of 2-hexene, an undesired byproduct. While the present experiment does not interrogate the possibility of a 1,2-H insertion, this process does not have an influence on the final olefin product and hence, does not affect the selectivity for 1-hexene in the C6 fraction.

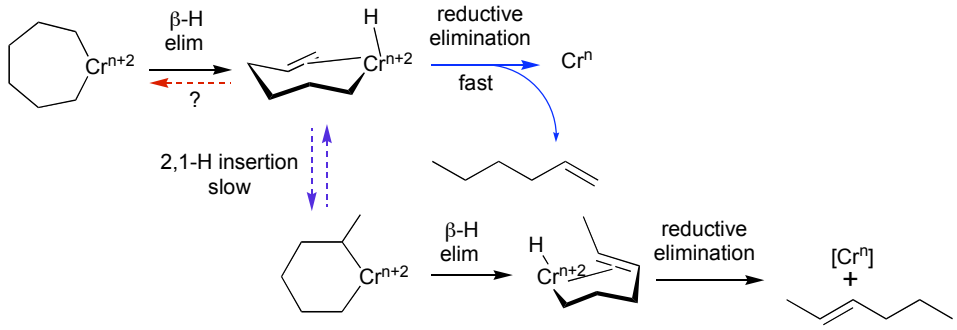

Scheme 12. Partial mechanism indicating the beneficial effect of fast reductive elimination vs. 2,1-H insertion on the purity of 1-hexene.

An alternative explanation for the selective formation of the observed isotopomers of 1-hexene in the trimerization of 1,2-ethylene-d_2 involves concerted 3,7-H (or D) shifts instead of stepwise β-H (or D) elimination followed by reductive elimination (Scheme 13).[33-40] It is clear that if a metal hydride is not formed at all, like in the 3,7-H shift mechanism, then no selectivity issues remain relative to hydride reinsertion. A number of computational studies have found that 3,7-H shift is more energetically favorable than a stepwise mechanism for titanium, tantalum, and chromium ethylene trimerization systems. It is

important to note, however, that catalytic systems closely related to the present system generate byproducts that have to involve intermediate β-H elimination.[9,20,30] The observed isotope effects may provide an indication of the mechanistic pathway occurring in these transformations. In the case of the stepwise mechanism, two situations can be envisioned. If β-H elimination is fast and reversible with respect to reductive elimination, then the observed ratio of isotopomers reflects a composite of an equilibrium isotope effect for the β-H elimination and the kinetic isotope effect for the reductive elimination. If β-H elimination is slow relative to the subsequent reductive elimination, then the ratio of isotopomers reflects the kinetic isotope effect of the β-H elimination. In the case of the 3,7-H shift, the ratio of isotopomers represents the kinetic isotope effect for this process. In either case, the ratio of isotopomers represents the intrinsic overall isotope effect for the formation of 1-hexene from the chromacycloheptane. Reasoning that a 3,7-H shift may have a significant tunneling contribution leading to unusual kinetic isotope effects, the isotope effect dependence on temperature was investigated. Only a modest variation was observed over 50 K which does not support this mechanistic proposal, but cannot rule it our either. Overall, the present experiments, while consistent with both possibilities, cannot distinguish between concerted and stepwise mechanisms. The difference between the observed isotope effect for the trimerization of *cis*-ethylene-d_2 (3.1(1)) vs *trans*-ethylene-d_2 (4.1(1)) is somewhat surprising, since both ethylenes should give the same value if only primary

isotope effects are involved. The difference could be due to a small steric isotope effect.

Interestingly, the present diphosphine framework (and more generally, PNP phosphines with either four *ortho*-alkyl substituents or at least one *ortho*-ether group) is capable of rendering the reaction very selective for the formation of 1-hexene in the C6 fraction without any isomerization coming from chain walking or insertions of the pendant olefin. Two explanations could be envisioned. One possibility invokes the steric bulk of the ligand facilitating the transition state for 3,7-H shift over β-H elimination. Conversely, if β-H elimination does occur, reductive elimination is very fast compared to isomerization. Again, the sterics of the ligand (or the ability of pendant donors to compete for coordination sites) would slow the coordination of the pendant olefin and the hydride reinsertion.

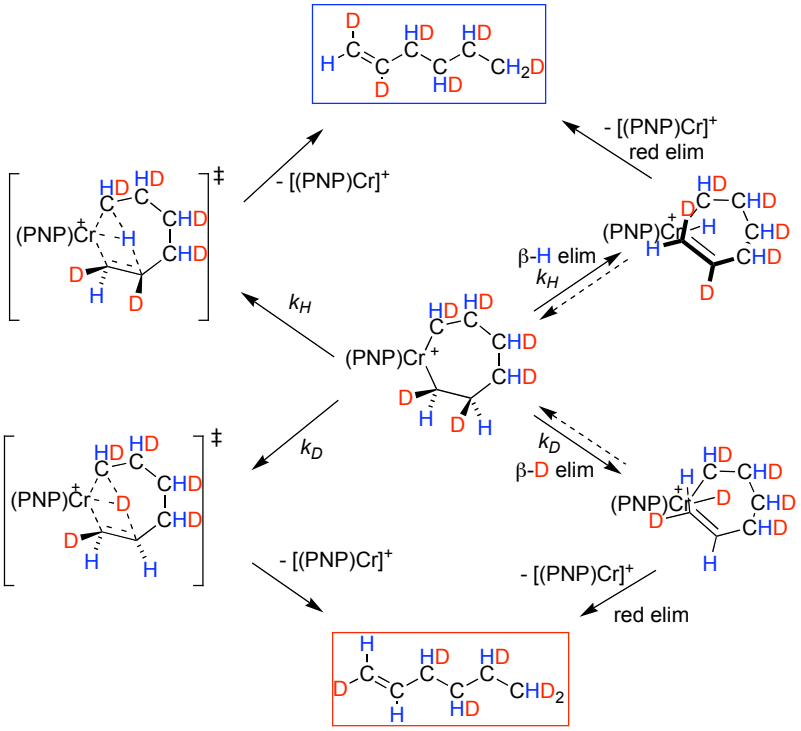

Scheme 13. Concerted and stepwise mechanisms for the formation of 1-hexene from chromacycloheptane.

Reactions with 1,1-dideuteroethylene

The trimerization of *gem*-ethylene-d_2 was performed under conditions identical to the ones for *cis*- and *trans*-ethylene-d_2. The formation of two types of olefin isotopomers of 1-hexene was observed, depending on the terminal methylene group, $=CD_2$ or $=CH_2$. Because in both cases the allylic position can bear either hydrogens or deuteriums, the corresponding signals are complicated by the overlap of different coupling patterns. The integrals corresponding to the peaks for the vinyllic protons provide the ratio between the two possible double

bond isotopomers. The integrals corresponding to the peaks for the vinyllic protons provide the ratio (1.3(1)) between the two possible double bond isotopomers.

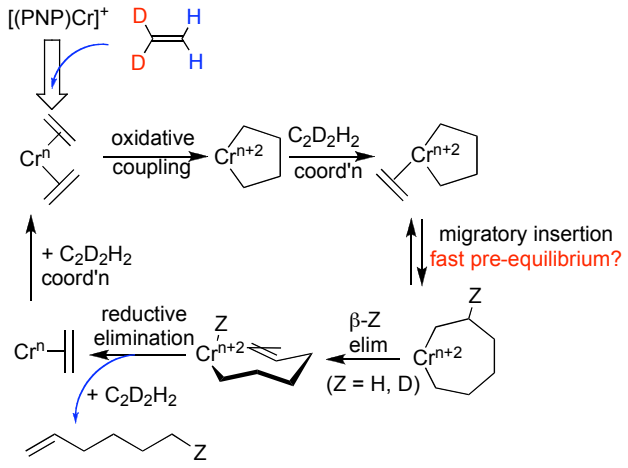

Scheme 14. Proposed mechanism for a fast and reversible formation of chromacycloheptane.

The outcome of the trimerization of *gem*-ethylene-d_2 can be used to investigate the reversibility of the formation of chromacycloheptane. In the context of the metallacyclic mechanism, the reverse process would involve an elimination of ethylene to generate a chromacyclopentane-ethylene species (Scheme 14). Three cases can be distinguished. If the formation of the chromacycloheptane is reversible and fast compared to subsequent steps then the various chromacyloheptane isotopomers can interconvert rapidly (Scheme 15). This will lead to a distribution of 1-hexene isotopomers according to the intrinsic isotope effect for the conversion of chromacycloheptane to 1-hexene which was

measured to be 3.1(1) for *cis*-ethylene-d_2 (4.1(1) for *trans*-ethylene-d_2) at room temperature. Conversely, if formation of chromacycloheptane is irreversible, and there is sufficient asymmetry such that β-H elimination occurs selectively from one end of the alkanediyl group (Scheme 16), no isotope effect is expected (assuming negligible secondary isotope effects). However, if formation of chromacycloheptane is irreversible and β-H elimination can occur equally from either end of the alkanediyl group then the different types chromacycloheptanes need to be treated separately (Scheme 17). The ones with all the same atoms (H or D) on the β-carbon can generate only one type of 1-hexene isotopomer leading to a 1:1 ratio of the two possible ones (stemming from the 1:1 probability of forming the two corresponding chromacycloheptane isotopomers). The metallacycloheptane displaying both hydrogens and deuteriums in the β-position are expected to β-eliminate according to the intrinsic isotope effect (3.1(1) to 4.1(1)). Upon accounting for the statistical populations of different chromacycloheptane isotopomers this analysis leads to an expected isotope effect of 2.1(1) to 2.5(1). The observed isotope effect is 1.3(1), indicating that the metallacycloheptane is formed irreversibly. This isotope effect is not conclusive with respect to symmetry of the two ends of the metallacycloheptane. It is possible that a dynamic process exchanges the two ends of the alkanediyl moiety at a rate similar to conversion to 1-hexene. This would lead to an isotope effect intermediate between the symmetric and the non-symmetric and static cases.

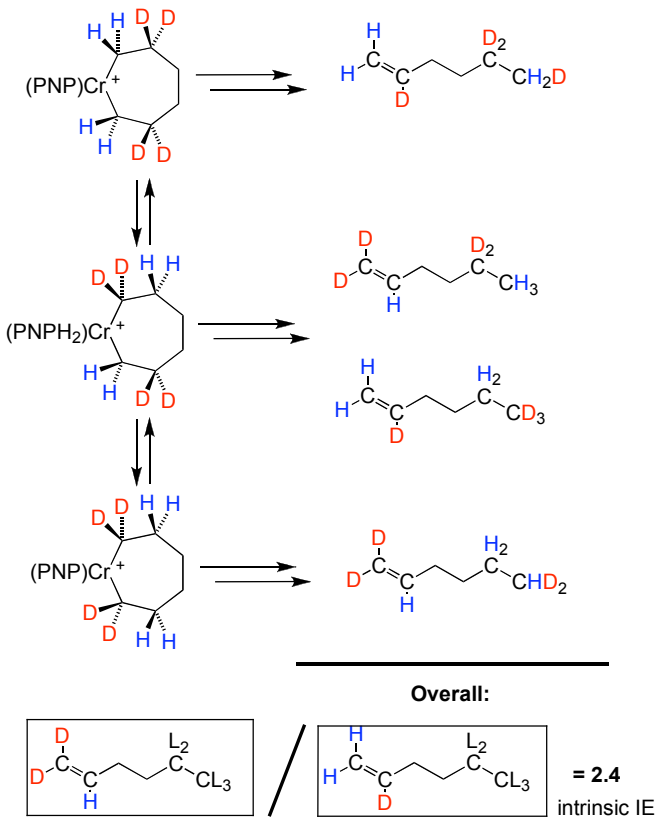

Scheme 15. Expected isotope effect for the reversible formation of chromacycloheptane.

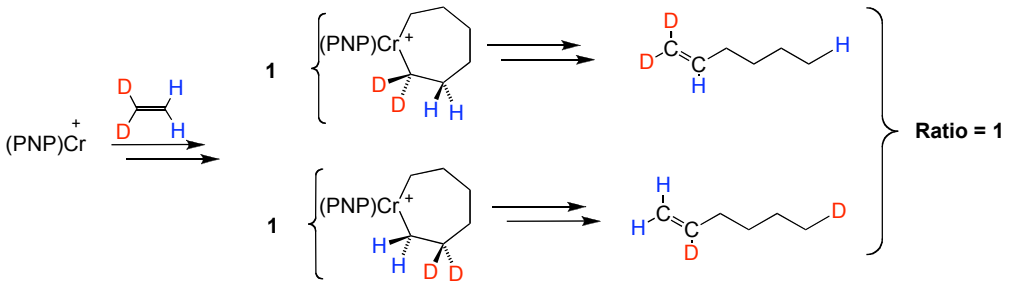

Scheme 16. Expected isotope effect for the irreversible formation of a asymmetric metallacycloheptane.

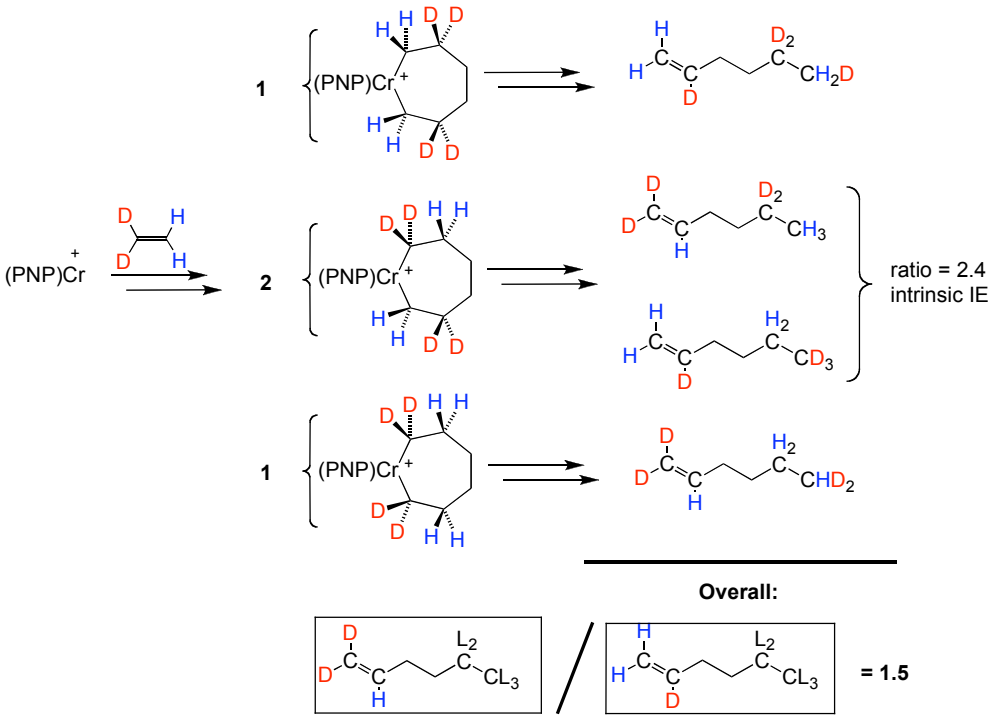

Scheme 17. Expected isotope effect for the irreversible formation of a symmetric metallacycloheptane.

Reaction of cationic species with α-olefins

Access to a chromabiphenyldiyl species, a model of the metallacyclopentane intermediate in the mechanism of the ethylene trimerization reaction, allows for selectivity studies relevant to olefin cotrimerization. In principle, olefin cotrimerization could lead to diverse olefin isomers of the same number of carbon atoms. For instance, cotrimerization of 1-butene with two ethylenes can lead to the formation of seven C8 isomers (not counting double bond stereoisomers) depending on the nature of the metallacyclopentane

formed, the regioselectivity of α-olefin insertion, and the regioselectivity of β-H elimination. While the preparation of olefin mixtures is desirable for some applications, the selective generation of only one isomer or mixture of isomers is more valuable. In this context, a better understanding of the selectivity of different steps of the cotrimerization reaction is desirable. Starting directly from a model of a chromacyclopentane allows for a systematic study of the α-olefin insertion and β-H elimination of a subset of cotrimerization possibilities (Scheme 18).

The cationic chromabiphenyldiyl species was prepared *in situ* as described above and was exposed to various olefins. The mixture was quenched and filtered through silicagel, and the nonvolatile species were analyzed by ^{1}H NMR spectroscopy and GC-MS. Only products stemming from stoichiometric olefin insertion into the chromabiphenyldiyl moiety were observed under these conditions. No α-olefin trimers were detectible. It is noteworthy that upon quenching the above mixture with water, it was found, by ^{31}P and ^{1}H NMR spectroscopy that the diphophine is altered to unidentified products. These products are not observed spectroscopically prior to quenching. Furthermore, the major phosphine species observed upon workup is also one of the compounds produced, according to ^{31}P NMR spectroscopy, if the same experiment is performed with phosphine and $Na[B(C_6H_3(CF_3)_2)_4]$ in the absence of chromium species. This suggests that any free phosphine produced may react with species stemming from $Na[B(C_6H_3(CF_3)_2)_4]$.

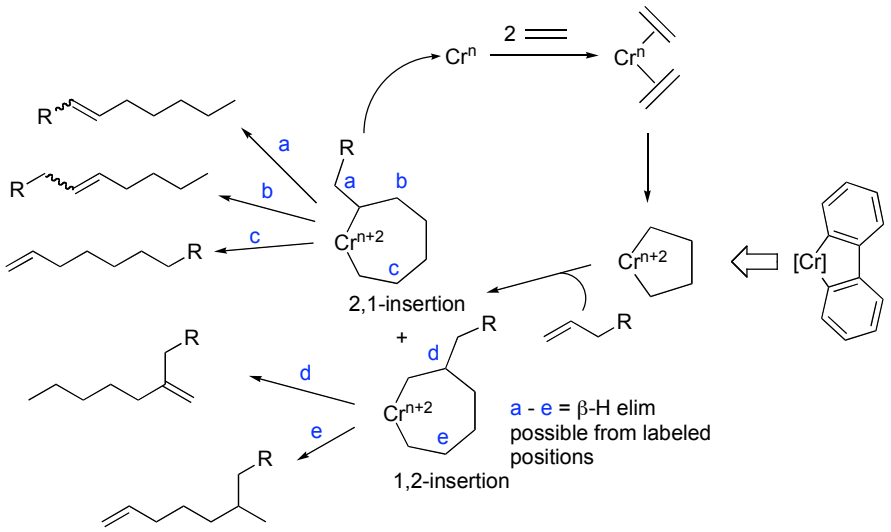

Scheme 18. Olefinic products stemming from the incorporation of an α-olefin into a chromacyclopentane.

The reaction of cationic chromabiphenyldiyl species with α-olefins, such as propene and 1-butene, leads to the formation of only one product, corresponding to the 1,2-insertion of olefin. The chromacycloheptane resulting from a 1,2-insertion of α-olefins has only one β-hydrogen hence the selectivity of β-H elimination cannot be tested in this process, given that the formation of the metallacycloheptane intermediate is irreversible. The reaction with internal olefins however, necessarily generates chromacycloheptanes with two types of β-hydrogens – on ring and exocyclic carbons (b and c in Scheme 19). Again formation of only one product is observed; this corresponds to β-H elimination from the ring position. It is interesting to note that the ring position is statistically disfavored vs the exocyclic position by three fold. However, in this case, the ring position also corresponds to a weaker, benzylic CH bond.

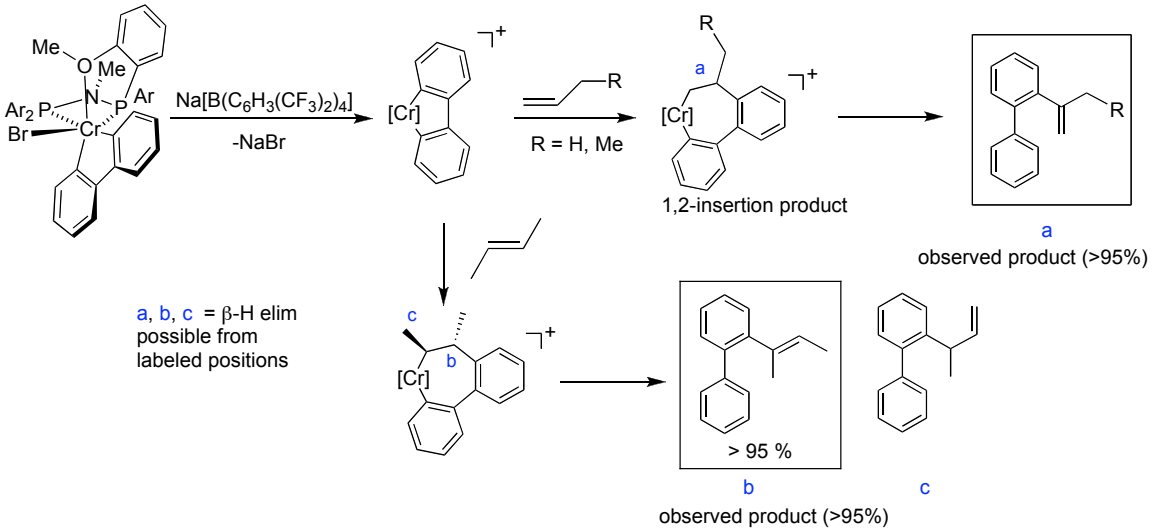

Scheme 19. Reaction of cationic chromabiphenyldiyl with a-olefins and internal olefins.

The above reaction, employing *E*-2-butene and forming *E*-2-biphenyl-2-butene, could occur via two mechanisms as described before (Scheme 13). The metallacycloheptane intermediate can undergo either a concerted hydride shift or β-H elimination followed by reductive elimination. These two possibilities apply for both β-positions (ring and exocyclic). The hydride shift could occur either in the cycle, as a 3,7-H shift (Scheme 20, top left), or exocyclic, as a reductive β-H abstraction (Scheme 20, bottom left). The exocyclic reductive β-H abstraction represents the acyclic version of the 3,7-H shift; this has not been commonly invoked over β-H elimination / reductive elimination of linear dialkyl species, but recently has been computed to be the preferred route for the conversion of titanium(IV)-methyl-ethyl species to titanium(II)-propylene and methane.[35] It is difficult to speculate which of the two positions would preferentially undergo reductive hydride shift; this is a problem well suited for

computation analysis. Alternatively, the β-H elimination mechanism could occur from both ring and exocyclic positions (Scheme 20, right). Since β-H elimination requires coplanarity of the β-C-H and Cr-C bonds, it is expected that the ring β-H elimination would encounter a higher barrier than the exocyclic process. In this context, the formation of only the product stemming from ring hydride shift / elimination may suggest that the working mechanism involves a 3,7-H shift.

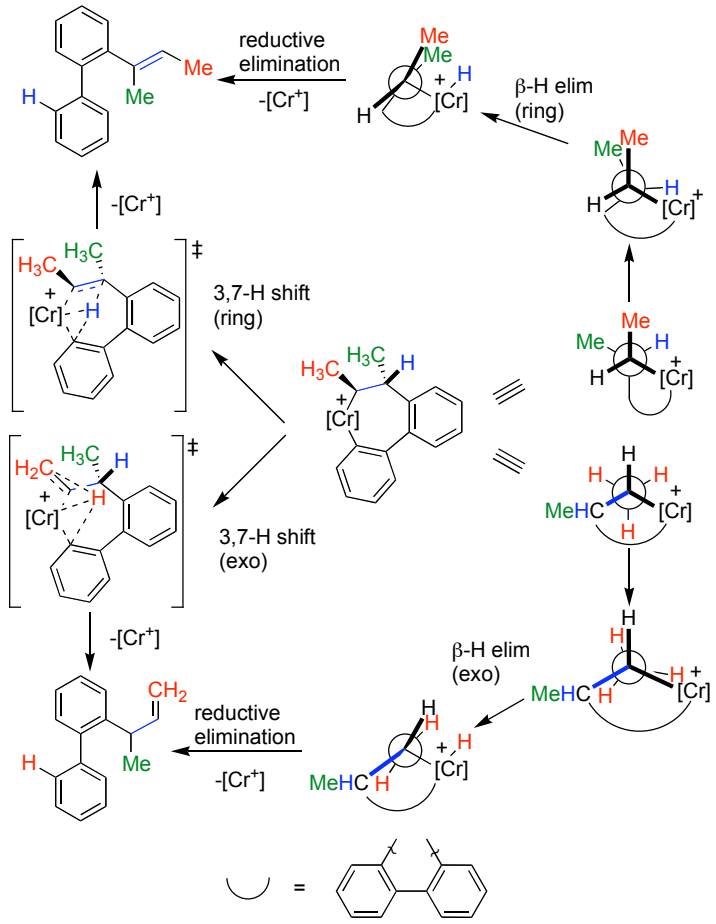

Scheme 20. Proposed mechanisms for the β-H elimination from different positions in a methyl-substituted chromacycloheptane model.

Competitive olefin insertion experiments

Envisioning that competition experiments may provide the relative rates of insertion of various olefins into a chromacyclopentane mimic, the chromabiphenyldiyl species was exposed to mixtures of two olefins. The cationic chromabiphenyldiyl complex was generated *in situ* in a J-Young tube and two olefins were condensed in at -178 °C. Excess larger than ten fold of olefin relative to chromabiphenyldiyl complex was utilized. This allowed the measurement of the approximate initial ratio in solution of the two olefins, the amounts consumed for the stoichiometric insertion reaction being negligible. Upon reaction completion, volatile materials were removed under vacuum and remaining biphenyl derivatives were inspected by ^{1}H NMR spectroscopy to provide the ratio of species generated by the insertion of different olefins. The relative rates of olefin insertion into the chromabiphenyldiyl moiety were calculated from the initial ratio of starting olefins and the final ratio of biphenyl olefin species (Table 1). The measurements involving ethylene present the problem that trimerization to generate 1-hexene occurs upon initiation via the chromabiphenyldiyl species leading to a decrease in the initial concentration of ethylene; this error was minimized by measuring the initial olefin ratio upon warming the sample to room temperature in the NMR probe. Since the formation of the chromacycloheptane species is irreversible, the present measurements reflect the relative insertion rates of these olefins and do not reflect any subsequent steps (3,7-H shifts or β-H elimination followed by reductive elimination).

Table 1. Relative insertion rates of various olefins in a cationic chroma-biphenyldiyl moiety.

Olefin	Relative insertion rate
Ethylene	13000
1-Butene	660
Propene	620
4-Methyl-1-pentene	190
3-Methyl-1-butene	62
Styrene	31
cis-2-Butene	16
trans-2-Butene	1

Generally, the relative insertion rates increase with decreasing size of the olefin. Ethylene inserts more than twenty times faster than linear α-olefins, consistent with the observed good selectivity of homotrimerization vs cotrimerization in the presence of α-olefin (1-hexene) product. The relative rates of insertion mirror the trends observed for the rates of olefin insertion into zirconium hydrides.[58] Internal olefins are slower that α-olefins with the *trans*-2-butene significantly slower than *cis*-2-butene. While the relative order of rates of insertions should probably remain the same, it is important to note that the

present model system is more sterically hindered, rigid, and involves different hybridization at the carbon centers compared to the parent chromacyclopentane which may lead to different values for the actual catalytic system.

Trimerization of a mixture of ethylene and propylene

To test the selectivity results obtained from stoichiometric reactions of α-olefins with a model of chromacyclopentane, the cotrimerization of ethylene and propylene was performed. A large excess of propylene was used to insure detectable levels of cotrimer. Propylene was chosen as a cotrimerization partner because all the C7 olefins are commercially available, allowing for comparison against original samples. The reaction was performed both starting with **1** upon halide abstraction (CH_2Cl_2) and with $Cr(PNP^{O4})Cl_3$ upon activation with MAO (toluene). Upon quenching, an aliquot was investigated by GC-MS. 3-Methyl-1-heptene, 4-methyl-1-heptene, 5-methyl-1-heptene, and 1-hexene were found to be the major products in both cases.

Analysis of various cotrimerization possibilities (Scheme 21) shows that three types of chromacylopentane and four types chromacycloheptanes can be formed (including the parent, unsubstituted ones). Multiple routes can be envisioned to some olefin products. None of the major products observed come from 2,1-insertions of propylene into chromacyclopentane or from β-H elimination / shift from exo-CH bonds, fact consistent with the selectivity conclusions above. It is worth noting however, that selectivities in the catalytic

system can be determined in part by steps prior to chromacycloheptane formation, such as the chromacyclopentane generation, which is not characterized in the present experiments.

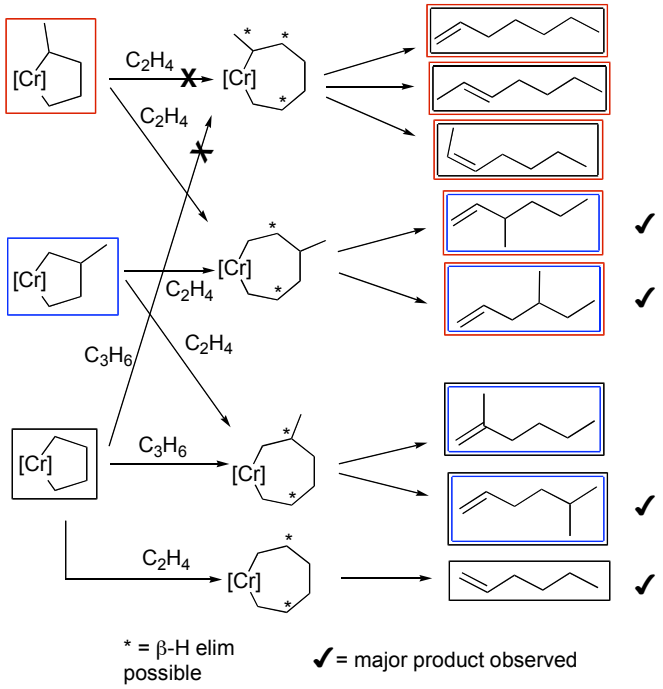

Scheme 21. Possible cotrimers of ethylene and propylene and the corresponding formation routes.

Conclusions

Mechanistic studies relevant to the catalytic ethylene trimerization reaction have been performed with using a chromium(III) system supported by diphosphine ligand PNP^{O4} = (*o*-MeO-C_6H_4)$_2$PN(Me)P(*o*-MeO-C_6H_4)$_2$. A model chromabiphenyldiyl complex was used as a well-defined precursor for a number of labeling studies. Catalytic trimerization of ethylene and 2-butyne is accomplished with a cationic chromium species but not with neutral one indicating that a cationic species is required for catalysis. Trimerization of a 1:1 mixture of C_2D_4 and C_2H_4 with the chromium system leads to isotopologs of 1-hexene without H/D scrambling, result that supports a metallacyclic mechanim and is inconsistent with a Cossee-type mechanism. When the same study is performed with a nickel non-selective oligomerization catalyst it gives a broader distribution of 1-hexene isotopologs (with H/D scrambling). These results indicate that oligomerization of mixtures of C_2D_4 and C_2H_4 and analysis of isotopolog distribution in the products is a versatile and useful test for distinguishing between metallacyclic and Cossee-type mechanisms of olefin oligomerization.

The trimerization of *trans*- and *cis*-ethylene-d_2 interrogates the formation of 1-hexene from chromacycloheptane. This experiment results in isotopomers corresponding to fast reductive elimination of the putative chromium-hydride-alkenyl species compared to isomerization pathways. It is also consistent with concerted 3,7-H shift. This effect probably stems from

the steric or coordinating properties of the *ortho* substituents and is important for the good selectivity for 1-hexene in the C6 fraction. The trimerization of *gem*-ethylene-d_2 occurres with an isotope effect consistent with the irreversible formation of chromacycloheptane.

Reaction of a chromabiphenyldiyl species with higher olefins has allowed for selectivity studies. α-Olefins insertion in the chromacyclopentane model occurs with 1,2-regioselectivity while β-H elimination in model chromacycloheptanes occurs from ring CH bonds over exo-CH bonds. While the selectivities observed in the stoichiometric system show some promise for the selective cotrimerization of olefins, our catalytic experiment with ethylene and propylene shows the complexity of the full system. Further experiments are needed to understand the selectivity of chromacyclopentane formation in mixtures of olefins as well as regioselectivity of insertion in asymmetric chromacycloheptane. Our measurements of relative rates of insertion into a chromabiphenyldiyl moiety for different olefins reveal that ethylene is significantly faster that α-olefins. This is consistent with the good selectivities for ethylene homotrimerization in the presence of 1-hexene product.

Experimental Section

General Considerations and Instrumentation. All air- and moisture-sensitive compounds were manipulated using standard vacuum line, Schlenk, or cannula techniques or in a drybox under a nitrogen atmosphere. Solvents for air- and moisture-sensitive reactions were dried over sodium benzophenone ketyl or by the method of Grubbs.[59] Dichloromethane-d_2 was purchased from Cambridge Isotopes and distilled from calcium hydride. Other materials were used as received. ^{1}H and ^{13}C NMR spectra were recorded on Varian Mercury 300, or Varian INOVA-500 spectrometers and unless otherwise indicated at room temperature. Chemical shifts are reported with respect to internal solvent: 7.27 and 77.23 (t) ppm ($CDCl_3$); 5.32 (t) and 54.00 (q) ppm (CD_2Cl_2); for ^{1}H and ^{13}C data.

Trimerization of ethylene with 1 upon halide abstraction. D_2-dichloromethane was vacuum transferred to a J-Young tube or Schlenk flask charged with **1** (8 - 34 mg, 10 - 42 μmol, 1 equiv) and $NaB[C_6H_3(CF_3)_2]_4$ (10.5-45 mg, 12-51 μmol, 1.2 equiv). The mixture was warmed to room temperature using a water bath followed by mixing (via mechanical rotation for NMR tubes or magnetic stirring for flasks) for 10 min. The mixture turned brown as the starting materials dissolved. Ethylene (128.2 mL at 30-125 Torr, 200 - 860 μmol, 17.5 - 23 equiv) was condensed in (~2.3 - 3.8 atm in the vessel at room temperature). The reaction mixture was mixed for 1 - 1.5 h at room temperature during which the mixture turned brown-green. *O*-vinyl-biphenyl and 1-hexene were detected by ^{1}H NMR spectroscopy. Relative to the amount of *o*-vinyl-biphenyl observed, about 3.5 equiv of 1-hexene is formed (ca 60%).

Reaction of 1 with ethylene. *D*2-dichloromethane was vacuum transferred to a J-Young tube charged with **1** (8.1 mg, 10.1 mmol, 1 equiv). Ethylene (43.48 mL at 87 Torr, 200 mmol, 20 equiv) was condensed in (~ 2 atm in the tube at room temperature). The mixture was warmed to room temperature using a water bath then mixed by mechanical rotation for 1 h. During this time the mixture achieved a brown-green color. *O*-vinyl-biphenyl was detected by ^{1}H NMR spectroscopy, but no 1-hexene was observed. After an additional 1 h of mixing the mixture turned brown-red, but no 1-hexene was formed according to ^{1}H NMR spectroscopy.

Trimerization of 2-butyne with 1 upon halide abstraction. Dichloromethane was vacuum transferred to a 10 mL round bottom Schelenk tube charged with **1** (31.8 mg, 39.6 μmol, 1 equiv) and $NaB[C_6H_3(CF_3)_2]_4$ (42 mg, 47.6 μmol, 1.2 equiv). The mixture was warmed up to room temperature using a water bath, followed by stirring for 10 min. 2-Butyne (128.2 mL at 160 torr, 1.1 mmol, 23.2 equiv) was condensed in. The reaction mixture was allowed to mix for 12 h. Upon opening to air, the mixture was quenched with 1 mL aqueous CO_3^{2-}/HCO_3^- solution. The mixture was transferred to a scintillation vial and centrifuged. The organic layer was separated and filtered through silica gel then volatile materials were removed under vacuum. The residue was analyzed by ^{1}H NMR spectroscopy in $CDCl_3$ and GC-MS. Hexamethyl benzene and 9,10-dimethylphenantrene were identified against commercially available samples.

Reaction of 2-butyne with 1. Dichloromethane was vacuum transferred to a 10 mL round bottom Schelenk tube charged with **1** (65.6 mg, 81.7 μmol, 1 equiv). 2-Butyne (128.2 mL at 220 torr, 1.5 mmol, 18.5 equiv) was condensed in. The

reaction mixture was allowed to mix for 12 h at room temperature. Upon opening to air, the mixture was quenched with 1 ml aqueous CO_3^{2-}/HCO_3^- solution. The mixture was transferred to a scintillation vial and centrifuged. The organic layer was separated in filtered through silica gel then volatile materials were removed under vacuum. The residue was analyzed by ^1H NMR spectroscopy in $CDCl_3$ and GC-MS. Hexamethyl benzene was absent by both analytical methods. 9,10-Dimethylphenantrene was identified as the major product by ^1H NMR spectroscopy in $CDCl_3$ and GC-MS.

Trimerization of a C_2D_4 / C_2H_4 mixture with 1 activated with $NaB[C_6H_3(CF_3)_2]_4$. D_2-dichloromethane was vacuum transferred to a J-Young tube charged with **1** (9.2 mg, 11.4 μmol, 1 equiv) and $NaB[C_6H_3(CF_3)_2]_4$ (12.2 mg, 13.8 μmol, 1.2 equiv). The mixture was warmed up to room temperature using a water bath, followed by mixing (via mechanical rotation) for 10 min. The mixture turned brown upon starting materials dissolving. A 1:1 mixture of C_2D_4 and C_2H_4 (128.2 mL at 29 torr, 200 μmol, 17.5 equiv) was condensed in (~2.4 atm in the tube at room temperature). The reaction mixture was allowed to mix for 1 h at room temperature during which time it achieved a brown green color. The reaction vessel was cooled in a dry ice / acetone bath and degassed. Following removal of ethylene, the mixture was allowed to reach room temperature and volatile materials were vacuum transferred to a round bottom flask and analyzed by GC-MS. The 1-hexene fraction shows a 1:3:3:1 distribution of isotopomers (C_6H_{12}, $C_6H_8D_4$, $C_6H_4D_8$, and C_6D_{12}). The solid residue was partitioned between water and dichloromethane and the organic fraction was analyzed by GC-MS to reveal the presence of d_0- and d_4-*o*-vinylbiphenyl and biphenyl.

Trimerization of a C_2D_4 / C_2H_4 mixture with 1 activated with MAO. Compound **1** (8.2 mg, 10.1 μmol, 1 equiv) was suspended in toluene (30 mL) and the mixture was cooled to –78 °C in a dry ice / acetone bath. Under counterflow of argon, the Teflon stopcock was replaced with a rubber septum, and MAO solution (10% in toluene, d = 0.875 g/mL, 2.4 mL, 300 equiv) was added via syringe. The septum was replaced with the Teflon stopcock. The mixture was degassed briefly and placed under 1:1 C_2D_4 / C_2H_4 mixture (~2.3 atm static pressure, 10 mmol, 1000 equiv) while warming up to room temperature in a water bath. The reaction mixture was allowed to stir for 1.5 h. An aliquot was collected, quenched with water and analyzed by GC-MS. The 1-hexene fraction resolves in a quartet showing a 1:3:3:1 distribution of isotopomers (C_6H_{12}, $C_6H_8D_4$, $C_6H_4D_8$, and C_6D_{12}). D_0- and d_4-*o*-vinylbiphenyl do not resolve on the GC trace but are both present according to the mass spectrum.

Trimerization of a C_2D_4 / C_2H_4 mixture with $CrCl_3(THF)_3$ / PNP^{O4} activated with MAO. A solution of $CrCl_3(THF)_3$ (6 mg, 16 μmol, 1 equiv) in dichloromethane (1 mL) was added to a dichloromethane solution (1 mL) of **1** (8.3 mg, 16 μmol, 1 equiv). The reaction mixture was allowed to stir for 1 h at room temperature. Volatile materials were removed *in vacuo*, and toluene (40 ml) was added. The resulting mixture was cooled down in a dry ice / acetone bath and the Teflon stopcock was replaced with a rubber septum under counterflow of argon. MAO solution (10% in toluene, d = 0.875 g/mL, 3.2 mL, 300 equiv) was added via syringe then the septum was replaced with the Teflon stopcock. The mixture was degassed briefly and placed under 1:1 C_2D_4 / C_2H_4 mixture (~1.4 atm static pressure at room temperature, 1.4 mmol, 875 equiv) while warming up to room

temperature in a water bath. It was allowed to stir for 2.5 h; the mixture turned pale green. An aliquot was collected, quenched with water and analyzed by GC-MS. The 1-hexene fraction displays a 1:3:3:1 distribution of isotopomers (C_6H_{12}, $C_6H_8D_4$, $C_6H_4D_8$, and C_6D_{12}).

Trimerization of *cis*-, *trans*-, and *gem*-$C_2H_2D_2$. D_2-dichloromethane was vacuum transferred to a J-Young tube or Schlenk flask charged with **1** (8-34 mg, 10-42 μmol, 1 equiv) and $NaB[C_6H_3(CF_3)_2]_4$ (10.5-45 mg, 12-51 μmol, 1.2 equiv). The mixture was warmed up to room temperature using a water bath followed by mixing (via mechanical rotation for NMR tubes or magnetic stirring for flasks) for 10 min. The mixture turned brown upon starting materials dissolving. Labeled ethylene (128.2 mL at 30-125 torr, 200-860 μmol, 17.5-23 equiv) was condensed in (~2.3-3.8 atm in the vessel at room temperature). The reaction mixture was allowed to mix for 1-1.5 h at room temperature during which the mixture turned brown-green. Subsequently, the reaction mixture was cooled in a dry ice / acetone bath and degassed. Following removal of ethylene, the mixture was allowed to warm to room temperature, and volatile materials were vacuum transferred to a round bottom flask and analyzed by ^1H and ^{13}C NMR spectroscopy. Isotope effects obtained: 3.1, 3.2, 3.1 (298 K, *cis*-$C_2H_2D_2$), 4.0, 4.1 (298 K, *trans*-$C_2H_2D_2$), 1.3, 1.3 (gem-$C_2H_2D_2$), 4.0, 3.4 (273 K, *cis*-$C_2H_2D_2$), 3.6, 3.6 (248 K, *cis*-$C_2H_2D_2$). The solid residue was partitioned between water and dichloromethane and the organic fraction was analyzed by GC-MS to reveal the presence of d_2-*o*-vinylbiphenyl and biphenyl. Figures 5, 6, and 7 show the olefin region of the ^1H NMR spectra of trimers resulted from different ethylene-d_2 isotopomers. Figure 8 shows couplings obtained from these spectra.

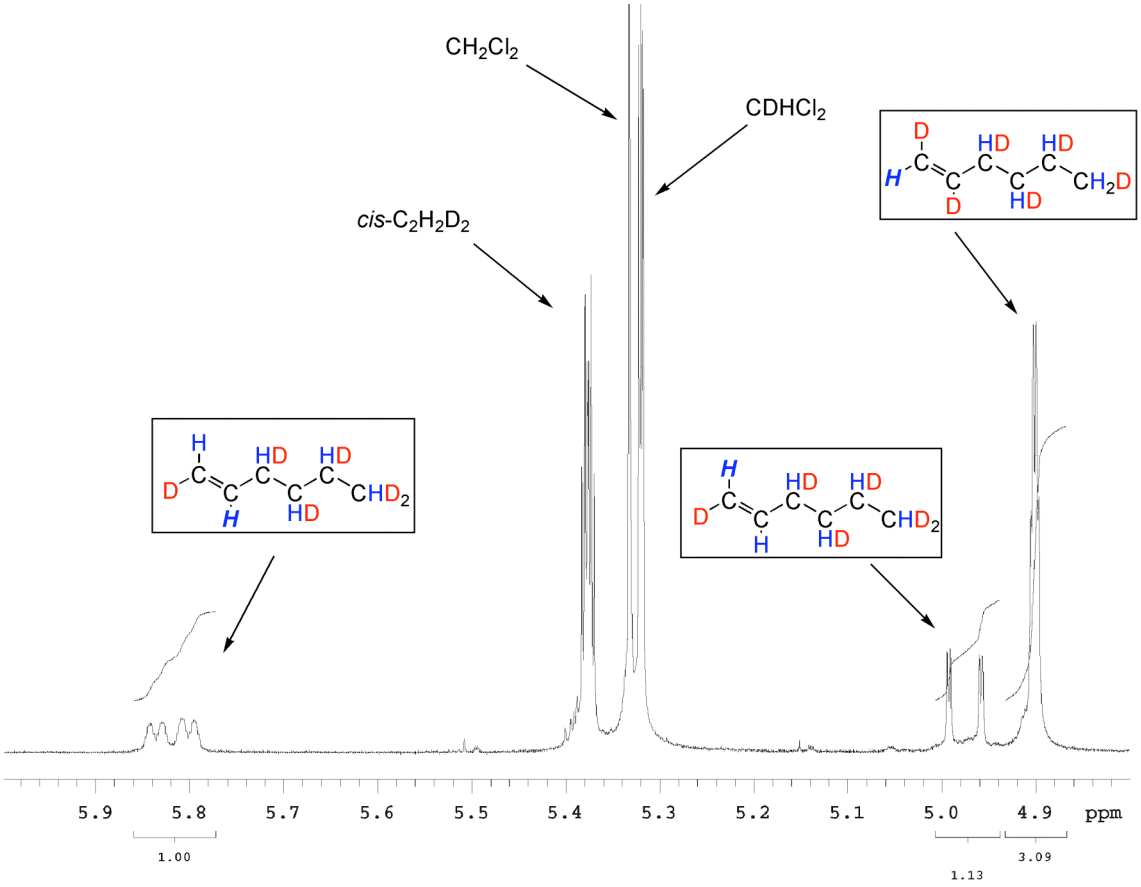

Figure 5. Olefinic region of the ^{1}H NMR spectrum of the volatile materials resulting from the trimerization of *cis*-dideuteroethylene.

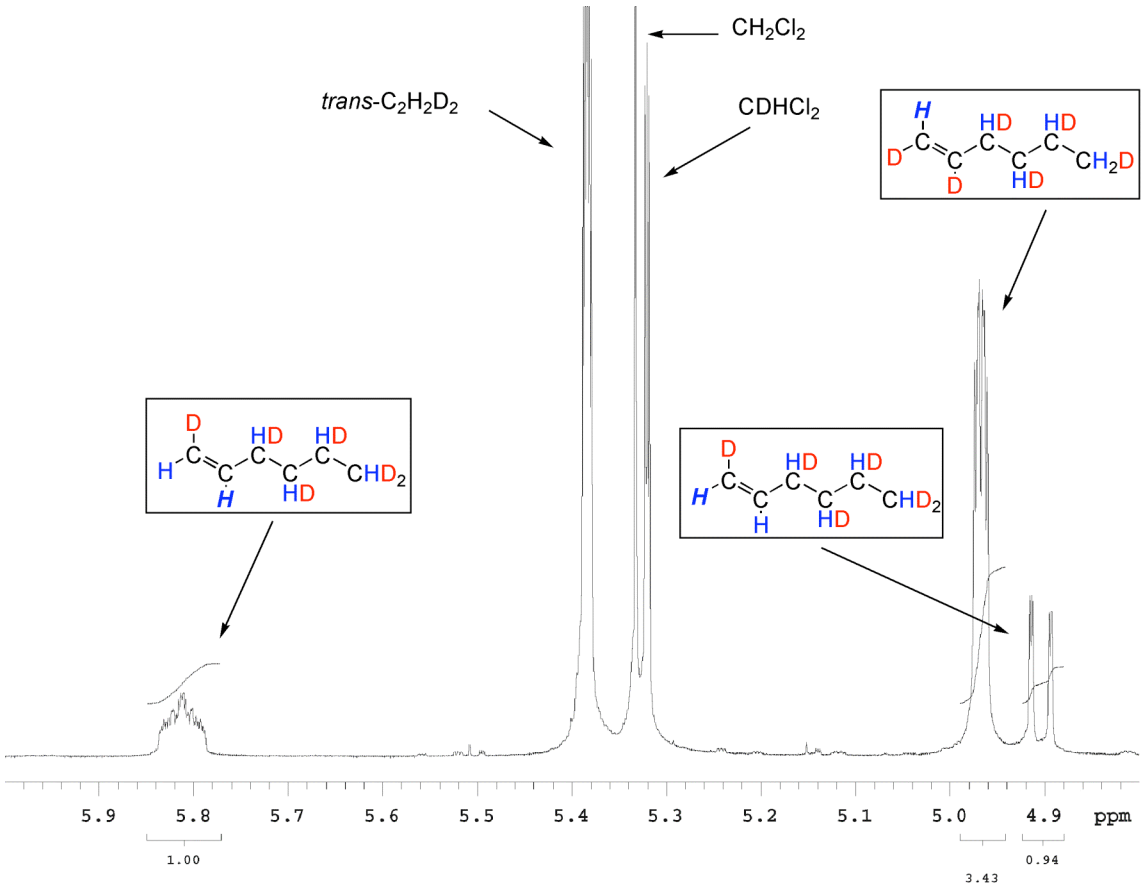

Figure 6. Olefinic region of the ^{1}H NMR spectrum of the volatile materials resulting from the trimerization of *trans*-dideuteroethylene.

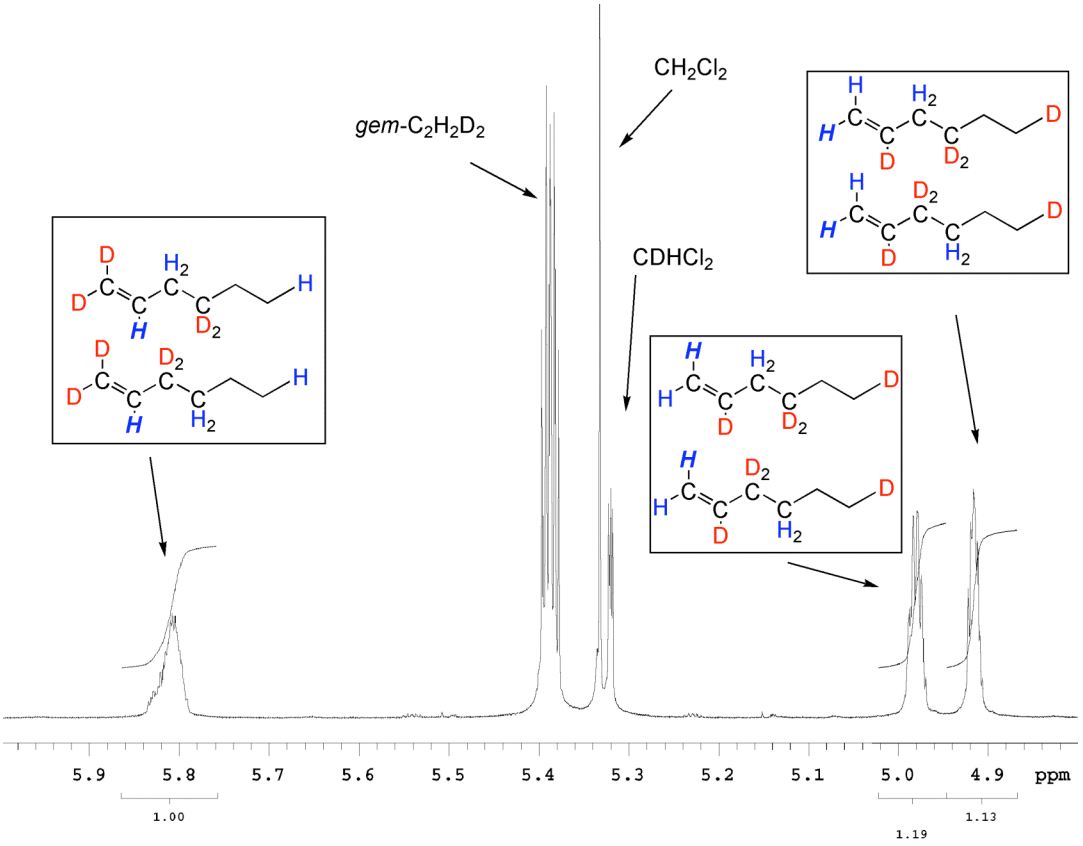

Figure 7. Olefinic region of the ^{1}H NMR spectrum of the volatile materials resulting from the trimerization of *gem*-dideuteroethylene.

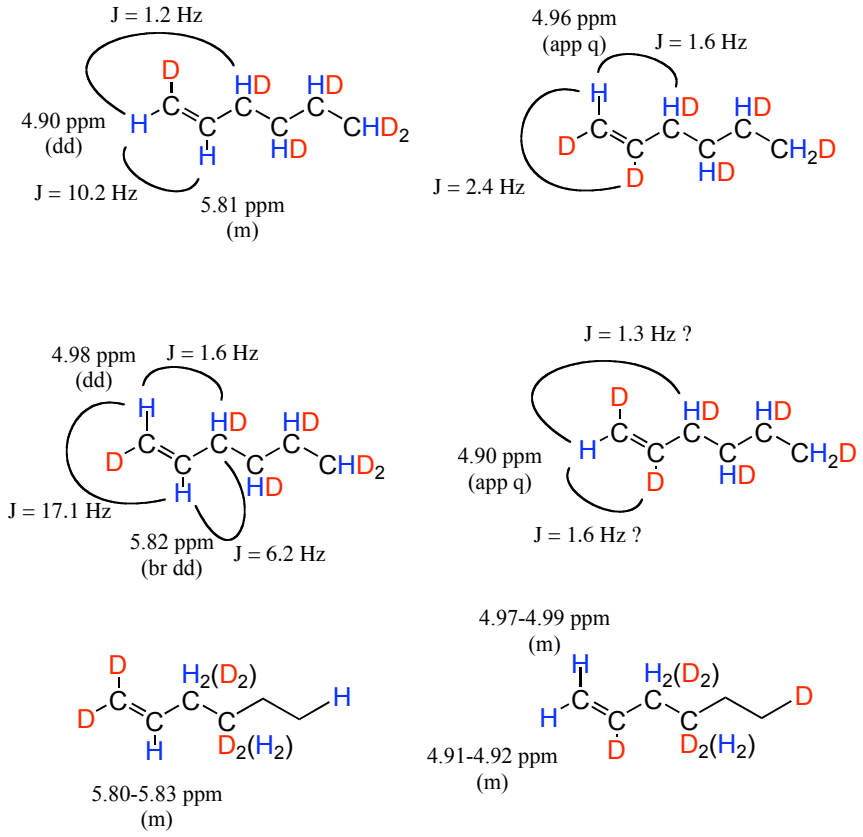

Figure 8. ^{1}H NMR data (CD_2Cl_2, 500 MHz) for the olefinic protons of various isotopomers of 1-hexene-d_6.

Reaction of 1 with higher olefins upon halide abstraction. These experiments were performed with propylene, 1-butene, *cis*- and *trans*-2-butene, and styrene. The following procedure is typical: Dichloromethane (2 mL) was vacuum transferred to a Schlenk flask charged with **1** (37 mg, 46.0 μmol, 1 equiv) and $NaB[C_6H_3(CF_3)_2]_4$ (49 mg, 55.3 μmol, 1.2 equiv). The mixture was warmed up to room temperature using a water bath followed by magnetic stirring for 10 min. The mixture turned brown upon starting materials dissolving. Propylene (128.2 mL at 160 torr, 1.1 mmol, 24.6 equiv) was condensed in. (In the case of styrene,

the olefin was added via syringe, in the glove box). The reaction mixture was allowed to mix for 24 h at room temperature during which the mixture turned green. Upon opening to air, the mixture was quenched with 1 ml aqueous CO_3^{2-} /HCO_3^- solution. The mixture was transferred to a scintillation vial and centrifuged. The organic layer was separated in filtered through silica gel then volatile materials were removed under vacuum. The residue was analyzed by NMR spectroscopy in $CDCl_3$ and GC-MS. With respect to diphosphine at the end of the reaction: ^{1}H NMR (300 MHz, $CDCl_3$) δ: 2.65, 2.68 (two br singlets, 3H, NC*H*), 3.66, 3.73 (two br singlets, 12H, OCH_3) ^{31}P NMR (121 MHz, $CDCl_3$) δ: 29.6, 54.9 (major, doublets, J_{PP}=122 Hz), 19.2, 37.9 (minor, doublets, J_{PP}=9 Hz). The same major peaks in ^{31}P NMR spectrum are observed when a solution (CH_2Cl_2) of PNP^{O4} and $NaB[C_6H_3(CF_3)_2]_4$ (1.1 equiv) is stirred for 36 h, then quenched with water. In the reactions with the olefins, GC-MS analysis shows the formation of one major biphenyl-olefin species along with biphenyl. The nature of the resulting biphenyl olefin was determined from the aliphatic and olefin peaks in the ^{1}H NMR spectrum. 2-Vinyl-biphenyl, 2-(1-phenyl-vinyl)-biphenyl, and 2-i-propenyl-biphenyl were identified using literature reports. The remaining of the biphenyl derivatives are presented below.

2-(1-i-Propyl-vinyl)-biphenyl. Obtained from 3-methyl-1-butene. ^{1}H NMR (500 MHz, $CDCl_3$) δ: 0.82 (d, $^3J_{HH}$=6.8 Hz, 6H, CH_3), 1.95 (app h, $^3J_{HH}$=6.8 Hz, 1H, C*H*(CH_3)$_2$), 5.10 (dd, $^3J_{HH}$=0.4 Hz, $^2J_{HH}$=1.5 Hz, 1H, =C*H*H), 5.14 (app t, $^2J_{HH}$=$^3J_{HH}$=1.5 Hz, 1H, =CH*H*).

2-(1-Ethyl-vinyl)-biphenyl. Obtained from 1-butene. ^{1}H NMR (500 MHz, $CDCl_3$)) δ: 0.82 (d, $^3J_{HH}$=7.3 Hz, 3H, C*H*$_3$), 1.91 (q, $^3J_{HH}$=7.3 Hz, 2H, C*H*$_2$CH$_3$), 5.08 (m, 1H, =C*H*H), 5.10 (app q, J_{HH}=1.4 Hz, 1H, =CH*H*).

2-(E-1-methyl-propenyl)-biphenyl. Obtained in the reaction with *trans*-2-butene. ^{1}H NMR (500 MHz, $CDCl_3$)) δ: 1.53 (app q, 3H, =C(Ar)C*H*$_3$), 1.67 (dq, $^5J_{HH}$=1.1, $^3J_{HH}$=6.8 Hz, 1H, =CH(C*H*$_3$)), 5.55 (qq, $^4J_{HH}$=1.5 Hz, $^3J_{HH}$=6.8 Hz, 1H, =C*H*CH$_3$). NOE experiment: magnetization of the 1.53 ppm signal does not transfer to the 5.55 ppm signal.

2-(Z-1-methyl-propenyl)-biphenyl. Obtained in the reaction with *cis*-2-butene. ^{1}H NMR (500 MHz, $CDCl_3$)) δ: 1.43 (app d, $^5J_{HH}$=1.2, $^3J_{HH}$=6.7 Hz, 3H, =CHC*H*$_3$), 1.73 (app q, $^5J_{HH}\approx{}^4J_{HH}$=1.2 Hz, 1H, C(Ar)C*H*$_3$), 5.44 (app q, $^4J_{HH}$=1.2 Hz, $^3J_{HH}$=6.6 Hz, 1H, =C*H*(CH$_3$)). NOE experiment: magnetization of the 1.73 ppm signal transfers at 5.44 ppm signal.

2-(1-i-Butyl-vinyl)-biphenyl. Obtained in the competition between 4-methyl-1-pentene and propene. ^{1}H NMR (500 MHz, $CDCl_3$) δ: 0.67 (d, $^3J_{HH}$=6.8 Hz, 6H, C*H*$_3$), 1.32 (m, C*H*(CH$_3$)$_2$), 1.68 (overlap with propylene peak, 2H, =C(Ar)C*H*$_2$), 5.10 (m, overlap with propylene peak 1H, =C*H*H), 5.14 (app d, J_{HH}=2.2 Hz, 1H, =CH*H*).

Reaction of 1 with mixtures of olefins upon halide abstraction. The following procedure is typical: d_2-Dichloromethane (~0.6 mL) was vacuum transferred to a J-Young tube charged with **1** (15.4 mg, 19.2 μmol, 1 equiv) and NaB[$C_6H_3(CF_3)_2$]$_4$ (25.5 mg, 28.8 μmol, 1.5 equiv). The mixture was warmed up to room temperature using a water bath followed by mechanical rotation of the tube for 10 min. The mixture turned brown upon starting materials dissolving. Propylene (55.39 mL at 80 torr, 0.24 mmol, 13 equiv) and 1-butene (55.39 mL at 80

torr, 0.24 mmol, 13 equiv) were condensed in. In the case of styrene, the olefin was added first via syringe, in the glove box, to a frozen dichlomethane mixture prepared as above. The mixture was kept frozen, connected to a high-vacuum line and the second olefin was condensed in. Upon adding in the second olefin, the NMR tube was sealed and warmed up to room temperature under water flow. The ^{1}H NMR spectrum of the crude mixture was recorded after 1-2 h of mechanical spinning to give the ratio of unreacted olefin starting materials dissolved in solution. The reaction mixture was allowed to spin for 24 h at room temperature, then the mixture was quenched with 1 mL aqueous CO_3^{2-}/HCO_3^- solution. The mixture was transferred to a scintillation vial and centrifuged. The organic layer was separated in filtered through silica gel then volatile materials were removed under vacuum. The residue was analyzed by ^{1}H NMR spectroscopy in $CDCl_3$ to give the ratio of biphenyl-olefin products and their identity. From the ratio of initial excess olefins in solution and the ratio of products, the relative insertion rate was calculated. Competition experiments between propylene and 1-butene, 4-methyl-1-pentene, styrene, 3-methyl-1-butene and *cis*-2-butene were performed. The order of addition was varied for 1-butene (ratio=1.1 in both cases) and 3-methyl-1-butene (ratio=10 and 13) and was found to have just a small influence on the results of the experiment. *Trans*-2-butene was found to be too slow to compete with propylene and the competition experiment was performed with *cis*-2-butene. The results are presented in Table 1. To check the relative rates obtained from propylene competition experiments, different mixtures of olefins were utilized – *cis*-2-butene and 3-methyl-1-butene (ratio=1/3.3); styrene and 3-methyl-1-butene (ratio=1/1.2).

Ethylene oligomerization with $Ni(Ph_2PCH_2COO)(PPh_3)(Ph)$. A benzene (2 mL) solution of the Ni complex (1 mg) was placed in a thick wall Schlenk tube equipped with a screw-in Teflon adaptor. The solution was degassed and then ethylene was condensed in (128.8 mL, 630 torr). The flask was immersed in a water bath an agitated until the solution was thawed then the reaction flask was immersed in an oil bath preheated at 73 °C. The reaction mixture was stirred vigorously for 5 min, then was frozen and quenched with water. The organic layer was analyzed by GC-MS. Fractions C_4 to C_{24} are observable, with the corresponding isotopologs.

Cotrimerization of ethylene and propylene using 1 as catalyst precursor. Dichloromethane (2 mL) was vacuum transferred to a 7 mL Schlenk tube charged with **1** (16.4 mg, 20.4 μmol, 1 equiv) and $NaB[C_6H_3(CF_3)_2]_4$ (22 mg, 24.8 μmol, 1.2 equiv). The mixture was warmed up to room temperature using a water bath followed by stirring for 10 min. The mixture turned brown upon starting materials dissolving. Propylene (55.39 mL at 430 torr, 1.29 mmol, 63 equiv) and ethylene (55.39 mL at 60 torr, 0.18 mmol, 8.8 equiv) were condensed in. The flask was sealed and warmed up to room temperature under water flow. The reaction mixture was stirred at room temperature for 24 h, then was quenched and analyzed by GC-MS. The major products formed are 1-hexene, 3-methyl-1-hexene, 4-methyl-1-hexene, and 5-methyl-1-hexene. These were compared against the GC-MS data of original samples, available commercially.

Cotrimerization of ethylene and propylene using $CrCl_3(PNP^{O4})$ as catalyst precursor. Compound $CrCl_3(PNP^{O4})$ (10.1 mg, 14.9 μmol, 1 equiv) was suspended in toluene (30 mL), in a 170 mL Schlenk tube fitted with a screw-in Teflon stopper.

The flask was connected to a high-vacuum line, placed under Ar and MAO (10% in toluene, d = 0.875g/mL, 3.0 mL, 300 equiv) was added via syringe. Then the reaction mixture was cooled to -78 °C and degassed. Propylene (3 times 128.2 mL at 800 torr, 16.6 mmol, $1.1 \bullet 10^3$ equiv) and ethylene (128.2 mL at 100 torr, 0.69 mmol, 46 equiv) were condensed in. The flask was sealed and warmed up to room temperature under water flow. The reaction mixture was stirred at room temperature for 36 h, then was quenched and analyzed by GC-MS. The major products formed are 1-hexene, 3-methyl-1-hexene, 4-methyl-1-hexene, and 5-methyl-1-hexene. These were compared against GC-MS data of original C7 samples, available commercially.

References

(1) Lappin, G. R.; Nemec, L. H.; Sauer, J. D.; Wagner, J. D. In *Kirk-Othmer Encyclopedia of Chemical Technology*; Wiley & Sons, Inc: 2005.

(2) Kissin, Y. V. In *Kirk-Othmer Encyclopedia of Chemical Technology*; Wiley & Sons, Inc: 2005.

(3) Skupinska, J. *Chem. Rev.* **1991**, *91*, 613-48.

(4) Dixon, J. T.; Green, M. J.; Hess, F. M.; Morgan, D. H. *J. Organomet. Chem.* **2004**, *689*, 3641-3668.

(5) Wang, C.; Huang, J. L. *Chin. J. Chem.* **2006**, *24*, 1397-1401.

(6) Walsh, R.; Morgan, D. H.; Bollmann, A.; Dixon, J. T. *Appl. Catal. A-Gen.* **2006**, *306*, 184-191.

(7) Schofer, S. J.; Day, M. W.; Henling, L. M.; Labinger, J. A.; Bercaw, J. E. *Organometallics* **2006**, *25*, 2743-2749.

(8) Overett, M. J.; Blann, K.; Bollmann, A.; Dixon, J. T.; Hess, F.; Killian, E.; Maumela, H.; Morgan, D. H.; Neveling, A.; Otto, S. *Chem. Commun.* **2005**, 622-624.

(9) Overett, M. J.; Blann, K.; Bollmann, A.; Dixon, J. T.; Haasbroek, D.; Killian, E.; Maumela, H.; McGuinness, D. S.; Morgan, D. H. *J. Am. Chem. Soc.* **2005**, *127*, 10723-10730.

(10) McGuinness, D. S.; Wasserscheid, P.; Morgan, D. H.; Dixon, J. T. *Organometallics* **2005**, *24*, 552-556.

(11) McGuinness, D. S.; Wasserscheid, P.; Keim, W.; Morgan, D.; Dixon, J. T.; Bollmann, A.; Maumela, H.; Hess, F.; Englert, U. *J. Am. Chem. Soc.* **2003**, *125*, 5272-5273.

(12) McGuinness, D. S.; Wasserscheid, P.; Keim, W.; Hu, C. H.; Englert, U.; Dixon, J. T.; Grove, C. *Chem. Commun.* **2003**, 334-335.

(13) McGuinness, D. S.; Brown, D. B.; Tooze, R. P.; Hess, F. M.; Dixon, J. T.; Slawin, A. M. Z. *Organometallics* **2006**, *25*, 3605-3610.

(14) Mahomed, H.; Bollmann, A.; Dixon, J. T.; Gokul, V.; Griesel, L.; Grove, C.; Hess, F.; Maumela, H.; Pepler, L. *Appl. Catal. A-Gen.* **2003**, *255*, 355-359.

(15) Hessen, B. *J. Mol. Catal. A-Chem.* **2004**, *213*, 129-135.

(16) Deckers, P. J. W.; Hessen, B.; Teuben, J. H. *Angew. Chem.-Int. Edit. Engl.* **2001**, *40*, 2516-2519.

(17) Deckers, P. J. W.; Hessen, B.; Teuben, J. H. *Organometallics* **2002**, *21*, 5122-5135.

(18) Crewdson, P.; Gambarotta, S.; Djoman, M. C.; Korobkov, I.; Duchateau, R. *Organometallics* **2005**, *24*, 5214-5216.

(19) Carter, A.; Cohen, S. A.; Cooley, N. A.; Murphy, A.; Scutt, J.; Wass, D. F. *Chem. Commun.* **2002**, 858-859.

(20) Bollmann, A.; Blann, K.; Dixon, J. T.; Hess, F. M.; Killian, E.; Maumela, H.; McGuinness, D. S.; Morgan, D. H.; Neveling, A.; Otto, S.; Overett, M.; Slawin, A. M. Z.; Wasserscheid, P.; Kuhlmann, S. *J. Am. Chem. Soc.* **2004**, *126*, 14712-14713.

(21) Andes, C.; Harkins, S. B.; Murtuza, S.; Oyler, K.; Sen, A. *J. Am. Chem. Soc.* **2001**, *123*, 7423-4.

(22) Deckers, P. J. W.; Hessen, B.; Teuben, J. H. *Angew. Chem.-Int. Edit. Engl.* **2001**, *40*, 2516-+.

(23) Reagen, W. K.; Conroy, B. K.; Phillips Petroleum Co.: CA 2020509, 1991.

(24) Wu, F.-j.; Amoco Corp.: US 5,744,677, 1998.

(25) Bluhm, M. E.; Walter, O.; Doring, M. *J. Organomet. Chem.* **2005**, *690*, 713-721.

(26) Kohn, R. D.; Haufe, M.; Kociok-Kohn, G.; Grimm, S.; Wasserscheid, P.; Keim, W. *Angew. Chem.-Int. Edit. Engl.* **2000**, *39*, 4337-4339.

(27) Wasserscheid, P.; Grimm, S.; Kohn, R. D.; Haufe, M. *Adv. Synth. Catal.* **2001**, *343*, 814-818.

(28) Kohn, R. D.; Haufe, M.; Mihan, S.; Lilge, D. *Chem. Commun.* **2000**, 1927-1928.

(29) Agapie, T.; Day, M. W.; Henling, L. M.; Labinger, J. A.; Bercaw, J. E. *Organometallics* **2006**, *25*, 2733-2742.

(30) Elowe, P. R.; McCann, C.; Pringle, P. G.; Spitzmesser, S. K.; Bercaw, J. E. *Organometallics* **2006**, *25*, 5255-5260.

(31) Agapie, T.; Schofer, S. J.; Labinger, J. A.; Bercaw, J. E. *J. Am. Chem. Soc.* **2004**, *126*, 1304-1305.

(32) Emrich, R.; Heinemann, O.; Jolly, P. W.; Krueger, C.; Verhovnik, G. P. J. *Organometallics* **1997**, *16*, 1511-1513.

(33) Blok, A. N. J.; Budzelaar, P. H. M.; Gal, A. W. *Organometallics* **2003**, *22*, 2564-2570.

(34) de Bruin, T. J. M.; Magna, L.; Raybaud, P.; Toulhoat, H. *Organometallics* **2003**, *22*, 3404-3413.

(35) Tobisch, S.; Ziegler, T. *Organometallics* **2003**, *22*, 5392-5405.

(36) van Rensburg, W. J.; Grove, C.; Steynberg, J. P.; Stark, K. B.; Huyser, J. J.; Steynberg, P. J. *Organometallics* **2004**, *23*, 1207-1222.

(37) Yu, Z. X.; Houk, K. N. *Angew. Chem.-Int. Edit. Engl.* **2003**, *42*, 808-811.

(38) Tobisch, S.; Ziegler, T. *Organometallics* **2005**, *24*, 256-265.

(39) Tobisch, S.; Ziegler, T. *Organometallics* **2004**, *23*, 4077-4088.

(40) Tobisch, S.; Ziegler, T. *J. Am. Chem. Soc.* **2004**, *126*, 9059-9071.

(41) Tomov, A. K.; Chirinos, J. J.; Long, R. J.; Gibson, V. C.; Elsegood, M. R. J. *J. Am. Chem. Soc.* **2006**, *128*, 7704-7705.

(42) Tomov, A. K.; Chirinos, J. J.; Jones, D. J.; Long, R. J.; Gibson, V. C. *J. Am. Chem. Soc.* **2005**, *127*, 10166-10167.

(43) Bowen, L. E.; Wass, D. F. *Organometallics* **2006**, *25*, 555-557.

(44) Temple, C.; Jabri, A.; Crewdson, P.; Gambarotta, S.; Korobkov, I.; Duchateau, R. *Angew. Chem.-Int. Edit. Engl.* **2006**, *45*, 7050-7053.

(45) Jabri, A.; Temple, C.; Crewdson, P.; Gambarotta, S.; Korobkov, I.; Duchateau, R. *J. Am. Chem. Soc.* **2006**, *128*, 9238-9247.

(46) Jabri, A.; Crewdson, P.; Gambarotta, S.; Korobkov, I.; Duchateau, R. *Organometallics* **2006**, *25*, 715-718.

(47) Blann, K.; Bollmann, A.; Dixon, J. T.; Hess, F. M.; Killian, E.; Maumela, H.; Morgan, D. H.; Neveling, A.; Otto, S.; Overett, M. J. *Chem. Commun.* **2005**, 620-621.

(48) McAlister, D. R.; Bercaw, J. E.; Bergman, R. G. *J. Am. Chem. Soc.* **1977**, *99*, 1666-1668.

(49) Schore, N. E. *Chem. Rev.* **1988**, *88*, 1081-1119.

(50) Johnson, E. S.; Balaich, G. J.; Rothwell, I. P. *J. Am. Chem. Soc.* **1997**, *119*, 7685-7693.

(51) Vollhardt, K. P. C. *Angew. Chem.-Int. Edit. Engl.* **1984**, *23*, 539-556.

(52) Zeiss, H. H.; Herwig, W. *J. Am. Chem. Soc.* **1958**, *80*, 2913-2913.

(53) Whitesides, G. M.; Ehmann, W. J. *J. Am. Chem. Soc.* **1970**, *92*, 5625.

(54) Whitesides, G. M.; Ehmann, W. J. *J. Am. Chem. Soc.* **1968**, *90*, 804.

(55) Kanno, K.; Liu, Y. H.; Iesato, A.; Nakajima, K.; Takahashi, T. *Org. Lett.* **2005**, *7*, 5453-5456.

(56) Takahashi, T.; Liu, Y. H.; Iesato, A.; Chaki, S.; Nakajima, K.; Kanno, K. *J. Am. Chem. Soc.* **2005**, *127*, 11928-11929.

(57) Peuckert, M.; Keim, W. *Organometallics* **1983**, *2*, 594-597.

(58) Chirik, P. J.; Bercaw, J. E. *Organometallics* **2005**, *24*, 5407-5423.

(59) Pangborn, A. B.; Giardello, M. A.; Grubbs, R. H.; Rosen, R. K.; Timmers, F. J. *Organometallics* **1996**, *15*, 1518-20.

Chapter 4

A Tantalum Example of Intramolecular C-H/M-CH_3 σ-Bond Metathesis Faster than O-H/M-CH_3 Protonolysis: Cyclometallated Tantalum Diphenolate Pincer Complexes – Study of Mechanism and Insertion Chemistry

Abstract

A diphenol connected at the *ortho* positions via semi-rigid, ring-ring (sp^2-sp^2) linkages to a benzene ring was efficiently prepared by palladium coupling chemistry from the protected bromo-phenol and 1,3-dibromobenzene. Tantalum complexes supported by these ligands were synthesized via alkane elimination or salt metathesis routes. Reaction of $TaCl_2(CH_3)_3$ with deprotonated diphenol affords a cyclometallated dimethyl tantalum phenyl diphenolate complex $Ta(CH_3)_2[(OC_6H_2\text{-}tBu_2)_2C_6H_3]$ (**5**). Free diphenol reacts with $TaCl_2(CH_3)_3$ to afford a tantalum methyl dichloride diphenolate complex $TaCl_2CH_3[(OC_6H_2\text{-}tBu_2)_2C_6H_4]$ (**6**). Deuterium labeling of the phenol hydrogens and of the linking phenyl ring allowed for the uncovering of the metallation mechanism which involves protonolysis of a methyl group followed by cyclometallation of the linking ring and then by protonation of the cyclometallated group by the pendant phenol. Starting with $TaCl_2CH_3[(OC_6H_2\text{-}tBu_2)_2C_6H_4]$ (**6**), the kinetics of the cyclometallation reaction to give the pincer complex $TaCl_2[(OC_6H_2\text{-}tBu_2)_2C_6H_3]$ (**7**) were studied at different temperatures. This process was found to obey first order kinetics in **6** with the activation parameters of $\Delta H^{\ddagger} = 27.1 \pm 0.9$ kcal/mol; $\Delta S^{\ddagger} = -2 \pm 2$ cal/mol·K, as extracted from an Eyring plot. A relatively constant (within the error of the measurements) isotope effect of 1.6 ± 0.2 was measured in the temperature interval from 91 to 125 °C. Species $Ta(CH_3)_2[(OC_6H_2\text{-}tBu_2)_2C_6H_3]$ (**5**) was found to react with tBuNC to insert into the Ta-CH_3 bonds and generate an imino-acyl species (**11**). Reaction of **5** with Ph_2CO, norcamphor, or PhCN leads to insertion into the Ta-Ph bond. Complexes **6**, **7**-

OEt_2, and **11** have been structurally characterized in the solid state and all show a mer binding mode of the diphenolate ligands. The ligand geometry, however, varies from *pseudo*-C_s-symmetric in **6** to *pseudo*-C_2-symmetric in the cyclometallated species **7-OEt_2** and **11**.

Introduction

Cyclometallated pincer-type complexes supported by LCL ligands (L=phosphine, amine, thioether, or ether) is an intense area of study.[1-6] Pincer based complexes have been used for catalysis, for fundamental studies of small molecule activation and of diverse organometallic structures and transformations, as well as for the design and development of novel materials and sensors. The versatility of these systems for a variety of applications relies on their specific balance of reactivity and stability conferred by this type of chelating ligand. Most of the reported systems are based on late transition metal complexes, but early metal and lanthanide pincer complexes have been reported as well.[5,7-19] In particular, 2,6-di(*o*-anisol)phenyl systems have been reported to support yttrium, samarium, and ytterbium complexes.[7-9] Diaminophenyl systems have been studied for supporting titanium, tantalum, lutetium, and yttrium chemistry.[5,10-19] The tantalum systems stand out for their organometallic chemistry derived from alkylidene and olefin complexes.[5,10-16] In the context of developing and studying new reactions supported by robust ligand frameworks, it is interesting to note that, to the authors' knowledge, no multiply charged

cyclometallated pincer ligands have been reported. In all the reported cases, the pendant ligands are based on neutral donors such as phosphines, amines, thioethers, ethers, and carbenes.[1-6] For early metal chemistry, in which higher oxidations states are accessible, the study of complexes supported by robust multianionic ligands that would complement the known monoanionic cyclometallated pincer ligands is an underdeveloped area.

We have investigated recently ligand architectures for non-metallocene polymerization catalysts based on diphenolates connected at the *ortho* positions via semi-rigid, ring-ring (sp^2-sp^2) linkages to a flat ring (pyridine, furan, thiophene) that presents a neutral ligand (Chapter 5). During the study of these systems we became interested in the related, trianionic, phenyl-diphenolate framework (Figure 1). Tantalum was selected as a starting metal for investigating this ligand architecture due to its rich chemistry supported by phenolates and, as mentioned above, by multidentate phenyl pincer ligands.[20-22] The use of terphenyl frameworks for pincer ligands has recently emerged as a route to chiral, C_2-symmetric pincer systems; systems of C_s symmetry have been reported as well.[7-9,23,24] This chapter presents the synthesis and structural characterization of pincer phenyl-diphenolate complexes of tantalum and their reactivity, along with mechanistic studies of the cyclometallation reaction.

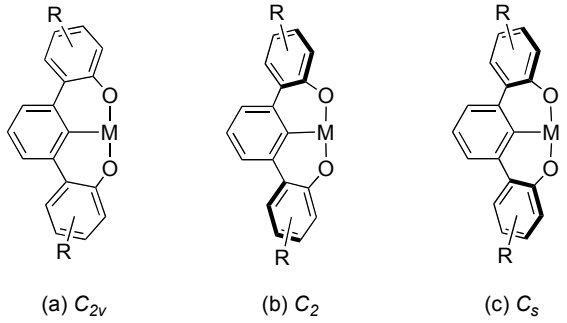

Figure 1. Phenyl-diphenolate framework showing possible binding geometries.

Results and Discussion

Preparation of diphenol

The present diphenol has been prepared using well precedented procedures. Starting from commercially available and cheap 2,4-di-t-butyl phenol, the desired linked diphenols can be accessed within four steps. Bromination and protection of the phenol functionality with methoxymethyl (MOM) or methyl generates compound **1a** and **1b**. Lithium-halogen exchange followed by salt metathesis with $ZnCl_2$ provides, *in situ*, aryl zinc reagents suitable for the Negishi cross-couping.[25] 1,3-Dibromobenzene has been used as a coupling partner with $Pd(PPh_3)_4$ as catalyst. Once the coupling reaction is complete, aqueous workup provides the crude organics upon extraction in CH_2Cl_2. Protected diphenol product (**2a** or **2b**) is obtained by precipitation with methanol from a concentrated CH_2Cl_2 solution, followed by one or two triturations with methanol. Collection by filtration and washing with cold methanol provides protected diphenols (**2a** or **2b**) as white powders. Standard

deprotecting procedures – EtSNa in DMF at 120 °C and acidic methanol at 80 °C – have been employed for removing methyl and MOM groups, respectively.[26] Analytically pure diphenol is obtained as a white solid by precipitation from methanol and collection by filtration.

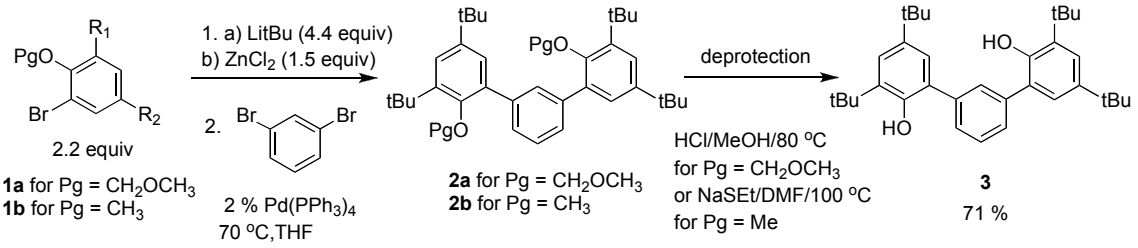

Scheme 1. Synthesis of benzene-1,3-diphenol.

Preparation of tantalum complexes supported by a phenyl linked diphenoxide $Ta(CH_3)_2[(OC_6H_2\text{-}tBu_2)_2C_6H_3]$ (5) and $Ta(CH_2Ph)_2[(OC_6H_2\text{-}tBu_2)_2C_6H_3]$ (6)

Two strategies have been used for the metallation of diphenol **3** – salt metathesis and alkane elimination. For the salt metathesis route, diphenol **3** was deprotonated *in situ* with KBn and then treated with a $TaCl_2(CH_3)_3$. Within hours, the reaction is complete with the generation of one major species according to ^{1}H NMR spectroscopy. Recrystallization from petroleum ether affords analytically clean material. The ^{1}H NMR shows a singlet corresponding to the Ta-CH_3 groups integrating to 6H, and only two peaks (a doublet and a triplet) for the linking phenyl group integrating to 3H. The ^{13}C NMR spectrum of the product presents two diagnostic peaks, at 60.6 and 198.5 ppm. A survey of some previously reported tantalum(V) methyls with at least two diphenolate ligands indicates

that the ^{13}C NMR chemical shift range for the methyl group is between 43 and 64 ppm.[27,28] The ^{13}C NMR chemical shift for Ta-*C*(*ipso*) is 190-210 ppm.[12,29-33] These data support the structural assigment of **5** as $Ta(CH_3)_2[(OC_6H_2\text{-}tBu_2)_2C_6H_3]$ (Scheme 2). Formation of **5** presumably occurs via intermediate generation of a simple salt metathesis product, complex **4**, bound through the oxygens (Scheme 2). This species then cyclometallates, with loss of methane. Utilization of $TaCl_2(CH_2Ph)_3$ instead of $TaCl_2(CH_3)_3$ as a metal precursor in this reaction leads to the formation of $Ta(CH_2Ph)_2[(OC_6H_2\text{-}tBu_2)_2C_6H_3]$ (**6**). Previous reports of cyclometallated pincer ligands complex of early metals rely on using starting materials in which the hydrogen connected to the metallated carbon had been already replaced with a transmetallating agent (Grignard reagents or lithium aryls). The CH (or CC) activation route for accessing cyclometallated pincer frameworks is, however, common for late transition metal systems.[34] The preparation described here relies on CH activation at the desired position upon coordination of the ligand to the metal center. These reactions are reminiscent of cyclometallations via σ-bond metathesis observed for tantalum systems with phenolate ligands *ortho*-substituted with t-butyl, i-propyl, or phenyl groups.[21,27,30,35-39] An interesting comparison is provided by the previously characterized $Ta(CH_3)_3(OC_6H_3\text{-}2,6\text{-}Ph_2)_2$ and $Ta(CH_2Ph)_3(OC_6H_3\text{-}2,6\text{-}Ph_2)_2$ which lose CH_4 only above 200 °C and toluene above 175 °C, respectively;[30] in contrast, the related proposed tantalum trialkyl species **4** is only transient toward the formation of the cyclometallated product **5** at room temperature. This suggests that the pincer nature of the ligand, with initial chelation of the two phenolates

facilitates the cyclometallation, possibly by locking the aryl group into the necessary orientation for σ-bond metathesis.

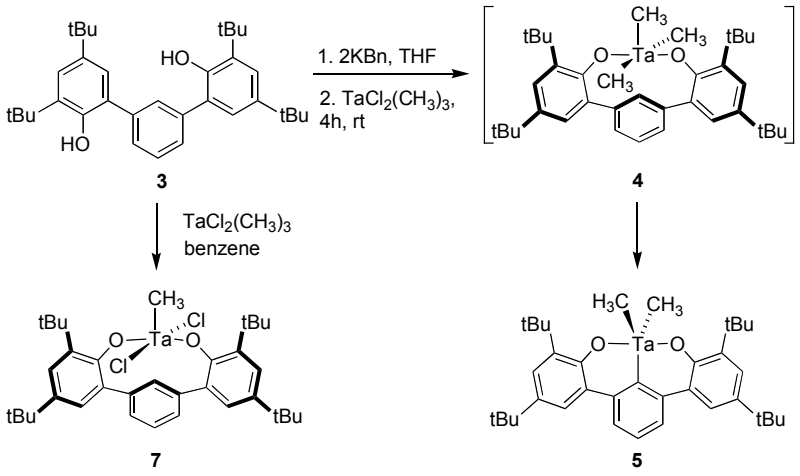

Scheme 2. Metallation of benzene-1,3-diphenol **3**.

Complex **6** was studied by single-crystal X-ray diffraction (Figure 2). Similar to the pyridine bridged systems (Chapter 5), this molecule displays *pseudo*-C_s symmetry. The angle between the Ta-C(phenyl) vector and the plane of the bridging benzene group is, however, about 10 ° larger than in the pyridine case. This correlates with the shorter Ta-C(phenyl) distance compared to the Ta-N distance. This is consistent with the fact that the anionic aryl donor is a better ligand than the pyridine donor and therefore can enforce better the appropriate orientation for good orbital overlap.

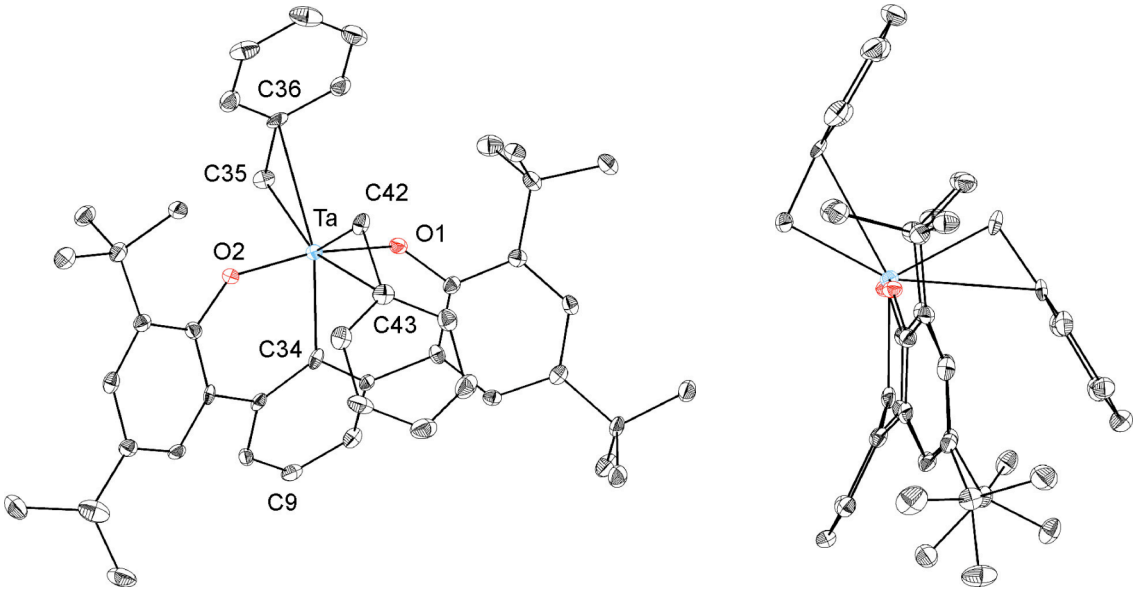

Figure 2. Structural drawing of **6**. Selected bond lengths (Å) and angles (°): Ta-O1 1.904(2); Ta-O2 1.903(2); Ta-C34 2.176(3); Ta-C35 2.190(4); Ta-C42 2.203(4); O1-Ta-O2 169.17(9); Ta-C35-C36 93.2(2); Ta-C42-C43 96.4(2); C17-O2-Ta 142.9(2); C1-O1-Ta 141.6(2); C34-Ta-C35 117.86(13); C34-Ta-C42 118.24(14); Ta-C34-C9 156.5.

Preparation of a tantalum complex supported by a benzene linked diphenoxide $TaCl_2(CH_3)[(OC_6H_2\text{-}tBu_2)_2C_6H_4]$ (7)

An alkane elimination route was explored for the metallation of **3** with $TaCl_2(CH_3)_3$ leading, at room temperature, to a species that still displays signals for a Ta*C*H_3 group and the C(*ipso*)-*H* in the ^{1}H and ^{13}C NMR spectra (species **7**, Scheme 2). A single crystal X-ray diffraction study supported the spectroscopic assignment of **7** (Figure 3). The tantalum center is six-coordinate, taking into account the weak interaction with the arene *ipso*-carbon (Ta-C bond length of 2.791(5) Å). The methyl group is located trans to the arene system, the position

with the smallest trans influence. The other bond lengths to tantalum are typical. The Ta-C18-C9 angle of 120° indicates a significant twist of the arene, probably to avoid a steric interaction between tantalum and the ring as well as to increase a bonding interaction between the metal center and the π-system. The O1-Ta-O2 angle of 152° indicates a significant deviation from an octahedral environment, possibly due to the connecting benzene ring which, by twisting, pulls the pendant phenolates down.

The isolation of compound **7** provides support for the proposed route for the formation of **5** (Scheme 2) by allowing the isolation of the diphenolate species without CH activation. In this case, the cyclometallation reaction is not as facile as for the putative $Ta(CH_3)_3[(OC_6H_2\text{-}tBu_2)_2C_6H_3]$ (**4**) and the intermediate is stable enough to be isolated. Access to **7** also provides an opportunity to perform kinetic studies of the cyclometallation reaction. To that end, the synthesis of isotopicaly labeled compounds was undertaken.

Preparation of deuterium labeled versions of 7

Labeling of the of the cyclometallation site in the ligand precursor was achieved starting from fully deuterated aniline (Scheme 3). Reaction with hexamethylenetetraamine bromine complex, starting from -78 °C, leads to the clean formation of the dibrominated product.[40] The amine functionality is replaced by hydrogen by formation of the diazonium salt and reduction with

H_3PO_2.[41] With 1,3-dibromobenzene-2,4,5-d_3 in hand, diphenol **3-*d*$_3$** was accessed using the procedure described above (Scheme 1).

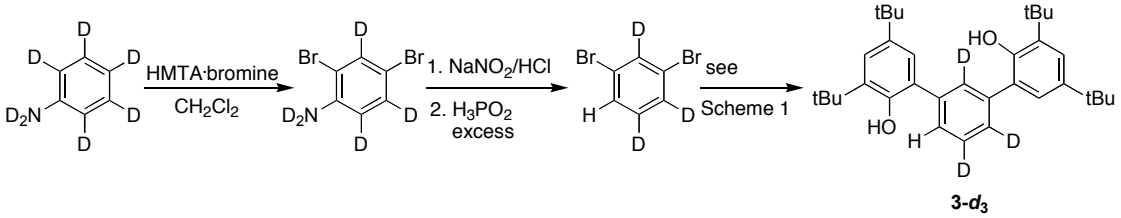

Scheme 3. Preparation of labeled diphenol **3-*d*$_3$**.

Surprisingly, the reaction of **3-*d*$_3$** with $TaCl_2(CH_3)_3$ did not provide the expected product isotopolog (eq 1). The ^{1}H NMR spectrum of the isolated product two major peaks for the connecting arene – two doublets with a four-bond coupling (Figure 4). The ^{1}H NMR chemical shifts correspond to the positions 2 and 4 of the unlabeled compound. Notably, when the experiment is performed in J-Young tube, formation of both CH_4 and CH_3D is observed. The formation of CH_3D indicates that somehow, one of the methyl groups leaves with a hydrogen from the connecting ring. Following a hypothesis that the proton at the *ipso*-carbon comes from the phenol groups, a derivative labeled at these positions was prepared (eq 2). Species **3-*d*$_2$** was afforded by repeated precipitations of diphenol **3** from dry THF solution with D_2O/DCl followed by removal of volatile materials under vacuum.

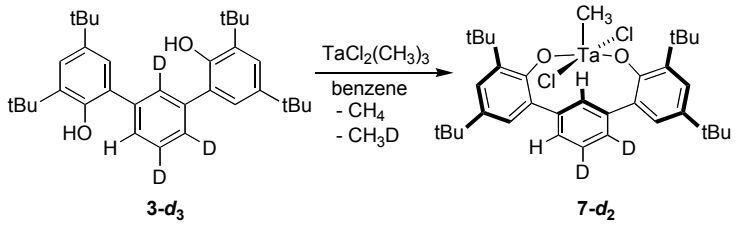

(1)

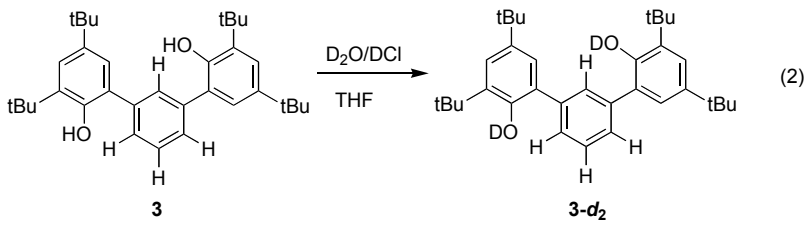

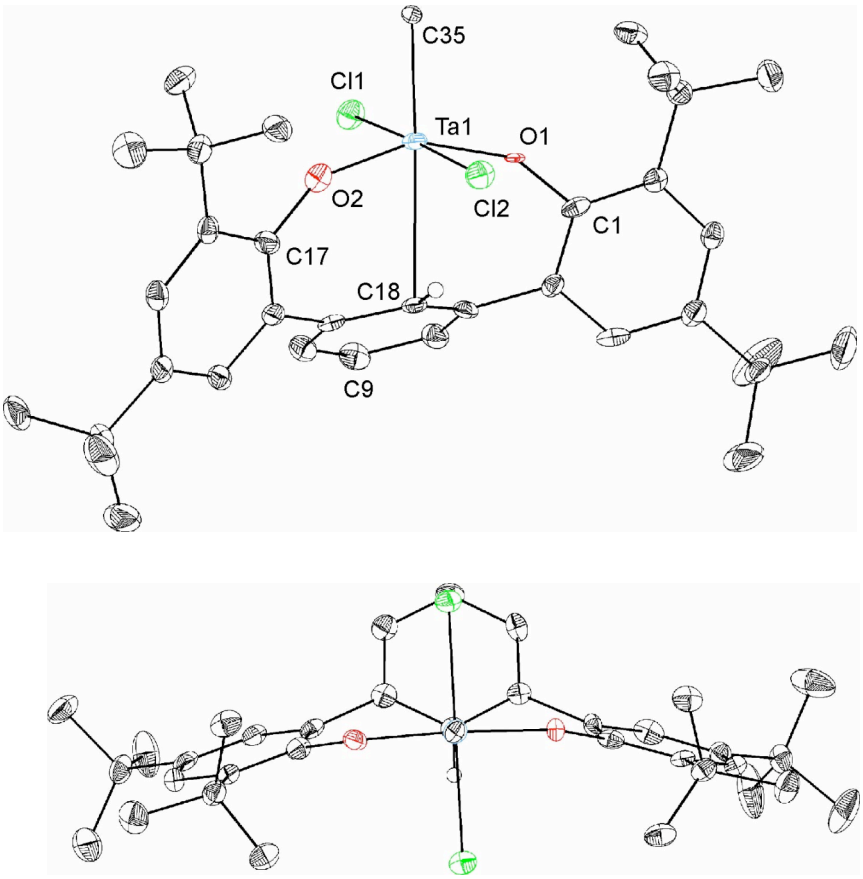

Figure 3. Structural drawing of **7**. Selected bond lengths (Å) and angles (°): Ta-O1 1.876(4); Ta-O2 1.859(4); Ta-C35 2.147(4); Ta-C18 2.7913(47); Ta-C18-C9 120°; O1-Ta-O2 152.45(15); Ta-O1-C1 151.7(3); Ta-O2-C17 149.1(4).

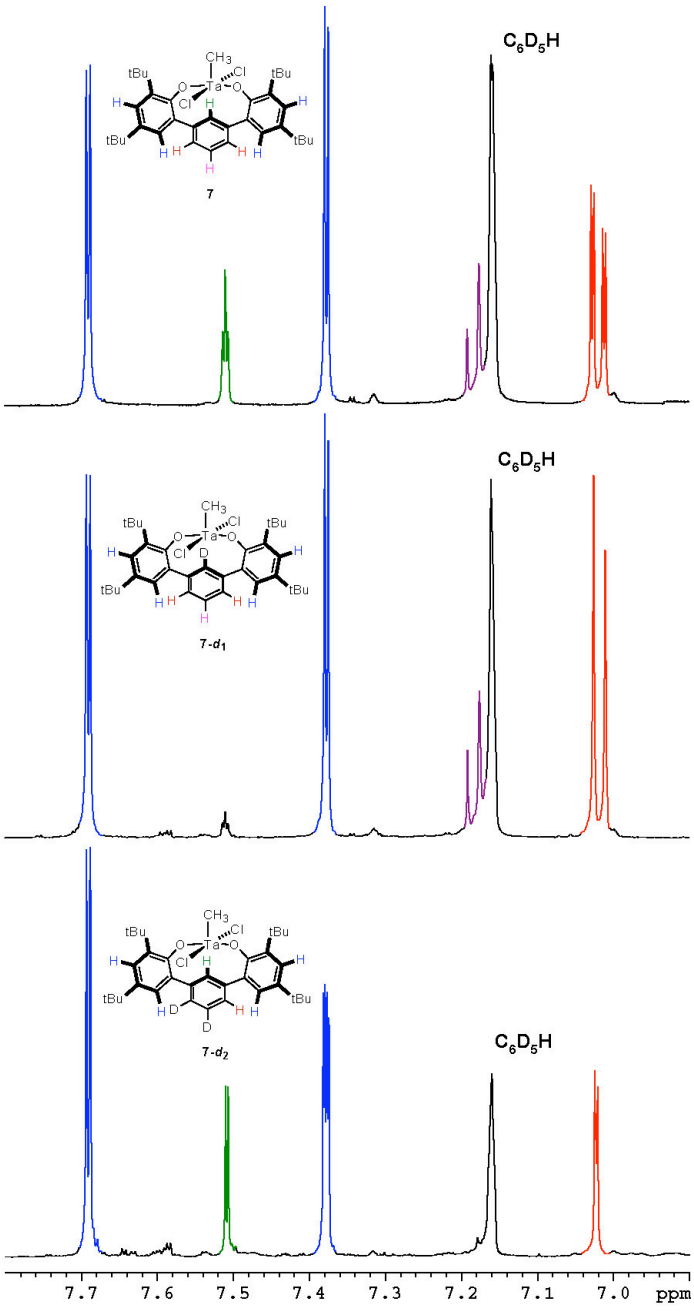

Figure 4. Aromatic reagion of the ^{1}H NMR spectra (C_6D_6) of different isotopologs of **7**.

The reaction of **3-*d*$_2$** with $TaCl_2(CH_3)_3$, performed in a J-Young tube, leads to the formation of both CH_4 and CH_3D, as indicated by ^1H NMR spectroscopy (eq 2). The peak corresponding the cyclometallation site is greatly diminished in the ^1H NMR spectrum (Figure 4). Furthermore the equivalent protons at positions 4 and 6 display only a doublet, without showing the expected four bond coupling with the proton at position 2. These data indicate that position 2 was deuterated. Given that in both labeling experiments formation of both CH_4 and CH_3D is observed indicates that part of the methyls leave with the proton (deuterium) from the phenol and part with the proton (deuterium) from the bridging arene ring.

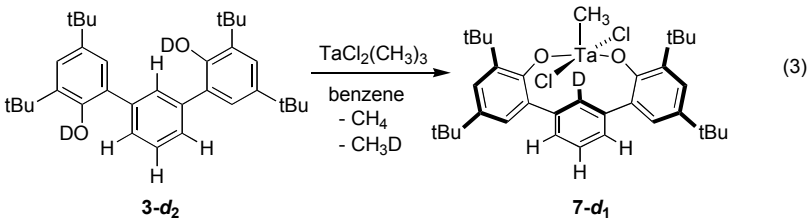

3-*d*$_2$ **7-*d*$_1$** (3)

The proposed mechanism that accounts for the observed labeling patterns involves first protonation of a methyl group to form CH_3H_e and a tantalum dimethyl dichloride phenolate complex (**A** and **B**, Scheme 4). In this intermediate, cyclometallation could occur at the two distinct *ortho* positions (H_a and H_b). Sterically, conformation **A** may be favored over **B**, due to steric interactions. This could actually favor cyclometallation at position H_b, which is not observed. However, cyclometallation probably does not occur at this stage, given that previously reported tantalum *ortho*-phenyl-phenolates require high temperatures for this reaction. In the present system, coordinatioin of the

pendant phenol could occur, without protonation, to give species **C**. In **C**, the CH_a bond is brought in close proximity to the metal in a conformation that may facilitate σ-bond metathesis to lose CH_3H_a and give cyclometallated species **D**. The coordinated phenol protonates the phenyl ring to generate the observed product **7**. The proposed mechanism takes advantage of the double chelation in **C** to facilitate CH bond activation. It is surprising, however, than the σ-bond metathesis with the aryl CH bond to give CH_3H_a is faster that protonation by the phenol to give CH_3H_f. This type of selectivity is unprecedented for early metals to the authors' knowledge.

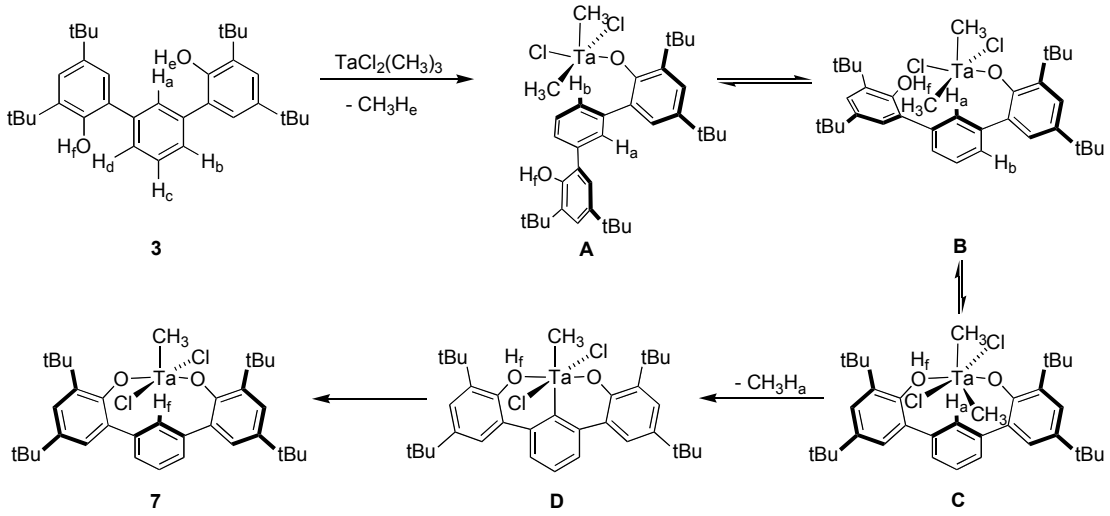

Scheme 4. Proposed mechanism for the formation of **7**, involving intermediate cyclometallation and protonation of the connecting benzene ring.

Conversion of $TaCl_2(CH_3)[(OC_6H_2\text{-}tBu_2)_2C_6H_4]$ (6) to $TaCl_2[(OC_6H_2\text{-}tBu_2)_2C_6H_3]$ (7) via methane elimination

The reactivity of **7** for σ-bond metathesis was investigated. Increased temperature does lead to the cyclometallated product **8** (Scheme 3) along with CH_4 according to an experiment performed in a J-Young tube, in a C_6D_6 solution, and monitored by ^1H NMR spectroscopy. Crystals of the cyclometallated product, suitable for an X-ray diffraction study, were obtained from a diethyl ether solution (Figure 5). An ether molecule coordinates to the metal center to satisfy six-coordination. In contrast with the structure of **7**, the TaC(*ipso*) vector almost lies in the cyclometallated aryl plane (Ta-C15-C18 angle is 164°) maximizing the interaction of the metal with carbon σ-orbital. The O1-Ta-O2 angle is 169°, significantly more linear than in **7** (152°). This could be due to the strong interaction with the cyclometallated phenyl ring which brings the entire terphenyl framework closer to the metal. Interestingly, the C_6D_6 solution of the crystallographically characterized species displays ^1H NMR chemical shifts for the ether molecule different from the ones of free diethyl ether suggesting that the ether remains coordinated even in solution state. This is not observed for complex **5** indicating a decrease in metal's eletrophilicity in that case, probably due to the presence of stronger σ-donors (methyls vs chlorides).

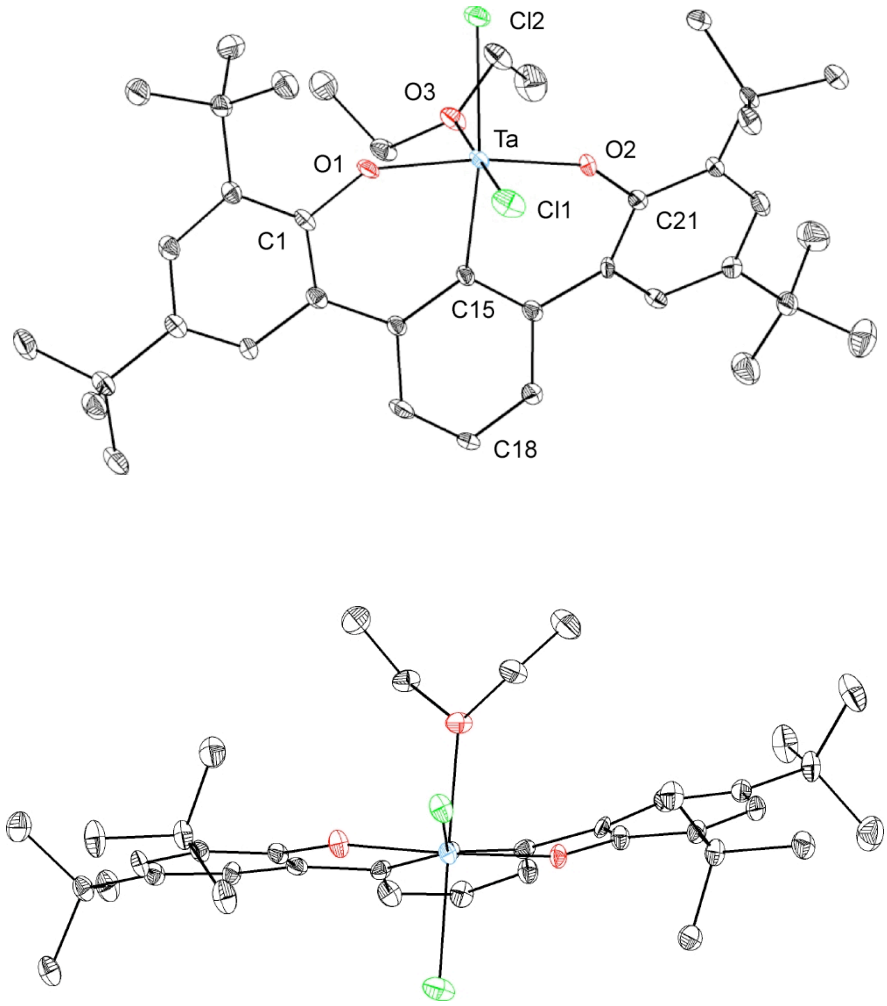

Figure 5. Structural drawing of **8**. Selected bond lengths (Å) and angles (°): Ta-O1 1.8828(13); Ta-O2 1.8755(13); Ta-O3 2.2446(14); Ta-C15 2.1870(19); Ta-C15-C18 164.2; O1-Ta-O2 168.75(6); C21-O2-Ta 145.34(13); C1-O1-Ta 142.51(13).

This reaction, proceeding via σ-bond metathesis, is quite unusual given that the methyl group and the CH bond are located trans to each other in the ground state structure. Hence the transformation requires first an isomerization to a species that displays the CH bond and the methyl in close vicinity, such as in

9 (Scheme 5). Alternatively, a bimolecular mechanism could be invoked. To further detail this transformation, a kinetic study was undertaken. The reaction was performed in C_6D_5Br over a range of 34°C (91-125 °C). The reaction was found to obey first order kinetics in the tantalum complex (Figure 6), consistent with a mechanism involving first an isomerization to bring the methyl group cis to the *ipso*-CH bond followed CH activation. The Eyring analysis yielded $\Delta H^{\ddagger}$ = 27.1 ± 0.9 kcal/mol; $\Delta S^{\ddagger}$ = -2 ± 2 cal/mol·K (Figure 7). The enthalpy value is similar to one observed for cyclometallations, with methane elimination, of tantalum supported by monodentate phenolates.[21] These studies gave entropies of activation of -7(3) and -6(4) eu for t-butyl substitution and -15(3) for phenyl substitution. This suggests that the phenyl substituted phenolates require more reorganization for the transition state compared to the t-butyl substituted ones, which is consistent with the fact that the phenyl group needs to rotate significantly from the ground state in order to achieve the required geometry for cyclometallation. For the present system, the entropy of activation of essentially 0 eu is consistent with a rate determining step involving the cyclometallation (**9** to **8**), given that the *ipso*-CH bond is already preorganized for the reaction. A rate determining step involving isomerization (**7** to **9**) is expected to involve some degree of reorganization and lead to a negative and significant entropy of activation, especially for a semirigid terphenyl system.[42,43]

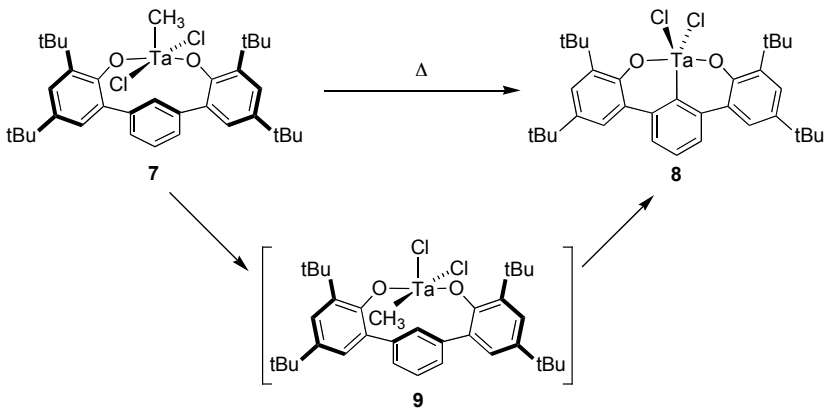

Scheme 5. Proposed mechanism for the preparation of **7** involving an intermediate cyclometallation of the connecting benzene ring.

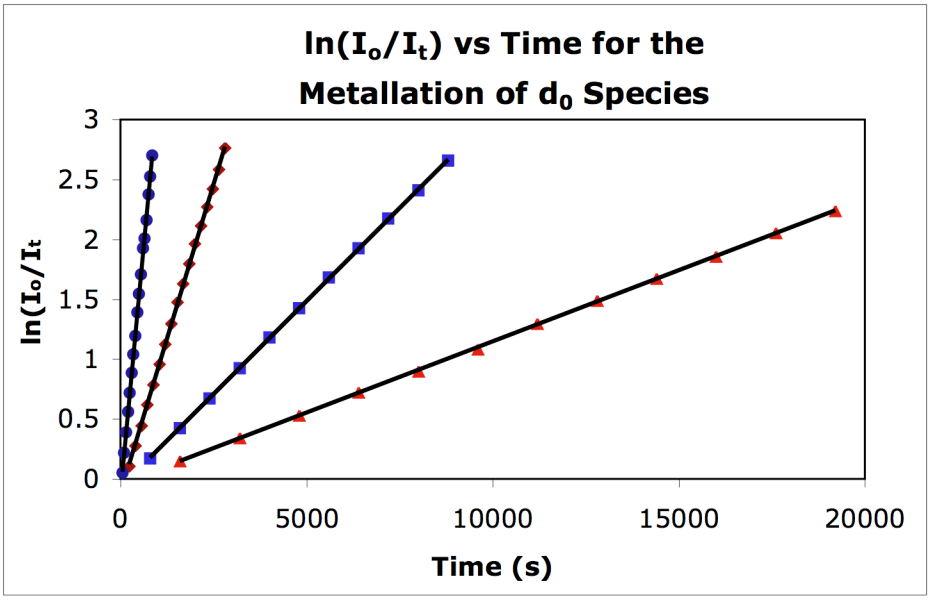

Figure 6. Kinetic plots for the cyclometallation of **7** at different temperatures (red triangles: 91 °C, blue squares: 101 °C, red diamonds: 111 °C, blue circles: 125 °C).

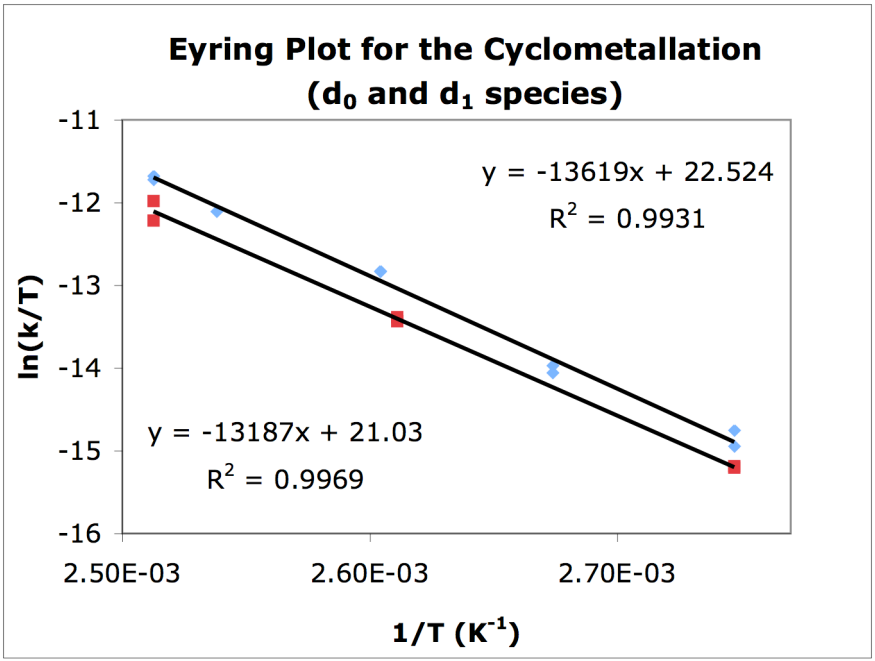

Figure 7. Eyring plots for the cyclometallation of **7** (blue) and **7-*d*$_1$** (red).

To investigate further the possibility that the isomerization from **7** to **9** is the rate determining step in this transformation, the cyclometallation position was labeled with deuterium (**7-*d*$_1$**). Kinetic data were obtained over the same temperature interval, allowing the derivation of the activation parameters. The experimental error does not allow distinguishing between the slopes of the cyclometallation reactions from **7** and **7-*d*$_1$** (Figure 6). As a result, the isotope effect is the same (k_H/k_D=1.6) over a range of 34 °C (91-125 °C). These isotope effects are smaller than the one observed for the intermolecular σ-bond metathesis reactions of $Cp^*_2ScCH_3$ with C_6H_6 and C_6D_6 (k_H/k_D=2.8(2) at 80°C).[44] They are also smaller than those observed in cyclometallations of t-butyl groups *ortho* to tantalum phenolates (k_H/k_D=5.2(4) at 180°C, k_H/k_D=2.3(5) at 118°C and k_H/k_D=1.9(5) at 135°C for different ligand sets, respectively).[21,38] The observation

of an isotope effect for the present system, even though relatively small, suggests that the rate determining step involves σ-bond metathesis (**9** to **8**). It is notable then that cyclometallation from the methyl dichloride **7** is slower than from the trimethyl species **4**. This could be due to the fact that in **4**, the ground state is destabilized by the proposed trans dimethyl species. In **7**, with a methyl trans to a weaker ligand, the ground state is lower in energy compared to **4**, hence the activation barrier could be higher. Interestingly, a reversed trend has been reported for TaPhY(OC_6H_2-2,6-tBu_2-4-X)(OC_6H_2-2-tBu-4-X-6-($C(CH_3)_2CH_2$)), Y=Ph or Cl, X=CH_3 or OCH_3, in which the diphenyl species cyclometallates slower than the phenyl chloride species.[38] The different behavior probably stems from the different ground state geometries in the present system (six coordinate, pseudo-octahedral) vs the previously reported ones (five coordinate, trigonal bipyramid). For the five coordinate species, the σ-bond metathesis process has to push two ligands trans to each other leading to a higher energy transition state for the case when the ligands are both carbyls vs a carbyl and a chloride.

Insertion chemistry of $Ta(CH_3)_2[(OC_6H_2$-$tBu_2)_2C_6H_3]$ (5) – Reactions with ketones

Compound **5**, with two types of Ta-C single bonds provides an interesting case for the study of insertion chemistry with various substrates. The reaction with excess (1.5 equiv) benzophenone was performed in C_6D_6 and 60 °C. Clean formation of a single product is observed after 12 h. The nature of the insertion

product can be determined based on ^{13}C and ^{1}H NMR spectroscopic data. In the ^{13}C NMR spectrum, the peak corresponding to the Ta-CH_3 groups of the starting material appears at 60.6 ppm (C_6D_6). In the product, this is replaced by two peaks with a similar chemical shift (60.8 and 62.7 ppm). If one of these methyl groups would be carbon bound, it should shift significantly upfield. Hence this suggests a loss of symmetry of the molecule, but no insertion into the Ta-CH_3 bonds, consistent with structure **10** (Scheme 6). Furthermore, the Ta-*C*(*ipso*) peak, which has a chemical shift of 198.5 ppm in the starting material, is absent from this region in the product. Finally a single crystal X-ray diffraction study confirmed the structural assignment (Figure 8), but the quality of the dataset precluded reliable determination of structural parameters. The phenyl groups show five distinct peaks in the aromatic region of the ^{1}H NMR spectrum. This indicates slow rotation on the NMR time scale around the OC-Ph bonds, consistent with the hindered structure observed in the solid-state. The clean formation of only one product suggests a significant preference for the insertion into the Ta-phenyl bond. The reasons behind the observed selectivity of insertion are currently not well understood. It is also interesting that the excess substrate does not insert into the Ta-CH_3 bonds still available after the first insertion into the Ta-aryl. This could be due to steric reasons.

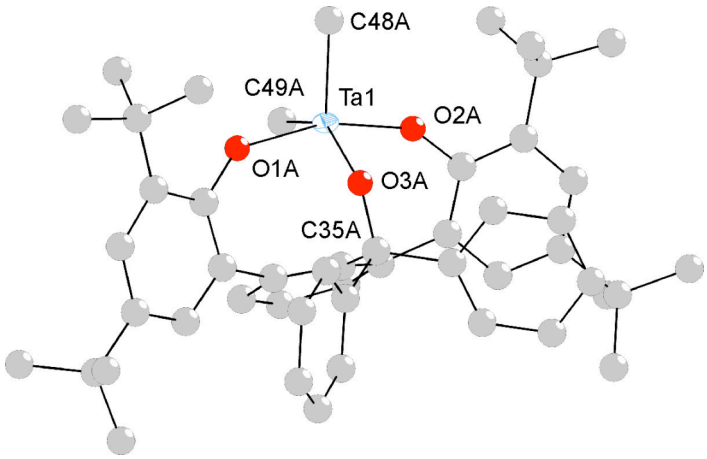

Figure 8. Structural drawing of **10**. Selected bond lengths (Å) and angles (°): Ta1-O1A 1.936(8); Ta1-O2A 1.939(8); Ta1-C48A 2.126(11); Ta1-C49A 2.208(11); Ta1-O3A 1.962(7); O1A-Ta1-O2A 160.5(3); Ta1-O3A-C48A 110.9(4); Ta1-O3A-C49A 143.1(4).

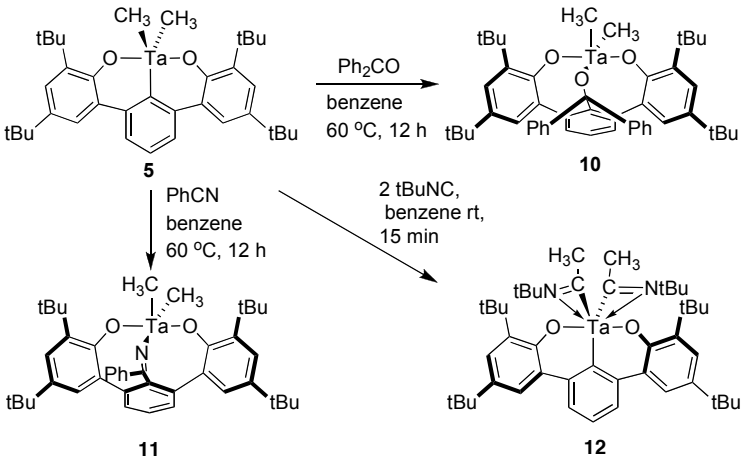

Scheme 7. Insertion chemistry of **5**.

Insertion chemistry of $Ta(CH_3)_2[(OC_6H_2\text{-}tBu_2)_2C_6H_3]$ (5) – Reaction with benzonitrile

The reaction of **5** with benzonitrile was performed under conditions similar to the ones with ketones. The ^{13}C NMR spectrum of the reaction product shows that the two Ta-CH_3 groups become inequivalent, but their chemical shifts (57.0 and 59.1 ppm) remain in the expected region for metal bound alkyls. No signal is observed in the Ta-*C*(phenyl) region. The ketimide peak appears at 169.9 ppm. These data are consistent with insertion into the Ta-phenyl bond to generate compound **11**. Interestingly, if less than one equivalent of PhCN is used, the reaction proceeds with the formation of an additional product. It may be possible that the imide functionality further reacts with another equivalent of tantalum starting material to give a species unidentified to date. The solid structure of **11** was determined by a single crystal X-ray diffraction study (Figure 9). The tantalum center is five coordinate, with a distorted trigonal bipyramid geometry. The Ta-N-C19 is very acute, due to the geometric constrains of this unusual chelating ligand. The angle between the Ta-C19 vector and the bridging benzene ring is acute as well, probably to accommodate the two atom bridge (CN) between Ta and C19 resulting from the insertion of PhCN.

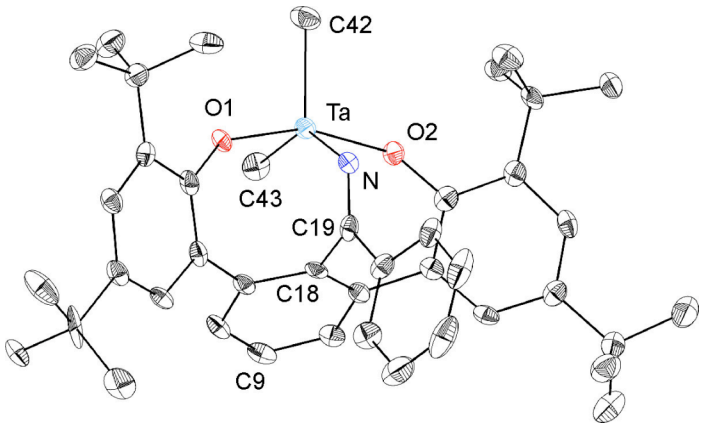

Figure 9. Structural drawing of **11**. Selected bond lengths (Å) and angles (°): Ta-O1 1.912(3); Ta-O2 1.919(4); Ta-N 2.037(4); Ta-C42 2.148(6); Ta-C43 2.163(6); O1-Ta-O2 156.34(15); Ta-N-C19 114.2(4); C17-O2-Ta 142.1(3); C1-O1-Ta 143.6(3); N-Ta-C42 114.7(2); N-Ta-C43 140.9(2); Ta-C18-C9 110.2.

Insertion chemistry of $Ta(CH_3)_2[(OC_6H_2\text{-}tBu_2)_2C_6H_3]$ (5) – Reaction with tBuNC

To investigate the scope of insertion chemistry with complex **5**, reactions with tBuNC have been explored. It was found that the reaction with two equivalents of isonitrile occurs quickly, reaching completion within 15 min at room temperature, to generate cleanly one species. The ^{1}H NMR spectrum of the product shows only one singlet corresponding to the Ta-CH_3 groups from the starting material. The ^{13}C NMR spectrum displays a peak at 179.6 ppm corresponding to Ta-*C*(phenyl). Furthermore, no peaks are observed in the Ta-CH_3 reagion (~55-65 ppm). Instead, one new peak is observed in the aliphatic region at 22.2 ppm. A new downfield peak (226.0 ppm) indicates the formation of the iminoacyl moiety. These data are consistent with 1,1-insertion of isonitrile

into the Ta-CH_3 bonds selectively, without any observable insertion into the Ta-phenyl bond. This assignment was confirmed by a single crystal X-ray diffraction study (Figure 10). The solid-state structure is essentially C_2-symmetric with the phenolate aryl rings significantly twisting away from each other. The O1-Ta-O2 angle is 166°, similar to the cyclometallated species **8** and significantly larger than in species **7**. The iminoacyl groups are both κ^2, with the nitrogen coordinated next to the aryl ligand. The structural parameters of the tantalum-iminoacyl units are similar to previously reported ones.[45-47]

The analyzed substrates indicate that 1,2-inserting substrates prefer insertion into the Ta-phenyl bond, while 1,1-inserting substrates prefer insertion into the Ta-Me bond. While currently not understood, the complete switch in selectivity observed for the two types of substrates may result from the geometrical requirements of the transition state for the insertion into the Ta-aryl bond. The chelated Ta-phenyl bond may be able to accommodate better a two-atom rather than a one-atom insertion.

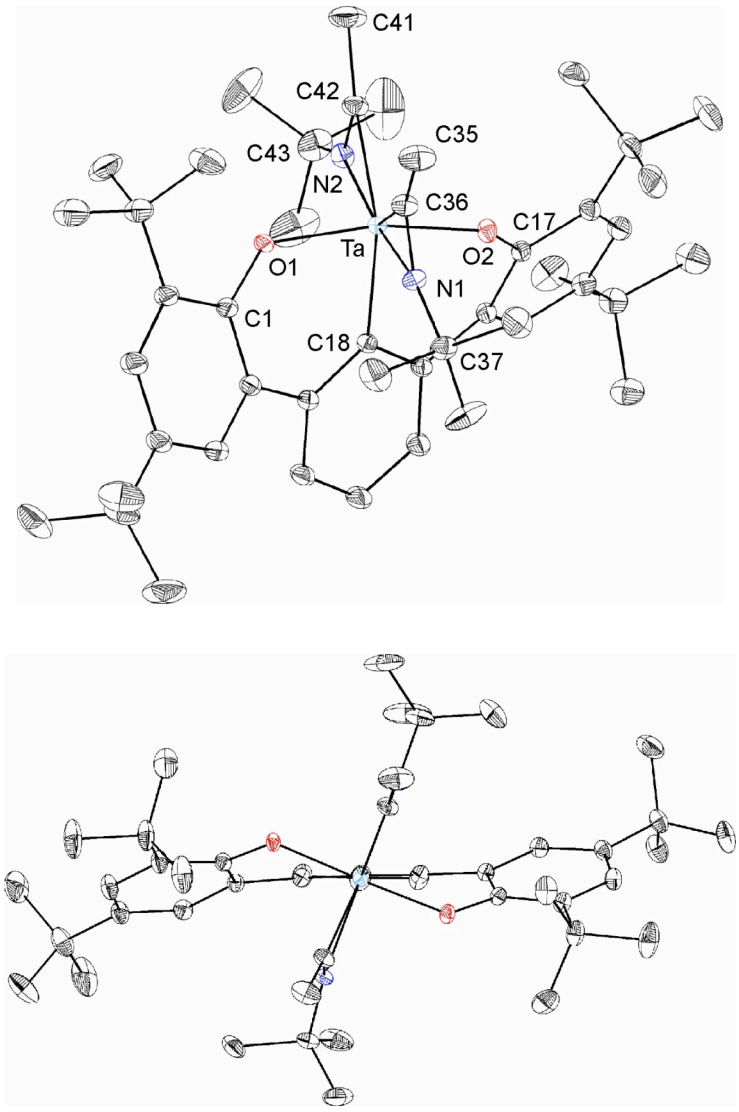

Figure 10. Structural drawing of **12**. Selected bond lengths (Å) and angles (°): Ta-O1 1.9517(11); Ta-O2 1.9415(11); Ta-N1 2.1414(12); Ta-N2 2.1494(13); Ta-C36 2.1574(15); Ta-C42 2.1576(15); Ta-C18 2.2256(14); N1-C36 1.275(2); N2-C42 1.278(2); C(36)-Ta(1)-C(42) 103.50(6); Ta-C36-N1 72.06(9); Ta-C42-N2 72.39(9); O1-Ta-O2 166.30(5); C17-O2-Ta 133.22(10); C1-O1-Ta 129.80(10).

Conclusion

A diphenol connected in the *ortho*-position via a 1,3-benzene group was prepared and its ability to support tantalum chemistry was investigated. An alkane elimination route with $Ta(CH_3)_3Cl_2$ lead to the isolation of $Ta(CH_3)Cl_2[(OC_6H_2\text{-}tBu_2)_2C_6H_4]$. Deuterium labeling studies indicated that this transformation involves protonolysis of a methyl group followed by cyclometallation of the linking ring and then by protonation of the cyclometallated group by the pendant phenol. This mechanism implicates that the C-H/Ta-CH_3 σ-bond metathesis is faster than the O-H/M-CH_3 protonolysis. High temperature kinetic and labeling studies of the cyclometallation of $Ta(CH_3)Cl_2[(OC_6H_2\text{-}tBu_2)_2C_6H_4]$ to give $TaCl_2[(OC_6H_2\text{-}tBu_2)_2C_6H_4]$ suggest that σ-bond metathesis is the rate determining step. Salt metathesis routes into tantalum chemistry afforded access to cyclometallated species $Ta(CH_3)_2[(OC_6H_2\text{-}tBu_2)_2C_6H_3]$ at room temperature. This species was found to selectively to undergo 1,2-insertions with ketones and benzonitrile and 1,1-insertions with t-butylisonitrile.

Experimental Section

General Considerations and Instrumentation. All air- and moisture-sensitive compounds were manipulated using standard vacuum line, Schlenk, or cannula techniques or in a drybox under a nitrogen atmosphere. Solvents for air- and moisture-sensitive reactions were dried over sodium benzophenone ketyl or by

the method of Grubbs.[48] Benzene-d_6 was purchased from Cambridge Isotopes and distilled from sodium benzophenone ketyl. Chloroform-d_1 and dichloromethne-d_2 were purchased from Cambridge Isotopes and distilled from calcium hydride. Other materials were used as received. Elemental analyses were performed by Desert Analytics, Tucson, AZ. ^{1}H and ^{13}C NMR spectra were recorded on Varian Mercury 300, or Varian INOVA-500 spectrometers and unless otherwise indicated at room temperature. Chemical shifts are reported with respect to internal solvent: 7.16 and 128.38 (t) ppm (C_6D_6); 7.27 and 77.23 (t) ppm ($CDCl_3$); 5.32 (t) and 54.00 (q) ppm (CD_2Cl_2); for ^{1}H and ^{13}C data.

Synthesis of (MOMO)BrC$_6$H$_2$-tBu$_2$ (1a). Bromine (3.7 mL, 11.6 g, 72.5 mmol, 1 equiv) was added via syringe to a solution of 2,4-di-t-butyl-phenol (15 g, 72.8 mmol, 1 equiv) in CH_2Cl_2 (200 mL). The brown color of Br_2 disappeared upon addition. GC-MS analysis after 5 min shows only the presence of the desired brominated product (M^+=286). The organic mixture was washed with water, then dried over $MgSO_4$, and filtered. Upon removal of volatile material by rotary evaporation, a golden oil is obtained which solidifies after placing under high vacuum (<1 mTorr). This material (4,6-di-t-butyl-2-bromophenol) was dissolved in dry THF (200 mL), under argon, and was deprotonated with NaH (1.92 g, 80 mmol, 1.1 equiv). After the addition of NaH the reaction mixture was stirred for 1 h at room temperature then MOMCl (6.1 mL, 6.5 g, 80.3 mmol, 1.1 equiv) was added via syringe. The reaction mixture was stirred at room temperature for 9 h. Water was added and the mixture was concentrated under vacuum. The desired product was extracted with CH_2Cl_2 (three times). The combined organic fractions

were dried over $MgSO_4$, filtered, and concentrated to ~50 mL. CaH_2 was added and stirred at room temperature for 6 h then at 100 °C, under vacuum, for 1 h. The reaction vessel was sealed with a needle valve and brought inside an inert atmosphere glove box. The mixture was filtered through a pad of activated alumina with the aid of some Et_2O. Volatiles were removed under vacuum to give 23.5 g (98% yield over two steps) of desired product **1a**, as a golden oil. ^{1}H NMR (300 MHz, $CDCl_3$) δ: 1.30 (s, 9H, C(CH_3)$_3$), 1.44 (s, 9H, C(CH_3)$_3$), 3.70 (s, 3H, OCH_3), 5.23 (s, 2H, OCH_2O), 7.32 (d, 2H, aryl-*H*), 7.41 (d, 2H, aryl-*H*). ^{13}C NMR (75 MHz, $CDCl_3$) δ: 31.0 (C(*C*H$_3$)$_3$), 31.5 (C(*C*H$_3$)$_3$), 34.8 (*C*(CH$_3$)$_3$), 36.1 (*C*(CH$_3$)$_3$), 57.9 (OCH$_3$), 99.5 (OCH$_2$O), 117.7, 124.1, 128.9, 144.6, 147.8, 150.7 (aryl). GC-MS: M^+=328.

Synthesis of (MeO)BrC$_6$H$_2$-tBu$_2$ (1b). A procedure analogous the synthesis of **1a** was employed. The MOMCl was replaced with Me_2SO_4 as alkylating agent. Starting from 20 g of 2,4-di-t-butyl-phenol, 26.8 g (92% yield over two steps) of **1b** were obtained. ^{1}H NMR (300 MHz, $CDCl_3$) δ: 1.30 (s, 9H, C(CH_3)$_3$), 1.41 (s, 9H, C(CH_3)$_3$), 3.92 (s, 3H, OCH_3), 7.29 (d, 2H, aryl-*H*), 7.42 (d, 2H, aryl-*H*). ^{13}C NMR (75 MHz, $CDCl_3$) δ: 31.1 (C(*C*H$_3$)$_3$), 31.6 (C(*C*H$_3$)$_3$), 34.8 (*C*(CH$_3$)$_3$), 35.9 (*C*(CH$_3$)$_3$), 61.5 (OCH$_3$), 117.8, 123.8, 129.0, 144.2, 147.4, 154.3 (aryl). GC-MS: M^+=298.

Synthesis of (HOC$_6$H$_2$-tBu$_2$)$_2$C$_6$H$_4$ (3). A mixture of **1b** (8.0 g, 26.8 mmol, 1 equiv) and THF (100 mL) in a Schlenk tube fitted with a screw-in Teflon stopper was frozen in a cold well, in an inert atmosphere glove box. This mixture was allowed to thaw and tBuLi solution (1.7 in pentanes, 33 mL, 56.1 mmol, 2.1 equiv) was added via syringe. The mixture was stirred for 1 h, allowing to reach

room temperature. $ZnCl_2$ (2.6 g, 20 mmol, 0.7 equiv) was added with the aid of 25 mL THF. After stirring the reaction mixture for 30 minutes, 1,3-dibromobenzene (2.84 g, 12.0 mmol, 0.45 equiv) and $Pd(PPh_3)_4$ (0.31 g, 0.27 mmol, 0.01 equiv) with the aid of some THF (~25 mL). The reaction vessel was placed in an oil bath preheated to 75 °C. Upon stirring for 16 h the mixture was allowed to cool to room temperature and was quenched with water. Volatile materials were removed under vacuum and water was added (~ 150 mL). This mixture was extracted with Et_2O (three times). The combined organics were dried over $MgSO_4$, filtered, and concentrated by rotary evaporation. The resulting residue was suspended in MeOH and cooled to -25 °C. The white precipitate was collected by filtration through a sintered glass funnel and washed with cold MeOH. This procedure generates 5.6 g of **2b** as a white powder. ^{1}H NMR (300 MHz, $CDCl_3$) δ: 1.35 (s, 18H, $C(CH_3)_3$), 1.45 (s, 18H, $C(CH_3)_3$), 3.34 (s, 6H, OCH_3), 7.22 (d, 2H, aryl-*H*), 7.36 (d, 2H, aryl-*H*), 7.45-7.51 (m, 1H, 5-C_6H_3-*H*), 7.56 (app dt, 2H, 4,6-C_6H_2-H_2), 7.81 (app t, 1H, 2-C_6H_3-*H*). ^{13}C NMR (75 MHz, $CDCl_3$) δ: 31.2 ($C(CH_3)_3$), 31.8 ($C(CH_3)_3$), 34.8 ($C(CH_3)_3$), 35.6 ($C(CH_3)_3$), 60.4 (OCH_3), 123.6, 126.9, 127.8, 128.6, 130.0, 134.6, 140.9, 142.2, 145.6, 155.2 (aryl). GC-MS: M^+=514. Compound **2b** (5.6 g, 10.9 mmol, 1 equiv) obtained above was suspended in DMF (60 mL). NaSEt was prepared *in situ* by the slow addition of EtSH (3.2 mL, 2.7 g, 43.3 mmol, 4 equiv) and NaH (1.04 g, 43.3 mmol, 4 equiv). The resulting mixture was heated to 110 °C for 5 hours, then cooled and an aliquot was collected and inspected by GC-MS to show the formation of the free phenol (M^+=486). Water (60 mL) was added and the resulting mixture was extracted

with Et_2O, dried over $MgSO_4$, and filtered. Volatile materials were removed by rotary evaporation with mild heating. The residue was triturated with MeOH a couple of times, then suspended in MeOH (20 mL) and cooled to -25 °C. A white precipitate was collected by filtration and washed with cold MeOH. The collected solid was placed under vacuum to give 4.77 g (9.8 mmol, 81% yield over two steps) desired product **3**.

Preparation of **3** using **1a** as starting material involves an analogous palladium coupling to give the terphenyl framework **2a**. This material was carried over to the step involving removal of protecting group. Compound **2a** was suspended in MeOH and concentrated HCl was added. This mixture was heated at 80 °C for 2-6 h. Upon cooling down, volatile materials were removed under vacuum and the desired product (**3**) was obtained as above. Starting from 1.24 g of 1,3-dibrombenzene led to the isolation of 1.83 g (72% yield) of **3**. ^{1}H NMR (300 MHz, $CDCl_3$) δ: 1.36 (s, 18H, C(C*H*$_3$)$_3$), 1.49 (s, 18H, C(C*H*$_3$)$_3$), 5.51 (s, 2H, O*H*), 7.15 (d, 2H, aryl-*H*), 7.39 (d, 2H, aryl-*H*), 7.55 (app dt, 1H, 2H, 4,6-C_6H_2-*H*$_2$), 7.61-7.66 (m, 2H, 2,5-C_6H_2-*H*$_2$). ^{13}C NMR (75 MHz, $CDCl_3$) δ: 30.0 (C(*C*H$_3$)$_3$), 31.9 (C(*C*H$_3$)$_3$), 34.6 (*C*(CH$_3$)$_3$), 35.4 (*C*(CH$_3$)$_3$), 124.3, 125.0, 127.8, 129.0, 130.4, 131.1, 135.9, 139.5, 142.5, 148.9 (aryl).

Preparation of $Ta(CH_3)_2[(OC_6H_2\text{-}tBu_2)_2C_6H_3]$ (5). KBn (234 mg, 1.8 mmol, 2 equiv) was added as a solid to an Et_2O / THF (17 / 1 mL respectively) solution of diphenol **3** (437 mg, 0.90 mmol, 1 equiv). Orange solid KBn dissolves and discolors over less than an hour. The reaction mixture was allowed to react for 2 h, then $TaCl_2Me_3$ (267 mg, 0.90 mmol, 1 equiv) was added. Within minutes, the

color of the reaction mixture turns brown. The mixture was stirred for 4 h then filtered through a bed of Celite. Volatile materials were removed under vacuum. Petroleum ether was added to the brown residue and the mixture was stirred for ~ 10 minutes. This mixture was filtered through Celite to remove dark solids. The pale brown filtrate was concentrated and cooled to -35 °C. The resulting white precipitate was collected by filtration, washed with cold petroleum ether, and dried under vacuum. This procedure affords 339 mg (0.49 mmol, 54% yield) of **5** as a white powder. ^{1}H NMR (500 MHz, C_6D_6) δ: 0.81 (s, 6H, Ta(CH_3)$_2$), 1.40 (s, 18H, C(CH_3)$_3$), 1.73 (s, 18H, C(CH_3)$_3$), 7.48 (t, 1H, C_6H_2-*H*), 7.69 (d, 2H, aryl-*H*), 8.04 (d, 2H, aryl-*H*), 8.23 (d, 2H, C_6H-H_2). ^{13}C NMR (125 MHz, C_6D_6) δ: 31.3 (C(*C*H$_3$)$_3$), 32.3 (C(*C*H$_3$)$_3$), 35.3 (*C*(CH$_3$)$_3$), 35.8 (*C*(CH$_3$)$_3$), 60.6 (TaCH$_3$), 123.8, 125.1, 131.2, 135.4, 137.4, 144.1, 144.8, 153.6 (aryl), 198.5 (aryl-*C*Ta). Anal. calcd. for $C_{36}H_{49}O_2Ta$ (%): C, 62.24; H, 7.11. Found: C, 60.88; H, 7.24.

Preparation of $TaCl_2(CH_3)[(OC_6H_2$-$tBu_2)_2C_6H_4]$ (6). An Et_2O (5 mL) solution of Diphenol **3** (152 mg, 0.31 mmol, 1 equiv) was added to an Et_2O (5 mL) solution of $TaCl_2(CH_3)_3$. The reaction mixture changes gradually from colorless to yellow. The mixture was stirred for 16 h, then volatile materials were removed under vacuum. The residue was suspended in petroleum ether and cooled to -35 °C. A yellow precipitate was collected by filtration and washed with cold petroleum ether. Drying under vacuum gives 131 mg (0.17 mmol, 56% yield) of **6** as a bright yellow powder. ^{1}H NMR (300 MHz, C_6D_6) δ: 1.31 (s, 18H, C(CH_3)$_3$), 1.74 (s, 18H, C(CH_3)$_3$), 2.27 (s, 3H, TaCH_3), 7.02 (dd, 2H, C_6H_2-H_2), 7.17 (t, overlap with C_6D_5H, 1H, C_6H_3-*H*), 7.38 (d, 2H, aryl-*H*), 7.52 (t, 1H, C_6H_3-*H*), 7.69 (d, 2H, aryl-*H*). ^{13}C

NMR (125 MHz, CD_2Cl_2) δ: 31.2 ($C(CH_3)_3$), 31.9 ($C(CH_3)_3$), 35.2 ($C(CH_3)_3$), 36.0 ($C(CH_3)_3$), 69.3 ($TaCH_3$), 112.6, 124.7, 125.0, 130.9, 133.4, 134.9, 138.4, 145.3, 147.7, 157.5 (aryl). Anal. calcd. for $C_{35}H_{47}Cl_2O_2Ta$ (%): C, 55.93; H, 6.30. Found: C, 54.81; H, 6.06.

Synthesis of $Ta(CH_2Ph)_2[(OC_6H_2\text{-}tBu_2)_2C_6H_3]$ (6). KBn (35.6 mg, 0.27 mmol, 2 equiv) was added as a solid to a slurry of **3** (66.5 mg, 0.136 mmol, 1 equiv) in benzene (10 mL). The reaction mixture was stirred for 1 h at room temperature during which the orange color of KBn disappears. A benzene (5 mL) solution of $TaCl_2(CH_2Ph)_3$ (71.8 mg, 0.136 mmol, 1 equiv) was added to the reaction mixture containing the deprotonated phenol. The reaction mixture was stirred for 10 h at room temperatures then filtered through a bed of Celite. Volatile materials were removed under vacuum. The residue was recrystallized from petroleum ether at -35 °C. The desired product was collected by filtrations as a white powder, washed with cold petroleum ether, and dried under vacuum (62.1 mg, 73.4 μmol, 54% yield). ^{1}H NMR (500 MHz, CD_2Cl_2) δ: 1.41 (s, 18H, $C(CH_3)_3$), 1.72 (s, 18H, $C(CH_3)_3$), 2.82 (s, 4H, $TaCH_2$), 6.70-6.83 (m, 10H, C_6H_5), 7.38 (t, 1H, 4-C_6H_2-*H*), 7.45 (d, 2H, aryl-*H*), 7.48 (d, 2H, aryl-*H*). ^{13}C NMR (125 MHz, CD_2Cl_2) δ: 31.5 ($C(CH_3)_3$), 32.0 ($C(CH_3)_3$), 35.1 ($C(CH_3)_3$), 35.8 ($C(CH_3)_3$), 71.7 ($TaCH_2$), 123.2, 125.6, 126.2, 127.1, 129.1, 129.3, 131.1, 131.6, 135.6, 135.9, 142.0, 144.4, 153.3 (aryl), 197.3 (aryl-*C*Ta)**.** Anal. calcd. for $C_{48}H_{57}O_2Ta$ (%): C, 68.07; H, 6.78. Found: C, 67.96; H, 6.72.

Synthesis of $(DOC_6H_2\text{-}tBu_2)_2C_6H_3$ (3-d_2). A dry THF (10 mL) solution of compound **3** (200 mg) was placed in a flask previously flame dried and rinsed

with D_2O. D_2O was added until precipitation was observed. Volatile materials were removed by rotary evaporation. Dry THF (10 mL) was added, followed by precipitation with D_2O. This procedure was repeated three times. The OH peaks are absent by ^1H NMR spectroscopy.

Synthesis of $(HOC_6H_2\text{-}tBu_2)_2C_6HD_3$ (3-d_3). 2,4-Dibromoaniline-d_5 was prepared according to the literature procedure for the non-deuterated version,[40,41] starting from aniline-d_7 (0.30 g, 3.0 mmol). Resulting 2,4-Dibromoaniline-d_5 was all submitted to the following step, by mixing with water, adding concentrated HCl (2 mL), and cooling in a ice / water bath. $NaNO_2$ (0.23 g, 3.3 mmol, 1.1 equiv) was added to the resulting cold mixture and the mixture was stirred for 1 h at 0 °C. H_3PO_2 was added (6 g 50% solution, 45 mmol, 15 equiv) and the reaction mixture was allowed to warm up to room temperature and was stirred for 3 hours. This solution was extracted with CH_2Cl_2. The organic fraction was dried over MgSO4 and filtered. Volatile materials were removed by rotary evaporation to generate $C_6Br_2D_3H$ as a colorless oil (0.1845 g, 0.77 mmol, 25% yield). ^1H NMR (300 MHz, $CDCl_3$) δ: 7.44 (s, $C_6Br_2D_3H$). GC-MS: M^+=239. This material was used as precursor for the synthesis of **3-d_3** by using the procedure above with **1a**. ^1H NMR (500 MHz, $CDCl_3$) δ: 1.34 (s, 18H, $C(CH_3)_3$), 1.47 (s, 18H, $C(CH_3)_3$), 5.37 (s, 2H, OH), 7.13 (d, 2H, aryl-H), 7.38 (d, 2H, aryl-H), 7.53 (s, 1H, 2H, 4-C_6D_3-H).

Reaction of 3-d_2 with $TaCl_2(CH_3)_3$. A solution of $TaCl_2(CH_3)_3$ (7.2 mg, 0.024 mmol, 1 equiv) in C_6D_6 (0.4 mL) was placed in a J-Young tube and a solution of **3-d_2** (11.9 mg, 0.024 mmol, 1 equiv) in C_6D_6 (0.4 mL) was added with the aid of C_6D_6 (~ 0.3 mL). The NMR tube was sealed and mechanically rotated for 10 hours after

which the reaction mixture was investigated by NMR spectroscopy. ^{1}H NMR (500 MHz, C_6D_6) aromatic region, δ: 7.02 (d, 2H, C_6HD-*H*$_2$, ^{3}J = 7.6 Hz), 7.17 (t, overlap with C_6D_5*H*, 1H, C_6DH_2-*H*, ^{3}J = 7.6 Hz), 7.38 (d, 2H, aryl-*H*, ^{4}J = 2.4 Hz), 7.51 (t, 0.16H, C_6H_3-*H*), 7.69 (d, 2H, aryl-*H*, ^{4}J = 2.4 Hz). Methane region, δ: 0.14 (t, 0.59H, CD*H*$_3$), 0.16 (s, 0.71H, C*H*$_4$). ^{2}H NMR (75 MHz, CH_2Cl_2, recorded upon product isolation): δ: 7.13 (br s).

Reaction of 3-*d*$_3$ with $TaCl_2(CH_3)_3$. A solution of $TaCl_2(CH_3)_3$ (7.3 mg, 0.025 mmol, 1 equiv) in C_6D_6 (0.4 mL) was placed in a J-Young tube and a solution of **3-*d*$_3$** (12.1 mg, 0.025 mmol, 1 equiv) in C_6D_6 (0.4 mL) was added with the aid of C_6D_6 (~ 0.3 mL). The NMR tube was sealed and mechanically rotated for 10 hours after which the reaction mixture was investigated by NMR spectroscopy. ^{1}H NMR (500 MHz, C_6D_6) aromatic region, δ: 7.02 (d, 1H, C_6D_2H-*H*, ^{4}J = 1.7 Hz), 7.38 (two d, 2H, aryl-*H*, ^{4}J = 2.4 Hz), 7.51 (d, 0.76H, C_6D_2H-*H*, ^{4}J = 1.7 Hz), 7.69 (d, 2H, aryl-*H*, ^{4}J = 2.4 Hz). Methane region, δ: 0.14 (t, 0.29H, CD*H*$_3$), 0.16 (s, 0.71H, C*H*$_4$). ^{2}H NMR (75 MHz, CH_2Cl_2, recorded upon product isolation): δ: 7.40, 7.80 (br s).

Preparation of 8. A C_6D_6 (0.6 mL) solution of **7** (15 mg) was placed in a J-Young tube, sealed, and immersed almost completely in an oil bath at 110 ^{o}C, behind a blast shield. After 10 h, the sample was cooled to room temperature. ^{1}H and ^{13}C spectroscopic analysis show the clean formation of the species assigned to **7**. ^{1}H NMR (500 MHz, C_6D_6) δ: 1.35 (s, 18H, C(C*H*$_3$)$_3$), 1.74 (s, 18H, C(C*H*$_3$)$_3$), 7.31 (t, 1H, C_6H_2-*H*), 7.66 (d, 2H, aryl-*H*), 7.85 (d, 2H, aryl-*H*), 8.04 (d, 2H, C_6H-*H*$_2$). ^{13}C NMR

(125 MHz, C_6D_6) δ: 31.4 ($C(CH_3)_3$), 32.2 ($C(CH_3)_3$), 35.3 ($C(CH_3)_3$), 35.9 ($C(CH_3)_3$), 124.4, 124.5, 128.3, 133.9, 135.2, 138.2, 144.2, 146.5, 154.0 (aryl), 205.4 (aryl-*C*Ta).

Kinetic measurements for the conversion of 7 to 8. Stock solutions containing **7** and Ph_2CH_2 as a standard were prepared in C_6D_5Br and stored at -35 °C. The NMR probe was brought to the desired temperature and calibrated with an ethylene glycol standard. After the NMR run was complete, the temperature was checked again. Deflections less than a degree were found indicating temperature stability during experiment. A J-Young tube charged with the solution of **4** was utilized in these experiments. The decay of the Ta-CH_3 peak was integrated against the methylene hydrogens of the standard Ph_2CH_2. Data was acquired for at least three half lives. The data was plotted using Microsoft Excel. The standard error for each rate constant measurement was found to be less than 1% using the regression function in Excel.

Compound 10 (Ph_2CO insertion). A toluene (5 mL) solution containing Ph_2CO (26 mg, 1.4 μmol, 1 equiv) and **5** (100 mg, 1.4 μmol, 1 equiv) was placed in a Schlenk flask with screw-in Teflon stopper. Upon sealing, the flask was immersed in an oil bath at 60 °C and stirred for 12 h. Volatile materials were removed under vacuum and the residue was triturated with petroleum ether. Recrystallization from petroleum ether at -35 °C allows the isolation of **10** (62.8 mg, 50%) by filtration, as a white powder. ^{1}H NMR (500 MHz, CD_2Cl_2) δ: 0.23 (s, 3H, TaCH_3), 1.22 (s, 18H, C(CH_3)$_3$), 1.31 (s, 3H, TaCH_3), 1.54 (s, 18H, C(CH_3)$_3$), 6.68 (app tt, 2H, 2 *p*-C_6H_4-*H*), 6.72 (app td, 2H, 2 *m*-C_6H_4-*H*), 6.76 (d, 2H, aryl-*H*), 6.86 (app td, 2H, 2 *m*-C_6H_4-*H*), 6.95 (app d, 2H, 2 *o*-C_6H_4-*H*), 7.03 (d, 2H, aryl-*H*), 7.26

(app dt, 2H, 2 *o*-C_6H_4-*H*), 7.28 (d, 2H, C_6H-H_2), 7.53 (d, 1H, C_6H_2-*H*). ^{13}C NMR (125 MHz, CD_2Cl_2) δ: 30.1 ($C(CH_3)_3$), 31.7 ($C(CH_3)_3$), 34.6 ($C(CH_3)_3$), 35.6 ($C(CH_3)_3$), 60.9 ($TaCH_3$), 62.0 ($TaCH_3$), 84.0 (O*C*), 123.2, 125.3, 126.1, 126.2, 126.4, 127.6, 127.9, 130.7, 133.7, 135.3, 135.7, 136.0, 142.6, 145.6, 151.0, 157.5 (aryl). Anal. calcd. for $C_{49}H_{59}O_3Ta$ (%): C, 67.11; H, 6.78. Found: C, 68.03; H, 6.95.

Compound 11 (PhCN insertion). A toluene (5 mL) solution containing PhCN (30 mg, 2.9 μmol, 2 equiv) and **5** (100 mg, 1.4 μmol, 1 equiv) was placed in a Schlenk flask with screw-in Teflon stopper. Upon sealing, the flask was immersed in an oil bath at 60 °C and stirred for 12 h. Volatile materials were removed under vacuum and the residue was triturated with petroleum ether. Recrystallization from petroleum ether at -35 °C allows the isolation of **11** (53.3 mg, 46%) by filtration, as a white powder. ^1H NMR (500 MHz, CD_2Cl_2) δ: 0.23 (s, 3H, $Ta(CH_3)$), 1.20 (s, 18H, $C(CH_3)_3$), 1.22 (s, 3H, $Ta(CH_3)_2$), 1.52 (s, 18H, $C(CH_3)_3$), 6.98 (d, 2H, aryl-*H*), 7.06 (t, 2H, C_6H-H_2), 7.12-7.16 (d and t overlapped, 3H, aryl-*H*), 7.16 (d, 2H, aryl-*H*), 7.35 (d, 2H, aryl-*H*), 7.68 (t, 1H, aryl-*H*). ^{13}C NMR (125 MHz, CD_2Cl_2) δ: 30.1 ($C(CH_3)_3$), 31.7 ($C(CH_3)_3$), 34.8 ($C(CH_3)_3$), 35.6 ($C(CH_3)_3$), 56.4 ($TaCH_3$), 59.2 ($TaCH_3$), 123.9, 125.0, 126.2, 126.3, 128.3, 130.5, 131.8, 132.2, 133.1, 138.2, 139.8, 141.5, 144.7, 158.5 (aryl), 169.8 (N*C*). Anal. calcd. for $C_{43}H_{54}NO_2Ta$ (%): C, 64.73; H, 6.82; N, 1.76. Found: C, 63.20; H, 6.84; N, 1.73.

Compound 12 (tBuNC insertion). A mixture of tBuNC (25 mg, 3.0 μmol, 2.7 equiv) and C_6H_6 (~1 mL) was added to a solution of **5** (72 mg, 1.1 μmol, 1 equiv) in C_6H_6 (5 mL) in a 20 mL vial. Upon addition, the colorless mixture turned yellow. The reaction mixture was stirred for 1.5 h and volatile materials were

removed under vacuum. ^{1}H NMR spectroscopic analysis shows clean formation of **12**. Recrystallization from petroleum ether at -35 °C followed by collection by filtration leads to the isolation of 28.5 mg (31%) of **12** as a yellow powder. ^{1}H NMR (300 MHz, C_6D_6) δ: 0.84 (s, 18H, C(CH_3)$_3$), 1.29 (s, 18H, C(CH_3)$_3$), 1.41 (s, 18H, C(CH_3)$_3$), 2.91 (s, 6H, TaCCH_3), 7.37 (d, 2H, aryl-*H*), 7.58 (t, 1H, C_6H_2-*H*), 8.05 (d, 2H, aryl-*H*), 8.23 (d, 2H, C_6H-H_2). ^{13}C NMR (75 MHz, C_6D_6) δ: 22.2 (TaCCH_3), 29.5 (C(*C*H$_3$)$_3$), 30.7 (C(*C*H$_3$)$_3$), 32.4 (C(*C*H$_3$)$_3$), 35.0 (aryl-*C*(CH$_3$)$_3$), 35.4 (aryl-*C*(CH$_3$)$_3$), 62.7 (N*C*(CH$_3$)$_3$), 121.5, 125.1, 125.6, 127.7, 134.9, 135.1, 141.9, 145.6, 153.2 (aryl), 198.5 (aryl-*C*Ta), 226.0 (Ta*C*CH$_3$). Anal. calcd. for $C_{46}H_{67}N_2O_2Ta$ (%): C, 64.17; H, 7.84; N, 3.25. Found: C, 63.87; H, 7.92; N, 3.21.

X-ray Crystal Data: General Procedure. Crystals grown from dichloromethane (**6**), benzene (**7** and **8**), petroleum ether (**10** and **11**) or a mixture of diethyl ether and petroleum ether (**12**) at -35 °C were removed quickly from a scintillation vial to a microscope slide coated with Paratone N oil. Samples were selected and mounted on a glass fiber with Paratone N oil. Data collection was carried out on a Bruker Smart 1000 CCD diffractometer. The structures were solved by direct methods. All non-hydrogen atoms were refined anisotropically. Some details regarding refined data and cell parameters are available in Table 1 and 2. Selected bond distances and angles are supplied in the captions for Figures 2, 3, 5, 8, 9, and 10.

Table 1. Crystal and refinement data for complexes **6**, **7**, and **8**.

	6	**7**	**8**
Empirical formula	$C_{48}H_{57}O_2Ta \bullet CH_2Cl_2$	$2(C_{35}H_{47}O_2Cl_2Ta) \bullet C_6H_6$	$C_{38}H_{53}O_3Cl_2Ta$
Formula weight	931.81	1581.26	809.65
T (K)	100(2)	100(2)	100(2)
a, Å	10.7524(5)	11.2683(7)	15.0003(3)
b, Å	11.2822(5)	17.5151(11)	15.1231(3)
c, Å	18.5744(8)	18.2677(12)	16.5600(4)
α, deg	88.9940(10)	88.7480(10)	95.7320(10)
β, deg	82.324(2)	88.5720(10)	97.0480(10)
γ, deg	74.9580(10)	89.2020(10)	91.9980(10)
Volume, Å^3	1649.7(5)	3603.1(4)	3705.40(14)
Z	2	2	4
Crystal system	Triclinic	Triclinic	Triclinic
Space group	P-1	P-1	P-1
d_{calc}, g/cm^3	1.435	1.457	1.451
θ range, deg	1.87 to 27.50	1.59 to 33.65	1.35 to 50.18
μ, mm^{-1}	2.710	3.229	3.144

Abs. Correction	Semi-empirical from equiv.	None	None
GOF	1.818	1.622	1.000
R_1,[a] wR_2[b] [I>2σ(I)]	0.0410, 0.0908	0.0605, 0.1014	0.0390, 0.0748

[a] $R_1 = \sum | |F_o| - |F_c| | / \sum |F_o|$. [b] $wR_2 = [\sum[w(F_o^2-F_c^2)^2] / \sum[w(F_o^2)^2]]^{1/2}$.

Table 2. Crystal and refinement data for complexes **10**, **11**, and **12**.

	10	**11**	**12**
Empirical formula	$C_{49}H_{59}O_3Ta \bullet C_5H_{12}$	$C_{43}H_{48}NO_2Ta \bullet C_5H_{12}$	$C_{46}H_{67}N_2O_2Ta$
Formula weight	949.06	863.92	860.97
T (K)	100(2)	100(2)	100(2)
a, Å	16.4299(8)	12.4786(8)	10.1483(3)
b, Å	17.0630(9)	28.9867(18)	14.5504(4)
c, Å	18.7829(9)	12.6931(8)	15.6639(4)
α, deg	74.600(2)		88.0490(10)
β, deg	89.357(2)	102.621(3)	86.7020(10)
γ, deg	73.670(2)		73.7530(10)
Volume, Å^3	4860.3(4)	4480.3(5)	2216.53(11)
Z	4	4	2

Crystal system	Triclinic	Monoclinic	Triclinic
Space group	P-1	$P2_1/c$	P-1
d_{calc}, g/cm^3	1.297	1.281	1.290
θ range, deg	1.46 to 20.07	1.40 to 29.03	1.94 to 45.15
μ, mm^{-1}	2.301	2.489	2.515
Abs. Correction	Gaussian	Gaussian	None
GOF	0.979	1.439	1.155
R_1,[a] wR_2[b] [I>2σ(I)]	0.0528, 0.0956	0.0556, 0.1045	0.0349, 0.0749

[a] $R_1 = \sum ||F_o| - |F_c|| / \sum |F_o|$. [b] $wR_2 = [\sum[w(F_o^2-F_c^2)^2] / \sum[w(F_o^2)^2]]^{1/2}$.

References

(1) Moulton, C. J.; Shaw, B. L. *J. Chem. Soc.-Dalton Trans.* **1976**, 1020-1024.

(2) van der Boom, M. E.; Milstein, D. *Chem. Rev.* **2003**, *103*, 1759-1792.

(3) Albrecht, M.; van Koten, G. *Angew. Chem., Int. Ed. Engl.* **2001**, *40*, 3750-3781.

(4) Crabtree, R. H. *Pure Appl. Chem.* **2003**, *75*, 435-443.

(5) Rietveld, M. H. P.; Grove, D. M.; van Koten, G. *New J. Chem.* **1997**, *21*, 751-771.

(6) Slagt, M. Q.; van Zwieten, D. A. P.; Moerkerk, A.; Gebbink, R.; van Koten, G. *Coord. Chem. Rev.* **2004**, *248*, 2275-2282.

(7) Rabe, G. W.; Berube, C. D.; Yap, G. P. A. *Inorg. Chem.* **2001**, *40*, 4780-4784.

(8) Rabe, G. W.; Zhang-Presse, M.; Riederer, F. A.; Golen, J. A.; Incarvito, C. D.; Rheingold, A. L. *Inorg. Chem.* **2003**, *42*, 7587-7592.

(9) Rabe, G. W.; Zhang-Presse, M.; Riederer, F. A.; Yap, G. P. A. *Inorg. Chem.* **2003**, *42*, 3527-3533.

(10) Rietveld, M. H. P.; Klumpers, E. G.; Jastrzebski, J.; Grove, D. M.; Veldman, N.; Spek, A. L.; van Koten, G. *Organometallics* **1997**, *16*, 4260-4267.

(11) Rietveld, M. H. P.; Lohner, P.; Nijkamp, M. G.; Grove, D. M.; Veldman, N.; Spek, A. L.; Pfeffer, M.; van Koten, G. *Chem.-Eur. J.* **1997**, *3*, 817-822.

(12) Abbenhuis, H. C. L.; Feiken, N.; Grove, D. M.; Jastrzebski, J.; Kooijman, H.; Vandersluis, P.; Smeets, W. J. J.; Spek, A. L.; van Koten, G. *J. Am. Chem. Soc.* **1992**, *114*, 9773-9781.

(13) Abbenhuis, H. C. L.; Feiken, N.; Haarman, H. F.; Grove, D. M.; Horn, E.; Kooijman, H.; Spek, A. L.; Van Koten, G. *Angew. Chem.-Int. Edit. Engl.* **1991**, *30*, 996-998.

(14) Abbenhuis, H. C. L.; Feiken, N.; Haarman, H. F.; Grove, D. M.; Horn, E.; Spek, A. L.; Pfeffer, M.; van Koten, G. *Organometallics* **1993**, *12*, 2227-2235.

(15) Abbenhuis, H. C. L.; Grove, D. M.; Vandersluis, P.; Spek, A. L.; Van Koten, G. *Recl. Trav. Chim. Pays-Bas-J. Roy. Neth. Chem. Soc.* **1990**, *109*, 446-448.

(16) Abbenhuis, H. C. L.; Rietveld, M. H. P.; Haarman, H. F.; Hogerheide, M. P.; Spek, A. L.; van Koten, G. *Organometallics* **1994**, *13*, 3259-3268.

(17) Hogerheide, M. P.; Boersma, J.; Spek, A. L.; van Koten, G. *Organometallics* **1996**, *15*, 1505-1507.

(18) Hogerheide, M. P.; Grove, D. M.; Boersma, J.; Jastrzebski, J.; Kooijman, H.; Spek, A. L.; van Koten, G. *Chem.-Eur. J.* **1995**, *1*, 343-350.

(19) Donkervoort, J. G.; Jastrzebski, J.; Deelman, B. J.; Kooijman, H.; Veldman, N.; Spek, A. L.; van Koten, G. *Organometallics* **1997**, *16*, 4174-4184.

(20) Bradley, D. C.; Mehrotra, R. C.; Singh, A.; Rothwell, I. P. *Alkoxo and Aryloxo Derivatives of Metals*; Academic Press: London, 2001.

(21) Rothwell, I. P. *Acc. Chem. Res.* **1988**, *21*, 153-159.

(22) Rothwell, I. P. *Chem. Commun.* **1997**, 1331-1338.

(23) Ma, L. Q.; Woloszynek, R. A.; Chen, W. Z.; Ren, T.; Protasiewicz, J. D. *Organometallics* **2006**, *25*, 3301-3304.

(24) Smith, R. C.; Protasiewicz, J. D. *Organometallics* **2004**, *23*, 4215-4222.

(25) Milne, J. E.; Buchwald, S. L. *J. Am. Chem. Soc.* **2004**, *126*, 13028-13032.

(26) Greene, T. W.; Wuts, P. G. M. *Protective Groups in Organic Synthesis*; Wiley & Sons: New York, 1999.

(27) Chesnut, R. W.; Yu, J. S.; Fanwick, P. E.; Rothwell, I. P.; Huffman, J. C. *Polyhedron* **1990**, *9*, 1051-1058.

(28) Chamberlain, L. R.; Rothwell, I. P.; Folting, K.; Huffman, J. C. *J. Chem. Soc.-Dalton Trans.* **1987**, 155-162.

(29) Steffey, B. D.; Fanwick, P. E.; Rothwell, I. P. *Polyhedron* **1990**, *9*, 963-968.

(30) Chesnut, R. W.; Steffey, B. D.; Rothwell, I. P.; Huffman, J. C. *Polyhedron* **1988**, *7*, 753-756.

(31) Bonanno, J. B.; Henry, T. P.; Neithamer, D. R.; Wolczanski, P. T.; Lobkovsky, E. B. *J. Am. Chem. Soc.* **1996**, *118*, 5132-5133.

(32) Rietveld, M. H. P.; Hagen, H.; van de Water, L.; Grove, D. M.; Kooijman, H.; Veldman, N.; Spek, A. L.; van Koten, G. *Organometallics* **1997**, *16*, 168-177.

(33) Rietveld, M. H. P.; Teunissen, W.; Hagen, H.; van de Water, L.; Grove, D. M.; vanderSchaaf, P. A.; Muhlebach, A.; Kooijman, H.; Smeets, W. J. J.; Veldman, N.; Spek, A. L.; van Koten, G. *Organometallics* **1997**, *16*, 1674-1684.

(34) Vigalok, A.; Milstein, D. *Acc. Chem. Res.* **2001**, *34*, 798-807.

(35) Mulford, D. R.; Clark, J. R.; Schweiger, S. W.; Fanwick, P. E.; Rothwell, I. P. *Organometallics* **1999**, *18*, 4448-4458.

(36) Baley, A. S.; Chauvin, Y.; Commereuc, D.; Hitchcock, P. B. *New J. Chem.* **1991**, *15*, 609-610.

(37) Steffey, B. D.; Chamberlain, L. R.; Chesnut, R. W.; Chebi, D. E.; Fanwick, P. E.; Rothwell, I. P. *Organometallics* **1989**, *8*, 1419-1423.

(38) Chamberlain, L. R.; Kerschner, J. L.; Rothwell, A. P.; Rothwell, I. P.; Huffman, J. C. *J. Am. Chem. Soc.* **1987**, *109*, 6471-6478.

(39) Chamberlain, L.; Keddington, J.; Rothwell, I. P.; Huffman, J. C. *Organometallics* **1982**, *1*, 1538-1540.

(40) Heravi, M. M.; Abdolhosseini, N.; Oskooie, H. A. *Tet. Lett.* **2005**, *46*, 8959-8963.

(41) Hilgetag, G.; Martini, A. *Preparative Organic Chemistry*; Wiley-Interscience: New York, 1972.

(42) Marinescu, S. M.; Agapie, T.; Day, M. W.; Bercaw, J. E. *Organometallics*, **2007**, *26*, 1178-1190.

(43) Fay, R. C.; Lindmark, A. F. *J. Am. Chem. Soc.* **1983**, *105*, 2118-2127.

(44) Thompson, M. E.; Baxter, S. M.; Bulls, A. R.; Burger, B. J.; Nolan, M. C.; Santarsiero, B. D.; Schaefer, W. P.; Bercaw, J. E. *J. Am. Chem. Soc.* **1987**, *109*, 203-219.

(45) Chamberlain, L. R.; Durfee, L. D.; Fanwick, P. E.; Kobriger, L.; Latesky, S. L.; McMullen, A. K.; Rothwell, I. P.; Folting, K.; Huffman, J. C.; Streib, W. E.; Wang, R. *J. Am. Chem. Soc.* **1987**, *109*, 390-402.

(46) Durfee, L. D.; Rothwell, I. P. *Chem. Rev.* **1988**, *88*, 1059-1079.

(47) Chamberlain, L. R.; Rothwell, I. P.; Huffman, J. C. *J. Chem. Soc.-Chem. Commun.* **1986**, 1203-1205.

(48) Pangborn, A. B.; Giardello, M. A.; Grubbs, R. H.; Rosen, R. K.; Timmers, F. J. *Organometallics* **1996**, *15*, 1518-1520.

Chapter 5

Synthetic, Structural, and Reactivity Studies of Tantalum Complexes Supported by Diphenolates Bridged via Pyridine, Thiophene, and Furan Linkers – Mechanistic Studies of the Formation of a Tantalum Benzylidene

Abstract

A series of diphenols connected at the *ortho* positions via semi-rigid, ring-ring (sp^2-sp^2) linkages to a flat ring (pyridine, furan, thiophene) that presents another ligand (L-type) was efficiently prepared by palladium coupling chemistry from the protected bromo-phenol and the corresponding 1,3-dibromo substituted linker. Tantalum complexes supported by these ligands were synthesized via alkane elimination or salt metathesis routes. Solid-state structures of these complexes show that in all cases the ligands bind in mer fashion, but with different geometries of the terphenyl framework. The pyridine linked system binds in a C_s-fashion, the furan linked system in a C_{2v}-fashion, and the thiophene linked system in a C_1-fashion. The observed solid-state structures have been reproduced well by DFT calculations. A tantalum tribenzyl species (**6**) supported by the pyridine linked system was prepared from tantalum pentabenzyl or tantalum tribenzyl dichloride. Upon heating in the presence of dimethylphenylphosphine species **6** generates a benzylidene, by α-hydrogen abstraction. This process was found to be independent of phosphine concentration. The activation parameters extracted from an Eyring plot, $\Delta H^{\ddagger}$ = 31.3 ± 0.6 kcal/mol and $\Delta S^{\ddagger}$ = 3 ± 2 cal/mol·K, and the kinetic isotope effect k_H/k_D = 4.9 ± 0.4 (125 °C) are consistent with a mechanism involving rate determining α-hydrogen abstraction from a six-coordinate species, followed by phosphine coordination to the resulting benzylidene. According to the solid-state structure, the benzylidene π-bond is oriented perpendicular to the oxygen-oxygen vector. This was correlated with the results of DFT calculations.

Introduction

Early transition metal complexes based on non-metallocene frameworks have emerged as important avenues for the development of both catalysts for a variety of reactions and platforms for the study of elementary organometallic transformations. [1-12] Non-metallocene systems are showing great potential for diverse reactions including olefin polymerizations, hydroaminations, hydrogenations, and olefin metathesis. Compared to their metallocene counterparts, however, early metal systems containing non-cyclopentadienyl ligands have been less explored and are less well understood.

In this context, the discovery of tunable and easily available ligand frameworks that could support new transformations and allow for reaction stereocontrol is desirable. Furthermore, to avoid ligand degradation and potential catalyst decomposition, robust ancillary ligand frameworks are of interest. Phenolates and anilides have been reported to be very tunable ligands with respect to sterics and electronics.[13] Multidentate phenolate systems have found applications in olefin polymerization catalysis as well as in the synthesis and study of fundamental organometallic transformations.[14-31] One drawback apparent for some of the reported mutidentate systems is the degradation of the groups connecting the ligating atoms.[21,25,32] For instance, the tripodal tetradentate diphenolate reported Kol *et al.* have been reported to be susceptible to β-H abstraction from the position next to the metal coordinated tertiary amine.[21]

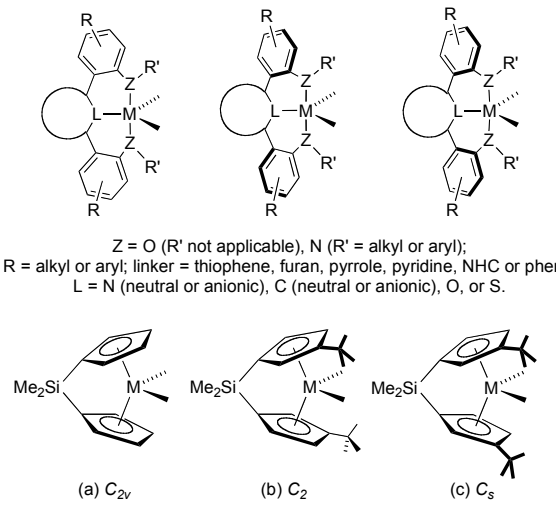

Figure 1. Geometrical analogy between the present tridentate framework and appropriately substituted metallocenes.

This chapter describes the synthesis and characterization of a series of tantalum complexes supported by diphenoxides linked via aryl-aryl linkages to flat rings that display another donor and the investigation of their reactivity (Figure 1). Anilide analogs of this framework have been studied in collaboration with undergraduate Daniel Tofan; these will not be described here. The motivation to study this ligand family stems from their resemblance to ubiquitous metallocene frameworks which have been used to support a variety of stoichiometric and catalytic transformations (Figure 1). Another reason to utilize this ligand framework is its relatively robust construction, without easily accessible positions for intramolecular CH activation. Assuming that the terphenyl unit will enforce a mer binding mode, the present framework could have binding geometries of C_2, C_{2v}, and C_s symmetry, depending on the direction of twisting around the aryl-aryl linkages. This geometrical versatility is of

interest in the context of developing stereoselective applications. Previous reports of boron and group 4 complexes supported by the pyridine diphenolate systems provide examples of C_s symmetric structures.[33-35] Crystallographically characterized complexes of Fe^{III}, Cu^{II}, and Al^{III} present the C_2 symmetric binding mode.[36]

Results and Discussion

Preparation of diphenols

The present diphenols have been prepared using well precedented procedures. Starting from commercially available and inexpensive 2,4-di-t-butyl phenol, the desired linked diphenols can be accessed within four steps. Bromination and suitable protection of the phenol functionality generates compounds **1**. Lithium-halogen exchange followed by salt metathesis with $ZnCl_2$ provides, *in situ*, aryl zinc reagents suitable for the Negishi cross-couping. 2,6-Dibromopyridine, 2,5-dibromothiophene, and 2,5-dibromofuran have been used as coupling partners with $Pd(PPh_3)_4$ as catalyst. Aqueous workup provides protected diphenols as white powders. Methyl and methoxymethyl (MOM) protecting groups have been used for making the pyridine and thiophene linked systems. Standard deprotecting procedure – acidic methanol at 80 °C – have been employed for removing MOM groups. For the furan linked system, acid mediated deprotection of the MOM groups proved difficult, leading to multiple products. Utilization of a SEM protecting group allowed both the palladium catalyzed coupling reaction and clean deprotection using Bu_4NF in HMPA.

Analytically pure diphenols are obtained as white solids by precipitation from methanol and collection by filtration.

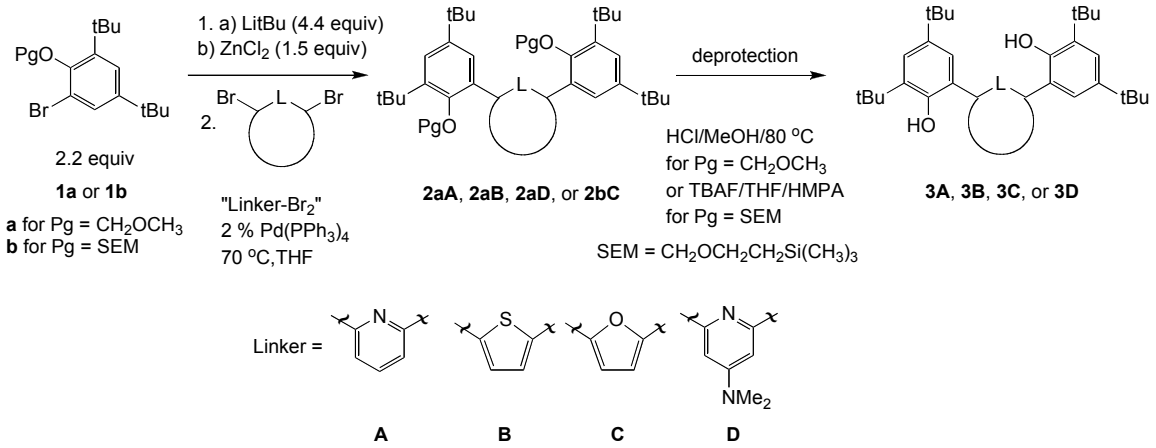

Scheme 1. Preparation of diphenols bridged by pyridine, thiophene, and furan linkers.

Preparation of tantalum alkyl complexes supported by the pyridine linked diphenoxide (3A)

With diphenols **3A-3D** in hand, tantalum metallations have been performed using either salt metathesis or alkane eliminations routes. Common tantalum alkyl starting materials such as $Ta(CH_2Ph)_5$, $TaCl_2(CH_2Ph)_3$, $TaCl_3(CH_2Ph)_2$, $TaCl_2Me_3$, or $TaCl_3Me_2$, have been used as precursors to phenoxide supported complexes (Scheme 2).[37,38] Deprotonation of the phenols has been performed *in situ* with KBn or $KN(SiMe_3)_2$. The tantalum precursors have been added to a slurry of potassium bisphenoxide in benzene or diethyl ether. The ^1H NMR spectra of the crude reaction mixtures show essentially clean formation of the desired products. Filtration to remove KCl byproduct, followed

by recrystallization provides analytically pure samples of the corresponding tantalum complexes. The ^{1}H NMR spectroscopic features of the prepared compounds are notable. Complex **4** displays one singlet integrating for 4 H corresponding to the benzyl CH_2 resonances. This suggests that the two benzyl groups are related by a mirror plane (Scheme 2). Another possible explanation involves a fast exchange process. Complex **5** shows a sharp singlet integrating to 9 H corresponding to the three tantalum coordinated methyl groups, in a variety of deuterated solvents. A variable temperature ^{1}H NMR study was undertaken to reveal that at –90 °C, the Ta-CH_3 give rise to two broad singlets in a two to one ratio. There is no geometry available to complex **5** which could lead to three chemically equivalent methyl groups. Hence, a fluxional process allows their exchange, consistent the variable temperature study. The low temperature spectrum indicates a favored structure with two equivalent methyls. This can be accomplished by the presence of a mirror plane such as in the C_{2v} structure in Scheme 2. A C_s structure, with a facial binding of the tridentate ligand is consistent with these data as well.

The solid-state structure of compound **5** shows mer coordination of the tridentate ligand (Figure 2). The Ta-N bond length is in the long range compared to other reported Ta-pyridine complexes, but the unexpected feature is the pyridine ring bent away from the Ta-N axis (Ta-N-C9 angle is 146.6 °). This distortion could be due to the inherent rigidity in the terphenyl framework which may not allow all groups to adopt the ideal conformation for metal binding. The Ta-CH_3 groups are clearly chemically different, with one trans to

the pyridine nitrogen and two roughly trans to each other. The Ta-CH_3 bond lengths are typical for tantalum methyl complexes. The C35-Ta-C34 and C35-Ta-C36 angles are 108.42(7)° and 104.62(8)°, respectively, with atoms C34 and C36 leaning toward the pyridine donor. With this distortion and the long Ta-N bond, the structure could be viewed as a trigonal bipyramid with an additional weak interaction with the pyridine. It is worth noting that the two methyl groups cis to the nitrogen donor are chemically different in the solid state due to the tilting of the pyridine plane. The low temperature spectrum observed for **5** could be accounted for by fast flipping of the pyridine ring between the two sides of the OON plane. Given that this cannot be frozen if at –90 °C, the energy of the trasition state C_{2v} structure is probably low compared to the ground state.

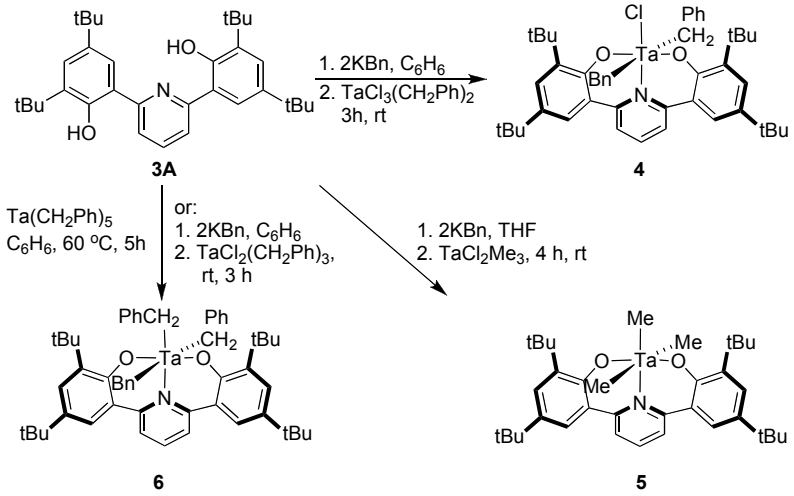

Scheme 2. Metallation strategies using diphenol **3A**.

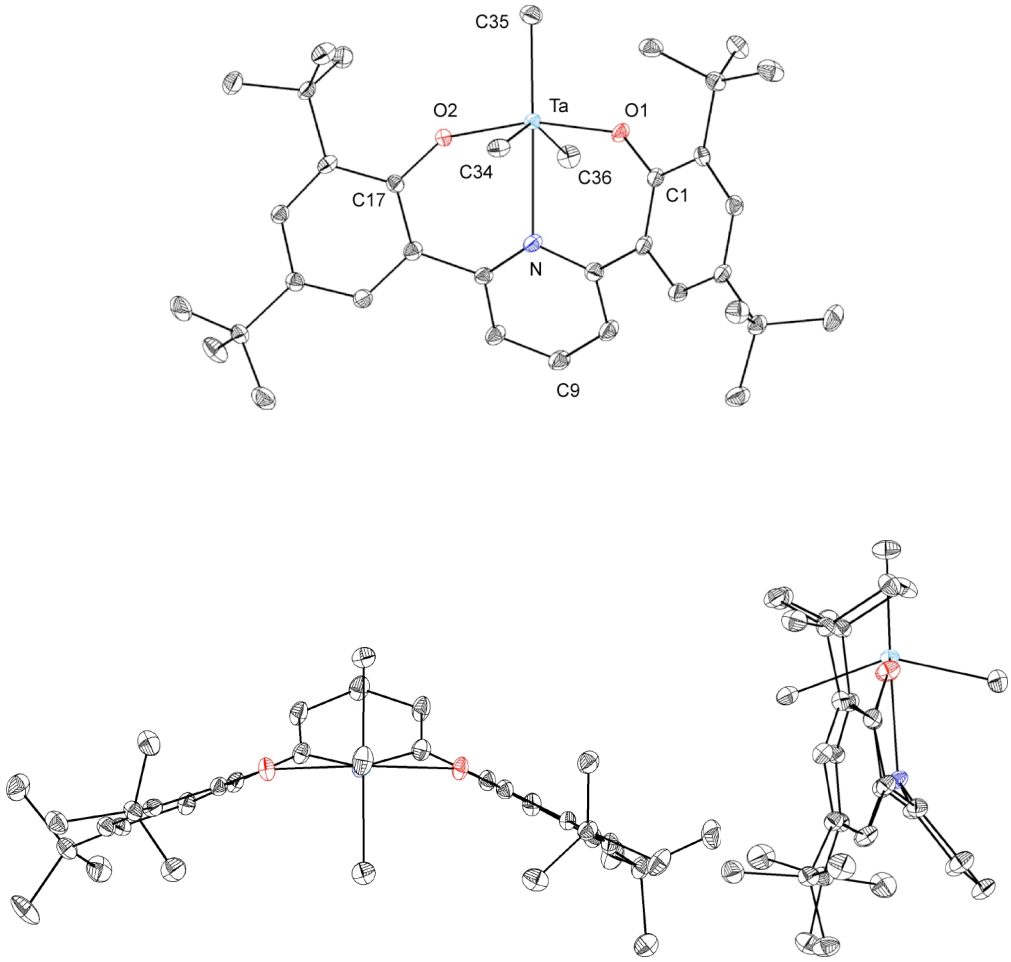

Figure 2. Structural drawing of **5**. Selected bond lengths (Å) and angles (°): Ta-O1 1.9113(13); Ta-O2 1.9020(13); Ta-C35 2.1573(18); Ta-C34 2.1931(18); Ta-C36 2.2032(19); Ta-N 2.4428(14); Ta-N-C9 146.6; O1-Ta-O2 163.45(5); C35-Ta-C34 108.42(7); C35-Ta-C36 104.62(8); Ta-O1-C1 138.09(11); Ta-O2-C17 141.66(11).

Alkane elimination routes were found to be facile for methyl tantalum starting materials. In those cases, the reaction is complete within hours at room temperature to give $TaCl_3[(OC_6H_2\text{-}tBu_2)_2NC_5H_3]$ (**7**) or $TaCl_2(CH_3)[(OC_6H_2\text{-}tBu_2)_2NC_5H_3]$ (**8**) if starting from $TaCl_3Me_2$ or $TaCl_2Me_3$, respectively. Tantalum

pentabenzyl requires heating at 60 °C for five hours for complete conversion to $Ta(CH_2Ph)_3[(OC_6H_2\text{-}tBu_2)_2NC_5H_3]$ (**6**); at room temperature this reaction is only 60% completed after 35 h. The lower reactivity for the precursor could be due to the decreased basicity of the benzyl vs the methyl groups as well as to a more hindered metal center in the tantalum benzyl vs tantalum methyl species. The ^1H NMR spectrum of compound **6** shows two singlets for the benzylic protons (Ta-CH_2Ph) in a two to one ratio. This is consistent with a mer binding mode. For a fac binding mode, the methylene protons trans to oxygen donors are diastereotopic and should display two distinct signals, which is not observed. A single crystal X-ray diffraction study of **6** (Figure 3) confirmed the meridional binding mode indicated by the ^1H NMR spectroscopic data. Compared to the trimetyl compound, the tantalum tribenzyl species shows a notable difference with respect to the binding of the alkyl groups – the C41-Ta-C34 and C41-Ta-C48 angles are about 30° smaller (75.14(7)° and 76.32(7)°, respectively). It is not clear if this orientation is adopted to avoid some steric interactions between the pyridine ring the bulkier benzyl groups or to facilitate some bonding interaction between the metal center and the π system of the benzyl group – one of the Ta-C-C(phenyl) angles is more acute than the others, at 97° vs 119° and 120°, and the Ta-C(ipso) bond length is 2.81 Å. Furthermore, this geometry allows one of the benzyl phenyls to be in close proximity to the pyridine ring indicating the possibility of some π -π stacking interactions.[39,40]

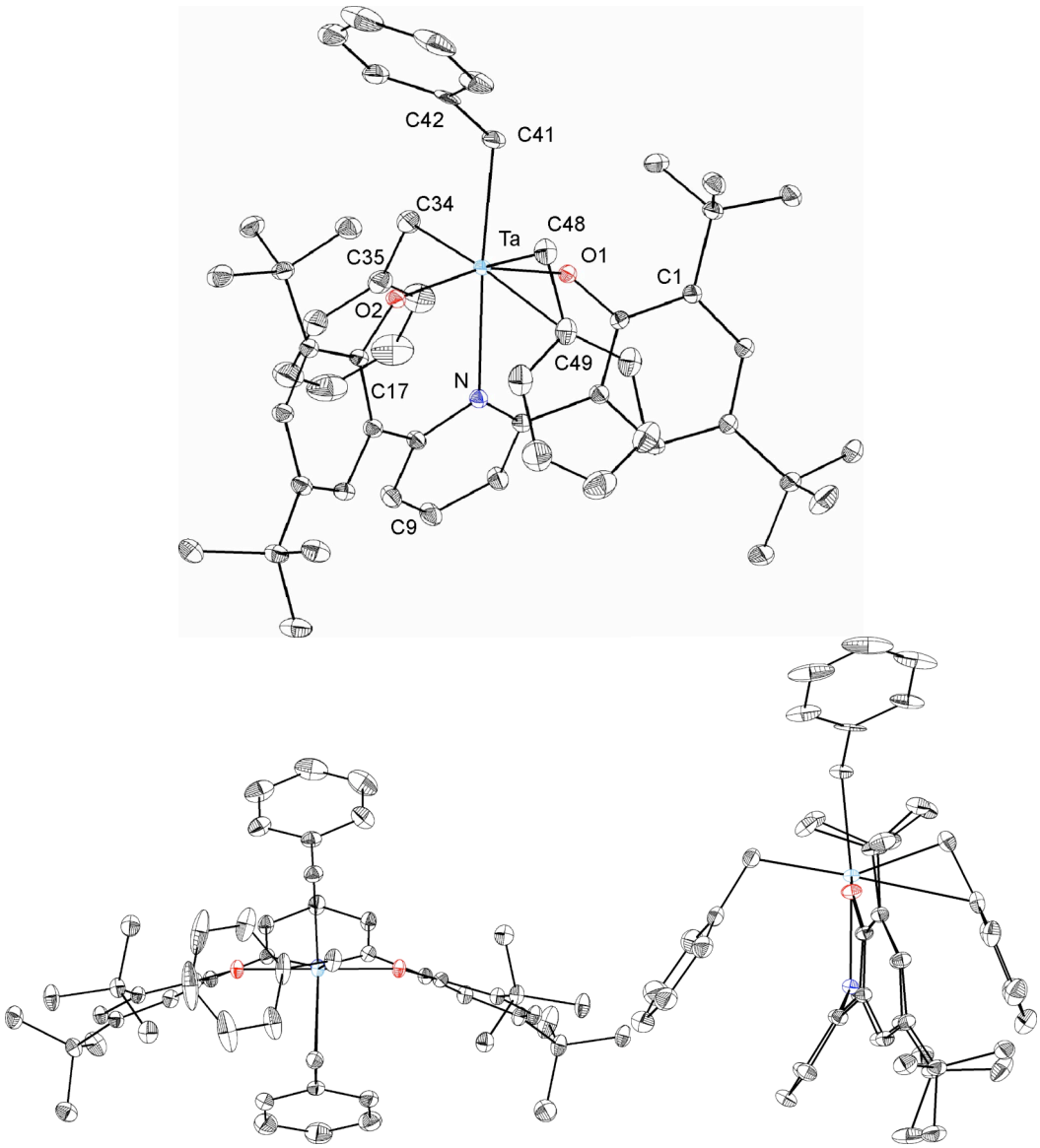

Figure 3. Structural drawing of **6**. Selected bond lengths (Å) and angles (°): Ta-O1 1.8961(11); Ta-O2 1.8972(11); Ta-C41 2.3088(16); Ta-C34 2.2243(18); Ta-C48 2.2269(18); Ta-N 2.4299(13); Ta-N-C9 150.5; O1-Ta-O2 158.89(5); C41-Ta-C34 75.14(7); C41-Ta-C48 76.32(7); Ta-O1-C1 145.20(11); Ta-O2-C17 145.45(10).

On route to a tantalum benzylidene – Formation of $TaF_2(CH_2Ph)[(OC_6H_2\text{-}tBu_2)_2NC_5H_3]$

An elegant route to tantalum alkylidenes involves cationic alkyl species (Scheme 3).[41] Deprotonation of these species with bases such as Me_3PCH_2 or $KN(SiMe_3)_2$ has been reported to lead to neutral alkylidenes. This strategy was attempted starting with $Ta(CH_2Ph)_3[(OC_6H_2\text{-}tBu_2)_2NC_5H_3]$ (**6**). Reaction with $[Ph_3C][BF_4]$, in toluene, leads to the clean formation of one species according to NMR spectroscopy. The ^1H NMR spectrum of the isolated product displays a triplet corresponding to a benzyl group which integrates to only 2 H (instead of expected 4 H) relative to the phenoxide ligand tBu groups. This species also displays a broad peak in the ^{19}F NMR spectrum. A single-crystal X-ray diffraction study allowed the identification of the product – a tantalum monobenzyl difluoride (Figure 4). In the solid-state, the benzyl binds trans to the pyridine ligand. This is consistent with the solution ^1H and ^{19}F NMR spectroscopic data. This species is possibly formed by fluoride abstraction by the electrophilic, cationic tantalum species, followed by a fluoride – benzyl swap. The target benzylidene species has been prepared by a different route (see below) and alternative procedures involving the cationic alkyl strategy have not been further explored.

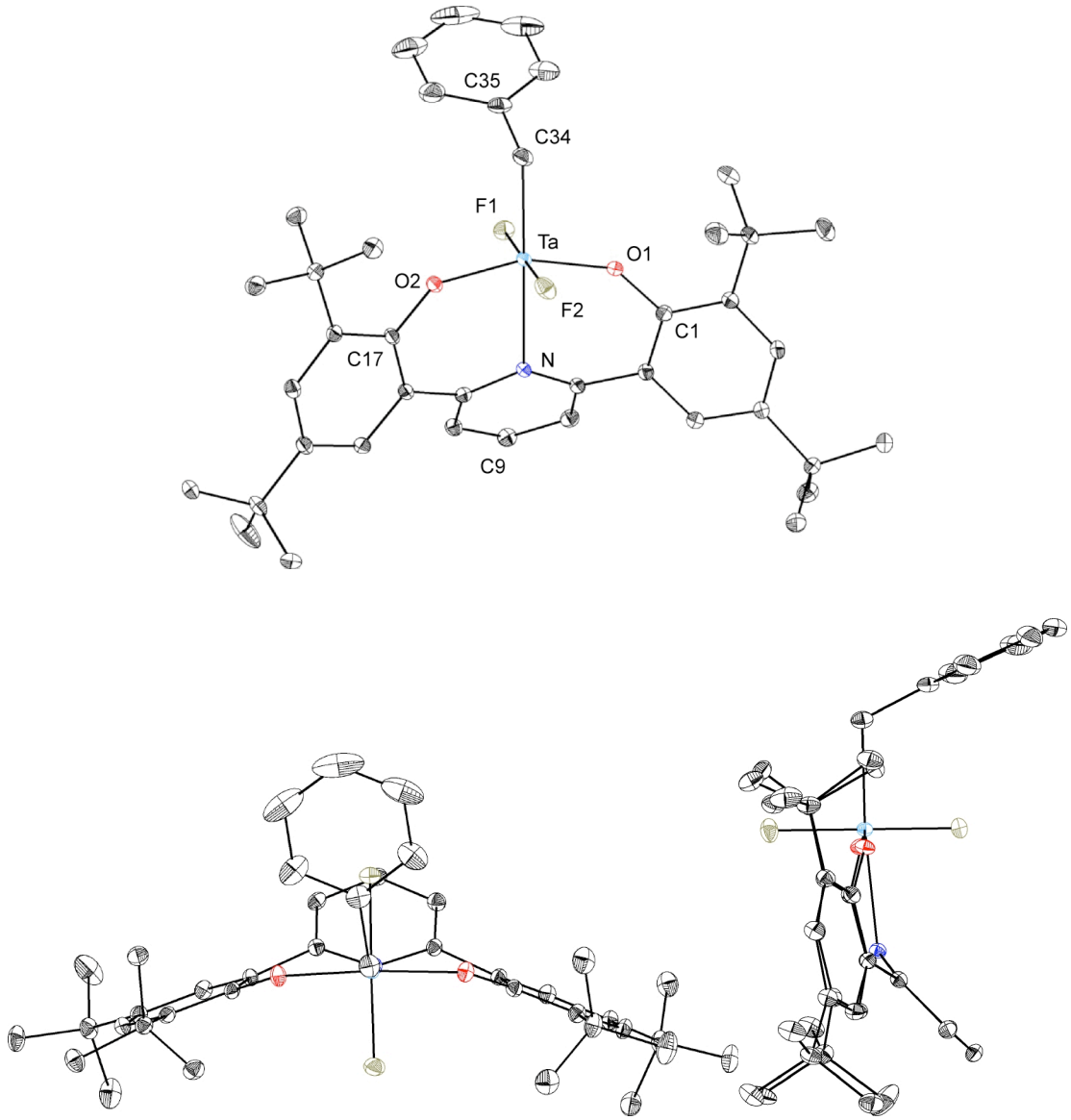

Figure 4. Structural drawing of **9**. Selected bond lengths (Å) and angles (°): Ta-O1 1.8906(13); Ta-O2 1.8908(13); Ta-F1 1.8927(10); Ta-C34 2.1872(19); Ta-F2 1.9110(11); Ta-N 2.4486(14); Ta-N-C9 142.8; O1-Ta-O2 158.28(5); F1-Ta-C34 90.74(6); F2-Ta-C34 89.21(6); Ta-O1-C1 143.78(12); Ta-O2-C17 144.38(11).

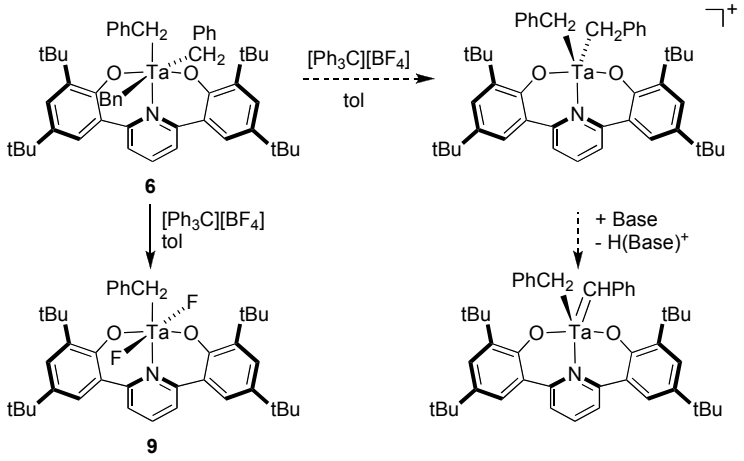

Scheme 3. Strategy to access an alkylidene via a cationic alkyl intermediate – unexpected formation of a tantalum difluoride.

Preparation of a tantalum benzylidene by alkane elimination – Formation of Ta(CHPh)(CH_2Ph)(PMe_2Ph)[$(OC_6H_2$-t$Bu_2)_2NC_5H_3$] (10-P)

Another common route to alkylidene complexes involves intramolecular α-H abstraction.[42-47] This strategy has been used intensively in particular in conjunction with the addition of a base, such as phosphines. Compound **6** was heated to temperatures over 90 °C in benzene-d_6 or toluene-d_8 in the presence of excess PMe_2Ph. Clean formation of a new species (**10-P**) was observed by ^{1}H NMR spectroscopy (eq 1). The singlet at 9.03 ppm is diagnostic for a benzylidene species. The reaction proceeds quite slowly at 90 °C, reaching completion after more that three days. At 125 °C however, the reaction is complete within hours. In the absence of phosphine, benzylidine formation still seems to occur, judging by the appearance of a peak at 9.20 ppm (^{1}H NMR spectroscopy), however, the reaction is not as clean. The use of other bases such as quiniclidine or PMe_3 has

been explored. The reaction occurs cleanly in the presence of PMe_3, but decomposition is observed in the presence of quiniclidine. Even for the phosphines that afford clean formation of the benzylidene, prolonged subsequent heating leads to decomposition. Preliminary studies with **10-P** indicate that it reacts with ethylene and diphenylacetilene suggesting promise for further exploration. Notably, the observed clean reactivity at high temperatures underlines the chemical robustness of this ligand framework. Even under milder conditions, other reported multidentate biphenoxides have shown reaction with the supporting ligands.[21]

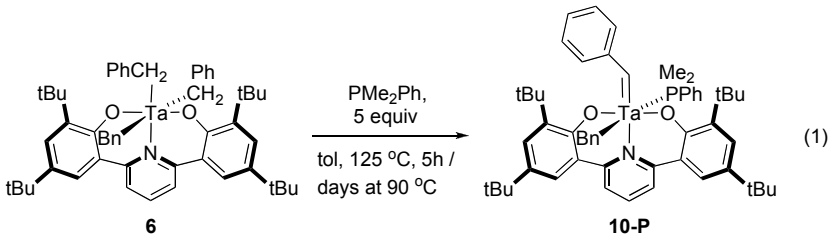

(1)

Further investigation into the nature of the tantalum benzylidene **10-P** involved single-crystal X-ray diffraction, NMR spectroscopy, and DFT calculations. The solid-state structure of **10-P** (Figure 5) displays hexacoordination at tantalum, with meridionally coordinated pyridine bisphenoxide, benzylidene trans to pyridine, and phosphine and benzyl groups trans to each other. Interestingly, the benzylidene lies such that the π-bond roughly bisects the O_2N plane. This orientation is sterically unfavorable, pointing the phenyl group toward the phenoxide t-butyl moiety. The ^1H coupled ^{13}C NMR spectrum of **10-P** shows a coupling constant $^1J_{CH}$ = 103 Hz for the alkylidene carbon. Both the TaCC and the alkylidene $^1J_{CH}$ coupling constants have been

used as indicators of the degree of α-agostic interaction. A large TaCC angle correlates with a small C-H coupling constant (due to increased p-character in the CH bond) and is indicative of increased degree of α-agostic interaction.[12,48] For instance, complex $Cp_2Ta(CHPh)(CH_2Ph)$, which does not present a low-energy orbital of appropriate symmetry for an α-agostic interaction, shows a coupling constant $^1J_{CH}$ = 127 Hz and a TaCC angle of 135.2°.[45] At the other end of the spectrum lies Cp*Ta(CHPh)(CH_2Ph) which has a coupling constant of $^1J_{CH}$ = 82 Hz with a TaCC angle of 166°.[49] The present value of $^1J_{CH}$ = 103 Hz is indicative of an average amount of α-agostic interaction. This correlates well with the Ta-C42-C43 angle of 149.7°. Interestingly, the benzylidines prepared by Kol *et al.* supported by bisamino-diphenolate ligands display significantly more acute alkylidine TaCC angles (140° and 142°).[21] However, for all those cases, the phenolates display either chloride or just hydrogen in the ortho-position to the phenolate oxygen. Hence, the observed larger alkylidene TaCC angle in the pyridine-diphenolate case could be due to a steric interaction between the phenyl group and the bulkyl ortho-t-butyl group of the phenolate. This possibility was explored computationally.

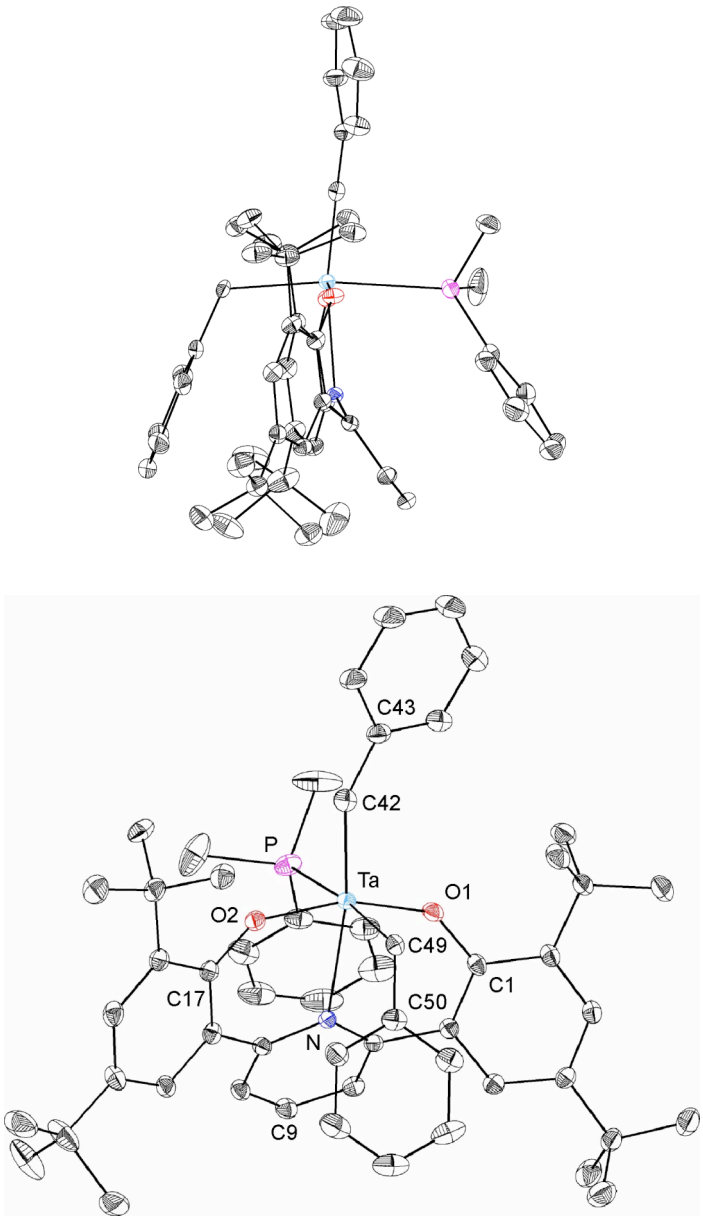

Figure 5. Structural drawing of **10-P**. Selected bond lengths (Å) and angles (°): Ta-O1 1.9355(18); Ta-O2 1.9095(18); Ta-C42 1.996(2); Ta-C49 2.279(2); Ta-P 2.7058(7); Ta-N 2.4827(17); O1-Ta-O2 159.17(6); Ta-C42-C43 149.7(2); Ta-O1-C1 137.10(15); Ta-O2-C17 145.33(15); Ta-N-C9 150.0.

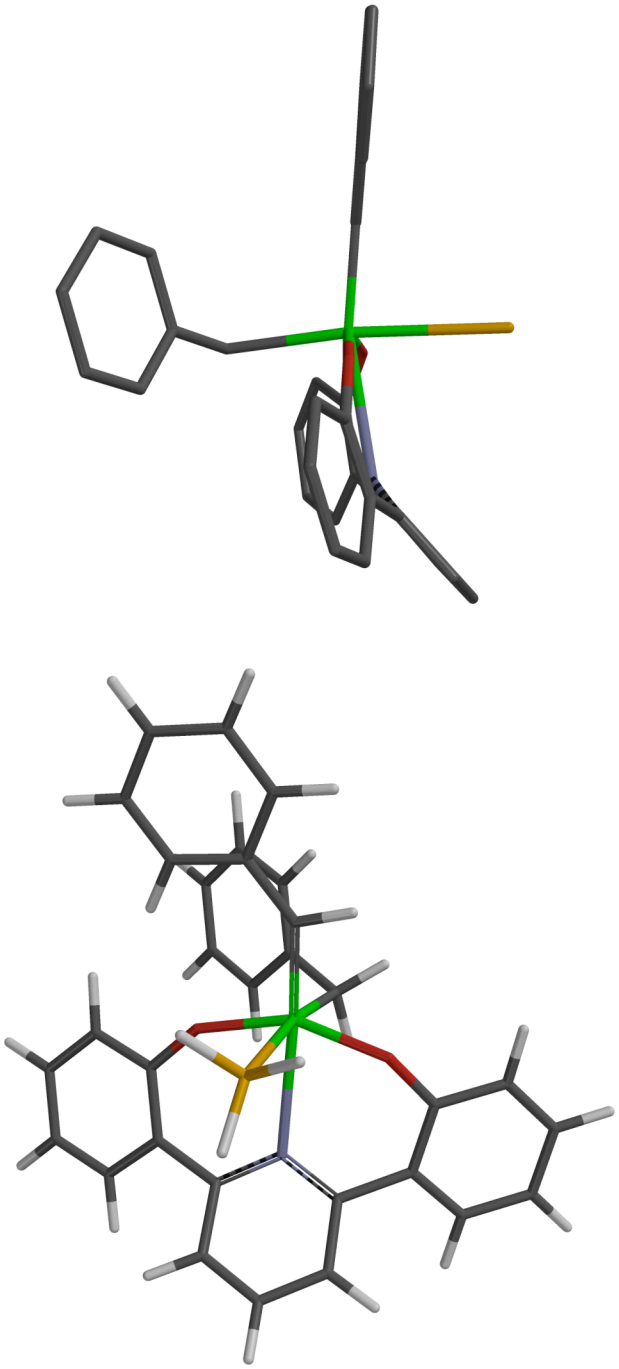

Figure 6. Optimized gas-phase structure of a simplified model (**10-Pm**) of complex **10-P**. Hydrogens are omitted in the top view, for clarity.

DFT calculations were performed on a model of **10-P** displaying hydrogens in the positions *ortho* to the phenolate oxygens (B3LYP, basis set LACVP**, model **10-Pm,** Figure 6). The unrestricted optimized geometry of **10-Pm** displays an alkylidene TaCC angle of 141°, more acute than the one observed in the solid-state for the tBu substituted species and similar to the ones observed in the Kol systems, bearing smaller substituents. This indicates that the intrinsic preference for α-agostic interaction is small based on the DFT calculation, almost as small as in the metallocene systems. However, sterically, the t-butyl *ortho* substituent pushes the phenyl group away from the tantalum center, increasing the TaCC angle. This enforces more p-character to the alkylidene CH bond and decreases $^{1}J_{CH}$ coupling. The alkylidene Ta-C π-interaction is apparent in the calculated HOMO (Figure 7). This interaction is roughly perpendicular to the Ta-O vectors using the tantalum. This correlates with the predicted interactions between the frontier orbitals of the tantalum fragment and of the carbene (Figure 8). The TaO_2N and $TaCp_2$ fragments are related electronically due to a structural asymmetry which differentiates the nature of the orthogonal orbitals available for interaction with additional ligands. The d-orbitals that have a contribution toward the Cp or O ligands are involved in π-bonding with the ancillary ligands and are destabilized with respect to interaction with additional ligands. The remaining d-orbitals, found perpedicular to the O-O and Cp-Cp vector, are available for bonding with an incoming ligand. Given that the carbene has a similar asymmetry – a p-orbital only available perpendicular to the plane of the fragment – a specific geometry is expected for binding to the tantalum center; the geometry that allows for the formation of a π-bond (Figure 8).

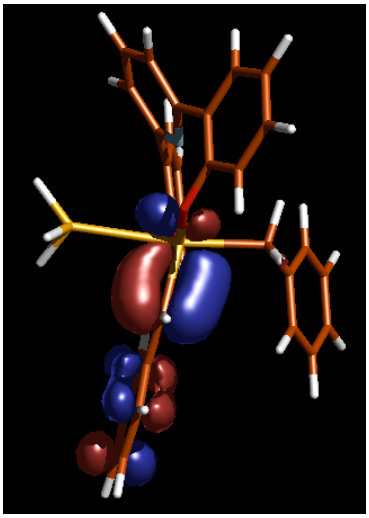

Figure 7. Depiction of HOMO of the optimized gas-phase structure of complex **10**.

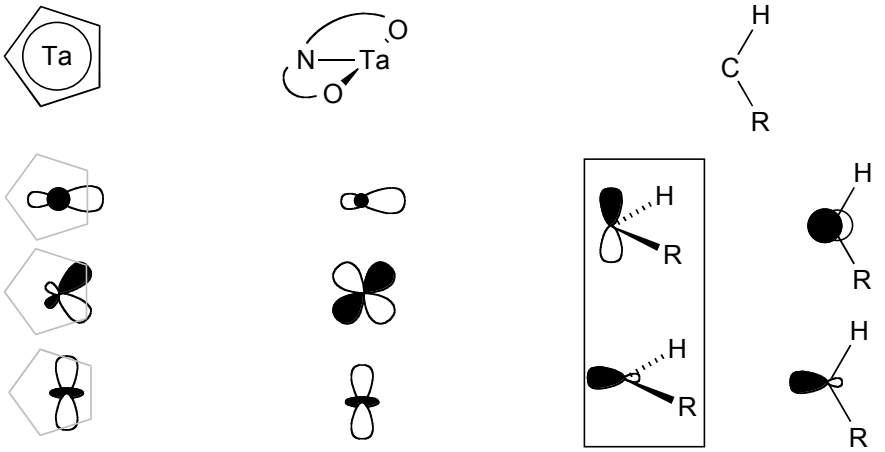

Figure 8. Frontier orbitals of tantalocene, tantalum pyridine-diphenolate, and carbene (in two perpendicular orientations) fragments. The orientation in the rectangle allows for symmetry matching of carbene and metal fragment frontier orbitals.

Mechanistic study of the formation of tantalum benzylidene Ta(CHPh)(CH_2Ph)(PMe_2Ph)[(OC_6H_2-tBu_2)$_2$$NC_5H_3$] (10-P)

A number of mechanisms could be envisioned for the formation of benzylidene **10-P**. One pathway, which has been proposed in the literature, involves first coordination of the phosphine to give rise to a crowded species **6-P**.[45,49,50] In this species, an α-H and a neighboring alkyl are brought in close proximity to facilitate α-H abstraction leading to alkylidene formation. Formation of species **6-P** could occur via a fast preequillibrium followed by a rate determining α-H abstraction (Mechanism 1). For this mechanism, the observed rate constant is expected to have a non-linear dependence on the phosphine concentration. Alternatively, **6-P** could be generated in a slow step followed by a fast α-H abstraction (Mechanism 2). For this pathway, the observed rate constant is expected to have a linear dependence on phosphine concentration. For mechanism 3, α-H abstraction occurs first, in a rate-determining step, followed by alkylidene trapping with the phosphine. For this mechanistic pathway, the reaction rate constant is independent of phosphine concentration.

To evaluate the mechanism of the benzylidene formation, a series of kinetic experiments was performed. Under pseudo-first-order conditions with respect to phosphine concentration (more than twenty fold excess vs. **6**), the reaction rate was found to be first order in the concentration of **6** (Figure 9). Provided that the rate of the reaction is predicted to be dependent on the phosphine concentration for two of the proposed mechanisms, kinetic measurements were performed at various concentrations of phosphine, at 115 °C.

Over a phosphine concentration range varied by fifteen fold, the reaction rate was found to remain constant (Figure 10). This indicates that the reaction rate has a zero order dependence on phosphine concentration, consistent with mechanism 3. Mechanism 1 could give rise to a similar dependence in phosphine concentration under saturation conditions ($k_1[PMe_2Ph] >> k_{-1}$). However, under these conditions, species **6-P** should be observable by spectroscopy, which is not the case. To further probe the nature of the rate determining step, the benzylic position was labeled with deuterium and the rate constant was measured at 115 °C (Figure 9). An isotope effect $k_H/k_D = 4.9 \pm 0.4$ was found, indicating that the rate determining step involves C-H bond cleavage. This is consistent with both mechanisms 1 and 3. Kinetic analysis of the present reaction was performed over a temperature range of 37 °C and the activation parameters were determined from an Eyring plot (Figure 11). The activation parameters were found to be $\Delta H^{\ddagger} = 31.3 \pm 0.6$ kcal/mol and $\Delta S^{\ddagger} = 3 \pm 2$ cal/mol·K for the non-deuterated species (for the deuterated species, **6-*d*$_6$**, they are $\Delta H^{\ddagger} = 34.4 \pm 0.6$ kcal/mol and $\Delta S^{\ddagger} = 8 \pm 2$ cal/mol·K). The small activation entropy is consistent with a unimolecular rate determining step (mechanisms 1 and 3). However, mechanism 3 is the only reaction pathway consistent with all the above experimental results.

Calculated rate constants (see Scheme 4):

Mechanism 1: $$k_{obs} = \frac{k_1 \bullet k_2 \bullet [PMe_2Ph]}{k_1 \bullet [PMe_2Ph] + k_{-1}}$$

Mechanism 2: $$k_{obs} = \frac{k_1 \bullet k_2 \bullet [PMe_2Ph]}{k_{-1} + k_2}$$

Mechanism 3: $k_{obs} = k_1$

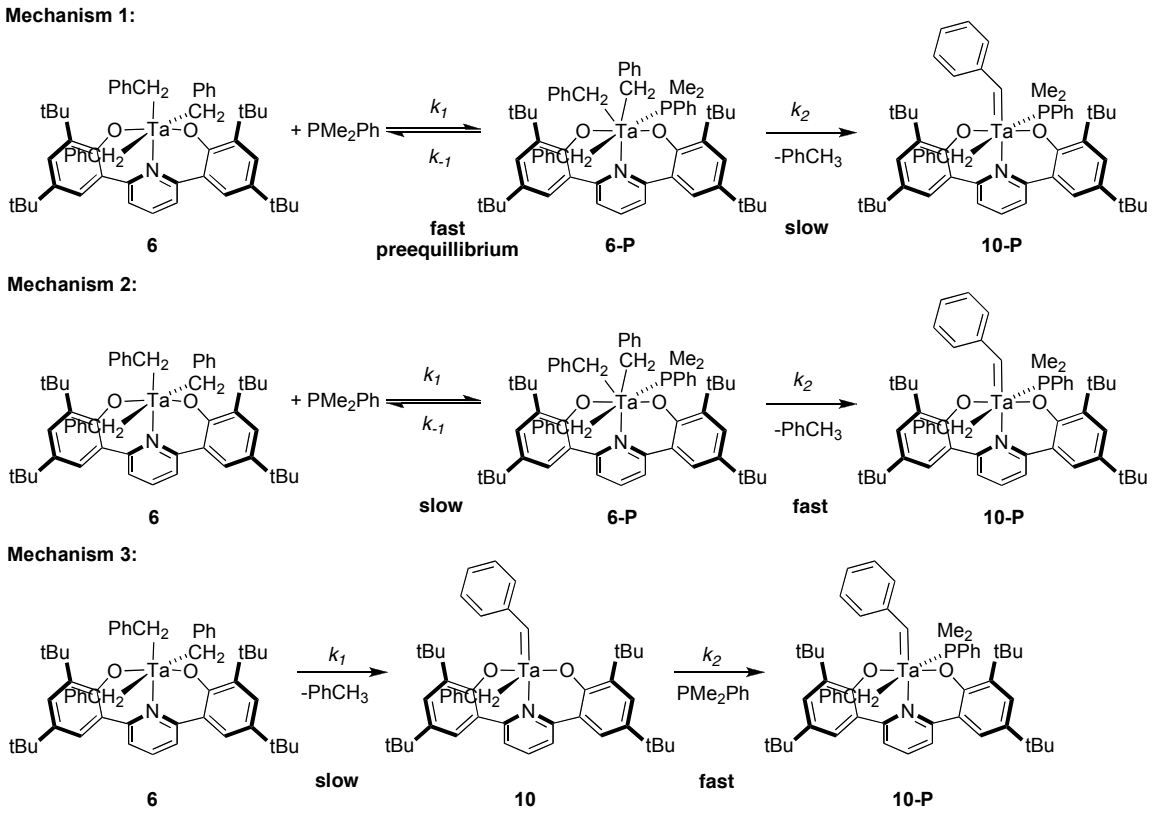

Scheme 4. Proposed mechanisms for the formation of benzylidene.

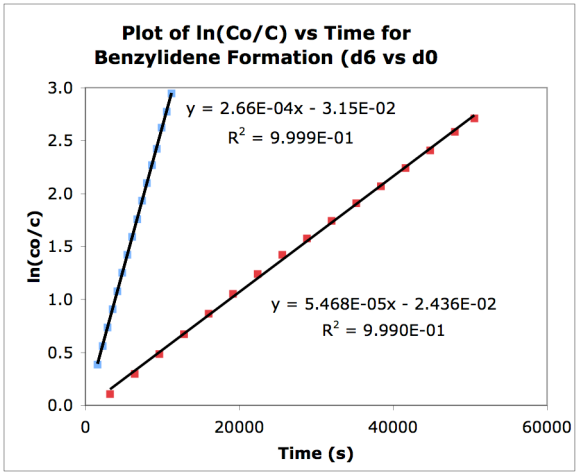

Figure 9. Kinetic plots for the conversion of **6** (blue) and **6-*d*$_6$** (red) into **10-P**.

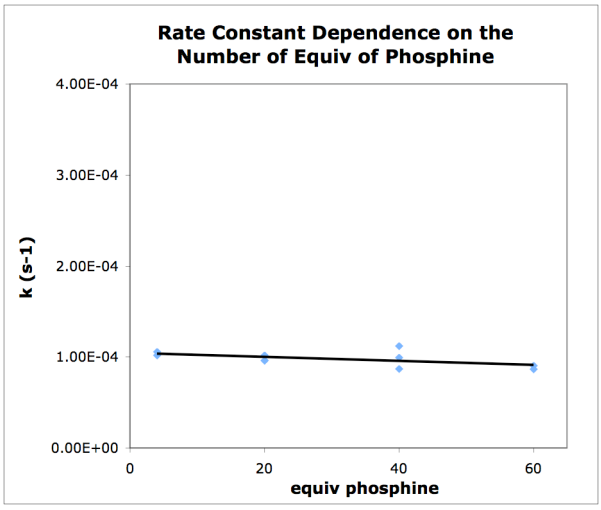

Figure 10. Plot of the dependence of the observed rate constant on the concentration of phosphine for conversion of **6** to **10-P**.

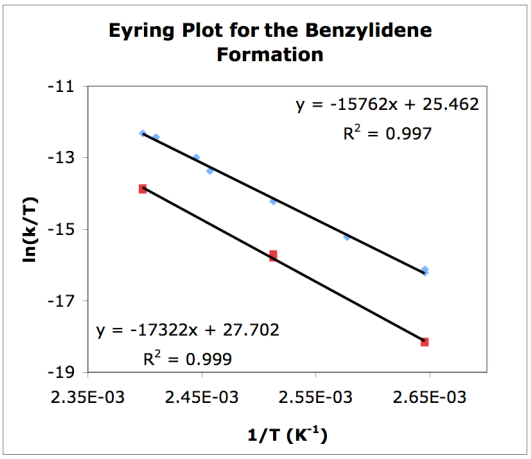

Figure 11. Eyring plots for the cyclometallation of **6** (blue) and **6-d_6** (red).

To explore the relevant electronic features of the α-abstraction reaction, the synthesis of compounds with mixed benzyl ligand sets was targeted. Compound **4** was used as a precursor for reaction with Grignard reagents substituted with OMe and CF_3 in the *para* position. Mixtures of products were

obtained in these cases. The reaction of **4** with deuterium labeled benzyl Grignard reagent leads to the tribenzyl species with label incorporation at all positions (Scheme 5). Addition of excess labeled Grignard causes further incorporation of deuterium into all positions of the tantalum complex. This suggests that an exchange occurs between the benzyl Grignard reagent and the tantalum bound benzyl groups in **6**. This process would clearly hinder the selective generation of mixed benzyl systems, hence no further attempts to synthetically access these were made.

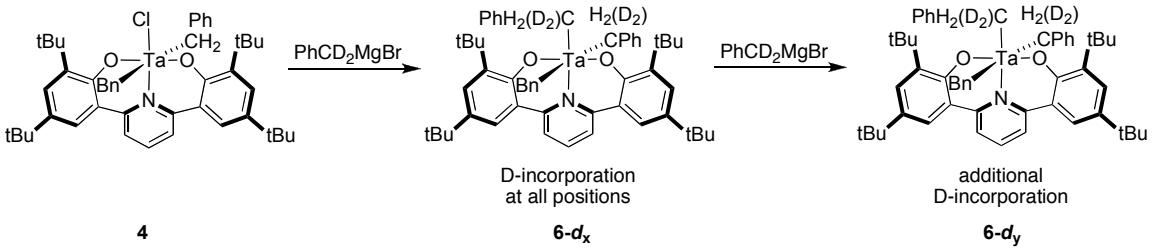

Scheme 5. Incorporation of labeled benzyl groups at all positions of **6**.

Synthesis of a tantalum complex supported by a thiophene linked diphenoxide $TaMe_3[(OC_6H_2\text{-}tBu_2)_2SC_4H_2]$ (11)

Following the success of metallating the pyridine-diphenolate ligand, five-member ring linkers have been investigated. A mixture of thiophene-2,5-diphenol (**3-B**) and $TaCl_2(CH_3)_3$ was allowed to stir at room temperature overnight. Only unreacted diphenol is observed by ^1H NMR spectroscopy. The increased steric bulk of the larger sulfur substituent is possibly the reason behind the reduced reactivity of the free phenol. The salt metathesis route proved

successful, however. Phenol deprotonation with KBn or $KN(SiMe_3)_2$, followed by reaction with $TaCl_2(CH_3)_3$ leads to the clean formation of one species assigned to $Ta(CH_3)_3[(OC_6H_2\text{-}tBu_2)_2SC_4H_2]$ (**11**, eq 2) based on ^1H NMR spectroscopy. Surprisingly, the ^1H NMR spectrum of **11** at room temperature shows only a broad peak corresponding to the TaCH_3 groups. A variable temperature ^1H NMR study revealed that at low temperatures (below –20 °C) the broad peak decoalesces into three singlets. This behavior is consistent with an exchange process for the methyl groups. The low temperature static structure displays three chemically different methyl groups.

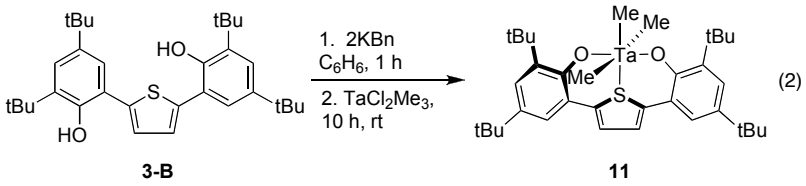

3-B **11** (2)

Complex **11** was characterizated crystallographically (Figure 12) and represents the first structurally characterized example of a thiophene tantalum complex. The Ta-S bond length (2.773(2) Å) is among the longest reported in the Cambridge Structural Database. Mononuclear tantalum(V) complexes displaying Ta-S bond lengths longer than 2.7 Å involve SEt_2 and $(PhSCH_2)_2$ adducts, trans to multiple bound ligands (alkylidene and sufide, respectively).[51,52] Complex **11** displays a meridional coordination mode of the thiophene-diphenolate moiety with a few notable features. The angle beween the thiophene plane and the TaS vector is 104°, significantly more acute than in the pyridine linked system. This could be due to two reasons. The bigger sulfur atom leads to a longer Ta-S distance which, in turn, rotates the thiophene ring away from tantalum.

Electronically, the degree of hybridization of sulfur is smaller compared to nitrogen and the involvement of the lone pair in aromatic delocalization is diminished. In consequence, the thiophene sulfur is more likely to coordinate to tantalum perpendicular to the ring rather than parallel. Another difference consists in the orientation of the tantalum methyl groups. Unlike in the pyridine-diphenolate system, the two methyl groups cis to the thiophene donor move closer to the methyl trans to sulfur (C34-Ta-C33 and C34-Ta-C35 are 76.2(2)° and 76.5(2)°, respectively). This could be due to the larger size of the sulfur compared to nitrogen which may force the methyl groups away from the thiophene donor. Interestingly, the three methyl groups and tantalum are not found in the same plane which leads to a lowering in symmetry from C_s to C_1. The solid-state structure is consistent with the low temperature ^{1}H NMR data, with all the tantalum methyl groups chemically different.

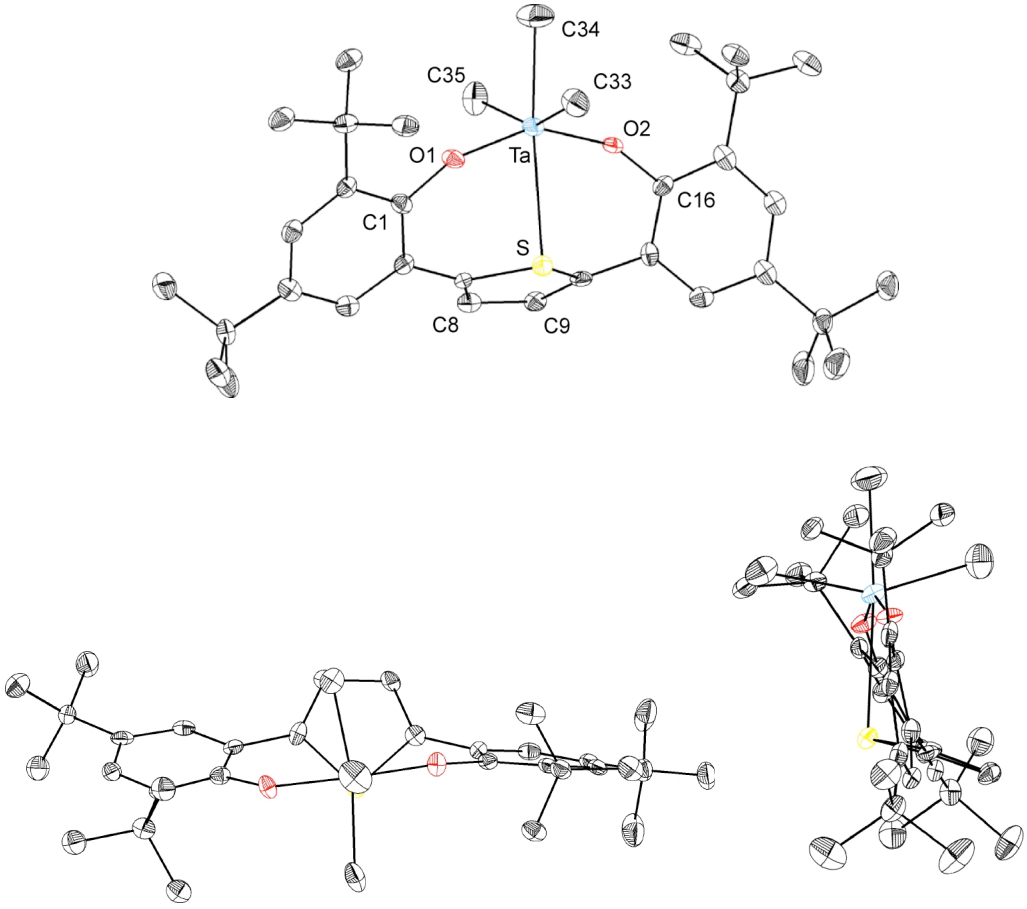

Figure 12. Structural drawing of **11**. Selected bond lengths (Å) and angles (°): Ta-O1 1.9119(38); Ta-O2 1.9136(34); Ta-C33 2.1676(66); Ta-C34 2.2164(65); Ta-C35 2.2179(62); Ta-S 2.7730(16); O2-Ta-O3 149.23(16); C34-Ta-C33 76.2(2); C34-Ta-C35 76.5(2); C16-O2-Ta 152.4(3); C1-O1-Ta 155.2(3); Ta-S-C8 103.6; Ta-S-C9 102.5.

Preparation of a tantalum complexes supported by the furan linked diphenoxide ligand

The furan linked diphenol (**3-C**) was found to metallate well via both alkane elimination and salt metathesis routes. A colorless benzene solution of $TaCl_2(CH_3)_3$ turns slightly orange upon addition of furan-2,5-diphenol and the color darkens upon stirring at room temperature for a few hours (eq 3). The desired product, $TaCl_2(CH_3)[(OC_6H_2\text{-}tBu_2)_2OC_4H_2]$ (**12**), was isolated as an orange powder upon precipitation from cold petroleum ether. The facile methane elimination route is in contrast to the behavior of the thiophene linked system lending further support to a steric argument for the observed reactivities. For the salt metathesis route, the potassium diphenolate was used in the reaction with $TaCl_2(CH_3)_3$, leading to the isolation of $Ta(CH_3)_3[(OC_6H_2\text{-}tBu_2)_2OC_4H_2]$ (**13**) as an off-white power. Similar to the trimethyl compounds supported by the pyridine and thiophene linked diphenolates, compound **13** displays an unexpected ^1H NMR spectrum; the three tantalum methyl groups show only one singlet at room temperature. A variable temperature ^1H NMR study revealed that lowering the temperature leads to a broadening of the Ta-CH_3 peak eventually leading to decoalescence around –55 °C. At –90 °C, the methyl groups display two sharp singlets in a two to one ratio. This behavior reflects a fluxional process as described above, which exchanges the methyl groups. The lowest energy structure relates to the one inferred for compound **5**, with two equivalent methyls and one different.

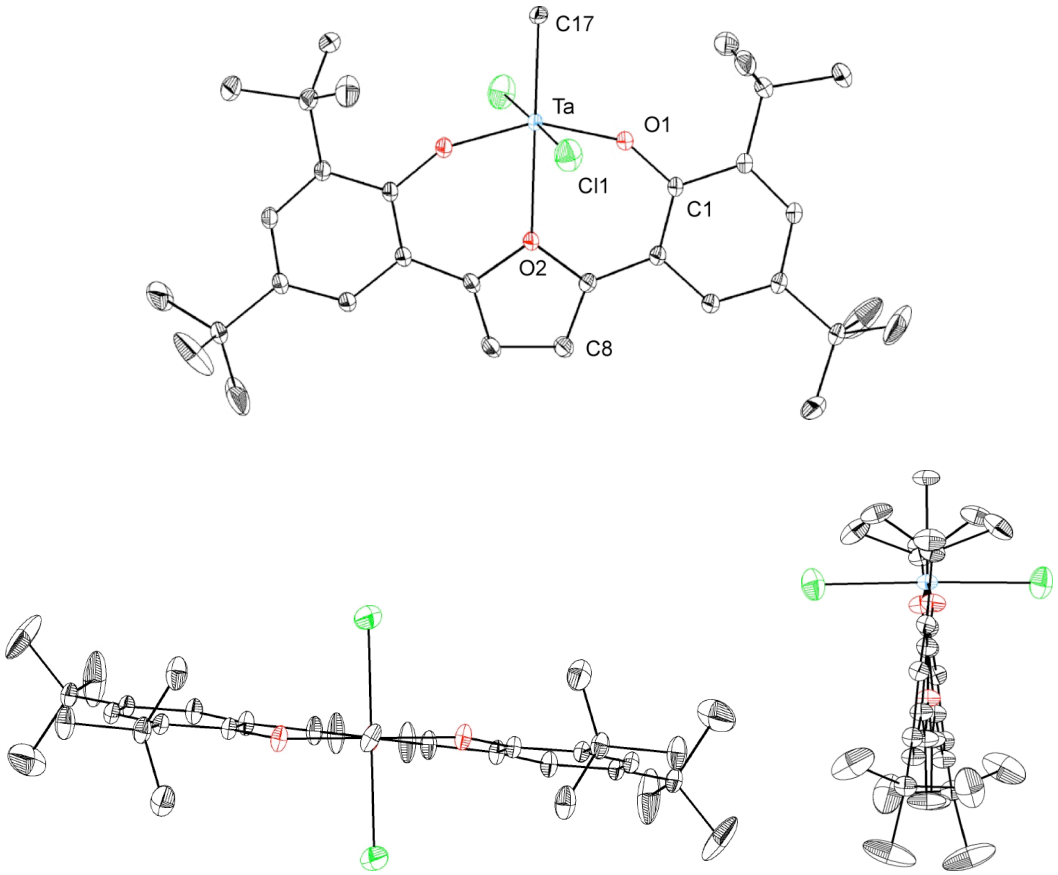

Figure 13. Structural drawing of **12**. Selected bond lengths (Å) and angles (°): Ta-O1 1.8692(14); Ta-C17 2.154(2); Ta-O3 2.4052(18); O1-Ta-O1A 152.34(9); C1-O1-Ta 150.10(12).

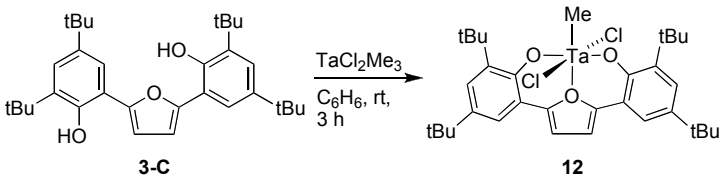

Complex **12**, which was studied by single-crystal X-ray diffraction (Figure 13), represents the first structurally characterized example of a furan tantalum complex. The Ta-O bond length (2.405(2) Å) is longer than a typical tantalum-

ether bond. Complex **12** displays a meridional coordination mode of the furan-diphenolate moiety. As the molecule is found on a C_2 crystallographic axis, the TaO vector lies in the plane of the furan ring. Given that the twist of the two phenolate rings is small (6° from the plane of the furan), this molecule is almost C_{2v} symmetric.

Solid-state binding modes of different diphenolate ligands

Single crystal X-ray diffraction studies allowed the determination of the solid-state structure and binding geometries for all the presented diphenolate ligands. In all the cases, the tridentate ligands were found to bind meridionally. However, different geometric distortions of the ligand framework were observed depending on the nature of the linker between the two phenoxides. The pyridine linked system has been crystallographically characterized in the context of several tantalum complexes displaying varied ligands, from different alkyls to halides to a benzylidine. For all these cases, the pyridine diphenolate framework adopts a C_s symmetric conformation. The pyridine bends away from the Ta-N vector to give angles of 143° to 151°. The N-Ta (2.43-2.48 Å) and O-Ta (1.89-1.94 Å) bond lengths remain relatively constant across the observed structures (Table 1). Changing the pyridine donor to a stronger, anionic, phenyl donor (Chapter 4) leads to a shortening of the Ta-donor bond (2.19-2.23 Å) and to an increase in the tantalum-donor-ring angle to 164-177°. This modification of structural parameters translates in a change in ligand geometry from C_s to C_2 symmetry indicating a strategy for affecting different ligand binding modes by altering the

binding abilities of the linker donor. The choice of a C_2 vs C_s structure seems to be a consequence of the strength of the interaction between the donor on the linked and the metal center. The distortion from a C_{2v} structure (all rings in the same plane) is probably due to the fact that the phenolate oxygens are too close together and the metal center cannot fit properly. Twisting around the aryl-aryl bonds to give either a C_2 or a C_s structure moves the oxygen donors further apart. Moving from six member ring linkers to five-member ring linkers while preserving the donor as a second row element (similar size) leads to an essentially C_{2v} symmetric structure (**12**). The angle between the Ta-O vector and the furan ring is 180°. The five-member ring increases the angle between the aryl-aryl linkages, essentially increasing the space between the two phenolate donors. This allows the metal center to fit in without significant rotation around the aryl-aryl bonds. The thiophene linked system displays the large sulfur donor which, in a C_{2v} geometry, is too close to the metal center. As a consequence, the thiophene ring tilts away from tantalum.

Table 1. Selected structural parameters for tantalum complexes supported by tridentate diphenolate ligands. The letters in square brackets refer to the types of donors in the diphenolate framework. C-C refers to the distance between the quaternary carbon atoms *ortho* to the phenolate oxygens.

Compound	Ta-O	Ta-Link	TaLC	OTaO	TaOC	C-C
$TaMe_3[NO_2]$	1.911(1) 1.902(1)	2.443(1)	147	163.45(5)	138.1(1) 141.7(1)	8.85
$TaBn_3[NO_2]$	1.896(1) 1.897(1)	2.430(1)	151	158.89(5)	145.2(1 145.5(1)	9.18
$TaBnF_2[NO_2]$	1.891(1) 1.891(1)	2.449(1)	143	158.28(5)	143.8(1) 144.4(1)	8.89
$Ta(CHPh)BnPR_3[NO_2]$	1.936(2) 1.910(2)	2.483(2)	150	159.17(6)	137.1(2) 145.3(2)	8.98
$TaCl_2(OEt_2)[CO_2]$*	1.883(1) 1.876(1)	2.187(2)	164	168.75(6)	145.3(1) 142.5(1)	9.02
$Ta(NCMetBu)_2[CO_2]$*	1.941(1) 1.952(1)	2.226(1)	177	166.30(5)	129.8(1) 133.2(1)	9.03
$TaCl_2Me[CHO_2]$*	1.859(4) 1.876(4)	2.801(2)	120	152.5(2)	149.9(4) 150.6(4)	8.84
$TaMe_3[SO_2]$	1.912(4) 1.914(3)	2.773(2)	104 103	149.2(2)	152.4(3) 155.2(3)	9.05
$TaCl_2Me[OO_2]$	1.869(1)	2.405(2)	180	152.34(9)	150.1(1)	9.02

* From Chapter 4

The ring parameters for a few studied and planned linkers were determined computationally in order to quantify some of the qualitative arguments in the above discussions (Table 2). The linker features relevant to the overall binding of the tridentate ligands include the angle (α) between the two ring-ring linkages, the distance (*b*) between the two atoms on the linker that bind to the phenolate ring, and the distance (*a*) between the donor on the linker and the "b" vector. The furan linker parameters represent the values for which a diphenolate system can accommodate a tantalum center without twist. Moving to the six-member ring donors (pyridine and phenyl), *b* becomes larger and *a* and α become smaller. While α changes in the direction of decreasing the space available for the metal center, parameters *a* and *b* change toward increasing it. Parameter α must be dominant in this case and bring the phenolates too close to the metal center for a C_{2v} geometry: the phenolate rings twist in order to accommodate the metal center, generating C_2 or C_s structures in the solid-state. Replacing the furan linker with thiophene increases significantly all three parameters above. The large value of *a* suggest that the tantalum center would not be able to bind to the ligand unless the sulfur moves away by tilting the thiophene ring, the observed structural feature.

Table 2. Ring parameters for various cyclic linkers (calculated with Spartan at the 6-31G** level of theory).

	α (°)	b (Å)	a (Å)
Pyridine	115	2.26	0.68
Benzene	120	2.40	0.69
Furan	126	2.16	0.80
Thiophene	149	2.47	1.21

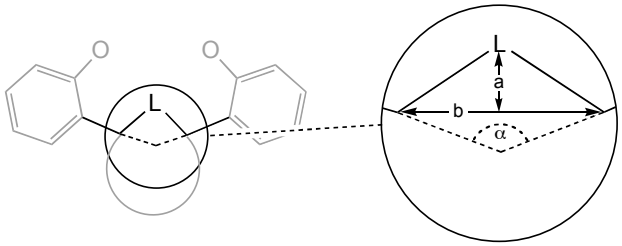

DFT studies

A computational study of models of compounds **5** and **11** was performed (Figures 15 and 16). Models with an ortho-t-butyl group and without t-butyl groups were employed. It was found that in both cases, the tilt of the linker was well reproduced. In the case of **5**, the solid-state structure displays a Ta-N distance of 2.44 Å. The computed values are 2.56 Å (no *ortho* substitution) and 2.49 Å (with *ortho* t-butyl groups). For **11**, the solid-state structure shows a Ta-S distance of 2.77 Å, while the calculated values are 2.95 Å (no *ortho* substitution) and 2.87 Å (with *ortho* t-butyl groups). The agreement between the experiment and computation is good and highlights the importance of using models similar to the real structure. In this case, the t-butyl groups are proposed to have a steric effect leading to a slight distortion of the ligand framework to bring the donor on the linker closer to the metal center. Interestingly, the calculations on models of

11 reproduce the distortion of the tantalum methyl groups but not the twist of one of the phenolates.

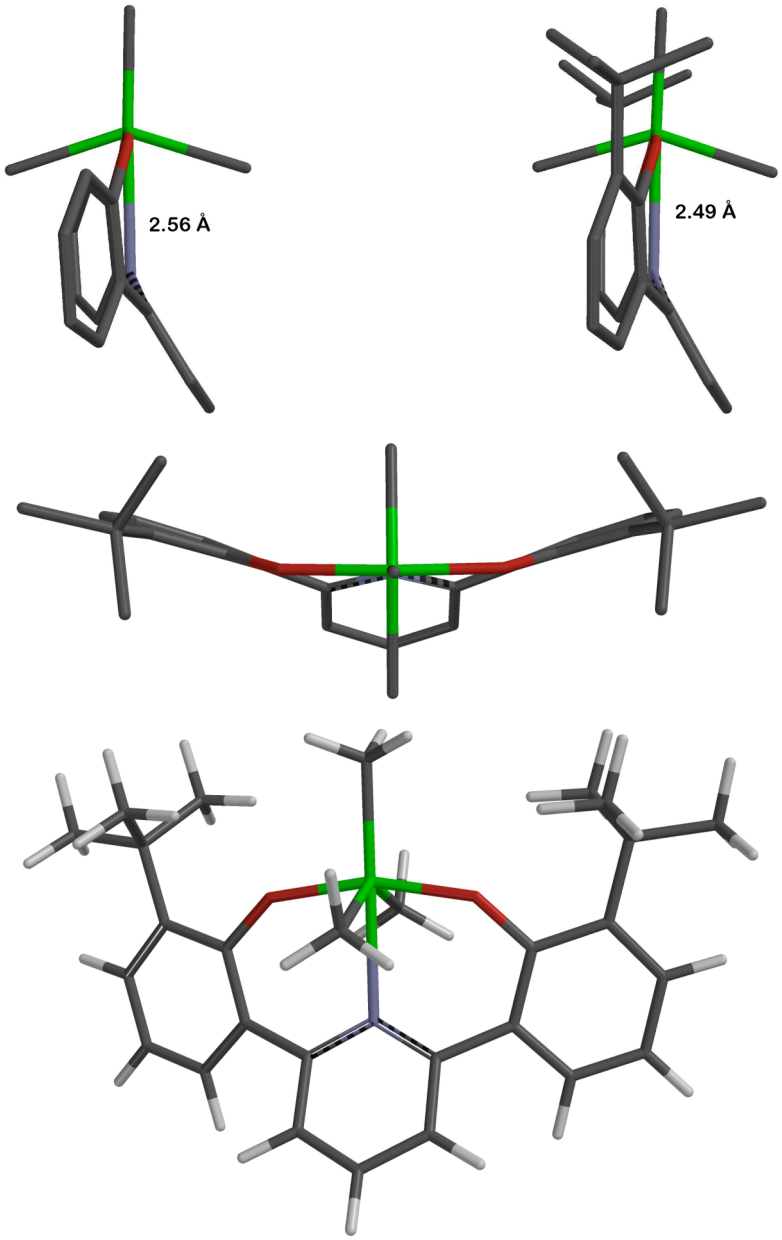

Figure 14. Optimized gas-phase structure of simplified models of complex **5** (with H and tBu substitution). Hydrogens are omitted in the top views, for clarity.

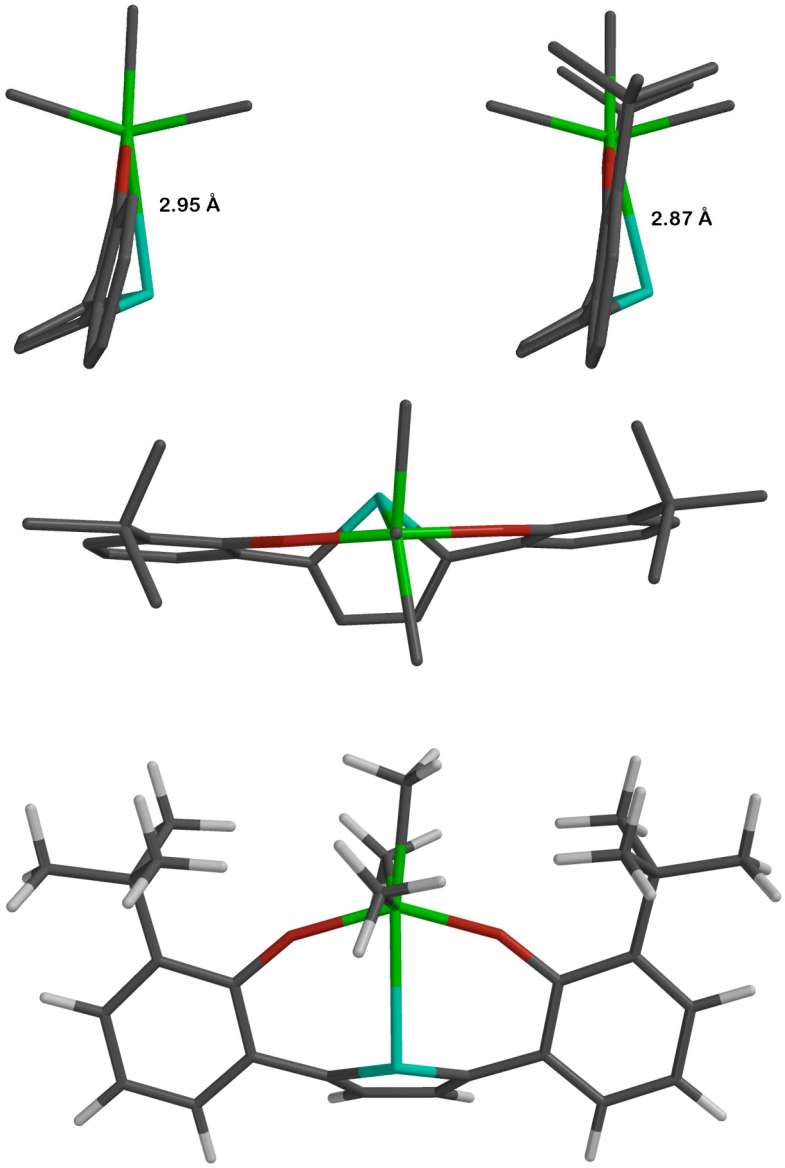

Figure 15. Optimized gas-phase structure of simplified models of complex **11** (with H and tBu substitution). Hydrogens are omitted in the top views, for clarity.

Exchange processes in the tantalum trimethyl species 5, 11, and 13

High temperature ^{1}H NMR spectra of compounds **5**, **11**, and **13**, show only one peak at high temperature, indicative of a fast exchange process. While the nature of this process is not well understood, it is noteworthy that a significant distortion of the diphenolate ligand framework is required for this process. The solid state structures display mer-binding of the tridentate ligand and, accordingly, mer binding of the three methyl groups. One mechanistic possibility involves twists of the trigonal faces of the octahedral structure (Scheme 6).[53,54] An alternative pathway could involve decoordination of the donor on the linker to generate a five-coordinate species which could undergo Berry pseudo-rotations. In order for the alkyl groups to exchange by either mechanism, they need to access a trigonal face of an octahedral (or trigonal bipyramid) structure. In this context, the two oxygens would have to be cis, a geometry that has not been documented in the present tantalum systems. Given the presence of aryl-aryl linkages in the multidentate framework, facial binding modes are expected to be strained and higher in energy than meridional binding modes. The observed sharp singlets at room temperature for **5** and **13** indicate that the present ligands are quite flexible, being able to attain easily transient facial geometries.

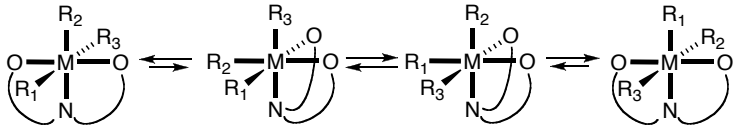

Scheme 6. Proposed mechanism for the exchange of alkyl groups (R) involving rotation of trigonal faces of the octahedron.

Conclusions

A series of diphenols connected at the *ortho* positions via semi-rigid, ring-ring linkages to a flat ring (pyridine, furan, thiophene) that presents another ligand was efficiently prepared and their ability to support tantalum chemistry has been investigated. Metallations were performed using salt metathesis and alkane elimination routes. The diphenolates were found to bind in a meridional fashion to give C_1, C_{2v}, and C_s ligand geometries. Variable temperature ^{1}H NMR studies of tantalum trimethyl species indicate that, in solution, these complexes are fluxional leading to exchange of the methyl groups. A tantalum tribenzyl species supported by the pyridine diphenolate framework undergoes α-H abstraction upon heating to over 90 °C in the presence of Lewis bases. The mechanism of this process was investigated kinetically at several temperatures and with different phosphine concentrations. The first order rate constant for the disappearance of the trialkyl species was found to be independent on phosphine concentration and the isotope effect at 125 °C was found to be $k_H/k_D = 4.9 \pm 0.4$. These findings are consistent with a mechanism involving rate determining α-H abstraction in the six-cordinate species to give a five-coordinate benzylidene which is trapped by the phosphine in a fast step. Overall, the present ligand frameworks have been found to be thermally robust and to support tantalum alkyl and alkylidene motifs lending promise to further studies and reaction development based on these architectures.

Experimental Section

General Considerations and Instrumentation. All air- and moisture-sensitive compounds were manipulated using standard vacuum line, Schlenk, or cannula techniques or in a drybox under a nitrogen atmosphere. Solvents for air- and moisture-sensitive reactions were dried over sodium benzophenone ketyl or by the method of Grubbs.[55] Benzene-d_6 was purchased from Cambridge Isotopes and distilled from sodium benzophenone ketyl. Chloroform-d_1 and dichloromethane-d_2 were purchased from Cambridge Isotopes and distilled from calcium hydride. MOM protected phenol **1a** was prepared as described in Chapter 4. Other materials were used as received. Elemental analyses were performed by Desert Analytics, Tucson, AZ. ^{1}H and ^{13}C NMR spectra were recorded on Varian Mercury 300, or Varian INOVA-500 spectrometers and unless otherwise indicated at room temperature. Chemical shifts are reported with respect to internal solvent: 7.16 and 128.38 (t) ppm (C_6D_6); 7.27 and 77.23 (t) ppm ($CDCl_3$); 5.32 (t) and 54.00 (q) ppm (CD_2Cl_2); for ^{1}H and ^{13}C data.

Preparation of 1b. A procedure similar to the preparation of **1a** (Chapter 4) was utilized. Yield 90% (16.9 g) starting from 2-bromo-4,6-di-t-butyl-phenol. ^{1}H NMR (300 MHz, $CDCl_3$) δ: 0.07 (s, 9H, Si(C*H*$_3$)$_3$), 1.06 (s, 2H, OCH$_2$C*H*$_2$Si), 1.30 (s, 9H, C(C*H*$_3$)$_3$), 1.44 (s, 9H, C(C*H*$_3$)$_3$), 3.98 (s, 2H, OC*H*$_2$CH$_2$Si), 5.26 (s, 2H, OC*H*$_2$O), 7.31 (d, 2H, aryl-*H*), 7.40 (d, 2H, aryl-*H*). ^{13}C NMR (75 MHz, $CDCl_3$) δ: -1.2 (Si(*C*H$_3$)$_3$), 18.4 (Si*C*H$_2$), 31.1 (C(*C*H$_3$)$_3$), 31.5 (C(*C*H$_3$)$_3$), 34.8 (*C*(CH$_3$)$_3$), 36.1 (*C*(CH$_3$)$_3$), 67.8 (OCH$_2$CH$_2$), 97.8 (OCH$_2$O), 117.8, 124.1, 128.9, 144.6, 147.6, 150.7 (aryl).

Preparation of protected diphenols. The Negishi coupling procedure (Chapter 4) was employed.

2aA. ^{1}H NMR (300 MHz, $CDCl_3$) δ: 1.37 (s, 18H, C(CH_3)$_3$), 1.51 (s, 18H, C(CH_3)$_3$), 3.41 (s, 6H, OCH_3), 4.64 (s, 4H, OCH_2O), 7.45 (d, 2H, aryl-*H*), 7.61 (d, 2H, aryl-*H*), 7.68-7.80 (m, 3H, NC$_5H_3$). ^{13}C NMR (75 MHz, $CDCl_3$) δ: 31.1 (C(*C*H$_3$)$_3$), 31.6 (C(*C*H$_3$)$_3$), 34.8 (*C*(CH$_3$)$_3$), 35.6 (*C*(CH$_3$)$_3$), 57.6 (OCH$_3$), 99.7 (OCH$_2$O), 123.2, 125.2, 126.7, 134.1, 136.1, 142.5, 146.1, 151.5, 158.4 (aryl).

2aB. ^{1}H NMR (300 MHz, $CDCl_3$) δ: 1.35 (s, 18H, C(CH_3)$_3$), 1.50 (s, 18H, C(CH_3)$_3$), 3.51 (s, 6H, OCH_3), 4.80 (s, 4H, OCH_2O), 7.28 (s, 2H, SC$_4H_2$), 7.31 (d, 2H, aryl-*H*), 7.38 (d, 2H, aryl-*H*). ^{13}C NMR (75 MHz, $CDCl_3$) δ: 31.1 (C(*C*H$_3$)$_3$), 31.7 (C(*C*H$_3$)$_3$), 34.8 (*C*(CH$_3$)$_3$), 35.7 (*C*(CH$_3$)$_3$), 57.7 (OCH$_3$), 98.5 (OCH$_2$O), 124.5, 126.5, 127.0, 128.2, 141,8, 143.0, 146.2, 151.1 (aryl).

2bC. ^{1}H NMR (300 MHz, $CDCl_3$) δ: 0.02 (s, 9H, Si(CH_3)$_3$), 0.97 (s, 2H, OCH$_2$CH_2Si), 1.34 (s, 9H, C(CH_3)$_3$), 1.48 (s, 9H, C(CH_3)$_3$), 3.83 (s, 2H, OCH_2CH$_2$Si), 4.93 (s, 2H, OCH_2O), 6.95 (s, 2H, OC$_4H_2$), 7.34 (d, 2H, aryl-*H*), 7.65 (d, 2H, aryl-*H*). ^{13}C NMR (75 MHz, $CDCl_3$) δ: -1.2 (Si(*C*H$_3$)$_3$), 18.4 (SiCH$_2$), 31.2 (C(*C*H$_3$)$_3$), 31.6 (C(*C*H$_3$)$_3$), 34.8 (*C*(CH$_3$)$_3$), 35.7 (*C*(CH$_3$)$_3$), 67.7 (OCH$_2$CH$_2$), 97.0 (OCH$_2$O), 111.3, 123.4, 124.4, 124.8, 143.1, 146.0, 150.3, 150.7 (aryl). HRMS $C_{44}H_{72}Si_2O_5$: Calcd mass: 736.4918. Measured mass: 736.4923.

2aD. ^{1}H NMR (300 MHz, $CDCl_3$) δ: 1.35 (s, 18H, C(CH_3)$_3$), 1.50 (s, 18H, C(CH_3)$_3$), 3.06 and 3.43 (singlets, 6H each, N(CH_3)$_2$ and OCH_3), 4.71 (s, 4H, OCH_2O) 6.95 (s, 2H, NC$_5H_2$), 7.43 (d, 2H, aryl-*H*), 7.55 (d, 2H, aryl-*H*). ^{13}C NMR (75 MHz, $CDCl_3$) δ: 31.1 (C(*C*H$_3$)$_3$), 31.7 (C(*C*H$_3$)$_3$), 34.8 (*C*(CH$_3$)$_3$), 35.6 (*C*(CH$_3$)$_3$), 39.6 (N(*C*H$_3$)$_2$), 57.5

(OCH_2O), 99.1 (OCH_3), 106.5, 124.6, 126.7, 134.9, 142.2, 145.7, 151.1, 155.0, 158.4 (aryl).

Removal of MOM protecting group. The procedure presented in Chapter 4 was employed.

3A. ^{1}H NMR (300 MHz, $CDCl_3$) δ: 1.39 (s, 18H, C(CH_3)$_3$), 1.48 (s, 18H, C(CH_3)$_3$), 7.46 (d, 2H, aryl-*H*), 7.51 (d, 2H, aryl-*H*), 7.67 (d, 2H, 3,5-NC_5H-H_2), 8.01 (t, 1H, 4-NC_5H_2-*H*), 10.59 (s, 2H, O*H*). ^{13}C NMR (75 MHz, $CDCl_3$) δ: 29.8 (C(*C*H$_3$)$_3$), 31.8 (C(*C*H$_3$)$_3$), 34.6 (*C*(CH$_3$)$_3$), 35.6 (*C*(CH$_3$)$_3$), 120.5, 121.3, 123.0, 126.4, 137.5, 140.0, 141.5, 153.3, 157.6 (aryl). HRMS $C_{33}H_{45}O_2N$: Calcd mass: 487.3450. Measured mass: 487.3446. Yield: 74% over two steps.

3B. ^{1}H NMR (300 MHz, C_6D_6) δ: 1.30 (s, 18H, C(CH_3)$_3$), 1.61 (s, 18H, C(CH_3)$_3$), 5.57 (s, 2H, O*H*). 6.72 (s, 2H, SC_4H_2), 7.41 (d, 2H, aryl-*H*), 7.54 (d, 2H, aryl-*H*). ^{13}C NMR (75 MHz, $CDCl_3$) δ: 29.9 (C(*C*H$_3$)$_3$), 31.8 (C(*C*H$_3$)$_3$), 34.6 (*C*(CH$_3$)$_3$), 35.4 (*C*(CH$_3$)$_3$), 120.4, 125.0, 125.4, 127.3, 136.0 (aryl). HRMS $C_{32}H_{44}O_2S$: Calcd mass: 492.3062. Measured mass: 492.3067. Yield: 69% over two steps.

3D. ^{1}H NMR (300 MHz, $CDCl_3$) δ: 1.43 (s, 18H, C(CH_3)$_3$), 1.52 (s, 18H, C(CH_3)$_3$), 3.20 (s, 6H, N(CH_3)$_2$), 6.82 (s, 2H, NC_5H_2), 7.46 (d, 2H, aryl-*H*), 7.51 (d, 2H, aryl-*H*), 11.1 (s, 2H, O*H*). ^{13}C NMR (75 MHz, $CDCl_3$) δ: 29.8 (C(*C*H$_3$)$_3$), 31.9 (C(*C*H$_3$)$_3$), 34.5 (*C*(CH$_3$)$_3$), 35.5 (*C*(CH$_3$)$_3$), 39.6 (N(*C*H$_3$)$_2$), 103.2, 122.4, 122.5, 125.7, 137.1, 140.9, 153.5, 156.9, 157.7 (aryl). HRMS $C_{35}H_{50}O_2N_2$: Calcd mass: 530.3872. Measured mass: 530.3863. Yield: 88% over two steps.

Preparation of compound 3C. Compound **2bC** (1.5 g, 2 mmol, 1 equiv) was dissolved in HMPA (50 mL) and a THF solution of $(nBu)_4NF$ (1 M in THF with 5% water, 20.4 mL, 10 equiv). The color of the mixture gradually changed from colorless to orange to green. After two days of stirring at room temperature, water was added and an CH_2Cl_2 extraction was performed. Organic fractions were dried over $MgSO_4$ and filtered, and volatile materials were removed by rotary evaporation. Remaining HMPA was removed Kugelrohr distillation. Recrystalization from CH_3CN provides the **3C** as a white powder (0.7645 g, 1.6 mmol, 80% yield). ^{1}H NMR (500 MHz, $CDCl_3$) δ: 1.35 (s, 18H, $C(CH_3)_3$), 1.48 (s, 18H, $C(CH_3)_3$), 6.58 and 6.79 (s, 2H each, O*H* and OC_4H_2), 7.35 (d, 2H, aryl-*H*), 7.39 (d, 2H, aryl-*H*). ^{13}C NMR (125 MHz, $CDCl_3$) δ: 29.9 ($C(CH_3)_3$), 31.7 ($C(CH_3)_3$), 34.6 ($C(CH_3)_3$), 35.4 ($C(CH_3)_3$), 109.1, 116.6, 122.0, 125.0, 136.8, 142.7, 149.6, 152.1 (aryl). HRMS $C_{32}H_{44}O_3$: Calcd mass: 476.3290. Measured mass: 476.3314.

Synthesis of 4. KBn (139 mg, 1.07 mmol, 2 equiv) was added with the aid of C_6H_6 (5 mL) to a solution of 3A (260 mg, 0.534 mmol, 1 equiv) in C_6H_6 (10 mL). This mixture was allowed to stir at room temperature for 2 h during which the orange KBn dissolved and discolored to lead to the formation of a colorless emulsion of phenolate. A C_6H_6 solution of $TaCl_3(CH_2Ph)_2$ (250 mg, 0.534 mmol, 1 equiv) was added and the reaction mixture was allowed to stir at room temperature for 5 h. Salts were removed by filtration through a bed of Celite and volatile materials were removed under vacuum. The resulting residue was suspended in petroleum ether and the mixture was cooled to -35 °C. The desired product was collected by filtration as an orange solid and was washed with cold petroleum

ether. This procedure affords 0.460 g (97% yield) of **4**. ^{1}H NMR (500 MHz, CD_2Cl_2) δ: 1.40 (s, 18H, C(CH_3)$_3$), 1.60 (s, 18H, C(CH_3)$_3$), 2.39 (s, 4H, Ta(CH_2)$_2$), 6.26 (d, 4H, *o*-C_6H_3-H_2), 6.60-6.67 (m, 6H, *m*- and *p*-C_6H_2-H_3), 7.23 (d, 2H, aryl-*H*), 7.60 (d, 2H, aryl-*H*), 7.74 (d, 2H, 3,5-NC_5H-H_2), 7.84 (t, 1H, NC_5H_2-*H*). ^{13}C NMR (125 MHz, CD_2Cl_2) δ: 30.6 (C(*C*H_3)$_3$), 31.9 (C(*C*H_3)$_3$), 35.2 (*C*(CH$_3$)$_3$), 35.7 (*C*(CH$_3$)$_3$), 75.2 (Ta*C*H$_2$), 125.3, 125.6, 127.2, 127.66, 127.68, 129.0, 131.2, 138.6, 139.0, 141.6, 145.1, 152.1, 156.1 (aryl). Anal. calcd. for $C_{47}H_{57}ClNO_2Ta$ (%): C, 63.83; H, 6.50; N, 1.58. Found: C, 63.53; H, 6.55; N, 1.58.

Synthesis of 5. KBn (85.2 mg, 0.66 mmol, 2 equiv) was added with the aid of C_6H_6 (4 mL) to a solution of **3A** (159.6 mg, 0.33 mmol, 1 equiv) in C_6H_6 (4 mL). This mixture was allowed to stir at room temperature for 0.5 h which afforded a pale gray mixture of deprotonated phenol. A C_6H_6 solution of $TaCl_2(CH_3)_3$ (97.3 mg, 0.33 mmol, 1 equiv) was added and the reaction mixture was allowed to stir at room temperature for 4 h. Salts were removed by filtration through a bed of Celite. Volatile materials were removed under vacuum to give the desired product as a white powder. ^{1}H NMR (500 MHz, CD_2Cl_2) δ: 0.40 (s, 9H, Ta(CH_3)$_3$), 1.37 (s, 18H, C(CH_3)$_3$), 1.61 (s, 18H, C(CH_3)$_3$), 7.37 (d, 2H, aryl-*H*), 7.56 (d, 2H, aryl-*H*), 7.70 (d, 2H, NC_5H-H_2), 7.92 (t, 1H, NC_5H_2-*H*). ^{1}H NMR (500 MHz, CD_2Cl_2 ,-90 °C) δ: -0.01 (s, 6H, Ta*C*H$_3$), 0.79 (s, 3H, Ta*C*H$_3$). ^{1}H NMR (500 MHz, C_6D_6) δ: 0.90 (s, 9H, Ta(CH_3)$_3$), 1.33 (s, 18H, C(CH_3)$_3$), 1.73 (s, 18H, C(CH_3)$_3$), 7.03 (t, 1H, NC_5H_2-*H*), 7.24 (d, 2H, NC_5H-H_2), 7.34 (d, 2H, aryl-*H*), 7.73 (d, 2H, aryl-*H*). ^{13}C NMR (125 MHz, CD_2Cl_2) δ: 30.2 (C(*C*H$_3$)$_3$), 31.9 (C(*C*H$_3$)$_3$), 35.0 (*C*(CH$_3$)$_3$), 35.9 (*C*(CH$_3$)$_3$), 56.1 (Ta*C*H$_3$), 124.8, 126.3, 127.4, 128.7, 138.9, 139.2, 144.2, 153.5, 156.9

(aryl). Anal. calcd. for $C_{36}H_{52}NO_2Ta$ (%): C, 60.75; H, 7.36; N, 1.97. Found: C, 60.77; H, 7.35; N, 1.97.

Synthesis of 6 from $TaCl_2(CH_2Ph)_3$. KBn (78.5 mg, 0.604 mmol, 2 equiv) was added with the aid of C_6H_6 (4 mL) to a solution of **3A** (147 mg, 0.302 mmol, 1 equiv) in C_6H_6 (4 mL). This mixture was allowed to stir at room temperature for 1.5 h which afforded a colorless mixture of deprotonated phenol. A C_6H_6 solution of $TaCl_2(CH_2Ph)_3$ (158.5 mg, 0.302 mmol, 1 equiv) was added and the reaction mixture was allowed to stir at room temperature for 10 h. Salts were removed by filtration through a bed of Celite and volatile materials were removed under vacuum. The resulting residue was suspended in petroleum ether and the mixture was cooled to -35 °C. The desired product was collected by filtration and washed with cold petroleum ether. This procedure affords 168 mg (59% yield) of **6** as an orange powder.

Synthesis of 6 from $Ta(CH_2Ph)_5$. A C_6H_6 solution of **3A** (314.6 mg, 0.646 mmol, 1 equiv) was added to a Schlenk bomb charged with a solution of $Ta(CH_2Ph)_5$ (411 mg, 0.646 mmol, 1 equiv) in C_6H_6 (20 mL total volume). The flask was sealed, immersed in an oil bath at 60 °C, and stirred for 5 h. Volatile materials were removed under vacuum and petroleum ether was added and the mixture was stored at -35 °C. Compound **6** was collected by filtration and washed with cold petroleum ether (484 mg, 79% yield). ^{1}H NMR (500 MHz, C_6D_6) δ: 1.35 (s, 18H, $C(CH_3)_3$), 1.78 (s, 18H, $C(CH_3)_3$), 3.08 (s, 4H, $TaCH_2$), 3.88 (s, 2H, $TaCH_2$), 6.25 (t, 2H, aryl-*H*), 6.36 (t, 4H, aryl-*H*), 6.45 (d, 4H, aryl-*H*), 6.69 (t, 1H, aryl-*H*), 7.04-7.06 (m, 3H, aryl-*H* overlap), 7.18 (d, 2H, aryl-*H*), 7.52 (t, 2H, aryl-*H*), 7.72 (t, 2H, aryl-

H), 7.78 (t, 2H, aryl-*H*). ^{13}C NMR (125 MHz, C_6D_6) δ: 31.1 (C(CH_3)$_3$), 32.1 (C(CH_3)$_3$), 35.0 (*C*(CH_3)$_3$), 36.0 (*C*(CH_3)$_3$), 73.5 (TaCH_2), 81.6 (TaCH_2), 122.9, 124.7, 125.2, 126.6, 127.2, 127.8, 128.0, 128.3, 129.2, 132.1, 138.1, 139.3, 143.1, 144.8, 152.3, 154.8, 156.9 (aryl). Anal. calcd. for $C_{54}H_{64}NO_2Ta$ (%): C, 68.99; H, 6.86; N, 1.49. Found: C, 69.10; H, 7.38; N, 1.49.

Synthesis of 7. A solution of phenol **3a** (100 mg, 0.205 mmol, 1 equiv) in C_6H_6 (3 mL) was added to a solution of $TaCl_2(CH_3)_3$ (31.2 mg, 0.205 mmol, 1 equiv) in C_6H_6 (3 mL). The reaction mixture was allowed to stir for 10 h at room temperature. Volatile materials were removed under vacuum and the desired product was crystallized precipitated from petroleum ether at -35 °C. Compound **7** was obtained as an orange powder (153 mg, 97% yield) upon collection by filtration. ^{1}H NMR (500 MHz, CD_2Cl_2) δ: 1.39 (s, 18H, C(CH_3)$_3$), 1.63 (s, 18H, C(CH_3)$_3$), 7.51 (d, 2H, aryl-*H*), 7.70 (d, 2H, aryl-*H*), 8.05 (d, 2H, NC_5H-H_2), 8.22 (t, 1H, NC_5H_2-*H*). ^{13}C NMR (125 MHz, CD_2Cl_2) δ: 30.4 (C(CH_3)$_3$), 31.9 (C(CH_3)$_3$), 35.3 (*C*(CH_3)$_3$), 35.7 (*C*(CH_3)$_3$), 126.0, 126.5, 127.7, 128.9, 138.7, 142.1, 147.4, 151.3, 157.3 (aryl).

Synthesis of 8. A solution of phenol **3A** (101 mg, 0.207 mmol, 1 equiv) in C_6H_6 (3 mL) was added to a solution of $TaCl_2(CH_3)_3$ (61.6 mg, 0.207 mmol, 1 equiv) in C_6H_6 (3 mL). The reaction mixture was allowed to stir at room temperature for 3 h. Volatile materials were removed under vacuum to give the desired product as a yellow powder. ^{1}H NMR (500 MHz, CD_2Cl_2) δ: 1.39 (s, 18H, C(CH_3)$_3$), 1.70 (s, 18H, C(CH_3)$_3$), 1.82 (s, 3H, TaCH_3), 7.45 (d, 2H, aryl-*H*), 7.68 (d, 2H, aryl-*H*), 7.86 (d, 2H, NC_5H-H_2), 8.10 (t, 1H, NC_5H_2-*H*). ^{13}C NMR (125 MHz, CD_2Cl_2) δ: 30.7

($C(CH_3)_3$), 31.9 ($C(CH_3)_3$), 35.2 ($C(CH_3)_3$), 35.9 ($C(CH_3)_3$), 68.3 ($TaCH_3$), 125.4, 126.7, 127.0, 128.2, 138.3, 141.3, 146.7, 151.8, 157.7 (aryl).

Reaction of 6 with $[Ph_3C][BF_4]$. A toluene solution of **6** (50.8 mg, 54 μmol, 1 equiv) was added to slurry of $[Ph_3C][BF_4]$ (17.8 mg, 54 μmol, 1 equiv) in toluene. The reaction mixture, initially cloudy and orange, changes to yellow within two hours, as the insoluble $[Ph_3C][BF_4]$ reacts and dissolves. Volatile materials were removed under vacuum and the residue was suspended in petroleum ether and cooled to -35 °C. A precipitate was collected by filtration, washed with cold petroleum ether, and dried under vacuum to give **9** as an off-white powder. ^{19}F NMR (282 MHz, toluene) δ: 148.7. ^1H NMR (300 MHz, C_6D_6) δ: 1.30 (s, 18H, $C(CH_3)_3$), 1.61 (s, 18H, $C(CH_3)_3$), 3.81 (br t, J_{HF}=5.3 Hz, 2H, $TaCH_2$), 6.86-6.96 (app t, 2H, aryl-*H*), 7.08 (d, 2H, aryl-*H*), 7.28 (t, 2H, aryl-*H*), 7.51 (d, 2H, aryl-*H*), 7.68 (d, 2H, aryl-*H*).

Synthesis of 10-P. A toluene (5 mL) solution of **6** (115 mg, 0.122 mmol, 1 equiv) and PMe_2Ph (84.5 mg, 0.612 mmol, 5 equiv) was placed in a Schlenk flask fitted with a Screw in Teflon stopper. The flask was sealed and immersed in an oil bath at 125 °C. Upon stirring for 5 hours, the mixture was allowed to cool to room temperature and volatile materials were removed under vacuum. Petroleum ether was added and desired product was recrystallized at -35 °C. Collection by filtration affords 55.4 mg (46% yield) of **10-P**. ^1H NMR (500 MHz, CD_2Cl_2) δ: 1.10 (br s, 6H, $P(CH_3)_2$), 1.41 (s, 18H, $C(CH_3)_3$), 1.60 (s, 18H, $C(CH_3)_3$), 2.20 (s, 2H, $TaCH_2$), 5.96 (d, 2H, aryl-*H*), 6.23 (t, 1H, aryl-*H*), 6.40 (t, 2H, aryl-*H*), 6.79 (t, 1H, aryl-*H*), 6.9-7.2 (br s and sharp d and t, 9H, aryl-*H*), 7.31 (t, 2H, aryl-*H*), 7.46 (d,

2H, aryl-*H*), 7.55 (d, 2H, aryl-*H*), 7.68 (t, 1H, aryl-*H*), 8.59 (s, 1H, TaCHPh). ^{13}C NMR (125 MHz, CD_2Cl_2) δ: 13.8 (br $P(CH_3)_2$), 30.6 ($C(CH_3)_3$), 32.0 ($C(CH_3)_3$), 35.0 ($C(CH_3)_3$), 35.9 ($C(CH_3)_3$), 60.6 (br $TaCH_2$), 119.7, 124.3, 124.6, 126.3, 126.6, 126.9, 127.1, 128.0, 128.4, 128.5, 129.1 (br), 130.8, 130.9, 131.0, 137.7, 139.0, 143.6, 148.3, 153.1, 153.7, 158.7 (aryl), 243.0 (TaCHPh).

Kinetic measurements for the conversion of 6 to 10-P. Stock solutions containing **6** ($1.22 \bullet 10^{-2}$ M) and PMe_2Ph ($4.88 \bullet 10^{-2}$ to $73.2 \bullet 10^{-2}$ M) were prepared in xylene-d_{10} and stored at -35 ºC. The NMR probe was brought to the desired temperature and calibrated with an ethylene glycol standard. A J-Young tube charged with the solution of **6** was utilized in these experiments. The decay of the Ta-CH_2Ph peak was integrated against residual CD_2H in the deuterated solvent. The data was plotted using Microsoft Excel. Typical NMR spectroscopic data for the kinetic runs is presented in Figure 16.

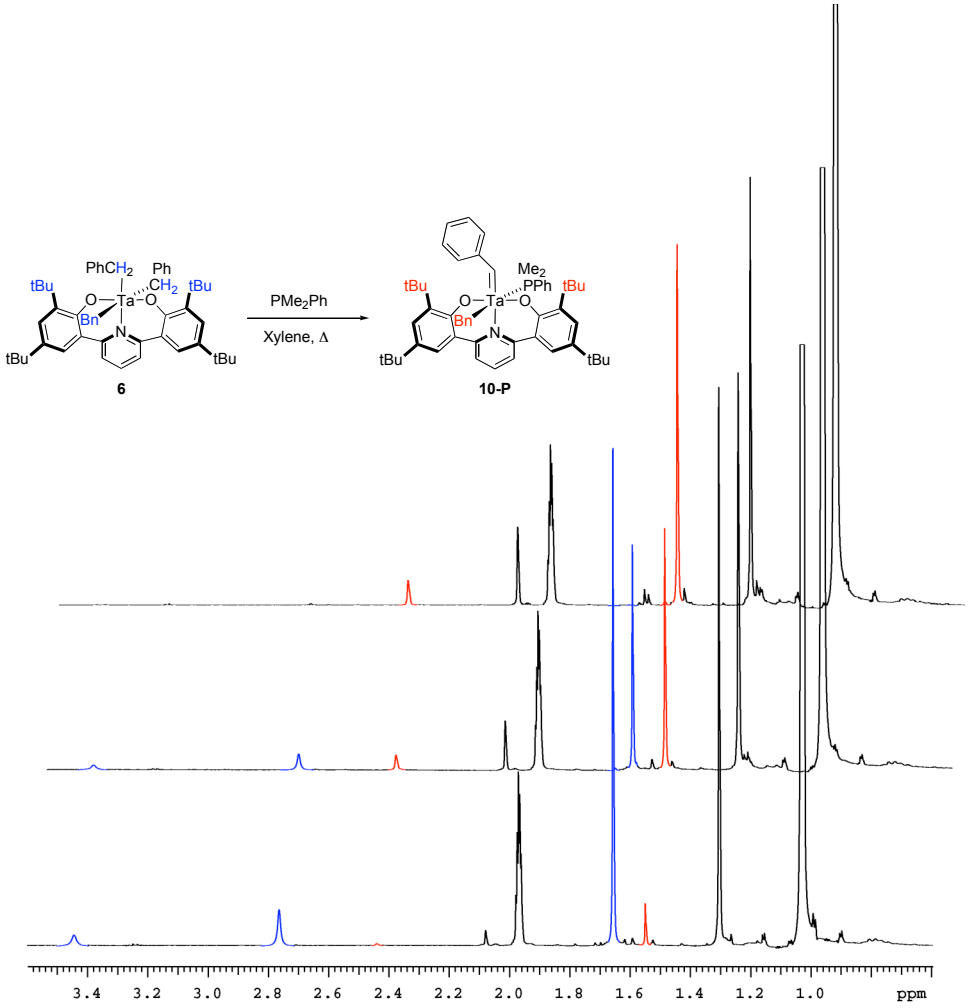

Figure 16. ^{1}H NMR spectra for the conversion of **6** to **10-P** (time increases from bottom to top).

Synthesis of 11. KBn (52.8 mg, 0.406 mmol, 2 equiv) was added with the aid of C_6H_6 (2 mL) to a solution of **3B** (100 mg, 0.203 mmol, 1 equiv) in C_6H_6 (5 mL). This mixture was allowed to stir at room temperature for 5 h. The orange KBn discolored to give a phosphorescent pale green mixture. $TaCl_2(CH_3)_3$ (60.4 mg, 0.203 mmol, 1 equiv) in C_6H_6 (5 mL) was added and the reaction mixture stirred

at room temperature to give a pale yellow solution. Salts were removed by filtration through a bed of Celite. Volatile materials were removed under vacuum and petroleum ether was added to the residue. Upon cooling to -35 °C, the desired product was collected as a very pale yellow powder (43.2 mg, 28%yield). ^{1}H NMR (500 MHz, CD_2Cl_2) δ: 1.01 (v br s, 9H, TaCH_3), 1.37 (s, 18H, C(CH_3)$_3$), 1.46 (s, 18H, C(CH_3)$_3$), 7.14 (s, 2H, SC$_4H_2$), 7.50 (d, 2H, aryl-*H*), 7.52 (d, 2H, aryl-*H*). ^{1}H NMR (500 MHz, CD_2Cl_2, -55 °C) δ: 0.40 (s, 3H, TaCH_3), 1.06 (s, 3H, TaCH_3), 1.25 (s, 3H, TaCH_3). ^{13}C NMR (125 MHz, CD_2Cl_2) δ: 30.4 (C(*C*H$_3$)$_3$), 31.8 (C(*C*H$_3$)$_3$), 35.1 (*C*(CH$_3$)$_3$), 35.8 (*C*(CH$_3$)$_3$), 123.3, 124.7, 126.1, 130.7, 139.2, 141.1, 145.4, 158.1 (aryl). Anal. calcd. for $C_{35}H_{51}O_2STa$ (%): C, 59.00; H, 6.91. Found: C, 58.65; H, 7.17.

Synthesis of 12. A solution of phenol **3C** (50.2 mg, 0.105 mmol, 1 equiv) in C_6H_6 (5 mL) was added to a solution of $TaCl_2(CH_3)_3$ (31.2 mg, 0.105 mmol, 1 equiv) in C_6H_6 (5 mL). The reaction mixture was allowed to stir at room temperature. Volatile materials were removed under vacuum and the desired product was crystallized as an orange solid (53 mg, 68% yield) from petroleum ether at -35 °C. ^{1}H NMR (500 MHz, CD_2Cl_2) δ: 1.42 (s, 18H, C(CH_3)$_3$), 1.75 (s, 18H, C(CH_3)$_3$), 2.11 (s, 3H, TaCH_3), 7.28 (s, 2H, OC$_4H_2$), 7.64 (d, 2H, aryl-*H*), 7.75 (d, 2H, aryl-*H*). ^{1}H NMR (500 MHz, CD_2Cl_2, -55 °C) δ: -0.16 (s, 6H, TaCH_3), 0.89 (s, 3H, TaCH_3). ^{13}C NMR (125 MHz, CD_2Cl_2) δ: 30.7 (C(*C*H$_3$)$_3$), 31.8 (C(*C*H$_3$)$_3$), 35.3 (*C*(CH$_3$)$_3$), 36.0 (*C*(CH$_3$)$_3$), 70.1 (TaCH_3), 110.9, 121.1, 122.2, 125.2, 139.4, 147.2, 150.8, 152.6 (aryl). Anal. calcd. for $C_{33}H_{45}Cl_2O_3Ta$ (%): C, 53.45; H, 6.12. Found: C, 53.50; H, 5.92.

Synthesis of 13. KBn (53.1 mg, 0.408 mmol, 2 equiv) was added with the aid of C_6H_6 (4 mL) to a solution of **3C** (97.3 mg, 0.204 mmol, 1 equiv) in C_6H_6 (4 mL). This mixture was allowed to stir at room temperature for 0.5 h which afforded a pale gray mixture of deprotonated phenol. A C_6H_6 solution of $TaCl_2(CH_3)_3$ (60.7 mg, 0.204 mmol, 1 equiv) was added and the reaction mixture was allowed to stir at room temperature for 1 h. Salts were removed by filtration through a bed of Celite. Volatile materials were removed under vacuum to give the desired product as a white powder. ^{1}H NMR (500 MHz, CD_2Cl_2) δ: 0.32 (s, 9H, Ta(CH_3)$_3$), 1.40 (s, 18H, C(CH_3)$_3$), 1.65 (s, 18H, C(CH_3)$_3$), 6.95 (s, 2H, OC_4H_2), 7.54 (d, 2H, aryl-*H*), 7.61 (d, 2H, aryl-*H*). ^{13}C NMR (125 MHz, CD_2Cl_2) δ: 30.3 (C(*C*H$_3$)$_3$), 31.8 (C(*C*H$_3$)$_3$), 35.1 (*C*(CH$_3$)$_3$), 36.0 (*C*(CH$_3$)$_3$), 58.2 (Ta*C*H$_3$), 110.8, 121.1, 123.6, 124.9, 139.9, 144.5, 151.8, 152.2 (aryl). Anal. calcd. for $C_{35}H_{51}O_3Ta$ (%): C, 59.99; H, 7.34. Found: C, 60.32; H, 7.53.

X-ray Crystal Data: General Procedure. Crystals were removed quickly from a scintillation vial to a microscope slide coated with Paratone N oil. Samples were selected and mounted on a glass fiber with Paratone N oil. Data collection was carried out on a Bruker Smart 1000 CCD diffractometer. The structures were solved by direct methods. All non-hydrogen atoms were refined anisotropically. Some details regarding refined data and cell parameters are available in Table 3 and 4. Selected bond distances and angles are supplied in the corresponding figure captions and in Table 1.

Table 3. Crystal and refinement data for complexes **5**, **6**, and **9**.

	5	**6**	**9**
Empirical formula	$C_{36}H_{52}NO_2Ta$	$C_{54}H_{64}NO_2Ta \bullet \frac{1}{2}C_6H_{14}$	$C_{40}H_{50}NO_2F_2Ta \bullet C_6H_6$
Formula weight	711.74	983.10	873.87
T (K)	100(2)	100(2)	100(2)
a, Å	11.1983(3)	11.6884(3)	13.6879(4)
b, Å	11.4259(3)	18.9587(4)	28.6266(7)
c, Å	14.4511(4)	21.6301(5)	11.3658(3)
α, deg	88.7580(10)		
β, deg	75.2440(10)	95.3950(10)	113.9359(10)
γ, deg	70.9590(10)		
Volume, Å^3	1686.39(8)	4771.93(19)	4070.57(19)
Z	2	4	4
Crystal system	Triclinic	Monoclinic	Monoclinic
Space group	P-1	$P2_1/n$	$P2_1/c$
d_{calc}, g/cm^3	1.402	1.368	1.426
θ range, deg	1.89 to 47.50	1.89 to 42.95	1.63 to 40.73
μ, mm^{-1}	3.289	2.346	2.747
Abs. correction	SADABS	SADABS	SADABS
GOF	1.206	1.216	1.229
R_1,[a] wR_2[b] [I>2σ(I)]	0.0392, 0.0703	0.0389, 0.0626	0.0398, 0.0580

[a] $R_1 = \sum | |F_o| - |F_c| | / \sum |F_o|$. [b] $wR_2 = [\sum[w(F_o^2-F_c^2)^2] / \sum[w(F_o^2)^2]]^{1/2}$.

Table 4. Crystal and Refinement data for complexes **10-P**, **11**, and **12**.

	10-P	**11**	**12**
Empirical formula	$C_{55}H_{68}NO_2PTa \bullet 2.5(C_6H_6)$	$C_{35}H_{51}O_2STa$	$C_{33}H_{45}O_3Cl_2Ta$
Formula weight	1182.29	716.77	809.65
T (K)	100(2)	100(2)	100(2)
a, Å	29.1034(6)	9.8813(16)	15.0003(3)
b, Å	43.7491(9)	11.3580(18)	15.1231(3)
c, Å	19.1359(4)	15.332(2)	16.5600(4)
α, deg		86.956(3)	95.7320(10)
β, deg		76.513(3)	97.0480(10)
γ, deg		80.423(3)	91.9980(10)
Volume, $Å^3$	24364.7(9)	1649.7(5)	3705.40(14)
Z	16	2	4
Crystal system	Orthorhombic	Triclinic	Triclinic
Space group	Fdd2	P-1	P-1
d_{calc}, g/cm^3	1.289	1.443	1.451
θ range, deg	1.68 to 41.03	1.82 to 28.41	1.35 to 50.18
μ, mm^{-1}	1.875	3.423	3.144
Abs. correction	None	Semi-empirical from equiv.	None
GOF	1.095	1.276	1.000
R_1,[a] wR_2[b] [I>2σ(I)]	0.0415, 0.0665	0.0421, 0.0665	0.0390, 0.0748

[a] $R_1 = \sum | |F_o| - |F_c| | / \sum |F_o|$. [b] $wR_2 = [\sum[w(F_o^2-F_c^2)^2] / \sum[w(F_o^2)^2]]^{1/2}$.

References

(1) Britovsek, G. J. P.; Gibson, V. C.; Wass, D. F. *Angew. Chem., Int. Ed. Engl.* **1999**, *38*, 428-447.

(2) Gibson, V. C.; Spitzmesser, S. K. *Chem. Rev.* **2003**, *103*, 283-315.

(3) Coates, G. W.; Hustad, P. D.; Reinartz, S. *Angew. Chem., Int. Ed. Engl.* **2002**, *41*, 2236-2257.

(4) Watson, D. A.; Chiu, M.; Bergman, R. G. *Organometallics* **2006**, *25*, 4731-4733.

(5) Anderson, L. L.; Arnold, J.; Bergman, R. G. *J. Am. Chem. Soc.* **2005**, *127*, 14542-14543.

(6) Ackermann, L.; Bergman, R. G.; Loy, R. N. *J. Am. Chem. Soc.* **2003**, *125*, 11956-11963.

(7) Rothwell, I. P. *Chem. Commun.* **1997**, 1331-1338.

(8) Wallace, K. C.; Liu, A. H.; Dewan, J. C.; Schrock, R. R. *J. Am. Chem. Soc.* **1988**, *110*, 4964-4977.

(9) Schrock, R. R. *Angew. Chem., Int. Ed. Engl.* **2006**, *45*, 3748-3759.

(10) Schrock, R. R.; Hoveyda, A. H. *Angew. Chem., Int. Ed. Engl.* **2003**, *42*, 4592-4633.

(11) Tsang, W. C. P.; Hultzsch, K. C.; Alexander, J. B.; Bonitatebus, P. J.; Schrock, R. R.; Hoveyda, A. H. *J. Am. Chem. Soc.* **2003**, *125*, 2652-2666.

(12) Schrock, R. R. *Chem. Rev.* **2002**, *102*, 145-179.

(13) Bradley, D. C.; Mehrotra, R. C.; Singh, A.; Rothwell, I. P. *Alkoxo and Aryloxo Derivatives of Metals*; Academic Press: London, 2001.

(14) Mason, A. F.; Coates, G. W. *J. Am. Chem. Soc.* **2004**, *126*, 16326-16327.

(15) Tian, J.; Hustad, P. D.; Coates, G. W. *J. Am. Chem. Soc.* **2001**, *123*, 5134-5135.

(16) Tshuva, E. Y.; Goldberg, I.; Kol, M. *J. Am. Chem. Soc.* **2000**, *122*, 10706-10707.

(17) Tshuva, E. Y.; Goldberg, I.; Kol, M.; Goldschmidt, Z. *Organometallics* **2001**, *20*, 3017-3028.

(18) Tshuva, E. Y.; Groysman, S.; Goldberg, I.; Kol, M.; Goldschmidt, Z. *Organometallics* **2002**, *21*, 662-670.

(19) Groysman, S.; Goldberg, I.; Kol, M.; Genizi, E.; Goldschmidt, Z. *Adv. Synth. Catal.* **2005**, *347*, 409-415.

(20) Groysman, S.; Segal, S.; Goldberg, I.; Kol, M.; Goldschmidt, Z. *Inorg. Chem. Commun.* **2004**, *7*, 938-941.

(21) Groysman, S.; Goldberg, I.; Kol, M.; Genizi, E.; Goldschmidt, Z. *Organometallics* **2004**, *23*, 1880-1890.

(22) Groysman, S.; Goldberg, I.; Kol, M.; Goldschmidt, Z. *Organometallics* **2003**, *22*, 3793-3795.

(23) Groysman, S.; Segal, S.; Shamis, M.; Goldberg, I.; Kol, M.; Goldschmidt, Z.; Hayut-Salant, E. *J. Chem. Soc.-Dalton Trans.* **2002**, 3425-3426.

(24) Freundlich, J. S.; Schrock, R. R.; Davis, W. M. *Organometallics* **1996**, *15*, 2777-2783.

(25) Freundlich, J. S.; Schrock, R. R.; Davis, W. M. *J. Am. Chem. Soc.* **1996**, *118*, 3643-3655.

(26) Baumann, R.; Davis, W. M.; Schrock, R. R. *J. Am. Chem. Soc.* **1997**, *119*, 3830-3831.

(27) Baumann, R.; Stumpf, R.; Davis, W. M.; Liang, L. C.; Schrock, R. R. *J. Am. Chem. Soc.* **1999**, *121*, 7822-7836.

(28) Liang, L. C.; Schrock, R. R.; Davis, W. M.; McConville, D. H. *J. Am. Chem. Soc.* **1999**, *121*, 5797-5798.

(29) Mehrkhodavandi, P.; Bonitatebus, P. J.; Schrock, R. R. *J. Am. Chem. Soc.* **2000**, *122*, 7841-7842.

(30) Mehrkhodavandi, P.; Schrock, R. R. *J. Am. Chem. Soc.* **2001**, *123*, 10746-10747.

(31) Mehrkhodavandi, P.; Schrock, R. R.; Pryor, L. L. *Organometallics* **2003**, *22*, 4569-4583.

(32) Schrock, R. R.; Seidel, S. W.; Schrodi, Y.; Davis, W. M. *Organometallics* **1999**, *18*, 428-437.

(33) Chan, M. C. W.; Tam, K. H.; Zhu, N. Y.; Chiu, P.; Matsui, S. *Organometallics* **2006**, *25*, 785-792.

(34) Chan, M. C. W.; Tam, K. H.; Pui, Y. L.; Zhu, N. Y. *J. Chem. Soc., Dalton Trans.* **2002**, 3085-3087.

(35) Li, Y. Q.; Liu, Y.; Bu, W. M.; Guo, J. H.; Wang, Y. *Chem. Commun.* **2000**, 1551-1552.

(36) Steinhauser, S.; Heinz, U.; Sander, J.; Hegetschweiler, K. *Z. Anorg. Allg. Chem.* **2004**, *630*, 1829-1838.

(37) Schrock, R. R.; Meakin, P. *J. Am. Chem. Soc.* **1974**, *96*, 5288-5290.

(38) Schrock, R. R. *J. Organomet. Chem.* **1976**, *122*, 209-225.

(39) Janiak, C. *J. Chem. Soc.-Dalton Trans.* **2000**, 3885-3896.

(40) Hunter, C. A.; Sanders, J. K. M. *J. Am. Chem. Soc.* **1990**, *112*, 5525-5534.

(41) Schrock, R. R. *J. Am. Chem. Soc.* **1975**, *97*, 6577-6578.

(42) Fellmann, J. D.; Rupprecht, G. A.; Wood, C. D.; Schrock, R. R. *J. Am. Chem. Soc.* **1978**, *100*, 5964-5966.

(43) McLain, S. J.; Wood, C. D.; Messerle, L. W.; Schrock, R. R.; Hollander, F. J.; Youngs, W. J.; Churchill, M. R. *J. Am. Chem. Soc.* **1978**, *100*, 5962-5964.

(44) Schrock, R. R.; Fellmann, J. D. *J. Am. Chem. Soc.* **1978**, *100*, 3359-3370.

(45) Schrock, R. R.; Messerle, L. W.; Wood, C. D.; Guggenberger, L. J. *J. Am. Chem. Soc.* **1978**, *100*, 3793-3800.

(46) Schrock, R. R. *Acc. Chem. Res.* **1979**, *12*, 98-104.

(47) Li, L.; Hung, M.; Xue, Z. *J. Am. Chem. Soc.* **1995**, *117*, 12746.

(48) Nugent, W. A.; Mayer, J. M. *Metal-ligand multiple bonds*; Wiley: New York, 1988.

(49) Messerle, L. W.; Jennische, P.; Schrock, R. R.; Stucky, G. *J. Am. Chem. Soc.* **1980**, *102*, 6744-6752.

(50) Rupprecht, G. A.; Messerle, L. W.; Fellmann, J. D.; Schrock, R. R. *J. Am. Chem. Soc.* **1980**, *102*, 6236-6244.

(51) Wallace, K. C.; Davis, W. M.; Schrock, R. R. *Inorg. Chem.* **1990**, *29*, 1104-1106.

(52) Drew, M. G. B.; Rice, D. A.; Williams, D. M. *J. Chem. Soc.-Dalton Trans.* **1984**, 845-848.

(53) Marinescu, S. M.; Agapie, T.; Day, M. W.; Bercaw, J. E. *Organometallics*, **2007**, *26*, 1178-1190.

(54) Fay, R. C.; Lindmark, A. F. *J. Am. Chem. Soc.* **1983**, *105*, 2118-2127.

(55) Pangborn, A. B.; Giardello, M. A.; Grubbs, R. H.; Rosen, R. K.; Timmers, F. J. *Organometallics* **1996**, *15*, 1518.

Chapter 6

Propylene Polymerization and Oligomerization Catalysis Based on Zirconium and Titanium Complexes Supported by Tridentate Diphenolate Frameworks with Furan, Thiophene, and Pyridine Donors

Abstract

A series of zirconium and titanium complexes with novel tridentate diphenolate ligands have been prepared and investigated for applications in propylene polymerization. The ligand framework is based on diphenolates connected at the *ortho* positions via semi-rigid, ring-ring (sp^2-sp^2) linkages to a flat heterocycle (pyridine, furan, or thiophene). The zirconium and titanium dibenzyl species have been prepared by toluene elimination. Titanium complexes with pyridine and furan diphenolates and zirconium complexes with pyridine and thiophene diphenolates have been characterized by single-crystal X-ray diffraction. The titanium solid-state structures are roughly C_2 symmetric while the zirconium ones are C_s symmetric. In the solid-state, the titanium pyridine diphenolate system was found to be structurally affected by the size of the substituents *ortho* to the oxygens – the larger group leading to a larger C_2 distortion. Both titanium and zirconium complexes were found to be active for the polymerization of propylene upon activation with MAO. The activities observed for the zirconium complexes are excellent, exceeding 10^6 g polypropylene / (mol Zr • h) in some cases. Titanium polymerization catalysts are about 10^3 less active, but generate polymers of higher molecular weight. The titanium diphenolate-furan and diphenolate-thiophene systems were found to generate active propylene oligomerization catalysts.

Introduction

Polymers represent one of the most important commodity chemicals.[1] They are produced in quantities of hundreds of billions of pounds per year. Polymer applications range from uses in the automotive and construction industries to food packaging and information age technologies. The wide utility of polymers stems from their useful and versatile material properties. The last half a century has seen great developments in the olefin polymerization catalysis and in particular in the ability to affect polymer architecture, and hence polymer's physical properties, by controlling the structure of the catalyst.[2] Design of well-defined, single-site catalysts has emerged as a powerful method to control polymer features such as tacticity, molecular weight, molecular weight distribution, level of comonomer incorporation, etc.

Early metal metallocene complexes have provided the most important and well-studied framework for single-site catalysts for olefin polymerization.[3,4] Recently, nonmetallocene frameworks have emerged as versatile alternatives.[5-7] Complexes based on iron, cobalt, nickel and palladium have been shown to polymerize and oligomerize olefins with good activities and sometimes in a living fashion.[8] In the realm of early metal polymerization catalysis, frameworks displaying only one or no cyclopentadienyl ligand have been developed. A broad range of multidentate ligands has been utilized as supporting architectures for olefin polymerization catalysts. In this context, a broad interest has been shown in generating polymers with controlled tacticity through the use of nonmetallocene catalysts.[5,7] Promising advances have been made in both the

development of single-site living polymerization catalysts and the design of ancillary ligands that have the appropriate symmetry for polymer tacticity control.[7] While the reasons behind the polymerization behaviors observed for various systems are not well understood, the interesting developments warrant further exploration into the area of nonmetallocene olefin polymerization catalysis. These frameworks also present the advantage of being relatively inexpensive and easy to prepare and modify.

Anilides and phenolates are common anionic donors found in multidentate ligands for polymerization catalysis. Some of the most successful nonmetallocene polymerization catalysts include bi-, tri-, and tetradentate anilide and phenolate ligands. Tridentate bisanilide ligands have been reported to support ethylene and α-olefin polymerization; in some cases living polymerization of 1-hexene was possible.[9-15] Bidentate imino-phenolate ligands have been shown to support C_2-symmetric architectures; these catalysts are able to generate syndiotactic or isotactic polypropylene depending on the nature of the substituents on the phenolate rings.[16-22] Tetradentate diphenolate frameworks have been reported to give very active catalysts for the polymerization of 1-hexene; again, tacticity control was possible by use of C_2-symmetric architectures.[23-32] Tridentate diphenolate frameworks have been successful as well in supporting olefin polymerization.[33-36]

This report describes the development of semirigid tridentate diphenolate architectures for the polymerization of propylene with titanium and zirconium. The utilized ligand framework is based on diphenolates connected at the *ortho*

positions via semi-rigid, ring-ring (sp^2-sp^2) linkages to a flat heterocycle (pyridine, furan, or thiophene). The ligand synthesis was described in Chapter 4. We have found that these ligands bind to tantalum meridionally giving rise to diverse geometries on the metal center. This relates them sterically to appropriately substituted metallocene systems (Chapter 4, Figure 1). The ligand involving a pyridine linker and two phenoxides was reported by other groups to bind to iron(III), copper(II), and aluminum(III) in a C_2 fashion.[37] When bound to boron or zirconium(IV) this ligand binds in a C_s fashion.[35,36,38]

With respect to olefin polymerization activity, a number of related systems have been investigated, based on the pyridine linker and phenoxides, alkoxides, or anilides anionic donors.[35,36,39-41] It was found that a zirconium pyridine bisphenoxide system can polymerize ethylene with high activities and also incorporate propylene.[35,36] A chiral cationic zirconium pyridine bisalkoxide was found to insert only one ethylene molecule,[41] while a related titanium pyridine bisalkoxide was reported to polymerize ethylene with good activity.[39] A zirconium pyridine bisanilide system was shown to polymerize ethylene upon activation with MAO.[40] Notably, computational studies on bisphenoxide-donor systems indicated that a strong interaction with the additional donor lowers the transition state for olefin insertion.[42] Here, we report the synthesis, characterization, and polymerization ability of group 4 systems (Figure 1) based on tridentate diphenolates connected by pyridine (this was recently reported, but homopolymerization of α-olefins was not), furan, and thiophene linkers.

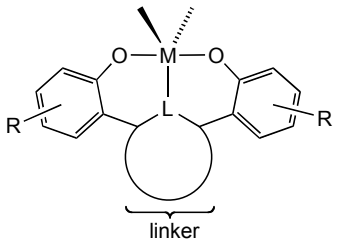

Linker = thiophene, furan, or pyridine;
L = N, O, or S; M = Ti or Zr; R = alkyl or aryl.

Figure 1. General formulation of group 4 systems supported by tridentate diphenolate ligands.

Results and Discussion

Preparation of zirconium and titanium complexes supported by tridentate diphenolates

As described before (Chapter 5), diphenols **1-H$_2$**, **2-H$_2$**, and **3-H$_2$** are conveniently accessed from easily available starting materials. Titanium and zirconium dibenzyl complexes have been prepared by toluene elimination between the tetrabenzyl precursors and diphenols (eq 1). These reactions have been performed in diethyl ether. The titanium complexes are obtained as red (**2-TiBn$_2$** and **3-TiBn$_2$**) or orange (**1a-TiBn$_2$** and **1b-TiBn$_2$**) solids while the zirconium one are pale yellow (**1a-ZrBn$_2$**, **1b-ZrBn$_2$**, and **3-ZrBn$_2$**) or colorless (**2-ZrBn$_2$**). Coordinated ether was not observed by NMR spectroscopy indicating that the products are five-coordinate. ^{1}H NMR spectra of the titanium and zirconium dibenzyl complexes show a singlet for the benzyl C*H*$_2$ protons. A

variable temperature ^{1}H NMR study was performed for **1a-TiBn$_2$**. The benzyl peak was found to remain a sharp singlet at temperatures as low as -80 °C.

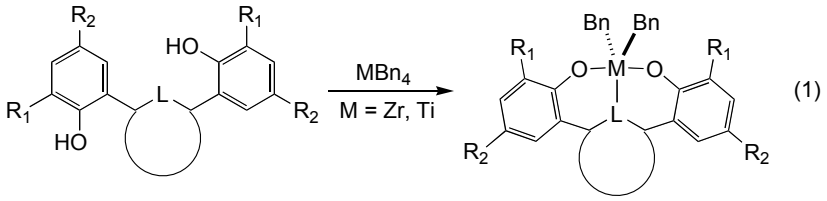

(1)

1a-H$_2$: R$_1$ = R$_2$ = tBu, Linker = Pyridine
1b-H$_2$: R$_1$ = CEt$_3$, R$_2$ = Me, Linker = Pyridine
2-H$_2$: R$_1$ = R$_2$ = tBu, Linker = Furan
3-H$_2$: R$_1$ = R$_2$ = tBu, Linker = Thiophene

1a-TiBn$_2$	**1a-ZrBn$_2$**
1b-TiBn$_2$	**1b-ZrBn$_2$**
2-TiBn$_2$	**2-ZrBn$_2$**
3-TiBn$_2$	**3-ZrBn$_2$**

As shown for tantalum, the present ligands can achieve a number of binding geometries (C_{2v}, C_s, C_2, C_1, Figure 2). These geometries may be distinguishable by ^{1}H NMR spectroscopy by analysis of the benzyl CH_2 protons. C_{2v} geometry is expected to lead to a singlet for these protons, while C_s geometry to two singlets. C_2 symmetry makes the CH_2 protons diastereotopic, which should lead to two doublets. C_1 geometry would make all four benzylic protons different, leading to four doublets. The observed ^{1}H NMR spectra of the titanium and zirconium dibenzyl complexes showing only a singlet for the benzyl CH_2 protons suggests that the solution structure is either C_{2v}-symetric or in fast exchange between different possible geometries (Figure 2). Scheme 2 shows the interconversion between the C_{2v}, C_s, and C_2 geometries, the C_1 geometry, not shown, being intermediate between the other three. While it is not clear which geometry should be preferred, the tantalum data suggest that this will be dependent on the type of linker involved. Exchange between C_2 enantiomers could occur via a C_{2v} structure, if both phenolate rings twist at the same time, or

via C_1 structures, if the rings twist separately. Similarly, exchange between the two C_s structures can occur via C_{2v} or C_1 intermediates.

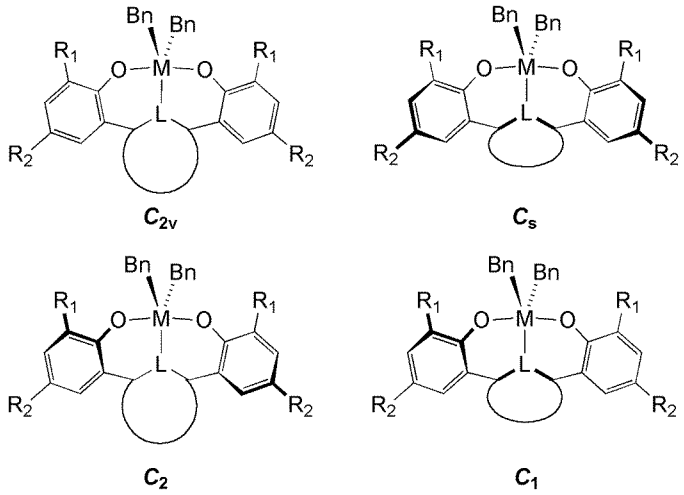

Figure 2. Possible geometries of group 4 dibenzyl complexes supported by tridentate diphenolate frameworks.

The solution symmetry of the present species and their ability to exchange between different geometries is important with regard to controlling polymer microstructure. For instance, a C_2 structure may enforce isotactic polymerization if the steric transfer to the metal site is efficient enough, while the above C_s and C_{2v} structures should give atactic polymers. If C_2 / C_s interconversion occurs at a rate slower than the insertion rates, stereoblock polymers could be obtained if enatiomorphic site control is operative. A similar type of oscillation of the catalyst has been proposed to lead to isotactic-atactic stereoblock polymers.[43] In a related process, inversion between the two C_2 structures could be controlled by the polymer chain end. In this case, syndiotactic polymer could be generated if the inversion occurs after each insertion.[44,45]

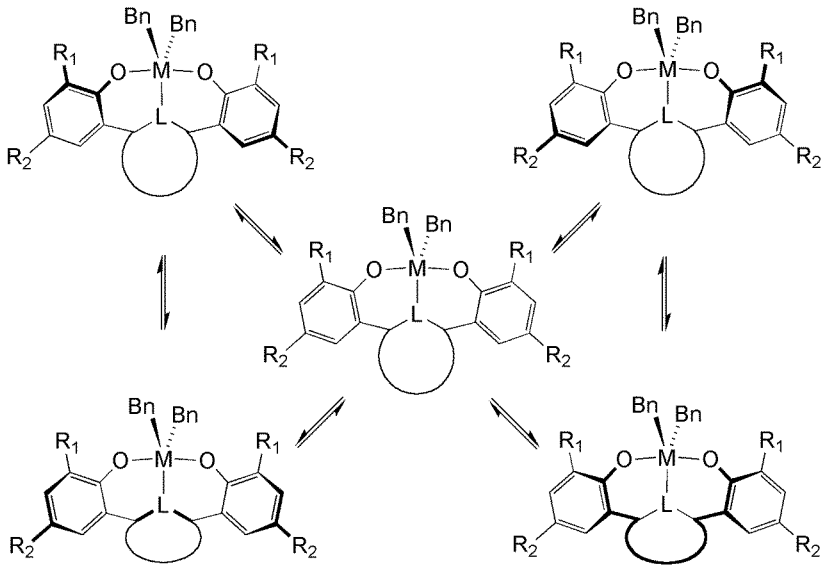

Scheme 2. Equillibria of interconversion of various geometrical isomers.

As a measure of the ligands steric demands, the ability to coordinate two diphenolates was investigated. The reaction of metal tetrabenzyl precursors was performed with two equivalents of phenol (**1a-H$_2$**). For zirconium, a mixture of species is generate within a few hours (^{1}H NMR spectroscopy), displaying the free phenol, **1a-ZrBn$_2$** as well as another species assigned as **(1a)$_2$-Zr**. Upon heating to 60 °C for 10.5 h this mixture funnels to one species displaying no benzyl peaks, but only phenolate ligand peaks. This is consistent with the clean formation of **(1a)$_2$-Zr**. The analogous experiment was performed with titanium. At room temperature the titanium reaction generates only the titanium dibenzyl species (**1a-Ti**) and leaves an equivalent of diphenol unreacted. Heating at 60 °C for 10.5 h leads to a new species with no benzyl peaks, but the reaction is not complete. Extending the reaction time by 24 h leads to complete conversion to the tetraphenolate complex **(1a)$_2$-Ti**. The fact that two of diphenolate ligands can

be coordinated to a metal center indicates that while the *ortho* substituents are quite bulky, the metal center still remains quite open. The titanium reaction is slower than the zirconium one indicating, not surprisingly, that the smaller titanium center is more hindered.

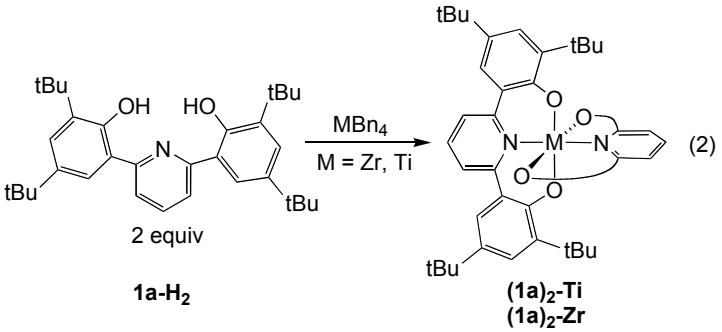

(2)

Structural characterization of group IV dibenzyl complexes with tridentate diphenolate ligands

Single-crystal X-ray diffraction studies have been instrumental in determining the binding modes of the diphenolate ligands, in the solid-state. Attempts to grow crystals adequate for these studies were successful for compounds **1a-TiBn$_2$**, **1b-TiBn$_2$**, **2-TiBn$_2$**, **1b-ZrBn$_2$**, and **3-ZrBn$_2$**. The titanium complexes were all found to be five-coordinate in the solid state, with a trigonal bipyramid geometry. The two phenolate rings twist away from each-other to give rise to C_2-symmetric structures. The dihedral angles between the Ti-O bonds and the plane of the linker can be used as a measure of the twisting leading to the C_2 structure. Also, the distance between the carbon substituents *ortho* to the phenolate oxygens (d_{CC}) gives a measure of how the steric bulk varies around the metal center (Table 1). Keeping the linker the same (pyridine, in **1a-TiBn$_2$**, Figure

3, and **1b-TiBn$_2$**, Figure 4) allows for a comparison of the effect of substituents *ortho* to the phenolate oxygen. Switching from tBu to CEt_3 leads to an increase in the twist angle by 8°, from about 28° to 36°. The distance between the substituents d_{CC} changes by less than 0.1 Å. Not surprisingly, the distance between the phenolate oxygens does not change significantly. The interaction of the metal with the benzyl groups is notable – in **1a-TiBn$_2$** the Ti-C-C_{ipso} angles are around 97° while in **1b-TiBn$_2$** they are 108° and 114°; the Ti-C_{ipso} varies accordingly (Table 1). These structural features indicate that the steric bulk of the substituent in the *ortho* position affects both the orientation of the diphenolate framework and the binding of the other ligands. Increasing the steric bulk forces the phenolate rings to twist further away from each other, but the distance between the substituents is not affected significantly. The bulkier CEt_3 group also has the effect of pushing the phenyl of the benzyl ligands away from the metal center. Interestingly, the orientation of the two benzyl groups is more propeller-like in the less bulky system, possibly indicating that the large radial extension of the CEt_3 group reaches to the alkyl substituent on both sides of the propeller of the diphenolate ligand. It is noteworthy that the C_2 binding mode of the ligand is in contrast to its C_s binding mode in all the tantalum complexes; this indicates that symmetry of the metal complex could be tuned, possibly by changing the size of the central atom via using different metals.

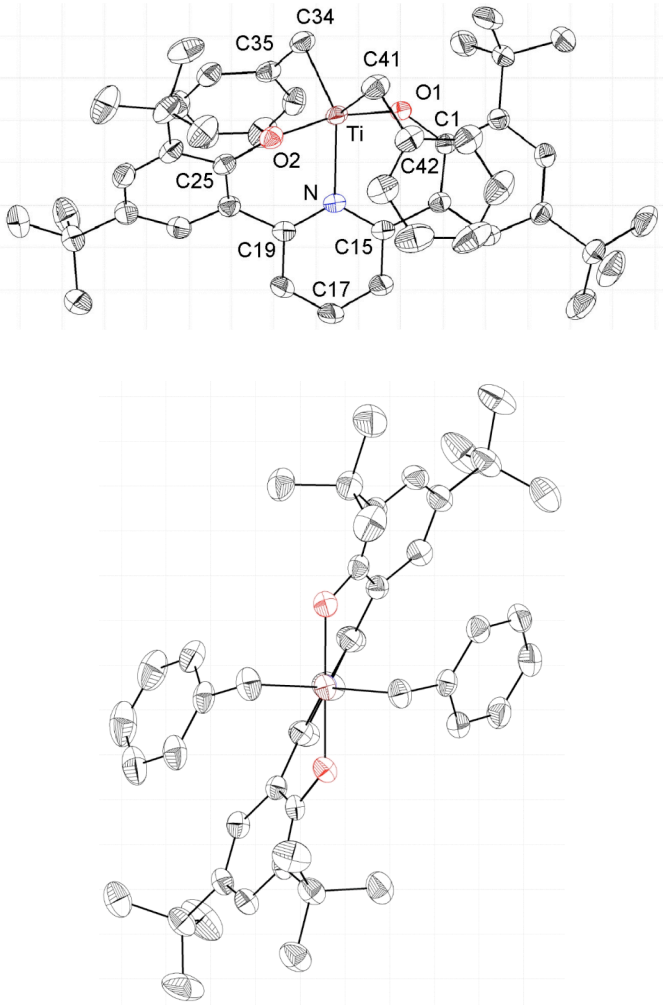

Figure 3. Structural drawing of **1a-TiBn$_2$**. Selected bond lengths (Å) and angles (°): N(1)-Ti(1) 2.2181(12); O(1)-Ti(1) 1.8688(11); O(2)-Ti(1) 1.8578(11); C(34)-Ti(1) 2.1222(17); C(41)-Ti(1) 2.1207(16); C(35)-C(34)-Ti(1) 96.92(10); C(42)-C(41)-Ti(1) 97.43(10); C(1)-O(1)-Ti(1) 132.47(10); C(25)-O(2)-Ti(1) 134.96(10).

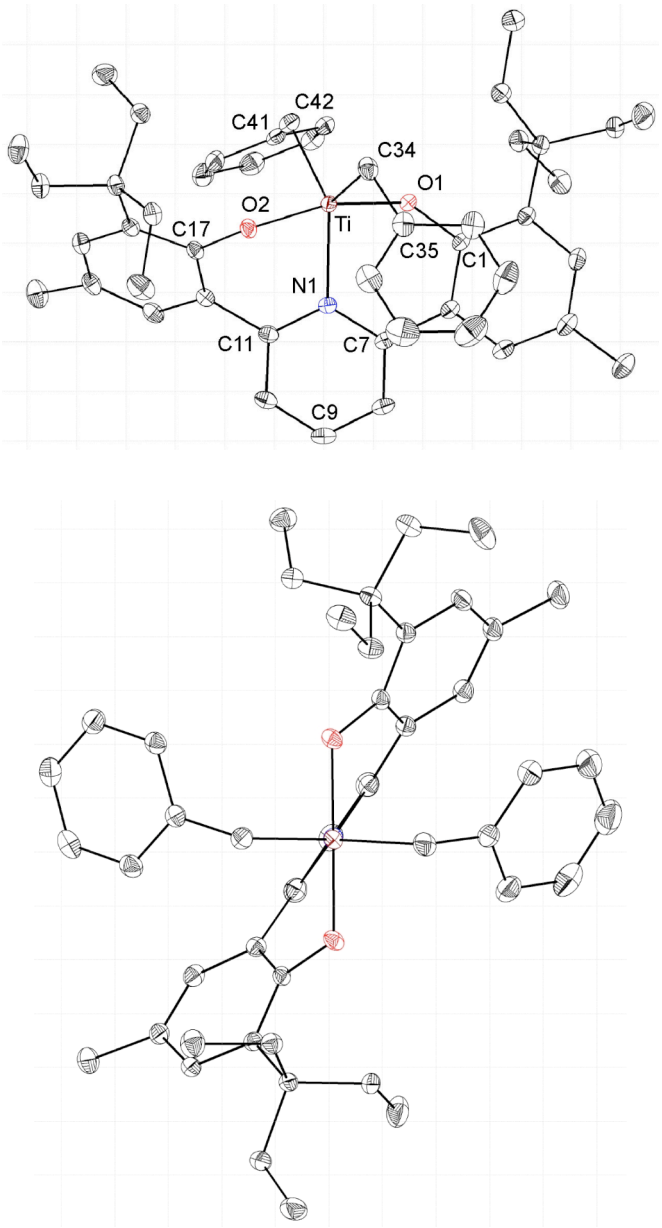

Figure 4. Structural drawing of **1b-TiBn$_2$**. Selected bond lengths (Å) and angles (°): Ti(1)-O(1) 1.8873(7); Ti(1)-O(2) 1.8935(8); Ti(1)-C(41) 2.1022(10); Ti(1)-C(34) 2.1167(10); Ti(1)-N(1) 2.1587(8); O(1)-Ti(1)-O(2) 164.93(3); C(35)-C(34)-Ti(1) 107.67(7); C(42)-C(41)-Ti(1) 114.04(7); C(1)-O(1)-Ti(1) 126.24(6); C(17)-O(2)-Ti(1) 123.38(6).

Comparison between **1a-TiBn$_2$** vs **2-TiBn$_2$** (Figure 5) allows for the study of the effect of changing the linker while keeping the *ortho* substituents the same (tBu). Moving from pyridine to furan causes a small decrease in the twist angle (from 28° to about 24°). However, the distance between the *ortho* stubstituents increases substantially, by more than 2 Å from 9.11 Å to 11.29 Å. With respect to the benzyls, the Ti-C-C$_{ipso}$ angles are slightly smaller in the furan based system. These structural trends indicate that the furan linker makes the metal center more sterically open by pulling the phenolate rings out. This is particularly emphasized by the significant increase in the distance between the two *ortho* substituents. The closer interaction between titanium and the phenyl of the benzyl ligands could be due to the less sterically hindered environment around the metal. Alternatively, this could be due to a more eletrophilic metal center with a furan donor instead of the pyridine donor.

The complexes characterized in the solid-state present C_s- (**1b-ZrBn$_2$**, Figure 6) and C_1-symmetric (**3-ZrBn$_2$**, Figure 7) binding modes of the ligand. Crystals of the pyridine based complex (**1b-ZrBn$_2$**) were obtained from a saturated diethyl ether solution, and a molecule of ether was found to coordinate to the metal leading to a distorted octahedral geometry. One of the Zr-C$_{ipso}$ distances is longer than the other by over 0.7 Å. The pyridine plane is tilted away from the Zr-N vector and the Zr-N bond length is long. As in the case of tantalum complexes supported by the same ligand, the metal interaction with the nitrogen is strained by a twist of the pyridine ring, leading to a C_s-symmetric structure. The long zirconium ether oxygen bond length is indicative of a weak

interaction – consistent with the fact that the ether can be removed under vacuum. The metal center's electrophilicity is indicated by the one relatively short Zr-C_{ipso} distance.

Table 1. Selected structural parameters for the crystallographically characterized group 4 compounds supported by tridentate diphenolate frameworks. C-C = distance between the *ortho*-substituents quaternary carbons.

Compound	O-Ti-L-C (°)	O-O (Å)	C-C (Å)	M-C (Å)	M-C_{ipso} (Å)	M-C-C_{ipso} (°)
1a-TiBn$_2$	27.6; 28.2	3.70	9.11	2.12 2.12	2.74 2.73	96.9 97.4
1b-TiBn$_2$	35.3; 36.1	3.74	9.15	2.10 2.12	3.03 2.93	114.0 107.6
2-TiBn$_2$	21.6; 25.4	3.64	11.29	2.09 2.11	2.61 2.64	91.8 93.4
1b-ZrBn$_2$(OEt$_2$)	--	3.9	9.44	2.29 2.33	2.676 3.41	103.9 125.8
3-ZrBn$_2$	--	3.86	9.38	2.26 2.27	2.60 2.95	85.3 102.4

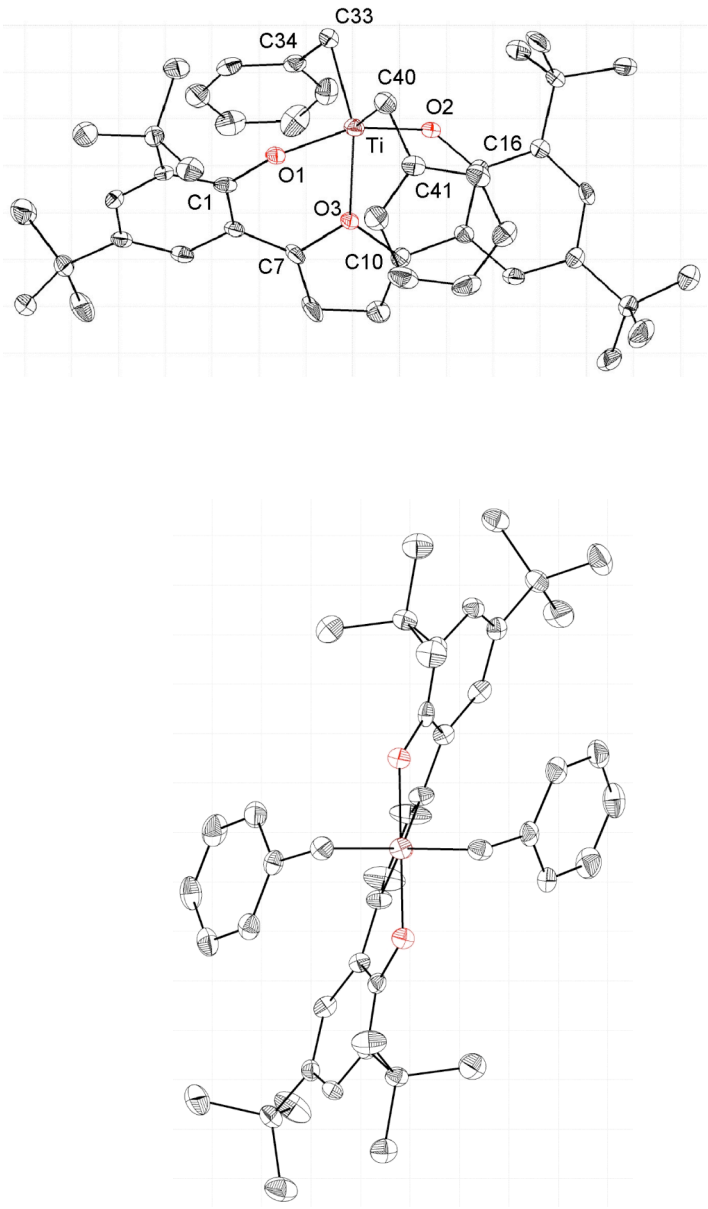

Figure 5. Structural drawing of **2-TiBn$_2$**. Selected bond lengths (Å) and angles (°): Ti(1)-O(2) 1.8605(16); Ti(1)-O(1) 1.8576(16); Ti(1)-C(33) 2.094(2); Ti(1)-C(40) 2.105(2); Ti(1)-O(3) 2.2510(15); Ti(1)-C(34) 2.605(3); Ti(1)-C(41) 2.641(2); O(2)-Ti(1)-O(1) 157.26(7); C(1)-O(1)-Ti(1) 140.67(15); C(16)-O(2)-Ti(1) 140.08(15); C(34)-C(33)-Ti(1) 91.80(14); C(41)-C(40)-Ti(1) 93.37(15).

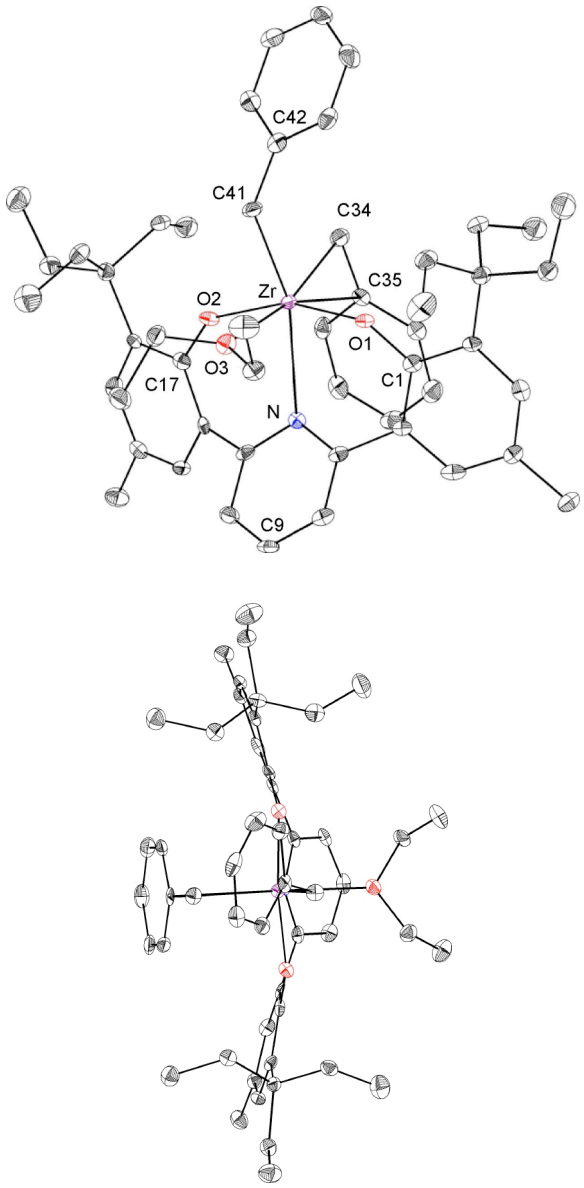

Figure 6. Structural drawing of **1b-ZrBn$_2$(OEt$_2$)**. Selected bond lengths (Å) and angles (°): Zr(1)-O(2) 1.9797(16); Zr(1)-O(1) 1.9897(15); Zr(1)-C(34) 2.289(3); Zr(1)-C(41) 2.334(3); Zr(1)-O(3) 2.3907(16); Zr(1)-N(1) 2.471(2); Zr(1)-C(35) 2.676(2); O(2)-Zr(1)-O(1) 158.67(7); C(1)-O(1)-Zr(1) 142.84(14); C(17)-O()-Zr(1) 143.80(16); C(36)-C(35)-Zr(1) 103.86(16); C(42)-C(41)-Zr(1) 125.62(18).

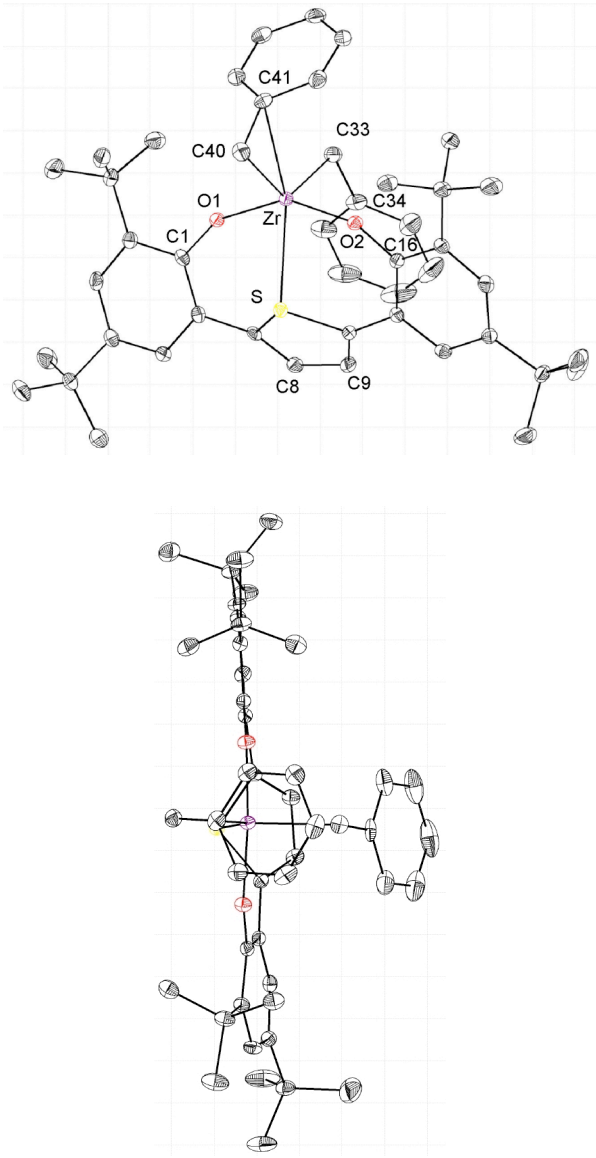

Figure 7. Structural drawing of **3-ZrBn$_2$**. Selected bond lengths (Å) and angles (°): Zr(1)-O(2) 1.9999(11); Zr(1)-O(1) 2.0052(11); Zr(1)-C(33) 2.259(2); Zr(1)-C(40) 2.273(2); Zr(1)-C(41) 2.5973(17); Zr(1)-S(1) 2.6411(5); O(2)-Zr(1)-O(1) 149.24(5); C(1)-O(1)-Zr(1) 153.07(11); C(16)-O(2)-Zr(1) 152.35(10); C(41)-C(40)-Zr(1) 85.25(11); C(34)-C(33)-Zr(1) 102.41(12).

The thiophene bridged zirconium complex was crystallized from toluene; in the solid-state, it is a distorted trigonal bipyramid with the diphenolate ligand binding is a C_1-fashion. The thiophene ring is almost perpendicular to the Zr-S vector. One of the benzyl groups significantly bends toward the metal center to give a Zr-C-C_{ipso} angle of 85.3° and a Zr-C_{ipso} distance of 2.60 Å. The structural features of the diphenolate ligand are similar to the ones observed for the tantalum complex supported by the same ligand (Chapter 4). The zirconium center supported by the thiophene diphenolate ligand is more electrophilic than in the pyridine based system, as indicated by the stronger interaction with benzyl ipso-carbon. This could be due to the fact the thiophene system is five-coordinate, but also to a weaker interaction of the metal center with the sulfur compared to the nitrogen donor.

Overall, from the perspective of diphenolate ligand binding, the zirconium complexes were found to be similar to the tantalum complexes, in contrast to the titanium species, suggesting that the semi-rigid ligand binding mode may be dependent on the size of the metal center. Importantly both titanium and zirconium complexes show meridional binding of the multidentate ligands. This should limit the number of possible accessible geometries. Related, more flexible bisanilide tridentate ligands, investigated by Schrock el al., were shown to bind in both fac and mer fashion (with some exceptions) which may have had a detrimental effect on controlling polymer tacticity.[9,12] It is noteworthy that the solution structure of the present complexes is fluxional, hence other geometries may be accessed in the solution state.

Propylene polymerization and oligomerization with zirconium complexes

Propylene polymerization trials have been performed with the present complexes at 0 °C, upon activation with excess methylaluminumoxane (MAO). The zirconium species generate waxy polymers which are separated from the quenched methanol / hydrochloric acid mixture by decantation. These materials are rinsed with water and placed under vacuum at 80 °C to remove volatile materials, then weighed and analyzed by various techniques including ^{1}H and ^{13}C NMR spectroscopy, GPS, and GC-MS. The MAO activated zirconium complexes have been found to be very active polymerization catalysts. In some cases, the activity exceeds 10^{6} g polypropylene / (mol Zr • h) which is comparable with activities observed for some of the most active propylene polymerization catalysts known.

Polymers obtained from the zirconium pyridine-diphenolate systems (**1a-ZrBn$_2$** and **1b-ZrBn$_2$**) were investigated by GPC. Interestingly, the polymer molecular weight distribution was found to be bimodal, with both fractions displaying low PDIs (Figure 8). For polymers obtained from **1a-ZrBn$_2$**, the high molecular weight fractions (MW=$1.6\bullet10^{5}$-$1.9\bullet10^{5}$) were found to have PDIs between 1.9 and 2.5 while the low molecular weight ones are around 1.5 (MW=~$1.3\bullet10^{5}$). An MAO dependence of the molecular weight distribution was observed. On varying the MAO excess from 2000 to 4000 equivalents, the molecular weight distribution shifts toward the low molecular weight polymers (Figure 8). ^{13}C NMR analysis of the resulting polymers shows significant peaks corresponding to *i*-butyl terminal groups, peaks that increased in propensity

with increasing MAO excess (Figure 9).[46,47] The polymerization activity was found to be dependent on MAO excess, with maximum activities at intermediate MAO excess. Polymers generated from **1b-ZrBn$_2$** or from **1a-ZrBn$_2$** with low 500 equiv MAO have few i-butyl end-groups (^{13}C NMR spectroscopy), but display terminal and internal olefin peaks as well as n-propyl end-groups. A GC-MS analysis revealed that polymers from **1b-ZrBn$_2$** display some low molecular weight oligomers of propylene (< C_{30}).

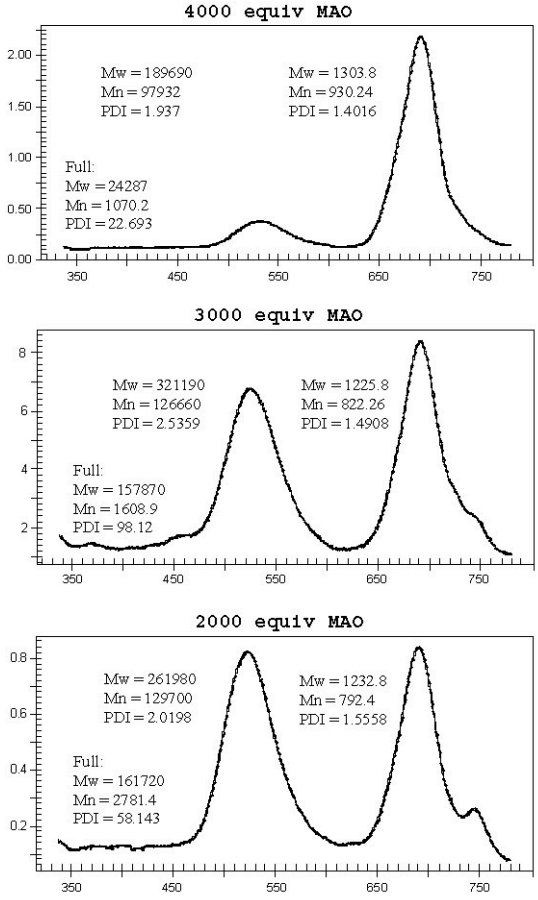

Figure 8. GPC for polymers obtained from **1a-ZrBn$_2$** upon activation with MAO (runs 6-8, Table 2).

Table 2. Polymerization runs with zirconium precatalysts.

Run #	Precatalyst	Cat mmols	Time (h)	Solvent (3+0.7 mL)	Liquid C3H6 (mL, 0C)	MAO (g)	MAO (equiv)	Polymer (mg)	Activity (g/mol.h)
1	**1a-ZrBn$_2$**	0.007	0.5	PhMe	34-39 mL	0.207	500	202	5.8E+04
2	**1a-ZrBn$_2$**	0.007	2	PhMe	34-39 mL	0.207	500	702	5.0E+04
3	**1a-ZrBn$_2$**	0.007	2	PhMe	34-39 mL	0.207	500	322	2.3E+04
4	**1a-ZrBn$_2$**	0.007	1.5	PhMe	34-39 mL	0.414	1000	11120	1.1E+06
5	**1a-ZrBn$_2$**	0.0035	0.5	PhMe	34-39 mL	0.207	1000	71	4.1E+04
6	**1a-ZrBn$_2$**	0.0035	0.5	PhMe	34-39 mL	0.414	2000	904	5.2E+05
7	**1a-ZrBn$_2$**	0.0035	0.5	PhMe	34-39 mL	0.621	3000	1717	9.8E+05
8	**1a-ZrBn$_2$**	0.0035	0.5	PhMe	34-39 mL	0.828	4000	404	2.3E+05
9	**1b-ZrBn$_2$**	0.007	2	PhMe	34-39 mL	0.207	500	9573	6.8E+05
10	**1b-ZrBn$_2$**	0.007	2	PhMe	34-39 mL	0.207	500	7096	5.1E+05
11	**1b-ZrBn$_2$**	0.0035	0.5	PhMe	34-39 mL	0.207	1000	2260	1.3E+06
12	**1b-ZrBn$_2$**	0.0035	0.5	PhMe	34-39 mL	0.207	1000	1940	1.1E+06
13	**1b-ZrBn$_2$**	0.0035	0.5	PhMe	34-39 mL	0.207	1000	2610	1.5E+06
14	**2-ZrBn$_2$**	0.0007	0.5	PhMe	34-39 mL	0.207	5000	417	1.2E+06
15	**2-ZrBn$_2$**	0.0007	0.5	PhMe	34-39 mL	0.207	5000	1621	4.6E+06
16	**3-ZrBn$_2$**	0.007	0.5	PhMe	34-39 mL	0.414	1000	3260	9.3E+05
17	**3-ZrBn$_2$**	0.007	0.5	PhMe	34-39 mL	0.207	500	5620	1.6E+06

Table 3. Polymerization runs with titanium precatalysts. *Oligomers are obtained for these runs.

Run #	Precatalyst	Cat mmols	Time (h)	Solvent (3+0.7 mL)	Liquid C3H6 (mL, 0C)	MAO (g)	MAO (equiv)	Polymer (mg)	Activity (g/mol.h)
1	**1a-TiBn$_2$**	0.007	0.5	PhMe	34-39 mL	0.207	500	3	8.6E+02
2	**1a-TiBn$_2$**	0.007	0.5	PhMe	34-39 mL	0.207	500	2	5.7E+02
3	**1a-TiBn$_2$**	0.007	2.6	PhMe	34-39 mL	0.207	500	14	7.7E+02
4	**1a-TiBn$_2$**	0.007	2	PhMe	34-39 mL	0.207	500	8	5.7E+02
5	**1a-TiBn$_2$**	0.007	2	PhMe	34-39 mL	0.207	500	7	5.0E+02
6	**1a-TiBn$_2$**	0.007	2	PhCl	34-39 mL	0.207	500	17	1.2E+03
7	**1a-TiBn$_2$**	0.007	2	PhCl	34-39 mL	0.207	500	20	1.4E+03
8	**1b-TiBn$_2$**	0.007	2	PhMe	34-39 mL	0.207	500	35	2.5E+03
9	**1b-TiBn$_2$**	0.007	2	PhMe	34-39 mL	0.207	500	32	2.3E+03
10	**1b-TiBn$_2$**	0.007	2	PhCl	34-39 mL	0.207	500	30	2.1E+03
11	**1b-TiBn$_2$**	0.007	2	PhCl	34-39 mL	0.207	500	30	2.1E+03
12	**1b-TiCl$_2$**	0.007	2	PhCl	34-39 mL	0.207	500	73	5.2E+03
13	**1b-TiCl$_2$**	0.007	2	PhCl	34-39 mL	0.207	500	42	3.0E+03
14	**2-TiBn$_2$***	0.007	0.5	PhMe	34-39 mL	0.207	500	870	2.5E+05
15	**2-TiBn$_2$***	0.007	0.5	PhMe	34-39 mL	0.207	500	1570	4.5E+05
16	**3-TiBn$_2$***	0.007	2	PhMe	34-39 mL	0.207	500	1940	1.4E+05
17	**3-TiBn$_2$***	0.007	2	PhMe	34-39 mL	0.207	500	2130	1.5E+05

The small PDIs observed for each polymer fraction indicates that single-site catalysts are involved. The observed bimodal distribution is probably due to the presence of two types of catalysts the relative distribution of which is dependent of the amount of MAO utilized. The presence of *i*-butyl terminal groups is indicative of chain trasfer to aluminum. If 1,2-insertion is the propagation regiochemistry, then i-butyl terminal groups could form at both ends of the polymer, by insertion into the initial Zr-Me bond as well as by chain transfer of a $CH_2CH(Me)$(Polymeryl) group from zirconium to aluminum followed by quenching by acid (Scheme 3). The increase in the i-butyl end-groups with increasing the excess of MAO is consistent with an increased amount of chain transfer to aluminum. The diverse set of olefin resonances observed in some of the samples may be indicative of metal chain-walking or possibly of acid catalyzed isomerization upon work-up. Samples that show olefin signals (^{13}C NMR spectroscopy) were also found to show a similar amount of n-propyl end groups, fact consistent with termination events based on β-H elimination event and with 1,2-insertion of propylene into the generated metal hydride (Scheme 4). The observed predominant end-groups are consistent with a preference for 1,2-insertion of propylene into both Zr-H and Zr-C bonds.

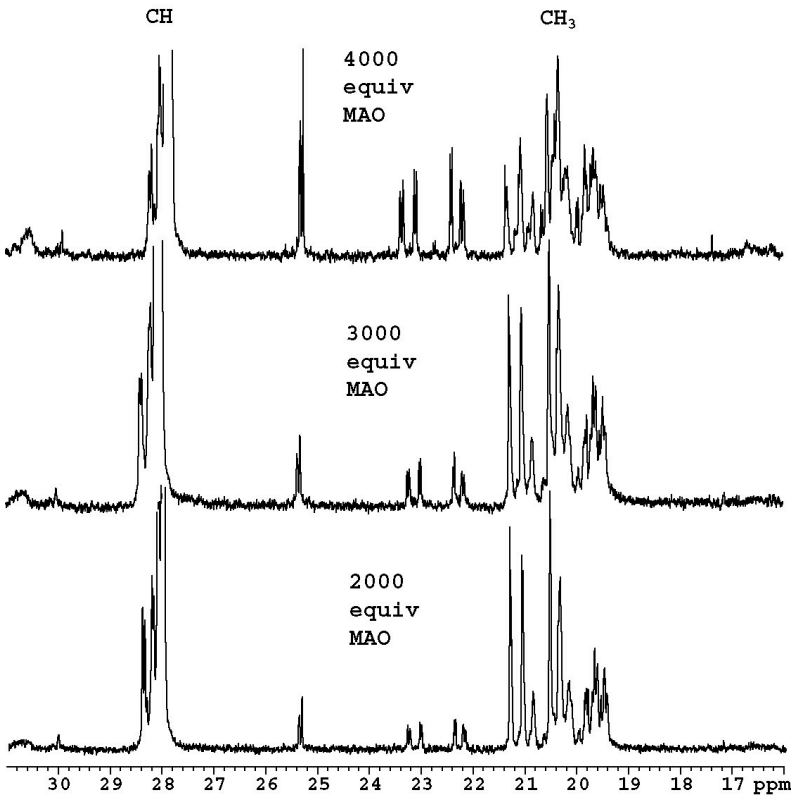

Figure 9. Selected region of ^{13}C NMR spectra for polymers obtained from **1a-ZrBn$_2$** upon activation with MAO (runs 6-8, Table 2).

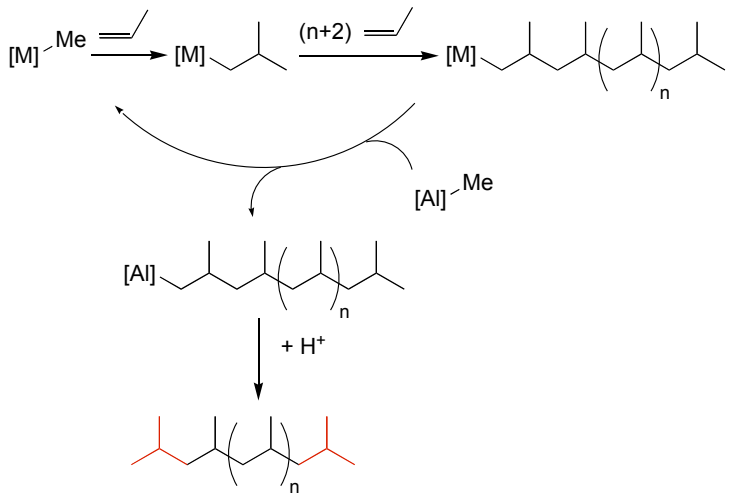

Scheme 3. Formation of i-butyl polymer end groups.

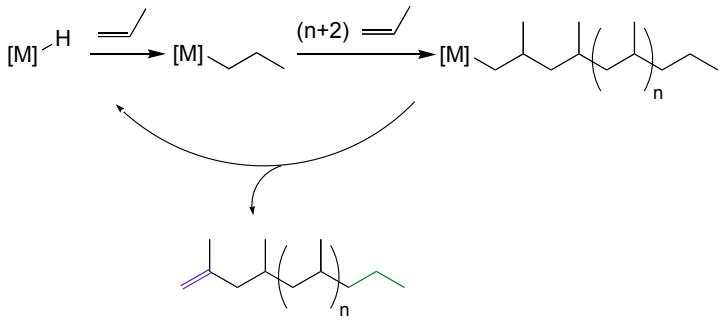

Scheme 4. Formation of olefin and n-propyl polymer end groups.

The differences in behavior between **1a-ZrBn$_2$** and **1b-ZrBn$_2$**, with regard to the presence of oligomers, i-butyl end-groups, effect of excess MAO, and propensity for β-H elimination could rise from a variety of reasons. For example the bulkier system **1b-ZrBn$_2$** may hinder chain transfer to aluminum and hence decrease the number of i-butyl end groups. However this does not account for the formation of light oligomers of propylene and increase in β-H elimination events. A broader pool of ligand frameworks needs to be explored before conclusions could be drawn.

To investigate the ability of the zirconium pyridine-diphenolate systems to support polymerization catalysis upon stoichiometric activation, the reaction of **1a-ZrBn$_2$** with $[Ph_3C][B(C_6F_5)_4]$ was performed in C_6D_5Cl, in a J-Young tube. This reaction is not clean, but formation of one major species was observed by ^{1}H NMR spectroscopy. Excess 1-hexene was added to the mixture and allowed to react for less than an hour. ^{1}H NMR spectroscopy shows almost complete disappearance of the 1-hexene peaks and appears of new signals in the olefin region. Upon adding another portion of 1-hexene and allowing to react for 12 h,

consumption of the monomer was observed again (the second time to a lower extent compared to the first). These observations indicate that the cationic zirconium species resulted from stoichiometric activation of **1b-ZrBn$_2$** is very active for the oligomerization of 1-hexene. While chain termination (or transfer) occurs frequently, the resulting zirconium species remain active for oligomerization for extended periods of time and even after the monomer is essentially consumed.

Complexes **2-ZrBn$_2$** and **3-ZrBn$_2$** show high polymerization activity as well. Complex **3-ZrBn$_2$** leads to atactic polymers with a small amount of olefin and n-propyl end groups (^{13}C NMR spectrum). GC analysis shows the absence of low propylene oligomers. This is in contrast with the outcome of the polymerization trials with **3-ZrBn$_2$** which leads to abundant formation of oily oligomers along with some higher polymers. A statistical distribution of C_9 to C_{45} oligomers was observed by GC and GC-MS analysis in this case. ^{13}C NMR spectra of these samples show olefin peaks and n-propyl terminal groups. These results, while not well understood, show that changing the nature of the linker leads to differences in the outcome of propylene polymerizations. This feature provides opportunities for further studies of the role of different ligand characteristics on the produced polymer.

Propylene polymerization and oligomerization with titanium complexes

The propylene polymerization reactivity of the present titanium dibenzyl species, upon activation with excess MAO has been investigated. Titanium pyridine diphenolate systems were found to be about three orders of magnitude less active than the zirconium counterparts. One polymer sample, obtained in quantities sufficient for analysis indicated that the obtained polymers are high molecular weight and show no olefin signals in the ^{13}C NMR spectra. The methyl region of the ^{13}C NMR spectrum shows a significant peak corresponding to the *mmmm* pentad overlapping with a distribution of peaks corresponding to atactic polymer. The nature of the solvent (toluene vs chlorobenzene) and of the titanium precursor was found not to influence activity significantly. The observed lower activity compared to zirconium could be attributed to a more crowded environment around the titanium center. Analysis of the precursors may hint to the features that control reactivity in these systems. Comparing the solid-state structures of the **1b-ZrBn$_2$** and **1b-TiBn$_2$** shows that the zirconium center accommodates a sixth ligand in its coordination sphere, unlike titanium. A more open metal center could possibly be more active for insertion but also for β-H elimination, which are observed for zirconium. Furthermore the zirconium precursor is C_s-symmetric while the titanium one is C_2-symmetric. The symmetry of the titanium system may have contributed to the observed fraction containing isotactic enrichment. It is important to note that while the precursors are well defined, the active cationic species are not, and may have geometries different from the ones observed in the precursors.

Titanium complexes supported by the furan (**2-TiBn$_2$**) and thiophene (**3-TiBn$_2$**) linked frameworks show high activity for the oligomerization of propylene. The oligomer products separate as oils upon quenching the MAO with HCl / MeOH and have been analyzed by GC, GC-MS, and NMR spectroscopy. The furan system was found to generate mainly C_9 to C_{21} oligomers, while the thiophene one generates a broader distribution of oligomers – C_9 to C_{33}. ^{13}C NMR spectra of the resulting oligomer mixtures show many olefin peaks along with a complicated aliphatic region. The complex spectra may be due to titanium chain-walking or to isomerization by acid catalysis during workup. Clearly, β-H elimination is a facile process in these systems. The increased activity of **2-TiBn$_2$** and **3-TiBn$_2$** compared to the pyridine based systems may be due to a more open metal center. This is apparent in the solid-state structures of **2-TiBn$_2$** and **1a-TiBn$_2$**. Compared to the pyridine system (**1a-TiBn$_2$**), the furan based system (**2-TiBn$_2$**) shows a significant increase in the distance between the bulky *ortho*-t-butyl groups from 9.1 to 11.3 A. This "opening" of the metal center could lead to faster insertion rates as well as the increased propensity for β-H elimination, both phenomena being observed.

Conclusions

Zirconium and titanium complexes supported by novel tridentate diphenolate ligands have been prepared and investigated for applications in propylene polymerization. The ligand architecture has been varied by changing the linker from pyridine, to furan, to thiophene and the size of the subtituents *ortho* to the phenol oxygen. The zirconium and titanium dibenzyl species have been prepared by toluene elimination. Titanium complexes with pyridine and furan diphenolates and zirconium complexes with pyridine and thiophene diphenolates have been characterized by single-crystal X-ray diffraction. The titanium solid-state structures are roughly C_2 symmetric while the zirconium ones are C_s symmetric. Both titanium and zirconium complexes were found to be active for the polymerization of propylene upon activation with MAO. The activities observed for the zirconium complexes are excellent, exceeding 10^6 g polypropylene / (mol Zr • h) in some cases. The excess of MAO was found to affect the polymerization activity and the level β-H elimination and chain transfer events. Titanium pyridine diphenolate systems are about 10^3 less active, but generate polymers of higher molecular weight. The titanium diphenolate-furan and diphenolate-thiophene systems were found to be active for propylene oligomerization catalysis. While in some cases, the observed catalytic behavior could be explained by catalyst structure and reaction conditions, there are still features not well understood. Further exploration of related systems should lead to a better understanding of the important characteristics of the present catalysts for controlling the polymerization outcomes.

Experimental Section

General Considerations and Instrumentation. All air- and moisture-sensitive compounds were manipulated using standard vacuum line, Schlenk, or cannula techniques or in a drybox under a nitrogen atmosphere. Solvents for air- and moisture-sensitive reactions were dried over sodium benzophenone ketyl or by the method of Grubbs.[48] Benzene-d_6 was purchased from Cambridge Isotopes and distilled from sodium benzophenone ketyl. Chloroform-d_1 and chlorobenzene-d_5 were purchased from Cambridge Isotopes and distilled from calcium hydride. Phenols **1a-H$_2$**, **b-H$_2$**, **c-H$_2$**, were prepared as described in Chapter 5. Other materials were used as received. Elemental analyses were performed by Desert Analytics, Tucson, AZ. ^{1}H and ^{13}C NMR spectra were recorded on Varian Mercury 300, or Varian INOVA-500 spectrometers and unless otherwise indicated at room temperature. Chemical shifts are reported with respect to internal solvent: 7.16 and 128.38 (t) ppm (C_6D_6); 7.27 and 77.23 (t) ppm ($CDCl_3$); 5.32 and 54.00 (q) ppm (CD_2Cl_2); 6.0 and 73.78 (t) ppm ($C_2D_2Cl_4$); for ^{1}H and ^{13}C data.

Preparation of protected diphenol 1b-Me$_2$. The procedure used in Chapter 4 (for **6**) was followed. **1b-Me$_2$**. Yield: 63% (1.16 g) for the palladium coupling reaction starting from 0.84 g dibromopyridine. ^{1}H NMR (300 MHz, $CDCl_3$) δ: 0.70 (t, 9H, CH_2CH_3), 1.85 (q, 6H, CH_2CH_3), 2.37 (s, 3H, aryl-CH_3), 3.32 (s, 6H, OCH_3), 7.05 (d, 2H, aryl-*H*), 7.42 (d, 2H, aryl-*H*), 7.65-7.75 (m, 3H, NC_5H_3). ^{13}C NMR (75 MHz,

$CDCl_3$) δ: 8.7 (CH_2CH_3), 21.4 (aryl-CH_3), 27.1 (CH_2CH_3), 44.9 (aryl-*C*), 61.0 (OCH_3), 123.0, 130.2, 131.0,132.4, 134.2, 136.2, 138.7,155.8,158.2 (aryl).

Preparation of diphenol 1b-H_2. Yield: 85% (0.935 g) for the removal of methyl protecting group from **1b-Me_2** (1.16 g). ^{1}H NMR (300 MHz, $CDCl_3$) δ: 0.71 (t, 9H, CH_2CH_3), 1.90 (q, 6H, CH_2CH_3), 2.35 (s, 3H, aryl-CH_3), 7.10 (d, 2H, aryl-*H*), 7.28 (d, 2H, aryl-*H*), 7.63 (d, 2H, NC_5H-3,5-H_2), 7.96 (t, 1H, NC_5H_2-4-*H*), 10.55 (br s, 2H, O*H*). ^{13}C NMR (75 MHz, $CDCl_3$) δ: 8.8 (CH_2CH_3), 21.4 (aryl-CH_3), 26.2 (CH_2CH_3), 44.9 (aryl-*C*), 120.2, 121.6, 126.5, 127.7, 132.9, 134.4, 140.0, 153.4, 157.3 (aryl). HRMS $C_{33}H_{45}O_2N$: Calcd mass: 487.3450. Measured mass: 487.3460.

Preparation of group 4 dibenzyl complexes. General procedure. 1a-$TiBn_2$. An Et_2O (10 mL) solution of phenol **1a** (100 mg, 206 μmol, 1 equiv) was added to a solution of $TiBn_4$ (86 mg, 206 μmol, 1 equiv) in Et_2O (5 mL). The mixture was stirred at room temperature for 5-12 h. Volatile materials were removed under vacuum and the residue was mixed with petroleum ether and recrystallized at -35 °C. The desired product was collected by filtration and washed with cold petroleum ether. This procedure gives 130 mg (181 μmol, 87%) of **1a-$TiBn_2$** as an orange powder. ^{1}H NMR (500 MHz, CD_2Cl_2) spectra recorded at 25 °C and -80 °C are shown in Figure 10 – no distereotopic hydrogens are observed at low temperature. ^{1}H NMR (500 MHz, CD_2Cl_2) δ: 1.41 (s, 18H, $C(CH_3)_3$), 1.94 (s, 18H, $C(CH_3)_3$), 3.48 (s, 4H, $TiCH_2$), 6.29-6.37 (m, 6H, *m*- and *p*-C_6H_2-H_3), 6.43 (d, 4H, *o*-C_6H_3-H_2), 7.16 (d, 2H, aryl-*H*), 7.43 (d, 2H, 3,5-NC_5H-H_2), 7.65 (t, 1H, 4-NC_5H_2-*H*), 7.68 (d, 2H, aryl-*H*). ^{13}C NMR (125 MHz, CD_2Cl_2) δ: 31.5 ($C(CH_3)_3$), 32.0 ($C(CH_3)_3$),

35.0 ($C(CH_3)_3$), 36.2 ($C(CH_3)_3$), 84.5 ($TiCH_2$), 122.8, 123.9, 126.1, 127.0, 127.2, 127.8, 129.4, 136.0, 138.3, 138.5, 141.7, 156.5, 157.3 (aryl). Anal. calcd. for $C_{47}H_{57}NO_2Ti$ (%): C, 78.86; H, 8.03; N, 1.96. Found: C, 77.62; H, 8.38; N, 1.95.

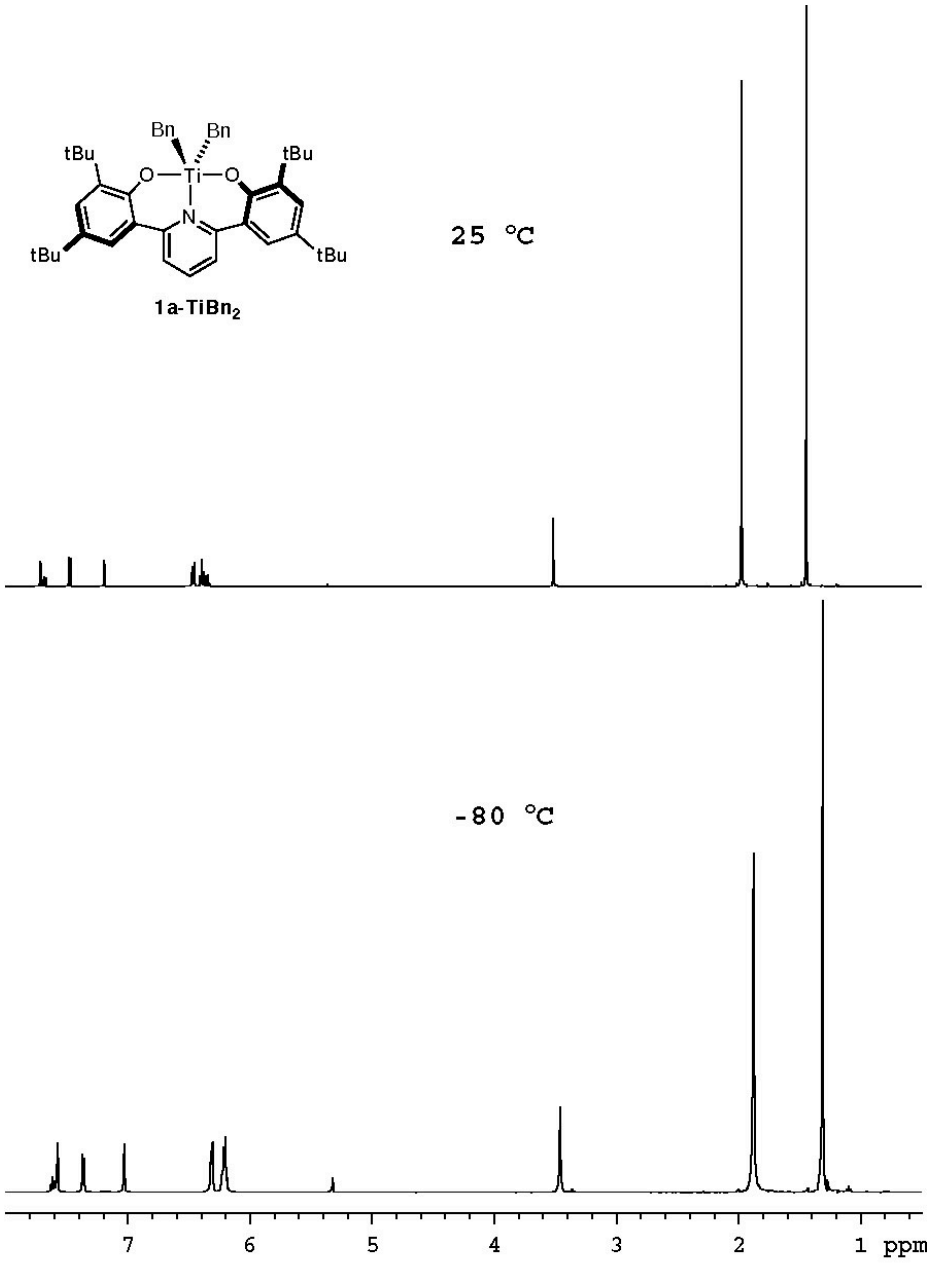

Figure 10. ^1H NMR spectra (CD_2Cl_2) of 1a-$TiBn_2$ at -80 °C and 25 °C.

1b-TiBn$_2$. ^{1}H NMR (500 MHz, C_6D_6) δ: 1.03 (t, 18H, CH_2CH_3), 2.34 (s, 6H, aryl-CH_3), 2.58 (q, 12H, CH_2CH_3), 3.83 (s, 4H, TiCH_2), 6.32 (t, 2H, *p*-C_6H_3-H_2), 6.51 (t, 4H, *m*-C_6H_3-H_2), 6.71 (t, 1H, 4-NC_5H_2-*H*), 6.77 (d, 4H, *o*-C_6H_3-H_2), 6.91 (d, 2H, 3,5-NC_5H-H_2), 6.93 (d, 2H, aryl-*H*), 7.43 (d, 2H, aryl-*H*). ^{13}C NMR (125 MHz, C_6D_6) δ: 9.4 (CH_2CH_3), 21.8 (aryl-CH_3), 27.3 (CH_2CH_3), 44.9 (aryl-*C*), 84.6 (TiCH_2), 123.2, 124.0, 127.9, 128.1, 128.6, 130.0, 130.2, 133.4, 133..8, 137.6, 138.8, 157.2, 157.5 (aryl). Anal. calcd. for $C_{47}H_{57}NO_2Ti$ (%): C, 78.86; H, 8.03; N, 1.96. Found: C, 78.53; H, 8.25; N, 2.10. 78% yield.

2-TiBn$_2$. ^{1}H NMR (500 MHz, C_6D_6) δ: 1.37 (s, 18H, $C(CH_3)_3$), 2.12 (s, 18H, $C(CH_3)_3$), 3.89 (s, 4H, TiCH_2), 6.37 (t, 2H, *p*-C_6H_3-H_2), 6.51-6.54 (m, 6H, overlap *m*-C_6H_3-H_2 and OC_4-H_2), 6.99 (d, 4H, *o*-C_6H_3-H_2), 7.49 (d, 2H, aryl-*H*), 7.73 (d, 2H, aryl-*H*). ^{13}C NMR (125 MHz, C_6D_6) δ: 32.0 ($C(CH_3)_3$), 32.1 ($C(CH_3)_3$), 35.0 ($C(CH_3)_3$), 36.6 ($C(CH_3)_3$), 88.2 (TaCH_2), 108.7, 121.3, 122.1, 124.1, 124.5, 128.4, 130.6, 137.9, 138.0, 143.1, 154.2, 155.7 (aryl). ^{13}C NMR (125 MHz, $CDCl_3$) δ: 31.5 ($C(CH_3)_3$), 31.9 ($C(CH_3)_3$), 34.8 ($C(CH_3)_3$), 36.1 ($C(CH_3)_3$), 87.4 (TiCH_2), 108.2, 120.7, 121.3, 123.3, 123.9, 127.9, 129.6, 137.2, 137.7, 142.7, 153.5, 155.0 (aryl). Anal. calcd. for $C_{46}H_{56}O_3Ti$ (%): C, 78.39; H, 8.01. Found: C, 77.84; H, 8.22. 62% yield.

3-TiBn$_2$. ^{1}H NMR (500 MHz, C_6D_6) δ: 1.33 (s, 18H, $C(CH_3)_3$), 2.06 (s, 18H, $C(CH_3)_3$), 3.93 (s, 4H, TiCH_2), 6.23 (s, 2H, SC_4H_2), 6.56 (t, 2H, *p*-C_6H_3-H_2), 6.3-6.5 (v br s, 4H, *m*-C_6H_3-H_2 or *o*-C_6H_3-H_2), 6.6-7.2 (v br s, 4H, *m*-C_6H_3-H_2 or *o*-C_6H_3-H_2), 7.41 (d, 2H, aryl-*H*), 7.74 (d, 2H, aryl-*H*). ^{1}H NMR (500 MHz, CD_2Cl_2) δ: 1.38 (s, 18H, $C(CH_3)_3$), 1.95 (s, 18H, $C(CH_3)_3$), 3.58 (br s, 4H, TiCH_2), 6.30 (s, 2H, SC_4H_2), 6.4-7.0 (br, 10H,

C_6H_5), 7.27 (d, 2H, aryl-*H*), 7.56 (d, 2H, aryl-*H*). ^{13}C NMR (125 MHz, CD_2Cl_2) δ: 31.9 (C(CH_3)$_3$), 32.0 (C(CH_3)$_3$), 34.9 (C(CH_3)$_3$), 36.6 (C(CH_3)$_3$), 88.4 (TiCH_2), 122.9, 124.0, 125.7, 126.3, 127.2, 128.7, 131.2, 135.5, 137.7, 139.9, 142.9, 160.5 (aryl). This was obtained as a glassy material which precluded recrystallization. Anal. calcd. for $C_{46}H_{56}O_2STi$ (%): C, 76.64; H, 7.83. Found: C, 76.61; H, 7.80.

1a-ZrBn$_2$. ^{1}H NMR (500 MHz, C_6D_6) δ: 1.39 (s, 18H, C(CH_3)$_3$), 1.79 (s, 18H, C(CH_3)$_3$), 2.70 (s, 4H, ZrCH_2), 6.63 (t, 2H, *p*-C_6H_3-H_2), 6.78 (t, 4H, *m*-C_6H_3-H_2), 6.83 (t, 1H, 4-NC_5H_2-*H*), 7.02 (d, 4H, *o*-C_6H_3-H_2), 7.06 (d, 2H, 3,5-NC_5H-H_2), 7.10 (d, 2H, aryl-*H*), 7.70 (d, 2H, aryl-*H*). ^{13}C NMR (125 MHz, C_6D_6) δ: 31.1 (C(CH_3)$_3$), 32.3 (C(CH_3)$_3$), 34.9 (C(CH_3)$_3$), 36.0 (C(CH_3)$_3$), 60.1 (ZrCH_2), 123.3, 124.8, 126.4, 127.5, 129.7, 130.1, 136.3, 139.0, 139.1, 141.7, 155.1, 160.5 (aryl). 88% yield.

1b-ZrBn$_2$. ^{1}H NMR (500 MHz, C_6D_6) δ: δ: 0.92 (t, 18H, CH_2CH_3), 2.29 (s, 6H, aryl-CH_3), 2.33 (q, 12H, CH_2CH_3), 2.83 (s, 4H, ZrCH_2), 6.53 (t, 2H, *p*-C_6H_3-H_2), 6.72 (t, 4H, *m*-C_6H_3-H_2), 6.79 (d, 2H, aryl-*H*), 6.83 (app t, 1H, 4-NC_5H_2-*H*), 6.94 (d, 2H, 3,5-NC_5H-H_2), 6.97 (d, 4H, *o*-C_6H_3-H_2), 7.29 (d, 2H, aryl-*H*). ^{13}C NMR (125 MHz, C_6D_6) δ: 9.3 (CH_2CH_3), 15.7, 21.6 (aryl-CH_3), 26.9 (CH_2CH_3), 45.4 (aryl-*C*), 61.2, 66.1, 123.1, 125.3, 127.9, 129.0, 129.7, 129.9, 131.0, 133.3, 133.5, 138.8, 138.9, 155.1, 160.0 (aryl). 58% yield.

2-ZrBn$_2$. ^{1}H NMR (500 MHz, C_6D_6) δ: 1.38 (s, 18H, C(CH_3)$_3$), 1.76 (s, 18H, C(CH_3)$_3$), 2.51 (s, 4H, ZrCH_2), 6.53 (s, 2H, OC_4H_2), 6.67 (t, 2H, *p*-C_6H_3-H_2), 6.82 (t, 4H, *m*-C_6H_3-H_2), 7.03 (d, 4H, *o*-C_6H_3-H_2), 7.48 (d, 2H, aryl-*H*), 7.59 (d, 2H, aryl-*H*). ^{13}C NMR (125 MHz, C_6D_6) δ: 31.0 (C(CH_3)$_3$), 32.1 (C(CH_3)$_3$), 34.9 (C(CH_3)$_3$), 36.1

($C(CH_3)_3$), 61.4 ($ZrCH_2$), 109.7, 121.4, 122.3, 124.1, 124.7, 129.6, 130.4, 137.5, 142.6, 152.9, 156.2 (aryl). 69% yield.

3-ZrBn$_2$. ^{1}H NMR (500 MHz, CD_2Cl_2) δ: 1.35 (s, 18H, $C(CH_3)_3$), 1.63 (s, 18H, $C(CH_3)_3$), 2.28 (br s, 4H, $ZrCH_2$), 6.51 (s, 2H, SC_4H_2), 6.68 (br s, 4H, *o*-C_6H_3-H_2), 6.85 (br t, 4H, *m*-C_6H_3-H_2), 6.99 (t, 1H, *p*-C_6H_4-*H*), 7.29 (d, 2H, aryl-*H*), 7.42 (d, xH, aryl-*H*). ^{13}C NMR (125 MHz, CD_2Cl_2) δ: 31.0 ($C(CH_3)_3$), 31.8 ($C(CH_3)_3$), 34.8 ($C(CH_3)_3$), 36.2 ($C(CH_3)_3$), 62.7 ($ZrCH_2$), 123.2, 123.9, 124.6, 125.5, 128.0, 130.0, 130.3, 137.5, 138.5, 142.4, 158.0 (aryl). Anal. calcd. for $C_{46}H_{56}O_2SZr$ (%): C, 72.29; H, 7.39. Found: C, 72.14; H, 7.17. 58% yield.

Preparation of (1a)$_2$-Ti. An Et_2O (3 mL) solution of $TiBn_4$ (12.7 mg, 30.8 μmol, 1 equiv) was added to a solution of **1a** (30 mg, 61.6, μmol, 2 equiv) in Et_2O (3 mL). The reaction mixture was allowed to stir at room temperature for 5 hours then volatile materials were removed under vacuum and the residue was analyzed by ^{1}H NMR spectroscopy to show the presence of **1a-TiBn$_2$** and **1a-H$_2$**. The crude residue was dissolved in toluene and transferred to a Schlenk tube equipped with a screw in Teflon stopper. The reaction flask was immersed in a oil bath at 60 °C and allowed to stir for 10.5 h. ^{1}H NMR spectrum of the residue upon volatile removal – one major species but reaction still not complete. The reaction mixture was resubmitted to heating with stirring for 24 h. Volatile materials were removed *in vacuo*. The residue shows clean formation of a species consistent with the formulation of **(1a)$_2$-Ti** by ^{1}H and ^{13}C NMR spectroscopy. ^{1}H NMR (500 MHz, C_6D_6) δ: 1.02 (s, 18H, $C(CH_3)_3$), 1.42 (s, 18H, $C(CH_3)_3$), 7.28 (t, 1H, NC_5H_2-*H*), 7.55 (d, 2H, aryl-*H*), 7.64 (d, , 2H, NC_5H-H_2), 7.76 (d, 2H, aryl-*H*). ^{13}C NMR (125 MHz,

C_6D_6) δ: 29.9 (C(*C*H_3)$_3$), 32.3 (C(*C*H_3)$_3$), 34.9 (*C*(CH$_3$)$_3$), 35.3 (*C*(CH$_3$)$_3$), 123.2, 125.4, 126.1, 126.6, 135.8, 139.0, 140.7, 155.9, 160.2 (aryl). Anal. calcd. for $C_{66}H_{86}N_2O_4Ti$ (%): C, 77.77; H, 8.50; N, 2.75. Found: C, 78.35; H, 8.53; N, 2.52.

Preparation of (1a)$_2$-Zr. An Et_2O (3 mL) solution of $TiBn_4$ (14 mg, 30.8 μmol, 1 equiv) was added to a solution of **1a** (30 mg, 61.6, μmol, 2 equiv) in Et_2O (3 mL). The reaction mixture was allowed to stir at room temperature for 5 hours then volatile materials were removed under vacuum and the residue was analyzed by ^{1}H NMR spectroscopy. Compounds **1a-ZrBn$_2$**, **1a-H$_2$**, and **(1a)$_2$-Zr** can be identified by 1H NMR spectroscopy. The crude residue was dissolved in toluene and transferred to a Schlenk tube equipped with a screw in Teflon stopper. The reaction flask was immersed in a oil bath at 60 °C and allowed to stir for 10.5 h. ^{1}H NMR spectrum of the residue upon volatile removal shows clean formation of a species consistent with the formulation of **(1a)$_2$-Zr** by ^{1}H and ^{13}C NMR spectroscopy. ^{1}H NMR (500 MHz, C_6D_6) δ: 1.17 (s, 18H, C(C*H*$_3$)$_3$), 1.43 (s, 18H, C(C*H*$_3$)$_3$), 7.21 (t, 1H, NC$_5$H$_2$-*H*), 7.47 (d, , 2H, NC$_5$H-*H*$_2$), 7.59 (d, 2H, aryl-*H*), 7.67 (d, 2H, aryl-*H*). ^{13}C NMR (125 MHz, C_6D_6) δ: 30.2 (C(*C*H$_3$)$_3$), 32.3 (C(*C*H$_3$)$_3$), 34.9 (*C*(CH$_3$)$_3$), 35.6 (*C*(CH$_3$)$_3$), 123.7, 125.6, 125.7, 127.2, 138.1, 139.6, 140.4, 156.8, 157.3 (aryl). Anal. calcd. for $C_{66}H_{86}N_2O_4Zr$ (%): C, 74.60; H, 8.16; N, 2.64. Found: C, 75.16; H, 8.26; N, 2.53.

General polymerization procedure. A high pressure glass reactor was charged with solid MAO (0.207 to 0.828 mg, 500 to 4000 equiv) and toluene (3 mL, distilled from Na/Ph_2CO) was added. The vessel was sealed and attached to a propylene tank and purged. Upon cooling to 0 °C, propylene (35-39 mL) was

condensed in. Zirconium or titanium precatalysts (0.7-7 μmol) were added via syringe, as a toluene solution (0.7 mL). The reaction mixture was stirred vigorously at 0 °C for the desired amount of time. Excess propylene was carefully vented then the cold bath was removed and a MeOH/HCl solution (10/1, 50 mL) was added slowly. The resulting mixture was transferred to an Erlenmeyer flask, additional MeOH/HCl solution was added (50 mL) and was allowed to stir at room temperature for at least four hours. The methanol solution was decanted and the polymer was rinsed with methanol. Upon decanting the methanol, the polymer was trasfered to a vial and volatile materials were removed by placing under vacuum and heating to 80 °C. The resulting materials were investigated by NMR spectroscopy and GPC. If oligomers rather than polymers were formed, the MeOH/HCl solution was extracted with pentane twice. t-Butyl-benzene (0.5 mL) was added to the combined organics and the mixture was investigated by GC and GC-MS.

X-ray Crystal Data: General Procedure. Crystals grown from diethyl ether (**1b-ZrBn$_2$**), toluene (**3-ZrBn$_2$**) or a mixture of diethyl ether and petroleum ether (**1a-TiBn$_2$**, **1b-TiBn$_2$**, and **2-TiBn$_2$**) at -35 °C were removed quickly from a scintillation vial to a microscope slide coated with Paratone N oil. Samples were selected and mounted on a glass fiber with Paratone N oil. Data collection was carried out on a Bruker Smart 1000 CCD diffractometer. The structures were solved by direct methods. All non-hydrogen atoms were refined anisotropically. Some details regarding refined data and cell parameters are available in Tables 4. Selected bond distances and angles are supplied in the captions of Figures 3 - 8.

Table 4. Crystal and refinement data for complexes **1b-ZrBn$_2$**, **3-ZrBn$_2$**, **1a-TiBn$_2$**, **1b-TiBn$_2$**, and **2-TiBn$_2$**.

	1b-ZrBn$_2$	**3-ZrBn$_2$**	**1a-TiBn$_2$**	**1b-TiBn$_2$**	**2-TiBn$_2$**
Empirical formula	$C_{51}H_{67}NO_3Zr \cdot C_4H_{10}O$	$C_{46}H_{56}O_2SZr \cdot 1.5(C_7H_8)$	$C_{47}H_{57}NO_2Ti$	$C_{47}H_{57}NO_2Ti$	$C_{46}H_{56}O_3Ti$
Formula weight	907.40	902.39	715.8	715.84	704.81
T (K)	100(2)	100(2)	100(2)	208(2)	100(2)
a, Å	15.8272(11)	32.9618(13)	11.2513(4)	9.6700(6)	9.5660(14)
b, Å	16.9637(11)	10.8886(4)	13.1612(4)	19.2570(12)	14.100(2)
c, Å	19.1982(12)	28.8405(12)	13.7639(4)	21.9500(14)	15.100(2)
α, deg			76.075(1)		85.053(3)
β, deg	107.911(3)	107.7780(10)	81.769(1)	102.2860(10)	76.411(3)
γ, deg			84.868(1)		85.591(3)
Volume, Å^3	4904.7(6)	9856.8(7)	1954.7(1)	3993.8(4)	1969.0(5)
Z	4	8	2	4	2
Crystal system	Monoclinic	Monoclinic	Triclinic	Monoclinic	Triclinic
Space group	$P2_1/n$	C2/c	$P\bar{1}$ (# 2)	P2(1)/c	$P\bar{1}$ (# 2)
d_{calc}, g/cm^3	1.229	1.216	1.216	1.191	1.189
θ range, deg	1.64 to 28.40	1.65 to 33.99	1.83 to 39.06	2.12 to 28.24	1.94 to 33.27
μ, mm^{-1}	0.269	0.305	0.258	0.252	0.256

Abs. correction	None	None	None	Semi-empir. from equiv.	TWINABS
GOF	1.128	1.258	1.329	1.035	1.730
R_1,[a] wR_2[b] [I>2σ(I)]	0.0468, 0.0731	0.0485, 0.0821	0.0471, 0.0966	0.0448, 0.1168	0.0516, 0.1067

[a] $R_1 = \sum | |F_o| - |F_c| | / \sum |F_o|$. [b] $wR_2 = [\sum[w(F_o^2-F_c^2)^2] / \sum[w(F_o^2)^2]]^{1/2}$.

References

(1) *Encyclopedia of Polymer Science and Technology*; on-line ed.; Wiley & Sons, Inc., 2006.

(2) Kissin, Y. V. In *Kirk-Othmer Encyclopedia of Chemical Technology Online*; Wiley & Sons, Inc: 2005.

(3) Coates, G. W. *Chem. Rev.* **2000**, *100*, 1223-1252.

(4) Resconi, L.; Cavallo, L.; Fait, A.; Piemontesi, F. *Chem. Rev.* **2000**, *100*, 1253-1345.

(5) Gibson, V. C.; Spitzmesser, S. K. *Chem. Rev.* **2003**, *103*, 283-315.

(6) Britovsek, G. J. P.; Gibson, V. C.; Wass, D. F. *Angew. Chem., Int. Ed. Engl.* **1999**, *38*, 428-447.

(7) Coates, G. W.; Hustad, P. D.; Reinartz, S. *Angew. Chem., Int. Ed. Engl.* **2002**, *41*, 2236-2257.

(8) Ittel, S. D.; Johnson, L. K.; Brookhart, M. *Chem. Rev.* **2000**, *100*, 1169-1203.

(9) Baumann, R.; Stumpf, R.; Davis, W. M.; Liang, L. C.; Schrock, R. R. *J. Am. Chem. Soc.* **1999**, *121*, 7822-7836.

(10) Liang, L. C.; Schrock, R. R.; Davis, W. M.; McConville, D. H. *J. Am. Chem. Soc.* **1999**, *121*, 5797-5798.

(11) Aizenberg, M.; Turculet, L.; Davis, W. M.; Schattenmann, F.; Schrock, R. R. *Organometallics* **1998**, *17*, 4795-4812.

(12) Baumann, R.; Davis, W. M.; Schrock, R. R. *J. Am. Chem. Soc.* **1997**, *119*, 3830-3831.

(13) Mehrkhodavandi, P.; Schrock, R. R.; Pryor, L. L. *Organometallics* **2003**, *22*, 4569-4583.

(14) Mehrkhodavandi, P.; Schrock, R. R. *J. Am. Chem. Soc.* **2001**, *123*, 10746-10747.

(15) Mehrkhodavandi, P.; Bonitatebus, P. J.; Schrock, R. R. *J. Am. Chem. Soc.* **2000**, *122*, 7841-7842.

(16) Mason, A. F.; Coates, G. W. *J. Am. Chem. Soc.* **2004**, *126*, 16326-16327.

(17) Mason, A. F.; Coates, G. W. *J. Am. Chem. Soc.* **2004**, *126*, 10798-10799.

(18) Reinartz, S.; Mason, A. F.; Lobkovsky, E. B.; Coates, G. W. *Organometallics* **2003**, *22*, 2542-2544.

(19) Mitani, M.; Furuyama, R.; Mohri, J.; Saito, J.; Ishii, S.; Terao, H.; Nakano, T.; Tanaka, H.; Fujita, T. *J. Am. Chem. Soc.* **2003**, *125*, 4293-4305.

(20) Tian, J.; Hustad, P. D.; Coates, G. W. *J. Am. Chem. Soc.* **2001**, *123*, 5134-5135.

(21) Tian, J.; Coates, G. W. *Angew. Chem., Int. Ed. Engl.* **2000**, *39*, 3626-3629.

(22) Matsui, S.; Tohi, Y.; Mitani, M.; Saito, J.; Makio, H.; Tanaka, H.; Nitabaru, M.; Nakano, T.; Fujita, T. *Chem. Lett.* **1999**, 1065-1066.

(23) Segal, S.; Goldberg, I.; Kol, M. *Organometallics* **2005**, *24*, 200-202.

(24) Groysman, S.; Tshuva, E. Y.; Goldberg, I.; Kol, M.; Goldschmidt, Z.; Shuster, M. *Organometallics* **2004**, *23*, 5291-5299.

(25) Tshuva, E. Y.; Groysman, S.; Goldberg, I.; Kol, M.; Goldschmidt, Z. *Organometallics* **2002**, *21*, 662-670.

(26) Tshuva, E. Y.; Goldberg, I.; Kol, M.; Goldschmidt, Z. *Chem. Commun.* **2001**, 2120-2121.

(27) Tshuva, E. Y.; Goldberg, I.; Kol, M.; Goldschmidt, Z. *Organometallics* **2001**, *20*, 3017-3028.

(28) Tshuva, E. Y.; Goldberg, I.; Kol, M. *J. Am. Chem. Soc.* **2001**, *123*, 3621-3621.

(29) Tshuva, E. Y.; Goldberg, I.; Kol, M.; Goldschmidt, Z. *Inorg. Chem. Commun.* **2000**, *3*, 611-614.

(30) Tshuva, E. Y.; Goldberg, I.; Kol, M. *J. Am. Chem. Soc.* **2000**, *122*, 10706-10707.

(31) Tshuva, E. Y.; Goldberg, I.; Kol, M.; Weitman, H.; Goldschmidt, Z. *Chem. Commun.* **2000**, 379-380.

(32) Tshuva, E. Y.; Versano, M.; Goldberg, I.; Kol, M.; Weitman, H.; Goldschmidt, Z. *Inorg. Chem. Commun.* **1999**, *2*, 371-373.

(33) Takaoki, K.; Miyatake, T. *Macromol. Symp.* **2000**, *157*, 251-257.

(34) Nakayama, Y.; Watanabe, K.; Ueyama, N.; Nakamura, A.; Harada, A.; Okuda, J. *Organometallics* **2000**, *19*, 2498-2503.

(35) Chan, M. C. W.; Tam, K. H.; Pui, Y. L.; Zhu, N. Y. *J. Chem. Soc., Dalton Trans.* **2002**, 3085-3087.

(36) Chan, M. C. W.; Tam, K. H.; Zhu, N. Y.; Chiu, P.; Matsui, S. *Organometallics* **2006**, *25*, 785-792.

(37) Steinhauser, S.; Heinz, U.; Sander, J.; Hegetschweiler, K. *Z. Anorg. Allg. Chem.* **2004**, *630*, 1829-1838.

(38) Li, Y. Q.; Liu, Y.; Bu, W. M.; Guo, J. H.; Wang, Y. *Chem. Commun.* **2000**, 1551-1552.

(39) Mack, H.; Eisen, M. S. *J. Chem. Soc., Dalton Trans.* **1998**, 917-921.

(40) Guerin, F.; McConville, D. H.; Vittal, J. J. *Organometallics* **1996**, *15*, 5586-5590.

(41) Gauvin, R. M.; Osborn, J. A.; Kress, J. *Organometallics* **2000**, *19*, 2944-2946.

(42) Froese, R. D. J.; Musaev, D. G.; Morokuma, K. *Organometallics* **1999**, *18*, 373-379.

(43) Coates, G. W.; Waymouth, R. M. *Science* **1995**, *267*, 217-219.

(44) Tian, J.; Hustad, P. D.; Coates, G. W. *J. Am. Chem. Soc.* **2001**, *123*, 5134-5135.

(45) Milano, G.; Cavallo, L.; Guerra, G. *J. Am. Chem. Soc.* **2002**, *124*, 13368-13369.

(46) Lin, S.; Waymouth, R. M. *Macromolecules* **1999**, *32*, 8283-8290.

(47) Cheng, H. N.; Smith, D. A. *Macromolecules* **1986**, *19*, 2065-2072.

(48) Pangborn, A. B.; Giardello, M. A.; Grubbs, R. H.; Rosen, R. K.; Timmers, F. J. *Organometallics* **1996**, *15*, 1518-20.

Chapter 7

Group 3 Dialkyl Complexes with Tetradentate (L, L, N, O; L = N, O, S) Phenolate Ligands – Synthesis and Reactivity

This work was done in collaboration with undergraduate Smaranda C. Marinescu and has been published:

Marinescu, S. M.; Agapie, T.; Day, M. W.; Bercaw, J. E. *Organometallics*, **2007**, *26*, 1178-1190.

Abstract

Tripodal, tetradentate phenols, $(LCH_2)_2NCH_2$-C_6H_2-3,5-$(CMe_3)_2$-2-OH (L = CH_2OCH_3 (**1**), CH_2NEt_2 (**2**), 2-C_5H_4N (**3**), CH_2SCMe_3 (**5**), CH_2NMe_2 (**6**)), were synthesized, and metallations were performed via alkane elimination from yttrium and scandium *tris*-alkyl complexes to generate the corresponding dialkyl complexes $[(LCH_2CH_2)_2NCH_2$-C_6H_2-3,5-$(CMe_3)_2$-2-O]MR_2 (M = Y, L = OCH_3, R = CH_2SiMe_2Ph (**7a**); M = Y, L = NEt_2, R = CH_2SiMe_2Ph (**7b**); M = Sc, L = OCH_3, R = CH_2SiMe_2Ph (**8a**), M = Sc, L = $SCMe_3$, R = CH_2SiMe_2Ph (**8b**); M = Y, L = OCH_3, R = CH_2SiMe_3 (**9**), M = Sc, L = OCH_3, R = CH_2SiMe_3 (**10**)). X-ray crystallographic studies show that **7a**, **7b**, and **8a** adopt, in the solid state, mononuclear structures of C_1 symmetry. The ^{1}H NMR spectra of these dialkyl complexes in benzene-d_6 at high temperatures reveal exchange processes involving the ether groups and the alkyl groups. The dynamic behavior of species **7a**, **8a** and **10** in toluene-d_8 was investigated by variable-temperature ^{1}H NMR spectroscopy. The activation parameters of the fluxional processes for **7a**, **8a** and **10** were determined by line-shape and Eyring analyses (for **7a**: $\Delta H^{\ddagger}$ = 7.3 ± 0.3 kcal/mol; $\Delta S^{\ddagger}$ = -16 ± 1.4 cal/mol·K; for **8a**: $\Delta H^{\ddagger}$ = 9.9 ± 0.5 kcal/mol; $\Delta S^{\ddagger}$ = -15.3 ± 1.8 cal/mol·K; for **10**: $\Delta H^{\ddagger}$ = 10.8 ± 0.6 kcal/mol; $\Delta S^{\ddagger}$ = -11.4 ± 1.9 cal/mol·K). These data establish that the dialkyl complexes **7a**, **8a** and **10** undergo a non-dissociative exchange process. The scandium dialkyl complex $[(C_5H_4N$-2-$CH_2)_2NCH_2$-C_6H_2-3,5-$(CMe_3)_2$-2-O]$Sc(CH_2SiMe_2Ph)_2$ (**11**) was found to cleanly undergo activation of a C-H bond of a methylene linking a pyridine to the central nitrogen donor. This process follows first order kinetics (k = 2.8(3) x

10^{-4} s^{-1} at 0 °C). The yttrium dialkyl complexes **7a** and **9** react with one equivalent of $[PhNHMe_2]^+[B(C_6F_5)_4]^-$ in chlorobenzene-d_5, to generate a solution that slowly polymerizes ethylene. Compounds **7** - **10** also polymerize ethylene with low activity upon activation with MAO.

Introduction

Cationic alkyl complexes of group 4 metals are the most common single-site olefin polymerization catalysts.[1-3] Isoelectronic, neutral alkyl complexes of group 3 metals generally show much lower polymerization activity.[4] One approach to increasing polymerization activity involves the generation of cationic alkyl species. The most common route to cationic alkyl species involves alkide abstraction from neutral dialkyl or trialkyl complexes. Over the last few years the synthesis of dialkyl and trialkyl complexes of group 3 metals supported by multidentate ligands has been an area of increasing interest.[5-21] Recent reports indicate that, upon activation, the resulting cationic alkyl complexes display promising polymerization activities.[8-10,13,20] However, group 3 still remains a relatively unexplored part of the transition series in the context of olefin polymerization.[2,3]

As part of our continuing interest in developing novel polymerization catalysts, we have explored new ligand designs to support cationic group 3 alkyl complexes. Accordingly, a series of $[L_2NO]$ (L = neutral donor; N = tertiary amine; O = phenolate) monoanionic, tripodal ligands was targeted. There is precedent in the literature for related $[N_3O]$ monoanionic ligands to support

zinc(II) and copper(I) complexes[22-25] as well as for [S_2NO] ligands to support copper(II) complexes.[26] Complexes supported by triazacyclononanes functionalized with one pendant phenolate arm have been reported as well.[15,27] Furthermore, related tetradentate amino phenolate ligands have been recently shown to support group 3, 4, and 5 alkyl complexes.[15,28-34] Group 4 dialkyls supported by diphenolate ligands were reported to be active olefin polymerization catalysts when activated, and, in some cases, isotactic poly-1-hexene and polypropylene are obtained.[34-36] These reports indicate that monoanionic [L_2NO] frameworks could be used as robust ancillary ligands. Inspired by the promising precedents, a new series of [L_2NO] ligands was prepared, and the ability of these to support group 3 dialkyl species was investigated (below). This report describes the synthesis and reactivity of a series of yttrium and scandium alkyl complexes with such tetradentate phenolate ligands. After we started work on this project, two of the ligands described herein were reported by others to support early metal complexes. Ligand **1**, $(CH_3OCH_2CH_2)_2NCH_2$-C_6H_2-3,5-$(CMe_3)_2$-2-OH, was recently reported by Kol *et al.* as part of a study of a number of zirconium complexes;[37] while ligand **2**, $(Et_2NCH_2CH_2)_2NCH_2$-C_6H_2-3,5-$(CMe_3)_2$-2-OH was reported by Arnold *et al.* as part of a study of group 3 catalysts for the polymerization of lactide and ε-caprolactone.[38]

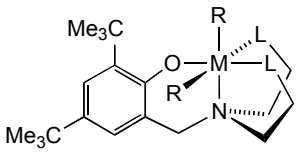

M = Y, Sc
L = OCH_3, NEt_2, NMe_2, $SCMe_3$
R = CH_2SiMe_2Ph, CH_2SiMe_3

Results and Discussion

Ligand and metal dialkyl complex syntheses. (a) Synthesis of $(LCH_2)_2NCH_2$-C_6H_2-3,5-$(CMe_3)_2$-2-OH (L = CH_2OCH_3, CH_2NEt_2, 2-C_5H_4N)

A modification of the Mannich condensation used by Kol *et al.* to synthesize tetradentate diphenolate ligands was employed for the synthesis of tetradentate monophenolate ligands **1** and **2** (eq 1).[39] Using a related strategy, compound **3** was prepared from the corresponding benzyl bromide and secondary amine (eq 2). Compounds **1**, **2** and **3** were synthesized using commercially available or easily accessible starting materials. These procedures afford the desired products in close to quantitative yields. The phenols obtained in this fashion do not require additional purification before metallation.

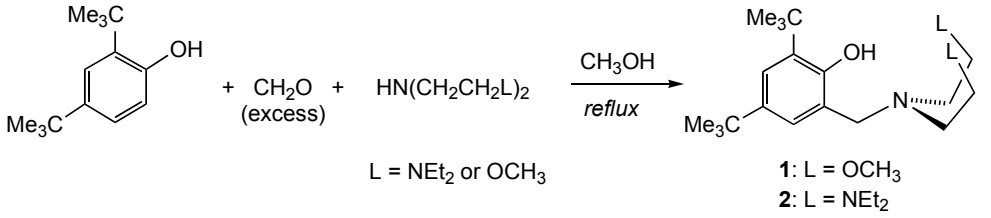

(1)

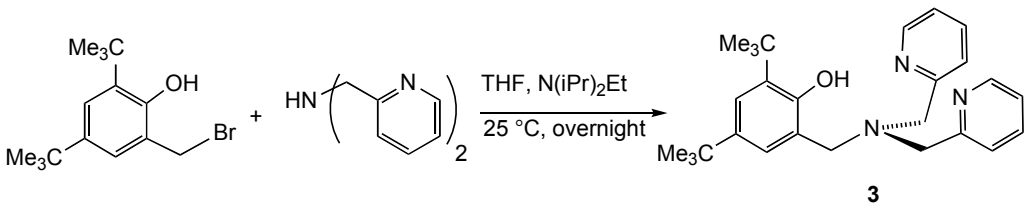

(2)

(b) Synthesis of $(LCH_2CH_2)_2NCH_2$-C_6H_2-3,5-$(CMe_3)_2$-2-OH (L = $SCMe_3$, NMe_2)

An alternative route to [L_2NO] ligand frameworks involves nucleophilic substitution on dichloride **4** (Scheme 1). This synthetic route was developed to gain access to ligand precursors for which the appropriate secondary amine starting materials required for the Mannich condensation are not commercially available. Compound **4** has been readily prepared in two steps from commercially available starting materials via Mannich condensation followed by chlorination with thionyl chloride. The nucleophilic substitution step could present a problem due to the unprotected phenol functionality; however, the example shown affords the desired product **5** cleanly upon purification by precipitation from CH_3OH, and compound **6** upon purification by column chromatography.

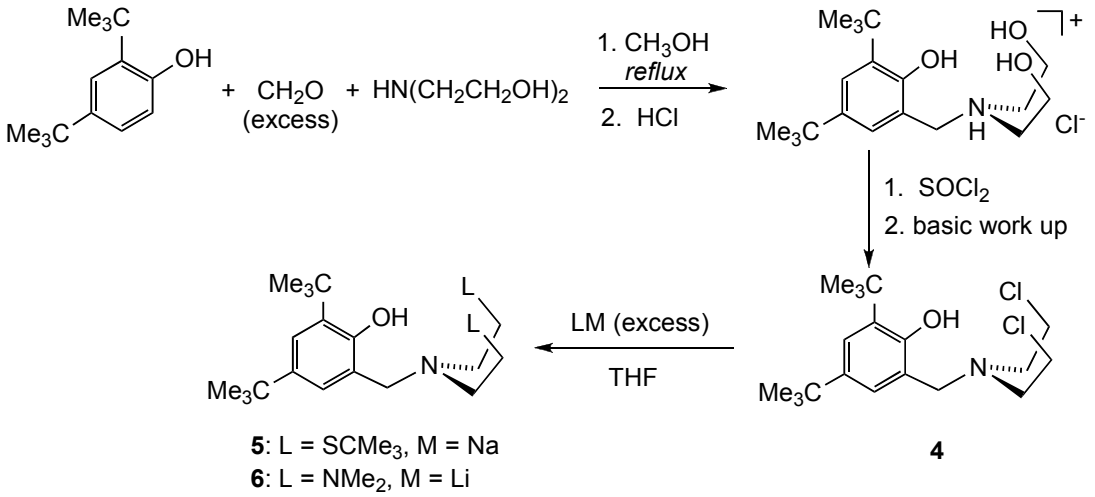

Scheme 1. Synthesis of phenols with pendant thioethers and amines.

The ligand syntheses described here offer the possibility of altering the nature of the two L groups. Such ligand architecture allows for steric and electronic variations on both the phenol and the L donor fragments.

(c) Synthesis of metal dialkyl complexes [$(LCH_2CH_2)_2NCH_2$-C_6H_2-3,5-$(CMe_3)_2$-2-O]MR_2 (M = Y, Sc; L = OCH_3, NEt_2, $SCMe_3$; R = CH_2SiMe_2Ph, CH_2SiMe_3)

Using *in situ* generated yttrium and scandium trialkyl starting materials, the preparation of target metal dialkyl complexes was accomplished via alkane elimination (eq 3). The starting materials, $M(THF)_2(CH_2SiMe_2Ph)_3$, M = Y, Sc, were expected to give more crystalline products,[17] while $M(THF)_2(CH_2SiMe_3)_3$ were preferred for ease of byproduct removal. For all compounds (eq 3) metallations occur cleanly with elimination of one equivalent of $SiMe_3Ph$ or $SiMe_4$, based on the ^1H NMR spectrum of the crude reaction mixture. The isolated yields are somewhat low due to the high solubility of the products. In general, the reactions occur more cleanly when the reaction mixture is started at low temperatures (< -70 °C) and allowed to warm to room temperature. Dialkyl complexes **7a**, **7b**, **8a**, and **8b** can be separated from the alkane byproduct by recrystallization from petroleum ether-diethyl ether mixtures. On the other hand, when the more volatile byproduct, $SiMe_4$, is formed, the purification is accomplished by removing the volatile materials under vacuum. All complexes are air and water-sensitive.

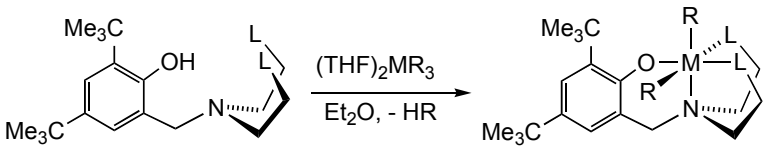

(3)

R = CH_2SiMe_2Ph
M = Y; L = OCH_3 (**7a**), NEt_2 (**7b**)
M = Sc; L = OCH_3 (**8a**), $SCMe_3$ (**8b**)

R = CH_2SiMe_3
M = Y; L = OCH_3 (**9**)
M = Sc; L = OCH_3 (**10**)

The reactions of yttrium and scandium trialkyl complexes, $M(THF)_2(CH_2SiMe_2Ph)_3$, with ligand $(Me_2NCH_2CH_2)_2NCH_2$-C_6H_2-3,5-$(CMe_3)_2$--2-OH (**6**) generate multiple, as yet unidentified, products according to the ^{1}H NMR spectroscopy. One possible decomposition pathway is the C-H activation of the methyl groups. A recent report indicates that group III complexes with pendant tertiary amine donors can undergo ligand C-H activation reactions.[21] The authors of this report state that the rate of this process is dependent on subtle ligand changes. If the reactions shown in eq 3 are similarly very dependent on ligand structure, we may reconcile why in some, but not all cases the targeted dialkyl product (**7b**) can be isolated with pendant amine donors. Reaction of phenol **3** with metal *tris*-alkyls will be discussed in a later section.

Assuming the formation of hexacoordinate metal complexes, the dialkyl species could present C_1 or C_s symmetry (Scheme 2). In order to determine the favored geometry in the solid state as well as solution, single crystal X-ray diffraction studies as well as variable temperature ^{1}H NMR spectroscopic studies were performed. These are discussed in the following sections.

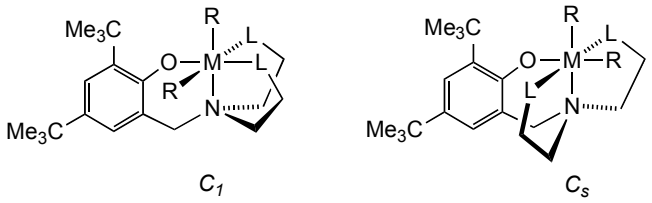

Scheme 2. Possible binding octahedral geometries for dialkyl complexes supported by tetradentate phenolate ligands.

Solid-State Structures of Dialkyl Complexes

The solid-state structures of **7a**, **7b**, and **8a** were determined by single crystal X-ray diffraction studies (Figures 1 - 3). In all three cases, a six-coordinate, distorted octahedral, monomeric, C_1-symmetric structure is displayed. One alkyl group is trans to the linking (axial) nitrogen, the other trans to a pendant neutral donor, rather than a phenolate oxygen, possible to avoid greater trans influence in the latter case. The metal-ether oxygen distances are larger that the metal-phenolate oxygen distances by 0.3 - 0.4 Å. Moreover, the M-O bonds to the ethers trans to the alkyls are longer than to the ones trans to the phenolates by 0.05 - 0.1 Å, as anticipated for a larger trans influence for the alkyls. A similar trend is observed for the pendant amines, with a difference of more than 0.2 Å between the one trans to the alkyl vs. the one trans to the phenolate. An analogous substantial bond length difference was observed for a related yttrium dialkyl triaminoamide complex reported recently.[21]

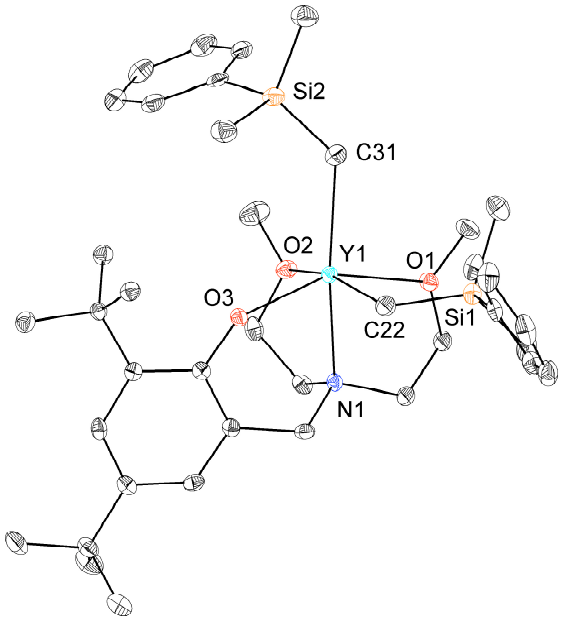

Figure 1. Structural drawing of **7a** $[(CH_3OCH_2CH_2)_2NCH_2\text{-}C_6H_2\text{-}3,5\text{-}(CMe_3)_2\text{-}2\text{-}O]Y(CH_2SiMe_2Ph)_2$ with thermal ellipsoids at the 50% probability level. Selected bond lengths (Å) and angles (°): Y-O_3 2.1140(11); Y-O_1 2.4038(11); Y-O_2 2.5040(11); Y-N 2.5345(14); Y-C_{22} 2.4453(19); Y-C_{31} 2.4557(19); N-Y-O_1 69.30(4); N-Y-O_2 65.89(4); N-Y-O_3 78.55(4); N-Y-C_{22} 99.28(6); O_3-Y-C_{22} 94.48(6).

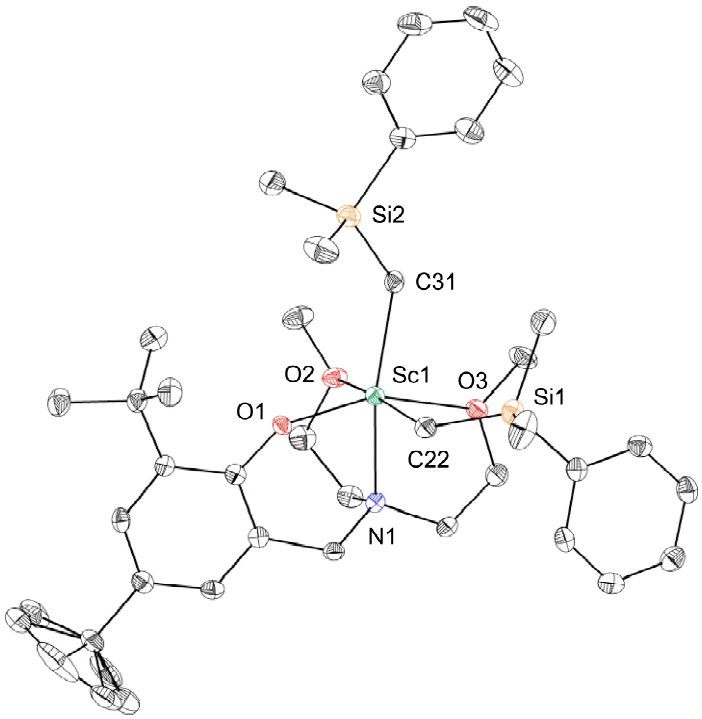

Figure 2. Structural drawing of **8a**, $[(CH_3OCH_2CH_2)_2NCH_2\text{-}C_6H_2\text{-}3,5\text{-}(CMe_3)_2\text{-}2\text{-}O]Sc(CH_2SiMe_2Ph)_2$, with thermal ellipsoids at the 50% probability level. Selected bond lengths (Å) and angles (°): Sc-O_1 1.9702(10); Sc-O_2 2.3494(11); Sc-O_3 2.3028(11); Sc-N 2.3721(13); Sc-C_{22} 2.2698(16); Sc-C_{31} 2.2636(16); N-Sc-O_1 82.50(4); N-Sc-O_2 71.98(4); N-Sc-O_3 70.16(4); N-Sc-C_{22} 99.58(5); O_1-Sc-C_{22} 95.90(5).

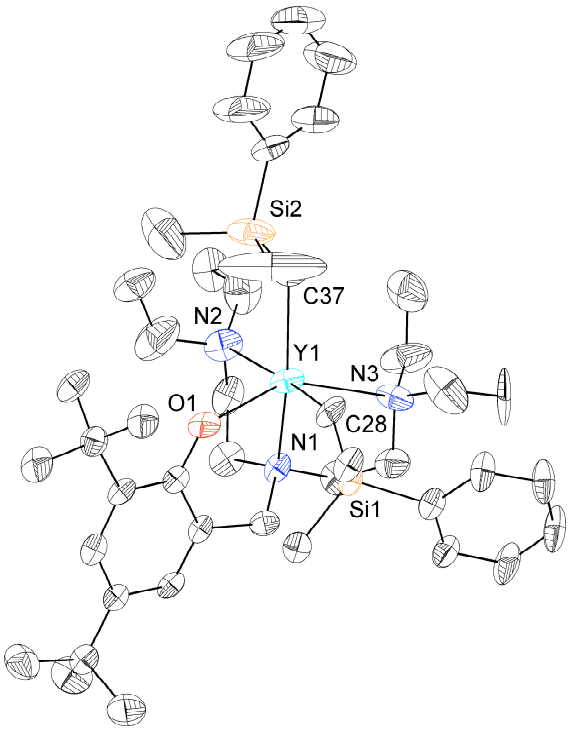

Figure 3. Structural drawing of **7b**, $[(Et_2NCH_2CH_2)_2NCH_2\text{-}C_6H_2\text{-}3,5\text{-}(CMe_3)_2\text{-}2\text{-}O]\text{-}Y(CH_2SiMe_2Ph)_2$, with thermal ellipsoids at the 50% probability level. Selected bond lengths (Å) and angles (°): Y-O_1 2.104(4); Y-N_1 2.538(4); Y-N_2 2.832(5); Y-N_3 2.594(5); Y-C_{28} 2.425(5); Y-C_{37} 2.430(5); N_1-Y-O_1 76.55(13); N_1-Y-N_2 66.81(14); N_1-Y-N_3 71.62(14); N_1-Y-C_{28} 114.41(16); O_1-Y-C_{37} 112.95(16). Only one of the two positions calculated for the ethyl methyl groups is shown.

Solution Structure of Dialkyl Complexes

Despite their C_1 solid-state structures, the room temperature (294 K) ^{1}H NMR spectra for both **7a** and **8a**, [$(CH_3OCH_2CH_2)_2NCH_2$-C_6H_2-3,5-$(CMe_3)_2$-2-O]-M$(CH_2SiMe_2Ph)_2$ (M = Y, Sc), in toluene-d_8 feature, among other peaks, a singlet corresponding to Si(CH_3)$_2$Ph, a singlet corresponding to MCH_2 (M = Y, Sc) and a singlet corresponding to OCH_3. At temperatures below 203 K, the ^{1}H NMR spectra feature two singlets corresponding to the OCH_3 groups (Figure 4), along with four singlets for Si(CH_3)$_2$Ph (Figure 5) and four doublets for MCH_2 (some overlapping). Upon increasing the temperature, the peaks corresponding to the Si(CH_3)$_2$Ph groups collapse first into two singlets and then, at higher temperatures into a singlet. Similar behavior is observed for **8b**, [$(Me_3CSCH_2CH_2)_2NCH_2$-C_6H_2-3,5-$(CMe_3)_2$-2-O]Sc$(CH_2SiMe_2Ph)_2$, (Figure 6). For compounds **9** and **10**, [$(CH_3OCH_2CH_2)_2NCH_2$-C_6H_2-3,5-$(CMe_3)_2$-2-O]-M$(CH_2SiMe_3)_2$ (M = Y, Sc), with a different alkyl, the methyls bound to each silicon are equivalent and give rise to only two singlets at low temperature and one singlet at high temperature. At room temperature, compound **7b**, [$(Et_2NCH_2CH_2)_2NCH_2$-C_6H_2-3,5-$(CMe_3)_2$-2-O]Y$(CH_2SiMe_2Ph)_2$, displays only one set of peaks for the metal bound alkyl groups; moreover the four ethyl groups display only one broad triplet/quartet combination.

Given the small number of peaks corresponding to the [CH_2SiMe_2Ph] groups, the room temperature spectra for **7a** and **8a** are neither consistent with C_s nor with C_1 structures (Scheme 2). For the C_s structure, the two metal alkyl

groups are chemically different and distinct peaks are expected in the ^{1}H NMR spectra – two singlets for the Si(CH_3)$_2$Ph protons and two singlets for MCH_2 (M = Y, Sc). On the other hand, for the C_1 structure, the silicon methyls are diastereotopic and should display four singlets. Furthermore, the Sc- or Y-bound methylene groups present diastereotopic hydrogens and should display four doublets in the ^{1}H NMR spectrum. The ether methyls are chemically different and should display two distinct singlets. Hence, the variable temperature ^{1}H NMR spectroscopy data are indicative of an exchange process. The ^{1}H NMR spectra at low temperatures (*vide infra*) do indicate that the lowest energy structure is the C_1-symmetric one, as established for the solid-state structures. The ^{1}H NMR spectroscopy data for **8b**, **9**, and **10** indicate the presence of a similar exchange process and a C_1-symmetric ground state structure.

Dynamic processes in 7a, 8a, and 10

In order to determine exchange rate constants, line-shape analyses were performed for **7a** (Figure 4), **8a**, and **10**. As shown in Figure 4, increasing the temperature from 203 K to 273 K results in broadening and coalescence of the OCH_3 resonances followed by sharpening of the resulting coalesced signal. For **7a** and **8a**, line-shape analyses were performed only for the ether methyl groups. The activation parameters for exchange of methoxy groups were obtained from Eyring plots (Figures 7 and 8) over a temperature range of greater than 60 K: $\Delta H^{\ddagger}$ = 7.3 ± 0.3 kcal/mol and $\Delta S^{\ddagger}$ = -16.2 ± 1.4 cal/(mol·K) for **7a** and $\Delta H^{\ddagger}$ = 9.9 ± 0.5

kcal/mol and $\Delta S^{\ddagger}$ = -15.3 ± 1.8 cal/(mol·K) for **8a**. Compound **10**, [$(CH_3OCH_2CH_2)_2NCH_2$-C_6H_2-3,5-$(CMe_3)_2$-2-O]Sc$(CH_2SiMe_3)_2$, provides an opportunity to inspect independently the exchange rates for both the ether methyl groups and the silicon methyl groups, because both display only two singlets in the slow exchange limit. The activation parameters determined for the exchange of the ether methyl groups are $\Delta H^{\ddagger}$ = 10.6 ± 0.4 kcal/mol and $\Delta S^{\ddagger}$ = -12.3 ± 1.4 cal/(mol·K), and the ones for the silicon methyl groups are $\Delta H^{\ddagger}$ = 11.1 ± 0.7 kcal/mol and $\Delta S^{\ddagger}$ = -10.4 ± 2.3 cal/(mol·K), values that are not significantly different and indicative of a single process for exchange of both methoxy and alkyl groups.

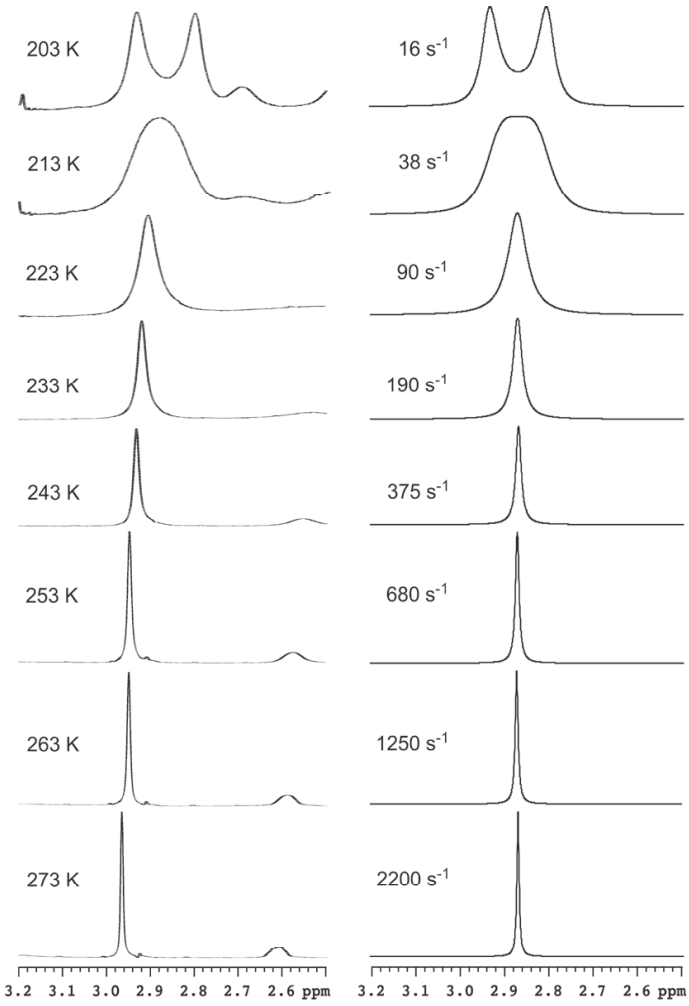

Figure 4. Experimental (left) and simulated (right) variable temperature ^{1}H NMR spectra of **7a** $[(CH_3OCH_2CH_2)_2NCH_2\text{-}C_6H_2\text{-}3,5\text{-}(CMe_3)_2\text{-}2\text{-}O]\text{-}Y(CH_2SiMe_2Ph)_2$, showing the O$CH_3$ (δ 2.94 and 2.8) resonances (toluene-d_8, 500 MHz). Best-fit first-order rate constants (k) are illustrated with the simulated spectra.

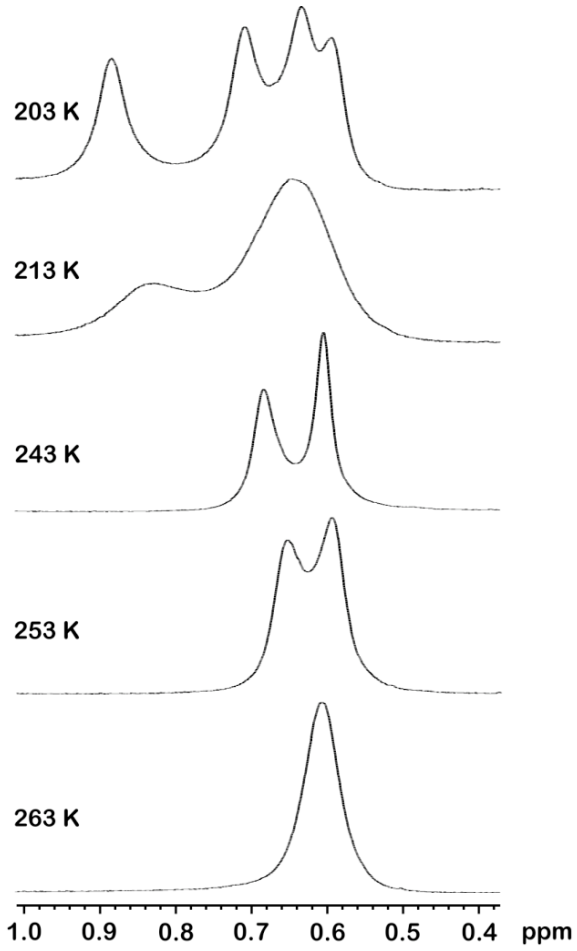

Figure 5. Variable temperature ^{1}H NMR spectra of **7a**, $[(CH_3OCH_2CH_2)_2NCH_2\text{-}C_6H_2\text{-}3,5\text{-}(CMe_3)_2\text{-}2\text{-}O]Y(CH_2SiMe_2Ph)_2$, showing the $Si(CH_3)_2Ph$ peaks (toluene-d_8, 500 MHz).

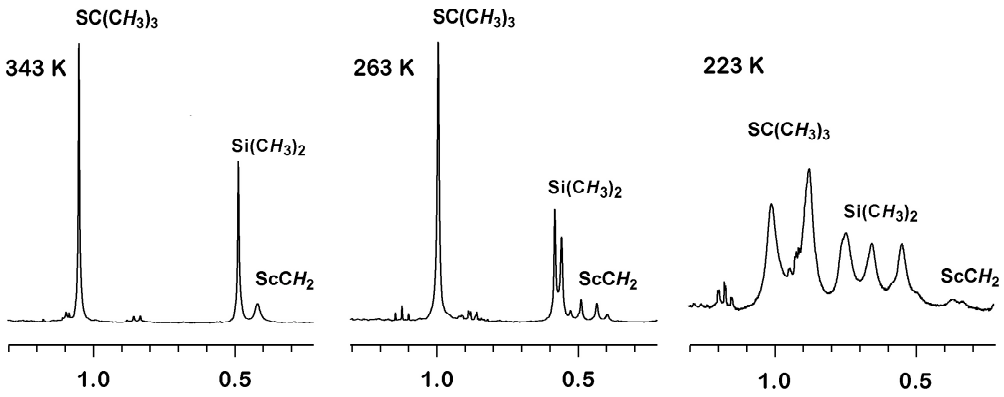

Figure 6. Selected aliphatic region of the ^{1}H NMR spectra of **8b,** $[(Me_3CSCH_2CH_2)_2NCH_2\text{-}C_6H_2\text{-}3,5\text{-}(CMe_3)_2\text{-}2\text{-}O]Sc(CH_2SiMe_2Ph)_2$, at different temperatures (toluene-d_8, 300 MHz).

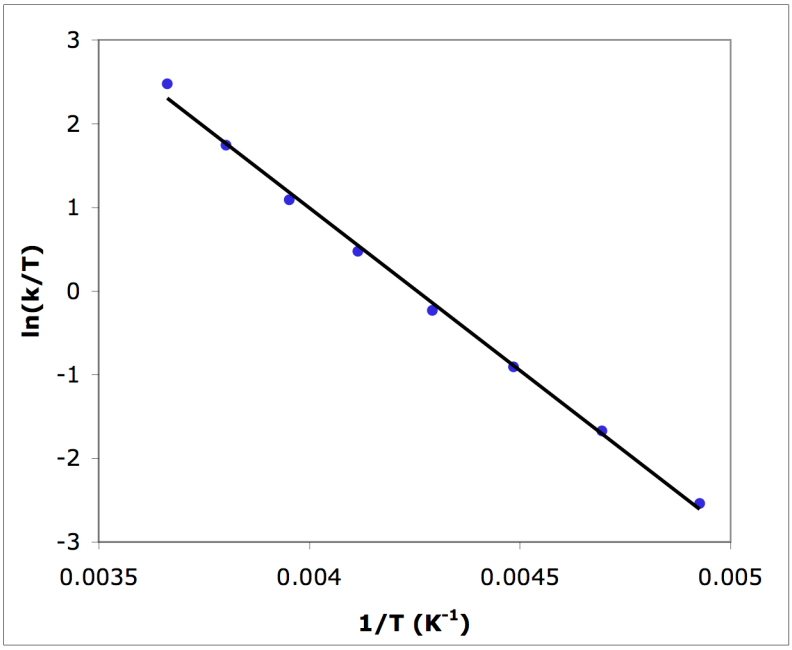

Figure 7. Eyring plot for $[(CH_3OCH_2CH_2)_2NCH_2\text{-}C_6H_2\text{-}3,5\text{-}(CMe_3)_2\text{-}2\text{-}O]\text{-}Y(CH_2SiMe_2Ph)_2$ (**7a**) (toluene-d_8, 500 MHz).

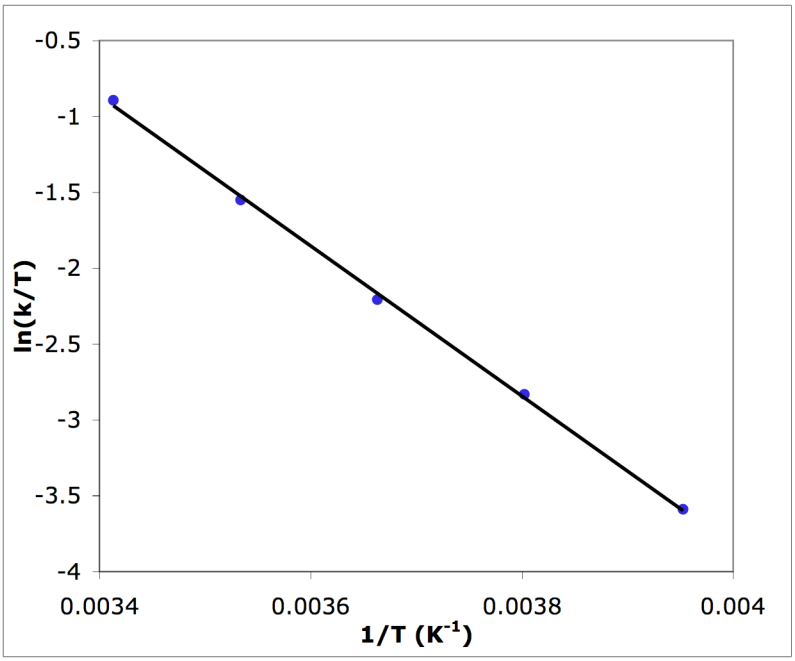

Figure 8. Eyring plot for $[(CH_3OCH_2CH_2)_2NCH_2\text{-}C_6H_2\text{-}3,5\text{-}(CMe_3)_2\text{-}2\text{-}O]\text{-}Sc(CH_2SiMe_2Ph)_2$ (**8a**) (toluene-d_8, 300 MHz).

The substantially negative values of the entropy of activation suggest that **7a**, **8a**, and **10** undergo a non-dissociative exchange process. The proposed mechanism that accommodates the dynamic NMR behavior involves twisting of the trigonal faces of the pseudo-octahedron (Scheme 3), resulting in the interconversion of three facial groups via trigonal prismatic intermediates. This type of mechanism has previously been proposed for dynamic processes in pseudo-octahedral complexes of titanium.[40]

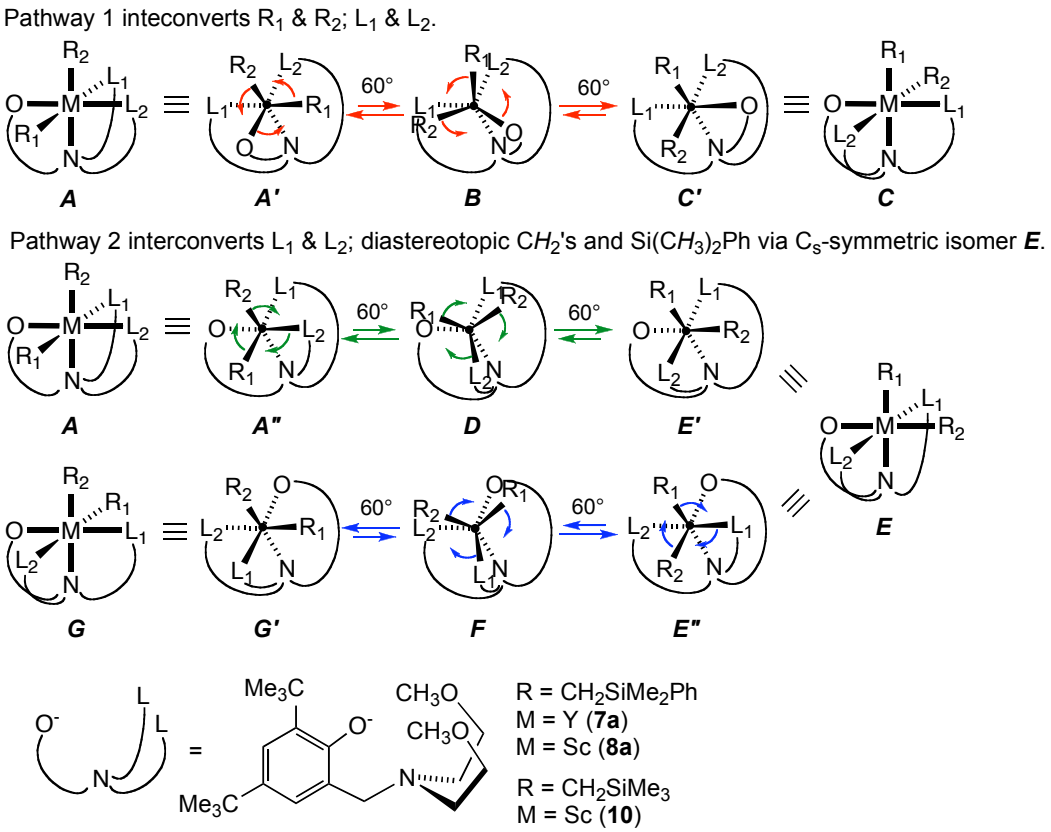

Scheme 3. Proposed mechanism for the exchange of R and L ligands.

Two reaction pathways are required from the ground state structure (***A***): one involves rotation around the pseudo-C_3 axis passing through the [R_1R_2O] and [NL_2L_1] trigonal faces, and a second involving rotation around the pseudo-C_3 axis passing through the [$R_1R_2L_2$] and [NOL_1] trigonal faces followed by rotation around the pseudo-C_3 axis passing through the [$R_1L_1R_2$] and [NL_2O] trigonal faces. Other possible pseudo-C_3 rotations would necessarily change the nature of the tetradentate [ONL_1L_2] coordination (N axial with O, L_1 and L_2 cis to N), and thus need not be considered for non-dissociative processes. Twisting of the [R_1R_2O] face (red arrow pathway) leads to the C_1 structure ***C*** via trigonal

prismatic intermediate ***B***. This process affords simultaneous exchange of the ligands L_1 and L_2 together with alkyls R_1 and R_2. However, this process does *not* exchange the diastereotopic groups of the alkyls (CH_2 and $Si(CH_3)_2Ph$). A pathway that interconverts these diastereotopic protons involves twisting of the $[R_1R_2L_2]$ face (green arrow pathway) to accesses C_s structure, ***E***, which, upon subsequent twisting of the $[R_1L_1R_2]$ face (blue arrow pathway), gives ***G*** (an enantiomer of ***A***). This process also interchanges L_1 and L_2, but does not change the chemical environment of the alkyl groups R_1 and R_2. Hence, either pathway can interconvert the neutral ligands L_1 and L_2, but neither one alone can exchange both the metal alkyl groups and the diastereotopic groups on each of the metal alkyls.

Significantly, for **7a**, $[(CH_3OCH_2CH_2)_2NCH_2\text{-}C_6H_2\text{-}3,5\text{-}(CMe_3)_2\text{-}2\text{-}O]\text{-}Y(CH_2SiMe_2Ph)_2$, exchange of $[Si(CH_3)_2Ph]$ methyl hydrogens occurs in two stages; first the four singlets collapse into two singlets and, at higher temperatures, into one singlet (Figure 5). This stepwise behavior suggests that the exchange involves two processes with different activation barriers. The diastereotopic methylene hydrogens for these alkyls (both CH_2SiMe_3 and CH_2SiMe_2Ph derivatives) appear to also exhibit stepwise exchange behavior that in some cases changes from four doublets to a singlet by way of *two doublets*, although in most cases it is not possible to unambiguously identify these small signals at intermediate temperatures. The 263 K spectrum for **8b** $[(Me_3CSCH_2CH_2)_2NCH_2\text{-}C_6H_2\text{-}3,5\text{-}(CMe_3)_2\text{-}2\text{-}O]Sc(CH_2SiMe_2Ph)_2$ (Figure 6) does clearly show one set of these two resonances as an AB quartet indicative of that

the alkyls are in rapid exchange, but the individual diastereotopic hydrogens on the two methylenes Sc(CH_aH_b)$_2$SiMe$_2$Ph are in slow exchange and thus still coupled to each other.[41] We infer therefore that the stepwise exchange of diastereotopic [Si(CH_3)$_2$Ph] groups gives rise to a similar situation: 4 singlets in slow exchange, followed by rapid alkyl exchange with slow diastereotopic [Si(CH_3)$_a$(CH_3)$_b$Ph] methyl exchange at intermediate temperatures giving rise to two singlets, and rapid alkyl and diastereotopic methyl exchange at high temperatures exhibiting one singlet. We attempted to simulate the observed spectra using two independent exchange rate constants at each temperature for the four peaks due to Si(CH_3)$_2$Ph of **7a**, but even for this relatively simple case we have been unsuccessful. Thus, we can conclude that interconversion ***A*** ⇔ ***C*** is sometimes faster than ***A*** ⇔ ***E*** ⇔ ***G*** (this is the case for **8b**), but we are unable to quantify the differences in rates and barriers.

The activation enthalpy for the yttrium complex **7a** is smaller than that for the scandium analog **8a**. Assuming that bond strengths are affected in a similar fashion along the reaction coordinate, it is likely that larger yttrium center renders the complex more sterically open, facilitating access to the strained trigonal prismatic intermediates. Supporting this hypothesis, increased steric bulk around the metal center has been shown to increase the activation enthalpy for a series of titanium/acac complexes that exchange via a similar mechanism.[40]

Interestingly, the room temperature ^{1}H NMR spectrum of **7b**, [(Et$_2$NCH$_2$CH$_2$)$_2$NCH$_2$-C$_6$H$_2$-3,5-(CMe$_3$)$_2$-2-O]Y(CH$_2$SiMe$_2$Ph)$_2$, shows only one set

of peaks for the ethyl groups suggesting fast exchange of ethyls bound to the same nitrogen. The mechanism proposed here for the complexes with ether donors (Scheme 3) cannot account for this exchange. However, a mechanism involving amine dissociation followed by inversion and recoordination would provide a pathway for exchanging the ethyl groups on each pendant nitrogen donor. This type of mechanism has been proposed recently for a related yttrium dialkyl triaminoamide complex.[21] Furthermore, a related yttrium complex supported by the same ligand but with bulkier amide ligands ($N(SiMe_2H)_2$ instead of CH_2SiMe_2Ph) has been reported to coordinate only via one of the two pendant amines suggesting that the amine coordination is not very strong.[38]

Metallation of $(C_5H_5N\text{-}2\text{-}CH_2)_2NCH_2\text{-}C_6H_2\text{-}3,5\text{-}(CMe_3)_2\text{-}2\text{-}OH$ (3) with Scandium *Tris*(alkyl)

Reaction of scandium *tris*-alkyl, $Sc(THF)_2(CH_2SiMe_2Ph)_3$, with ligand $(C_5H_5N\text{-}2\text{-}CH_2)_2NCH_2\text{-}C_6H_2\text{-}3,5\text{-}(CMe_3)_2\text{-}2\text{-}OH$ (**3**) in diethyl ether, at room temperature, generates first a green solution that, within seconds, becomes deep red. The reaction occurs cleanly; only one set of peaks corresponding to the multidentate ligand is observed in the ^1H NMR spectrum at room temperature after 1 h. The reaction was repeated at low temperature (-45 ^oC) and the outcome investigated using ^1H, ^1H-^1H COSY, ^{13}C, DEPT, and HETCOR NMR spectroscopic studies. At -45 ^oC, the ^1H NMR spectrum shows only one set of peaks corresponding to the multidentate ligand, along with four singlets corresponding

to Si(CH_3)$_2$Ph and four doublets corresponding to ScCH_2. The benzylic hydrogen atoms, [(C_5H_5N-2-CH_2)$_2$NCH_2-C_6H_2-3,5-(CMe_3)$_2$-2-O], show six doublets (two distinct doublets and four overlapped) that correlate with three CH_2 peaks (DEPT study) with chemical shifts between δ 60 and 63 ppm. One equivalent of $PhSiMe_3$, along with free THF released from the starting material, are observed as well. These data are consistent with the formation of dialkyl species **11** having a C_1 symmetry structure at -45 °C (Scheme 4), similar to the structures above.

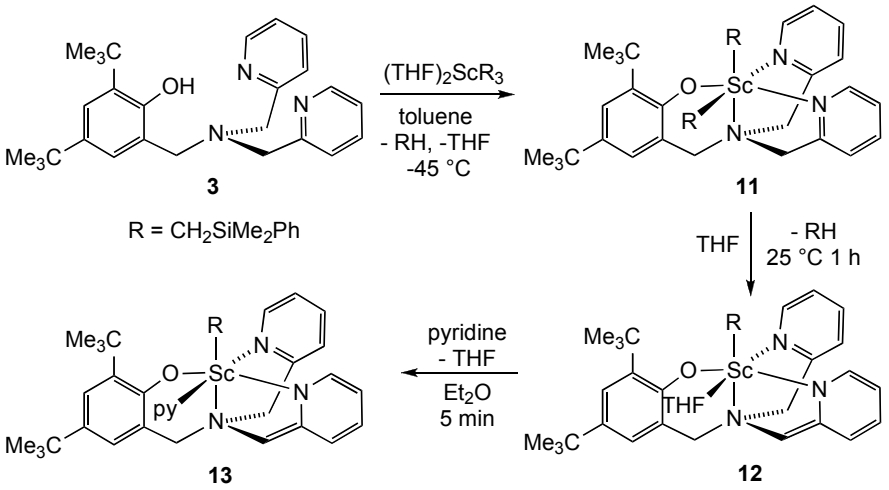

Scheme 4. Metallation and CH activation of phenol **3**.

The reaction mixture generated at -45 °C was allowed to warm to room temperature and, after one hour, was interrogated by NMR spectroscopy. The formation of one additional equivalent of $PhSiMe_3$ was observed. The ^{1}H NMR spectrum shows two singlets corresponding to Si(CH_3)$_2$Ph and two doublets corresponding to ScCH_2. In the benzylic region, four doublets and one singlet are observed. This singlet correlates with a methine carbon at 100.9 ppm as

determined by a HETCOR experiment. The $^{1}J_{C-H}$ value of 170 Hz is indicative of an sp^2 hybridized carbon.[45] A tautomeric binding mode through the carbon is possible, but not consistent with the observed coupling constant. The THF peak is broadened and shifted indicating ether coordination. These data are consistent with the decomposition of **11** via C-H activation of a methylene group linking a pyridine to the central nitrogen to give **12** with loss of another equivalent of silane. Confirmation that the activated methylene position does link a pyridine arm was made by quenching a THF solution of **12** with methanol-d_4 and checking for deuterium incorporation (^{2}H NMR spectroscopy) in the phenol found in the resulting mixture. A similar activation of a ligand benzylic C-H bond was reported as well for a tantalum system supported by a related tetradentate diphenolate ligand.[29] However, a scandium alkyl complex supported by a dianionic ligand displaying the same pyridine arm as here was stable enough for isolation at room temperature.[15] THF may be displaced by addition of pyridine to afford **13** (Scheme 4), but not by softer donors such as ethylene, 2-butyne, and trimethylphosphine.[42] Compound **12** is thermally unstable, decomposing in solution even at -35 °C over a few days.

Transformation of **11** into **12** was monitored by ^{1}H NMR spectroscopy in toluene-d_8 at 0 °C. Both the disappearance of **11** and the formation of **12** were followed over time by measuring the integrals for selected, baseline separated proton peaks. As expected, these processes were found to follow first order

kinetics with similar rate constants (Figure 9, SI, k = 2.8(3) x 10^{-4} s^{-1} for the decay of **11** and k = 2.3(1) x 10^{-4} s^{-1} for the formation of **12**).

Attempts to cleanly metallate **3** with $Y(THF)_2(CH_2SiMe_2Ph)_3$ have been unsuccessful. NMR scale reactions of the yttrium trialkyl complex and compound **3**, in toluene-d_8, when monitored by ^{1}H NMR spectroscopy at -35 °C, reveal multiple, unidentified products.

Generation of Cationic Alkyls for Ethylene Polymerizations

Generation and characterization of cationic monoalkyl yttrium species was attempted. In order to allow characterization by ^{1}H NMR spectroscopy, a stoichiometric activator, $[PhNHMe_2]^+[B(C_6F_5)_4]^-$, was utilized (eq 5). NMR scale reactions of $[(CH_3OCH_2CH_2)_2NCH_2\text{-}C_6H_2\text{-}3,5\text{-}(CMe_3)_2\text{-}2\text{-}O]YR_2$, R = CH_2SiMe_2Ph (**7a**), and R = CH_2SiMe_3 (**9**) with one equivalent anilinium salt in chlorobenzene-d_5 occur with formation of a major new species, but not cleanly at -35 °C. For **9**, formation of $SiMe_4$ is observed, along with one major set of peaks corresponding to the phenoxide $C(CH_3)_3$ groups. The metal bound alkyl group displays two doublets for YCH_2, while the ether groups display two singlets for the OCH_3 protons. Upon warming to room temperature, the doublets for the metal bound methylene group collapse into a singlet, as do the two peaks for the ether methyl groups. These observations are consistent with the protonation of one of the alkyl groups to generate a C_1 symmetric monoalkyl species (**15**) at -35 °C. The

$N(CH_3)_2$ resonances are shifted from free dimethyl aniline suggesting coordination to the metal center. Compound **15** seems to be involved in a dynamic process that exchanges the ether groups and the diastereotopic YCH_2 protons. The cationic species decomposes within hours at room temperature. Slow consumption of ethylene (7.5 equivalents in 7 h) was observed with **15** generated at low temperature.

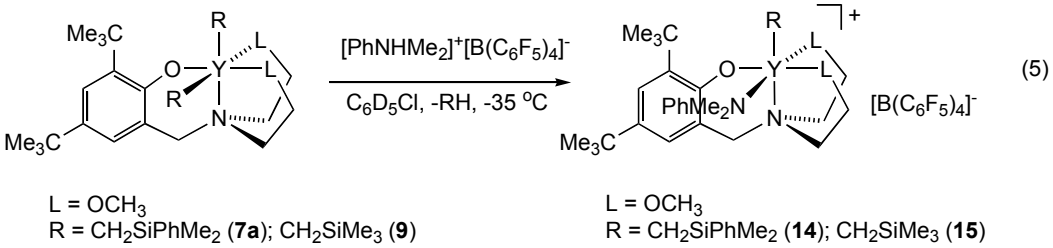

(5)

L = OCH_3
R = $CH_2SiPhMe_2$ (**7a**); CH_2SiMe_3 (**9**)

L = OCH_3
R = $CH_2SiPhMe_2$ (**14**); CH_2SiMe_3 (**15**)

The dialkyl complexes were investigated for ethylene polymerization activity more generally. Medium scale polymerizations with **7a** or **9** and activation with $[PhNHMe_2]^+[B(C_6F_5)_4]^-$ in a closed system with excess ethylene (initial pressure of 4 atm) led to the isolation of small amounts of polymer upon workup with MeOH/HCl. The polymerization was repeated as above, but with addition of excess MAO, as well as with MAO as sole activator. Only minor changes in polymerization activity arose on changing the nature of activator. Polymerization trials with dialkyls **7a**, **7b**, **8a**, **8b**, **9**, and **10** were performed upon activation with excess MAO (500 equivalents), under 5 bar of ethylene, using 3.3 x 10^{-4} *M* concentrations of precatalyst. Under these conditions, all complexes serve as sluggish polymerization precatalysts, displaying productivities between 0.5 and 2.5 Kg PE/mol M·bar (M = Y, Sc), after 1 h reaction times. The very low

polymerization activities in these systems with pendant, unconstrained, donor groups may relate to the results reported by Hessen *et al.* who studied tetradentate monoanionic ligands based on one amide donor and three amine donors.[21] A system competent for ethylene polymerization was obtained when the neutral donors were linked in a macrocycle (1,4,7-triazacyclononane), but the polymerization activity decreases twenty fold when the NN macrocyclic linkage is removed. This reduction in activity was attributed to a reduced stability of the complexes with "open" triamine ligands, and, indeed, that may well be the case here.

Conclusions

Yttrium and scandium dialkyl complexes supported by readily available tetradentate, monoanionic phenolate ligands can be prepared by alkane elimination from *tris*-alkyl precursors. ^{1}H NMR spectroscopy studies show fluxional behavior in solution. C_1 symmetric structures are favored for all alkyls in solid state as well as in solution. The dynamic behavior of dialkyl complexes with pendant ether donors was investigated by variable-temperature ^{1}H NMR spectroscopy, and the fluxional rates and activation parameters were determined by line-shape analysis. A mechanism involving non-dissociative ligand exchange, likely via trigonal prismatic intermediates generated via twists of pseudooctahedral trigonal faces containing both alkyls and another donor ligand. The ligand with pendant pyridine donors $(C_5H_4N\text{-}2\text{-}CH_2)_2NCH_2\text{-}C_6H_2\text{-}3,5\text{-}(CMe_3)_2\text{-}2\text{-}OH$ (**3**) presents a different reactivity.

Low temperature NMR studies indicate intermediate formation of dialkyl species at -45 °C, that decomposes cleanly by activation of a C-H bond of a methylene connecting the pyridine to the nitrogen linker position at 0 °C. The yttrium dialkyl complexes **7a** and **9** react quite cleanly (^{1}H NMR spectroscopy), at low temperatures with one equivalent of $[PhNHMe_2]^+[B(C_6F_5)_4]^-$ in chlorobenzene-d_5 to generate one equivalent of alkane and, presumably, a cationic monoalkyl species. Solutions of these cations slowly polymerize ethylene. Compounds **7** - **10** also polymerize ethylene upon activation with MAO, but with very low activities.

Experimental Section

General Considerations and Instrumentation. All air- and moisture-sensitive compounds were manipulated using standard vacuum line, Schlenk, or cannula techniques or in a drybox under a nitrogen atmosphere. Solvents for air- and moisture-sensitive reactions were dried over sodium benzophenone ketyl or by the method of Grubbs.[43] Benzene-d_6 was purchased from Cambridge Isotopes and distilled from sodium benzophenone ketyl. Chloroform-d_1 and chlorobenzene-d_5 were purchased from Cambridge Isotopes and distilled from calcium hydride. 2-Hydroxy-3,5-di(*t*-butyl)benzyl bromide was prepared according to the literature procedure.[44] Other materials were used as received. ^{1}H and ^{13}C NMR spectra were recorded on Varian Mercury 300, or Varian INOVA-500 spectrometers and unless otherwise indicated at room temperature. Chemical shifts are reported with respect to internal solvent: 7.16 and 128.38 (t)

ppm (C_6D_6); 7.27 and 77.23 (t) ppm ($CDCl_3$), for ^1H and ^{13}C data. ^1H NMR data recorded in C_6D_5Cl was referenced with respect with the most upfield peak for Ph_2CH_2 (3.8 ppm) or with respect to the alkane byproduct, $Si(CH_3)_4$ (0 ppm), where appropriate. ^2H NMR spectra were recorded on a Varian INOVA-500 spectrometer, the chemical shifts being reported with respect to an external D_2O reference (4.8 ppm).

Synthesis of $(MeOCH_2CH_2)_2NCH_2$-C_6H_2-3,5-$(CMe_3)_2$-2-OH (1). A methanol (10 mL) solution of 2,4-di(*t*-butyl)phenol (2 g, 9.7 mmol, 1 equiv), bis(2-methoxyethyl)amine (1.3 g, 9.7 mmol, 1 equiv), and formaldehyde (3.5 g 37% aqueous solution, 38.9 mmol, 4 equiv) was refluxed. After allowing cooling down to room temperature, volatile material was removed via rotary evaporation. The resulting pale yellow oil was placed under high vacuum for six hours to remove remaining excess amine. The resulting material was pure by ^1H NMR spectroscopy (3.08 g, 8.7 mmol, 90%). HRMS: calcd, 351.2773 (M^+); found, 351.2766. ^1H NMR (300 MHz, C_6D_6) δ: 1.37 (s, 9H, $C(CH_3)_3$), 1.73 (s, 9H, $C(CH_3)_3$), 2.60 (t, 4H, *J* = 5.7 Hz, NCH_2CH_2O), 3.21 (t, 4H, *J* = 5.7 Hz, NCH_2CH_2O), 3.01 (s, 6H, OCH_3), 3.63 (s, 2H, aryl-CH_2), 6.94 (d, 1H, *J* = 2.4 Hz, aryl-*H*), 7.51 (d, 1H, *J* = 2.4 Hz, aryl-*H*), 10.91 (s, 1H, O*H*). ^1H NMR (300 MHz, $CDCl_3$) δ: 1.29 (s, 9H, $C(CH_3)_3$), 1.43 (s, 9H, $C(CH_3)_3$), 2.82 (t, 4H, *J* = 5.7 Hz, NCH_2CH_2O), 3.54 (t, 4H, *J* = 5.7 Hz, NCH_2CH_2O), 3.33 (s, 6H, OCH_3), 3.85 (s, 2H, aryl-CH_2), 6.74 (d, 1H, *J* = 2.4 Hz, aryl-*H*), 7.21 (d, 1H, *J* = 2.4 Hz, aryl-*H*), 10.59 (br s, 1H, O*H*). ^{13}C NMR (75 MHz, $CDCl_3$) δ: 29.8 ($C(CH_3)_3$), 31.9 ($C(CH_3)_3$), 34.3 (CMe_3), 35.0 (CMe_3), 53.5

(CH_2), 59.0 (OCH_3), 59.7 (CH_2) , 70.6 (CH_2), 121.7 (*aryl*), 123.0 (*aryl*-H), 123.7 (*aryl*-H), 135.8 (*aryl*), 140.5 (*aryl*), 154.5 (*aryl*).

Synthesis of $(Et_2NCH_2CH_2)_2NCH_2$-C_6H_2-3,5-$(CMe_3)_2$-2-OH (2). A methanol (15 mL) solution of 2,4-di(*t*-butyl)phenol (3.68 g, 17.8 mmol, 1.1 equiv), *N*,*N*,*N'*,*N'*-tetraethyldiethylenetriamine (3.9 g 90% purity, 16.2 mmol, 1 equiv), and formaldehyde (5.3 g 37% aqueous solution, 64.8 mmol, 4 equiv) was refluxed for 14 h. After allowing cooling down to room temperature, volatile material was removed via rotary evaporation. 8 mL HCl 36.5% were added to the reaction mixture. The aqueous phase was washed with petroleum ether (3 x 50 mL). The aqueous layer was neutralized with KOH solution and extracted with diethyl ether (3 x 50 mL). The organic phase was dried over anhydrous $MgSO_4$. The volatile materials were removed via rotary evaporation to yield the desired product as a yellow oil (6.56 g, 15.2 mmol, 94%). ^{1}H NMR data in C_6D_6 match literature report.[38] ^{1}H NMR (300 MHz, $CDCl_3$) δ: 0.97 (t, *J* = 7.1 Hz, 12H, CH_2CH_3), 1.27 (s, 9H, $C(CH_3)_3$), 1.41 (s, 9H, $C(CH_3)_3$), 2.48 (q, *J* = 7.1 Hz, 8H, CH_2CH_3), 2.57-2.64 (m, 8H, NCH_2CH_2N), 3.73 (s, 2H, aryl-CH_2), 6.83 (d, *J* = 2.3 Hz, 1H, aryl-*H*), 7.18 (d, *J* = 2.3 Hz , 1H, aryl-*H*), 10.56 (br s, 1H, O*H*). ^{13}C NMR (75 MHz, $CDCl_3$) δ: 11.8 (NCH_2CH_3), 29.8 ($C(CH_3)_3$), 31.9 ($C(CH_3)_3$), 34.3 ($C(CH_3)_3$), 35.0 (CMe_3), 47.4 (NCH_2), 50.6 (NCH_2), 52.3 (NCH_2), 59.0 (NCH_2), 122.0 (*aryl*), 122.9 (*aryl*-H), 123.9 (*aryl*-H), 135.7 (*aryl*), 140.4 (*aryl*), 154.3 (*aryl*).

Synthesis of $(C_5H_4N$-2-$CH_2)_2NCH_2$-C_6H_2-3,5-$(CMe_3)_2$-2-OH (3). A THF (20 mL) solution of 2-hydroxy-3,5-di(*t*-butyl)benzyl bromide (1.49 g, 5.0 mmol, 1 equiv) was added dropwise to a THF (20 mL) solution of di-(2-picolyl) amine (0.99 g, 5.0

mmol, 1 equiv) and N,N-diisopropylethylamine (0.62 g, 5.0 mmol, 1 equiv). The reaction mixture was stirred at room temperature overnight. The volatile materials were removed via rotary evaporation. A solution of NaOH was added to the reaction mixture and the organic phase was extracted with CH_2Cl_2. The organic phase was dried over anhydrous $MgSO_4$. The volatile materials were removed via rotary evaporation to yield a golden oil (1.77 g, 4.2 mmol, 84%). HRMS: calcd, 418.2858 (MH^+); found, 418.2852. ^{1}H NMR (500 MHz, C_6D_6) δ: 1.36 (s, 9H, C(C*H*$_3$)$_3$), 1.77 (s, 9H, C(C*H*$_3$)$_3$), 3.68 (s, 2H, aryl-C*H*$_2$N), 3.82 (s, 4H, NC*H*$_2$C$_5$H$_4$N), 6.52-6.56 (m, 2H, aryl-*H*), 6.95-7.01 (m, 3H, aryl-*H*), 7.12 (d, 2H, aryl-*H*), 7.53 (d, *J* = 2.4 Hz, 1H, aryl-*H*), 8.41-8.44 (m, 2H, aryl-*H*), 11.07 (s, 1H, O*H*). ^{1}H NMR (300 MHz, $CDCl_3$) δ: 1.28 (s, 9H, C(C*H*$_3$)$_3$), 1.48 (s, 9H, C(C*H*$_3$)$_3$), 3.82 (s, 2H, aryl-C*H*$_2$N), 3.89 (s, 4H, NC*H*$_2$C$_5$H$_4$N), 6.90 (d, *J* = 2.4 Hz, 1H, aryl-*H*), 7.13-7.19 (m, 2H, aryl-*H*), 7.22 (d, *J* = 2.4 Hz, 1H, aryl-*H*), 7.39 (d, 2H, aryl-*H*), 7.60-7.67 (m, 2H, aryl-*H*), 8.57 (m, 2H, aryl-*H*), 10.66 (s, 1H, O*H*). ^{1}H NMR (300 MHz, CD_2Cl_2) δ: 1.26 (s, 9H, C(C*H*$_3$)$_3$), 1.44 (s, 9H, C(C*H*$_3$)$_3$), 3.78 (s, 2H, aryl-C*H*$_2$N), 3.83 (s, 4H, NC*H*$_2$C$_5$H$_4$N), 6.90 (d, 1H, aryl-*H*), 7.13-7.21 (m, 3H, aryl-*H*), 7.33 (d, 2H, aryl-*H*), 7.63 (td, 2H, aryl-*H*), 8.54 (m, 2H, aryl-*H*), 10.67 (s, 1H, O*H*). ^{13}C NMR (75 MHz, $CDCl_3$) δ: 29.8 (C(*C*H$_3$)$_3$), 31.9 (C(CH$_3$)$_3$), 34.3 (*C*Me$_3$), 35.2 (*C*Me$_3$), 58.4 (NCH$_2$), 59.7 (NCH$_2$), 121.8 (*aryl*), 122.4 (*aryl*-H), 123.3 (*aryl*-H), 123.8 (*aryl*-H), 124.7 (*aryl*-H), 135.7 (*aryl*), 136.8 (*aryl*-H), 140.5 (*aryl*), 149.2 (*aryl*-H), 154.0 (*aryl*), 158.3 (*aryl*).

Synthesis of (ClCH$_2$CH$_2$)$_2$NCH$_2$-C$_6$H$_2$-3,5-(CMe$_3$)$_2$-2-OH (4). A methanol (40 mL) solution of 2,4-di(*t*-butyl)phenol (20.3 g, 98.3 mmol, 1 equiv),

diethanolamine (15.5 g, 147.4 mmol, 1.5 equiv) and formaldehyde (31.9 g of 37% aqueous solution, 393.1 mmol, 4 equiv) was refluxed overnight. After allowing cooling down to room temperature, volatile material was removed via rotary evaporation. The oily residue was dissolved in 200 mL diethyl ether and treated with 14 mL concentrated hydrochloric acid (37%). Abundant precipitation of a white solid was observed. The product was collected on the sintered glass funnel and washed with diethyl ether and water. The solid prepared by the above procedure was dissolved in CH_2Cl_2. Thionyl chloride (46.5 mL, 75.8 g, 637.5 mmol, 6.5 equiv) was added via volumetric pipet and the reaction mixture was allowed to stir overnight. A 10% solution of KOH was added to the reaction mixture until basic pH. The organic phase was extracted with CH_2Cl_2 (3 x 400 mL). The organic phase was dried over anhydrous $MgSO_4$. The volatile materials were removed via rotary evaporation to yield a yellowish solid (26.7 g, 74.2 mmol, 75%). HRMS: calcd, 359.1783 (M^+); found, 359.1765. ^{1}H NMR (300 MHz, C_6D_6) δ: 1.35 (s, 9H, C(CH_3)$_3$), 1.68 (s, 9H, C(CH_3)$_3$), 2.28 (t, 4H, *J* = 6.6 Hz, NCH_2CH_2Cl), 2.97 (t, 4H, *J* = 6.6 Hz, NCH_2CH_2Cl), 3.22 (s, 2H, aryl-CH_2), 6.82 (d, 1H, *J* = 2.7 Hz, aryl-*H*), 7.50 (d, 1H, *J* = 2.7 Hz, aryl-*H*), 9.61 (s, 1H, O*H*). ^{1}H NMR (300 MHz, $CDCl_3$) δ: 1.31 (s, 9H, C(CH_3)$_3$), 1.45 (s, 9H, C(CH_3)$_3$), 3.00 (t, 4H, *J* = 6.6 Hz, NCH_2CH_2Cl), 3.64 (t, 4H, *J* = 6.6 Hz, NCH_2CH_2Cl), 3.87 (s, 2H, aryl-CH_2), 6.87 (d, 1H, *J* = 2.4 Hz, aryl-*H*), 7.28 (d, 1H, *J* = 2.4 Hz, aryl-*H*), 9.45 (br s, 1H, O*H*). ^{13}C NMR (75 MHz, $CDCl_3$) δ: 29.8 (C(*C*H_3)$_3$), 31.9 (C(*C*H_3)$_3$), 34.4 (*C*Me$_3$), 35.1 (*C*Me$_3$), 41.2 (*C*H_2), 55.9 (*C*H_2), 59.5 (*C*H_2), 120.8 (*aryl*), 123.8 (*aryl*-H), 123.9 (*aryl*-H), 136.4 (*aryl*), 141.3 (*aryl*), 153.9 (*aryl*).

Synthesis of $(Me_3CSCH_2CH_2)_2NCH_2$-C_6H_2-3,5-$(CMe_3)_2$-2-OH (5). A THF (~50 mL) solution of Me_3CSH (3.3 g, 36.7 mmol, 3.3 equiv) was added under argon atmosphere to a suspension of sodium hydride (1.3 g, 53.3 mmol, 4.8 equiv) in THF (~50 mL). A THF (~60 mL) solution of **4** (4 g, 11.1 mmol, 1 equiv) was added to the reaction mixture and allowed to stir overnight. The reaction mixture was quenched with distilled water (150 mL) and extracted with diethyl ether (3 x 100 mL). The organic fraction was dried over $MgSO_4$ and filtered. Volatile materials were removed via rotary evaporation. The resulting yellow solid was recrystallized from methanol to give a white solid (2.8 g, 6.1 mmol, 55%). HRMS: calcd, 466.3177 ([MH^+]-H_2); found, 466.3161. ^{1}H NMR (300 MHz, C_6D_6) δ: 1.13 (s, 18H, SC(CH_3)$_3$), 1.36 (s, 9H, aryl-C(CH_3)$_3$), 1.70 (s, 9H, aryl-C(CH_3)$_3$), 2.46-2.61 (m, 8H, NCH_2CH_2S), 3.43 (s, 2H, aryl-CH_2), 6.88 (d, J = 2.4 Hz, 1H, aryl-*H*), 7.48 (d, J = 2.4 Hz , 1H, aryl-*H*), 10.39 (s, 1H, O*H*). ^{1}H NMR (300 MHz, $CDCl_3$) δ: 1.26 (s, 18H, SC(CH_3)$_3$), 1.28 (s, 9H, aryl-C(CH_3)$_3$), 1.43 (s, 9H, aryl-C(CH_3)$_3$), 2.62-2.82 (m, 8H, NCH_2CH_2S), 3.80 (s, 2H, aryl-CH_2), 6.84 (d, J = 2.6 Hz, 1H, aryl-*H*), 7.22 (d, J = 2.6 Hz , 1H, aryl-*H*), 10.20 (br s, 1H, O*H*). ^{13}C NMR (75 MHz, $CDCl_3$) δ: 25.8 (CH_2), 29.8 (C(CH_3)$_3$), 31.2 (C(CH_3)$_3$), 31.9 (C(CH_3)$_3$), 34.3 (CMe_3), 35.0 (CMe_3), 42.5 (CMe_3), 54.7 (CH_2), 59.3 (CH_2), 121.4 (*aryl*), 123.3 (*aryl*-H), 123.7 (*aryl*-H), 136.0 (*aryl*), 141.0 (*aryl*), 154.2 (*aryl*).

Synthesis of $(Me_2NCH_2CH_2)_2NCH_2$-C_6H_2-3,5-$(CMe_3)_2$-2-OH (6). Compound **4** (4 g, 11.2 mmol, 1 equiv) and lithium dimethylamide (2.9 g, 56.2 mmol, 5 equiv) were placed in a Schlenk tube, in the drybox. THF (~50 mL) was vacuum transferred over the starting materials. The reaction mixture was allowed to

warm up to room temperature and was stirred overnight. The reaction mixture was quenched with water and extracted with diethyl ether. The organic fraction was dried over $MgSO_4$ and filtered. Volatile materials were removed via rotary evaporation. The resulting oil consists of three species. A diethyl ether solution of the product mixture was acidified with hydrochloric acid. The aqueous layer was washed with diethyl ether, then basified with sodium hydroxide and extracted with diethyl ether. The organic fraction was dried over $MgSO_4$, filtered, then volatile materials were removed via rotary evaporation. The resulting material consists of a mixture of only two species. Purification by column chromatography with ethylacetate as eluent provided pure product (0.4 g, 0.9 mmol, 8%). Because this phenol did not give clean metallation reactions, no optimization was attempted. HRMS: calcd, 332.2828 (M-[$HNMe_2$]); found, 332.2818. ^{1}H NMR (300 MHz, C_6D_6) δ: 1.39 (s, 9H, C(CH_3)$_3$), 1.75 (s, 9H, C(CH_3)$_3$), 1.86 (s, 12H, NCH_3), 1.96 (t, 4H, *J* = 5.7 Hz, NCH_2CH_2N), 2.24 (t, 4H, *J* = 5.7 Hz, NCH_2CH_2N), 3.59 (s, 2H, aryl-CH_2), 6.93 (d, 1H, *J* = 2.4 Hz, aryl-*H*), 7.52 (d, 1H, *J* = 2.4 Hz, aryl-*H*), 11.61 (br s, 1H, O*H*). ^{1}H NMR (300 MHz, $CDCl_3$) δ: 1.27 (s, 9H, C(CH_3)$_3$), 1.41 (s, 9H, C(CH_3)$_3$), 2.18 (s, 12H, NCH_3), 2.45 (t, 4H, *J* = 5.9 Hz, NCH_2CH_2N), 2.65 (t, 4H, *J* = 5.9 Hz, NCH_2CH_2N), 3.73 (s, 2H, aryl-CH_2), 6.83 (d, 1H, *J* = 2.4 Hz, aryl-*H*), 7.18 (d, 1H, *J* = 2.4 Hz, aryl-*H*), 10.51 (br s, 1H, O*H*). ^{13}C NMR (75 MHz, $CDCl_3$) δ: 29.8 (C(CH_3)$_3$), 31.9 (C(CH_3)$_3$), 34.3 (CMe_3), 35.0 (CMe_3), 45.6 (NCH_3), 46.1 (NCH_2), 53.6 (NCH_2), 58.4 (NCH_2), 122.3 (*aryl*), 122.9 (*aryl*-H), 123.3 (*aryl*-H), 135.9 (*aryl*), 140.4 (*aryl*), 155.0 (*aryl*).

Synthesis of [(LCH$_2$CH$_2$)$_2$NCH$_2$-C$_6$H$_2$-3,5-(CMe$_3$)$_2$-2-O]M(CH$_2$SiMe$_2$Ph)$_2$ (M = Y, Sc; L = OMe, NEt$_2$, SCMe$_3$). In a typical procedure, a THF (5 mL) solution of phenol (1 equiv) was added dropwise to an *in situ* generated THF (5 mL) solution of M(THF)$_2$(CH$_2$SiMe$_2$C$_6$H$_5$)$_3$ (1 equiv) and allowed to stir for 4 h at room temperature. ^{1}H NMR spectra of the crude reaction mixtures show clean formation of the desired yttrium and scandium dialkyl products along with SiMe$_3$Ph. The volatile materials were removed under vacuum. Diethyl ether (5 mL) was added, and the mixture filtered through Celite to remove insoluble salts. The filtrate was concentrated under vacuum.

Synthesis of [(MeOCH$_2$CH$_2$)$_2$NCH$_2$-C$_6$H$_2$-3,5-(CMe$_3$)$_2$-2-O]Y(CH$_2$SiMe$_2$Ph)$_2$ (7a). Recrystallization from petroleum ether or petroleum ether/diethyl ether mixtures, followed by collection on a sintered glass funnel and washing with cold petroleum ether provides desired product as a white solid (57% yield) carrying only traces of alkane impurity. Anal. Calcd for C$_{39}$H$_{62}$NO$_3$Si$_2$Y: C, 63.47; H, 8.47; N, 1.90. Found: C, 64.46; H, 9.01; N, 2.08. ^{1}H NMR (300 MHz, C$_6$D$_6$) δ: -0.38 (d, ^{2}J$_{YH}$ = 2.9 Hz, 4H, YC*H*$_2$), 0.65 (s, 12H, Si(C*H*$_3$)$_2$), 1.43 (s, 9H, C(C*H*$_3$)$_3$), 1.82 (s, 9H, C(C*H*$_3$)$_3$), 1.39, 2.24, 2.33, 2.60 (br m, 8H, NC*H*$_2$C*H*$_2$O), 3.24 (br s, 2H, aryl-C*H*$_2$), 2.94 (s, 6H, OC*H*$_3$), 6.86 (d, 1H, *J* = 2.4 Hz, aryl-*H*), 7.59 (d, 1H, *J* = 2.4 Hz, aryl-*H*), 7.23 (t, 2H, *p*-Ph*H*), 7.31 (t, 4H, *m*-Ph*H*), 7.88 (d, 4H, *o*-Ph*H*). ^{13}C NMR (75 MHz, C$_6$D$_6$) δ: 3.5 (s, Si(*C*H$_3$)$_2$), 27.6 (d, Y*C*H$_2$, ^{1}J$_{YC}$ = 39.8 Hz), 30.6 (C(*C*H$_3$)$_3$), 32.6 (C(*C*H$_3$)$_3$), 34.6 (*C*Me$_3$), 36.0 (*C*Me$_3$), 52.6, 61.3, 63.6, 72.0 (OC*H*$_3$, aryl-*C*H$_2$, NCH$_2$*C*H$_2$O), 123.7, 125.1, 125.9, 127.9, 128.0, 134.3, 136.8, 137.5, 148.3 (*aryls*), 162.2 (d, ^{2}J$_{YC}$ = 3.1 Hz, *C*OY). ^{1}H NMR (500 MHz, C$_6$D$_5$CD$_3$, -75°C) δ: -0.51 (br app d,

1H, YCH_2), -0.35 (br app t, 2H, YCH_2), -0.24 (br app d, 1H, YCH_2), 0.63 (s, 3H, SiCH_3), 0.67 (s, 3H, SiCH_3), 0.75 (s, 3H, SiCH_3), 0.95 (s, 3H, SiCH_3), 1.51 (s, 9H, C(CH_3)$_3$), 1.92 (s, 9H, C(CH_3)$_3$), 1.06, 1.37, 1.74, 2.20, 2.36, 2.47, 2.70 (m, 9H, NCH_2CH_2O and aryl-CH_2), 2.80 (br s, 3H, OCH_3), 2.94 (br s, 3H, OCH_3), 3.84 (br app d, 1H, aryl-CH_2), 6.92 (s, 1H, aryl-*H*), 7.23 (br s, 4H, aryl-*H*), 7.40 (br s, 2H, aryl-*H*), 7.62 (s, 1H, aryl-*H*), 7.73 (br s, 2H, aryl-*H*), 8.00 (br s, 2H, aryl-*H*) .

Synthesis of [(Et$_2$NCH$_2$CH$_2$)$_2$NCH$_2$-C$_6$H$_2$-3,5-(CMe$_3$)$_2$-2-O]Y(CH$_2$SiMe$_2$Ph)$_2$ (7b). Recrystallization from petroleum ether, followed by collection on a sintered glass funnel and washing with cold petroleum ether provides desired product as a white solid (32% yield) carrying only traces of alkane residue. Anal. Calcd for $C_{45}H_{76}ON_3Si_2Y$: C, 65.90; H, 9.34; N, 5.12. Found: C, 66.20; H, 8.85; N, 5.49. ^{1}H NMR (300 MHz, C_6D_6, 40°C) δ: -0.21 (d, $^2J_{YH}$ = 2.7 Hz, 4H, YCH_2), 0.57 (s, 12H, Si(CH_3)$_2$), 0.68 (t, 12H, NCH$_2$CH_3), 1.43 (s, 9H, C(CH_3)$_3$), 1.81 (s, 9H, C(CH_3)$_3$), 2.36 (q, 8H, NCH_2CH$_3$), 1.20-1.32, 1.88-2.10, 2.14-2.22 (m, 8H, NCH_2CH_2N), 3.34 (br s, 2H, aryl-CH_2), 6.95 (d, *J* = 2.6 Hz, 1H, aryl-*H*), 7.58 (d, *J* = 2.6 Hz, 1H, aryl-*H*), 7.18-7.30 (m, 6H, *p*-Ph*H* and *m*-Ph*H*), 7.80 (d, 4H, *o*-Ph*H*). ^{13}C NMR (75 MHz, C_6D_6, 40°C) δ: 3.4 (Si(*C*H$_3$)$_2$), 9.7 (NCH$_2$*C*H$_3$), 31.4 (d, $^1J_{YC}$ = 41.9 Hz, YCH$_2$), 31.0 (C(*C*H$_3$)$_3$), 32.5 (C(*C*H$_3$)$_3$), 34.6 (*C*Me$_3$), 36.1 (*C*Me$_3$), 46.4 (NCH$_2$), 49.3 (NCH$_2$), 51.0 (NCH$_2$), 61.4 (NCH$_2$), 123.4, 125.1, 125.7, 127.9, 128.0, 134.3, 137.3, 138.0, 147.9 (*aryls*), 161.5 (d, $^2J_{YC}$ = 3.3 Hz, *C*OY). ^{1}H NMR (300 MHz, $C_6D_5CD_3$, -75°C, selected peaks) δ: -0.52 (br app d, 1H, YCH_2), -0.33 (br app d, 1H, YCH_2), -0.13 (br app d, 1H, YCH_2), 0.10 (br app d, 1H, YCH_2), 1.50 (s, 9H, C(CH_3)$_3$), 1.95 (s, 9H, C(CH_3)$_3$).

Synthesis of [(MeOCH$_2$CH$_2$)$_2$NCH$_2$-C$_6$H$_2$-3,5-(CMe$_3$)$_2$-2-O]Sc(CH$_2$SiMe$_2$Ph)$_2$ (8a). Recrystallization from diethyl ether, followed by collection on a sintered glass funnel and washing with cold diethyl ether provides desired product as a white solid (26% yield) carrying only traces of alkane byproduct. Anal. Calcd for $C_{39}H_{62}NO_3Si_2Sc$: C, 67.49; H, 9.00; N, 2.02. Found: C, 67.81; H, 8.66; N, 2.31. ^{1}H NMR (300 MHz, C_6D_6, 55 °C) δ: -0.03 (s, 4H, ScC*H*$_2$), 0.59 (s, 12H, Si(C*H*$_3$)$_2$), 1.40 (s, 9H, C(C*H*$_3$)$_3$), 1.81 (s, 9H, C(C*H*$_3$)$_3$), 1.43-1.54, 2.33-2.59, 2.72-2.80, 3.21-3.44 (m, 10H, NC*H*$_2$C*H*$_2$O and aryl-C*H*$_2$), 3.07 (s, 6H, OC*H*$_3$), 6.83 (d, *J* = 2.4 Hz, 1H, aryl-*H*), 7.56 (d, *J* = 2.4 Hz, 1H, aryl-*H*), 7.17-7.24 (m, 2H, *p*-Ph*H*), 7.25-7.32 (m, 4H, Ph*H*), 7.82 (m, 4H, Ph*H*). ^{13}C NMR (75 MHz, C_6D_6, 55 °C) δ: 3.1 (Si(*C*H$_3$)$_2$), 30.7 (Sc*C*H$_2$), 30.8 (C(*C*H$_3$)$_3$), 32.5 (C(*C*H$_3$)$_3$), 34.6 (*C*Me$_3$), 36.0 (*C*Me$_3$), 53.4 (br s, O*C*H$_3$), 61.9 (*C*H$_2$), 64.1 (*C*H$_2$), 71.9 (*C*H$_2$), 123.9, 124.9, 125.3, 127.9, 128.0, 134.4, 136.7, 138.2, 148.0 (*aryls*), 161.8 (*C*OSc). ^{1}H NMR (300 MHz, $C_6D_5CD_3$, -60 °C, selected peaks) δ: -0.22 (br app d, 1H, ScC*H*$_2$), -0.05 (br app d, 1H, ScC*H*$_2$), 0.16 (br app d, 1H, ScC*H*$_2$), 0.70 (br app d, 1H, ScC*H*$_2$), 0.53 (s, 3H, SiCH$_3$), 0.62 (s, 3H, SiCH$_3$), 0.80 (s, 3H, SiCH$_3$), 0.90 (s, 3H, SiCH$_3$), 1.48 (s, 9H, C(C*H*$_3$)$_3$), 1.92 (s, 9H, C(C*H*$_3$)$_3$), 2.80 (s, 3H, OC*H*$_3$), 3.10 (s, 3H, OC*H*$_3$).

Synthesis of [(Me$_3$CSCH$_2$CH$_2$)$_2$NCH$_2$-C$_6$H$_2$-3,5-(CMe$_3$)$_2$-2-O]Sc(CH$_2$SiMe$_2$Ph)$_2$ (8b). Recrystallization from petroleum ether, followed by collection on a sintered glass funnel and washing with cold petroleum ether provides desired product as a white solid (16% yield) carrying only traces of alkane residue. Anal. Calcd for $C_{45}H_{74}NOS_2Si_2Sc$: C, 66.70; H, 9.20; N, 1.73. Found: C, 67.70; H, 8.99; N, 1.76. ^{1}H NMR (300 MHz, C_6D_6) δ: 0.49 (br d, *J* = 12 Hz, 2H, ScC*H*$_2$), 0.58 (br d, *J* = 12 Hz,

2H, ScCH_2), 0.62 (s, 6H, Si(CH_3)$_2$), 0.64 (s, 6H, Si(CH_3)$_2$), 1.01 (s, 18H, SC(CH_3)$_3$), 1.40 (s, 9H, C(CH_3)$_3$), 1.81 (s, 9H, C(CH_3)$_3$), 1.93-2.16, 2.19-2.32, 2.34-2.47 (m, 8H, NCH_2CH_2N), 3.17 (br s, 2H, aryl-CH_2), 6.85 (d, J = 2.4 Hz, 1H, aryl-*H*), 7.54 (d, J = 2.4 Hz, 1H, aryl-*H*), 7.19-7.29 (m, 6H, Ph*H*), 7.79 (m, 4H, Ph*H*). ^{1}H NMR (300 MHz, C_6D_6, 70 °C) δ: 0.48 (br s, 4H, ScCH_2), 0.55 (s, 12H, Si(CH_3)$_2$), 1.06 (s, 18H, SC(CH_3)$_3$), 1.38 (s, 9H, C(CH_3)$_3$), 1.76 (s, 9H, C(CH_3)$_3$), 2.07-2.43, 2.45-2.60 (m, 8H, NCH_2CH_2N), 3.23 (s, 2H, aryl-CH_2), 6.84 (d, J = 2.4 Hz, 1H, aryl-*H*), 7.51 (d, J = 2.4 Hz, 1H, aryl-*H*), 7.17-7.26 (m, 6H, Ph*H*), 7.74 (m, 4H, Ph*H*). ^{13}C NMR (75 MHz, C_6D_6, 70 °C) δ: 3.1 (s, Si(*C*H$_3$)$_2$), 27.6 (Sc*C*H$_2$), 31.0 (C(*C*H$_3$)$_3$), 31.1 (C(*C*H$_3$)$_3$), 32.5 (C(*C*H$_3$)$_3$), 34.7 (*C*Me$_3$), 36.0 (*C*Me$_3$), 40.5 (br s, S*C*Me$_3$), 46.3 (*C*H$_2$), 51.6 (*C*H$_2$), 60.8 (*C*H$_2$), 123.3 (*aryl*), 124.9 (*aryl*-H), 125.4 (*aryl*-H), 128.0 (*aryl*-H), 128.1 (*aryl*-H), 134.4 (*aryl*-H), 137.5 (*aryl*), 146.9 (*aryl*), 160.8 (*C*OSc). ^{1}H NMR (300 MHz, $C_6D_5CD_3$, -50 °C, selected peaks) δ: 0.35 (br app d, 1H, ScCH_2), 0.55 (br s, 3H, SiCH_3), 0.66 (br s, 3H, SiCH_3), 0.75 (br s, 3H, SiCH_3), 0.88 (s, 9H, SC(CH_3)$_3$), 1.01 (s, 9H, SC(CH_3)$_3$), 1.42 (s, 9H, C(CH_3)$_3$), 1.86 (s, 9H, C(CH_3)$_3$).

Synthesis of [(MeOCH$_2$CH$_2$)$_2$NCH$_2$-C$_6$H$_2$-3,5-(CMe$_3$)$_2$-2-O]Y(CH$_2$SiMe$_3$)$_2$ (9). A thawing THF (5 mL) solution of phenol (MeOCH$_2$CH$_2$)$_2$NCH$_2$-C$_6$H$_2$-3,5-(CMe$_3$)$_2$-2-OH (0.36 g, 1.0 mmol, 1 equiv) was added dropwise to an *in situ* generated thawing THF (5 mL) solution of Y(THF)$_2$(CH$_2$SiMe$_3$)$_3$ (1 equiv) and allowed to stir for 4 h at room temperature. The volatile materials along with the byproduct, tetramethylsilane, were removed under vacuum. ^{1}H NMR spectra of the crude reaction mixtures show clean formation of the desired yttrium dialkyl product. Diethyl ether (5 mL) was

added, and the mixture filtered through Celite to remove insoluble salts. The filtrate was concentrated under vacuum. Recrystallization from petroleum ether, followed by collection on a sintered glass funnel and washing with cold petroleum ether provides desired product as a white solid (0.24g, 0.4 mmol, 38%). Anal. Calcd for $C_{29}H_{58}NO_3Si_2Y$: C, 56.74; H, 9.52; N, 2.28. Found: C, 55.62; H, 9.34; N, 2.36. ^{1}H NMR (300 MHz, C_6D_6, 40 °C) δ: -0.58 (d, $^2J_{YH}$ = 2.7 Hz, 4H, YCH_2), 0.44 (s, 18H, Si(CH_3)$_3$), 1.41 (s, 9H, C(CH_3)$_3$), 1.79 (s, 9H, C(CH_3)$_3$), 1.56-1.67, 2.44-2.58, 2.76-2.85 (m, 8H, NCH_2CH_2O), 3.48 (br s, 2H, aryl-CH_2), 3.19 (s, 6H, OCH_3), 6.90 (d, *J* = 2.6 Hz, 1H, aryl-*H*), 7.56 (d, *J* = 2.6 Hz, 1H, aryl-*H*). ^{13}C NMR (75 MHz, C_6D_6, 40 °C) δ: 5.1 (Si(*C*H$_3$)$_3$), 30.8 (d, Y*C*H$_2$, $^1J_{YC}$ = 40.1 Hz), 30.7 (C(*C*H$_3$)$_3$), 32.6 (C(*C*H$_3$)$_3$), 34.6 (*C*Me$_3$), 36.0 (*C*Me$_3$), 52.9 (br s, OCH$_3$), 61.4 (*C*H$_2$), 63.8 (*C*H$_2$), 72.1 (*C*H$_2$), 123.5, 125.2, 125.9, 137.0, 137.4 (*aryls*), 162.4 (d, $^2J_{YC}$ = 3.3 Hz, *C*OY).

Synthesis of [(MeOCH$_2$CH$_2$)$_2$NCH$_2$-C$_6$H$_2$-3,5-(CMe$_3$)$_2$-2-O]Sc(CH$_2$SiMe$_3$)$_2$ (10). A thawing THF (5 mL) solution of phenol (MeOCH$_2$CH$_2$)$_2$NCH$_2$-C$_6$H$_2$-3,5-(CMe$_3$)$_2$-2-OH (**1**) (0.30 g, 0.9 mmol, 1 equiv) was added dropwise to the *in situ* generated thawing THF (5 mL) solution of Sc(THF)$_2$(CH$_2$SiMe$_3$)$_3$ (1 equiv) and allowed to stir for 4 h at room temperature. The volatile materials along with the byproduct, tetramethylsilane, were removed under vacuum. ^{1}H NMR spectra of the crude reaction mixtures show clean formation of the desired yttrium dialkyl product. Diethyl ether (5 mL) was added, and the mixture filtered through Celite to remove insoluble salts. The filtrate was concentrated under vacuum. Recrystallization from petroleum ether,

followed by collection on a sintered glass funnel and washing with cold petroleum ether provides desired product as a white solid (0.22g, 0.4 mmol, 45%). Anal. Calcd for $C_{29}H_{58}NO_3Si_2Sc$: C, 61.12; H, 10.26; N, 2.46. Found: C, 58.66; H, 9.01; N, 2.22. ^{1}H NMR (300 MHz, C_6D_6, 60 °C) δ: -0.22 (s, 4H, ScCH_2), 0.38 (s, 18H, Si(CH_3)$_3$), 1.39 (s, 9H, C(CH_3)$_3$), 1.79 (s, 9H, C(CH_3)$_3$), 1.62-1.72, 2.63, 2.86-2.95 (m, 8H, NCH_2CH_2O), 3.56 (br s, 2H, aryl-CH_2), 3.19 (s, 6H, OCH_3), 6.89 (d, J = 2.7 Hz, 1H, aryl-*H*), 7.54 (d, J = 2.7 Hz, 1H, aryl-*H*). ^{13}C NMR (75 MHz, C_6D_6, 60 °C) δ: 4.7 (Si(*C*H$_3$)$_3$), 30.7 (Sc*C*H$_2$), 30.9 (C(*C*H$_3$)$_3$), 32.5 (C(*C*H$_3$)$_3$), 34.6 (*C*Me$_3$), 36.0 (*C*Me$_3$), 53.5 (br s, OCH$_3$), 61.9 (*C*H$_2$), 64.3 (*C*H$_2$), 72.0 (*C*H$_2$), 123.8, 125.0, 125.3, 136.8, 138.0 (*aryls*), 162.0 (*C*OSc). ^{1}H NMR (300 MHz, $C_6D_5CD_3$, -50 °C, selected peaks) δ: -0.35 (br app d, 1H, ScCH_2), -0.22 (br app d, 1H, ScCH_2), -0.15 (br app d, 1H, ScCH_2), -0.08 (br app d, 1H, ScCH_2), 0.45 (s, 9H, Si(CH_3)$_3$), 0.64 (s, 9H, Si(CH_3)$_3$), 1.46 (s, 9H, C(CH_3)$_3$), 1.89 (s, 9H, C(CH_3)$_3$), 2.85 (s, 3H, OCH_3), 3.20 (s, 3H, OCH_3), 6.93 (br d, 1H, aryl-*H*), 7.61 (br d, 1H, aryl-*H*).

Synthesis of [(C$_5$H$_4$N-2-CH$_2$)$_2$NCH$_2$-C$_6$H$_2$-3,5-(CMe$_3$)$_2$-2-O]-Sc(CH$_2$SiMe$_2$Ph)$_2$ (11). Under a nitrogen atmosphere, a toluene-d_8 solution (0.4 mL) of Sc(CH$_2$SiMe$_2$Ph)$_3$(THF)$_2$ (68.4 mg, 0.1074 mmol, 1 equiv) was frozen in an J-Young tube. Toluene-d_8 (0.1 mL) was added to separate the toluene-d_8 solution (0.4 mL each) of *tris*-alkyl complex from the phenol (C$_5$H$_4$N-2-CH$_2$)$_2$NCH$_2$-C$_6$H$_2$-3,5-(CMe$_3$)$_2$-2-OH (**3**) (44.8 mg, 0.1074 mmol, 1 equiv.). Before recording the ^{1}H NMR spectrum, the sample was allowed to warm up for 5 - 10 seconds and mixed. After recording the ^{1}H and ^{13}C NMR spectra, the sample was allowed to warm up to room temperature and to stir for

1 h. The ^{1}H NMR spectrum shows formation of one species containing the phenolate ligand. The kinetics of this process were studied by ^{1}H NMR spectroscopy at 0 °C. ^{1}H NMR (300 MHz, $C_6D_5CD_3$, -45 °C) δ: 0.21 (s, 9H, PhSi(CH_3)$_3$, 1 equiv), -0.09 (br app d, J = 11.2 Hz, 1H, ScCH-H), 0.17 (br app d, J = 11.2 Hz, 1H, ScCH-H), 0.45 (br app d, J = 11.2 Hz, 1H, ScCH-H), 0.64 (br app d, J = 11.2 Hz, 1H, ScCH-H), 0.29 (s, 3H, SiCH_3), 0.54 (s, 3H, SiCH_3), 0.92 (s, 3H, SiCH_3), 0.96 (s, 3H, SiCH_3), 1.40 (m, 17H, C(CH_3)$_3$ and O(CH$_2$CH_2)$_2$, THF, 2 equiv), 1.65 (s, 9H, C(CH_3)$_3$), 3.57 (t, 8H, O(CH_2CH$_2$)$_2$, THF, 2 equiv.), 2.60-2.83 (m, 4H, NCH_2), 4.01 (d, J = 14.4 Hz, 1H, NCH_2), 4.37 (d, J = 11.1 Hz, 1H, NCH_2), 5.76 (d, 1H, aryl-H), 6.21 (t, 1H, aryl-H), 6.36-6.48 (m, 4H, aryl-H), 6.72-7.63 (15H, aryl-H), 8.17 (d, 2H, aryl-H), 8.66 (d, 1H, aryl-H), 8.91 (d, 1H, aryl-H). ^{13}C NMR (75 MHz, $C_6D_5CD_3$, -45 °C) δ: -1.3 (PhSi(*C*H$_3$)$_3$), 2.3 (Si*C*H$_3$), 2.6 (Si*C*H$_3$), 2.7 (Si*C*H$_3$), 3.8 (Si*C*H$_3$), 25.6 (O(CH$_2$*C*H$_2$)$_2$, THF), 28.7 (br, Sc*C*H$_2$), 30.3 (br, Sc*C*H$_2$), 30.5 (C(*C*H$_3$)$_3$), 32.1 (C(*C*H$_3$)$_3$), 34.0 (*C*Me$_3$), 35.3 (*C*Me$_3$), 60.3 (N*C*H$_2$), 61.9 (N*C*H$_2$), 62.3 (N*C*H$_2$), 67.6 (O(*C*H$_2$CH$_2$)$_2$, THF), 119.9, 121.8, 122.7, 123.4, 123.5, 127.9, 129.0, 133.4, 133.5, 133.8, 134.1, 134.3, 135.1, 136.4, 136.9, 137.7, 138.8, 139.9, 147.4, 147.6, 149.5, 156.6, 156.7, 161.3 (*aryls* and *C*$_6$H$_5$SiMe$_3$).

Spectroscopic characterization of 12. ^{1}H NMR (300 MHz, $C_6D_5CD_3$,) δ: 0.20 (s, 18H, PhSi(CH_3)$_3$, 2 equiv), 0.27 (d, J = 11 Hz, 1H, ScCH-H), 0.41 (d, J = 11 Hz, 1H, ScCH-H), 0.61 (s, 3H, SiCH_3), 0.62 (s, 3H, SiCH_3), 1.36 (m, 17H, C(CH_3)$_3$ and O(CH$_2$CH_2)$_2$, THF, 2 equiv), 1.65 (s, 9H, C(CH_3)$_3$), 3.72 (br s, 8H, O(CH_2CH$_2$)$_2$, THF, 2 equiv), 2.91 (d, J = 14.8 Hz, 1H, NCH-H), 3.32 (d, J = 13.5 Hz, 1H, NCH-H), 3.86 (d, J = 13.5 Hz, 1H, NCH-H), 4.19 (d, J = 14.8 Hz, 1H, NCH-H), 4.08

(s, 1H, NC-*H*), 5.01 (t, 1H, aryl-*H*), 5.74 (d, 1H, aryl-*H*), 6.05-6.12 (m, 1H, aryl-*H*), 6.16-6.24 (d, 1H, aryl-*H*), 6.24-6.30 (t, 1H, aryl-*H*), 6.56-6.63 (td, 1H, aryl-*H*), 7.02 (d, 1H, aryl-*H*), 7.16-7.23 (m, 7H, aryl-*H*), 7.28-7.35 (t, 2H, aryl-*H*), 7.39-7.46 (m, 5H, aryl-*H*), 7.52 (d, 1H, aryl-*H*), 7.90 (dd, 2H, aryl-*H*), 8.72 (d, 1H, aryl-*H*). ^{13}C NMR (75 MHz, $C_6D_5CD_3$,) δ: -1.2 (PhSi(*C*H_3)$_3$), 3.0 (Si*C*H_3), 3.1 (Si*C*H_3), 25.6 (O(*C*H_2*C*H_2)$_2$, THF), 27.7 (Sc*C*H_2), 30.3 (C(*C*H_3)$_3$), 32.1 (C(*C*H_3)$_3$), 34.3 (*C*Me$_3$), 35.5 (*C*Me$_3$), 62.1 (N*C*H_2), 64.4 (N*C*H_2), 68.8 (br s, O(*C*H_2*C*H_2)$_2$, THF), 96.6 (*aryl*-H), 100.9 (N*C*H, J_{CH} = 170 Hz), 114.0 (*aryl*-H), 122.3, 122.5, 123.7, 123.9, 124.9, 127.7, 127.8, 128.0, 129.0, 131.0, 133.5, 136.6, 137.9, 138.3, 140.2, 143.5, 143.8, 146.9, 149.0, 151.9, 159.8, 160.3 (*aryls* and *C*$_6$H$_5$SiMe$_3$). A diethyl ether solution of **12** was quenched with CD_3OD and filtered through alumina. The volatile materials were removed under vacuum. ^{1}H NMR (500 MHz, $CDCl_3$, peaks in the 3.5-4.0 ppm region) δ: 3.80 (d, *J* = 13.5 Hz, 1H, aryl-C*H*-H), 3.83 (d, *J* = 13.5 Hz, 1H, aryl-C*H*-H), 3.86 (br s, 1H, NC*H*DC$_5$H$_4$N), 3.88 (br s, 2H, NC*H*$_2$C$_5$H$_4$N). ^{2}H NMR (75 MHz, CH_2Cl_2) δ: 3.83.

Synthesis of 13. Under a nitrogen atmosphere, dry pyridine (10.7 μL, 0.13 mmol, 1 equiv) was added dropwise to a diethyl ether solution (3 mL) of **12** (1 equiv) previously generated. The reaction mixture was allowed to stir for 5 minutes. The volatile materials were removed under vacuum. The ^{1}H NMR spectrum shows formation of one species containing the phenolate ligand. ^{1}H NMR (300 MHz, $C_6D_5CD_3$,) δ: 0.42 (d, *J* = 11 Hz, 1H, Sc*C*H-H), 0.60 (d, *J* = 11 Hz, 1H, Sc*C*H-H), 0.31 (s, 3H, Si*C*H_3), 0.38 (s, 3H, Si*C*H_3), 1.33 (m, 9H, C(*C*H_3)$_3$), 1.73 (s, 9H, C(*C*H_3)$_3$), 2.98 (d, *J* = 14.4 Hz, 1H, NCH-*H*), 3.12 (br d, *J* = 14.4 Hz, 1H,

NCH-*H*), 3.61 (br d, *J* = 14.4 Hz, 1H, NCH-*H*), 4.20 (d, *J* = 14.4 Hz, 1H, NCH-*H*), 4.07 (s, 1H, NC-*H*), 5.07 (br t, 1H, aryl-*H*), 5.78 (d, 1H, aryl-*H*), 6.12-6.23 (m, 2H, aryl-*H*), 6.30 (t, 1H, aryl-*H*), 6.48 (br t, 2H, C_5H_5N), 6.63 (t, 1H, aryl-*H*), 6.78 (br t, 1H, C_5H_5N), 6.88 (br s, 1H, aryl-*H*), 7.17-7.46 (m, 4H, aryl-*H*), 7.65 (br s, 1H, aryl-*H*), 7.73 (br s, 2H, aryl-*H*), 8.77 (d, 1H, aryl-*H*), 8.97 (br s, 2H, C_5H_5N). ^{13}C NMR (75 MHz, $C_6D_5CD_3$,) δ: -1.2 ($PhSi(CH_3)_3$), 2.3 ($SiCH_3$), 2.5 ($SiCH_3$), 30.4 ($C(CH_3)_3$), 32.0 ($C(CH_3)_3$), 32.2 ($ScCH_2$), 34.2 (CMe_3), 35.6 (CMe_3), 62.7 (NCH_2), 64.4 (NCH_2), 101.4 (NCH), 96.9 (*aryl*-H), 114.2 (*aryl*-H), 122.3, 122.5, 123.8, 124.9, 125.2, 127.6, 128.0, 129.0, 131.1, 133.5, 133.8, 135.7, 136.6, 137.9, 138.3, 138.6, 140.2, 144.0. 146.9, 149.0, 150.8, 151.8, 152.7, 159.8, 160.4 (*aryls*, C_5H_5N, and $C_6H_5SiMe_3$).

Activation of 7a with $[PhNHMe_2]^+[B(C_6F_5)_4]^-$ and NMR-Scale Ethylene Polymerizations. Under nitrogen atmosphere, chlorobenzene-d_5 solution (0.4 mL) of yttrium dialkyl complex (13.5 mg, 0.018 mmol, 1 equiv) was frozen in a J-Young tube. Chlorobenzene-d_5 solution (0.3 mL) of diphenylmethane (3.1 mg, 0.018 mmol, 1 equiv) was added as internal standard and to separate the chlorobenzene-d_5 solution (0.4 mL each) of yttrium dialkyl complex from the solution of stoichiometric activator $[PhNHMe_2]^+[B(C_6F_5)_4]^-$ (14.6 mg, 0.018 mmol, 1 equiv). Before recording the ^1H NMR spectrum, the sample was allowed to warm up for 5 - 10 seconds and mixed. The ^1H NMR spectrum shows formation of mainly one species containing the phenolate ligand along with the alkane byproduct. After activation, ethylene (0.166 mmol, 9.3 equiv) was condensed in the J-Young tube. Using diphenylmethane as internal standard, slow consumption of ethylene (< 4 equiv) was observed over 6 h. **Spectroscopic**

characterization of 14: ^{1}H NMR (300 MHz, C_6D_5Cl, -40 °C) Tentatively assigned to the activated species (major) δ: -0.75 (br d, *J* = 10.8 Hz, 1H, YCH-*H*), -0.54 (br d, *J* = 10.8 Hz, 1H, YCH-*H*), 0.37 (br s, 3H, SiCH_3), 0.49 (br s, 3H, SiCH_3), 1.36 (s, 9H, C(CH_3)$_3$), 1.68 (s, 9H, C(CH_3)$_3$), 2.09-3.50 (m, NCH_2CH_2O and aryl-CH_2 – overlapping broad peaks), 3.11 (s, 3H, OCH_3), 3.38 (s, 3H, OCH_3), 2.62 (s, 6H, C_6H_5N(CH_3)$_2$). Not assigned δ: 0.85 (t, 1H), 0.89 (t, 1H), 1.61 (s, not C(CH_3)$_3$ from the starting material), 6.55-7.79 (aryl-*H* peaks for $YCH_2SiMe_2C_6H_5$, C_6H_2-OY, $C_6H_5SiMe_3$, and $C_6H_5NMe_2$). ^{1}H NMR (300 MHz, C_6D_5Cl) Tentatively assigned to the activated species (major) - δ: -0.60 (br s, 2H, YCH_2), 0.40 (br s, 6H, Si(CH_3)$_2$), 1.32 (s, 9H, C(CH_3)$_3$), 1.57 (br s, 9H, C(CH_3)$_3$), 2.08-3.08 (br m, 10H, NCH_2CH_2O and aryl-CH_2), 3.23 (s, 6H, OCH_3), 2.65 (s, 6H, C_6H_5N(CH_3)$_2$,), remaining peaks are broad and overlap. Not assigned δ: 0.85 (m, ~2H), 1.22 (s, not C(CH_3)$_3$ from the starting material), 6.67-7.71 (aryl-*H* peaks for $YCH_2SiMe_2C_6H_5$, C_6H_2-OY, $C_6H_5SiMe_3$, and $C_6H_5NMe_2$).

Activation of 9 with $[PhNHMe_2]^+[B(C_6F_5)_4]^-$ and NMR Scale Ethylene Polymerizations. Under a nitrogen atmosphere, chlorobenzene-d_5 solution (0.4 mL) of yttrium dialkyl complex (9.1 mg, 0.015 mmol, 1 equiv) was frozen in a J Young tube. Chlorobenzene-d_5 solution (0.3 mL) of diphenylmethane (2.5 mg, 0.015 mmol, 1 equiv) was added as internal standard and to separate the chlorobenzene-d_5 solution (0.4 mL each) of yttrium dialkyl complex from the stoichiometric activator $[PhNHMe_2]^+[B(C_6F_5)_4]^-$ (11.9 mg, 0.015 mmol, 1 equiv). Before recording the ^{1}H NMR spectrum, the sample was allowed to warm up for 5 - 10 seconds and mixed. The ^{1}H NMR spectrum shows formation of mainly

one species containing the phenolate ligand, along with the alkane byproduct. After activation, ethylene (0.166 mmol, 11.1 equiv) was condensed into the J Young tube. Using diphenylmethane as internal standard, slow consumption of ethylene (< 7.5 equiv) was observed over 7 h. **Spectroscopic characterization of 15:** ^{1}H NMR (300 MHz, C_6D_5Cl, -40 °C). Tentatively assigned to the activated species (major) δ: -0.98 (br d, *J* = 11.1 Hz, 1H, YCH-*H*), -0.77 (br d, *J* = 11.1 Hz, 1H, YCH-*H*), 0.19 (br s, 9H, Si(C*H*$_3$)$_3$), 1.30 (s, 9H, C(C*H*$_3$)$_3$), 1.60 (s, 9H, C(C*H*$_3$)$_3$), 1.70-3.00 (br m, NC*H*$_2$C*H*$_2$O and aryl-C*H*$_2$), 3.15 (s, 3H, OC*H*$_3$), 3.37 (s, 3H, OC*H*$_3$), 2.59 (s, 6H, $C_6H_5N(CH_3)_2$). Not assigned δ: 0.83 (m), 1.22 (s), 6.54 - 7.62 (aryl-*H* peaks for C_6H_2-OY, and $C_6H_5NMe_2$). ^{1}H NMR (300 MHz, C_6D_5Cl) Tentatively assigned to the activated species (major) δ: -0.81 (br s, 2H, YC*H*$_2$), 0.15 (br s, 9H, Si(C*H*$_3$)$_3$), 1.30 (s, 9H, C(C*H*$_3$)$_3$), 1.58 (br s, 9H, C(C*H*$_3$)$_3$), 1.80-4.00 (br m, NC*H*$_2$C*H*$_2$O and aryl-C*H*$_2$ – overlapping broad peaks), 3.33 (s, 6H, OC*H*$_3$), 2.69 (s, 6H, $C_6H_5N(CH_3)_2$). Not assigned δ: 0.84 (m), 1.22, 6.67-7.51 (aryl-*H* peaks for C_6H_2-OY, and $C_6H_5NMe_2$).

Line shape and Eyring analysis. NMR spectral simulations were performed using gNMR version 3.6. The chemical shifts observed in the slow limit exchange (203 K) were used to set up the spin systems. The relative population ratio was fixed at 1:1 for **7a**, **8a** and **10**. Lorentzian line shapes with line widths of 2 Hz were utilized. Small changes to the line width did not visibly affect the activation parameters of the exchange process. As the chemical shifts of the different hydrogens vary slightly with temperature, the difference in the chemical shifts was used to compare simulated with experimental spectra. For

different temperatures, the exchange rate was varied to get the best fit between the simulated and the experimental spectra. Activation parameters were determined by a standard Eyring analysis, and the standard deviations from the chi-squares fit were used to estimate the uncertainties in $\Delta H^{\ddagger}$ and $\Delta S^{\ddagger}$.

Ethylene Polymerizations. Ethylene polymerizations were performed in a high-pressure glass vessel equipped with a magnetic stirrer. In a typical procedure, under nitrogen atmosphere, solid MAO (48.3 mg, 0.833 mmol, 500 equiv) was added to 4.5 mL chlorobenzene. The mixture was pressurized to 1 bar of ethylene. A chlorobenzene (0.5 mL) solution of catalyst precursor (1.67 μmol, 1 equiv) was added by syringe. The ethylene pressure was immediately increased to 5 bar and the solution was stirred for 1 h. The polymerization was stopped by venting of the vessel and quenching with a mixture of 37% HCl solution and methanol (1:12 v:v). The polymer was collected by filtration, washed with methanol (3 x 10 mL) and dried under high vacuum overnight. Productivities of less than 3 Kg PE•(mol M)$^{-1}$•h^{-1}•bar^{-1} were obtained.

X-ray Crystal Data: General Procedure. Crystals grown from diethyl ether (**7a** and **8a**) or a mixture of diethyl ether and petroleum ether (**7b**) at -35 °C were removed quickly from a scintillation vial to a microscope slide coated with Paratone N oil. Samples were selected and mounted on a glass fiber with Paratone N oil. Data collection was carried out on a Bruker Smart 1000 CCD diffractometer. The structures were solved by direct methods. All non-hydrogen atoms were refined anisotropically. Some details regarding

refined data and cell parameters are available in Table 1. Selected bond distances and angles are supplied in the captions of Figures 3 - 5.

Table 1. Crystal and refinement data for complexes **7a**, **7b**, and **8a**.

	7a	**7b**	**8a**
Empirical formula	$C_{39}H_{62}NO_3Si_2Y$	$C_{45}H_{76}N_3OSi_2Y$	$C_{39}H_{62}NO_3Si_2Sc$
Formula weight	737.99	820.18	694.04
T (K)	98(2)	100(2)	100(2)
a, Å	11.3640(4)	18.3292(16)	12.8434(5)
b, Å	14.2999(5)	10.1929(8)	18.7067(7)
c, Å	25.4993(9)	28.733(2)	33.6484(12)
α, deg			
β, deg	100.2310(10)	103.571(2)	
γ, deg			
Volume, Å^3	4077.9(2)	5218.2(8)	8084.3(5)
Z	4	4	8
Crystal system	Monoclinic	Monoclinic	Orthorhombic
Space group	$P2_1/n$	$P2_1/c$	Pbca

d_{calc}, g/cm^3	1.202	1.044	1.140
θ range, deg	1.62 to 28.41	1.46 to 22.49	1.99 to 28.50
μ, mm^{-1}	1.523	1.194	0.276
Abs. Correction	None	None	None
GOF	1.446	2.059	2.272
R_1,[a] wR_2 [b] [I>2σ(I)]	0.0323, 0.0535	0.0640, 0.1126	0.0447, 0.0693

[a] $R_1 = \sum | |F_o| - |F_c| | / \sum |F_o|$. [b] $wR_2 = [\sum[w(F_o^2-F_c^2)^2] / \sum[w(F_o^2)^2]]^{1/2}$.

References

(1) McKnight, A.; Waymouth, R., M. *Chem. Rev.* **1998**, *98*, 2587.

(2) Gibson, V. C.; Spitzmesser, S. K. *Chem. Rev.* **2003**, *103*, 283.

(3) Britovsek, G. J. P.; Gibson, V. C.; Wass, D. F. *Angew. Chem. Int. Ed.* **1999**, *38*, 428.

(4) Shapiro, P. J.; Schaefer, W. P.; Labinger, J. A.; Bercaw, J. E.; Cotter, W. D. *J. Am. Chem. Soc.* **1994**, *116*, 4623.

(5) Zeimentz, P. M.; Arndt, S.; Elvidge, B. R.; Okuda, J. *Chem. Rev.* **2006**, *106*, 2404-2433.

(6) Arndt, S.; Okuda, J. *Adv. Synth. Catal.* **2005**, *347*, 339-354.

(7) Gromada, J.; Carpentier, J. F.; Mortreux, A. *Coord. Chem. Rev.* **2004**, *248*, 397-410.

(8) Hayes, P. G.; Piers, W. E.; McDonald, R. *J. Am. Chem. Soc.* **2002**, *124*, 2132.

(9) Bambirra, S.; van Leusen, D.; Meetsma, A.; Hessen, B.; Teuben, J. H. *Chem. Commun.* **2003**, 522.

(10) Bambirra, S.; van Leusen, D.; Meetsma, A.; Hessen, B.; Teuben, J. H. *Chem. Commun.* **2001**, 637.

(11) Lee, L. W. M.; Piers, W. E.; Elsegood, M. R. J.; Clegg, W.; Parvez, M. *Organometallics* **1999**, *18*, 2947.

(12) Lee, L.; Berg, D. J.; Einstein, F. W.; Batchelor, R. J. *Organometallics* **1997**, *16*, 1819.

(13) Hajela, S.; Schaefer, W. P.; Bercaw, J. E. *J. Organomet. Chem.* **1997**, *532*, 45.

(14) Fryzuk, M. D.; Giesbrecht, G.; Rettig, S. J. *Organometallics* **1996**, *15*, 3329.

(15) Skinner, M. E. G.; Tyrrell, B. R.; Ward, B. D.; Mountford, P. *J. Organomet. Chem.* **2002**, *647*, 145.

(16) Evans, W. J.; Broomhall-Dillard, R. N. R.; Ziller, J. W. *Organometallics* **1996**, *15*, 1351.

(17) Emslie, D. J. H.; Piers, W. E.; Parvez, M.; McDonald, R. *Organometallics* **2002**, *21*, 4226.

(18) Bambirra, S.; Brandsma, M. J. R.; Brussee, E. A. C.; Meetsma, A.; Hessen, B.; Teuben, J. H. *Organometallics* **2000**, *19*, 3197.

(19) Hayes, P. G.; Piers, W. E.; Lee, L. W. M.; Knight, L. K.; Parvez, M.; Elsegood, M. R. J.; Clegg, W. *Organometallics* **2001**, *20*, 2533.

(20) Ward, B. D.; Bellemin-Laponnaz, S.; Gade, L. H. *Angew. Chem. Int. Ed. Engl.* **2005**, *44*, 2.

(21) Bambirra, S.; Boot, S.; van Leusen, D.; Meetsma, A.; Hessen, B. *Organometallics* **2004**, *23*, 1891.

(22) Trosch, A.; Vahrenkamp, H. *Eur. J. Inorg. Chem.* **1998**, 827.

(23) Trosch, A.; Vahrenkamp, H. *Inorg. Chem.* **2001**, *40*, 2305.

(24) Abufarag, A. V., H. *Inorg. Chem.* **1995**, *34*, 329.

(25) Inoue, Y.; Matyjaszewski, K. *Macromolecules* **2003**, *36*, 7432-7438.

(26) Takahashi, K.; Ogawa, E.; Oishi, N.; Nishida, Y.; Kida, S. *Inor. Chim. Acta* **1982**, *66*, 97.

(27) Bylikin, S. Y.; Robson, D. A.; Male, N. A. H.; Rees, L. H.; Mountford, P.; Schroder, M. *J. Chem. Soc., Dalton Trans.* **2001**, 170.

(28) Groysman, S.; Goldberg, I.; Kol, M.; Goldschmidt, Z. *Organometallics* **2003**, *22*, 3793-3795.

(29) Groysman, S.; Goldberg, I.; Kol, M.; Genizi, E.; Goldschmidt, Z. *Organometallics* **2004**, *23*, 1880-1890.

(30) Tshuva, E. Y.; Goldberg, I.; Kol, M.; Goldschmidt, Z. *Chem. Commun.* **2001**, 2120-2121.

(31) Tshuva, E. Y.; Goldberg, I.; Kol, M.; Goldschmidt, Z. *Inor. Chem.* **2001**, *40*, 4263-4270.

(32) Tshuva, E. Y.; Goldberg, I.; Kol, M.; Goldschmidt, Z. *Organometallics* **2001**, *20*, 3017-3028.

(33) Tshuva, E. Y.; Groysman, S.; Goldberg, I.; Kol, M.; Goldschmidt, Z. *Organometallics* **2002**, *21*, 662-670.

(34) Tshuva, E. Y.; Goldberg, I.; Kol, M. *J. Am. Chem. Soc.* **2000**, *122*, 10706-10707.

(35) Segal, S.; Goldberg, I.; Kol, M. *Organometallics* **2005**, *24*, 200-202.

(36) Busico, V.; Cipullo, R.; Ronca, S.; Budzelaar, P. H. M. *Macromol. Rapid Commun.* **2001**, *22*, 1405-1410.

(37) Groysman, S.; Sergeeva, E.; Goldberg, I.; Kol, M. *Inor. Chem.* **2005**, *44*, 8188-8190.

(38) Westmoreland, I.; Arnold, J. *Dalton Transactions* **2006**, 4155-4163.

(39) Tshuva, E. Y.; Goldberg, I.; Kol, M.; Goldschmidt, Z. *Organometallics* **2001**, *20*, 3017.

(40) Fay, R. C.; Lindmark, A. F. *J. Am. Chem. Soc.* **1983**, *105*, 2118.

(41) Cationic Zr species generated from ligand precursor **1** were reported, at room temperature, to display ^{1}H NMR spectroscopy characteristics related to the phenomena reported here – the ether CH_3 groups show only one singlet, while the metal bound benzyl group show two doublets for the methylene groups.(ref 33) This is consistent both with the Cs structure proposed by Kol et al., with the two benzyls reflecting into each other via the mirror plane, and with a dynamic process which, in this case, exchanges the ether groups (via B), but not the diastereotopic hydrogens (via D - F). A variable temperature ^{1}H NMR spectroscopy study would distinguish between the two possibilities.

(42) Dialkyl complexes **7a** and **8a** do not show a reaction upon treatment with pyridine, suggesting that the intramolecular ether donors are preferred to the added base. While no reactivity was observed toward ethylene, **7b** reacts with acetonitrile and diphenylacetylene to afford multiple unidentified products.

(43) Pangborn, A. B.; Giardello, M. A.; Grubbs, R. H.; Rosen, R. K.; Timmers, F. J. *Organometallics* **1996**, *15*, 1518.

(44) Sokolowski, A.; Muller, J.; Weyhermuller, T.; Schnepf, R.; Hildebrandt, P.; Hildenbrand, K.; Bothe, E.; Wieghardt, K. *J. Am. Chem. Soc.* **1997**, *119*, 8889-8900.

(45) Silverstein, R. M.; Webster, F. X. *Spectroscopic Identification of Organic Compounds*, 6th ed., **1998**.

Appendix 1

Enantiopure Non-Metallocene Olefin Polymerization Catalysts: Toward the Kinetic Resolution of Chiral Monomers

Abstract

The syntheses of chiral tetradentate tripodal diphenolate ligands have been accomplished starting from readily available chiral building blocks. Metallations have been performed using zirconium tetrabenzyl ($ZrBn_4$) as a starting material. Polymerization studies carried out with a chiral zirconium dibenzyldiphenolate show very high polymerization activity, but no enantioselectivity for polymerization of racemic 3-methyl-1-pentene. A second-generation chiral ligand, displaying different substitution of the phenol groups, has been synthesized, but separation of the diastereomers has been unsuccessful. In order to avoid generating a mixture of diastereomers, a ligand having chiral phenol groups has been prepared. Metallation using $ZrBn_4$ leads to the clean formation of one metal complex. Decreased polymerization activity and no enantioselectivity have been observed for polymerization of racemic 3-methyl-1-pentene with this species.

Introduction

Chiral olefins have great potential as synthons in asymmetric synthesis and as monomers for new specialty polymers with previously inaccessible optical and physical properties.[1,2] High yield methods for the production of enantiomerically pure chiral olefins remain elusive, however, kinetic resolution via trasition metal mediated catalysis is an attractive approach.[3] The potential for generating a useful polymer compensates for the low maximum theoretical yield of 50% for the resolved, unreacted monomer. Furthermore, chiral resolution of a-

olefins via polymerization may provide a general route to enantiomerically pure unfunctionalized and functionalized alkenes.[4-11]

In general terms, an optically active catalyst would react fast with one enantiomer of a racemic mixture to convert it to product, while leaving the other enantiomer unreacted (Eq 1). Kinetic resolution is the result of energy differences between diastereomeric transition states or intermediates that are accessible for each enantiomer along the reaction pathway. Most reported examples of kinetic resolution of olefins involve species containing functional groups like alcohols or ethers, which increase the chelating ability of the substrate and differentiate better the diastereotopic intermediate structures.[12-15] The only report involving kinetic resolution of an unfuctinalized olefin involves a dihydroxylation reaction.[16]

$$(R,S)\text{-A} \xrightarrow[\text{chiral reagent or catalyst}]{k_R > k_S} \text{B} + (S)\text{-A} \qquad (1)$$

In this context, Ziegler-Natta catalysts are promising candidates for the kinetic resolution of a-olefins (Eq 2), given the large pool of systems that display high activity and high level of stereocontrol.[17-19] Preferential polymerization of one enantiomer of a racemic mixture has been documented for chiral sites in heterogeneous systems as well as for single-site metallocene catalysts.[20-26] Considering that single-site catalysts are well defined and can be finely tuned, they are good candidates for performing kinetic resolutions. Rational choice and structural modification of a Ziegler-Natta catalyst may provide an effective system for kinetic resolution of α-olefins. Work by Bercaw *et al.* using a doubly linked *ansa*-metallocene catalyst indicates that this is a viable approach.[27] The

very active catalysts employed in that study were able to polymerize relatively bulky 3-substituted a-olefins and promising selectivities for polymerization of one enantiomer of racemic mixtures were observed in a number of cases. On the downside, steric modifications of the initial catalyst did not significantly improve the selectivity, triggering a search for alternate systems.

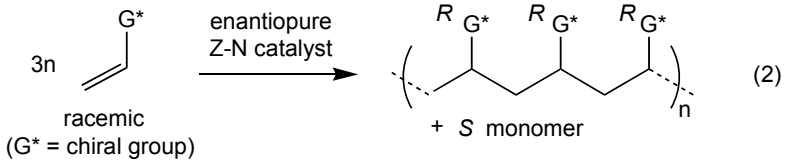

(2)

The required qualities of an efficient catalyst for kinetic resolution of chiral monomers are high polymerization activity and high enantioselectivity. Recently it was reported that non-metallocene catalysts might satisfy the required qualities for efficient kinetic resolution of chiral monomers. For example, Kol *et al.* describe a catalytic system that is both very active for 1-hexene polymerization and has potential for diverse variation of the ligand framework towards chiral versions (Figure 1).[28-31] We have confirmed these reports, and further, have established that **1b** readily polymerizes 3-methyl-1-pentene under Kol's conditions. We anticipate that **1a** will have even greater activity based on the finding that the complex having an ether donor coordinated to the metal has the highest activity in the series.[28]

In this work, we report the synthesis and characterization of a chiral version of the Kol catalyst and experiments assessing its enantioselectivity for the polymerization of chiral monomers. Unfortunatelly no kinetic resolution was observed for the studied systems for the polymerization of 3-methyl-1-pentene.

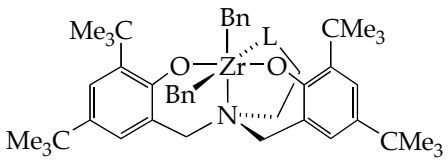

(**1a**, L = OMe; **1b**, L = NMe_2; **1c**, L = NEt_2; **1d**, L = SMe)

Figure 1. Zirconium dialkyl complexes supported by biphenolate ligands.

Results and Discussion

Ligand design

As mentioned in the preceding section, a number of strategies could be envisioned for the desymmetrization of the Kol catalysts. A problematic feature of the Kol system is the dramatic dependence of activity towards 1-hexene polymerization on small changes in the ligand framework. For instance, changing the ligand from **1b** to **1c** decreases the activity by more than three orders of magnitude (from 21000 to 60 g(mmol cat)$^{-1}$h^{-1}).[30] Hence, in designing chiral versions of the Kol ligands, it is important to ensure preservation of high polymerization activity.

Considering the possible geometries of the active cationic catalyst in the Kol system (Figure 2), some predictions could be attempted regarding the possible effect of the position of a chiral center on relaying the chirality to the incoming monomer. A trigonal-bipyramidal (**a**) structure is more likely than a square-pyramid (**b**) due to reduced steric strain in the former. In that case, the olefin would approach the metal center (**a**) in the equatorial plane. Ideally, only

one face of the olefin will be able to coordinate and insert, to give an isotactic polymer.

For a trigonal-bipyramidal structure (**a**, Figure 2), a chiral group on L would probably have a close interaction with the polymer chain, affecting the incoming monomer mostly in an indirect fashion. Stereofacial control for olefin coordination and insertion would be limited with that strategy. An alternative strategy is to make the backbone between the L and N chiral, which may induce a propeller-like arrangement of the ligand around the metal center.[32,33] Modification of the substituents ortho to phenolate oxygens is another approach to render the molecule asymmetric.

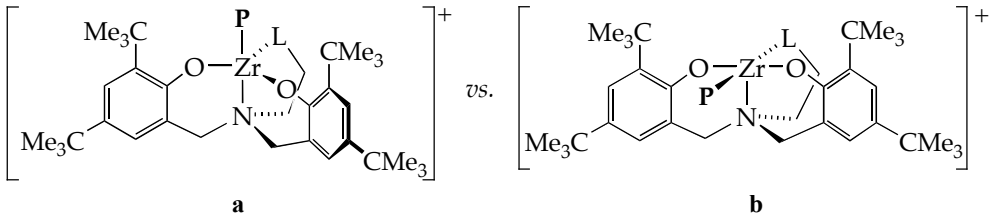

a **b**

Figure 2. Possible geometries for the propagating species. P = polymer chain; L = neutral donor.

Ligand synthesis

A synthetic protocol was designed for the preparation of chiral tetradentate diphenols with bulky *o*-substituents ligands (Scheme 1). This synthetic route, even thought slightly longer, was found to work considerably better than the Mannich condensation procedure used by Kol *et al*.[14] The only problematic step is the selective methylation of the alcohol vs. the phenol in **1**, but limiting the amount of MeI used, and purifying the product (**2**) by column chromatography was found to give yields of ~60%. The procedure mentioned

above can be modified to prepare ligands that contain different phenol groups (**15**, Scheme 2).

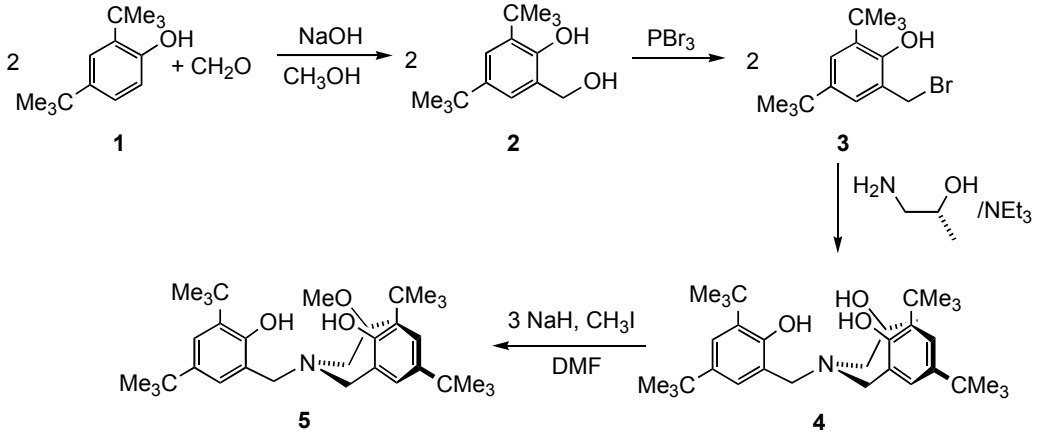

Scheme 1. Synthesis of chiral bisphenol with a chiral center on the neutral backbone.

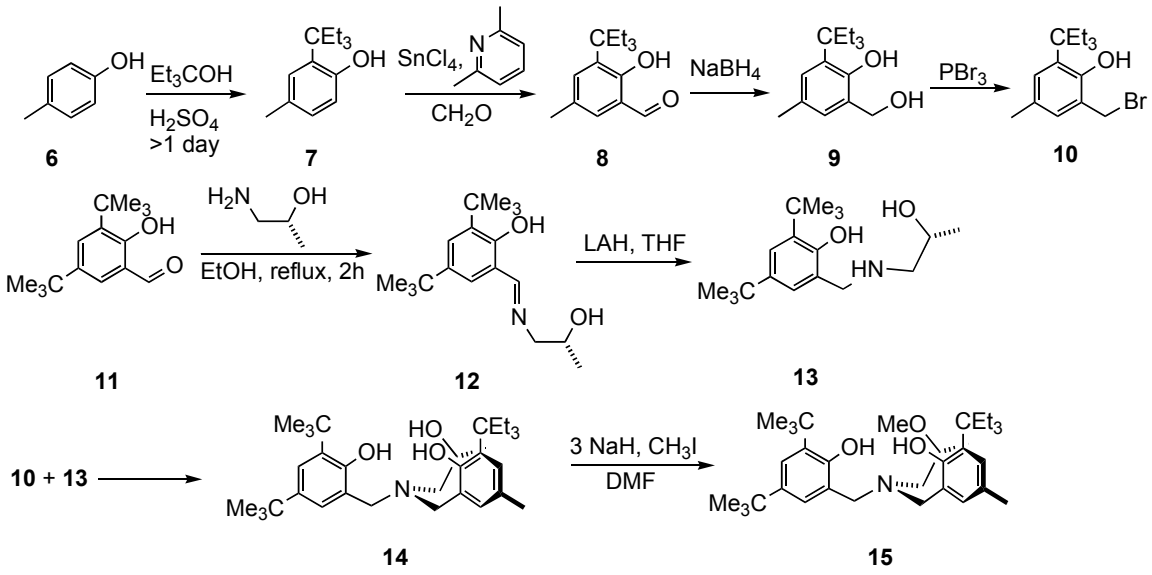

Scheme 2. Synthesis of bisphenol with different substitution of the phenol rings.

Synthesis of zirconium dialkyl complexes

Synthesis of target zirconium dialkyl complexes has been accomplished via an alkane elimination route starting from $Zr(CH_2C_6H_5)_4$ (Scheme 3). The four

t-butyl groups in **16** show distinct peaks in the ^{1}H NMR spectrum indicating that the chiral backbone renders them to different chemical environments. Metallation of **15** gives rise to a 1:1 mixture of diastereomers whose separation has been unsuccessful to date.

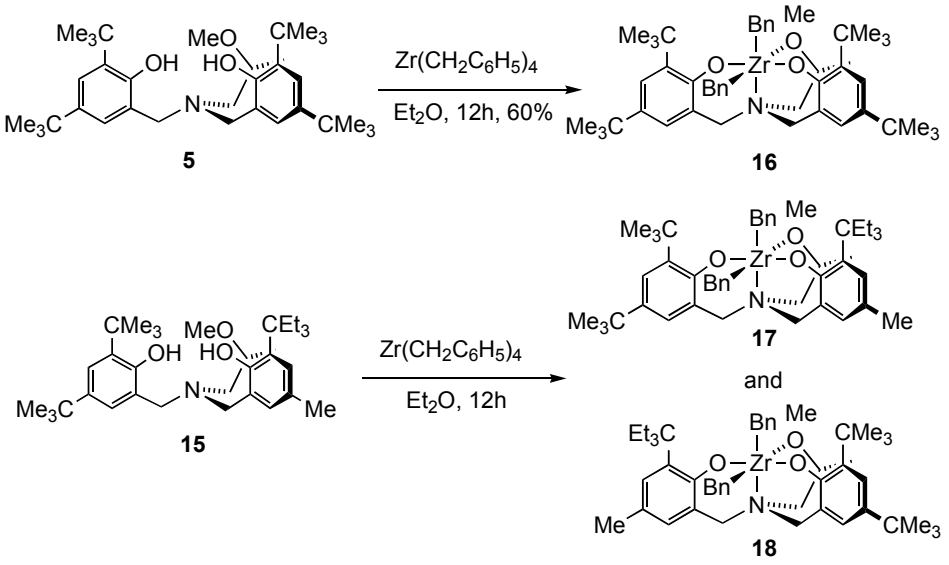

Scheme 3. Metallation of bisphenols **5** and **15** with $ZrBn_4$.

Complex **16** has been structurally characterized by single crystal X-ray diffraction (Figure 3). All Zr-ligand bond lengths are similar to the related nonchiral complex **1a**.[12] The methyl group on the chiral center points away from the metal. The two phenolate aryl rings are almost related by a mirror plane, indicating that in the solid state, the chiral backbone does not differentiate them significantly.

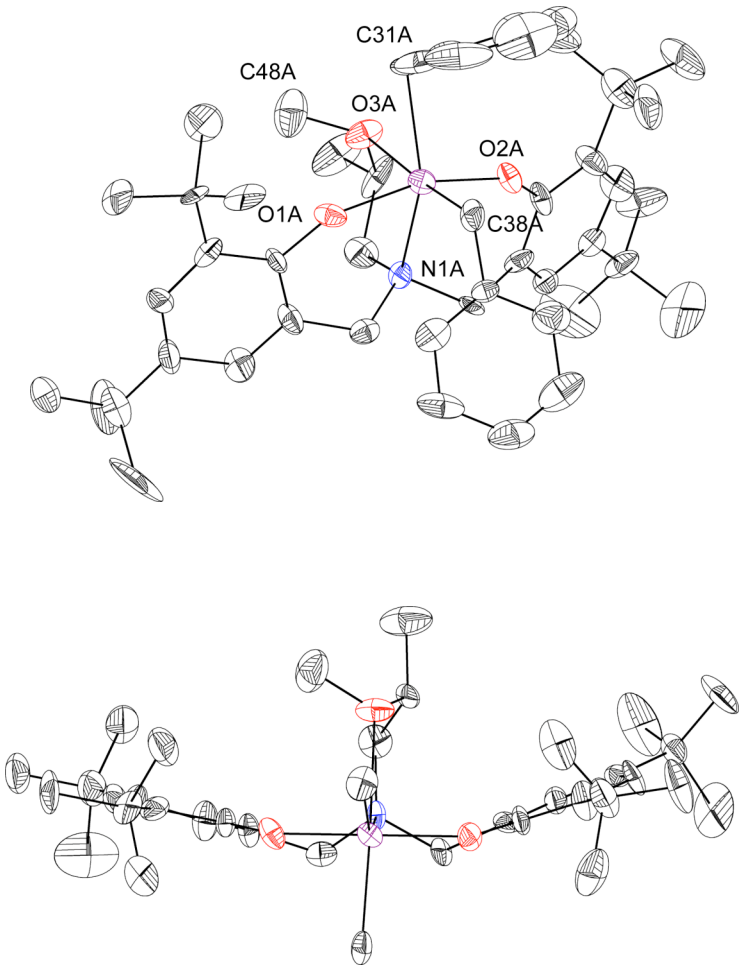

Figure 3. Left: Structural drawing of **16** with thermal ellipsoids at the 50% probability level. Selected bond lengths (Å) and angles (°): Zr-O_{1A} 1.974(4); Zr-O_{2A} 1.972(5); Zr-O_{3A} 2.447(5); Zr-N_{1A} 2.454(7); Zr-C_{31A} 2.303(7); Zr-C_{28A} 2.266(8); O_{2A}-Zr-O_{1A} 159.7(2); O_{3A}-Zr-O_{1A} 89.0(2); N_{1A}-Zr-O_{1A} 70.6(2); N_{1A}-Zr-O_{2A} 80.4(2); C_{31A}-Zr-O_{38A} 99.3(3). Right: view along the Zr-N vector; for clarity, phenyl groups are not shown.

Polymerization experiments with 3-methyl-1-pentene

Inspired by promising preliminary NMR scale experiments, bulk polymerizations were performed with 3-methyl-1-pentene. Activation of compound **3** with $[Ph_3C][B(C_6F_5)_4]$ in chlorobenzene, at room temperature, was followed by addition of monomer containing a known amount of tetradecane. After stirring for 20 min the mixture became cloudy and viscous indicating polymer formation. GC analysis of this mixture shows 28% conversion of the monomer. This conversion rate corresponds to an activity of ~1200 turnovers h^{-1} (~100 g (mmol cat)$^{-1}$ h^{-1}), being superior the those of zirconocene catalysts currently explored for kinetic resolution (72 turnovers h^{-1} on average after 12 h).[16] The reaction was quenched and a fraction of the unreacted monomer was converted to 2-methylbutanoic ester and analyzed by chiral GC.[16] The analysis showed no enantioselectivity. A similar polymerization experiment was performed at –18°C, where a better energetic differentiation of the transition states or intermediates may be in effect, but again, no enantionselectivity was observed.

Next generation ligand – Synthesis

A ligand design that displays two different phenol moieties was shown to give rise to complications at the metallation step by generating a mixture of diastereomers (Scheme 3). In order to avoid this problem, a ligand asymmetric at the phenol group was envisioned which, upon metallation, would form only one possible isomer (assuming that the phenoxides will bind trans, as observed for all related compounds that have been crystallographically characterized). This ligand framework is based on the binaphthalene motif and its synthesis was

accomplished starting from enantiomerically pure 1,1'-bi-2-naphthol (binol), which is commercially available (Scheme 4). The lowest yielding step in the synthetic scheme is the nickel catalyzed aryl-aryl coupling reaction. Also, the aryl to substitute for the triflate has to be substituted with bulky groups in order to avoid bromination in a subsequent step.

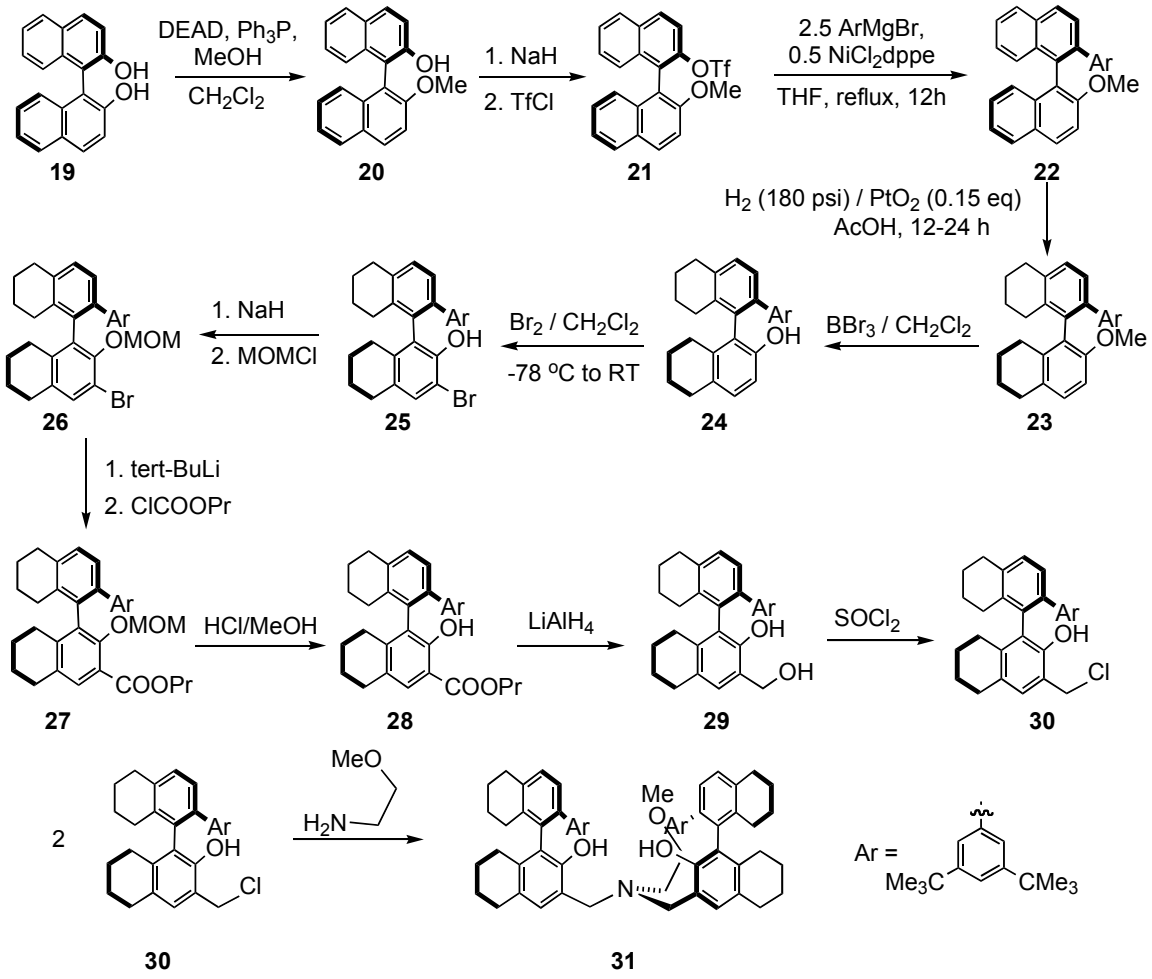

Scheme 4. Preparation of bisphenol with axial chirality on the phenol arms.

Metallation of **35** was performed using $Zr(CH_2C_6H_5)_4$ (Eq 3). The ^1H NMR spectrum of the product is consistent with the formation of only one species based on the number of O*C*H_3 peaks (Figure 3). The aryl *tert*-butyl groups

display two singlets, indicating that the front and the back (as drawn) of the molecule are different enough to differentiate their chemical shifts. Also, the aryl C*H* groups on the phenoxide ring display two singlets, indicating that the left and right sides of the molecule are chemically different. Activation with $[Ph_3C][B(C_6F_5)_4]$ in PhCl generated a catalyst active for the polymerization of 3-methyl-1-pentene, albeit with lower activity (~0.5 g(mmol cat)$^{-1}$·h^{-1}). No enantioselectivity was observed.

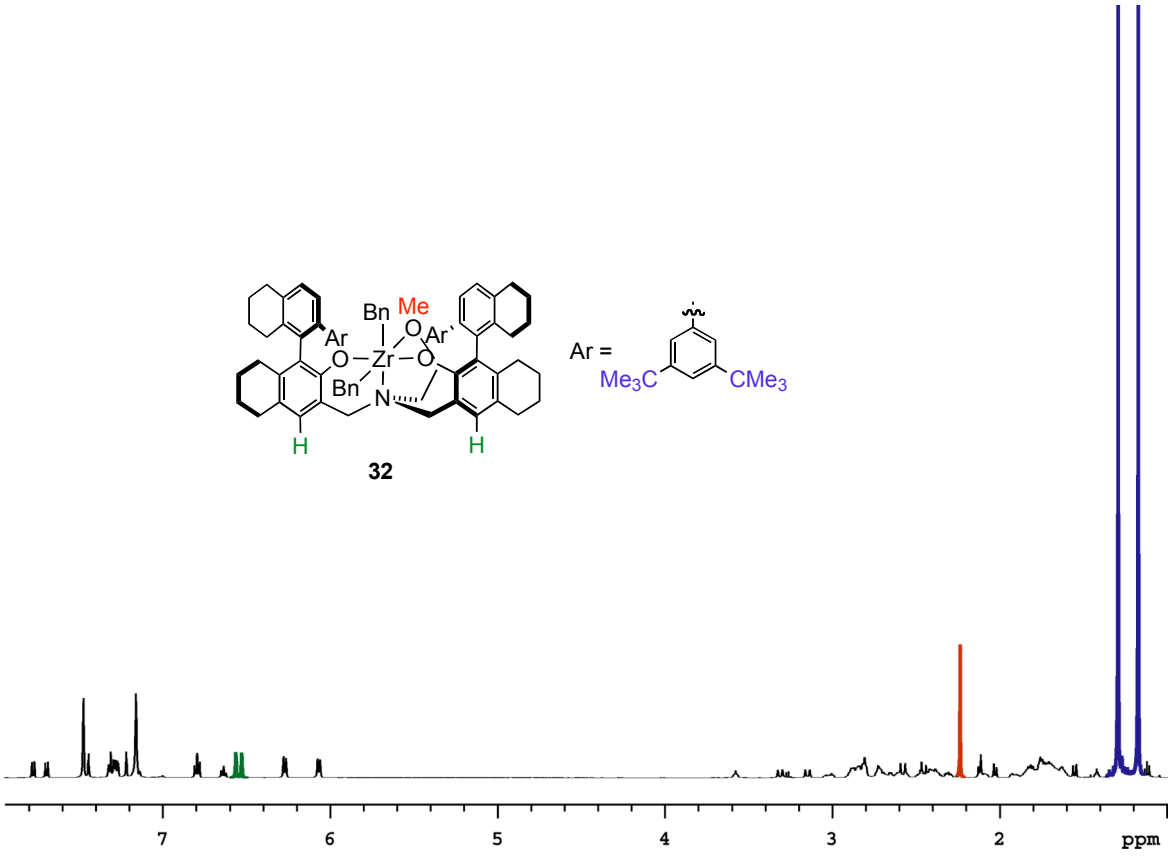

Figure 4. ^{1}H NMR (C_6D_6) of compound **32**.

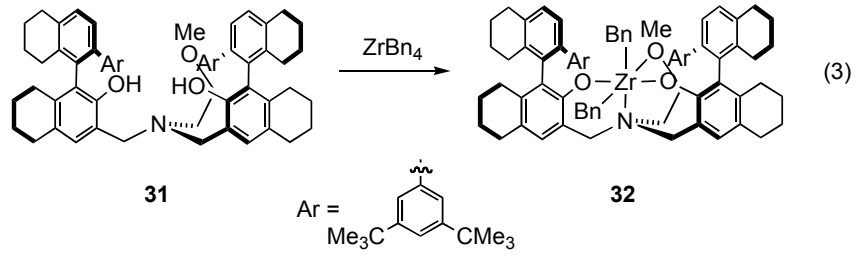

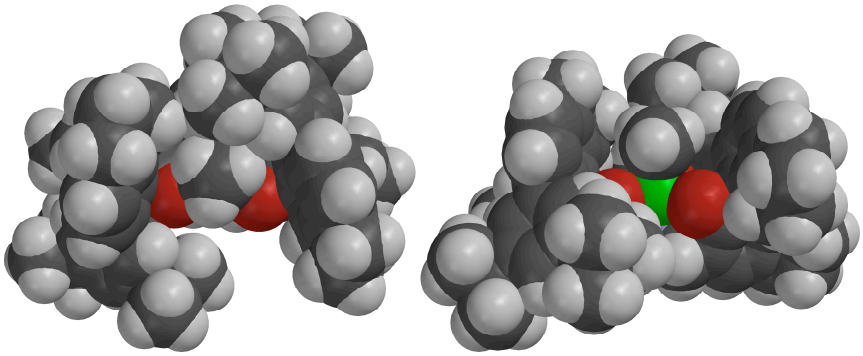

Figure 5. Spartan model of **32** with methyl instead of benzyl group: top view (left) and side view (right).

Inspection of a Spartan model reveals the asymmetry of the molecule, as expected from the asymmetry of the solution NMR spectroscopy structure. The center is significantly more hindered compared to complex **16**. The increased steric bulk could be the reason behind the observed decrease in polymerization activity. The reasons behind the lack of enantioselectivity are not clear, but it could stem from the inherent flexibility of the molecule. Change of conformation could occur at all the sp^3 carbons connecting the axial nitrogen and the rest of the donors. A low barrier to adopting different conformations may translate into small differences in reactivity toward the two olefin enantiomers. To explore this proposal, more rigid bisphenolate ligand frameworks are targeted.

Conclusions

Tripodal, tetradentate biphenols with chiral backbones can be synthesized in four steps from readily available chiral building blocks. Characterization of a zirconium dialkyl complex shows coordination of the ether group (solid-state structure) and diastereaotopic *t*-butyl groups in solution (^{1}H NMR spectroscopy). Activation with $[Ph_3C][B(C_6F_5)_4]$ in chlorobenzene generates a very active polymerization catalyst (more active than the zirconocene catalysts currently explored for kinetic resolution). However, no enantioselectivity was achieved with the reported precatalyst for polymerization of 3-methyl-1-pentene. A bisphenol with different substitution on the two phenol rings was prepared but was found to metallation to zirconium to give a 1:1 mixture of diastereomers. A system with enantiopure chiral phenol groups was prepared based on the binol framework. This system was found to metallate with $ZrBn_4$ to give only one isomer. Activation with $[Ph_3C][B(C_6F_5)_4]$ leads to a catalyst less active than more open analogs for the polymerization of 3-methyl-1-pentene. No enantioselectivity was observed for the polymerization of 3-methyl-1-pentene. The lack of selectivity may be due the flexibility of this system, stemming from the presence of sp^3 linkers between the axial nitrogen and the phenolate rings.

Experimental Section

General Considerations and Instrumentation. All air- and moisture-sensitive compounds were manipulated using standard vacuum line, Schlenk, or cannula techniques or in a drybox under a nitrogen atmosphere. Solvents for air- and moisture-sensitive reactions were dried over sodium benzophenone ketyl or by the method of Grubbs.[34] Benzene-d_6 was purchased from Cambridge Isotopes and distilled from sodium benzophenone ketyl. Chloroform-d_1 and dichloromethane-d_2 were purchased from Cambridge Isotopes and distilled from calcium hydride. MOM protected phenol **1a** was prepared as described in Chapter 4. Other materials were used as received. ^{1}H and ^{13}C NMR spectra were recorded on Varian Mercury 300, or Varian INOVA-500 spectrometers and unless otherwise indicated at room temperature. Chemical shifts are reported with respect to internal solvent: 7.16 and 128.38 (t) ppm (C_6D_6); 7.27 and 77.23 (t) ppm ($CDCl_3$), for ^{1}H and ^{13}C data.

Typical procedure for the polymerization of 3-methyl-1-pentene

In the glove box, a chlorobenzene solution (0.5 mL) of $[Ph_3C][B(C_6F_5)_4]$ (6.6 mg, 0.0071 mmol, 1.5 equiv) was added to a chlorobenzene solution (0.5 mL) of **16** (4.7 mg, 0.0058 mmol, 1 equiv) in a Schlenk tube. The addition was completed with the aid of some chlorobenzene (1 mL). 3-methyl-1-pentene (1 mL, 8.59 mmol, ca. 1500 equiv) mixed with a known amount of tetradecane was added via volumetric pipet. The Schlenk was sealed and the reaction mixture allowed to stir. After 20 min, an aliquot was collected via syringe, quenched in 1-butanol, and investigated by GC. The ratio of olefin to tetradecane standard indicated a 29% conversion. Et_2O (5 mL) was added to the reaction mixture, then a portion of

the volatile materials was vacuum transferred to a round bottom flask. This material was oxidized to the corresponding acid and methylated following standard procedures.[4] Chiral GC analysis of the resulting mixture indicated the presence of a one to one mixture of enantiomers. The above procedure was adapted for low temperature polymerization trials. The initial activated catalyst solution was frozen using a liquid nitrogen cooled cold well, a layer of solvent was added and frozen as well, then the monomer was added and frozen. The reaction flask was sealed and placed in an ethanol bath at –18°C. After 7 h 50 min of stirring (to 25% conversion) the mixture was quenched with water and analyzed as before. Again, no enantioselectivity was observed.

Spectroscopic characterization of 5. ^{1}H NMR (300 MHz, C_6D_6) δ: 0.50 (d, 3H, C*H*$_3$), 1.33, 1.69 (singlets, 18H, C(C*H*$_3$)$_3$), 2.25 (m, 2H, CHC*H*$_2$), 3.10 (s, 3H, OC*H*$_3$), 3.25 (m, 1H, C*H*CH$_3$), 3.46, 3.72 (doublets, 4H, aryl-C*H*$_2$N), 6.97, 7.51 (doublets, 2H, aryl-*H*), 8.89 (s, 1H, O*H*).

Spectroscopic characterization of 13. ^{1}H NMR (300 MHz, $CDCl_3$) δ: 0.93 (d, 3H, C*H*$_3$), 1.29 (s, 9H, C(C*H*$_3$)$_3$), 1.43 (s, 9H, C(C*H*$_3$)$_3$), 2.57-2.80 (m, 2H, NC*H*$_2$CH), 3.68-3.80 (m, 1H, C*H*), 3.99 (s, 2H, aryl-C*H*$_2$), 6.86 (d, 1H, aryl-*H*), 7.24 (d, 1H, aryl-*H*).

Spectroscopic characterization of 15. ^{1}H NMR (300 MHz, C_6D_6) δ: 0.53 (d, 3H, CHC*H*$_3$), 0.85 (t, 9H, CH$_2$C*H*$_3$), 1.33 (s, 9H, C(C*H*$_3$)$_3$), 1.68 (s, 9H, C(C*H*$_3$)$_3$), 2.15 (q, 6H, C*H*$_2$CH$_3$), 2.24 (app d, 2H, NC*H*$_2$), 2.26 (s, 3H, aryl-C*H*$_3$), 3.11 (s, 3H, OC*H*$_3$), 3.20-3.31 (m, 1H, C*H*CH$_3$), 3.38 (d, 2H, NC*H*$_2$), 3.62-3.71 (m, 2H, NC*H*$_2$), 6.69 (d, 1H, aryl-*H*), 6.94 (d, 1H, aryl-*H*), 7.14 (app d, 1H, aryl-*H*), 7.48 (d, 1H, aryl-*H*), 8.73 (br s, 2H, O*H*).

Spectroscopic characterization of 16. ^{1}H NMR (500 MHz, C_6D_6) δ: -0.07 (d, 3H, CHC*H*$_3$), 1.34, 1.37, 1.82, 1.88 (singlets, 18H, C(C*H*$_3$)$_3$), 1.29, 2.36 (dd, 1H; t, 1H, NC*H*$_2$CH), 2.55 (s, 3H, OC*H*$_3$), 2.56 (d, 1H), 2.64 (d, 1H), 2.72 (dd, 2H), 2.94 (dd, 2H), 3.14 (br m, 1H, C*H*CH$_3$), 3.27 (d, 1H), 3.57 (d, 1H), 6.61, 7.03 (triplets, 2H, *p*-Ph-*H*), 6.79, 7.36 (triplets, 4H, *m*-Ph-*H*), 6.87, 6.93, 7.55, 7.61 (doublets, 4H, aryl-*H*), 6.99, 7.68 (doublets, 4H, *o*-Ph-*H*). ^{13}C NMR (126 MHz, C_6D_6) δ: 15.5, (CHCH$_3$) 30.7, 32.3 (C(*C*H$_3$)$_3$), 34.7, 34.8, 35.9, 36.0 (*C*(CH$_3$)$_3$), 54.8, 58.3, 64.5, 65.3, 67.7, 68.4 (Zr-*C*H$_2$, NCH$_2$, OCH), 76.2 (*C*H$_3$), 121.2, 122.8, 124.7, 124.8, 124.9, 125.4, 125.5, 126.0, 128.6, 128.8, 129.4, 136.7, 137.2, 141.4, 141.6, 147.1, 148.7 (aryl), 158.1, 158.9 (*C*OZr).

Spectroscopic characterization of a mixture of 17 and 18. ^{1}H NMR (300 MHz, C_6D_6) δ: -0.06 (d, 3H, CHC*H*$_3$), 0.03 (d, 3H, CHC*H*$_3$), 1.34, 1.37, 1.81, 1.86 (singlets, 9H each, C(C*H*$_3$)$_3$), 2.23, 2.26 (singlets, 3H each, aryl-C*H*$_3$), 2.55, 2.62 (singlets, 3H each, OC*H*$_3$), 0.80-0.94, 2.2-3.2 (m, overlapping CH) 3.16 (d, 1H), 3.34 (d, 1H), 3.45 (d, 1H), 3.68 (d, 1H), 6.85-6.68 (m, 3H, aryl-*H*), 6.79-6.83 (m, 4H, aryl-*H*), 6.93 (d, 1H, aryl-*H*), 6.96-7.07 (m, 4H, aryl-*H*), 7.32-7.41 (m, 4H, aryl-*H*), 7.56 (d, 1H, aryl-*H*), 7.62 (d, 1H, aryl-*H*), 7.64-7.71 (m, 3H, aryl-*H*).

Spectroscopic characterization of 22. ^{1}H NMR (300 MHz, $CDCl_3$,) δ: 1.00 (s, 18H, C(C*H*$_3$)$_3$), 3.49 (s, 3H, OC*H*$_3$), 6.91 (d, 2H, aryl-*H*), 7.04 (t, 1H, aryl-*H*), 7.16 (d, 1H, aryl-*H*), 7.19-7.34 (m, 5H, aryl-*H*), 7.42-7.48 (m, 1H, aryl-*H*), 7.70-7.82 (m, 3H, aryl-*H*), 7.95 (d, 1H, aryl-*H*), 8.03 (d, 1H, aryl-*H*).

Spectroscopic characterization of 23. ^{1}H NMR (300 MHz, $CDCl_3$,) δ: 1.17 (s, 18H, C(C*H*$_3$)$_3$), 1.20-2.96 (m, 16H, C*H*$_2$), 3.64 (s, 3H, OC*H*$_3$), 6.61 (d, 1H, aryl-*H*), 6.87 (d,

1H, aryl-*H*), 6.94 (d, 2H, aryl-*H*), 7.12 (t, 1H, aryl-*H*), 7.17 (d, 1H, aryl-*H*), 7.24 (d, 1H, aryl-*H*).

Spectroscopic characterization of 24. ^{1}H NMR (300 MHz, $CDCl_3$,) δ: 1.19 (s, 18H, C(CH_3)$_3$), 1.20-2.96 (m, 16H, CH_2), 4.57 (s, 1H, O*H*), 6.67 (d, 1H, aryl-*H*), 6.84 (d, 1H, aryl-*H*), 6.94 (d, 2H, aryl-*H*), 7.18 (t, 1H, aryl-*H*), 7.24 (d, 1H, aryl-*H*), 7.33 (d, 1H, aryl-*H*).

Spectroscopic characterization of 25. ^{1}H NMR (300 MHz, $CDCl_3$,) δ: 1.20 (s, 18H, C(CH_3)$_3$), 1.20-2.96 (m, 16H, CH_2), 6.95 (d, 2H, aryl-*H*), 7.05 (s, 1H, aryl-*H*), 7.18 (t, 1H, aryl-*H*), 7.23 (d, 1H, aryl-*H*), 7.29 (d, 1H, aryl-*H*).

Spectroscopic characterization of 26. ^{1}H NMR (300 MHz, $CDCl_3$,) δ: 1.20 (s, 18H, C(CH_3)$_3$), 1.20-2.96 (m, 16H, CH_2), 2.91 (s, 3H, OCH_3), 4.87 (d, 1H, OCH_2O), 4.94 (d, 1H, OCH_2O), 7.00 (d, 2H, aryl-*H*), 7.15-7.19 (m, 3H, aryl-*H*), 7.26 (d, 1H, aryl-*H*).

Spectroscopic characterization of 27. ^{1}H NMR (300 MHz, $CDCl_3$,) δ: 1.01 (t, 3H, CH_2CH_3), 1.17 (s, 18H, C(CH_3)$_3$), 1.30-2.92 (m, 18H, CH_2), 2.80 (s, 3H, OCH_3), 4.23 (t, 2H, OC$H_2$$CH_2$), 4.90 (d, 1H, OC$H_2$O), 4.95 (d, 1H, OC$H_2$*O*), 7.03 (d, 2H, aryl-*H*), 7.14-7.20 (m, 2H, aryl-*H*), 7.26 (d, 1H, aryl-*H*), 7.47 (s, 1H, aryl-*H*).

Spectroscopic characterization of 28. ^{1}H NMR (300 MHz, $CDCl_3$,) δ: 1.04 (t, 3H, CH_2CH_3), 1.17 (s, 18H, C(CH_3)$_3$), 1.30-3.00 (m, 18H, CH_2), 4.21-4.40 (m, 2H, OC$H_2$$CH_2$), 7.04 (d, 2H, aryl-*H*), 7.14 (t, 1H, aryl-*H*), 7.21 (d, 1H, aryl-*H*), 7.26 (d, 1H, aryl-*H*), 7.42 (s, 1H, aryl-*H*), 10.89 (s, 1H, O*H*).

Spectroscopic characterization of 29. ^{1}H NMR (300 MHz, $CDCl_3$,) δ: 1.18 (s, 18H, C(CH_3)$_3$), 1.30-2.80 (m, 16H, CH_2), 2.90 (t, 1H, CH_2O*H*), 4.58-4.78 (2 dd, 2H,

CH_2OH), 5.50 (s, 1H, aryl-O*H*), 6.76 (s, 1H, aryl-*H*), 6.94 (d, 2H, aryl-*H*), 7.17 (t, 1H, aryl-*H*), 7.24 (d, 1H, aryl-*H*), 7.31 (d, 1H, aryl-*H*).

Spectroscopic characterization of 30. ^{1}H NMR (300 MHz, $CDCl_3$,) d: 1.18 (s, 18H, C(CH_3)$_3$), 1.30-3.00 (m, 16H, CH_2), 4.54 (d, 1H, CH_2Cl), 4.71 (d, 1H, CH_2Cl), 4.84 (br s, 1H, O*H*), 6.92 (s, 1H, aryl-*H*), 6.89 (d, 2H, aryl-*H*), 7.18 (t, 1H, aryl-*H*), 7.25 (d, 1H, aryl-*H*), 7.32 (d, 1H, aryl-*H*).

Spectroscopic characterization of 31. ^{1}H NMR (300 MHz, C_6D_6,) δ: 1.26 (s, 36H, C(CH_3)$_3$), 1.00-3.50 (m, 36H, CH_2), 3.04 (s, 3H, OCH_3), 3.02 (d, 2H, arylCH_2N), 4.34 (d, 2H, arylCH_2N), 6.66 (s, 2H, aryl-*H*), 7.11 (d, 2H, aryl-*H*), 7.31-7.34 (m, 6H, aryl-*H*), 7.41 (d, 2H, aryl-*H*), 7.98 (br s, 2H, O*H*).

Spectroscopic characterization of 32. ^{1}H NMR (500 MHz, C_6D_6,) δ: 1.17 (s, 18H, C(CH_3)$_3$), 1.29 (s, 18H, C(CH_3)$_3$), 1.55 (d, 1H), 1.58-1.95 (m, overlapping), 2.03 (d, 1H), 2.06-2.14 (m, 2H), 2.24 (s, 3H, OCH_3), 2.27-3.07 (m, overlapping), 3.15 (d, 1H), 3.31 (d, 1H), 6.07 (d, 2H, aryl-*H*), 6.27 (d, 2H, aryl-*H*), 6.53 (s, 1H, aryl-*H*), 6.56 (s, 1H, aryl-*H*), 6.64 (t, 1H, aryl-*H*), 6.79 (t, 2H, aryl-*H*), 7.22 (t, 1H, aryl-*H*), 7.25-7.34 (m, 5H, aryl-*H*), 7.44 (t, 1H, aryl-*H*), 7.47 (t, 4H, aryl-*H*), 7.69 (d, 1H, aryl-*H*), 7.78 (d, 1H, aryl-*H*).

References

(1) March, J. *Advanced Organic Chemistry. Reactions, Mechanisms and Structure*; 4th ed.; Wiley & Sons: New York, 1992.

(2) Eliel, A. L.; Wilen, S. H.; Mander, L. N. *Stereochemistry of Organic Compounds*; Wiley & Sons: New York, 1992.

(3) Hoveyda, A. H.; Didiuk, M. T. *Curr. Org. Chem* **1998**, *2*, 489.

(4) Kesti, M. R.; Coates, G. W.; Waymouth, R. M. *J. Am. Chem. Soc.* **1992**, *114*, 9679.

(5) Stehling, U. M.; Stein, K. M.; Kesti, M. R.; Waymouth, R. M. *Macromolecules* **1998**, *31*, 2019.

(6) Chung, T. C.; Rhubright, D. *Macromolecules* **1993**, *26*, 3019.

(7) Aaltonen, P.; Lofgren, B. *Macromolecules* **1995**, *28*, 5353.

(8) Aaltonen, P.; Fink, G.; Lofgren, B.; Seppala, J. *Macromolecules* **1996**, *29*, 5255.

(9) Bruzaud, S.; Cramail, H.; Duvignac, L.; Deffieux, A. *Macromol. Chem. Phys.* **1997**, *198*, 291.

(10) Schneider, M. J.; Schafer, R.; Mulhaupt, R. *Polymer* **1997**, *38*, 2455.

(11) Wilen, C.-E.; Nasman, J. H. *Macromolecules* **1994**, *27*, 4051.

(12) Martin, V. S.; Woodard, S. S.; Yamada, Y.; Ikeda, M.; Sharpless, K. B. *J. Am. Chem. Soc.* **1981**, *103*, 6237.

(13) Kitamura, M.; Kasahara, I.; Manbe, K.; Noyori, R.; Takaya, H. *J. Org. Chem.* **1988**, *53*, 708.

(14) Hayashi, T.; Yamamoto, A.; Ito, Y. *Chem. Commun.* **1986**, 1090.

(15) La, D. S.; Alexander, J. B.; Cefalo, D. R.; Graf, D. D.; Hoveyda, A. H.; Schrock, R. R. *J. Am. Chem. Soc.* **1998**, *120*, 9720.

(16) VanNieuwenhze, M. S.; Sharpless, K. B. *J. Am. Chem. Soc.* **1993**, *115*, 7864.

(17) Resconi, L.; Cavallo, L.; Fait, A.; Piemontesi, F. *Chem. Rev.* **2000**, *100*, 1253.

(18) Coates, G. W. *Chem. Rev.* **2000**, *100*, 1223.

(19) Brintzinger, H. H.; Fischer, D.; Mülhaupt, R.; Rieger, B.; Waymouth, R., M. *Angew. Chem. Int. Ed. Engl.* **1995**, 1143.

(20) Pino, P. *Adv. Polymer Sci.* **1965**, *4*, 393.

(21) Carlini, C.; Altomare, A.; Menconi, F.; Ciardelli, F. *Macromolecules* **1987**, *20*, 464.

(22) Vizzini, J.; Ciardelli, F.; Chien, J. C. W. *Macromolecules* **1992**, *25*, 108.

(23) Zambelli, A.; Proto, A.; Pasquale, L. In *Ziegler Catalysis*; Springer-Verlag, 1995, p 218.

(24) Zambelli, A.; Ammendola, P.; Sacchi, M. C.; Locatelli, P.; Zannoni, G. *Macromolecules* **1983**, *16*, 341.

(25) Chien, J. C. W.; Vizzini, J. C.; Kaminsky, W. *Makromol. Chem., Rapid Commun.* **1992**, *13*, 479.

(26) Ciardelli, F.; Carlini, C.; Altomare, A. In *Ziegler Catalysis*; Springer-Verlag, 1995, p 455.

(27) Baar, C.; Levy, C. J.; Min, E.; Henling, L. M.; Day, M. W.; Bercaw, J. E. *J. Am. Chem. Soc.* **2004**, *126*, 8216.

(28) Tshuva, E. Y.; Groysman, S.; Goldberg, I.; Kol, M.; Goldschmidt, Z. *Organometallics* **2002**, *21*, 662.

(29) Tshuva, E. Y.; Goldberg, I.; Kol, M.; Weitman, H.; Goldschmidt, Z. *Chem. Commun.* **2000**, 379.

(30) Tshuva, E. Y.; Goldberg, I.; Kol, M.; Goldschmidt, Z. *Organometallics* **2001**, *20*, 3017.

(31) Tshuva, E. Y.; Goldberg, I.; Kol, M.; Goldschmidt, Z. *Chem. Commun.* **2001**, 2120.

(32) Zahn, S.; Canary, J. W. *J. Am. Chem. Soc.* **2002**, *124*, 9204, and references herein.

(33) Canary, J. W.; Allen, C. S.; Castagnetto, J. M.; Chiu, Y.-H.; Toscano, P. J.; Wang, Y. *Inorg. Chem.* **1998**, *37*, 6255.

(34) Pangborn, A. B.; Giardello, M. A.; Grubbs, R. H.; Rosen, R. K.; Timmers, F. J. *Organometallics* **1996**, *15*, 1518.

Appendix 2

Tables for X-ray Crystal Structures

Structures for Chapter 2

Compound 23 (CCDC 187372)

Special Refinement Details

The crystals contain disordered THF solvent molecules cocrystallized with the species of interest. It was possible to obtain and refine a satisfactory model for the THF molecules using anisotropic displacement parameters for the heavy atoms and riding parameters for the hydrogen atoms. All non-hydrogen atoms were refined with anisotropic displacement parameters and all non-solvent hydrogen atoms were refined without restraint.

Refinement of F^2 against ALL reflections. The weighted R-factor (*w*R) and goodness of fit (S) are based on F^2, conventional R-factors (R) are based on F, with F set to zero for negative F^2. The threshold expression of $F^2 > 2\sigma(F^2)$ is used only for calculating R-factors(gt) etc. and is not relevant to the choice of reflections for refinement. R-factors based on F^2 are statistically about twice as large as those based on F, and R-factors based on ALL data will be even larger. All esds (except the esd in the dihedral angle between two l.s. planes) are estimated using the full covariance matrix. The cell esds are taken into account individually in the estimation of esds in distances, angles and torsion angles; correlations between esds in cell parameters are only used when they are defined by crystal symmetry. An approximate (isotropic) treatment of cell esds is used for estimating esds involving l.s. planes.

Table 2. Atomic coordinates (x 10^4) and equivalent isotropic displacement parameters (Å^{2}x 10^3) for TA01 (CCDC 187372). U(eq) is defined as the trace of the orthogonalized U^{ij} tensor.

	x	y	z	U_{eq}
Cr(1)	499(1)	8615(1)	2467(1)	14(1)
P(1)	389(1)	10012(1)	2150(1)	13(1)
P(2)	1902(1)	9423(1)	3240(1)	14(1)
O(1)	-1340(1)	8849(1)	3329(1)	32(1)
O(2)	-1436(1)	7866(1)	1383(1)	26(1)
O(3)	1947(1)	8082(1)	1423(1)	27(1)
O(4)	1000(1)	6963(1)	3159(1)	28(1)
O(5)	-2105(1)	9720(1)	1502(1)	23(1)
O(6)	2576(1)	9868(1)	1637(1)	18(1)
O(7)	3913(1)	10476(1)	4000(1)	24(1)
O(8)	2293(1)	8213(1)	4276(1)	28(1)
N	1503(1)	10324(1)	2809(1)	13(1)
C(1)	-611(2)	8787(1)	3018(1)	18(1)
C(2)	-693(2)	8177(1)	1798(1)	18(1)
C(3)	1448(2)	8331(1)	1833(1)	19(1)
C(4)	834(2)	7608(1)	2904(1)	19(1)
C(5)	-3237(2)	9354(2)	1257(2)	35(1)
C(6)	3699(2)	9729(2)	1483(1)	27(1)
C(7)	4744(2)	11076(2)	4332(1)	36(1)
C(8)	2650(3)	7500(2)	4687(2)	51(1)
C(9)	2164(2)	11093(1)	2806(1)	19(1)
C(10)	-878(2)	10607(1)	2276(1)	14(1)
C(11)	-2022(2)	10350(1)	1975(1)	18(1)
C(12)	-2977(2)	10734(1)	2149(1)	22(1)
C(13)	-2816(2)	11399(1)	2602(1)	24(1)

C(14)	-1705(2)	11676(1)	2891(1)	21(1)
C(15)	-744(2)	11275(1)	2738(1)	18(1)
C(16)	688(2)	10424(1)	1332(1)	14(1)
C(17)	1747(2)	10241(1)	1133(1)	16(1)
C(18)	1903(2)	10435(1)	462(1)	20(1)
C(19)	1024(2)	10834(1)	-11(1)	22(1)
C(20)	9(2)	11064(1)	187(1)	21(1)
C(21)	-154(2)	10854(1)	855(1)	19(1)
C(22)	3468(2)	9261(1)	3344(1)	17(1)
C(23)	4316(2)	9800(1)	3717(1)	22(1)
C(24)	5499(2)	9618(2)	3790(1)	33(1)
C(25)	5833(2)	8903(2)	3518(1)	39(1)
C(26)	5020(2)	8352(2)	3174(1)	35(1)
C(27)	3844(2)	8535(1)	3088(1)	25(1)
C(28)	1764(2)	9578(1)	4149(1)	14(1)
C(29)	1994(2)	8897(1)	4599(1)	18(1)
C(30)	1916(2)	8949(1)	5301(1)	22(1)
C(31)	1594(2)	9683(1)	5559(1)	22(1)
C(32)	1347(2)	10356(1)	5122(1)	21(1)
C(33)	1431(2)	10301(1)	4420(1)	17(1)
O(41)	5099(2)	1762(1)	-329(1)	55(1)
C(42A)	5341(6)	1959(8)	461(4)	40(3)
C(42B)	5694(8)	1476(5)	352(3)	62(2)
C(43)	6610(2)	2081(2)	625(1)	51(1)
C(44)	6927(2)	2401(1)	-32(1)	37(1)
C(45)	5771(2)	2389(1)	-559(1)	34(1)

Table 5. Anisotropic displacement parameters ($Å^2 x\ 10^4$) for TA01 (CCDC 187372). The anisotropic displacement factor exponent takes the form: $-2\pi^2$ [$h^2 a^{*2} U^{11}$ + ... + 2 h k a* b* U^{12}]

	U^{11}	U^{22}	U^{33}	U^{23}	U^{13}	U^{12}
Cr(1)	149(2)	140(2)	128(2)	-5(1)	37(1)	-8(1)
P(1)	119(2)	151(3)	119(2)	1(2)	21(2)	-3(2)
P(2)	125(3)	144(3)	139(2)	6(2)	23(2)	8(2)
O(1)	259(9)	441(10)	303(8)	-62(7)	170(7)	-47(7)
O(2)	325(9)	253(8)	174(7)	0(6)	-11(7)	-109(7)
O(3)	317(9)	277(8)	272(8)	-44(7)	161(7)	19(7)
O(4)	389(9)	177(8)	273(8)	39(6)	75(7)	26(7)
O(5)	137(7)	283(8)	271(8)	-105(6)	17(6)	-27(6)
O(6)	146(7)	233(8)	193(7)	34(6)	78(6)	30(6)
O(7)	159(7)	251(8)	290(8)	-67(6)	7(6)	-41(6)
O(8)	453(10)	172(8)	188(7)	52(6)	5(7)	90(7)
N	116(8)	129(8)	125(8)	1(6)	4(6)	-29(6)
C(1)	197(11)	180(11)	138(10)	-13(8)	3(8)	-19(8)
C(2)	237(11)	158(10)	147(10)	32(8)	79(9)	-8(9)
C(3)	195(11)	155(10)	201(10)	13(8)	32(9)	-18(8)
C(4)	198(11)	219(11)	147(10)	-18(9)	55(8)	-17(9)
C(5)	173(12)	384(15)	468(16)	-175(13)	13(12)	-62(11)
C(6)	211(12)	316(14)	323(14)	66(12)	139(11)	46(11)
C(7)	278(14)	352(15)	416(16)	-98(13)	-2(12)	-98(12)

C(8)	930(30)	180(14)	308(15)	39(12)	-148(17)	123(15)
C(9)	202(12)	184(11)	190(11)	-7(9)	36(9)	-48(9)
C(10)	159(10)	140(10)	118(9)	33(8)	38(8)	28(8)
C(11)	196(11)	175(11)	170(10)	-7(8)	50(8)	4(8)
C(12)	128(11)	299(13)	221(11)	-8(9)	26(9)	13(9)
C(13)	211(12)	288(12)	234(11)	27(10)	91(9)	118(10)
C(14)	304(13)	167(11)	181(11)	-14(9)	70(9)	55(9)
C(15)	210(11)	175(11)	146(10)	29(8)	36(8)	12(9)
C(16)	165(10)	131(10)	121(9)	-12(8)	25(8)	-26(8)
C(17)	179(11)	129(10)	161(10)	-12(8)	18(8)	-30(8)
C(18)	221(12)	180(11)	217(11)	-28(9)	92(9)	-67(9)
C(19)	320(13)	211(12)	135(10)	8(9)	66(9)	-95(9)
C(20)	246(12)	205(11)	155(10)	49(9)	-17(9)	-33(9)
C(21)	169(11)	191(11)	192(11)	-15(8)	27(9)	-39(9)
C(22)	123(10)	218(11)	173(10)	27(8)	19(8)	20(8)
C(23)	175(11)	277(12)	213(11)	21(9)	29(9)	10(9)
C(24)	148(12)	420(15)	386(14)	-14(12)	11(10)	-40(11)
C(25)	135(13)	525(17)	502(16)	4(13)	75(11)	93(12)
C(26)	262(13)	354(15)	421(14)	-50(12)	72(11)	142(11)
C(27)	201(12)	284(13)	253(11)	-13(10)	29(9)	40(10)
C(28)	103(10)	173(10)	132(9)	6(8)	0(7)	-15(8)
C(29)	163(10)	154(10)	187(10)	-10(8)	-6(8)	-19(8)
C(30)	195(11)	252(12)	172(11)	81(9)	-21(9)	-41(9)
C(31)	167(11)	358(13)	127(10)	5(9)	26(8)	-47(9)
C(32)	184(11)	239(12)	197(11)	-34(9)	53(9)	23(9)
C(33)	145(10)	193(11)	172(10)	35(9)	20(8)	17(8)
O(41)	627(12)	523(12)	438(10)	41(9)	-19(9)	-318(9)
C(42A)	380(40)	550(70)	320(40)	180(40)	210(30)	80(40)
C(42B)	1090(60)	460(40)	350(30)	100(30)	230(30)	-180(40)
C(43)	542(19)	660(20)	328(14)	61(13)	88(13)	-7(15)
C(44)	337(14)	407(15)	367(13)	60(11)	105(11)	59(11)
C(45)	429(15)	324(14)	285(12)	20(11)	89(11)	11(11)

Compound 25 (CCDC 205652)

Special Refinement Details

Refinement of F^2 against ALL reflections. The weighted R-factor (*w*R) and goodness of fit (S) are based on F^2, conventional R-factors (R) are based on F, with F set to zero for negative F^2. The threshold expression of $F^2 > 2\sigma(F^2)$ is used only for calculating R-factors(gt) etc. and is not relevant to the choice of reflections for refinement. R-factors based on F^2 are statistically about twice as large as those based on F, and R-factors based on ALL data will be even larger. All esds (except the esd in the dihedral angle between two l.s. planes) are estimated using the full covariance matrix. The cell esds are taken into account individually in the estimation of esds in distances, angles and torsion angles; correlations between esds in cell parameters are only used when they are defined by crystal symmetry. An approximate (isotropic) treatment of cell esds is used for estimating esds involving l.s. planes.

Table 2. Atomic coordinates (x 10^4) and equivalent isotropic displacement parameters ($Å^2$x 10^3) for TA02 (CCDC 205652). U(eq) is defined as the trace of the orthogonalized U^{ij} tensor.

	x	y	z	U_{eq}
Cr(1)	5993(1)	6899(1)	777(1)	12(1)
Cl(1)	5211(1)	7029(1)	-256(1)	17(1)
Cl(2)	7360(1)	8061(1)	760(1)	15(1)
Cl(3)	7455(1)	5779(1)	678(1)	17(1)
P(1)	4517(1)	7857(1)	1199(1)	12(1)
P(2)	6178(1)	6898(1)	1952(1)	12(1)
O(1)	4385(1)	6057(1)	856(1)	14(1)
O(2)	3344(2)	8854(1)	130(1)	25(1)
O(3)	6667(2)	7911(1)	3180(1)	25(1)
O(4)	3670(1)	5966(1)	2133(1)	17(1)
N(1)	4982(2)	7640(1)	1962(1)	12(1)
C(1)	4472(3)	5087(2)	813(1)	20(1)
C(2)	3161(2)	6409(2)	801(1)	15(1)
C(3)	3046(2)	7298(2)	982(1)	13(1)
C(4)	1854(2)	7669(2)	958(1)	18(1)
C(5)	798(2)	7175(2)	762(1)	22(1)
C(6)	938(2)	6300(2)	579(1)	22(1)
C(7)	2120(2)	5910(2)	585(1)	19(1)
C(8)	4321(2)	9043(2)	1142(1)	15(1)
C(9)	4830(2)	9588(2)	1629(1)	18(1)
C(10)	4769(2)	10511(2)	1577(1)	24(1)
C(11)	4209(3)	10881(2)	1034(1)	29(1)
C(12)	3714(3)	10366(2)	536(1)	27(1)
C(13)	3771(2)	9435(2)	585(1)	20(1)
C(14)	2760(3)	9220(2)	-447(1)	35(1)
C(15)	7647(2)	7332(1)	2341(1)	14(1)
C(16)	8729(2)	7161(2)	2057(1)	17(1)
C(17)	9896(2)	7431(2)	2331(1)	19(1)
C(18)	9989(2)	7884(2)	2894(1)	22(1)
C(19)	8930(2)	8062(2)	3186(1)	22(1)
C(20)	7755(2)	7782(2)	2914(1)	18(1)

C(21)	6757(3)	8388(2)	3767(2)	39(1)
C(22)	5856(2)	5944(1)	2440(1)	13(1)
C(23)	6890(2)	5529(2)	2777(1)	17(1)
C(24)	6740(2)	4812(2)	3167(1)	20(1)
C(25)	5548(2)	4518(2)	3250(1)	20(1)
C(26)	4507(2)	4908(2)	2920(1)	19(1)
C(27)	4656(2)	5597(2)	2501(1)	15(1)
C(28)	2436(2)	5695(2)	2238(1)	24(1)
C(29)	4202(3)	7830(2)	2472(1)	18(1)
Cl(4)	3217(1)	8579(1)	3856(1)	32(1)
Cl(5)	4123(1)	6760(1)	4097(1)	45(1)
C(31)	3336(3)	7674(2)	4385(1)	29(1)

Table 5. Anisotropic displacement parameters ($Å^2 x\ 10^4$) for TA02 (CCDC 205652). The anisotropic displacement factor exponent takes the form: $-2\pi^2$ [$h^2 a^{*2} U^{11}$ + ... + 2 h k a* b* U^{12}]

	U^{11}	U^{22}	U^{33}	U^{23}	U^{13}	U^{12}
Cr(1)	129(2)	107(2)	105(2)	-7(2)	-13(1)	3(2)
Cl(1)	198(3)	192(3)	111(3)	-6(2)	-21(2)	-1(3)
Cl(2)	165(3)	136(3)	147(3)	4(2)	-4(2)	-15(2)
Cl(3)	150(3)	143(3)	209(3)	-33(2)	-4(2)	28(2)
P(1)	142(3)	116(3)	111(3)	3(2)	-13(2)	14(2)
P(2)	141(3)	114(3)	109(3)	4(2)	-17(2)	1(3)
O(1)	130(9)	106(8)	166(8)	-19(6)	-21(7)	-1(7)
O(2)	323(11)	268(10)	137(9)	46(7)	-48(8)	57(8)
O(3)	242(10)	330(11)	163(9)	-117(8)	17(7)	-69(8)
O(4)	118(9)	192(9)	183(9)	49(7)	-20(7)	4(7)
N(1)	146(11)	137(10)	82(10)	14(8)	-3(8)	10(8)
C(1)	185(15)	113(13)	291(16)	-7(11)	18(12)	15(11)
C(2)	129(13)	211(13)	107(12)	8(10)	-4(9)	29(10)
C(3)	147(13)	160(12)	80(11)	3(9)	-9(9)	12(10)
C(4)	195(14)	169(14)	171(13)	-14(10)	-3(10)	39(11)
C(5)	119(13)	335(16)	199(14)	-5(11)	10(11)	52(12)
C(6)	157(14)	271(15)	212(14)	-14(11)	-33(11)	-41(12)
C(7)	188(14)	177(13)	188(13)	-31(10)	0(10)	-2(11)
C(8)	147(13)	134(12)	167(12)	12(10)	38(10)	34(10)
C(9)	174(13)	165(13)	215(14)	14(11)	25(11)	24(10)
C(10)	202(14)	165(14)	346(16)	-39(12)	47(12)	2(11)
C(11)	277(16)	132(14)	470(19)	40(13)	60(13)	17(12)
C(12)	261(16)	264(16)	291(16)	149(13)	37(13)	71(12)
C(13)	189(13)	203(13)	206(13)	35(11)	10(11)	30(11)
C(14)	410(20)	430(20)	175(15)	76(14)	-75(14)	80(17)
C(15)	164(13)	119(12)	122(12)	48(9)	-25(10)	-22(10)
C(16)	201(14)	130(12)	152(13)	32(10)	-30(10)	6(10)
C(17)	153(14)	190(13)	221(14)	59(10)	-10(11)	-4(11)
C(18)	201(14)	198(14)	235(14)	64(11)	-96(11)	-65(11)
C(19)	291(15)	209(13)	131(13)	2(11)	-53(11)	-34(12)
C(20)	191(13)	164(12)	168(13)	33(10)	-21(10)	-19(10)
C(21)	350(20)	560(20)	269(17)	-231(15)	40(15)	-82(17)
C(22)	154(12)	109(12)	120(11)	11(9)	-3(9)	8(10)

C(23)	183(14)	140(12)	167(13)	5(10)	-37(10)	-6(11)
C(24)	234(15)	156(13)	199(14)	37(10)	-63(11)	38(11)
C(25)	292(15)	137(13)	149(13)	40(10)	-15(11)	-40(11)
C(26)	202(14)	167(13)	195(13)	18(10)	3(11)	-45(11)
C(27)	184(13)	121(12)	124(12)	-18(9)	-28(10)	15(10)
C(28)	171(14)	287(17)	277(16)	61(13)	36(12)	3(12)
C(29)	230(15)	192(14)	130(13)	12(11)	34(11)	49(11)
Cl(4)	349(4)	345(4)	271(4)	48(3)	80(3)	122(3)
Cl(5)	503(5)	328(4)	548(5)	135(4)	226(4)	104(4)
C(31)	317(18)	372(17)	192(16)	11(13)	43(13)	-3(14)

Compound 27 (CCDC 217064)

Special Refinement Details

Refinement of F^2 against ALL reflections. The weighted R-factor (*w*R) and goodness of fit (S) are based on F^2, conventional R-factors (R) are based on F, with F set to zero for negative F^2. The threshold expression of $F^2 > 2\sigma(F^2)$ is used only for calculating R-factors(gt) etc. and is not relevant to the choice of reflections for refinement. R-factors based on F^2 are statistically about twice as large as those based on F, and R-factors based on ALL data will be even larger. All esds (except the esd in the dihedral angle between two l.s. planes) are estimated using the full covariance matrix. The cell esds are taken into account individually in the estimation of esds in distances, angles and torsion angles; correlations between esds in cell parameters are only used when they are defined by crystal symmetry. An approximate (isotropic) treatment of cell esds is used for estimating esds involving l.s. planes.

Table 2. Atomic coordinates (x 10^4) and equivalent isotropic displacement parameters (Å^{2}x 10^3) for TA13 (CCDC 217064). U(eq) is defined as the trace of the orthogonalized U^{ij} tensor.

	x	y	z	U_{eq}
Cr	6003(1)	8480(1)	7573(1)	10(1)
I(1)	7423(1)	8550(1)	6915(1)	18(1)
I(2)	7310(1)	8642(1)	8855(1)	15(1)
I(3)	5567(1)	10392(1)	7425(1)	17(1)
P(1)	4506(1)	8200(1)	6600(1)	11(1)
P(2)	4409(1)	8032(1)	7902(1)	11(1)
O(1)	6012(1)	6883(1)	7419(1)	12(1)
O(2)	4707(1)	8437(1)	5161(1)	21(1)
O(3)	2329(1)	7855(1)	8166(1)	22(1)
O(4)	5330(1)	7329(1)	9299(1)	17(1)
N	3663(1)	8037(1)	7060(1)	11(1)
C(1)	4724(2)	6982(2)	6314(1)	11(1)
C(2)	4154(2)	6549(2)	5692(1)	14(1)
C(3)	4358(2)	5583(2)	5547(1)	17(1)
C(4)	5124(2)	5054(2)	6017(1)	18(1)
C(5)	5710(2)	5462(2)	6645(1)	14(1)
C(6)	5493(2)	6428(2)	6790(1)	13(1)
C(7)	6717(2)	6241(2)	7931(1)	18(1)
C(8)	3810(2)	8999(2)	5895(1)	19(1)
C(9)	3100(2)	9691(2)	6048(1)	15(1)
C(10)	2573(2)	10353(2)	5557(1)	23(1)
C(11)	2727(2)	10357(2)	4908(1)	26(1)
C(12)	3413(2)	9717(2)	4757(1)	23(1)
C(13)	3976(2)	9050(2)	5252(1)	21(1)
C(14)	4783(2)	8379(2)	4469(1)	29(1)
C(15)	3847(2)	8809(2)	8417(1)	13(1)
C(16)	4448(2)	9594(2)	8772(1)	17(1)
C(17)	4091(2)	10216(2)	9190(1)	20(1)
C(18)	3121(2)	10059(2)	9255(1)	19(1)
C(19)	2504(2)	9283(2)	8910(1)	18(1)
C(20)	2872(2)	8651(2)	8504(1)	14(1)

C(21)	1392(2)	7588(2)	8315(1)	33(1)
C(22)	4394(2)	6766(2)	8201(1)	13(1)
C(23)	3992(2)	5981(2)	7752(1)	17(1)
C(24)	4117(2)	5009(2)	7974(1)	23(1)
C(25)	4682(2)	4798(2)	8648(1)	24(1)
C(26)	5095(2)	5559(2)	9113(1)	21(1)
C(27)	4946(2)	6533(2)	8891(1)	14(1)
C(28)	6083(2)	7145(2)	9950(1)	21(1)
C(29)	2585(2)	7686(2)	6747(1)	17(1)
C(31)	8092(2)	6545(2)	5770(1)	27(1)
Cl(1)	8834(1)	7295(1)	5380(1)	39(1)
Cl(2)	6755(1)	6703(1)	5365(1)	28(1)

Table 5. Anisotropic displacement parameters ($Å^2 x\ 10^4$) for TA13 (CCDC 217064). The anisotropic displacement factor exponent takes the form: $-2\pi^2$ [$h^2 a^{*2} U^{11}$ + ... + 2 h k a* b* U^{12}]

	U^{11}	U^{22}	U^{33}	U^{23}	U^{13}	U^{12}
Cr	97(2)	105(2)	89(1)	-2(1)	18(1)	1(1)
I(1)	210(1)	186(1)	180(1)	-39(1)	119(1)	-52(1)
I(2)	130(1)	186(1)	104(1)	-11(1)	2(1)	-8(1)
I(3)	189(1)	110(1)	181(1)	5(1)	30(1)	11(1)
P(1)	117(3)	108(3)	85(2)	5(2)	20(2)	0(2)
P(2)	105(3)	119(3)	92(2)	-5(2)	23(2)	5(2)
O(1)	153(7)	101(7)	85(6)	4(5)	7(5)	26(6)
O(2)	219(8)	218(8)	199(7)	34(6)	94(6)	39(7)
O(3)	187(8)	230(9)	286(8)	-95(7)	133(7)	-96(7)
O(4)	175(8)	186(8)	123(7)	12(6)	-2(6)	12(6)
N	90(8)	144(9)	98(7)	-1(6)	18(6)	6(7)
C(1)	118(10)	128(10)	110(9)	0(7)	53(7)	-21(8)
C(2)	130(10)	188(11)	119(9)	-6(8)	47(7)	-18(8)
C(3)	184(11)	204(11)	148(10)	-79(8)	77(8)	-68(9)
C(4)	171(11)	155(11)	240(11)	-68(8)	120(9)	-32(9)
C(5)	148(10)	126(10)	146(9)	2(7)	67(8)	4(8)
C(6)	106(10)	150(10)	136(9)	-22(7)	60(7)	-22(8)
C(7)	199(12)	137(11)	141(10)	11(7)	-18(8)	64(8)
C(8)	189(12)	179(11)	151(10)	20(8)	-3(8)	-52(9)
C(9)	143(10)	133(10)	149(10)	20(7)	17(8)	-6(8)
C(10)	190(12)	196(12)	282(12)	41(9)	36(9)	20(9)
C(11)	243(13)	238(13)	244(12)	76(9)	-1(9)	-33(10)
C(12)	204(12)	235(12)	200(11)	98(9)	-32(9)	-41(10)
C(13)	180(12)	190(11)	238(11)	-4(9)	47(9)	-15(9)
C(14)	338(14)	365(15)	190(11)	15(10)	119(10)	-27(11)
C(15)	137(10)	137(10)	103(9)	1(7)	37(7)	7(8)
C(16)	155(11)	204(11)	171(10)	-46(8)	74(8)	-18(9)
C(17)	218(12)	187(11)	199(10)	-67(8)	70(9)	-15(9)
C(18)	212(12)	190(11)	193(11)	-12(8)	109(9)	42(9)
C(19)	158(11)	203(11)	213(11)	16(8)	108(9)	14(9)
C(20)	150(10)	142(10)	144(9)	11(8)	53(8)	-31(8)
C(21)	261(14)	322(15)	474(15)	-110(12)	221(12)	-165(11)
C(22)	119(10)	143(10)	139(9)	16(7)	49(8)	14(8)

C(23)	184(11)	181(11)	143(10)	-10(8)	40(8)	-38(9)
C(24)	279(13)	149(11)	221(11)	-8(8)	41(9)	-60(10)
C(25)	271(13)	148(11)	292(12)	71(9)	75(10)	-23(9)
C(26)	208(12)	231(12)	176(10)	70(8)	49(9)	-3(9)
C(27)	115(10)	177(11)	142(9)	6(8)	47(7)	-14(8)
C(28)	192(12)	272(13)	114(10)	16(8)	-30(8)	-5(9)
C(29)	109(10)	230(12)	145(10)	-37(8)	14(8)	-8(8)
C(31)	281(14)	213(13)	299(12)	46(9)	63(10)	51(10)
Cl(1)	267(3)	293(4)	641(4)	12(3)	185(3)	-16(3)
Cl(2)	248(3)	315(3)	310(3)	-68(2)	120(2)	-38(3)

Compound 29 (CCDC 205423)

Special Refinement Details

Refinement of F^2 against ALL reflections. The weighted R-factor (*w*R) and goodness of fit (S) are based on F^2, conventional R-factors (R) are based on F, with F set to zero for negative F^2. The threshold expression of $F^2 > 2\sigma(F^2)$ is used only for calculating R-factors(gt) etc. and is not relevant to the choice of reflections for refinement. R-factors based on F^2 are statistically about twice as large as those based on F, and R-factors based on ALL data will be even larger. All esds (except the esd in the dihedral angle between two l.s. planes) are estimated using the full covariance matrix. The cell esds are taken into account individually in the estimation of esds in distances, angles and torsion angles; correlations between esds in cell parameters are only used when they are defined by crystal symmetry. An approximate (isotropic) treatment of cell esds is used for estimating esds involving l.s. planes.

Table 2. Atomic coordinates (x 10^4) and equivalent isotropic displacement parameters (Å^{2}x 10^3) for TA07 (CCDC 205423). U(eq) is defined as the trace of the orthogonalized U^{ij} tensor.

	x	y	z	U_{eq}
Cr(1)	3660(1)	-1234(1)	2115(1)	22(1)
Cl(1)	3742(1)	-2357(1)	2752(1)	33(1)
Cl(2)	2768(1)	-1844(1)	1186(1)	30(1)
P(1)	3200(1)	134(1)	1798(1)	17(1)
P(2)	4387(1)	-225(1)	2974(1)	22(1)
O(1)	1264(2)	-951(1)	2265(1)	24(1)
O(2)	2210(2)	77(1)	459(1)	30(1)
O(3)	4629(2)	960(1)	4090(1)	28(1)
O(4)	6250(2)	-1284(1)	3639(1)	28(1)
N(1)	3859(3)	555(2)	2497(1)	19(1)
C(1)	1382(3)	319(2)	1767(1)	21(1)
C(2)	759(4)	1021(2)	1528(2)	29(1)
C(3)	-650(4)	1122(3)	1526(2)	38(1)
C(4)	-1415(4)	514(3)	1747(2)	42(1)
C(5)	-838(4)	-191(3)	1987(2)	31(1)
C(6)	574(3)	-281(2)	2006(1)	24(1)
C(7)	426(4)	-1631(2)	2420(2)	36(1)
C(8)	3868(3)	693(2)	1159(1)	19(1)
C(9)	5009(3)	1178(2)	1265(2)	23(1)
C(10)	5604(4)	1538(2)	759(2)	29(1)
C(11)	5058(4)	1398(2)	147(2)	30(1)
C(12)	3930(4)	921(2)	20(2)	30(1)
C(13)	3319(3)	565(2)	524(2)	23(1)
C(14)	1711(4)	-166(3)	-176(2)	36(1)
C(15)	3506(3)	-212(2)	3700(1)	21(1)
C(16)	2637(4)	-850(2)	3792(2)	25(1)
C(17)	1972(4)	-926(2)	4347(2)	29(1)
C(18)	2192(4)	-353(2)	4816(2)	34(1)
C(19)	3070(4)	280(2)	4747(2)	30(1)
C(20)	3739(3)	357(2)	4195(1)	23(1)
C(21)	4926(5)	1542(3)	4580(2)	33(1)
C(22)	6204(4)	11(2)	3223(1)	26(1)

C(23)	6826(3)	723(2)	3106(1)	19(1)
C(24)	8198(4)	870(2)	3275(2)	29(1)
C(25)	8985(4)	235(2)	3560(2)	32(1)
C(26)	8374(3)	-494(2)	3681(1)	22(1)
C(27)	6987(4)	-591(2)	3519(2)	26(1)
C(28)	7040(5)	-1958(3)	3843(2)	38(1)
C(29)	3459(4)	1372(2)	2697(2)	29(1)
C(30)	5663(4)	-1214(3)	1878(2)	30(1)
C(40)	156(5)	2886(3)	9454(2)	68(2)
Cl(3)	1439(1)	2790(1)	8972(1)	90(1)
Cl(4)	262(1)	2180(1)	10104(1)	57(1)

Table 5. Anisotropic displacement parameters ($Å^2 x\ 10^4$) for TA07 (CCDC 205423). The anisotropic displacement factor exponent takes the form: $-2\pi^2$ [$h^2 a^{*2} U^{11}$ + ... + 2 h k a* b* U^{12}]

	U^{11}	U^{22}	U^{33}	U^{23}	U^{13}	U^{12}
Cr(1)	270(3)	220(3)	169(3)	-1(2)	43(2)	27(2)
Cl(1)	492(6)	225(5)	284(5)	15(4)	63(4)	42(4)
Cl(2)	341(5)	339(5)	225(4)	-68(4)	65(4)	-46(4)
P(1)	157(4)	225(4)	135(4)	4(3)	-2(3)	4(4)
P(2)	220(5)	284(5)	140(4)	15(4)	11(3)	50(4)
O(1)	228(12)	275(13)	225(12)	1(10)	52(10)	-54(10)
O(2)	342(14)	388(15)	165(11)	-40(10)	-41(10)	-50(12)
O(3)	292(14)	350(14)	211(12)	-38(10)	37(10)	-65(11)
O(4)	270(13)	238(13)	321(13)	70(10)	1(11)	11(11)
N(1)	211(15)	205(14)	137(13)	-4(11)	6(11)	-15(11)
C(1)	183(17)	291(19)	157(15)	-26(14)	7(13)	36(14)
C(2)	250(20)	410(20)	223(18)	34(16)	6(16)	70(17)
C(3)	380(20)	480(30)	280(20)	19(18)	-19(18)	190(20)
C(4)	210(20)	880(40)	161(18)	-30(20)	-1(16)	100(20)
C(5)	207(19)	570(30)	159(17)	-74(17)	14(14)	-47(19)
C(6)	200(18)	380(20)	128(15)	-64(14)	-14(13)	-21(15)
C(7)	320(20)	370(20)	410(20)	-29(19)	130(20)	-122(19)
C(8)	211(18)	205(18)	170(16)	16(13)	41(13)	43(14)
C(9)	209(18)	269(19)	206(18)	10(15)	-2(14)	42(15)
C(10)	220(20)	260(20)	390(20)	23(16)	97(17)	21(16)
C(11)	320(20)	340(20)	260(20)	119(16)	120(17)	87(17)
C(12)	360(20)	360(20)	167(18)	27(15)	15(16)	96(17)
C(13)	252(19)	252(18)	180(16)	11(14)	13(14)	47(15)
C(14)	370(20)	490(30)	220(19)	-120(19)	-36(17)	80(20)
C(15)	222(18)	260(18)	162(16)	17(14)	21(13)	67(15)
C(16)	290(20)	290(20)	157(17)	-26(15)	2(14)	37(16)
C(17)	350(20)	310(20)	213(18)	28(16)	47(16)	-94(18)
C(18)	420(20)	430(20)	183(18)	5(16)	137(17)	-19(18)
C(19)	370(20)	350(20)	186(18)	-61(16)	59(16)	-36(17)
C(20)	225(19)	294(19)	156(16)	-4(14)	-8(14)	22(15)
C(21)	320(20)	410(30)	250(20)	-39(18)	20(18)	-90(20)
C(22)	330(20)	300(20)	133(16)	-28(14)	35(14)	7(16)
C(23)	209(18)	208(18)	148(16)	10(13)	8(13)	-10(14)
C(24)	320(20)	350(20)	201(18)	-21(16)	30(16)	-96(18)
C(25)	280(20)	460(20)	231(18)	-58(17)	17(16)	-35(18)

C(26)	250(20)	235(19)	162(16)	-30(14)	9(14)	13(15)
C(27)	270(20)	320(20)	200(17)	-61(15)	48(15)	11(16)
C(28)	340(20)	360(30)	420(30)	30(20)	0(20)	90(20)
C(29)	370(20)	270(20)	230(20)	-24(17)	38(18)	-40(17)
C(30)	300(20)	350(30)	250(20)	-10(20)	57(18)	87(19)
C(40)	660(30)	990(40)	370(30)	190(20)	-70(20)	190(30)
Cl(3)	566(8)	1552(14)	586(8)	-149(9)	61(7)	-426(9)
Cl(4)	697(8)	578(7)	399(6)	97(5)	-204(6)	-175(6)

Compound 30 (CCDC 604085)

Special Refinement Details

Refinement of F^2 against ALL reflections. The weighted R-factor (*w*R) and goodness of fit (S) are based on F^2, conventional R-factors (R) are based on F, with F set to zero for negative F^2. The threshold expression of $F^2 > 2\sigma(F^2)$ is used only for calculating R-factors(gt) etc. and is not relevant to the choice of reflections for refinement. R-factors based on F^2 are statistically about twice as large as those based on F, and R-factors based on ALL data will be even larger. All esds (except the esd in the dihedral angle between two l.s. planes) are estimated using the full covariance matrix. The cell esds are taken into account individually in the estimation of esds in distances, angles and torsion angles; correlations between esds in cell parameters are only used when they are defined by crystal symmetry. An approximate (isotropic) treatment of cell esds is used for estimating esds involving l.s. planes.

Table 2. Atomic coordinates (x 10^4) and equivalent isotropic displacement parameters (Å^{2}x 10^3) for TA11 (CCDC 604085). U(eq) is defined as the trace of the orthogonalized U^{ij} tensor.

	x	y	z		U_{eq}
Cr(1)	7149(1)	-1310(1)	3336(1)	15(1)	1
Cl(1)	8764(1)	-1307(1)	3694(1)	19(1)	1
Cl(2)	7121(1)	-2687(1)	2866(1)	25(1)	1
Cl(3)	5533(1)	-1218(1)	2970(1)	21(1)	1
P(1)	7161(1)	73(1)	3787(1)	14(1)	1
P(2)	8149(1)	1650(1)	3565(1)	19(1)	1
N(1)	7018(1)	-623(1)	2119(1)	19(1)	1
N(2)	6996(1)	-1553(1)	4643(1)	18(1)	1
N(3)	8058(1)	734(1)	4102(1)	16(1)	1
N(4)	6811(2)	2739(1)	4163(2)	43(1)	1
N(5)	9035(1)	2940(1)	2849(1)	26(1)	1
C(1)	6409(2)	519(1)	2845(1)	16(1)	1
C(2)	5821(2)	1196(1)	2832(2)	23(1)	1
C(3)	5253(2)	1468(2)	2077(2)	36(1)	1
C(4)	5286(2)	1074(2)	1326(2)	53(1)	1
C(5)	5850(2)	395(2)	1332(2)	42(1)	1
C(6)	6401(2)	104(1)	2089(2)	22(1)	1
C(7)	7929(2)	-307(1)	1996(2)	24(1)	1
C(8)	6641(2)	-1212(1)	1406(2)	25(1)	1
C(9)	6662(2)	-30(1)	4688(2)	18(1)	1
C(10)	6393(2)	657(2)	5091(2)	24(1)	1
C(11)	6079(2)	555(2)	5811(2)	30(1)	1
C(12)	6059(2)	-226(2)	6149(2)	35(1)	1
C(13)	6348(2)	-909(2)	5774(2)	29(1)	1
C(14)	6650(2)	-819(1)	5029(2)	19(1)	1
C(15)	7903(2)	-1824(1)	5219(2)	23(1)	1
C(16)	6339(2)	-2268(1)	4618(2)	24(1)	1
C(17)	8718(2)	529(1)	4925(1)	20(1)	1
C(18)	8463(2)	2394(1)	4448(2)	20(1)	1
C(19)	9375(2)	2526(1)	4912(2)	21(1)	1
C(20)	9597(2)	3101(1)	5562(2)	26(1)	1
C(21)	8897(2)	3565(2)	5756(2)	30(1)	1
C(22)	7981(2)	3449(2)	5303(2)	32(1)	1

C(23)	7750(2)	2867(1)	4650(2)	27(1)	1
C(24)	6638(2)	3159(2)	3316(2)	67(1)	1
C(25)	6092(2)	2951(2)	4603(3)	79(1)	1
C(26)	9281(2)	1511(1)	3316(1)	19(1)	1
C(27)	9764(2)	780(1)	3376(1)	21(1)	1
C(28)	10577(2)	719(2)	3096(2)	24(1)	1
C(29)	10909(2)	1403(2)	2753(2)	26(1)	1
C(30)	10426(2)	2143(2)	2678(2)	26(1)	1
C(31)	9597(2)	2202(1)	2935(2)	22(1)	1
C(32)	9577(2)	3689(2)	3131(2)	49(1)	1
C(33)	8453(2)	3051(2)	1987(2)	50(1)	1
C11	7922(3)	5419(3)	4074(3)	43(1)	0.698(2)
Cl11	8611(1)	5783(1)	5039(1)	52(1)	0.698(2)
Cl21	6734(1)	5374(1)	4081(1)	38(1)	0.698(2)
C12	8336(4)	5178(8)	4069(5)	60(4)	0.302(2)
Cl12	7994(3)	5755(2)	4846(2)	66(1)	0.302(2)
Cl22	7440(2)	5121(1)	3124(2)	50(1)	0.302(2)

Table 5. Anisotropic displacement parameters ($Å^2 x\ 10^4$) for TA11 (CCDC 604085). The anisotropic displacement factor exponent takes the form: $-2\pi^2$ [$h^2 a^{*2} U^{11}$ + ... + 2 h k a* b* U^{12}]

	U^{11}	U^{22}	U^{33}	U^{23}	U^{13}	U^{12}
Cr(1)	147(2)	124(2)	191(2)	-17(2)	40(2)	6(2)
Cl(1)	154(3)	185(3)	243(3)	-18(3)	54(2)	26(2)
Cl(2)	262(3)	159(3)	337(4)	-60(3)	80(3)	11(2)
Cl(3)	146(3)	181(3)	281(3)	-27(3)	31(3)	-6(2)
P(1)	146(3)	124(3)	165(3)	-2(3)	44(3)	4(2)
P(2)	234(3)	144(3)	180(3)	20(3)	13(3)	-40(3)
N(1)	222(11)	156(10)	184(11)	-38(8)	40(9)	16(8)
N(2)	179(10)	143(10)	219(11)	-2(8)	44(9)	-24(8)
N(3)	168(10)	140(10)	141(10)	18(8)	1(8)	-25(8)
N(4)	263(13)	244(12)	673(19)	-170(13)	-106(12)	79(10)
N(5)	400(13)	170(11)	209(12)	7(9)	89(10)	-45(9)
C(1)	154(12)	129(12)	194(13)	4(10)	15(10)	-4(9)
C(2)	220(13)	167(13)	271(15)	-27(11)	29(11)	8(10)
C(3)	371(16)	242(15)	390(18)	-64(13)	-72(14)	150(12)
C(4)	670(20)	418(19)	329(19)	-33(15)	-209(16)	266(16)
C(5)	610(20)	318(16)	240(16)	-76(13)	-87(14)	174(14)
C(6)	236(13)	152(12)	251(14)	7(11)	11(11)	3(10)
C(7)	289(14)	226(13)	214(14)	5(11)	95(12)	-38(11)
C(8)	321(14)	215(13)	205(14)	-60(11)	43(12)	-9(11)
C(9)	146(12)	202(13)	206(13)	-5(11)	58(10)	2(10)
C(10)	222(13)	218(13)	281(15)	-22(11)	89(12)	23(10)
C(11)	286(15)	330(16)	330(16)	-113(13)	174(13)	2(12)
C(12)	372(16)	431(18)	325(17)	-69(14)	256(14)	-96(13)
C(13)	341(15)	265(14)	323(16)	1(12)	172(13)	-82(12)
C(14)	174(12)	174(12)	221(14)	-30(11)	53(11)	-38(10)
C(15)	233(13)	221(13)	226(14)	39(11)	26(11)	-11(10)
C(16)	278(14)	171(13)	274(15)	25(11)	74(12)	-70(10)

C(17)	209(13)	192(13)	172(13)	30(10)	21(11)	-36(10)
C(18)	264(13)	119(12)	188(14)	22(10)	28(11)	-20(10)
C(19)	272(14)	214(13)	154(13)	14(10)	68(11)	-45(11)
C(20)	283(15)	262(14)	194(14)	1(11)	-1(12)	-61(11)
C(21)	414(16)	220(14)	238(15)	-44(11)	9(13)	22(12)
C(22)	359(16)	209(14)	372(17)	-11(12)	33(13)	91(12)
C(23)	285(14)	140(13)	317(16)	14(11)	-37(12)	20(11)
C(24)	670(20)	206(16)	790(30)	-36(16)	-439(19)	82(15)
C(25)	284(17)	440(20)	1560(40)	-560(20)	100(20)	67(15)
C(26)	251(13)	210(13)	98(12)	-39(10)	21(10)	-112(10)
C(27)	255(14)	233(14)	139(13)	9(11)	23(11)	-103(11)
C(28)	284(14)	237(13)	182(14)	-33(11)	30(11)	-18(11)
C(29)	273(14)	345(16)	157(13)	-55(12)	61(11)	-68(12)
C(30)	351(15)	270(14)	160(14)	-1(11)	67(12)	-134(12)
C(31)	325(14)	183(13)	146(13)	-12(10)	30(11)	-78(11)
C(32)	610(20)	223(15)	690(20)	-53(15)	286(18)	-72(15)
C(33)	810(20)	355(18)	299(19)	75(14)	57(17)	190(16)
C11	520(30)	440(40)	370(30)	20(20)	210(30)	130(20)
Cl11	474(8)	598(8)	463(8)	118(6)	70(7)	-184(7)
Cl21	393(6)	239(5)	496(7)	-19(5)	111(5)	26(4)
C12	1090(130)	360(70)	450(80)	-110(60)	400(90)	40(80)
Cl12	1230(40)	386(17)	480(20)	53(15)	420(20)	200(20)
Cl22	514(17)	296(14)	660(20)	27(13)	79(14)	-13(11)

Compound 31 (CCDC 236661)

Special Refinement Details

The crystals contain a significant amount of solvent, which occupies approximately 31% of the total unit cell volume. This solvent is disordered and appears to be an illdefined mixture of dichloromethane and petroleum ether. Solvent flattening was employed using SQUEEZE as implemented in Platon. The difference Fourier routine in SQUEEZE assigned 380 electrons to the solvent void.

Refinement of F^2 against ALL reflections. The weighted R-factor (*w*R) and goodness of fit (S) are based on F^2, conventional R-factors (R) are based on F, with F set to zero for negative F^2. The threshold expression of $F^2 > 2\sigma(F^2)$ is used only for calculating R-factors(gt) etc. and is not relevant to the choice of reflections for refinement. R-factors based on F^2 are statistically about twice as large as those based on F, and R-factors based on ALL data will be even larger. All esds (except the esd in the dihedral angle between two l.s. planes) are estimated using the full covariance matrix. The cell esds are taken into account individually in the estimation of esds in distances, angles and torsion angles; correlations between esds in cell parameters are only used when they are defined by crystal symmetry. An approximate (isotropic) treatment of cell esds is used for estimating esds involving l.s. planes.

Table 2. Atomic coordinates (x 10^4) and equivalent isotropic displacement parameters (Å^{2}x 10^3) for TA14 (CCDC 236661). U(eq) is defined as the trace of the orthogonalized U^{ij} tensor.

	x	y	z	U_{eq}
Cr(1)	5748(1)	481(1)	721(1)	33(1)
Cl(1)	6911(1)	-736(1)	961(1)	40(1)
Cl(2)	5377(1)	467(1)	1661(1)	38(1)
Cl(3)	4142(1)	-481(1)	306(1)	33(1)
P(1)	7308(1)	1499(1)	1084(1)	31(1)
P(2)	9766(1)	1499(1)	1607(1)	33(1)
O(1)	8440(2)	730(2)	248(1)	41(1)
O(2)	9571(2)	3300(1)	1950(1)	39(1)
O(3)	12095(2)	1310(2)	1870(1)	42(1)
N(1)	4887(2)	1818(2)	617(1)	34(1)
N(2)	8427(2)	1181(2)	1631(1)	31(1)
C(1)	3676(2)	1649(2)	571(1)	43(1)
C(2)	4925(2)	2333(2)	54(1)	38(1)
C(3)	5391(2)	2384(2)	1152(1)	34(1)
C(4)	4778(3)	2978(2)	1405(2)	44(1)
C(5)	5286(3)	3467(2)	1917(2)	50(1)
C(6)	6403(3)	3393(2)	2180(2)	48(1)
C(7)	7037(3)	2834(2)	1920(1)	41(1)
C(8)	6548(2)	2326(2)	1404(1)	33(1)
C(9)	7859(2)	2120(2)	539(1)	35(1)
C(10)	7802(2)	3032(2)	485(1)	41(1)
C(11)	8197(3)	3486(3)	47(2)	52(1)
C(12)	8642(3)	2994(3)	-347(2)	58(1)
C(13)	8730(2)	2076(3)	-312(1)	49(1)
C(14)	8349(2)	1619(3)	139(1)	40(1)
C(15)	8557(2)	146(2)	-240(1)	56(1)
C(16)	10257(2)	1935(2)	2393(1)	31(1)
C(17)	10759(2)	1421(2)	2903(1)	37(1)
C(18)	11050(2)	1804(2)	3484(1)	40(1)
C(19)	10823(2)	2679(2)	3552(1)	41(1)

C(20)	10320(2)	3217(2)	3054(1)	38(1)
C(21)	10059(2)	2833(2)	2477(1)	32(1)
C(22)	9341(3)	4229(2)	2004(2)	50(1)
C(23)	10496(2)	428(2)	1695(1)	33(1)
C(24)	9994(2)	-408(2)	1603(1)	37(1)
C(25)	10622(3)	-1192(2)	1676(1)	44(1)
C(26)	11768(3)	-1124(2)	1836(1)	44(1)
C(27)	12285(3)	-307(2)	1904(1)	43(1)
C(28)	11669(2)	469(2)	1835(1)	34(1)
C(29)	13154(2)	1459(2)	2286(1)	52(1)
C(30)	8216(2)	714(2)	2165(1)	37(1)

Table 5. Anisotropic displacement parameters ($Å^2 x\ 10^4$) for TA14 (CCDC 236661). The anisotropic displacement factor exponent takes the form: $-2\pi^2$ [$h^2 a^{*2} U^{11}$ + ... + 2 h k a* b* U^{12}]

	U^{11}	U^{22}	U^{33}	U^{23}	U^{13}	U^{12}
Cr(1)	234(2)	425(3)	325(3)	12(3)	86(2)	50(2)
Cl(1)	300(4)	465(5)	414(5)	2(4)	51(3)	75(4)
Cl(2)	347(4)	458(5)	369(5)	8(4)	143(3)	10(4)
Cl(3)	235(3)	431(5)	341(4)	8(4)	90(3)	26(4)
P(1)	245(4)	431(5)	264(5)	8(4)	71(3)	49(4)
P(2)	260(4)	482(6)	237(5)	-17(4)	26(3)	36(4)
O(1)	254(11)	733(18)	217(12)	-82(12)	40(9)	44(11)
O(2)	350(12)	409(15)	375(14)	-21(11)	40(10)	28(11)
O(3)	280(12)	515(16)	440(14)	-42(12)	45(10)	59(11)
N(1)	254(13)	464(17)	327(15)	23(14)	107(12)	59(12)
N(2)	279(13)	477(17)	181(13)	36(12)	45(11)	29(12)
C(1)	205(15)	540(20)	550(20)	-47(18)	121(15)	48(15)
C(2)	301(17)	460(20)	390(20)	30(17)	91(15)	80(15)
C(3)	290(17)	325(19)	420(20)	14(16)	130(15)	2(15)
C(4)	360(19)	470(20)	510(20)	-43(19)	168(17)	56(17)
C(5)	470(20)	480(20)	630(30)	-90(20)	270(20)	64(19)
C(6)	510(20)	490(20)	440(20)	-157(18)	143(18)	-47(19)
C(7)	350(18)	470(20)	420(20)	-53(18)	134(16)	-17(16)
C(8)	356(17)	294(19)	400(20)	39(16)	181(15)	46(15)
C(9)	149(15)	610(20)	257(18)	24(17)	-1(13)	15(15)
C(10)	302(18)	560(30)	310(20)	59(18)	-34(15)	-37(17)
C(11)	370(20)	750(30)	380(20)	180(20)	-34(17)	-70(20)
C(12)	410(20)	950(40)	310(20)	210(20)	-30(17)	-170(20)
C(13)	240(17)	990(30)	224(19)	0(20)	15(14)	-70(20)
C(14)	224(16)	610(30)	300(20)	25(19)	-63(14)	10(17)
C(15)	277(18)	1000(30)	390(20)	-230(20)	76(16)	78(18)
C(16)	228(15)	460(20)	220(17)	-42(15)	23(13)	44(14)
C(17)	297(17)	510(20)	298(19)	-55(17)	53(14)	37(16)
C(18)	280(17)	620(30)	245(19)	-7(17)	-6(14)	-27(17)
C(19)	320(18)	560(30)	310(20)	-88(18)	45(15)	-78(17)
C(20)	274(16)	440(20)	410(20)	-84(18)	81(15)	-63(15)
C(21)	214(16)	450(20)	280(19)	9(17)	33(13)	-37(15)
C(22)	460(20)	470(20)	500(20)	-11(18)	-8(17)	38(17)
C(23)	359(17)	440(20)	197(16)	-62(16)	84(13)	35(17)
C(24)	345(17)	550(20)	218(17)	-20(17)	63(14)	60(18)

C(25)	560(20)	440(20)	310(20)	-53(17)	111(17)	57(18)
C(26)	440(20)	560(30)	300(20)	-21(17)	71(16)	168(18)
C(27)	328(18)	620(30)	321(19)	-67(18)	39(15)	121(18)
C(28)	325(17)	450(20)	211(17)	-12(17)	35(13)	86(17)
C(29)	293(18)	810(30)	440(20)	-90(20)	57(16)	3(19)
C(30)	375(18)	440(20)	315(19)	2(16)	101(15)	38(15)

Compound 32 (CCDC 208405)

Special Refinement Details

The crystals contain dichloromethane as a solvent of crystallization. There is one solvent site per asymmetric unit. The dichloromethane in this site is disordered between two orientations with relative occupancies of approximately 80:20 (see Table 2). The non-hydrogen atoms of both orientations were refined anisotropically. All hydrogen atoms in the structure were restrained to ride on the atoms to which they are bonded.

Refinement of F^2 against ALL reflections. The weighted R-factor (*w*R) and goodness of fit (S) are based on F^2, conventional R-factors (R) are based on F, with F set to zero for negative F^2. The threshold expression of $F^2 > 2\sigma(F^2)$ is used only for calculating R-factors(gt) etc. and is not relevant to the choice of reflections for refinement. R-factors based on F^2 are statistically about twice as large as those based on F, and R-factors based on ALL data will be even larger. All esds (except the esd in the dihedral angle between two l.s. planes) are estimated using the full covariance matrix. The cell esds are taken into account individually in the estimation of esds in distances, angles and torsion angles; correlations between esds in cell parameters are only used when they are defined by crystal symmetry. An approximate (isotropic) treatment of cell esds is used for estimating esds involving l.s. planes.

Table 2. Atomic coordinates (x 10^4) and equivalent isotropic displacement parameters (Å² x 10^3) for TA10 (CCDC 208405). U(eq) is defined as the trace of the orthogonalized U^{ij} tensor.

	x	y	z	U_{eq}	Occ
Cr(1)	8942(1)	8259(1)	1854(1)	15(1)	1
Br(1)	9932(1)	9902(1)	1865(1)	22(1)	1
P(1)	7332(1)	7132(1)	1821(1)	15(1)	1
P(2)	6368(1)	8830(1)	2778(1)	15(1)	1
O(1)	7653(2)	9266(2)	850(1)	15(1)	1
O(2)	9422(2)	5153(2)	1140(1)	22(1)	1
O(3)	7145(2)	9783(2)	3856(1)	24(1)	1
O(4)	3154(2)	9653(2)	3397(1)	26(1)	1
N(1)	5833(2)	7901(2)	2386(1)	16(1)	1
C(1)	6911(3)	7580(2)	854(2)	14(1)	1
C(2)	6385(3)	6943(3)	490(2)	18(1)	1
C(3)	6068(3)	7381(3)	-250(2)	19(1)	1
C(4)	6306(3)	8452(3)	-631(2)	20(1)	1
C(5)	6826(3)	9103(2)	-290(2)	17(1)	1
C(6)	7123(3)	8668(2)	455(2)	13(1)	1
C(7)	7850(3)	10396(2)	434(2)	19(1)	1
C(8)	7384(3)	5576(2)	2101(2)	18(1)	1
C(9)	6374(3)	5205(3)	2700(2)	21(1)	1
C(10)	6494(3)	3998(3)	2933(2)	25(1)	1
C(11)	7665(3)	3148(3)	2569(2)	25(1)	1
C(12)	8681(3)	3484(3)	1981(2)	22(1)	1
C(13)	8533(3)	4705(3)	1734(2)	19(1)	1
C(14)	10711(3)	4314(3)	799(2)	26(1)	1
C(15)	5986(3)	8402(2)	3830(2)	19(1)	1
C(16)	5264(4)	7569(3)	4204(2)	33(1)	1
C(17)	5071(4)	7266(3)	5004(2)	40(1)	1
C(18)	5647(4)	7776(3)	5432(2)	37(1)	1

C(19)	6353(3)	8624(3)	5073(2)	24(1)	1
C(20)	6495(3)	8946(2)	4277(2)	18(1)	1
C(21)	7961(4)	10183(3)	4244(2)	37(1)	1
C(22)	5096(3)	10322(2)	2641(2)	16(1)	1
C(23)	5645(3)	11252(2)	2229(2)	17(1)	1
C(24)	4742(3)	12418(3)	2124(2)	23(1)	1
C(25)	3270(3)	12647(3)	2424(2)	26(1)	1
C(26)	2700(3)	11749(3)	2831(2)	24(1)	1
C(27)	3600(3)	10585(3)	2960(2)	19(1)	1
C(28)	1655(3)	9780(3)	3634(2)	30(1)	1
C(29)	4339(3)	8003(3)	2291(2)	21(1)	1
C(30)	10162(3)	7095(3)	2620(2)	20(1)	1
C(31)	9896(3)	6997(3)	3422(2)	29(1)	1
C(32)	10899(3)	6254(3)	3873(2)	33(1)	1
C(33)	12237(3)	5578(3)	3510(2)	29(1)	1
C(34)	12535(3)	5650(3)	2721(2)	24(1)	1
C(35)	11526(3)	6391(2)	2261(2)	18(1)	1
C(36)	11764(3)	6540(2)	1413(2)	19(1)	1
C(37)	13018(3)	5914(3)	959(2)	22(1)	1
C(38)	13125(3)	6110(3)	151(2)	26(1)	1
C(39)	12033(3)	6886(3)	-195(2)	22(1)	1
C(40)	10761(3)	7525(2)	268(2)	20(1)	1
C(41)	10607(3)	7379(2)	1067(2)	15(1)	1
C(51)	9223(11)	4067(8)	3880(6)	32(2)	0.808(2)
Cl(1)	7689(1)	5096(1)	4350(1)	34(1)	0.808(2)
Cl(2)	9251(1)	2575(1)	4336(1)	36(1)	0.808(2)
C(51B)	8800(50)	4220(60)	4050(30)	90(20)	0.192(2)
Cl(1B)	7334(11)	3765(8)	4655(5)	123(4)	0.192(2)
Cl(2B)	10471(12)	3352(9)	4230(6)	137(4)	0.192(2)

Table 5. Anisotropic displacement parameters ($Å^2 x\ 10^4$) for TA10 (CCDC 208405). The anisotropic displacement factor exponent takes the form: $-2\pi^2$ [$h^2 a^{*2} U^{11}$ + ... + 2 h k a* b* U^{12}]

	U^{11}	U^{22}	U^{33}	U^{23}	U^{13}	U^{12}
Cr(1)	114(2)	142(3)	196(3)	-37(2)	-45(2)	-11(2)
Br(1)	193(2)	196(2)	298(2)	-52(1)	-83(1)	-61(1)
P(1)	143(4)	131(4)	159(4)	-28(3)	-22(3)	-28(3)
P(2)	158(4)	133(4)	157(4)	-28(3)	-22(3)	-29(3)
O(1)	139(10)	106(10)	224(11)	-14(8)	-65(8)	-44(8)
O(2)	168(10)	164(11)	286(12)	-53(9)	20(9)	-19(9)
O(3)	249(11)	300(12)	227(12)	-23(10)	-69(9)	-148(10)
O(4)	169(11)	231(12)	322(13)	-48(10)	63(9)	-57(9)
N(1)	122(12)	169(13)	188(13)	-65(10)	-8(10)	-28(10)
C(1)	84(13)	139(15)	173(16)	-26(12)	-18(12)	9(11)
C(2)	158(14)	168(16)	224(17)	-46(13)	-25(13)	-60(12)
C(3)	156(15)	214(17)	209(17)	-66(14)	-54(13)	-45(13)
C(4)	126(14)	262(17)	184(16)	-44(14)	-53(12)	6(13)
C(5)	112(14)	134(15)	232(17)	-17(13)	-9(12)	-17(12)

C(6)	57(13)	157(15)	170(16)	-53(12)	-17(11)	7(11)
C(7)	186(15)	144(16)	227(17)	35(13)	-35(13)	-67(13)
C(8)	208(15)	172(16)	174(16)	-43(13)	-63(13)	-61(13)
C(9)	241(16)	195(17)	241(18)	-31(14)	-90(14)	-77(13)
C(10)	295(18)	261(18)	194(17)	41(14)	-54(14)	-143(15)
C(11)	393(19)	167(17)	239(18)	34(14)	-151(15)	-117(15)
C(12)	256(17)	161(16)	278(19)	-70(14)	-99(14)	-35(13)
C(13)	219(16)	205(17)	174(16)	-6(13)	-62(13)	-95(13)
C(14)	169(15)	192(17)	380(20)	-88(15)	-18(14)	1(13)
C(15)	208(15)	159(16)	162(16)	-33(13)	-20(13)	-20(13)
C(16)	540(20)	310(20)	205(19)	-26(15)	-49(17)	-213(17)
C(17)	600(20)	370(20)	290(20)	15(17)	-28(18)	-286(19)
C(18)	600(20)	380(20)	164(18)	1(16)	-55(17)	-216(19)
C(19)	278(17)	258(18)	198(18)	-54(14)	-41(14)	-72(14)
C(20)	136(14)	152(16)	208(17)	-30(13)	-15(12)	1(12)
C(21)	400(20)	530(20)	330(20)	18(18)	-149(17)	-326(19)
C(22)	174(15)	162(16)	142(16)	-42(12)	-19(12)	-26(12)
C(23)	163(14)	183(16)	189(16)	-34(13)	-69(12)	-50(12)
C(24)	313(18)	153(16)	251(18)	-32(14)	-75(14)	-75(14)
C(25)	246(17)	165(17)	340(20)	-85(15)	-123(15)	48(14)
C(26)	150(15)	276(19)	271(18)	-107(15)	-40(13)	-3(14)
C(27)	199(15)	202(17)	173(16)	-69(13)	-21(13)	-36(13)
C(28)	184(16)	430(20)	286(19)	-133(16)	62(14)	-131(15)
C(29)	139(15)	235(17)	288(18)	-89(14)	-17(13)	-66(13)
C(30)	171(15)	208(17)	237(17)	-57(14)	-70(13)	-25(13)
C(31)	231(17)	300(19)	270(19)	-58(15)	-86(14)	48(14)
C(32)	317(19)	350(20)	261(19)	-53(16)	-119(15)	21(16)
C(33)	280(18)	233(18)	330(20)	26(15)	-182(15)	-18(14)
C(34)	172(15)	157(16)	380(20)	-65(14)	-82(14)	-3(13)
C(35)	135(14)	133(15)	283(18)	-36(13)	-68(13)	-34(12)
C(36)	129(14)	178(16)	287(18)	-59(14)	-40(13)	-69(12)
C(37)	116(14)	180(17)	360(20)	-91(14)	3(14)	-27(12)
C(38)	133(15)	199(17)	420(20)	-146(15)	97(14)	-50(13)
C(39)	236(16)	239(17)	201(17)	-51(14)	13(13)	-132(14)
C(40)	148(15)	171(16)	293(19)	-43(14)	-46(13)	-50(12)
C(41)	125(14)	130(15)	221(17)	-26(12)	-38(12)	-63(12)
C(51)	370(50)	260(30)	310(40)	-70(30)	-110(30)	-10(30)
Cl(1)	380(6)	263(6)	316(6)	-87(5)	-134(5)	42(5)
Cl(2)	402(6)	232(6)	424(7)	-105(5)	-71(5)	-16(5)
C(51B)	700(400)	1500(500)	900(400)	-100(300)	-100(300)	-700(400)
Cl(1B)	1570(80)	1140(70)	1260(80)	-90(60)	-680(70)	-540(60)
Cl(2B)	1480(90)	1250(80)	1110(70)	-510(60)	320(70)	-200(70)

Compound 33 (CCDC 604086)

Special Refinement Details

The crystal is a twin containing two domains which were defined using CELL_NOW, with the following results;

862 reflections read from file: ta151.p4p

619 reflections within 0.100 of an integer index assigned to domain 1,
619 of them exclusively; 243 reflections not yet assigned to a domain

Rotated from first domain by 179.9 degrees about
reciprocal axis 0.000 0.001 1.000 and real axis 0.259 0.170 1.000

412 reflections within 0.100 of an integer index assigned to domain 2,
236 of them exclusively; 7 reflections not yet assigned to a domain

The data were integrated with SAINT using the following twin law;

Transforms h1 -> h2
-0.99924 0.00004 0.00002
-0.00003 -1.00019 0.00009
0.51182 0.33871 0.99927

The integrated data was processed with TWINABS to produce and HKLF 5 type file for least-squares refinement in SHELXL. From TWINABS;

3570 data (1596 unique) involve component 1 only, mean I/sigma 8.5
3577 data (1593 unique) involve component 2 only, mean I/sigma 6.5
23224 data (7619 unique) involve 2 components, mean I/sigma 6.3
1 data (1 unique) involve 3 components, mean I/sigma 25.9

Refinement of F^2 against ALL reflections. The weighted R-factor (*w*R) and goodness of fit (S) are based on F^2, conventional R-factors (R) are based on F, with F set to zero for negative F^2. The threshold expression of $F^2 > 2\sigma(F^2)$ is used only for calculating R-factors(gt) etc. and is not relevant to the choice of reflections for refinement. R-factors based on F^2 are statistically about twice as large as those based on F, and R-factors based on ALL data will be even larger.

Table 2. Atomic coordinates (x 10^4) and equivalent isotropic displacement parameters (Å^{2}x 10^3) for TA15 (CCDC 604086). U(eq) is defined as the trace of the orthogonalized U^{ij} tensor.

	x	y	z	U_{eq}
Cr(1)	1283(1)	4210(1)	1858(1)	17(1)
Cl(1)	-396(1)	4502(1)	1087(1)	21(1)
S(1)	2415(1)	4437(1)	680(1)	20(1)
P(1)	2850(1)	6666(1)	2169(1)	17(1)
P(2)	3730(1)	4694(1)	2309(1)	18(1)
O(1)	666(2)	7180(2)	2538(1)	26(1)
O(2)	4892(2)	9540(2)	2353(1)	26(1)
O(3)	3435(2)	2241(2)	2863(1)	30(1)
N(1)	4267(2)	6345(2)	2281(1)	16(1)
C(1)	2826(3)	7484(3)	3059(2)	17(1)
C(2)	3883(3)	7934(3)	3648(2)	27(1)
C(3)	3735(3)	8451(3)	4326(2)	32(1)
C(4)	2532(4)	8508(3)	4418(2)	37(1)

C(5)	1455(3)	8066(3)	3842(2)	31(1)
C(6)	1613(3)	7581(3)	3154(2)	22(1)
C(7)	-679(3)	7019(3)	2626(2)	38(1)
C(8)	3161(3)	7907(3)	1512(2)	16(1)
C(9)	2352(3)	7552(3)	829(2)	19(1)
C(10)	2481(3)	8420(3)	281(2)	22(1)
C(11)	3435(3)	9697(3)	446(2)	28(1)
C(12)	4242(3)	10076(3)	1131(2)	30(1)
C(13)	4123(3)	9205(3)	1670(2)	21(1)
C(14)	5859(3)	10880(3)	2540(2)	37(1)
C(15)	5635(2)	7205(3)	2125(2)	22(1)
C(16)	4641(3)	4500(3)	3168(2)	18(1)
C(17)	5583(3)	5543(3)	3649(2)	24(1)
C(18)	6205(3)	5364(3)	4314(2)	35(1)
C(19)	5871(3)	4117(3)	4505(2)	30(1)
C(20)	4932(3)	3033(3)	4048(2)	29(1)
C(21)	4333(3)	3226(3)	3374(2)	24(1)
C(22)	2902(3)	920(3)	3071(2)	46(1)
C(23)	4456(3)	4171(2)	1564(2)	15(1)
C(24)	5641(3)	3965(2)	1686(2)	19(1)
C(25)	6110(3)	3534(3)	1096(2)	23(1)
C(26)	5401(3)	3285(3)	383(2)	26(1)
C(27)	4244(3)	3511(2)	248(2)	21(1)
C(28)	3797(3)	3973(2)	838(2)	15(1)
C(29)	1276(3)	3250(3)	-49(2)	28(1)
C(30)	526(3)	4168(3)	2847(2)	18(1)
C(31)	1246(3)	4263(3)	3547(2)	27(1)
C(32)	661(3)	4161(3)	4204(2)	34(1)
C(33)	-684(3)	3938(3)	4182(2)	30(1)
C(34)	-1410(3)	3870(3)	3499(2)	28(1)
C(35)	-834(3)	3985(3)	2854(2)	23(1)
C(36)	409(3)	2173(2)	1677(2)	14(1)
C(37)	1073(3)	1384(3)	1511(2)	30(1)
C(38)	394(3)	16(3)	1365(2)	35(1)
C(39)	-989(3)	-596(3)	1366(2)	31(1)
C(40)	-1689(3)	136(3)	1499(2)	34(1)
C(41)	-977(3)	1509(3)	1652(2)	26(1)
C(42)	9556(3)	892(3)	3601(2)	47(1)
Cl(2)	8064(1)	-440(1)	3684(1)	62(1)
Cl(3)	10771(1)	1214(1)	4409(1)	59(1)

Table 5. Anisotropic displacement parameters ($Å^2 x\ 10^4$) for TA15 (CCDC 604086). The anisotropic displacement factor exponent takes the form: $-2\pi^2$ [$h^2 a^{*2} U^{11}$ + ... + 2 h k a* b* U^{12}]

	U^{11}	U^{22}	U^{33}	U^{23}	U^{13}	U^{12}
Cr(1)	169(3)	142(3)	230(3)	39(2)	53(2)	86(2)
Cl(1)	185(4)	200(5)	265(5)	63(4)	41(4)	102(4)
S(1)	212(5)	203(5)	239(5)	44(4)	63(4)	134(4)
P(1)	174(4)	138(5)	231(5)	40(4)	49(4)	82(4)
P(2)	171(5)	137(5)	247(5)	36(4)	46(4)	85(4)

O(1)	239(13)	240(13)	377(15)	52(11)	106(11)	158(11)
O(2)	264(13)	137(13)	344(15)	16(11)	14(11)	57(10)
O(3)	302(14)	205(13)	438(16)	148(12)	58(12)	124(11)
N(1)	106(13)	82(13)	286(16)	22(12)	10(11)	32(11)
C(1)	285(19)	72(17)	193(19)	15(14)	52(15)	98(15)
C(2)	420(20)	163(19)	310(20)	15(17)	33(18)	193(17)
C(3)	540(30)	210(20)	220(20)	40(16)	-61(18)	191(19)
C(4)	790(30)	170(20)	230(20)	91(17)	170(20)	240(20)
C(5)	560(30)	167(19)	340(20)	100(17)	260(20)	214(19)
C(6)	310(20)	83(18)	290(20)	78(16)	98(17)	80(16)
C(7)	197(19)	280(20)	730(30)	100(20)	173(19)	133(17)
C(8)	175(18)	166(18)	185(19)	28(15)	75(15)	95(15)
C(9)	160(17)	119(17)	350(20)	41(16)	111(16)	98(14)
C(10)	220(19)	230(20)	240(20)	25(17)	69(15)	111(16)
C(11)	400(20)	170(20)	320(20)	121(17)	138(18)	131(18)
C(12)	310(20)	127(19)	470(30)	37(19)	149(19)	59(16)
C(13)	165(17)	173(19)	300(20)	13(17)	48(15)	77(15)
C(14)	290(20)	134(19)	550(30)	-63(18)	-41(18)	1(17)
C(15)	160(17)	199(18)	320(20)	24(16)	23(15)	85(15)
C(16)	203(18)	222(19)	191(19)	47(16)	54(15)	152(16)
C(17)	270(20)	230(20)	250(20)	-19(17)	-19(16)	152(17)
C(18)	350(20)	480(30)	380(20)	30(20)	90(18)	320(20)
C(19)	310(20)	530(30)	210(20)	60(20)	77(17)	320(20)
C(20)	380(20)	380(20)	270(20)	118(19)	107(17)	293(19)
C(21)	215(19)	280(20)	260(20)	-29(18)	11(16)	151(17)
C(22)	380(20)	190(20)	810(30)	280(20)	200(20)	59(18)
C(23)	169(17)	75(16)	240(20)	83(15)	129(14)	43(14)
C(24)	154(16)	148(17)	270(20)	73(15)	49(15)	72(14)
C(25)	141(17)	132(18)	450(20)	78(17)	89(17)	59(15)
C(26)	360(20)	130(18)	380(20)	88(16)	268(17)	142(16)
C(27)	252(19)	104(18)	290(20)	100(15)	73(16)	63(15)
C(28)	104(16)	70(16)	260(20)	42(15)	52(14)	15(13)
C(29)	272(19)	380(20)	290(20)	74(17)	90(16)	214(17)
C(30)	205(19)	114(17)	230(20)	18(15)	37(15)	64(15)
C(31)	250(20)	260(20)	330(20)	46(18)	98(17)	121(16)
C(32)	380(20)	390(20)	270(20)	-30(18)	3(17)	196(19)
C(33)	310(20)	320(20)	270(20)	-35(17)	100(17)	133(18)
C(34)	240(19)	330(20)	290(20)	-10(18)	79(17)	143(17)
C(35)	250(19)	239(19)	220(20)	57(16)	55(15)	117(16)
C(36)	154(17)	95(16)	180(19)	59(14)	77(14)	47(14)
C(37)	290(20)	250(20)	360(20)	92(18)	117(17)	91(17)
C(38)	410(20)	200(20)	460(30)	0(18)	81(19)	156(19)
C(39)	480(20)	116(19)	330(20)	-5(16)	164(18)	89(18)
C(40)	310(20)	290(20)	320(20)	19(18)	52(17)	32(18)
C(41)	310(20)	128(19)	300(20)	8(16)	62(16)	61(16)
C(42)	570(30)	540(30)	370(30)	-10(20)	-60(20)	330(20)
Cl(2)	671(7)	428(7)	612(8)	-9(6)	-42(6)	113(6)
Cl(3)	612(7)	586(7)	624(8)	93(6)	-29(6)	324(6)

Structures for Chapter 4

Compound 6 (CCDC 641994)

Special Refinement Details

The crystal is a twin. The orientation of two domains of the twin were defined using CELL_NOW from 999 reflections picked from four different runs. The domains are related to each other by a 180º rotation about the real *a* axis. Data were integrated (allowing for twinning) with SAINT and corrected for absorption with TWINABS producing a file suitable for twin refinement in SHELX.

Refinement of F^2 against ALL reflections. The weighted R-factor (*w*R) and goodness of fit (S) are based on F^2, conventional R-factors (R) are based on F, with F set to zero for negative F^2. The threshold expression of $F^2 > 2\sigma(F^2)$ is used only for calculating R-factors(gt) etc. and is not relevant to the choice of reflections for refinement. R-factors based on F^2 are statistically about twice as large as those based on F, and R-factors based on ALL data will be even larger.

All esds (except the esd in the dihedral angle between two l.s. planes) are estimated using the full covariance matrix. The cell esds are taken into account individually in the estimation of esds in distances, angles and torsion angles; correlations between esds in cell parameters are only used when they are defined by crystal symmetry. An approximate (isotropic) treatment of cell esds is used for estimating esds involving l.s. planes.

Table 2. Atomic coordinates (x 10^4) and equivalent isotropic displacement parameters (Å^{2}x 10^3) for TA32 (CCDC 641994). U(eq) is defined as the trace of the orthogonalized U^{ij} tensor.

	x	y	z	U_{eq}
Ta(1)	7216(1)	8093(1)	6985(1)	11(1)
O(1)	7092(2)	9577(2)	6463(1)	13(1)
O(2)	7684(2)	6579(2)	7476(1)	12(1)
C(1)	7777(3)	10428(3)	6257(2)	12(1)
C(2)	7151(3)	11653(3)	6130(2)	12(1)
C(3)	7940(3)	12481(4)	6023(2)	13(1)
C(4)	9289(3)	12111(3)	6013(2)	12(1)
C(5)	9860(3)	10881(3)	6082(2)	11(1)
C(6)	9139(3)	10005(3)	6203(2)	11(1)
C(7)	9818(3)	8690(3)	6284(2)	10(1)
C(8)	11056(3)	8282(4)	5885(2)	14(1)
C(9)	11828(3)	7124(4)	5978(2)	15(1)
C(10)	11430(3)	6383(3)	6517(2)	12(1)
C(11)	10197(3)	6759(3)	6930(2)	12(1)
C(12)	9937(3)	5936(3)	7537(2)	12(1)
C(13)	10954(3)	5249(3)	7886(2)	13(1)
C(14)	10784(3)	4427(3)	8428(2)	13(1)
C(15)	9523(3)	4286(4)	8620(2)	14(1)
C(16)	8449(3)	4955(3)	8312(2)	13(1)
C(17)	8677(3)	5814(3)	7777(2)	12(1)
C(18)	5683(3)	12088(4)	6090(2)	15(1)
C(19)	4893(3)	11893(4)	6817(2)	18(1)
C(20)	5240(4)	13466(4)	5925(3)	23(1)
C(21)	5382(4)	11377(4)	5469(2)	22(1)

C(22)	10135(3)	13034(4)	5947(2)	14(1)
C(23)	10790(4)	12976(4)	6630(2)	19(1)
C(24)	9320(4)	14360(4)	5870(2)	18(1)
C(25)	11167(4)	12708(4)	5278(2)	21(1)
C(26)	11904(4)	3635(4)	8799(2)	17(1)
C(27)	13168(4)	4026(4)	8588(3)	28(1)
C(28)	12132(4)	2293(4)	8562(3)	30(1)
C(29)	11574(4)	3750(5)	9624(2)	28(1)
C(30)	7101(3)	4700(4)	8508(2)	15(1)
C(31)	6048(3)	5880(4)	8767(2)	16(1)
C(32)	6777(4)	4144(4)	7830(2)	19(1)
C(33)	7095(4)	3777(4)	9126(2)	21(1)
C(34)	9304(3)	7870(3)	6769(2)	12(1)
C(35)	6299(3)	7310(4)	6195(2)	14(1)
C(36)	4982(3)	7712(4)	6625(2)	15(1)
C(37)	4531(4)	6944(4)	7147(2)	20(1)
C(38)	3366(4)	7352(4)	7583(2)	24(1)
C(39)	2592(4)	8523(5)	7517(2)	28(1)
C(40)	3028(4)	9305(4)	7018(3)	24(1)
C(41)	4200(4)	8912(4)	6572(2)	19(1)
C(42)	6156(4)	9064(4)	7992(2)	14(1)
C(43)	7305(4)	9324(4)	8263(2)	15(1)
C(44)	7712(4)	10392(4)	8050(2)	18(1)
C(45)	8826(4)	10587(4)	8263(2)	22(1)
C(46)	9548(4)	9762(4)	8706(2)	25(1)
C(47)	9168(4)	8704(4)	8925(2)	21(1)
C(48)	8057(4)	8495(4)	8702(2)	18(1)
C(51)	6613(4)	818(4)	-17(3)	36(1)
Cl(1)	5047(1)	1561(1)	-219(1)	35(1)
Cl(2)	7055(2)	1540(2)	670(1)	84(1)

Table 5. Anisotropic displacement parameters ($Å^2 x\ 10^4$) for TA32 (CCDC 641994). The anisotropic displacement factor exponent takes the form: $-2\pi^2[\ h^2a^{*2}U^{11} + ... + 2\ h\ k\ a^*\ b^*\ U^{12}\ ]$

	U^{11}	U^{22}	U^{33}	U^{23}	U^{13}	U^{12}
Ta(1)	95(1)	110(1)	129(1)	-7(1)	-20(1)	-29(1)
O(1)	106(11)	132(13)	148(14)	31(11)	-34(11)	-29(11)
O(2)	94(11)	109(12)	154(14)	1(11)	-21(11)	-19(10)
C(1)	127(16)	120(18)	115(19)	-22(16)	-10(14)	-44(15)
C(2)	124(16)	138(18)	102(18)	-29(15)	-19(15)	-28(16)
C(3)	156(17)	97(18)	115(19)	-9(16)	-35(15)	-4(15)
C(4)	160(17)	144(18)	81(18)	-9(15)	-15(15)	-67(16)
C(5)	103(16)	141(18)	99(18)	-13(16)	-29(14)	-25(15)
C(6)	134(16)	98(18)	95(19)	13(15)	-1(15)	-10(15)
C(7)	116(16)	100(18)	109(19)	-18(16)	-38(14)	-42(14)
C(8)	170(17)	160(20)	120(20)	-9(17)	-1(16)	-82(16)
C(9)	117(16)	190(20)	170(20)	-23(18)	-14(15)	-68(16)
C(10)	136(17)	83(18)	150(20)	-5(16)	-56(15)	-15(15)
C(11)	147(17)	109(18)	118(19)	-9(16)	-41(15)	-73(15)
C(12)	164(17)	58(16)	131(19)	-38(15)	-15(15)	-43(15)

C(13)	101(16)	125(18)	170(20)	-49(16)	-32(15)	-43(15)
C(14)	133(16)	139(18)	122(19)	-22(16)	-36(15)	-36(15)
C(15)	197(18)	119(19)	110(20)	15(16)	-28(16)	-68(16)
C(16)	119(16)	122(18)	140(20)	-50(16)	7(15)	-38(15)
C(17)	119(16)	112(18)	123(19)	-7(16)	-27(15)	-20(14)
C(18)	143(17)	130(19)	170(20)	14(17)	-35(16)	-2(16)
C(19)	125(17)	180(20)	220(20)	-8(18)	-13(16)	-16(16)
C(20)	151(18)	160(20)	370(30)	30(20)	-29(18)	2(17)
C(21)	190(19)	290(20)	190(20)	20(20)	-44(17)	-67(18)
C(22)	166(17)	97(19)	180(20)	-29(17)	-21(16)	-57(16)
C(23)	231(19)	142(19)	230(20)	-11(18)	-96(18)	-54(17)
C(24)	216(19)	133(19)	200(20)	10(17)	-74(17)	-65(16)
C(25)	205(19)	200(20)	220(20)	-51(18)	33(17)	-109(17)
C(26)	173(18)	160(20)	190(20)	40(18)	-40(16)	-42(16)
C(27)	153(19)	340(30)	330(30)	150(20)	-85(19)	-37(19)
C(28)	250(20)	190(20)	430(30)	10(20)	-140(20)	21(19)
C(29)	200(20)	380(30)	210(20)	10(20)	-51(18)	-10(20)
C(30)	155(17)	136(19)	160(20)	0(17)	-14(16)	-62(16)
C(31)	115(17)	145(19)	220(20)	-29(18)	-17(16)	-24(15)
C(32)	174(18)	180(20)	210(20)	-46(19)	-18(17)	-80(17)
C(33)	191(19)	200(20)	250(20)	28(19)	-18(17)	-81(17)
C(34)	181(17)	105(19)	96(19)	-25(16)	-8(15)	-78(15)
C(35)	143(17)	190(20)	96(19)	-2(17)	-16(15)	-57(16)
C(36)	129(17)	190(20)	160(20)	-53(18)	-50(15)	-82(16)
C(37)	230(20)	180(20)	230(20)	29(19)	-104(18)	-92(18)
C(38)	185(19)	370(30)	200(20)	30(20)	-69(17)	-131(19)
C(39)	147(19)	430(30)	210(20)	-50(20)	-2(18)	-10(20)
C(40)	176(19)	250(20)	280(30)	-70(20)	-91(18)	12(18)
C(41)	187(19)	180(20)	220(20)	36(19)	-95(17)	-81(17)
C(42)	218(18)	133(19)	91(19)	-1(16)	-63(16)	-82(16)
C(43)	160(17)	180(20)	101(19)	-82(17)	-7(16)	-32(16)
C(44)	200(19)	150(20)	170(20)	-14(18)	-31(17)	-25(16)
C(45)	228(19)	210(20)	240(20)	-80(19)	20(18)	-99(18)
C(46)	170(19)	290(20)	290(20)	-120(20)	-20(18)	-63(18)
C(47)	135(17)	260(20)	220(20)	-60(20)	-59(16)	14(17)
C(48)	222(19)	180(20)	130(20)	-34(17)	-15(17)	-57(17)
C(51)	200(20)	260(20)	590(40)	-50(30)	-70(20)	-10(20)
Cl(1)	276(5)	243(6)	531(8)	70(6)	-76(5)	-45(5)
Cl(2)	909(13)	769(13)	690(12)	-404(11)	-595(11)	310(10)

Compound 7 (CCDC 626578)

Special Refinement Details

Visual inspection of the diffraction images show the crystal is an obvious twin. The two components of the twin are related by an approximate 2-fold around the *a*-axis (*a** in reciprocal space) and orientation matrices for each component were calculated using CELL_NOW. However, attempts to integrate intensities separately for each to incorporated in least-squares refinement as a twinned crystal were unsuccessful. The four molecules in the unit cell have coordinates that are related to each with approximate $P2_1/c$ symmetry. The Laue symmetry of the diffraction pattern does not reflect 2/m symmetry as would be required by $P2_1/c$. Additionally, O(1) in each molecule refined as non-positive definite so a restraint was imposed on these oxygens causing the anisotropic displacement parameters to approximate isotropic behavior.

Refinement of F^2 against ALL reflections. The weighted R-factor (*w*R) and goodness of fit (S) are based on F^2, conventional R-factors (R) are based on F, with F set to zero for negative F^2. The threshold expression of $F^2 > 2\sigma(F^2)$ is used only for calculating R-factors(gt) etc. and is not relevant to the choice of reflections for refinement. R-factors based on F^2 are statistically about twice as large as those based on F, and R-factors based on ALL data will be even larger. All esds (except the esd in the dihedral angle between two l.s. planes) are estimated using the full covariance matrix. The cell esds are taken into account individually in the estimation of esds in distances, angles and torsion angles; correlations between esds in cell parameters are only used when they are defined by crystal symmetry. An approximate (isotropic) treatment of cell esds is used for estimating esds involving l.s. planes.

Table 2. Atomic coordinates (x 10^4) and equivalent isotropic displacement parameters (Å^{2}x 10^3) for TA19 (CCDC 626578). U(eq) is defined as the trace of the orthogonalized U^{ij} tensor.

	x	y	z	U_{eq}
Ta(1)	8977(1)	4766(1)	1808(1)	15(1)
Cl(1A)	10547(1)	4743(1)	2633(1)	22(1)
Cl(2A)	7323(1)	4795(1)	1024(1)	22(1)
O(1A)	8700(3)	5812(2)	1943(2)	11(1)
O(2A)	8661(3)	3741(2)	2002(2)	19(1)
C(1A)	8046(4)	6406(3)	2221(3)	17(1)
C(2A)	8026(4)	7121(3)	1875(3)	15(1)
C(3A)	7348(4)	7691(3)	2217(3)	17(1)
C(4A)	6718(4)	7580(3)	2868(3)	19(1)
C(5A)	6793(4)	6866(3)	3209(3)	21(1)
C(6A)	7444(4)	6263(3)	2893(3)	15(1)
C(7A)	7614(4)	5531(3)	3310(3)	14(1)
C(8A)	8022(5)	5552(3)	4016(3)	20(1)
C(9A)	8234(5)	4887(3)	4413(3)	22(1)
C(10A)	8069(5)	4189(4)	4100(3)	21(1)
C(11A)	7640(4)	4137(3)	3389(3)	17(1)
C(12A)	7487(4)	3372(3)	3069(3)	16(1)
C(13A)	6876(4)	2803(3)	3466(3)	18(1)
C(14A)	6784(4)	2077(3)	3202(3)	19(1)
C(15A)	7337(5)	1915(3)	2530(3)	20(1)
C(16A)	7971(5)	2447(3)	2103(3)	18(1)
C(17A)	8014(4)	3187(3)	2397(3)	18(1)

C(18A)	7395(4)	4825(3)	3006(3)	15(1)
C(19A)	8747(5)	7291(3)	1162(3)	19(1)
C(20A)	8309(5)	6800(4)	539(3)	26(1)
C(21A)	8636(6)	8133(3)	914(3)	29(1)
C(22A)	10063(5)	7125(4)	1292(3)	24(1)
C(23A)	6024(5)	8233(3)	3237(3)	22(1)
C(24A)	5643(7)	8849(4)	2672(4)	49(2)
C(25A)	6824(6)	8600(5)	3768(4)	53(2)
C(26A)	4893(6)	7947(4)	3605(5)	52(2)
C(27A)	6120(5)	1439(3)	3627(3)	23(1)
C(28A)	5450(6)	1748(4)	4320(4)	42(2)
C(29A)	7036(5)	857(4)	3921(4)	33(2)
C(30A)	5237(6)	1064(4)	3164(4)	41(2)
C(31A)	8595(5)	2246(3)	1382(3)	21(1)
C(32A)	8446(6)	1404(4)	1200(3)	33(2)
C(33A)	8099(5)	2723(4)	742(3)	25(1)
C(34A)	9950(5)	2371(4)	1432(3)	27(1)
C(35A)	10218(4)	4697(3)	899(3)	12(1)
Ta(2)	992(1)	9705(1)	3195(1)	15(1)
Cl(1B)	-594(1)	9731(1)	2385(1)	24(1)
Cl(2B)	2655(1)	9678(1)	3969(1)	22(1)
O(1B)	1293(3)	10744(2)	3034(2)	12(1)
O(2B)	1298(3)	8685(2)	3007(2)	18(1)
C(1B)	1945(4)	11316(3)	2723(3)	17(1)
C(2B)	1989(4)	12028(3)	3048(3)	17(1)
C(3B)	2650(4)	12589(3)	2673(3)	21(1)
C(4B)	3244(4)	12468(3)	2001(3)	19(1)
C(5B)	3146(4)	11756(3)	1696(3)	19(1)
C(6B)	2502(4)	11170(3)	2043(3)	15(1)
C(7B)	2332(4)	10448(3)	1665(3)	17(1)
C(8B)	1907(5)	10469(3)	951(3)	20(1)
C(9B)	1706(5)	9809(3)	585(3)	25(1)
C(10B)	1907(5)	9101(4)	922(3)	22(1)
C(11B)	2330(4)	9051(3)	1628(3)	18(1)
C(12B)	2482(4)	8296(3)	1982(3)	16(1)
C(13B)	3108(4)	7703(3)	1624(3)	18(1)
C(14B)	3197(4)	6973(3)	1915(3)	17(1)
C(15B)	2579(5)	6821(3)	2568(3)	19(1)
C(16B)	1940(5)	7368(3)	2957(3)	18(1)
C(17B)	1934(4)	8108(3)	2665(3)	16(1)
C(18B)	2567(4)	9730(3)	1985(3)	14(1)
C(19B)	1318(5)	12207(4)	3776(3)	20(1)
C(20B)	1761(5)	11687(4)	4394(3)	24(1)
C(21B)	1496(6)	13037(4)	4006(3)	32(2)
C(22B)	-24(5)	12105(4)	3678(3)	27(1)
C(23B)	3931(5)	13120(3)	1629(3)	24(1)
C(24B)	4736(6)	13492(4)	2140(4)	49(2)
C(25B)	3032(5)	13719(4)	1332(3)	29(2)
C(26B)	4648(6)	12841(4)	949(4)	50(2)
C(27B)	3880(5)	6343(3)	1502(3)	24(1)
C(28B)	4962(7)	6656(4)	1117(6)	80(4)
C(29B)	3070(6)	5994(4)	974(4)	47(2)
C(30B)	4299(7)	5709(4)	2036(4)	53(2)

C(31B)	1265(5)	7171(3)	3682(3)	19(1)
C(32B)	1335(6)	6323(4)	3873(3)	31(2)
C(33B)	-63(5)	7388(4)	3624(3)	26(1)
C(34B)	1816(5)	7596(4)	4318(3)	24(1)
C(35B)	-241(4)	9647(3)	4116(3)	12(1)
C(1C)	4742(8)	5384(8)	4368(6)	77(4)
C(2C)	4799(8)	4600(9)	4385(6)	84(4)
C(3C)	5055(7)	4222(7)	5024(7)	76(3)
C(1D)	4794(7)	9267(6)	-146(7)	70(3)
C(2D)	5113(7)	9464(7)	543(6)	66(3)
C(3D)	5302(7)	10203(8)	678(5)	66(3)

Table 5. Anisotropic displacement parameters ($Å^2 x 10^4$) for TA19 (CCDC 626578). The anisotropic displacement factor exponent takes the form: $-2\pi^2[h^2 a^{*2} U^{11} + ... + 2 h k a^* b^* U^{12}]$

	U^{11}	U^{22}	U^{33}	U^{23}	U^{13}	U^{12}
Ta(1)	124(1)	198(2)	136(1)	2(1)	50(1)	13(1)
Cl(1A)	171(6)	243(8)	255(8)	-10(6)	-48(6)	10(6)
Cl(2A)	212(6)	266(9)	192(7)	0(6)	-25(6)	14(6)
O(1A)	79(10)	110(11)	122(10)	3(8)	74(8)	-6(8)
O(2A)	163(17)	190(20)	220(20)	-45(16)	-48(15)	0(16)
C(1A)	80(20)	240(30)	180(30)	-50(20)	0(20)	10(20)
C(2A)	120(20)	200(30)	130(30)	0(20)	-50(20)	20(20)
C(3A)	150(20)	170(30)	200(30)	0(20)	-50(20)	10(20)
C(4A)	160(20)	160(30)	260(30)	-30(20)	0(20)	10(20)
C(5A)	130(20)	310(40)	200(30)	-60(20)	60(20)	-20(20)
C(6A)	120(20)	120(30)	210(30)	-30(20)	10(20)	0(20)
C(7A)	140(20)	200(30)	90(20)	10(20)	34(19)	-10(20)
C(8A)	230(30)	160(30)	210(30)	-20(20)	40(20)	-40(20)
C(9A)	240(30)	290(40)	120(30)	-10(20)	-20(20)	-30(30)
C(10A)	240(30)	230(30)	150(30)	20(20)	10(20)	0(30)
C(11A)	100(20)	220(30)	190(30)	-20(20)	60(20)	20(20)
C(12A)	110(20)	200(30)	170(30)	40(20)	-10(20)	30(20)
C(13A)	140(20)	210(30)	190(30)	60(20)	-20(20)	0(20)
C(14A)	120(20)	210(30)	230(30)	60(20)	-50(20)	30(20)
C(15A)	210(30)	140(30)	240(30)	0(20)	-50(20)	-10(20)
C(16A)	160(20)	160(30)	210(30)	20(20)	-50(20)	10(20)
C(17A)	140(20)	210(30)	190(30)	40(20)	10(20)	-10(20)
C(18A)	90(20)	200(30)	160(30)	0(20)	50(20)	0(20)
C(19A)	200(30)	220(30)	140(30)	10(20)	0(20)	30(20)
C(20A)	250(30)	350(40)	170(30)	10(30)	-50(20)	10(30)
C(21A)	390(40)	220(40)	250(30)	50(30)	30(30)	40(30)
C(22A)	180(30)	320(40)	220(30)	30(30)	30(20)	-60(30)
C(23A)	190(30)	170(30)	290(30)	-50(20)	50(20)	30(20)
C(24A)	640(50)	340(50)	480(50)	40(40)	50(40)	300(40)
C(25A)	360(40)	640(60)	610(50)	-430(40)	-170(40)	160(40)
C(26A)	490(40)	220(40)	840(60)	-140(40)	390(40)	-20(30)
C(27A)	230(30)	190(30)	270(30)	80(20)	30(20)	-10(20)
C(28A)	460(40)	250(40)	530(50)	-30(30)	250(30)	-80(30)

C(29A)	250(30)	340(40)	390(40)	200(30)	-60(30)	-10(30)
C(30A)	420(40)	310(40)	510(50)	100(30)	-70(30)	-160(30)
C(31A)	250(30)	190(30)	190(30)	-10(20)	-20(20)	40(20)
C(32A)	490(40)	290(40)	210(30)	-80(30)	0(30)	10(30)
C(33A)	250(30)	310(40)	170(30)	50(30)	10(20)	20(30)
C(34A)	230(30)	330(40)	240(30)	-50(30)	0(20)	90(30)
C(35A)	150(20)	140(30)	70(20)	10(20)	28(19)	20(20)
Ta(2)	120(1)	197(2)	142(1)	-4(1)	46(1)	10(1)
Cl(1B)	185(6)	254(9)	272(8)	-8(6)	-52(6)	11(6)
Cl(2B)	190(6)	268(9)	199(7)	4(6)	-20(5)	23(6)
O(1B)	130(10)	96(11)	127(11)	-24(8)	56(8)	21(8)
O(2B)	243(19)	130(20)	154(19)	29(15)	38(15)	-16(16)
C(1B)	90(20)	270(30)	150(30)	50(20)	-33(19)	10(20)
C(2B)	100(20)	210(30)	200(30)	30(20)	0(20)	60(20)
C(3B)	150(20)	220(30)	260(30)	40(20)	-10(20)	40(20)
C(4B)	100(20)	200(30)	260(30)	70(20)	10(20)	30(20)
C(5B)	130(20)	240(30)	200(30)	50(20)	50(20)	30(20)
C(6B)	110(20)	170(30)	170(30)	40(20)	20(20)	30(20)
C(7B)	140(20)	190(30)	170(30)	40(20)	50(20)	10(20)
C(8B)	250(30)	200(30)	150(30)	60(20)	10(20)	40(20)
C(9B)	380(30)	180(30)	200(30)	-30(20)	0(30)	-10(30)
C(10B)	250(30)	290(40)	120(30)	-20(20)	-30(20)	0(30)
C(11B)	110(20)	210(30)	210(30)	10(20)	40(20)	50(20)
C(12B)	110(20)	250(30)	110(20)	-10(20)	0(19)	-10(20)
C(13B)	120(20)	260(30)	160(30)	-60(20)	10(20)	10(20)
C(14B)	100(20)	170(30)	260(30)	-70(20)	-30(20)	30(20)
C(15B)	200(30)	200(30)	160(30)	-20(20)	-90(20)	0(20)
C(16B)	150(20)	220(30)	160(30)	0(20)	-40(20)	20(20)
C(17B)	140(20)	190(30)	150(30)	-10(20)	-30(20)	-20(20)
C(18B)	140(20)	200(30)	90(20)	20(20)	20(20)	70(20)
C(19B)	180(20)	300(40)	110(30)	-10(20)	-10(20)	-20(20)
C(20B)	220(30)	330(40)	160(30)	10(30)	0(20)	20(30)
C(21B)	440(40)	300(40)	220(30)	-10(30)	50(30)	-10(30)
C(22B)	160(30)	430(40)	200(30)	-30(30)	20(20)	80(30)
C(23B)	140(20)	200(30)	380(40)	70(30)	60(20)	20(20)
C(24B)	490(40)	410(50)	580(50)	280(40)	-200(40)	-280(40)
C(25B)	280(30)	270(40)	330(40)	80(30)	-100(30)	-60(30)
C(26B)	490(40)	220(40)	750(60)	50(40)	430(40)	-40(30)
C(27B)	160(20)	240(30)	320(30)	-60(30)	20(20)	20(20)
C(28B)	690(60)	180(40)	1490(90)	-190(50)	830(60)	-10(40)
C(29B)	470(40)	410(50)	550(50)	-290(40)	-210(40)	250(40)
C(30B)	640(50)	440(50)	510(50)	-40(40)	-110(40)	370(40)
C(31B)	200(30)	200(30)	170(30)	-20(20)	10(20)	-30(20)
C(32B)	420(40)	230(40)	270(30)	40(30)	30(30)	30(30)
C(33B)	220(30)	260(40)	280(30)	30(30)	-20(20)	-40(30)
C(34B)	270(30)	330(40)	120(30)	20(20)	-10(20)	-10(30)
C(35B)	140(20)	100(30)	100(20)	-7(19)	20(19)	-30(20)
C(1C)	380(50)	1460(120)	460(60)	150(70)	150(40)	-120(70)
C(2C)	400(50)	1600(130)	530(60)	-300(80)	260(40)	-340(70)
C(3C)	500(50)	890(80)	850(80)	150(70)	420(50)	50(50)
C(1D)	490(50)	580(60)	1030(80)	-300(60)	390(50)	-90(50)

C(2D)	400(50)	1000(90)	570(60)	260(60)	70(40)	50(50)
C(3D)	390(40)	1290(100)	310(50)	-130(60)	80(40)	-160(60)

Compound 8 (CCDC 601396)

Special Refinement Details

Residual peaks in the final electron density difference Fourier map lie near the metal centers. Absorption corrections did not appreciably account for these peaks therefore the corrections were not applied.

Refinement of F^2 against ALL reflections. The weighted R-factor (*w*R) and goodness of fit (S) are based on F^2, conventional R-factors (R) are based on F, with F set to zero for negative F^2. The threshold expression of $F^2 > 2\sigma(F^2)$ is used only for calculating R-factors(gt) etc. and is not relevant to the choice of reflections for refinement. R-factors based on F^2 are statistically about twice as large as those based on F, and R-factors based on ALL data will be even larger. All esds (except the esd in the dihedral angle between two l.s. planes) are estimated using the full covariance matrix. The cell esds are taken into account individually in the estimation of esds in distances, angles and torsion angles; correlations between esds in cell parameters are only used when they are defined by crystal symmetry. An approximate (isotropic) treatment of cell esds is used for estimating esds involving l.s. planes.

Table 2. Atomic coordinates (x 10^4) and equivalent isotropic displacement parameters (Å^{2}x 10^3) for TA18 (CCDC 601396). U(eq) is defined as the trace of the orthogonalized U^{ij} tensor.

	x	y	z	U_{eq}
Ta(1)	275(1)	-352(1)	2674(1)	9(1)
Cl(1A)	801(1)	-1652(1)	2073(1)	21(1)
Cl(2A)	-171(1)	-874(1)	3898(1)	15(1)
O(1A)	-863(1)	-535(1)	2046(1)	13(1)
O(2A)	1425(1)	31(1)	3192(1)	13(1)
O(3A)	-250(1)	914(1)	3222(1)	14(1)
C(1A)	-1447(1)	-155(1)	1505(1)	11(1)
C(2A)	-2355(1)	-464(1)	1366(1)	12(1)
C(3A)	-2925(1)	-4(1)	840(1)	14(1)
C(4A)	-2626(1)	724(1)	465(1)	13(1)
C(5A)	-1718(1)	977(1)	606(1)	13(1)
C(6A)	-1091(1)	525(1)	1103(1)	12(1)
C(7A)	-2704(1)	-1272(1)	1754(1)	13(1)
C(8A)	-2185(1)	-2098(1)	1506(1)	17(1)
C(9A)	-2606(1)	-1088(2)	2693(1)	18(1)
C(10A)	-3707(1)	-1495(1)	1463(1)	18(1)
C(11A)	-3304(1)	1180(1)	-111(1)	15(1)
C(12A)	-3673(2)	519(2)	-842(2)	28(1)
C(13A)	-4099(2)	1488(2)	351(2)	26(1)
C(14A)	-2898(2)	1990(2)	-420(2)	25(1)
C(15A)	582(1)	548(1)	1780(1)	10(1)
C(16A)	-103(1)	723(1)	1131(1)	11(1)
C(17A)	148(1)	1076(1)	433(1)	13(1)
C(18A)	1033(1)	1279(1)	364(1)	15(1)
C(19A)	1698(1)	1165(1)	994(1)	14(1)
C(20A)	1496(1)	836(1)	1721(1)	11(1)
C(21A)	2227(1)	408(1)	3097(1)	12(1)
C(22A)	2959(1)	361(1)	3714(1)	13(1)
C(23A)	3777(1)	740(1)	3581(1)	14(1)

C(24A)	3878(1)	1183(1)	2890(1)	14(1)
C(25A)	3128(1)	1226(1)	2313(1)	13(1)
C(26A)	2283(1)	817(1)	2378(1)	11(1)
C(27A)	2846(1)	-72(1)	4499(1)	15(1)
C(28A)	2186(2)	440(2)	4984(1)	21(1)
C(29A)	3743(2)	-72(2)	5056(1)	23(1)
C(30A)	2493(2)	-1055(2)	4301(2)	21(1)
C(31A)	4812(1)	1567(1)	2785(1)	14(1)
C(32A)	5239(1)	2133(2)	3567(1)	21(1)
C(33A)	4774(1)	2153(2)	2081(2)	20(1)
C(34A)	5416(1)	785(2)	2604(2)	20(1)
C(35A)	295(1)	1752(1)	3359(1)	16(1)
C(36A)	500(2)	2091(2)	4249(1)	20(1)
C(37A)	-1115(1)	967(1)	3529(1)	18(1)
C(38A)	-1697(2)	1658(2)	3163(2)	29(1)
Ta(2)	138(1)	4671(1)	2571(1)	9(1)
Cl(1B)	214(1)	3314(1)	1791(1)	18(1)
Cl(2B)	-375(1)	4120(1)	3759(1)	16(1)
O(1B)	-1037(1)	4823(1)	2098(1)	13(1)
O(2B)	1386(1)	4717(1)	2940(1)	12(1)
O(3B)	97(1)	5957(1)	3346(1)	16(1)
C(1B)	-1562(1)	5106(1)	1459(1)	12(1)
C(2B)	-2499(1)	4911(1)	1387(1)	14(1)
C(3B)	-3005(1)	5193(1)	700(1)	16(1)
C(4B)	-2619(1)	5645(1)	126(1)	15(1)
C(5B)	-1699(1)	5832(1)	241(1)	14(1)
C(6B)	-1134(1)	5557(1)	913(1)	12(1)
C(7B)	-2927(1)	4408(1)	2004(1)	17(1)
C(8B)	-2733(2)	4902(2)	2869(2)	24(1)
C(9B)	-2572(2)	3456(2)	2014(2)	25(1)
C(10B)	-3956(2)	4317(2)	1800(2)	25(1)
C(11B)	-3230(1)	5928(2)	-610(1)	18(1)
C(12B)	-3910(2)	6580(2)	-300(2)	24(1)
C(13B)	-3746(2)	5110(2)	-1088(1)	24(1)
C(14B)	-2695(2)	6371(2)	-1198(2)	29(1)
C(15B)	484(1)	5592(1)	1709(1)	9(1)
C(16B)	-137(1)	5748(1)	1009(1)	11(1)
C(17B)	195(1)	6127(1)	357(1)	14(1)
C(18B)	1089(1)	6382(1)	379(1)	15(1)
C(19B)	1682(1)	6306(1)	1076(1)	12(1)
C(20B)	1396(1)	5939(1)	1750(1)	10(1)
C(21B)	2134(1)	5257(1)	2993(1)	11(1)
C(22B)	2892(1)	5128(1)	3566(1)	13(1)
C(23B)	3608(1)	5752(1)	3617(1)	14(1)
C(24B)	3600(1)	6479(1)	3149(1)	13(1)
C(25B)	2851(1)	6548(1)	2579(1)	12(1)
C(26B)	2120(1)	5919(1)	2460(1)	11(1)
C(27B)	2924(1)	4340(1)	4086(1)	16(1)
C(28B)	2801(2)	3459(2)	3521(2)	22(1)
C(29B)	3839(2)	4328(2)	4619(2)	26(1)
C(30B)	2192(2)	4381(2)	4663(1)	21(1)
C(31B)	4429(1)	7120(1)	3259(1)	16(1)
C(32B)	4666(2)	7479(2)	4162(1)	21(1)
C(33B)	4294(2)	7909(2)	2748(2)	22(1)

C(34B)	5229(2)	6607(2)	2977(2)	27(1)
C(35B)	539(2)	6122(1)	4191(1)	18(1)
C(36B)	1194(2)	6921(2)	4325(2)	24(1)
C(37B)	-437(2)	6691(1)	3076(1)	17(1)
C(38B)	-1178(2)	6896(2)	3591(2)	22(1)

Table 5. Anisotropic displacement parameters ($Å^2 x\ 10^4$) for TA18 (CCDC 601396). The anisotropic displacement factor exponent takes the form: $-2\pi^2$ [$h^2 a^{*2} U^{11}$ + ... + 2 h k a* b* U^{12}]

	U^{11}	U^{22}	U^{33}	U^{23}	U^{13}	U^{12}
Ta(1)	73(1)	97(1)	100(1)	29(1)	12(1)	-2(1)
Cl(1A)	245(2)	143(2)	274(3)	21(2)	108(2)	52(2)
Cl(2A)	139(2)	185(2)	147(2)	76(2)	36(1)	8(1)
O(1A)	100(5)	152(6)	122(5)	47(5)	-4(4)	-17(4)
O(2A)	76(4)	182(6)	144(6)	85(5)	7(4)	-14(4)
O(3A)	139(5)	104(5)	186(6)	-3(5)	74(5)	-17(4)
C(1A)	89(6)	138(7)	109(7)	23(6)	2(5)	-14(5)
C(2A)	96(6)	138(7)	112(7)	14(6)	3(5)	-29(5)
C(3A)	93(6)	165(8)	159(8)	21(7)	-6(6)	-17(5)
C(4A)	102(6)	157(7)	116(7)	33(6)	-6(5)	-9(5)
C(5A)	100(6)	160(7)	129(7)	45(6)	3(5)	-12(5)
C(6A)	87(6)	144(7)	108(7)	6(6)	-7(5)	-19(5)
C(7A)	106(6)	144(7)	144(7)	21(6)	6(5)	-26(5)
C(8A)	149(7)	130(7)	230(9)	0(7)	30(7)	-13(6)
C(9A)	162(8)	211(9)	155(8)	38(7)	22(6)	-25(6)
C(10A)	116(7)	195(8)	213(9)	36(8)	21(6)	-39(6)
C(11A)	125(7)	182(8)	145(8)	53(7)	-28(6)	-8(6)
C(12A)	284(12)	279(12)	241(11)	38(10)	-101(9)	-1(9)
C(13A)	158(8)	326(12)	303(12)	110(10)	36(8)	58(8)
C(14A)	178(9)	284(11)	281(12)	124(10)	-27(8)	-30(8)
C(15A)	90(5)	113(6)	94(6)	10(6)	5(5)	-5(5)
C(16A)	95(6)	128(7)	90(6)	6(6)	10(5)	-13(5)
C(17A)	115(6)	180(8)	106(7)	32(7)	6(5)	-10(5)
C(18A)	125(7)	226(9)	103(7)	51(7)	22(6)	-26(6)
C(19A)	103(6)	212(9)	125(7)	42(7)	22(5)	-25(6)
C(20A)	92(6)	133(7)	105(7)	22(6)	9(5)	-4(5)
C(21A)	78(5)	147(7)	124(7)	32(6)	14(5)	1(5)
C(22A)	92(6)	159(7)	124(7)	36(6)	-2(5)	-7(5)
C(23A)	91(6)	166(8)	151(8)	39(7)	-1(5)	5(5)
C(24A)	86(6)	164(7)	155(8)	31(7)	2(5)	-2(5)
C(25A)	89(6)	161(7)	128(7)	32(6)	3(5)	-12(5)
C(26A)	88(6)	128(7)	109(7)	13(6)	10(5)	0(5)
C(27A)	114(6)	202(8)	142(8)	68(7)	-8(6)	-1(6)
C(28A)	191(9)	299(11)	163(9)	57(9)	42(7)	19(8)
C(29A)	160(8)	330(12)	203(10)	124(9)	-49(7)	-31(8)
C(30A)	171(8)	210(9)	266(11)	128(9)	-17(8)	5(7)
C(31A)	95(6)	159(7)	168(8)	32(7)	11(6)	-5(5)
C(32A)	152(8)	228(10)	237(10)	-25(9)	-1(7)	-67(7)
C(33A)	128(7)	236(10)	259(10)	103(9)	18(7)	-26(6)
C(34A)	108(7)	231(9)	253(10)	41(8)	37(7)	27(6)

C(35A)	196(8)	124(7)	166(8)	-2(7)	60(7)	-31(6)
C(36A)	249(10)	158(8)	184(9)	-4(8)	5(8)	-2(7)
C(37A)	145(7)	151(8)	255(10)	16(8)	84(7)	15(6)
C(38A)	217(10)	262(11)	383(14)	39(11)	15(10)	92(8)
Ta(2)	81(1)	99(1)	79(1)	26(1)	-9(1)	-2(1)
Cl(1B)	274(2)	123(2)	133(2)	4(2)	13(2)	4(2)
Cl(2B)	173(2)	182(2)	120(2)	62(2)	21(2)	-15(1)
O(1B)	106(5)	167(6)	126(6)	67(5)	-28(4)	-17(4)
O(2B)	98(5)	147(6)	124(5)	54(5)	-22(4)	3(4)
O(3B)	269(7)	138(6)	76(5)	23(5)	-4(5)	64(5)
C(1B)	95(6)	144(7)	116(7)	17(6)	-32(5)	5(5)
C(2B)	99(6)	151(7)	176(8)	30(7)	-28(6)	4(5)
C(3B)	99(6)	181(8)	172(8)	2(7)	-48(6)	17(5)
C(4B)	108(6)	177(8)	150(8)	8(7)	-45(6)	25(5)
C(5B)	111(6)	176(8)	127(7)	27(7)	-25(5)	26(5)
C(6B)	98(6)	135(7)	112(7)	13(6)	-24(5)	7(5)
C(7B)	102(6)	178(8)	215(9)	49(7)	-15(6)	-29(5)
C(8B)	160(8)	324(12)	222(10)	38(9)	31(7)	-12(8)
C(9B)	189(9)	186(9)	359(13)	101(9)	-40(9)	-34(7)
C(10B)	121(8)	285(11)	358(13)	121(10)	-17(8)	-57(7)
C(11B)	126(7)	247(9)	146(8)	30(8)	-37(6)	59(6)
C(12B)	220(9)	268(11)	220(10)	-10(9)	-57(8)	124(8)
C(13B)	182(9)	293(11)	206(10)	-53(9)	-88(7)	62(8)
C(14B)	197(10)	443(15)	221(11)	138(11)	-54(8)	67(9)
C(15B)	92(5)	99(6)	83(6)	24(6)	6(5)	11(4)
C(16B)	89(6)	137(7)	87(6)	9(6)	-15(5)	4(5)
C(17B)	122(7)	212(9)	102(7)	49(7)	-13(6)	-2(6)
C(18B)	146(7)	213(9)	102(7)	64(7)	3(6)	-9(6)
C(19B)	110(6)	156(7)	100(7)	38(6)	3(5)	-1(5)
C(20B)	88(5)	119(6)	81(6)	24(6)	-4(5)	4(5)
C(21B)	84(5)	148(7)	98(6)	26(6)	-3(5)	9(5)
C(22B)	100(6)	169(8)	121(7)	52(7)	-18(5)	22(5)
C(23B)	108(6)	187(8)	123(7)	37(7)	-22(5)	7(5)
C(24B)	99(6)	161(7)	127(7)	4(6)	-12(5)	-9(5)
C(25B)	114(6)	146(7)	106(7)	23(6)	-9(5)	2(5)
C(26B)	81(5)	134(7)	98(6)	17(6)	-8(5)	14(5)
C(27B)	131(7)	190(8)	170(8)	80(7)	-31(6)	15(6)
C(28B)	258(10)	174(9)	231(10)	65(8)	-17(8)	62(7)
C(29B)	162(9)	332(12)	275(11)	170(10)	-75(8)	20(8)
C(30B)	190(9)	276(11)	171(9)	112(9)	8(7)	17(7)
C(31B)	111(6)	194(8)	162(8)	6(7)	-2(6)	-32(6)
C(32B)	216(9)	189(9)	193(9)	-8(8)	-67(8)	-16(7)
C(33B)	182(9)	252(10)	229(10)	76(9)	-15(8)	-77(7)
C(34B)	147(8)	287(12)	369(13)	1(11)	66(9)	-3(7)
C(35B)	275(10)	151(8)	104(7)	1(7)	-36(7)	18(7)
C(36B)	259(10)	212(10)	237(10)	-55(9)	24(8)	-36(8)
C(37B)	262(9)	130(7)	125(8)	33(7)	31(7)	56(7)
C(38B)	221(9)	202(9)	235(10)	10(9)	44(8)	29(7)

Compound 10 (CCDC 641995)

Special Refinement Details

There are two molecules in the asymmetric unit along with two molecules of solvent. Diffraction quality is poor, peaks are broad and have shoulders. Intensity falls of quickly past $2\theta=35^{\circ}$ therefore refinement included data with $2\theta \leq 40^{\circ}$ only. All atoms except Ta were refined isotropically and hydrogens were included as riding atoms.

Refinement of F^2 against ALL reflections. The weighted R-factor (*w*R) and goodness of fit (S) are based on F^2, conventional R-factors (R) are based on F, with F set to zero for negative F^2. The threshold expression of $F^2 > 2\sigma(F^2)$ is used only for calculating R-factors(gt) etc. and is not relevant to the choice of reflections for refinement. R-factors based on F^2 are statistically about twice as large as those based on F, and R-factors based on ALL data will be even larger.

All esds (except the esd in the dihedral angle between two l.s. planes) are estimated using the full covariance matrix. The cell esds are taken into account individually in the estimation of esds in distances, angles and torsion angles; correlations between esds in cell parameters are only used when they are defined by crystal symmetry. An approximate (isotropic) treatment of cell esds is used for estimating esds involving l.s. planes.

Table 2. Atomic coordinates (x 10^4) and equivalent isotropic displacement parameters (Å^{2}x 10^3) for TA33 (CCDC 641995). U(eq) is defined as the trace of the orthogonalized U^{ij} tensor.

	x	y	z	U_{eq}
Ta(1)	259(1)	10103(1)	3278(1)	20(1)
O(1A)	231(5)	11244(5)	2725(4)	21(2)
O(2A)	668(5)	8884(5)	3705(4)	23(2)
O(3A)	200(5)	9889(5)	2306(4)	19(2)
C(1A)	503(7)	11666(8)	2091(6)	20(3)
C(2A)	-28(8)	12479(8)	1701(7)	27(3)
C(3A)	278(8)	12900(9)	1046(7)	24(4)
C(4A)	1052(8)	12547(8)	783(6)	23(3)
C(5A)	1542(8)	11740(8)	1184(6)	23(3)
C(6A)	1280(8)	11270(8)	1837(7)	28(3)
C(7A)	1853(7)	10423(8)	2297(6)	17(3)
C(8A)	2576(7)	10519(8)	2637(6)	21(3)
C(9A)	3116(8)	9821(8)	3137(6)	22(3)
C(10A)	2914(7)	9072(8)	3337(6)	16(3)
C(11A)	2203(8)	8936(8)	3022(6)	21(3)
C(12A)	1994(8)	8148(8)	3382(6)	23(3)
C(13A)	2616(8)	7371(8)	3399(6)	28(3)
C(14A)	2488(7)	6608(7)	3773(6)	18(3)
C(15A)	1714(8)	6621(9)	4125(7)	30(4)
C(16A)	1110(7)	7377(8)	4137(6)	19(3)
C(17A)	1247(8)	8133(8)	3739(6)	20(3)
C(18A)	-897(8)	12882(8)	1956(6)	23(3)
C(19A)	-822(8)	12950(8)	2755(6)	30(4)
C(20A)	-1497(8)	12347(8)	1900(7)	30(3)
C(21A)	-1312(8)	13800(8)	1450(6)	31(3)

C(22A)	1352(8)	13057(8)	61(7)	30(3)
C(23A)	1431(9)	13901(9)	167(7)	42(4)
C(24A)	2176(8)	12556(8)	-176(7)	37(4)
C(25A)	656(8)	13252(8)	-580(6)	34(4)
C(26A)	3177(8)	5734(8)	3806(7)	31(4)
C(27A)	3611(11)	5786(11)	3069(9)	78(6)
C(28A)	3828(11)	5553(11)	4429(8)	72(5)
C(29A)	2779(10)	4990(10)	3926(8)	63(5)
C(30A)	300(8)	7370(8)	4557(7)	30(3)
C(31A)	-510(8)	7792(8)	4021(6)	27(3)
C(32A)	285(9)	6447(9)	4962(7)	42(4)
C(33A)	291(9)	7818(9)	5159(7)	42(4)
C(34A)	1723(7)	9639(8)	2454(6)	18(3)
C(35A)	973(7)	9531(8)	2003(6)	20(3)
C(36A)	923(8)	10060(8)	1157(6)	26(3)
C(37A)	152(8)	10571(8)	809(6)	23(3)
C(38A)	62(8)	11022(8)	51(6)	26(3)
C(39A)	821(8)	10906(8)	-334(7)	24(3)
C(40A)	1572(8)	10401(8)	2(6)	23(3)
C(41A)	1661(8)	9965(8)	763(6)	25(3)
C(42A)	1016(8)	8635(8)	1965(6)	17(3)
C(43A)	320(8)	8325(8)	2166(6)	29(4)
C(44A)	324(9)	7534(9)	2106(7)	36(4)
C(45A)	1019(8)	7030(9)	1851(7)	37(4)
C(46A)	1706(8)	7323(8)	1657(6)	30(3)
C(47A)	1704(8)	8125(8)	1727(6)	28(3)
C(48A)	-959(7)	10337(8)	3715(6)	21(3)
C(49A)	1137(7)	10206(8)	4106(6)	22(3)
Ta(2)	5238(1)	10170(1)	1649(1)	21(1)
O(1B)	5663(5)	8988(5)	1780(4)	27(2)
O(2B)	5209(5)	11316(5)	1660(4)	28(2)
O(3B)	5155(4)	9955(4)	2715(4)	11(2)
C(1B)	6235(8)	8206(8)	2088(6)	21(3)
C(2B)	6108(8)	7457(8)	2040(7)	27(3)
C(3B)	6726(8)	6686(8)	2395(6)	22(3)
C(4B)	7467(8)	6651(8)	2788(6)	27(3)
C(5B)	7567(8)	7437(8)	2789(6)	24(3)
C(6B)	6972(7)	8222(7)	2449(6)	16(3)
C(7B)	7191(7)	9009(7)	2439(6)	18(3)
C(8B)	7904(8)	9135(8)	2088(6)	20(3)
C(9B)	8109(8)	9870(8)	1931(6)	26(3)
C(10B)	7545(7)	10567(8)	2089(6)	22(3)
C(11B)	6814(7)	10493(8)	2453(6)	18(3)
C(12B)	6227(8)	11343(8)	2516(6)	20(3)
C(13B)	6503(8)	11769(8)	2974(6)	19(3)
C(14B)	6013(8)	12558(8)	3024(6)	22(3)
C(15B)	5217(8)	12906(9)	2614(7)	29(4)
C(16B)	4943(8)	12523(8)	2142(6)	22(3)
C(17B)	5460(8)	11722(8)	2113(6)	22(3)
C(18B)	5310(8)	7445(8)	1593(7)	28(3)
C(19B)	4479(8)	7830(9)	1919(7)	40(4)
C(20B)	5311(8)	7933(8)	781(6)	28(3)
C(21B)	5313(9)	6530(9)	1594(7)	42(4)

C(22B)	8084(8)	5777(8)	3178(7)	29(3)
C(23B)	8836(9)	5878(9)	3568(7)	45(4)
C(24B)	8413(10)	5266(10)	2655(8)	63(5)
C(25B)	7606(10)	5317(10)	3780(8)	59(5)
C(26B)	6288(8)	13052(8)	3505(7)	30(3)
C(27B)	6361(9)	13890(8)	3029(7)	41(4)
C(28B)	7118(8)	12573(8)	3966(7)	34(4)
C(29B)	5589(9)	13247(9)	4056(7)	43(4)
C(30B)	4064(8)	12947(8)	1699(7)	29(3)
C(31B)	3471(8)	12383(8)	1982(7)	28(3)
C(32B)	3603(9)	13835(8)	1816(7)	39(4)
C(33B)	4161(8)	13076(8)	866(6)	29(4)
C(34B)	6672(7)	9688(7)	2696(6)	14(3)
C(35B)	5907(7)	9585(7)	3200(6)	9(3)
C(36B)	5947(8)	8663(8)	3633(6)	18(3)
C(37B)	5286(8)	8347(8)	3565(6)	19(3)
C(38B)	5278(8)	7544(8)	3992(6)	26(4)
C(39B)	5948(8)	7060(8)	4471(6)	25(3)
C(40B)	6642(9)	7339(9)	4563(7)	41(4)
C(41B)	6648(8)	8157(8)	4131(6)	24(3)
C(42B)	5881(7)	10096(7)	3805(6)	18(3)
C(43B)	6589(8)	9989(7)	4213(6)	17(3)
C(44B)	6538(8)	10415(7)	4773(6)	23(3)
C(45B)	5759(8)	10923(8)	4897(6)	25(3)
C(46B)	5026(8)	11013(8)	4470(6)	22(3)
C(47B)	5080(8)	10598(7)	3928(6)	18(3)
C(48B)	4034(7)	10417(8)	1094(6)	25(3)
C(49B)	6141(8)	10269(9)	798(7)	36(4)
C(1C)	2336(10)	1937(10)	3975(8)	62(5)
C(2C)	1672(10)	2585(9)	3394(8)	50(4)
C(3C)	1655(12)	3501(11)	3400(9)	78(6)
C(4C)	920(13)	4267(13)	2995(10)	94(7)
C(5C)	999(13)	4343(13)	2186(10)	103(7)
C(1D)	7351(11)	1958(11)	89(9)	75(5)
C(2D)	6672(12)	2610(12)	362(10)	83(6)
C(3D)	6676(15)	3490(15)	20(12)	117(8)
C(4D)	6090(30)	4230(30)	150(20)	300(20)
C(5D)	6123(16)	4273(16)	854(13)	137(9)

Table 5. Anisotropic displacement parameters ($Å^2 x 10^4$) for TA33 (CCDC 641995). The anisotropic displacement factor exponent takes the form: $-2\pi^2[h^2a^{*2}U^{11} + ... + 2 h k a^* b^* U^{12}]$

	U^{11}	U^{22}	U^{33}	U^{23}	U^{13}	U^{12}
Ta(1)	256(4)	264(4)	74(3)	-33(3)	19(3)	-59(3)
Ta(2)	268(4)	271(4)	68(4)	-34(3)	-8(3)	-60(3)

Compound 11 (CCDC 641996)

Special Refinement Details

This crystal is twinned. Incorporation of the twinning produced unsatisfactory results. Results of refinement as a single crystal did NOT produce the usual pattern of $Fo^2 > Fc^2$ for the reflections with the largest ΔF/esd. In fact, many low angle reflections that calculate large were observed very small with unreasonably large esd's. Presumably the orientation of twins is close enough that one reflection overlaps the background of another and results in a low count and high uncertainty. When the data was reintegrated using a simple sum over a set box size for intensity measurement and a user defined background function applied, this phenomena disappears and refinement gives more satisfactory results. When this is applied to twin integration still produces unsatisfactory results.

During least-squares refinement the anisotropic displacement parameters of the solvent and of C(30) were restrained to simulate isotropic behavior. Reflection 1 2 0 was omitted to bad agreement. The largest peaks in the final difference Fourier are near Ta, near solvent or near C(30).

Refinement of F^2 against ALL reflections. The weighted R-factor (*w*R) and goodness of fit (S) are based on F^2, conventional R-factors (R) are based on F, with F set to zero for negative F^2. The threshold expression of $F^2 > 2\sigma(F^2)$ is used only for calculating R-factors(gt) etc. and is not relevant to the choice of reflections for refinement. R-factors based on F^2 are statistically about twice as large as those based on F, and R-factors based on ALL data will be even larger.

All esds (except the esd in the dihedral angle between two l.s. planes) are estimated using the full covariance matrix. The cell esds are taken into account individually in the estimation of esds in distances, angles and torsion angles; correlations between esds in cell parameters are only used when they are defined by crystal symmetry. An approximate (isotropic) treatment of cell esds is used for estimating esds involving l.s. planes.

Table 2. Atomic coordinates (x 10^4) and equivalent isotropic displacement parameters (Å^{2}x 10^3) for TA34 (CCDC 641996). U(eq) is defined as the trace of the orthogonalized U^{ij} tensor.

	x	y	z	U_{eq}
Ta(1)	2588(1)	1249(1)	1489(1)	18(1)
O(1)	3299(3)	1837(1)	1617(3)	18(1)
O(2)	1380(3)	826(1)	1142(3)	20(1)
N(1)	1534(4)	1588(2)	2239(4)	19(1)
C(1)	3115(5)	2303(2)	1555(5)	19(1)
C(2)	3819(4)	2605(2)	2252(4)	18(1)
C(3)	3608(5)	3077(2)	2096(5)	21(1)
C(4)	2766(5)	3257(2)	1283(5)	21(1)
C(5)	2098(5)	2942(2)	619(4)	19(1)
C(6)	2249(5)	2466(2)	750(4)	19(1)
C(7)	1504(4)	2149(2)	7(4)	18(1)
C(8)	1441(5)	2158(2)	-1095(5)	23(1)
C(9)	762(5)	1848(2)	-1774(5)	23(1)
C(10)	157(5)	1513(2)	-1354(4)	20(1)
C(11)	208(4)	1496(2)	-252(4)	18(1)
C(12)	-354(4)	1134(2)	248(4)	18(1)
C(13)	-1500(5)	1118(2)	60(4)	20(1)
C(14)	-2044(4)	780(2)	523(5)	22(1)
C(15)	-1408(5)	458(2)	1183(5)	23(1)
C(16)	-238(5)	453(2)	1429(5)	21(1)

C(17)	267(4)	808(2)	937(5)	21(1)
C(18)	834(4)	1827(2)	418(4)	17(1)
C(19)	800(4)	1820(2)	1607(5)	20(1)
C(20)	-117(4)	2070(2)	1936(5)	22(1)
C(21)	-723(5)	2403(2)	1277(5)	28(1)
C(22)	-1573(5)	2640(2)	1593(6)	39(2)
C(23)	-1808(5)	2544(3)	2573(7)	45(2)
C(24)	-1227(5)	2204(3)	3219(6)	40(2)
C(25)	-383(5)	1961(2)	2916(5)	26(1)
C(26)	4764(5)	2425(2)	3159(5)	23(1)
C(27)	4273(5)	2147(2)	3978(5)	32(2)
C(28)	5546(5)	2126(2)	2672(5)	32(2)
C(29)	5445(5)	2821(2)	3769(5)	31(2)
C(30)	2576(5)	3780(2)	1005(6)	35(2)
C(31)	1394(5)	3915(2)	867(6)	34(2)
C(32)	3047(5)	3893(2)	51(5)	26(1)
C(33)	3254(6)	4068(2)	2003(5)	40(2)
C(34)	-3305(5)	790(2)	344(5)	26(1)
C(35)	-3626(5)	1226(2)	887(5)	35(2)
C(36)	-3747(5)	367(2)	855(6)	39(2)
C(37)	-3835(5)	794(3)	-844(6)	43(2)
C(38)	410(5)	100(2)	2194(5)	22(1)
C(39)	997(5)	350(2)	3228(5)	30(2)
C(40)	-337(5)	-278(2)	2518(5)	30(2)
C(41)	1238(5)	-149(2)	1665(5)	25(1)
C(42)	3810(5)	842(2)	2542(5)	30(2)
C(43)	2923(5)	1148(2)	-97(5)	26(1)
C(51)	6379(10)	1345(4)	6385(9)	102(4)
C(52)	6604(12)	1193(5)	5331(12)	136(5)
C(53)	7253(14)	816(6)	5289(14)	153(6)
C(54)	7374(18)	626(8)	4236(18)	210(9)
C(55)	8222(16)	926(7)	4054(17)	199(8)

Table 5. Anisotropic displacement parameters ($Å^2 x 10^4$) for TA34 (CCDC 641996). The anisotropic displacement factor exponent takes the form: $-2\pi^2[h^2a^{*2}U^{11} + ... + 2 h k a^* b^* U^{12}]$

	U^{11}	U^{22}	U^{33}	U^{23}	U^{13}	U^{12}
Ta(1)	190(1)	122(1)	219(1)	9(1)	30(1)	0(1)
O(1)	230(20)	73(18)	240(20)	21(16)	52(17)	-15(16)
O(2)	210(20)	121(19)	260(20)	-11(17)	19(17)	-38(16)
N(1)	190(20)	180(20)	200(30)	40(20)	40(20)	-10(20)
C(1)	220(30)	80(30)	280(30)	0(20)	100(20)	0(20)
C(2)	180(30)	180(30)	200(30)	-30(20)	60(20)	-40(20)
C(3)	280(30)	160(30)	200(30)	-10(20)	50(30)	-50(20)
C(4)	280(30)	110(30)	280(30)	20(20)	130(30)	30(20)
C(5)	280(30)	110(30)	170(30)	20(20)	70(20)	30(20)
C(6)	220(30)	130(30)	230(30)	0(20)	100(30)	-30(20)

C(7)	210(30)	110(30)	210(30)	30(20)	70(20)	50(20)
C(8)	320(30)	140(30)	230(30)	60(30)	90(30)	20(30)
C(9)	340(30)	190(30)	150(30)	10(20)	40(30)	70(30)
C(10)	260(30)	150(30)	190(30)	-20(20)	30(20)	30(20)
C(11)	200(30)	110(30)	230(30)	20(20)	40(20)	20(20)
C(12)	250(30)	130(30)	160(30)	-30(20)	30(20)	0(20)
C(13)	280(30)	170(30)	120(30)	10(20)	0(20)	20(20)
C(14)	210(30)	190(30)	240(30)	-80(30)	20(20)	-40(20)
C(15)	300(30)	170(30)	230(30)	-10(30)	90(30)	-80(30)
C(16)	230(30)	120(30)	280(30)	-50(30)	60(30)	-20(20)
C(17)	220(30)	160(30)	230(30)	-70(20)	30(20)	-20(20)
C(18)	190(30)	110(30)	200(30)	50(20)	40(20)	70(20)
C(19)	190(30)	130(30)	270(30)	-50(20)	60(20)	-70(20)
C(20)	170(30)	170(30)	300(30)	-70(30)	30(30)	-10(20)
C(21)	290(30)	260(30)	300(40)	-30(30)	60(30)	20(30)
C(22)	260(30)	370(40)	510(50)	-40(40)	0(30)	30(30)
C(23)	240(40)	510(50)	650(50)	-250(40)	220(40)	-70(30)
C(24)	290(40)	550(50)	390(40)	-210(40)	150(30)	-180(40)
C(25)	220(30)	340(40)	220(30)	-70(30)	70(30)	-90(30)
C(26)	210(30)	150(30)	310(30)	-10(30)	10(30)	-10(20)
C(27)	370(40)	310(40)	230(30)	30(30)	-40(30)	70(30)
C(28)	230(30)	300(40)	410(40)	-40(30)	30(30)	20(30)
C(29)	240(30)	270(40)	380(40)	-30(30)	-20(30)	-20(30)
C(30)	450(30)	120(30)	670(40)	-10(30)	540(30)	0(30)
C(31)	430(40)	160(30)	460(40)	-10(30)	170(30)	100(30)
C(32)	380(30)	210(30)	210(30)	70(30)	110(30)	-30(30)
C(33)	770(50)	170(30)	270(40)	0(30)	140(40)	-40(30)
C(34)	230(30)	270(30)	290(30)	10(30)	70(30)	-20(30)
C(35)	250(30)	340(40)	450(40)	-10(40)	60(30)	50(30)
C(36)	270(40)	390(40)	490(40)	20(40)	70(30)	-50(30)
C(37)	230(30)	540(50)	490(50)	-30(40)	30(30)	-10(30)
C(38)	300(30)	100(30)	230(30)	20(20)	0(30)	-60(20)
C(39)	420(40)	270(40)	180(30)	-20(30)	0(30)	-20(30)
C(40)	270(30)	260(40)	390(40)	120(30)	100(30)	0(30)
C(41)	280(30)	170(30)	280(30)	20(30)	10(30)	20(30)
C(42)	360(40)	200(30)	320(40)	50(30)	10(30)	50(30)
C(43)	270(30)	250(40)	290(30)	-50(30)	120(30)	60(30)
C(51)	1070(70)	1190(80)	760(60)	30(60)	90(60)	-120(60)
C(52)	1410(80)	1430(90)	1200(80)	-210(70)	170(70)	300(70)
C(53)	1720(90)	1450(90)	1440(90)	20(80)	380(80)	640(80)
C(54)	2310(120)	2090(120)	1830(110)	-80(90)	340(90)	160(90)
C(55)	1840(110)	2150(120)	2030(110)	60(90)	520(90)	-230(90)

Compound 12 (CCDC 626579)

Special Refinement Details

Two tertiary butyl groups exhibit a common type of disorder; rotation about the C-C bond to the central carbon, in this structure the C(24)-C(4) and C(43)-N(2) bond. The disorder was included in the model with the minor component refined isotropically and the C-C distances in both components restrained to be similar without imposing a target value. The relative populations are listed in Table 2 and the distances are listed in Table 4. The third figure illustrates both components together with the minor component in cyan.

Refinement of F^2 against ALL reflections. The weighted R-factor (*w*R) and goodness of fit (S) are based on F^2, conventional R-factors (R) are based on F, with F set to zero for negative F^2. The threshold expression of $F^2 > 2\sigma(F^2)$ is used only for calculating R-factors(gt) etc. and is not relevant to the choice of reflections for refinement. R-factors based on F^2 are statistically about twice as large as those based on F, and R-factors based on ALL data will be even larger. All esds (except the esd in the dihedral angle between two l.s. planes) are estimated using the full covariance matrix. The cell esds are taken into account individually in the estimation of esds in distances, angles and torsion angles; correlations between esds in cell parameters are only used when they are defined by crystal symmetry. An approximate (isotropic) treatment of cell esds is used for estimating esds involving l.s. planes.

Table 2. Atomic coordinates (x 10^4) and equivalent isotropic displacement parameters (Å^{2}x 10^3) for TA28 (CCDC 626579). U(eq) is defined as the trace of the orthogonalized U^{ij} tensor.

	x	y	z	U_{eq}	Occ
Ta(1)	7042(1)	5215(1)	7361(1)	10(1)	1
O(1)	6257(1)	6158(1)	6479(1)	12(1)	1
O(2)	7394(1)	4223(1)	8247(1)	13(1)	1
N(1)	6602(1)	6263(1)	8342(1)	13(1)	1
N(2)	7758(2)	4179(1)	6372(1)	16(1)	1
C(1)	5105(2)	6900(1)	6515(1)	14(1)	1
C(2)	5153(2)	7788(1)	6141(1)	17(1)	1
C(3)	3978(2)	8561(1)	6245(1)	21(1)	1
C(4)	2789(2)	8488(1)	6703(1)	18(1)	1
C(5)	2767(2)	7594(1)	7035(1)	16(1)	1
C(6)	3896(2)	6774(1)	6931(1)	13(1)	1
C(7)	3774(2)	5819(1)	7254(1)	14(1)	1
C(8)	2437(2)	5714(1)	7341(1)	18(1)	1
C(9)	2199(2)	4899(1)	7722(1)	20(1)	1
C(10)	3299(2)	4154(1)	7976(1)	18(1)	1
C(11)	4660(2)	4204(1)	7835(1)	13(1)	1
C(12)	5766(2)	3341(1)	8102(1)	12(1)	1
C(13)	5519(2)	2438(1)	8136(1)	15(1)	1
C(14)	6442(2)	1621(1)	8466(1)	16(1)	1
C(15)	7654(2)	1725(1)	8773(1)	17(1)	1
C(16)	7997(2)	2593(1)	8727(1)	15(1)	1
C(17)	7054(2)	3389(1)	8360(1)	12(1)	1
C(18)	4922(2)	5052(1)	7485(1)	12(1)	1
C(19)	6461(2)	7903(1)	5647(2)	25(1)	1
C(20)	7678(2)	7703(2)	6226(2)	33(1)	1

C(21)	6254(2)	8928(2)	5284(2)	38(1)	1
C(22)	6820(3)	7229(2)	4884(2)	35(1)	1
C(23)	1557(2)	9383(1)	6812(1)	27(1)	1
C(24A)	933(3)	9663(2)	5945(2)	38(1)	0.819(5)
C(25A)	2032(3)	10226(2)	7098(3)	38(1)	0.819(5)
C(26A)	438(3)	9214(2)	7438(3)	45(1)	0.819(5)
C(24B)	234(8)	9149(10)	6613(9)	35(3)	0.181(5)
C(25B)	1700(20)	10363(7)	6522(14)	57(5)	0.181(5)
C(26B)	1280(20)	9445(16)	7779(3)	62(6)	0.181(5)
C(27)	6104(2)	656(1)	8468(1)	19(1)	1
C(28)	4670(2)	752(1)	8899(2)	25(1)	1
C(29)	7142(2)	-121(1)	8962(2)	29(1)	1
C(30)	6103(3)	339(2)	7543(2)	32(1)	1
C(31)	9359(2)	2678(1)	9060(1)	20(1)	1
C(32)	10168(2)	1743(2)	9501(2)	34(1)	1
C(33)	10288(2)	2889(2)	8312(1)	24(1)	1
C(34)	9092(2)	3475(2)	9721(1)	29(1)	1
C(35)	8815(2)	6741(2)	8251(2)	26(1)	1
C(36)	7802(2)	6223(1)	8024(1)	15(1)	1
C(37)	5749(2)	6806(1)	9068(1)	18(1)	1
C(38)	6639(2)	6773(2)	9832(1)	32(1)	1
C(39)	5116(2)	7834(1)	8759(1)	28(1)	1
C(40)	4616(3)	6334(2)	9312(2)	33(1)	1
C(41)	10187(2)	4316(2)	6130(2)	34(1)	1
C(42)	8763(2)	4508(1)	6523(1)	17(1)	1
C(43)	7596(2)	3471(1)	5752(1)	27(1)	1
C(44A)	8124(5)	3677(3)	4856(1)	46(1)	0.871(5)
C(45A)	6074(3)	3526(3)	5749(2)	52(1)	0.871(5)
C(46A)	8404(5)	2478(2)	6064(2)	63(1)	0.871(5)
C(44B)	6420(20)	4165(16)	5299(16)	55(7)	0.129(5)
C(45B)	7080(30)	2639(13)	6109(17)	52(6)	0.129(5)
C(46B)	8681(16)	3289(14)	5015(9)	29(4)	0.129(5)

Table 5. Anisotropic displacement parameters ($Å^2$x 10^4) for TA28 (CCDC 626579). The anisotropic displacement factor exponent takes the form: $-2\pi^2[h^2a^{*2}U^{11} + ... + 2 h k a^* b^* U^{12}]$

	U^{11}	U^{22}	U^{33}	U^{23}	U^{13}	U^{12}
Ta(1)	90(1)	92(1)	110(1)	-8(1)	3(1)	-26(1)
O(1)	98(4)	97(4)	141(5)	14(3)	10(3)	3(3)
O(2)	147(5)	116(5)	150(5)	29(3)	-28(4)	-54(4)
N(1)	144(5)	122(5)	131(5)	-35(4)	15(4)	-45(4)
N(2)	180(6)	127(5)	142(6)	-40(4)	-17(4)	-6(4)
C(1)	121(5)	129(6)	144(6)	-2(4)	11(4)	-11(4)
C(2)	147(6)	135(6)	213(7)	32(5)	37(5)	-10(5)
C(3)	172(7)	132(7)	279(9)	31(5)	38(6)	0(5)
C(4)	148(6)	144(7)	230(8)	7(5)	6(5)	5(5)
C(5)	122(6)	169(7)	177(7)	-1(5)	11(5)	-20(5)
C(6)	122(5)	132(6)	144(6)	2(4)	-7(4)	-30(4)
C(7)	116(5)	149(6)	138(6)	11(4)	-7(4)	-37(4)
C(8)	107(6)	194(7)	223(7)	32(5)	-25(5)	-42(5)
C(9)	115(6)	239(8)	259(8)	54(6)	-24(5)	-71(5)

C(10)	133(6)	195(7)	219(7)	47(5)	-28(5)	-76(5)
C(11)	115(5)	148(6)	145(6)	11(4)	-23(4)	-58(4)
C(12)	115(5)	126(6)	137(6)	9(4)	-14(4)	-50(4)
C(13)	147(6)	153(6)	175(7)	5(5)	-5(5)	-69(5)
C(14)	174(6)	124(6)	188(7)	1(4)	11(5)	-59(5)
C(15)	160(6)	141(6)	208(7)	34(5)	-10(5)	-49(5)
C(16)	129(6)	160(6)	164(6)	24(5)	-22(5)	-50(5)
C(17)	120(5)	132(6)	127(6)	15(4)	-10(4)	-49(4)
C(18)	101(5)	135(6)	136(6)	-3(4)	-13(4)	-39(4)
C(19)	198(8)	161(8)	355(10)	105(6)	79(7)	-5(6)
C(20)	185(8)	234(9)	580(15)	132(9)	4(9)	-73(7)
C(21)	274(10)	218(10)	575(16)	188(9)	126(10)	-11(7)
C(22)	334(11)	300(11)	327(11)	61(8)	183(9)	11(8)
C(23)	165(7)	183(8)	423(12)	-38(7)	20(7)	25(6)
C(24A)	276(13)	280(14)	482(18)	5(12)	-101(12)	87(10)
C(25A)	302(13)	237(13)	570(20)	-176(12)	62(13)	-15(10)
C(26A)	289(14)	294(15)	640(20)	50(13)	237(15)	76(11)
C(27)	198(7)	123(6)	265(8)	-7(5)	12(6)	-62(5)
C(28)	222(8)	174(8)	367(11)	1(6)	30(7)	-98(6)
C(29)	256(9)	142(8)	463(13)	54(7)	-15(8)	-67(6)
C(30)	428(13)	228(10)	320(11)	-94(7)	62(9)	-147(9)
C(31)	147(6)	190(7)	257(8)	65(6)	-71(6)	-57(5)
C(32)	235(9)	296(11)	504(14)	183(9)	-190(9)	-92(8)
C(33)	143(7)	245(9)	349(10)	52(7)	-19(6)	-64(6)
C(34)	265(9)	366(11)	246(9)	1(7)	-127(7)	-98(8)
C(35)	194(8)	302(10)	332(10)	-111(7)	14(7)	-137(7)
C(36)	135(6)	150(6)	190(7)	-39(5)	0(5)	-58(5)
C(37)	181(7)	190(7)	157(7)	-65(5)	19(5)	-43(5)
C(38)	289(10)	412(12)	185(9)	-108(8)	-29(7)	12(8)
C(39)	316(10)	173(8)	295(10)	-85(6)	-32(8)	24(7)
C(40)	372(11)	384(12)	285(10)	-146(8)	188(9)	-210(9)
C(41)	160(8)	538(15)	282(10)	-148(9)	53(7)	-36(8)
C(42)	134(6)	173(7)	178(7)	-47(5)	16(5)	-8(5)
C(43)	337(10)	296(10)	214(9)	-140(7)	16(7)	-117(8)
C(44A)	720(30)	640(20)	161(11)	-150(12)	84(13)	-420(20)
C(45A)	520(20)	870(30)	339(16)	-310(17)	72(13)	-440(20)
C(46A)	1150(40)	192(14)	510(20)	-110(12)	-170(20)	-74(18)

Structures for Chapter 5

Compound 5 (CCDC 279741)

Special Refinement Details

All residual electron density peaks lie within 1Å of Ta and may be accounted for by an incomplete absorption correction model. Absorption corrections were based on measured faces and then finished with SADABS.

Refinement of F^2 against ALL reflections. The weighted R-factor (*w*R) and goodness of fit (S) are based on F^2, conventional R-factors (R) are based on F, with F set to zero for negative F^2. The threshold expression of $F^2 > 2\sigma(F^2)$ is used only for calculating R-factors(gt) etc. and is not relevant to the choice of reflections for refinement. R-factors based on F^2 are statistically about twice as large as those based on F, and R-factors based on ALL data will be even larger. All esds (except the esd in the dihedral angle between two l.s. planes) are estimated using the full covariance matrix. The cell esds are taken into account individually in the estimation of esds in distances, angles and torsion angles; correlations between esds in cell parameters are only used when they are defined by crystal symmetry. An approximate (isotropic) treatment of cell esds is used for estimating esds involving l.s. planes.

Table 2. Atomic coordinates (x 10^4) and equivalent isotropic displacement parameters (Å^{2}x 10^3) for TA17 (CCDC 279741). U(eq) is defined as the trace of the orthogonalized U^{ij} tensor.

	x	y	z	U_{eq}
Ta	6849(1)	8658(1)	6829(1)	11(1)
O(1)	5091(1)	8995(1)	7589(1)	14(1)
O(2)	8702(1)	8008(1)	6355(1)	13(1)
N(1)	7358(1)	7615(1)	8244(1)	13(1)
C(1)	4430(2)	8496(2)	8319(1)	13(1)
C(2)	3164(2)	8486(2)	8337(1)	14(1)
C(3)	2565(2)	7911(2)	9091(1)	15(1)
C(4)	3148(2)	7359(2)	9818(1)	14(1)
C(5)	4375(2)	7424(2)	9783(1)	15(1)
C(6)	5031(2)	7984(2)	9046(1)	14(1)
C(7)	6376(2)	7915(2)	9067(1)	14(1)
C(8)	6623(2)	8075(2)	9948(1)	18(1)
C(9)	7908(2)	7845(2)	9985(1)	19(1)
C(10)	8912(2)	7381(2)	9164(1)	16(1)
C(11)	8617(2)	7257(2)	8292(1)	13(1)
C(12)	9719(2)	6700(2)	7427(1)	13(1)
C(13)	10799(2)	5723(2)	7567(1)	14(1)
C(14)	11921(2)	5193(2)	6823(1)	14(1)
C(15)	11940(2)	5682(2)	5925(1)	14(1)
C(16)	10892(2)	6628(2)	5732(1)	13(1)
C(17)	9759(2)	7117(2)	6501(1)	12(1)
C(18)	2506(2)	9047(2)	7540(1)	14(1)

C(19)	3297(2)	8310(2)	6572(1)	20(1)
C(20)	2400(2)	10418(2)	7457(2)	19(1)
C(21)	1112(2)	8989(2)	7742(2)	22(1)
C(22)	2447(2)	6687(2)	10590(1)	16(1)
C(23)	2236(2)	5611(2)	10114(2)	22(1)
C(24)	1114(2)	7606(2)	11142(2)	26(1)
C(25)	3244(2)	6148(2)	11316(1)	23(1)
C(26)	13115(2)	4158(2)	6975(1)	17(1)
C(27)	12753(2)	3458(2)	7859(2)	24(1)
C(28)	14125(2)	4744(2)	7124(2)	26(1)
C(29)	13755(3)	3207(2)	6108(2)	30(1)
C(30)	10965(2)	7102(2)	4721(1)	14(1)
C(31)	12363(2)	6600(2)	4063(1)	20(1)
C(32)	10582(2)	8524(2)	4752(2)	21(1)
C(33)	10041(2)	6682(2)	4277(1)	21(1)
C(34)	6888(2)	6747(2)	6633(1)	17(1)
C(35)	6451(2)	9623(2)	5584(2)	21(1)
C(36)	7058(2)	10045(2)	7756(2)	20(1)

Table 5. Anisotropic displacement parameters ($Å^2 x\ 10^4$) for TA17 (CCDC 279741). The anisotropic displacement factor exponent takes the form: $-2\pi^2 [h^2 a^{*2} U^{11} + ... + 2 h k a^* b^* U^{12}]$

	U^{11}	U^{22}	U^{33}	U^{23}	U^{13}	U^{12}
Ta	104(1)	125(1)	105(1)	19(1)	-29(1)	-32(1)
O(1)	107(5)	173(5)	138(5)	32(4)	-22(4)	-52(4)
O(2)	92(5)	167(5)	117(5)	25(4)	-17(4)	-16(4)
N(1)	109(5)	176(6)	116(5)	16(4)	-31(4)	-56(5)
C(1)	121(6)	148(6)	116(6)	8(4)	-25(5)	-46(5)
C(2)	118(6)	154(6)	142(6)	12(5)	-41(5)	-44(5)
C(3)	117(6)	190(7)	154(7)	20(5)	-34(5)	-66(5)
C(4)	128(6)	176(6)	111(6)	11(5)	-15(5)	-53(5)
C(5)	133(7)	212(7)	114(6)	12(5)	-34(5)	-57(6)
C(6)	110(6)	194(7)	120(6)	0(5)	-20(5)	-47(5)
C(7)	111(6)	192(7)	116(6)	14(5)	-24(5)	-56(5)
C(8)	132(7)	290(9)	116(7)	-5(6)	-15(5)	-85(6)
C(9)	151(7)	318(9)	124(7)	16(6)	-57(6)	-95(7)
C(10)	130(7)	277(8)	115(6)	25(5)	-54(5)	-92(6)
C(11)	124(6)	178(6)	108(6)	22(5)	-44(5)	-58(5)
C(12)	109(6)	157(6)	120(6)	20(5)	-35(5)	-48(5)
C(13)	133(6)	174(6)	133(6)	30(5)	-47(5)	-48(5)
C(14)	132(6)	129(6)	154(7)	10(5)	-47(5)	-32(5)
C(15)	129(6)	140(6)	138(6)	10(5)	-25(5)	-33(5)
C(16)	130(6)	123(5)	118(6)	11(4)	-22(5)	-46(5)
C(17)	113(6)	133(5)	113(6)	2(4)	-27(5)	-33(5)
C(18)	140(7)	141(6)	171(7)	27(5)	-68(5)	-55(5)
C(19)	252(9)	201(7)	161(7)	6(6)	-96(7)	-64(7)
C(20)	178(8)	152(6)	256(9)	31(6)	-83(7)	-49(6)
C(21)	183(8)	275(9)	281(9)	110(7)	-132(7)	-123(7)
C(22)	132(7)	211(7)	128(7)	18(5)	-13(5)	-63(6)
C(23)	235(9)	213(8)	233(9)	43(7)	-84(7)	-96(7)

C(24)	193(9)	286(10)	226(10)	10(7)	44(7)	-57(8)
C(25)	232(9)	329(10)	156(8)	84(7)	-57(7)	-131(8)
C(26)	161(7)	147(6)	183(7)	4(5)	-64(6)	-6(5)
C(27)	256(10)	176(7)	260(10)	66(7)	-78(8)	-26(7)
C(28)	169(8)	249(9)	365(11)	63(8)	-123(8)	-55(7)
C(29)	331(12)	220(8)	229(10)	-53(7)	-100(9)	75(8)
C(30)	164(7)	135(6)	117(6)	15(5)	-15(5)	-42(5)
C(31)	192(8)	190(7)	156(8)	4(6)	19(6)	-35(6)
C(32)	234(9)	146(7)	200(8)	34(6)	13(7)	-44(6)
C(33)	234(9)	270(9)	148(8)	1(6)	-64(7)	-85(7)
C(34)	189(8)	167(6)	160(7)	8(5)	-65(6)	-46(6)
C(35)	180(8)	237(8)	200(8)	84(6)	-67(7)	-38(7)
C(36)	214(9)	193(7)	216(8)	6(6)	-53(7)	-87(7)

Compound 6 (CCDC 619638)

Special Refinement Details

The axial benzyl group is slightly disordered as shown (the minor component is represented by the cyan) in the third figure. No restraints were used on the disordered group. The disorder ratio is approximately 70:30, see Table 2. Additionally a solvent of crystallization sits at a center of symmetry. This molecule was modeled as hexane. Based solely on the crystallographic evidence it is not possible to unambiguously exclude disordered diethylether.

Refinement of F^2 against ALL reflections. The weighted R-factor (*w*R) and goodness of fit (S) are based on F^2, conventional R-factors (R) are based on F, with F set to zero for negative F^2. The threshold expression of $F^2 > 2\sigma(F^2)$ is used only for calculating R-factors(gt) etc. and is not relevant to the choice of reflections for refinement. R-factors based on F^2 are statistically about twice as large as those based on F, and R-factors based on ALL data will be even larger.

All esds (except the esd in the dihedral angle between two l.s. planes) are estimated using the full covariance matrix. The cell esds are taken into account individually in the estimation of esds in distances, angles and torsion angles; correlations between esds in cell parameters are only used when they are defined by crystal symmetry. An approximate (isotropic) treatment of cell esds is used for estimating esds involving l.s. planes.

Table 2. Atomic coordinates (x 10^4) and equivalent isotropic displacement parameters (Å^{2}x 10^3) for TA23 (CCDC 619638). U(eq) is defined as the trace of the orthogonalized U^{ij} tensor.

	x	y	z		U_{eq}
Ta(1)	1387(1)	7854(1)	2709(1)	10(1)	1
O(1)	1734(1)	8274(1)	3500(1)	13(1)	1
O(2)	1024(1)	7139(1)	2109(1)	13(1)	1
N(1)	1353(1)	6823(1)	3376(1)	12(1)	1
C(1)	1664(1)	8202(1)	4118(1)	12(1)	1
C(2)	1597(2)	8800(1)	4503(1)	13(1)	1
C(3)	1369(2)	8668(1)	5115(1)	15(1)	1
C(4)	1237(2)	7992(1)	5357(1)	15(1)	1
C(5)	1408(2)	7423(1)	4974(1)	14(1)	1
C(6)	1633(1)	7518(1)	4353(1)	13(1)	1
C(7)	1805(2)	6876(1)	3980(1)	13(1)	1
C(8)	2396(2)	6317(1)	4285(1)	16(1)	1
C(9)	2475(2)	5674(1)	3993(1)	18(1)	1
C(10)	1890(2)	5593(1)	3412(1)	16(1)	1
C(11)	1320(1)	6163(1)	3116(1)	13(1)	1
C(12)	652(1)	6014(1)	2511(1)	13(1)	1
C(13)	66(2)	5368(1)	2444(1)	14(1)	1
C(14)	-555(2)	5178(1)	1892(1)	14(1)	1
C(15)	-496(2)	5634(1)	1382(1)	14(1)	1
C(16)	81(2)	6279(1)	1416(1)	13(1)	1
C(17)	590(1)	6479(1)	2007(1)	12(1)	1
C(18)	1755(2)	9556(1)	4262(1)	15(1)	1
C(19)	728(2)	9762(1)	3799(1)	18(1)	1
C(20)	1833(2)	10095(1)	4795(1)	20(1)	1
C(21)	2875(2)	9616(1)	3943(1)	19(1)	1
C(22)	816(2)	7884(1)	6003(1)	18(1)	1

C(23)	-501(2)	7923(1)	5925(1)	29(1)	1
C(24)	1283(2)	8460(1)	6458(1)	19(1)	1
C(25)	1173(2)	7162(1)	6286(1)	32(1)	1
C(26)	-1307(2)	4511(1)	1823(1)	16(1)	1
C(27)	-2567(2)	4741(1)	1701(1)	22(1)	1
C(28)	-1186(2)	4049(1)	2406(1)	24(1)	1
C(29)	-980(2)	4069(1)	1271(1)	23(1)	1
C(30)	176(2)	6735(1)	834(1)	16(1)	1
C(31)	-294(2)	6349(1)	239(1)	23(1)	1
C(32)	-521(2)	7421(1)	875(1)	21(1)	1
C(33)	1447(2)	6909(1)	772(1)	22(1)	1
C(34)	3211(2)	7810(1)	2496(1)	19(1)	1
C(35)	3832(2)	7196(1)	2802(1)	19(1)	1
C(36)	4456(2)	7283(1)	3382(1)	29(1)	1
C(37)	5094(2)	6741(1)	3668(1)	39(1)	1
C(38)	5118(2)	6094(1)	3387(1)	38(1)	1
C(39)	4484(2)	5978(1)	2820(1)	33(1)	1
C(40)	3839(2)	6525(1)	2533(1)	25(1)	1
C(41)	1687(2)	8903(1)	2207(1)	18(1)	1
C(42A)	1332(9)	8972(5)	1516(3)	24(2)	0.703(19)
C(43A)	2038(8)	8762(3)	1078(3)	33(1)	0.703(19)
C(44A)	1721(10)	8828(3)	445(3)	49(2)	0.703(19)
C(45A)	659(12)	9108(3)	237(3)	55(3)	0.703(19)
C(46A)	-73(8)	9314(2)	675(3)	45(2)	0.703(19)
C(47A)	253(7)	9241(3)	1309(2)	30(1)	0.703(19)
C(42B)	1590(20)	8897(12)	1540(10)	29(4)	0.297(19)
C(43B)	2531(17)	8784(6)	1164(6)	28(3)	0.297(19)
C(44B)	2440(30)	8821(6)	530(7)	57(5)	0.297(19)
C(45B)	1440(30)	8989(8)	213(6)	58(7)	0.297(19)
C(46B)	480(20)	9149(9)	517(8)	53(7)	0.297(19)
C(47B)	556(16)	9115(9)	1170(7)	39(4)	0.297(19)
C(48)	-368(2)	8313(1)	2539(1)	19(1)	1
C(49)	-944(2)	7810(1)	2936(1)	18(1)	1
C(50)	-1444(2)	7182(1)	2693(1)	23(1)	1
C(51)	-1910(2)	6691(1)	3073(1)	31(1)	1
C(52)	-1880(2)	6808(1)	3710(1)	33(1)	1
C(53)	-1408(2)	7429(1)	3960(1)	28(1)	1
C(54)	-946(2)	7919(1)	3581(1)	21(1)	1
C(61)	1933(9)	5185(4)	5871(5)	262(7)	1
C(62)	686(4)	5106(2)	5835(2)	80(1)	1
C(63)	85(6)	5242(2)	5214(2)	121(2)	1

Table 5. Anisotropic displacement parameters ($Å^2 x\ 10^4$) for TA23 (CCDC 619638). The anisotropic displacement factorexponent takes the form: $-2\pi^2[\ h^2 a^{*2} U^{11} + ... + 2\ h\ k\ a^*\ b^*\ U^{12}\ ]$

	U^{11}	U^{22}	U^{33}	U^{23}	U^{13}	U^{12}
Ta(1)	142(1)	81(1)	85(1)	6(1)	13(1)	-6(1)
O(1)	184(6)	105(5)	90(4)	0(4)	16(4)	-10(4)
O(2)	183(5)	100(4)	108(4)	-10(4)	14(4)	-27(4)
N(1)	135(6)	108(5)	109(5)	3(4)	8(4)	2(4)

C(1)	132(7)	123(6)	110(6)	11(5)	21(5)	0(5)
C(2)	161(7)	116(6)	117(6)	3(5)	18(5)	-7(5)
C(3)	206(8)	133(7)	115(6)	0(5)	24(5)	-5(6)
C(4)	199(8)	132(7)	113(6)	2(5)	25(5)	1(5)
C(5)	189(8)	116(6)	123(6)	21(5)	20(5)	-6(5)
C(6)	144(7)	121(6)	116(6)	4(5)	3(5)	3(5)
C(7)	150(7)	115(6)	120(6)	14(5)	17(5)	7(5)
C(8)	209(8)	148(7)	130(6)	-3(5)	-17(6)	39(6)
C(9)	232(9)	134(7)	156(7)	11(5)	-13(6)	50(6)
C(10)	204(8)	121(6)	163(7)	-10(5)	0(6)	19(6)
C(11)	137(7)	106(6)	146(6)	-9(5)	21(5)	-5(5)
C(12)	148(7)	116(6)	119(6)	0(5)	6(5)	-11(5)
C(13)	178(8)	113(6)	142(6)	13(5)	25(5)	-10(5)
C(14)	149(7)	108(6)	165(6)	-3(5)	13(5)	-22(5)
C(15)	176(8)	126(6)	132(6)	0(5)	8(5)	-24(5)
C(16)	158(7)	120(6)	119(6)	-2(5)	20(5)	-10(5)
C(17)	152(7)	95(6)	123(6)	1(5)	23(5)	-16(5)
C(18)	215(8)	103(6)	122(6)	9(5)	15(6)	-7(5)
C(19)	228(9)	142(7)	179(7)	8(6)	1(6)	30(6)
C(20)	330(10)	127(7)	156(7)	-22(6)	36(7)	-28(7)
C(21)	230(9)	161(7)	181(7)	32(6)	41(6)	-30(6)
C(22)	267(9)	148(6)	120(6)	8(6)	49(6)	-17(7)
C(23)	257(10)	414(12)	213(8)	-7(8)	90(7)	-97(9)
C(24)	267(9)	200(8)	119(6)	-6(6)	43(6)	-3(7)
C(25)	626(15)	186(8)	163(7)	45(7)	123(8)	8(10)
C(26)	182(8)	121(6)	174(7)	15(5)	-1(6)	-33(5)
C(27)	199(9)	172(8)	282(9)	29(7)	1(7)	-32(6)
C(28)	286(11)	180(8)	243(9)	66(7)	-24(7)	-79(7)
C(29)	291(10)	146(7)	254(9)	-41(6)	39(7)	-50(7)
C(30)	211(8)	141(7)	115(6)	14(5)	15(6)	-44(6)
C(31)	356(11)	218(8)	123(7)	-5(6)	12(7)	-88(8)
C(32)	279(10)	180(8)	178(7)	36(6)	-5(7)	14(7)
C(33)	249(10)	215(8)	194(8)	-3(6)	80(7)	-75(7)
C(34)	162(7)	183(7)	217(7)	2(6)	53(6)	-9(6)
C(35)	146(7)	208(8)	235(7)	15(7)	61(6)	-13(7)
C(36)	241(10)	295(11)	325(10)	5(8)	-27(8)	-42(8)
C(37)	310(13)	426(14)	418(13)	123(11)	-90(10)	-36(10)
C(38)	265(12)	374(13)	497(15)	201(11)	35(10)	25(9)
C(39)	318(12)	218(9)	488(14)	60(9)	166(10)	35(8)
C(40)	245(10)	239(9)	275(9)	11(7)	97(8)	20(7)
C(41)	291(10)	111(6)	147(7)	30(5)	21(6)	-3(6)
C(42A)	550(50)	51(17)	101(14)	50(10)	-20(20)	-10(20)
C(43A)	660(40)	151(13)	194(18)	15(12)	140(20)	-60(20)
C(44A)	1160(70)	197(18)	148(18)	-10(14)	190(30)	-130(30)
C(45A)	1270(80)	210(17)	136(16)	35(15)	-170(30)	-200(30)
C(46A)	860(50)	150(16)	270(20)	62(14)	-240(20)	-80(20)
C(47A)	550(30)	166(15)	154(17)	66(13)	-119(17)	-46(17)
C(42B)	420(80)	70(50)	330(50)	80(30)	-150(50)	0(40)
C(43B)	590(80)	130(30)	160(40)	10(30)	190(50)	20(50)
C(44B)	1310(170)	150(40)	270(50)	20(30)	210(80)	-40(70)
C(45B)	1310(190)	250(50)	160(40)	20(40)	-70(80)	-360(80)
C(46B)	970(150)	270(70)	290(60)	150(60)	-350(90)	-290(80)
C(47B)	570(90)	300(70)	290(60)	90(50)	30(50)	-220(60)
C(48)	177(8)	203(8)	172(7)	-17(6)	-7(6)	33(6)

C(49)	126(7)	221(8)	191(7)	-21(7)	7(5)	39(6)
C(50)	160(8)	283(9)	250(8)	-75(8)	18(6)	-16(7)
C(51)	248(11)	304(11)	381(12)	-49(9)	69(9)	-62(8)
C(52)	256(11)	380(12)	367(12)	60(10)	93(9)	-36(9)
C(53)	228(10)	382(11)	221(8)	14(8)	41(7)	44(8)
C(54)	159(8)	270(9)	197(7)	-22(7)	-1(6)	46(7)
C(61)	3760(160)	1340(70)	3140(140)	210(80)	2380(130)	530(90)
C(62)	1030(40)	690(30)	700(30)	130(20)	220(30)	-140(30)
C(63)	2240(70)	690(30)	650(30)	140(20)	-150(40)	-520(40)

Compound 9 (CCDC 618859)

Special Refinement Details

Refinement of F^2 against ALL reflections. The weighted R-factor (*w*R) and goodness of fit (S) are based on F^2, conventional R-factors (R) are based on F, with F set to zero for negative F^2. The threshold expression of $F^2 > 2\sigma(F^2)$ is used only for calculating R-factors(gt) etc. and is not relevant to the choice of reflections for refinement. R-factors based on F^2 are statistically about twice as large as those based on F, and R-factors based on ALL data will be even larger.

All esds (except the esd in the dihedral angle between two l.s. planes) are estimated using the full covariance matrix. The cell esds are taken into account individually in the estimation of esds in distances, angles and torsion angles; correlations between esds in cell parameters are only used when they are defined by crystal symmetry. An approximate (isotropic) treatment of cell esds is used for estimating esds involving l.s. planes.

Table 2. Atomic coordinates (x 10^4) and equivalent isotropic displacement parameters ($Å^2$x 10^3) for TA22 (CCDC 618859). U(eq) is defined as the trace of the orthogonalized U_{ij} tensor.

	x	y	z	U_{eq}
Ta(1)	1893(1)	1412(1)	1243(1)	10(1)
F(1)	1349(1)	1374(1)	2528(1)	16(1)
F(2)	2457(1)	1444(1)	-42(1)	19(1)
O(1)	3020(1)	1000(1)	2177(1)	13(1)
O(2)	1184(1)	1987(1)	640(1)	13(1)
N(1)	3187(1)	1957(1)	2732(1)	10(1)
C(1)	4093(1)	972(1)	2883(2)	12(1)
C(2)	4673(1)	574(1)	2838(2)	13(1)
C(3)	5778(1)	580(1)	3605(2)	14(1)
C(4)	6304(1)	958(1)	4385(2)	13(1)
C(5)	5688(1)	1341(1)	4408(2)	13(1)
C(6)	4578(1)	1353(1)	3680(2)	11(1)
C(7)	3979(1)	1767(1)	3800(2)	11(1)
C(8)	4283(1)	1966(1)	5016(2)	14(1)
C(9)	3806(2)	2376(1)	5161(2)	14(1)
C(10)	3086(1)	2594(1)	4073(2)	13(1)
C(11)	2808(1)	2386(1)	2863(2)	11(1)
C(12)	2123(1)	2659(1)	1714(2)	11(1)
C(13)	2262(1)	3144(1)	1750(2)	13(1)
C(14)	1613(2)	3432(1)	747(2)	13(1)
C(15)	817(1)	3214(1)	-305(2)	13(1)
C(16)	638(1)	2733(1)	-407(2)	12(1)
C(17)	1319(1)	2457(1)	630(2)	11(1)
C(18)	4131(2)	157(1)	1963(2)	17(1)
C(19)	3203(2)	-28(1)	2262(2)	22(1)
C(20)	4900(2)	-252(1)	2149(2)	27(1)
C(21)	3726(2)	313(1)	546(2)	22(1)
C(22)	7520(1)	975(1)	5155(2)	15(1)
C(23)	7990(2)	1333(1)	4519(2)	21(1)
C(24)	8054(2)	498(1)	5192(2)	21(1)
C(25)	7790(2)	1129(1)	6553(2)	20(1)
C(26)	1796(2)	3962(1)	814(2)	16(1)

C(27)	2795(2)	4066(1)	563(2)	24(1)
C(28)	1960(2)	4150(1)	2147(2)	36(1)
C(29)	853(2)	4223(1)	-205(2)	20(1)
C(30)	-298(1)	2524(1)	-1568(2)	13(1)
C(31)	-813(2)	2893(1)	-2621(2)	18(1)
C(32)	58(2)	2118(1)	-2195(2)	17(1)
C(33)	-1145(2)	2349(1)	-1103(2)	17(1)
C(34)	688(2)	916(1)	36(2)	17(1)
C(35)	-164(2)	782(1)	496(2)	19(1)
C(36)	-1064(2)	1059(1)	220(2)	29(1)
C(37)	-1822(2)	955(1)	708(3)	43(1)
C(38)	-1685(2)	568(1)	1482(3)	50(1)
C(39)	-810(2)	282(1)	1744(2)	41(1)
C(40)	-57(2)	387(1)	1256(2)	28(1)

C(51)	5821(2)	2926(1)	3957(3)	45(1)
C(52)	6342(2)	2764(1)	5204(3)	45(1)
C(53)	6228(2)	2999(1)	6204(3)	39(1)
C(54)	5580(2)	3390(1)	5954(2)	32(1)
C(55)	5064(2)	3546(1)	4708(2)	31(1)
C(56)	5190(2)	3315(1)	3720(2)	40(1)

Table 5. Anisotropic displacement parameters ($Å^2 x\ 10^4$) for TA22 (CCDC 618859). The anisotropic displacement factorexponent takes the form: $-2\pi^2[h^2 a^{*2} U_{11} + ... + 2\ h\ k\ a^*\ b^*\ U_{12}]$

	U_{11}	U_{22}	U_{33}	U_{23}	U_{13}	U_{12}
Ta(1)	103(1)	76(1)	106(1)	-4(1)	38(1)	-8(1)
F(1)	161(5)	178(6)	157(5)	3(4)	92(4)	-12(5)
F(2)	266(6)	137(5)	215(5)	21(5)	159(5)	9(5)
O(1)	104(5)	92(6)	166(6)	-11(4)	39(5)	-12(5)
O(2)	125(6)	92(6)	140(6)	-1(4)	21(5)	1(5)
N(1)	105(6)	81(6)	123(6)	-8(5)	44(5)	-2(5)
C(1)	114(7)	115(8)	126(7)	11(6)	49(6)	0(6)
C(2)	131(7)	105(8)	159(8)	-2(6)	64(6)	-4(6)
C(3)	127(7)	108(8)	192(8)	6(6)	68(7)	25(6)
C(4)	120(7)	108(8)	156(8)	6(6)	49(6)	10(6)
C(5)	125(7)	119(9)	144(7)	-6(6)	47(6)	-3(6)
C(6)	115(7)	103(8)	123(7)	-2(5)	52(6)	7(6)
C(7)	114(7)	90(7)	137(7)	-2(6)	57(6)	1(6)
C(8)	126(7)	154(8)	120(7)	2(6)	42(6)	-5(6)
C(9)	144(8)	153(8)	116(7)	-26(6)	58(6)	-7(7)
C(10)	139(8)	112(8)	143(7)	-36(6)	68(6)	0(6)
C(11)	97(7)	115(8)	122(7)	1(6)	40(6)	-8(6)
C(12)	118(7)	91(7)	117(7)	7(5)	45(6)	3(6)
C(13)	125(7)	108(8)	140(7)	-21(6)	48(6)	-8(6)
C(14)	153(8)	100(7)	155(8)	-2(6)	81(6)	4(6)
C(15)	149(8)	116(8)	137(7)	21(6)	66(6)	19(6)
C(16)	110(7)	121(8)	136(7)	-1(6)	61(6)	9(6)
C(17)	128(7)	80(7)	145(7)	1(6)	68(6)	7(6)
C(18)	166(8)	98(8)	211(9)	-38(6)	54(7)	2(7)
C(19)	226(10)	125(9)	292(10)	-18(7)	90(8)	-31(8)
C(20)	252(11)	133(9)	351(12)	-77(8)	54(9)	30(8)
C(21)	256(10)	183(10)	200(9)	-66(7)	72(8)	-10(8)
C(22)	103(7)	130(8)	190(8)	13(6)	37(6)	2(6)
C(23)	158(8)	165(10)	310(10)	35(7)	104(8)	-6(7)
C(24)	140(8)	141(9)	311(11)	16(8)	51(8)	23(7)
C(25)	153(9)	208(10)	204(9)	9(7)	23(7)	-12(8)
C(26)	213(9)	87(8)	168(8)	-4(6)	74(7)	8(7)
C(27)	161(9)	136(9)	377(12)	-5(8)	57(9)	-46(8)
C(28)	726(19)	142(10)	219(10)	-29(8)	197(12)	43(11)
C(29)	175(9)	99(8)	302(10)	27(7)	80(8)	14(7)
C(30)	117(7)	131(8)	135(7)	0(6)	53(6)	1(6)
C(31)	154(8)	182(9)	156(8)	24(7)	15(7)	-10(7)
C(32)	174(8)	191(10)	142(8)	-31(7)	65(7)	7(7)
C(33)	143(8)	185(9)	195(9)	10(7)	81(7)	-10(7)
C(34)	192(9)	126(9)	187(9)	-30(6)	62(7)	-27(7)
C(35)	172(8)	183(9)	185(8)	-68(7)	57(7)	-75(7)

C(36)	224(10)	237(12)	403(13)	-131(10)	132(10)	-61(9)
C(37)	254(12)	469(17)	613(18)	-344(15)	236(13)	-166(12)
C(38)	467(16)	710(20)	447(16)	-374(15)	321(14)	-436(16)
C(39)	489(16)	471(17)	262(12)	-54(11)	154(12)	-319(14)
C(40)	292(12)	259(12)	258(11)	-3(9)	69(9)	-119(9)
C(51)	252(12)	600(20)	455(16)	-294(14)	118(12)	11(13)
C(52)	187(11)	237(13)	770(20)	-77(13)	33(13)	4(10)
C(53)	263(12)	425(16)	331(13)	102(11)	-30(10)	-139(11)
C(54)	316(12)	386(14)	292(12)	-112(10)	162(10)	-124(11)
C(55)	243(10)	314(13)	381(12)	-1(10)	127(9)	42(10)
C(56)	270(12)	670(20)	227(11)	-9(12)	63(10)	59(13)

Compound 10-P (CCDC 618398)

Special Refinement Details

The tBu group defined by C(26)-C(29) is disordered. The model includes the disorder without geometric restrainsts. The total site occupancy was restrained to one.Refinement of F2 against ALL reflections. The weighted R-factor (*w*R) and goodness of fit (S) are based on F2, conventional R-factors (R) are based on F, with F set to zero for negative F2. The threshold expression of F2 >2σ(F2) is used only for calculating R-factors(gt) etc. and is not relevant to the choice of reflections for refinement. R-factors based on F2 are statistically about twice as large as those based on F, and R-factors based on ALL data will be even larger. All esds (except the esd in the dihedral angle between two l.s. planes) are estimated using the fullcovariance matrix. The cell esds are taken into account individually in the estimation of esds in distances, angles and torsion angles; correlations between esds in cell parameters are only used when they are defined by crystal symmetry. An approximate (isotropic) treatment of cell esds is used for estimating esds involving l.s. planes.

Table 2. Atomic coordinates (x 104) and equivalent isotropic displacement parameters (Å2x 103) for TA21 (CCDC 618398). U(eq) is defined as the trace of the orthogonalized Uij tensor.

	x	y	z	U_{eq}	Occ
Ta(1)	2669(1)	179(1)	7973(1)	13(1)	1
P(1)	3177(1)	560(1)	7168(1)	21(1)	1
O(1)	3118(1)	-135(1)	7774(1)	17(1)	1
O(2)	2167(1)	453(1)	7830(1)	16(1)	1
N(1)	2368(1)	10(1)	6822(1)	13(1)	1
C(1)	3127(1)	-408(1)	7440(1)	16(1)	1
C(2)	3369(1)	-661(1)	7720(1)	17(1)	1
C(3)	3353(1)	-937(1)	7356(1)	18(1)	1
C(4)	3108(1)	-976(1)	6729(1)	16(1)	1
C(5)	2880(1)	-721(1)	6467(1)	16(1)	1
C(6)	2890(1)	-438(1)	6803(1)	15(1)	1
C(7)	2638(1)	-185(1)	6450(1)	14(1)	1
C(8)	2662(1)	-173(1)	5719(1)	16(1)	1
C(9)	2395(1)	32(1)	5360(1)	17(1)	1
C(10)	2088(1)	210(1)	5730(1)	16(1)	1
C(11)	2074(1)	193(1)	6461(1)	14(1)	1
C(12)	1709(1)	370(1)	6824(1)	15(1)	1
C(13)	1285(1)	410(1)	6484(1)	18(1)	1
C(14)	934(1)	583(1)	6765(1)	21(1)	1
C(15)	1010(1)	714(1)	7429(1)	21(1)	1
C(16)	1418(1)	676(1)	7803(1)	17(1)	1
C(17)	1767(1)	499(1)	7488(1)	15(1)	1
C(18)	3660(1)	-634(1)	8392(1)	21(1)	1
C(19)	4057(1)	-408(1)	8246(1)	25(1)	1
C(20)	3368(1)	-524(1)	9013(1)	25(1)	1
C(21)	3874(1)	-940(1)	8608(1)	30(1)	1
C(22)	3088(1)	-1277(1)	6334(1)	21(1)	1
C(23)	2597(1)	-1402(1)	6364(2)	32(1)	1
C(24)	3415(1)	-1516(1)	6617(2)	31(1)	1
C(25)	3207(1)	-1223(1)	5557(1)	31(1)	1
C(26)	482(1)	634(1)	6373(2)	37(1)	1
C(27A)	264(2)	273(2)	6250(4)	38(2)	0.496(7)
C(28A)	555(3)	754(2)	5682(4)	51(2)	0.496(7)

C(29A)	104(3)	776(2)	6792(5)	42(2)	0.496(7)
C(27B)	509(3)	1014(2)	6161(4)	49(2)	0.504(7)
C(28B)	81(2)	605(2)	6812(4)	37(2)	0.504(7)
C(29B)	455(2)	489(2)	5697(3)	42(2)	0.504(7)
C(30)	1491(1)	826(1)	8527(1)	20(1)	1
C(31)	1071(1)	1011(1)	8753(2)	31(1)	1
C(32)	1565(1)	577(1)	9092(1)	24(1)	1
C(33)	1903(1)	1047(1)	8502(1)	25(1)	1
C(34)	3726(1)	660(1)	7562(2)	47(1)	1
C(35)	2888(2)	925(1)	7046(2)	46(1)	1
C(36)	3356(1)	449(1)	6290(1)	22(1)	1
C(37)	3641(1)	196(1)	6222(1)	25(1)	1
C(38)	3796(1)	97(1)	5569(2)	36(1)	1
C(39)	3655(1)	253(1)	4973(2)	39(1)	1
C(40)	3367(1)	497(1)	5024(1)	36(1)	1
C(41)	3212(1)	601(1)	5689(1)	30(1)	1
C(42)	2932(1)	396(1)	8798(1)	19(1)	1
C(43)	3286(1)	424(1)	9324(1)	20(1)	1
C(44)	3692(1)	254(1)	9293(2)	27(1)	1
C(45)	4013(1)	258(1)	9831(2)	36(1)	1
C(46)	3932(1)	438(1)	10422(2)	40(1)	1
C(47)	3541(1)	616(1)	10453(2)	36(1)	1
C(48)	3225(1)	614(1)	9910(1)	26(1)	1
C(49)	2208(1)	-166(1)	8523(1)	14(1)	1
C(50)	1885(1)	-341(1)	8095(1)	20(1)	1
C(51)	1999(1)	-624(1)	7828(1)	23(1)	1
C(52)	1700(1)	-787(1)	7394(1)	30(1)	1
C(53)	1274(1)	-666(1)	7228(1)	31(1)	1
C(54)	1141(1)	-386(1)	7502(1)	31(1)	1
C(55)	1445(1)	-224(1)	7931(2)	23(1)	1
C(61)	1945(1)	1505(1)	6502(2)	42(1)	1
C(62)	2261(1)	1636(1)	6061(2)	49(1)	1
C(63)	2376(1)	1493(1)	5432(2)	48(1)	1
C(64)	2172(1)	1226(1)	5256(2)	43(1)	1
C(65)	1856(2)	1092(1)	5694(2)	45(1)	1
C(66)	1741(1)	1231(1)	6315(2)	44(1)	1
C(71)	-329(1)	758(1)	1047(2)	45(1)	1
C(72)	-131(1)	494(1)	1301(2)	46(1)	1
C(73)	342(1)	482(1)	1408(2)	43(1)	1
C(74)	612(1)	734(1)	1270(2)	46(1)	1
C(75)	411(2)	1001(1)	1019(2)	49(1)	1
C(76)	-58(1)	1010(1)	908(2)	47(1)	1
C(81)	0 0 9751(3)	53(2)	1		
C(82)	233(2)	226(1)	9391(2)	53(1)	1
C(83)	238(2)	221(1)	8683(2)	58(1)	1
C(84)	0 0 8331(3)	74(2)	1		

Table 5. Anisotropic displacement parameters (Å ^{2}x 10^4) for TA21 (CCDC 618398). The anisotropic displacement factor exponent takes the form: -2π ^{2}[h^{2}a*^{2}U$_{11}$ + ... + 2 h k a* b* U$_{12}$]

	U$_{11}$	U$_{22}$	U$_{33}$	U$_{23}$	U$_{13}$	U$_{12}$
Ta(1)	145(1)	139(1)	108(1)	-12(1)	-10(1)	-3(1)

P(1)	214(3)	209(3)	191(3)	-31(2)	35(2)	-70(3)
O(1)	180(8)	201(8)	136(7)	-26(5)	-36(5)	29(7)
O(2)	177(7)	158(7)	147(7)	-19(5)	2(6)	8(6)
N(1)	145(8)	115(7)	117(7)	4(5)	-16(7)	-3(7)
C(1)	129(10)	192(10)	147(9)	6(7)	4(8)	36(8)
C(2)	159(10)	205(11)	139(8)	2(7)	0(8)	42(9)
C(3)	181(11)	182(11)	182(10)	14(8)	0(9)	36(9)
C(4)	181(11)	148(10)	166(9)	-9(7)	27(8)	2(8)
C(5)	166(10)	178(10)	143(9)	-18(7)	9(8)	10(8)
C(6)	149(10)	160(10)	140(9)	-5(7)	8(8)	18(8)
C(7)	142(9)	138(8)	132(7)	-7(7)	-15(7)	-17(8)
C(8)	174(10)	175(10)	130(8)	-20(8)	23(8)	-3(9)
C(9)	194(10)	193(10)	121(10)	5(7)	-5(8)	-3(9)
C(10)	185(11)	178(11)	131(8)	12(7)	-17(8)	23(9)
C(11)	138(9)	140(9)	126(8)	1(7)	-14(7)	-5(8)
C(12)	186(11)	138(10)	128(8)	20(7)	21(8)	9(8)
C(13)	202(11)	176(11)	150(9)	6(8)	-19(8)	28(9)
C(14)	188(12)	256(13)	194(10)	20(9)	-20(9)	54(10)
C(15)	219(12)	198(11)	221(10)	-18(8)	27(9)	66(10)
C(16)	169(10)	155(10)	172(10)	1(7)	25(8)	18(8)
C(17)	159(10)	131(9)	149(9)	15(7)	18(8)	0(8)
C(18)	244(13)	210(12)	176(10)	-17(8)	-67(9)	57(10)
C(19)	197(12)	298(14)	262(11)	-71(10)	-59(10)	48(11)
C(20)	302(14)	296(14)	155(10)	7(9)	-36(10)	64(12)
C(21)	365(16)	293(14)	241(12)	-8(10)	-120(11)	105(13)
C(22)	260(13)	158(10)	207(10)	-17(8)	-3(9)	28(9)
C(23)	324(16)	243(14)	385(15)	-41(11)	-11(13)	-55(12)
C(24)	421(18)	199(13)	308(13)	-27(10)	-27(13)	57(12)
C(25)	426(16)	249(12)	241(13)	-66(10)	21(12)	75(12)
C(26)	223(14)	620(20)	262(13)	-20(13)	-45(11)	185(15)
C(27A)	180(30)	380(40)	560(40)	-130(30)	-140(30)	30(20)
C(28A)	350(40)	780(70)	400(40)	260(40)	-100(30)	80(40)
C(29A)	240(30)	550(50)	480(40)	-180(40)	-120(30)	130(40)
C(27B)	380(40)	340(40)	740(50)	220(30)	-220(40)	80(30)
C(28B)	180(30)	610(50)	320(30)	-40(40)	-30(20)	10(40)
C(29B)	280(30)	690(60)	300(30)	-120(30)	-60(20)	180(40)
C(30)	231(12)	181(11)	199(10)	-45(8)	20(9)	46(10)
C(31)	344(16)	305(15)	275(13)	-94(11)	23(12)	123(13)
C(32)	303(14)	225(12)	185(10)	-30(9)	22(10)	33(11)
C(33)	332(15)	180(12)	236(11)	-67(9)	22(11)	-26(11)
C(34)	372(19)	790(30)	246(13)	-152(15)	58(13)	-341(19)
C(35)	680(30)	205(14)	501(18)	74(13)	290(18)	-18(16)
C(36)	207(12)	268(13)	185(10)	2(9)	0(9)	-110(10)
C(37)	209(12)	313(14)	235(11)	-46(10)	25(10)	-57(11)
C(38)	259(13)	476(18)	355(16)	-141(13)	91(12)	-78(13)
C(39)	385(18)	570(20)	220(12)	-104(13)	65(12)	-216(16)
C(40)	422(19)	452(19)	192(12)	61(11)	-45(12)	-213(16)
C(41)	306(15)	336(16)	253(12)	75(10)	-29(11)	-122(13)
C(42)	200(11)	203(11)	164(9)	29(8)	14(9)	-38(9)
C(43)	251(13)	190(11)	156(9)	-14(8)	-19(9)	-39(10)
C(44)	272(14)	268(14)	276(12)	-57(10)	-80(11)	6(11)
C(45)	347(17)	321(16)	427(16)	-43(12)	-176(14)	56(13)
C(46)	496(19)	368(15)	320(14)	-3(14)	-228(16)	-30(14)
C(47)	504(18)	354(14)	222(11)	-62(13)	-128(15)	-40(13)
C(48)	352(15)	247(13)	185(10)	-52(9)	-41(11)	-22(11)
C(49)	145(9)	155(9)	114(8)	38(7)	17(7)	-4(8)
C(50)	219(11)	213(11)	160(11)	40(7)	7(8)	-79(9)
C(51)	180(11)	282(13)	236(12)	28(9)	32(9)	-53(10)

C(52)	376(17)	280(14)	251(12)	-84(10)	71(12)	-132(13)
C(53)	362(16)	399(17)	178(11)	3(10)	13(11)	-204(14)
C(54)	292(15)	371(16)	264(12)	98(11)	-64(11)	-121(13)
C(55)	210(10)	227(12)	242(11)	36(11)	-27(13)	-19(9)
C(61)	470(20)	450(20)	344(15)	25(13)	-61(15)	24(17)
C(62)	420(20)	500(20)	540(20)	-3(17)	-102(17)	-164(18)
C(63)	306(15)	720(30)	412(16)	130(19)	-36(18)	-104(16)
C(64)	470(20)	480(20)	352(16)	21(14)	-10(14)	78(17)
C(65)	630(30)	267(16)	465(18)	101(13)	-56(17)	-18(17)
C(66)	540(20)	368(18)	413(17)	183(14)	53(16)	-73(17)
C(71)	292(17)	720(30)	349(16)	-14(16)	-13(13)	-49(18)
C(72)	440(20)	580(20)	370(16)	-62(15)	-33(15)	-153(19)
C(73)	460(20)	470(20)	376(16)	-70(14)	-43(15)	11(17)
C(74)	297(17)	720(30)	361(16)	-50(16)	-42(14)	-96(18)
C(75)	500(20)	600(30)	365(17)	62(16)	-32(16)	-220(20)
C(76)	460(20)	620(30)	323(15)	90(15)	-38(15)	-5(19)
C(81)	630(40)	650(40)	320(20)	0	0	-150(30)
C(82)	580(30)	540(30)	470(20)	52(17)	-121(19)	-180(20)
C(83)	810(30)	470(20)	449(19)	143(16)	20(20)	-50(20)
C(84)	1470(80)	410(30)	330(20)	0	0	20(40)

Compound 11 (CCDC 607404)

Special Refinement Details

Refinement of F^2 against ALL reflections. The weighted R-factor (*w*R) and goodness of fit (S) are based on F^2, conventional R-factors (R) are based on F, with F set to zero for negative F^2. The threshold expression of $F^2 > 2\sigma(F^2)$ is used only for calculating R-factors(gt) etc. and is not relevant to the choice of reflections for refinement. R-factors based on F^2 are statistically about twice as large as those based on F, and R-factors based on ALL data will be even larger. All esds (except the esd in the dihedral angle between two l.s. planes) are estimated using the full covariance matrix. The cell esds are taken into account individually in the estimation of esds in distances, angles and torsion angles; correlations between esds in cell parameters are only used when they are defined by crystal symmetry. An approximate (isotropic) treatment of cell esds is used for estimating esds involving l.s. planes.

Table 2. Atomic coordinates (x 10^4) and equivalent isotropic displacement parameters ($Å^2$x 10^3) for TA20 (CCDC 607404). U(eq) is defined as the trace of the orthogonalized U^{ij} tensor.

	x	y	z	U_{eq}
Ta(1)	7895(1)	5616(1)	7513(1)	19(1)
S(1)	10446(1)	4787(1)	6362(1)	16(1)
O(1)	8898(3)	4632(3)	8262(2)	18(1)
O(2)	7879(3)	6409(3)	6385(2)	18(1)
C(1)	10011(5)	3843(4)	8448(3)	16(1)
C(2)	9829(5)	3144(4)	9236(3)	19(1)
C(3)	10990(5)	2294(4)	9336(3)	18(1)
C(4)	12285(5)	2152(4)	8721(3)	20(1)
C(5)	12460(5)	2945(4)	7997(3)	19(1)
C(6)	11338(5)	3802(4)	7858(3)	17(1)
C(7)	11514(4)	4687(4)	7127(3)	16(1)
C(8)	12232(5)	5627(4)	6999(3)	17(1)
C(9)	11842(5)	6476(4)	6358(3)	19(1)
C(10)	10812(5)	6197(4)	5981(3)	17(1)
C(11)	9978(5)	6904(4)	5411(3)	16(1)
C(12)	10598(5)	7601(4)	4698(3)	18(1)
C(13)	9816(5)	8321(4)	4177(3)	19(1)
C(14)	8375(5)	8262(4)	4366(3)	19(1)
C(15)	7681(5)	7600(4)	5075(3)	16(1)
C(16)	8513(5)	6963(4)	5619(3)	17(1)
C(17)	8450(5)	3280(4)	9956(3)	21(1)
C(18)	7274(5)	2910(5)	9573(3)	23(1)
C(19)	8022(5)	4579(5)	10272(3)	29(1)
C(20)	8570(5)	2490(5)	10783(3)	29(1)
C(21)	13489(5)	1143(4)	8803(3)	23(1)
C(22)	14838(5)	1647(5)	8745(4)	40(2)
C(23)	13716(6)	277(5)	8032(4)	39(2)
C(24)	13174(5)	431(5)	9676(3)	30(1)
C(25)	10454(5)	9139(4)	3427(3)	20(1)
C(26)	11921(5)	9342(5)	3500(4)	33(1)
C(27)	10583(6)	8609(5)	2521(3)	29(1)
C(28)	9515(5)	10367(4)	3476(4)	30(1)
C(29)	6080(5)	7582(4)	5244(3)	21(1)

C(30)	5436(5)	8298(5)	4526(3)	26(1)
C(31)	5343(5)	8148(5)	6162(3)	25(1)
C(32)	5828(5)	6285(4)	5219(3)	24(1)
C(33)	8038(6)	7290(5)	8079(4)	35(1)
C(34)	5840(5)	6080(6)	8451(4)	43(2)
C(35)	6642(5)	4345(5)	7197(4)	32(1)

Table 5. Anisotropic displacement parameters ($Å^2 x\ 10^4$) for TA20 (CCDC 607404). The anisotropic displacement factor exponent takes the form: $-2\pi^2$ [$h^2 a^{*2} U^{11}$ + ... + 2 h k a* b* U^{12}]

	U^{11}	U^{22}	U^{33}	U^{23}	U^{13}	U^{12}
Ta(1)	125(1)	221(1)	200(1)	13(1)	-18(1)	-31(1)
S(1)	137(6)	176(7)	185(7)	8(5)	-55(5)	-39(5)
O(1)	111(17)	226(19)	169(19)	34(15)	17(14)	-9(14)
O(2)	113(17)	280(20)	149(19)	34(15)	-33(14)	-30(14)
C(1)	120(20)	150(30)	220(30)	-20(20)	-70(20)	-20(20)
C(2)	230(30)	220(30)	170(30)	10(20)	-90(20)	-120(20)
C(3)	210(30)	210(30)	170(30)	0(20)	-90(20)	-90(20)
C(4)	220(30)	230(30)	170(30)	20(20)	-80(20)	-110(20)
C(5)	140(30)	210(30)	240(30)	-40(20)	-40(20)	-60(20)
C(6)	210(30)	150(30)	180(30)	20(20)	-70(20)	-50(20)
C(7)	80(20)	210(30)	180(30)	-10(20)	0(20)	-10(20)
C(8)	90(20)	240(30)	210(30)	10(20)	-70(20)	-30(20)
C(9)	160(30)	210(30)	200(30)	-40(20)	-20(20)	-30(20)
C(10)	130(20)	140(30)	180(30)	20(20)	20(20)	20(20)
C(11)	140(20)	120(30)	220(30)	-30(20)	-50(20)	-30(20)
C(12)	150(30)	180(30)	210(30)	-50(20)	-40(20)	-60(20)
C(13)	240(30)	180(30)	170(30)	-50(20)	-30(20)	-100(20)
C(14)	160(30)	170(30)	250(30)	0(20)	-100(20)	-20(20)
C(15)	160(30)	130(30)	200(30)	-30(20)	-60(20)	-20(20)
C(16)	170(30)	180(30)	170(30)	-10(20)	-20(20)	-60(20)
C(17)	200(30)	240(30)	200(30)	0(20)	-60(20)	-70(20)
C(18)	180(30)	320(30)	220(30)	-10(20)	-30(20)	-120(20)
C(19)	230(30)	370(30)	250(30)	-80(30)	10(20)	-110(20)
C(20)	260(30)	410(40)	210(30)	30(30)	-20(20)	-140(30)
C(21)	200(30)	230(30)	280(30)	70(20)	-110(20)	-50(20)
C(22)	280(30)	350(40)	610(40)	240(30)	-190(30)	-90(30)
C(23)	470(40)	350(40)	310(40)	20(30)	-110(30)	100(30)
C(24)	300(30)	310(30)	290(30)	100(30)	-140(30)	-40(30)
C(25)	260(30)	170(30)	180(30)	30(20)	-80(20)	-60(20)
C(26)	320(30)	380(40)	370(40)	160(30)	-160(30)	-200(30)
C(27)	360(30)	300(30)	220(30)	40(20)	-60(30)	-110(30)
C(28)	320(30)	250(30)	320(30)	40(30)	-40(30)	-90(30)
C(29)	140(30)	240(30)	220(30)	-30(20)	-30(20)	-10(20)
C(30)	180(30)	270(30)	330(30)	-20(30)	-80(20)	0(20)
C(31)	170(30)	270(30)	320(30)	-30(30)	-70(20)	0(20)
C(32)	150(30)	310(30)	270(30)	-10(20)	-30(20)	-60(20)
C(33)	440(40)	270(30)	380(40)	40(30)	-150(30)	-80(30)
C(34)	210(30)	610(50)	430(40)	-50(30)	0(30)	-40(30)
C(35)	260(30)	460(40)	260(30)	100(30)	-120(30)	-60(30)

Compound 12 (CCDC 620252)

Special Refinement Details

Refinement of F^2 against ALL reflections. The weighted R-factor (*w*R) and goodness of fit (S) are based on F^2, conventional R-factors (R) are based on F, with F set to zero for negative F^2. The threshold expression of $F^2 > 2\sigma(F^2)$ is used only for calculating R-factors(gt) etc. and is not relevant to the choice of reflections for refinement. R-factors based on F^2 are statistically about twice as large as those based on F, and R-factors based on ALL data will be even larger. All esds (except the esd in the dihedral angle between two l.s. planes) are estimated using the full covariance matrix. The cell esds are taken into account individually in the estimation of esds in distances, angles and torsion angles; correlations between esds in cell parameters are only used when they are defined by crystal symmetry. An approximate (isotropic) treatment of cell esds is used for estimating esds involving l.s. planes.

Table 2. Atomic coordinates (x 10^4) and equivalent isotropic displacement parameters ($Å^2$x 10^3) for TA26 (CCDC 620252). U(eq) is defined as the trace of the orthogonalized U^{ij} tensor.

	x	y	z	U_{eq}
Ta(1)	0	2879(1)	2500	14(1)
Cl(1)	466(1)	2849(1)	4538(1)	34(1)
O(1)	517(1)	2467(1)	1746(1)	18(1)
O(2)	0	657(2)	2500	17(1)
C(1)	838(1)	1629(2)	1515(2)	14(1)
C(2)	1240(1)	2043(2)	1049(2)	15(1)
C(3)	1557(1)	1137(2)	841(2)	16(1)
C(4)	1498(1)	-124(2)	1075(2)	16(1)
C(5)	1100(1)	-488(2)	1528(2)	18(1)
C(6)	761(1)	378(2)	1744(2)	16(1)
C(7)	349(1)	-120(2)	2162(2)	19(1)
C(8)	218(1)	-1311(2)	2293(3)	31(1)
C(9)	1320(1)	3408(2)	793(2)	20(1)
C(10)	1782(1)	3630(2)	303(2)	29(1)
C(11)	940(1)	3890(2)	-250(2)	31(1)
C(12)	1336(1)	4162(2)	2044(2)	28(1)
C(13)	1864(1)	-1062(2)	803(2)	18(1)
C(14)	1861(1)	-1109(4)	-653(3)	58(1)
C(15)	1781(1)	-2338(3)	1280(5)	60(1)
C(16)	2338(1)	-638(3)	1427(4)	58(1)
C(17)	0	4869(2)	2500	20(1)

Table 5. Anisotropic displacement parameters ($Å^2$x 10^4) for TA26 (CCDC 620252). The anisotropic displacement factor exponent takes the form: $-2\pi^2[h^2a^{*2}U^{11} + ... + 2 h k a^* b^* U^{12}]$

	U^{11}	U^{22}	U^{33}	U^{23}	U^{13}	U^{12}
Ta(1)	92(1)	107(1)	218(1)	0	44(1)	0
Cl(1)	257(2)	455(3)	281(2)	50(2)	-14(2)	-6(2)
O(1)	129(5)	138(5)	276(7)	18(5)	80(4)	4(4)

O(2)	135(7)	123(7)	259(9)	0	97(6)	0
C(1)	113(6)	143(7)	188(7)	5(6)	56(5)	4(5)
C(2)	114(6)	161(7)	173(7)	5(6)	39(4)	-1(5)
C(3)	113(6)	181(7)	188(7)	5(6)	47(5)	3(5)
C(4)	121(6)	173(7)	185(7)	-5(6)	50(5)	21(5)
C(5)	152(6)	138(6)	251(8)	2(6)	84(5)	7(5)
C(6)	131(6)	145(6)	227(8)	-7(6)	76(5)	9(5)
C(7)	169(7)	133(6)	308(9)	-4(6)	129(6)	24(5)
C(8)	284(9)	129(7)	596(15)	-5(9)	300(10)	17(7)
C(9)	162(7)	170(8)	285(9)	39(7)	83(6)	-11(5)
C(10)	229(8)	222(8)	440(12)	32(9)	169(8)	-38(7)
C(11)	248(9)	304(11)	392(12)	182(9)	87(8)	47(7)
C(12)	232(8)	191(8)	433(12)	-87(8)	146(8)	-63(7)
C(13)	131(6)	186(7)	236(8)	-4(6)	62(5)	31(5)
C(14)	669(19)	720(20)	340(13)	-91(14)	77(12)	468(18)
C(15)	462(16)	329(14)	1140(30)	318(17)	520(20)	239(12)
C(16)	146(9)	447(16)	1110(30)	-340(18)	-51(12)	85(9)
C(17)	127(9)	102(8)	384(15)	0	42(8)	0

Structures for Chapter 6

Compound 1a-$TiBn_2$

Special Refinement Details

All non-hydrogen atoms were refined anisotropically by full-matrix least-squares (SHELXL-97). All hydrogen atoms were placed using a riding model. Their positions were constrained relative to their parent atom using the appropriate HFIX command in SHELXL-97. The ^{t}Bu groups (C11, C12, C13, C14) and (C26, C27, C28, C29) are rotationally disordered about their quaternary carbon atoms (C11 and C26, respectively). C12, C13, and C14 are occupationally disordered with C12a, C13a, and C14a in a 76.0(5):24.0(5) ratio. Similarly, C27, C28, and C29 are occupationally disordered with C27a, C28a, and C29a in a 77.8(6):22.2(6) ratio.

Table 2. Atomic coordinates (x 10^4) and equivalent isotropic displacement parameters ($Å^2$x 10^3) for bercaw01. U(eq) is defined as one third of the trace of the orthogonalized U^{ij} tensor.

	x	y	z	U(eq)
C(1)	3353(2)	2653(1)	9436(1)	29(1)
C(2)	3137(2)	3286(1)	9727(1)	34(1)
C(3)	4231(2)	3525(1)	10193(1)	38(1)
C(4)	5512(2)	3174(1)	10387(1)	38(1)
C(5)	5707(2)	2582(1)	10065(1)	34(1)
C(6)	4677(2)	2320(1)	9571(1)	28(1)
C(7)	1736(2)	3691(1)	9532(1)	42(1)
C(8)	507(2)	3273(1)	9682(1)	55(1)
C(9)	1450(2)	3854(1)	8833(1)	51(1)
C(10)	1788(3)	4388(1)	9876(1)	65(1)
C(11)	6697(2)	3437(1)	10921(1)	46(1)
C(12)	6315(3)	4153(2)	11168(2)	63(1)
C(12A)	6240(13)	3521(9)	11503(5)	85(5)
C(13)	6875(4)	2935(2)	11461(1)	64(1)
C(13A)	8103(11)	2926(6)	11045(7)	90(5)
C(14)	8015(3)	3524(2)	10670(2)	74(1)
C(14A)	7366(13)	4108(5)	10748(5)	72(3)
C(15)	5058(2)	1747(1)	9186(1)	27(1)
C(16)	6491(2)	1689(1)	9170(1)	35(1)
C(17)	6944(2)	1171(1)	8833(1)	40(1)
C(18)	5969(2)	725(1)	8497(1)	36(1)
C(19)	4529(2)	803(1)	8490(1)	26(1)
C(20)	3568(2)	275(1)	8129(1)	26(1)
C(21)	4000(2)	-97(1)	7654(1)	30(1)
C(22)	3299(2)	-680(1)	7385(1)	31(1)
C(23)	2114(2)	-899(1)	7606(1)	33(1)
C(24)	1597(2)	-544(1)	8060(1)	29(1)
C(25)	2306(1)	71(1)	8297(1)	25(1)
C(26)	3832(2)	-1086(1)	6877(1)	41(1)
C(27)	5420(3)	-1183(3)	7065(2)	73(1)
C(27A)	4600(30)	-1732(11)	7165(6)	140(12)
C(28)	3136(4)	-1799(2)	6762(2)	70(1)
C(28A)	2674(13)	-1246(7)	6331(5)	71(4)
C(29)	3458(4)	-680(2)	6268(1)	66(1)
C(29A)	4900(20)	-623(11)	6570(10)	132(10)
C(30)	346(2)	-824(1)	8320(1)	37(1)

C(31)	-204(2)	-1516(1)	8024(1)	49(1)
C(32)	-909(2)	-324(1)	8202(1)	54(1)
C(33)	857(2)	-948(1)	9024(1)	51(1)
C(34)	137(2)	1693(1)	8103(1)	41(1)
C(35)	931(2)	1591(1)	7604(1)	38(1)
C(36)	659(2)	1029(1)	7195(1)	46(1)
C(37)	1433(2)	923(1)	6743(1)	57(1)
C(38)	2523(3)	1371(2)	6698(1)	68(1)
C(39)	2840(3)	1912(1)	7107(1)	64(1)
C(40)	2051(2)	2030(1)	7554(1)	47(1)
C(41)	852(2)	1242(1)	9633(1)	35(1)
C(42)	2171(2)	1206(1)	10119(1)	31(1)
C(43)	3118(2)	652(1)	10140(1)	37(1)
C(44)	4404(2)	644(1)	10566(1)	44(1)
C(45)	4764(2)	1173(1)	10990(1)	45(1)
C(46)	3836(2)	1720(1)	10982(1)	42(1)
C(47)	2568(2)	1739(1)	10551(1)	36(1)
N(1)	4077(1)	1309(1)	8840(1)	24(1)
O(1)	2290(1)	2348(1)	9031(1)	31(1)
O(2)	1780(1)	473(1)	8690(1)	29(1)
Ti(1)	1804(1)	1418(1)	8861(1)	26(1)

Table 4. Anisotropic displacement parameters ($Å^2$x 10^3)for bercaw01. The anisotropic displacement factor exponent takes the form: $-2\pi^2[h^2a^{*2}U^{11} + ... + 2\ h\ k\ a^*\ b^*\ U^{12}]$

	U^{11}	U^{22}	U^{33}	U^{23}	U^{13}	U^{12}
C(1)	32(1)	32(1)	25(1)	3(1)	10(1)	2(1)
C(2)	42(1)	32(1)	30(1)	2(1)	16(1)	5(1)
C(3)	49(1)	33(1)	36(1)	-5(1)	18(1)	-2(1)
C(4)	41(1)	40(1)	34(1)	-5(1)	14(1)	-10(1)
C(5)	30(1)	38(1)	35(1)	-1(1)	9(1)	-3(1)
C(6)	29(1)	29(1)	28(1)	1(1)	9(1)	-1(1)
C(7)	50(1)	41(1)	38(1)	2(1)	16(1)	16(1)
C(8)	47(1)	62(1)	63(1)	12(1)	26(1)	23(1)
C(9)	63(1)	50(1)	42(1)	7(1)	15(1)	24(1)
C(10)	86(2)	53(1)	57(1)	-9(1)	18(1)	29(1)
C(11)	42(1)	54(1)	43(1)	-15(1)	10(1)	-13(1)
C(12)	61(2)	61(2)	65(2)	-30(2)	12(2)	-16(1)
C(12A)	65(7)	133(14)	53(6)	-21(7)	0(5)	-32(7)
C(13)	61(2)	73(2)	47(2)	-12(2)	-12(1)	-12(2)
C(13A)	59(6)	69(7)	111(10)	-31(7)	-52(7)	22(5)
C(14)	41(2)	113(4)	71(2)	-43(2)	20(2)	-29(2)
C(14A)	88(8)	54(6)	69(7)	-12(5)	4(6)	-24(6)
C(15)	24(1)	28(1)	29(1)	4(1)	8(1)	1(1)
C(16)	24(1)	37(1)	44(1)	-6(1)	8(1)	-5(1)
C(17)	22(1)	46(1)	56(1)	-8(1)	14(1)	-1(1)
C(18)	26(1)	37(1)	48(1)	-8(1)	14(1)	2(1)
C(19)	23(1)	28(1)	28(1)	3(1)	8(1)	2(1)
C(20)	24(1)	29(1)	25(1)	3(1)	6(1)	3(1)
C(21)	26(1)	37(1)	28(1)	2(1)	10(1)	4(1)
C(22)	30(1)	39(1)	25(1)	-3(1)	6(1)	4(1)
C(23)	31(1)	38(1)	28(1)	-5(1)	4(1)	-2(1)
C(24)	25(1)	37(1)	24(1)	-1(1)	4(1)	-2(1)
C(25)	23(1)	33(1)	20(1)	1(1)	4(1)	1(1)
C(26)	40(1)	49(1)	37(1)	-13(1)	14(1)	1(1)
C(27)	45(2)	102(3)	75(2)	-41(2)	19(2)	16(2)
C(27A)	220(30)	133(16)	50(7)	-29(9)	-14(11)	136(18)

C(28)	92(2)	50(2)	84(3)	-31(2)	54(2)	-11(2)
C(28A)	75(7)	98(11)	40(6)	-28(6)	13(5)	2(7)
C(29)	98(3)	70(2)	37(2)	-9(1)	30(2)	2(2)
C(29A)	163(19)	142(16)	133(17)	-82(14)	123(17)	-63(14)
C(30)	31(1)	43(1)	37(1)	-8(1)	11(1)	-12(1)
C(31)	47(1)	55(1)	48(1)	-13(1)	16(1)	-21(1)
C(32)	30(1)	59(1)	77(2)	-11(1)	18(1)	-10(1)
C(33)	57(1)	63(1)	37(1)	-5(1)	19(1)	-25(1)
C(34)	30(1)	58(1)	33(1)	0(1)	4(1)	9(1)
C(35)	34(1)	49(1)	28(1)	10(1)	2(1)	16(1)
C(36)	41(1)	63(1)	30(1)	4(1)	1(1)	11(1)
C(37)	60(1)	77(2)	31(1)	-1(1)	4(1)	25(1)
C(38)	68(2)	101(2)	42(1)	14(1)	26(1)	29(1)
C(39)	67(1)	78(2)	55(1)	23(1)	30(1)	6(1)
C(40)	52(1)	47(1)	42(1)	14(1)	13(1)	9(1)
C(41)	32(1)	47(1)	29(1)	-1(1)	12(1)	0(1)
C(42)	35(1)	38(1)	25(1)	4(1)	14(1)	-1(1)
C(43)	49(1)	35(1)	28(1)	0(1)	7(1)	3(1)
C(44)	50(1)	48(1)	33(1)	7(1)	6(1)	14(1)
C(45)	45(1)	56(1)	30(1)	5(1)	0(1)	2(1)
C(46)	52(1)	45(1)	29(1)	-3(1)	8(1)	-7(1)
C(47)	42(1)	39(1)	30(1)	1(1)	14(1)	2(1)
N(1)	22(1)	27(1)	25(1)	4(1)	7(1)	2(1)
O(1)	28(1)	34(1)	30(1)	-1(1)	6(1)	6(1)
O(2)	24(1)	37(1)	28(1)	-6(1)	9(1)	-3(1)
Ti(1)	20(1)	35(1)	25(1)	-1(1)	7(1)	3(1)

Compound 1b-$TiBn_2$ (CCDC 622562)

Special Refinement Details

Refinement of F^2 against ALL reflections. The weighted R-factor (*w*R) and goodness of fit (S) are based on F^2, conventional R-factors (R) are based on F, with F set to zero for negative F^2. The threshold expression of $F^2 > 2\sigma(F^2)$ is used only for calculating R-factors(gt) etc. and is not relevant to the choice of reflections for refinement. R-factors based on F^2 are statistically about twice as large as those based on F, and R-factors based on ALL data will be even larger. All esds (except the esd in the dihedral angle between two l.s. planes) are estimated using the full covariance matrix. The cell esds are taken into account individually in the estimation of esds in distances, angles and torsion angles; correlations between esds in cell parameters are only used when they are defined by crystal symmetry. An approximate (isotropic) treatment of cell esds is used for estimating esds involving l.s. planes.

Table 2. Atomic coordinates (x 10^4) and equivalent isotropic displacement parameters ($Å^2$x 10^3) for TA25 (CCDC 622562). U(eq) is defined as the trace of the orthogonalized U^{ij} tensor.

	x	y	z	U_{eq}
Ti(1)	7656(1)	2696(1)	227(1)	12(1)
O(1)	8374(1)	2062(1)	1400(1)	15(1)
O(2)	7072(1)	2993(1)	-1041(1)	15(1)
N(1)	8214(1)	1208(1)	-146(1)	13(1)
C(1)	8072(1)	1156(1)	2059(1)	14(1)
C(2)	7996(1)	1061(1)	3116(1)	14(1)
C(3)	7557(1)	128(1)	3732(1)	18(1)
C(4)	7199(1)	-682(1)	3366(1)	18(1)
C(5)	7378(1)	-597(1)	2333(1)	17(1)
C(6)	7847(1)	302(1)	1667(1)	14(1)
C(7)	8194(1)	298(1)	588(1)	15(1)
C(8)	8574(1)	-662(1)	337(1)	18(1)
C(9)	8952(1)	-693(1)	-658(1)	20(1)
C(10)	8967(1)	229(1)	-1393(1)	18(1)
C(11)	8611(1)	1180(1)	-1127(1)	14(1)
C(12)	8654(1)	2147(1)	-1940(1)	14(1)
C(13)	9538(1)	2212(1)	-2782(1)	17(1)
C(14)	9536(1)	3066(1)	-3596(1)	17(1)
C(15)	8574(1)	3818(1)	-3601(1)	16(1)
C(16)	7660(1)	3794(1)	-2794(1)	14(1)
C(17)	7783(1)	2986(1)	-1916(1)	13(1)
C(18)	8437(1)	1914(1)	3560(1)	15(1)
C(19)	7797(1)	3002(1)	3157(1)	19(1)
C(20)	8099(1)	3907(1)	3575(1)	25(1)
C(21)	9811(1)	1978(1)	3222(1)	18(1)
C(22)	10593(1)	1015(1)	3683(1)	24(1)
C(23)	8222(1)	1650(1)	4726(1)	20(1)
C(24)	6924(1)	1752(1)	5206(1)	31(1)
C(25)	6607(1)	-1612(1)	4077(1)	25(1)
C(26)	10550(1)	3204(1)	-4458(1)	24(1)
C(27)	6581(1)	4614(1)	-2855(1)	14(1)
C(28)	5391(1)	4076(1)	-2387(1)	17(1)

C(29)	5155(1)	3151(1)	-2806(1)	29(1)
C(30)	6481(1)	5162(1)	-3974(1)	19(1)
C(31)	5415(1)	5953(1)	-4157(1)	26(1)
C(32)	6739(1)	5435(1)	-2254(1)	17(1)
C(33)	7805(1)	6123(1)	-2669(1)	25(1)
C(34)	5956(1)	3096(1)	960(1)	20(1)
C(35)	5283(1)	2128(1)	1308(1)	20(1)
C(36)	4880(1)	1647(1)	620(1)	27(1)
C(37)	4272(1)	725(1)	951(1)	37(1)
C(38)	4056(1)	264(1)	1972(1)	40(1)
C(39)	4452(1)	724(1)	2664(1)	35(1)
C(40)	5061(1)	1639(1)	2338(1)	26(1)
C(41)	8708(1)	4008(1)	-105(1)	17(1)
C(42)	10010(1)	3767(1)	-372(1)	16(1)
C(43)	10785(1)	3481(1)	377(1)	17(1)
C(44)	12006(1)	3246(1)	131(1)	21(1)
C(45)	12485(1)	3284(1)	-861(1)	24(1)
C(46)	11732(1)	3563(1)	-1614(1)	24(1)
C(47)	10508(1)	3803(1)	-1373(1)	20(1)

Table 5. Anisotropic displacement parameters ($Å^2 x\ 10^4$) for TA25 (CCDC 622562). The anisotropic displacement factor exponent takes the form: $-2\pi^2[\ h^2 a^{*2} U^{11} + ... + 2\ h\ k\ a^*\ b^*\ U^{12}\ ]$

	U^{11}	U^{22}	U^{33}	U^{23}	U^{13}	U^{12}
Ti(1)	133(1)	107(1)	114(1)	-25(1)	-4(1)	4(1)
O(1)	198(3)	109(3)	129(3)	-15(3)	-16(3)	-20(3)
O(2)	156(3)	160(3)	109(3)	-33(3)	13(2)	20(3)
N(1)	139(4)	118(4)	152(4)	-38(3)	-24(3)	-5(3)
C(1)	133(4)	107(4)	152(5)	-4(4)	-10(3)	-9(3)
C(2)	141(4)	126(4)	151(5)	-11(4)	-17(3)	0(3)
C(3)	185(5)	174(5)	147(5)	5(4)	-3(4)	-7(4)
C(4)	166(5)	143(4)	211(5)	19(4)	-17(4)	-23(4)
C(5)	168(4)	125(4)	212(5)	-17(4)	-28(4)	-24(4)
C(6)	148(4)	119(4)	159(5)	-14(4)	-21(3)	-4(3)
C(7)	145(4)	115(4)	178(5)	-27(4)	-30(3)	-13(3)
C(8)	195(5)	105(4)	238(6)	-42(4)	-38(4)	-6(4)
C(9)	212(5)	140(4)	273(6)	-93(4)	-31(4)	-4(4)
C(10)	182(5)	178(5)	206(5)	-98(4)	-15(4)	8(4)
C(11)	128(4)	146(4)	169(5)	-59(4)	-17(3)	-1(3)
C(12)	145(4)	152(4)	134(5)	-49(4)	-18(3)	-6(3)
C(13)	134(4)	209(5)	171(5)	-89(4)	-10(3)	14(4)
C(14)	134(4)	249(5)	136(5)	-71(4)	5(3)	-8(4)
C(15)	143(4)	213(5)	124(5)	-33(4)	-9(3)	-13(4)
C(16)	124(4)	167(4)	129(4)	-44(4)	-17(3)	-5(3)
C(17)	122(4)	155(4)	116(4)	-46(4)	4(3)	-16(3)
C(18)	184(5)	141(4)	128(5)	-17(4)	-21(3)	2(4)
C(19)	236(5)	152(5)	171(5)	-33(4)	-48(4)	14(4)
C(20)	343(6)	185(5)	228(6)	-52(5)	-46(5)	9(5)
C(21)	180(5)	201(5)	161(5)	-30(4)	-30(4)	-17(4)
C(22)	217(5)	271(6)	224(6)	-78(5)	-47(4)	37(4)
C(23)	267(5)	186(5)	146(5)	-22(4)	-17(4)	-1(4)

C(24)	337(7)	293(6)	236(6)	-38(5)	102(5)	4(5)
C(25)	243(6)	195(5)	269(6)	29(5)	2(4)	-70(4)
C(26)	167(5)	345(6)	191(5)	-67(5)	42(4)	6(4)
C(27)	123(4)	180(4)	119(4)	-29(4)	-10(3)	2(3)
C(28)	119(4)	223(5)	150(5)	-35(4)	-5(3)	-10(4)
C(29)	231(6)	386(7)	291(7)	-154(6)	26(5)	-126(5)
C(30)	166(5)	241(5)	137(5)	-12(4)	-23(4)	1(4)
C(31)	241(6)	298(6)	207(6)	23(5)	-45(4)	42(5)
C(32)	169(4)	182(5)	158(5)	-45(4)	-20(4)	5(4)
C(33)	253(6)	232(5)	268(6)	-75(5)	-16(4)	-61(4)
C(34)	178(5)	228(5)	168(5)	-56(4)	9(4)	24(4)
C(35)	129(4)	247(5)	205(5)	-34(5)	-13(4)	39(4)
C(36)	180(5)	355(7)	280(6)	-84(6)	-51(4)	2(5)
C(37)	256(6)	429(8)	480(9)	-165(7)	-99(6)	-57(6)
C(38)	291(7)	328(7)	537(10)	-6(7)	-73(6)	-96(6)
C(39)	277(6)	357(7)	338(7)	57(6)	-37(5)	-62(5)
C(40)	212(5)	305(6)	242(6)	-19(5)	-30(4)	-16(5)
C(41)	181(5)	127(4)	201(5)	-15(4)	-42(4)	-12(4)
C(42)	185(5)	96(4)	187(5)	-9(4)	-28(4)	-34(3)
C(43)	208(5)	135(4)	171(5)	-16(4)	-22(4)	-39(4)
C(44)	199(5)	172(5)	260(6)	-12(5)	-48(4)	-19(4)
C(45)	195(5)	205(5)	293(6)	-39(5)	16(4)	-23(4)
C(46)	272(6)	215(5)	210(6)	-37(5)	49(4)	-44(4)
C(47)	246(5)	170(5)	183(5)	-10(4)	-31(4)	-51(4)

Compound 2-$TiBn_2$ (CCDC 631415)

Special Refinement Details

The crystals are twinned with the two domains related by rotation around the real axis 0.230 1.000 -0.923. Of 999 reflections used to establish the twin law, 778 contribute to one domain, 636 to the other and both domains have 429 reflections in common.

Refinement of F^2 against ALL reflections. The weighted R-factor (*w*R) and goodness of fit (S) are based on F^2, conventional R-factors (R) are based on F, with F set to zero for negative F^2. The threshold expression of $F^2 > 2\sigma(F^2)$ is used only for calculating R-factors(gt) etc. and is not relevant to the choice of reflections for refinement. R-factors based on F^2 are statistically about twice as large as those based on F, and R-factors based on ALL data will be even larger. All esds (except the esd in the dihedral angle between two l.s. planes) are estimated using the full covariance matrix. The cell esds are taken into account individually in the estimation of esds in distances, angles and torsion angles; correlations between esds in cell parameters are only used when they are defined by crystal symmetry. An approximate (isotropic) treatment of cell esds is used for estimating esds involving l.s. planes.

Table 2. Atomic coordinates (x 10^4) and equivalent isotropic displacement parameters ($Å^2$x 10^3) for TA29 (CCDC 631415). U(eq) is defined as the trace of the orthogonalized U^{ij} tensor.

	x	y	z	U_{eq}
Ti(1)	7845(1)	7317(1)	5197(1)	18(1)
O(1)	8061(2)	8119(1)	4137(1)	18(1)
O(2)	6887(2)	6571(1)	6200(1)	17(1)
O(3)	5574(2)	7481(1)	5004(1)	17(1)
C(1)	7604(3)	8246(2)	3349(2)	17(1)
C(2)	8482(3)	8651(2)	2547(2)	17(1)
C(3)	7998(3)	8652(2)	1743(2)	19(1)
C(4)	6682(3)	8315(2)	1702(2)	18(1)
C(5)	5817(3)	7985(2)	2513(2)	19(1)
C(6)	6220(3)	7961(2)	3347(2)	16(1)
C(7)	5170(3)	7701(2)	4173(2)	20(1)
C(8)	3716(3)	7679(2)	4341(2)	37(1)
C(9)	3199(3)	7443(2)	5284(2)	37(1)
C(10)	4318(3)	7333(2)	5687(2)	20(1)
C(11)	4405(3)	7043(2)	6613(2)	17(1)
C(12)	3156(3)	7161(2)	7302(2)	19(1)
C(13)	3067(3)	6808(2)	8190(2)	18(1)
C(14)	4287(2)	6276(2)	8371(2)	19(1)
C(15)	5560(3)	6120(2)	7725(2)	16(1)
C(16)	5645(3)	6579(2)	6838(2)	18(1)
C(17)	9869(3)	9140(2)	2561(2)	19(1)
C(18)	11009(2)	8443(2)	2867(2)	32(1)
C(19)	9462(3)	9940(2)	3228(2)	32(1)
C(20)	10579(2)	9593(2)	1622(2)	26(1)
C(21)	6223(3)	8300(2)	798(2)	22(1)
C(22)	6512(3)	7293(2)	465(2)	41(1)
C(23)	7015(3)	9001(2)	58(2)	35(1)
C(24)	4599(2)	8578(2)	934(2)	40(1)
C(25)	1722(3)	6942(2)	8958(2)	22(1)

C(26)	1138(3)	5973(2)	9332(2)	26(1)
C(27)	536(3)	7559(2)	8620(2)	35(1)
C(28)	2090(3)	7444(2)	9734(2)	36(1)
C(29)	6799(3)	5429(2)	7923(2)	20(1)
C(30)	6422(3)	4953(2)	8887(2)	31(1)
C(31)	8187(2)	5936(2)	7831(2)	29(1)
C(32)	7061(3)	4632(2)	7257(2)	28(1)
C(33)	9519(2)	6300(2)	4744(2)	23(1)
C(34)	8717(3)	5929(2)	4129(2)	20(1)
C(35)	7526(3)	5381(2)	4475(2)	28(1)
C(36)	6705(3)	5109(2)	3899(2)	35(1)
C(37)	7055(3)	5366(2)	2981(2)	32(1)
C(38)	8233(3)	5906(2)	2618(2)	27(1)
C(39)	9026(3)	6191(2)	3189(2)	24(1)
C(40)	8913(2)	8165(2)	5879(2)	22(1)
C(41)	7566(3)	8677(2)	6334(2)	21(1)
C(42)	6810(3)	9337(2)	5838(2)	28(1)
C(43)	5480(3)	9752(2)	6244(2)	36(1)
C(44)	4864(3)	9533(2)	7149(2)	34(1)
C(45)	5583(3)	8896(2)	7658(2)	30(1)
C(46)	6914(3)	8473(2)	7257(2)	24(1)

Table 5. Anisotropic displacement parameters ($Å^2 x\ 10^4$) for TA29 (CCDC 631415). The anisotropic displacement factor exponent takes the form: $-2\pi^2[\ h^2 a^{*2} U^{11} + ... + 2\ h\ k\ a^*\ b^*\ U^{12}\ ]$

	U^{11}	U^{22}	U^{33}	U^{23}	U^{13}	U^{12}
Ti(1)	132(3)	206(3)	215(3)	-4(2)	-52(2)	-19(2)
O(1)	143(10)	224(10)	191(11)	-3(9)	-56(9)	-56(8)
O(2)	107(9)	217(10)	187(11)	1(8)	-39(8)	4(8)
O(3)	102(9)	229(10)	165(11)	-4(9)	-25(8)	-5(8)
C(1)	200(15)	132(14)	184(17)	-14(13)	-55(13)	26(12)
C(2)	161(15)	149(14)	188(17)	-7(13)	-39(13)	0(12)
C(3)	169(15)	210(15)	152(16)	-19(13)	44(13)	-20(12)
C(4)	198(15)	163(14)	174(16)	-33(13)	-48(13)	16(12)
C(5)	148(14)	181(15)	243(17)	14(14)	-75(13)	-28(12)
C(6)	140(14)	165(14)	184(17)	8(13)	-41(13)	2(12)
C(7)	185(16)	241(16)	186(17)	49(14)	-76(13)	-29(13)
C(8)	155(16)	670(20)	300(20)	176(17)	-138(15)	-51(15)
C(9)	110(15)	630(20)	300(20)	214(17)	-12(14)	-47(15)
C(10)	116(15)	224(15)	220(17)	44(14)	-4(13)	-36(12)
C(11)	119(14)	185(15)	201(17)	-4(13)	-44(13)	-36(12)
C(12)	128(15)	188(15)	272(18)	9(14)	-72(13)	-21(12)
C(13)	151(15)	188(15)	222(17)	-34(13)	-48(13)	-48(12)
C(14)	213(15)	229(15)	155(16)	-6(12)	-72(13)	-39(13)
C(15)	157(15)	188(14)	176(16)	-26(13)	-72(13)	-40(12)
C(16)	142(15)	159(14)	248(18)	-87(13)	-53(14)	-10(12)
C(17)	165(15)	224(15)	189(17)	10(13)	-25(13)	-67(12)
C(18)	148(15)	427(19)	350(20)	102(16)	-35(14)	-95(14)
C(19)	313(17)	345(18)	306(19)	-25(15)	-63(15)	-170(14)
C(20)	226(15)	291(17)	284(19)	9(14)	-95(14)	-93(13)
C(21)	214(16)	272(16)	168(16)	-35(14)	-44(13)	-21(13)

C(22)	580(20)	413(19)	268(19)	-116(16)	-128(17)	-103(17)
C(23)	371(19)	448(19)	248(19)	54(16)	-119(15)	-88(16)
C(24)	244(17)	750(20)	249(18)	-51(17)	-116(15)	-55(16)
C(25)	166(14)	267(16)	194(17)	-24(14)	-7(13)	-5(13)
C(26)	214(16)	338(17)	230(17)	3(14)	-41(13)	-65(13)
C(27)	202(16)	400(18)	355(19)	-11(16)	81(15)	35(14)
C(28)	307(17)	437(19)	325(19)	-158(16)	29(15)	-73(15)
C(29)	160(15)	253(15)	184(17)	25(14)	-55(13)	24(13)
C(30)	259(16)	347(17)	313(19)	52(15)	-113(15)	17(14)
C(31)	175(15)	376(18)	330(19)	13(15)	-105(14)	12(14)
C(32)	231(16)	263(16)	360(19)	8(15)	-112(14)	52(13)
C(33)	186(15)	227(15)	253(17)	-19(13)	-36(13)	6(12)
C(34)	163(15)	169(15)	269(18)	-48(14)	-52(14)	23(12)
C(35)	295(18)	249(16)	282(18)	-57(14)	-36(15)	-28(14)
C(36)	291(18)	308(18)	460(20)	-104(17)	-59(17)	-114(14)
C(37)	320(18)	338(18)	360(20)	-165(17)	-139(16)	-22(15)
C(38)	295(17)	276(17)	255(18)	-92(14)	-89(15)	69(14)
C(39)	182(15)	233(16)	291(19)	-62(15)	-7(14)	11(13)
C(40)	195(14)	260(16)	204(17)	11(13)	-45(13)	-74(13)
C(41)	220(16)	212(15)	232(18)	-76(14)	-64(14)	-64(13)
C(42)	398(19)	187(15)	236(18)	-59(14)	-51(15)	-22(14)
C(43)	450(20)	278(17)	380(20)	-51(17)	-176(17)	142(15)
C(44)	284(17)	328(18)	410(20)	-168(17)	-107(17)	85(15)
C(45)	315(19)	294(17)	287(19)	-111(15)	-22(15)	-68(15)
C(46)	274(17)	236(16)	272(19)	-64(15)	-134(15)	-42(13)

Compound 1b-$ZrBn_2$ (CCDC 631414)

Special Refinement Details

Refinement of F^2 against ALL reflections. The weighted R-factor (*w*R) and goodness of fit (S) are based on F^2, conventional R-factors (R) are based on F, with F set to zero for negative F^2. The threshold expression of $F^2 > 2\sigma(F^2)$ is used only for calculating R-factors(gt) etc. and is not relevant to the choice of reflections for refinement. R-factors based on F^2 are statistically about twice as large as those based on F, and R-factors based on ALL data will be even larger. All esds (except the esd in the dihedral angle between two l.s. planes) are estimated using the full covariance matrix. The cell esds are taken into account individually in the estimation of esds in distances, angles and torsion angles; correlations between esds in cell parameters are only used when they are defined by crystal symmetry. An approximate (isotropic) treatment of cell esds is used for estimating esds involving l.s. planes.

Table 2. Atomic coordinates (x 10^4) and equivalent isotropic displacement parameters ($Å^2$x 10^3) for TA27 (CCDC 631414). U(eq) is defined as the trace of the orthogonalized U^{ij} tensor.

	x	y	z	U_{eq}
Zr(1)	7873(1)	9000(1)	8380(1)	12(1)
O(1)	7369(1)	8924(1)	9208(1)	13(1)
O(2)	8038(1)	9388(1)	7458(1)	13(1)
O(3)	8284(1)	10302(1)	8837(1)	16(1)
N(1)	6499(1)	9778(1)	7878(1)	12(1)
C(1)	6602(2)	8974(2)	9376(1)	14(1)
C(2)	6490(2)	8567(1)	9988(1)	14(1)
C(3)	5647(2)	8584(2)	10071(1)	16(1)
C(4)	4927(2)	8976(2)	9589(1)	15(1)
C(5)	5081(2)	9409(2)	9032(1)	16(1)
C(6)	5912(2)	9425(1)	8917(1)	13(1)
C(7)	6017(2)	9969(1)	8334(1)	13(1)
C(8)	5562(2)	10686(2)	8268(1)	17(1)
C(9)	5552(2)	11191(2)	7709(2)	17(1)
C(10)	5957(2)	10967(2)	7210(1)	16(1)
C(11)	6423(2)	10258(1)	7285(1)	14(1)
C(12)	6790(2)	10046(1)	6682(1)	12(1)
C(13)	6305(2)	10280(2)	5971(1)	16(1)
C(14)	6606(2)	10149(1)	5382(1)	15(1)
C(15)	7444(2)	9813(2)	5513(1)	16(1)
C(16)	7976(2)	9583(1)	6203(1)	14(1)
C(17)	7609(2)	9667(1)	6786(1)	13(1)
C(18)	7267(2)	8122(1)	10540(1)	14(1)
C(19)	7556(2)	7418(2)	10146(2)	17(1)
C(20)	6869(2)	6762(2)	9904(2)	24(1)
C(21)	8090(2)	8671(2)	10833(2)	19(1)
C(22)	7943(2)	9421(2)	11204(2)	30(1)
C(23)	6985(2)	7813(2)	11193(2)	19(1)
C(24)	7691(2)	7351(2)	11773(2)	28(1)
C(25)	4018(2)	8959(2)	9688(2)	20(1)
C(26)	6072(2)	10397(2)	4617(2)	21(1)
C(27)	8925(2)	9261(1)	6327(1)	16(1)

C(28)	8986(2)	8391(2)	6580(2)	18(1)
C(29)	8448(2)	7817(2)	6008(2)	28(1)
C(30)	9600(2)	9752(2)	6931(2)	20(1)
C(31)	9604(3)	10637(2)	6778(2)	32(1)
C(32)	9180(2)	9322(2)	5612(2)	21(1)
C(33)	10113(2)	9047(2)	5653(2)	34(1)
C(34)	7834(2)	7683(2)	8113(2)	17(1)
C(35)	6885(2)	7783(1)	7700(1)	15(1)
C(36)	6214(2)	7730(2)	8032(2)	18(1)
C(37)	5351(2)	7931(2)	7669(2)	22(1)
C(38)	5109(2)	8203(2)	6954(2)	22(1)
C(39)	5756(2)	8256(2)	6606(2)	22(1)
C(40)	6624(2)	8054(2)	6972(2)	18(1)
C(41)	9360(2)	8842(2)	9070(2)	18(1)
C(42)	9917(2)	8160(2)	9041(1)	16(1)
C(43)	10003(2)	7512(2)	9513(2)	19(1)
C(44)	10581(2)	6894(2)	9512(2)	21(1)
C(45)	11083(2)	6900(2)	9035(2)	25(1)
C(46)	10997(2)	7527(2)	8554(2)	25(1)
C(47)	10422(2)	8137(2)	8559(2)	21(1)
C(48)	7963(2)	11158(2)	9762(2)	28(1)
C(49)	8497(2)	10481(2)	9611(1)	19(1)
C(50)	8474(2)	10941(2)	8402(1)	19(1)
C(51)	9448(2)	11150(2)	8619(2)	27(1)
O(61)	7878(2)	9305(1)	3714(1)	53(1)
C(61)	6659(2)	9972(2)	2790(2)	40(1)
C(62)	7602(2)	9992(2)	3295(2)	44(1)
C(63)	8036(3)	8694(2)	3318(2)	56(1)
C(64)	8500(2)	8019(2)	3823(2)	42(1)

Table 5. Anisotropic displacement parameters ($Å^2 x\ 10^4$) for TA27 (CCDC 631414). The anisotropic displacement factor exponent takes the form: $-2\pi^2[\ h^2 a^{*2} U^{11} + ... + 2\ h\ k\ a^*\ b^*\ U^{12}\ ]$

	U^{11}	U^{22}	U^{33}	U^{23}	U^{13}	U^{12}
Zr(1)	107(1)	125(1)	119(1)	11(1)	23(1)	18(1)
O(1)	101(9)	144(9)	136(8)	17(8)	36(7)	18(8)
O(2)	108(10)	155(9)	124(9)	23(7)	30(8)	29(8)
O(3)	185(11)	144(9)	150(9)	6(8)	41(8)	-28(8)
N(1)	83(12)	116(11)	145(11)	-1(9)	24(9)	-20(9)
C(1)	139(14)	124(12)	142(12)	-43(12)	31(10)	8(12)
C(2)	158(15)	128(13)	142(14)	-17(11)	50(12)	27(11)
C(3)	206(16)	145(14)	129(14)	11(11)	70(12)	-4(12)
C(4)	151(14)	135(12)	177(13)	-37(12)	56(11)	13(12)
C(5)	149(15)	145(14)	152(14)	-24(11)	19(12)	46(12)
C(6)	157(15)	105(13)	102(13)	-49(10)	23(11)	12(11)
C(7)	99(14)	121(13)	127(13)	-12(10)	-6(11)	0(11)
C(8)	144(15)	185(14)	169(14)	-30(12)	40(12)	32(12)
C(9)	144(15)	102(15)	235(15)	-23(11)	12(12)	22(11)
C(10)	143(14)	151(13)	152(13)	20(13)	5(11)	-24(13)
C(11)	99(14)	153(13)	142(13)	-1(11)	15(11)	-25(11)

C(12)	100(14)	90(12)	167(13)	3(10)	46(11)	-23(10)
C(13)	114(15)	121(13)	233(15)	26(11)	30(12)	1(11)
C(14)	133(15)	146(13)	167(14)	2(11)	24(12)	-34(11)
C(15)	187(16)	126(13)	174(14)	6(11)	76(13)	-18(12)
C(16)	135(15)	106(13)	170(14)	15(11)	46(12)	-6(11)
C(17)	145(15)	91(13)	129(13)	15(10)	28(11)	-11(11)
C(18)	167(15)	140(13)	125(13)	36(11)	44(12)	10(11)
C(19)	174(16)	164(14)	167(15)	33(12)	46(13)	33(12)
C(20)	270(19)	189(16)	222(17)	-2(13)	37(15)	24(14)
C(21)	195(17)	213(15)	140(15)	48(12)	34(13)	-2(13)
C(22)	310(20)	262(18)	310(20)	-49(15)	54(17)	-33(16)
C(23)	154(16)	213(16)	187(15)	19(12)	50(13)	-7(13)
C(24)	290(20)	341(19)	199(16)	50(15)	58(15)	2(16)
C(25)	182(16)	198(15)	234(15)	-3(15)	88(13)	21(14)
C(26)	181(18)	247(17)	177(16)	44(13)	5(14)	13(14)
C(27)	138(15)	190(14)	168(14)	20(11)	66(12)	31(11)
C(28)	192(17)	186(15)	164(15)	35(12)	45(14)	63(13)
C(29)	320(20)	200(17)	279(18)	-10(14)	39(17)	24(15)
C(30)	126(16)	283(16)	174(15)	13(13)	24(13)	-11(13)
C(31)	340(20)	248(17)	330(20)	5(15)	43(17)	-113(16)
C(32)	187(17)	263(16)	164(15)	25(13)	47(13)	35(13)
C(33)	257(19)	520(20)	238(17)	32(19)	97(15)	62(19)
C(34)	205(17)	175(14)	139(14)	21(12)	46(13)	27(12)
C(35)	195(16)	71(12)	167(14)	-31(11)	18(12)	-2(11)
C(36)	263(18)	148(14)	128(14)	-1(12)	52(13)	-25(12)
C(37)	219(18)	221(16)	248(17)	-64(13)	107(15)	-56(13)
C(38)	143(17)	195(15)	259(17)	-39(13)	-37(14)	-11(12)
C(39)	258(18)	196(15)	171(16)	-10(12)	-6(14)	-17(13)
C(40)	210(18)	116(14)	208(15)	-16(12)	81(14)	-36(12)
C(41)	160(16)	186(16)	172(15)	29(12)	33(12)	26(12)
C(42)	50(14)	219(15)	154(14)	-24(11)	-30(11)	-31(11)
C(43)	158(16)	225(16)	197(15)	-44(12)	73(13)	-30(12)
C(44)	178(16)	169(15)	238(16)	-8(13)	-23(13)	23(12)
C(45)	209(18)	233(16)	268(16)	-91(14)	19(14)	53(13)
C(46)	176(17)	370(19)	222(16)	-43(14)	85(14)	18(14)
C(47)	168(16)	275(17)	173(15)	17(13)	28(13)	2(13)
C(48)	219(19)	330(20)	271(18)	-87(15)	47(15)	14(15)
C(49)	211(18)	212(16)	140(14)	-18(12)	25(13)	-14(13)
C(50)	243(16)	140(14)	190(14)	16(13)	62(12)	-12(13)
C(51)	262(19)	203(18)	313(18)	33(15)	60(15)	-58(14)
O(61)	665(19)	472(15)	492(16)	120(13)	230(14)	37(13)
C(61)	400(20)	440(20)	291(18)	16(16)	20(16)	35(17)
C(62)	450(20)	430(20)	370(20)	110(17)	2(18)	25(17)
C(63)	990(40)	470(20)	330(20)	-19(18)	360(20)	-200(20)
C(64)	440(20)	480(20)	318(19)	5(16)	105(17)	73(18)

Compound 3-$ZrBn_2$ (CCDC 631416)

Special Refinement Details

Refinement of F^2 against ALL reflections. The weighted R-factor (*w*R) and goodness of fit (S) are based on F^2, conventional R-factors (R) are based on F, with F set to zero for negative F^2. The threshold expression of $F^2 > 2\sigma(F^2)$ is used only for calculating R-factors(gt) etc. and is not relevant to the choice of reflections for refinement. R-factors based on F^2 are statistically about twice as large as those based on F, and R-factors based on ALL data will be even larger. All esds (except the esd in the dihedral angle between two l.s. planes) are estimated using the full covariance matrix. The cell esds are taken into account individually in the estimation of esds in distances, angles and torsion angles; correlations between esds in cell parameters are only used when they are defined by crystal symmetry. An approximate (isotropic) treatment of cell esds is used for estimating esds involving l.s. planes.

Table 2. Atomic coordinates (x 10^4) and equivalent isotropic displacement parameters ($Å^2$x 10^3) for TA31 (CCDC 631416). U(eq) is defined as the trace of the orthogonalized U^{ij} tensor.

	x	y	z	U_{eq}	Occ
Zr(1)	2401(1)	4953(1)	950(1)	12(1)	1
S(1)	2160(1)	7074(1)	507(1)	12(1)	1
O(1)	1803(1)	5174(1)	973(1)	14(1)	1
O(2)	2910(1)	5638(1)	801(1)	13(1)	1
C(1)	1442(1)	5849(2)	921(1)	14(1)	1
C(2)	1070(1)	5295(2)	973(1)	15(1)	1
C(3)	714(1)	6046(2)	909(1)	17(1)	1
C(4)	706(1)	7300(2)	810(1)	15(1)	1
C(5)	1076(1)	7827(2)	772(1)	15(1)	1
C(6)	1442(1)	7114(2)	824(1)	13(1)	1
C(7)	1833(1)	7745(2)	809(1)	12(1)	1
C(8)	2022(1)	8784(2)	1036(1)	15(1)	1
C(9)	2446(1)	8966(2)	1016(1)	16(1)	1
C(10)	2586(1)	8062(2)	776(1)	12(1)	1
C(11)	3010(1)	7813(2)	737(1)	12(1)	1
C(12)	3282(1)	8796(2)	728(1)	14(1)	1
C(13)	3688(1)	8608(2)	695(1)	14(1)	1
C(14)	3806(1)	7395(2)	648(1)	16(1)	1
C(15)	3554(1)	6378(2)	662(1)	14(1)	1
C(16)	3153(1)	6592(2)	730(1)	13(1)	1
C(17)	1055(1)	3921(2)	1106(1)	19(1)	1
C(18)	1396(1)	3653(2)	1591(1)	22(1)	1
C(19)	1120(1)	3119(2)	697(1)	23(1)	1
C(20)	623(1)	3559(2)	1166(1)	28(1)	1
C(21)	289(1)	8043(2)	723(1)	18(1)	1
C(22)	85(1)	7759(2)	1123(1)	25(1)	1
C(23)	-12(1)	7672(2)	225(1)	25(1)	1
C(24)	367(1)	9422(2)	720(1)	25(1)	1
C(25)	3999(1)	9680(2)	726(1)	17(1)	1
C(26)	4188(1)	10036(3)	1258(1)	43(1)	1
C(27)	3762(1)	10789(2)	442(1)	36(1)	1
C(28)	4352(1)	9351(2)	509(1)	31(1)	1

C(29)	3714(1)	5069(2)	612(1)	18(1)	1
C(30)	3802(1)	4401(2)	1103(1)	21(1)	1
C(31)	4134(1)	5084(2)	485(1)	26(1)	1
C(32)	3390(1)	4389(2)	199(1)	20(1)	1
C(33)	2716(1)	4781(2)	1762(1)	18(1)	1
C(34)	2743(1)	6067(2)	1924(1)	19(1)	1
C(35)	2397(1)	6634(2)	2030(1)	26(1)	1
C(36)	2413(1)	7840(2)	2187(1)	37(1)	1
C(37)	2772(1)	8526(2)	2232(1)	43(1)	1
C(38)	3111(1)	8034(2)	2117(1)	41(1)	1
C(39)	3101(1)	6802(2)	1959(1)	28(1)	1
C(40)	2277(1)	3316(2)	437(1)	18(1)	1
C(41)	2492(1)	2601(2)	870(1)	17(1)	1
C(42)	2940(1)	2460(2)	1033(1)	20(1)	1
C(43)	3152(1)	1987(2)	1487(1)	22(1)	1
C(44)	2929(1)	1634(2)	1801(1)	23(1)	1
C(45)	2488(1)	1742(2)	1654(1)	20(1)	1
C(46)	2277(1)	2223(2)	1200(1)	18(1)	1
C(51)	1091(1)	8559(3)	2226(1)	51(1)	1
C(52)	837(1)	8838(3)	2519(1)	60(1)	1
C(53)	624(1)	7932(3)	2678(1)	63(1)	1
C(54)	660(1)	6712(3)	2565(1)	66(1)	1
C(55)	922(1)	6432(3)	2277(1)	61(1)	1
C(56)	1131(1)	7354(3)	2115(1)	57(1)	1
C(57)	1313(1)	9548(3)	2042(1)	67(1)	1
C(61)	4686(2)	7414(4)	2319(2)	194(11)	0.50
C(62)	4767(2)	6843(5)	1925(2)	95(3)	0.50
C(63)	5176(2)	6591(5)	1933(2)	152(6)	0.50
C(64)	5521(2)	6890(6)	2328(3)	210(8)	0.50
C(65)	5438(2)	7464(7)	2724(3)	239(13)	0.50
C(66)	5026(2)	7713(5)	2712(2)	212(10)	0.50
C(67)	4242(2)	7687(7)	2310(3)	130(5)	0.50

Table 5. Anisotropic displacement parameters ($Å^2 x\ 10^4$) for TA31 (CCDC 631416). The anisotropic displacement factor exponent takes the form: $-2\pi^2[\ h^2 a^{*2} U^{11} + ... + 2\ h\ k\ a^*\ b^*\ U^{12}\ ]$

	U^{11}	U^{22}	U^{33}	U^{23}	U^{13}	U^{12}
Zr(1)	108(1)	98(1)	143(1)	-12(1)	43(1)	5(1)
S(1)	107(2)	121(2)	139(2)	-13(2)	40(2)	0(2)
O(1)	115(5)	107(6)	188(7)	-2(5)	55(5)	11(4)
O(2)	132(6)	105(6)	171(7)	-2(5)	63(5)	13(5)
C(1)	115(8)	166(9)	120(10)	-17(7)	27(7)	25(6)
C(2)	140(8)	165(10)	133(10)	-13(7)	40(7)	-15(6)
C(3)	107(8)	213(10)	191(11)	5(8)	56(7)	-30(7)
C(4)	120(8)	196(10)	147(10)	-12(7)	42(7)	17(7)
C(5)	138(8)	135(9)	163(10)	5(7)	29(7)	12(7)
C(6)	117(8)	162(9)	121(10)	-14(7)	36(7)	-5(7)

C(7)	95(8)	129(9)	150(10)	10(7)	50(7)	44(6)
C(8)	140(8)	127(9)	185(11)	-5(7)	66(7)	31(7)
C(9)	152(9)	116(9)	203(11)	-16(8)	49(8)	-7(7)
C(10)	120(8)	112(8)	134(10)	4(7)	30(7)	-6(6)
C(11)	119(8)	132(9)	112(9)	-14(7)	28(7)	8(6)
C(12)	163(8)	122(9)	131(10)	-11(7)	36(7)	23(7)
C(13)	144(8)	149(9)	140(10)	14(7)	40(7)	-9(7)
C(14)	118(8)	189(10)	199(11)	11(8)	81(7)	21(7)
C(15)	124(8)	147(9)	152(10)	-7(7)	52(7)	25(6)
C(16)	135(8)	135(9)	107(10)	4(7)	35(7)	-12(6)
C(17)	140(8)	176(10)	250(12)	19(8)	66(8)	-26(7)
C(18)	244(11)	196(11)	247(13)	37(9)	98(9)	15(8)
C(19)	177(10)	194(11)	301(13)	-31(9)	52(9)	-30(8)
C(20)	216(11)	235(12)	420(16)	62(11)	128(11)	-26(9)
C(21)	116(8)	191(10)	229(11)	4(8)	57(7)	29(7)
C(22)	180(10)	301(12)	290(14)	39(10)	117(9)	43(9)
C(23)	162(10)	291(13)	265(13)	-1(10)	27(9)	67(8)
C(24)	160(10)	224(11)	374(15)	20(10)	103(10)	46(8)
C(25)	156(8)	146(10)	228(11)	-9(7)	77(8)	-30(6)
C(26)	442(14)	507(17)	313(14)	-64(14)	83(11)	-280(15)
C(27)	250(11)	196(12)	680(20)	144(12)	232(13)	22(9)
C(28)	213(11)	218(12)	558(19)	-27(11)	210(11)	-47(9)
C(29)	162(8)	147(9)	245(10)	9(9)	102(7)	38(8)
C(30)	172(10)	179(10)	266(13)	26(9)	65(9)	25(8)
C(31)	232(9)	176(10)	424(14)	30(11)	194(9)	68(9)
C(32)	234(10)	151(10)	239(12)	-15(9)	120(9)	34(8)
C(33)	190(9)	148(10)	179(10)	11(7)	47(7)	12(7)
C(34)	298(10)	157(10)	72(10)	-6(7)	2(8)	-11(8)
C(35)	399(12)	207(11)	149(11)	4(8)	62(9)	75(9)
C(36)	670(17)	207(12)	196(13)	1(9)	97(12)	121(11)
C(37)	870(20)	196(13)	190(14)	-19(10)	118(13)	11(13)
C(38)	593(17)	344(14)	207(13)	35(10)	18(12)	-261(13)
C(39)	354(12)	279(12)	181(12)	-11(9)	38(9)	-75(9)
C(40)	176(9)	198(10)	174(11)	-29(8)	47(8)	7(7)
C(41)	220(9)	66(8)	222(11)	-67(7)	55(8)	1(7)
C(42)	193(9)	158(10)	257(12)	-36(8)	89(9)	-12(7)
C(43)	171(9)	129(9)	332(13)	-17(8)	23(9)	11(7)
C(44)	299(11)	114(10)	226(12)	7(8)	-2(9)	1(8)
C(45)	267(10)	114(9)	232(12)	-36(8)	88(9)	-13(7)
C(46)	174(9)	124(9)	236(12)	-55(8)	47(8)	9(7)
C(51)	377(14)	810(20)	262(15)	-159(14)	-26(11)	90(14)
C(52)	563(18)	820(20)	377(18)	-249(16)	89(14)	54(16)
C(53)	604(19)	920(30)	350(18)	-168(17)	124(15)	139(18)
C(54)	640(20)	880(30)	315(18)	18(16)	-39(15)	40(17)
C(55)	610(19)	710(20)	333(17)	-109(15)	-110(14)	311(16)
C(56)	374(15)	940(30)	296(16)	-75(16)	-26(12)	219(15)
C(57)	471(17)	1050(30)	433(19)	-181(17)	44(14)	6(17)
C(61)	1950(160)	1470(140)	1660(170)	150(110)	-520(130)	-1280(120)
C(62)	1700(90)	600(50)	730(60)	-290(40)	600(60)	-460(50)
C(63)	680(60)	1640(110)	2150(140)	1170(100)	300(80)	110(70)
C(64)	910(90)	3400(200)	2130(180)	1210(160)	610(100)	200(110)
C(65)	3700(300)	750(80)	4200(300)	-1230(130)	3500(300)	-540(110)

C(66)	1450(100)	2300(150)	1640(150)	-1570(130)	-950(100)	960(110)
C(67)	760(60)	980(70)	2020(130)	850(80)	220(60)	-270(50)

Structures for Chapter 7

Compound 7a (CCDC 208195)

Special Refinement Details

Refinement of F^2 against ALL reflections. The weighted R-factor (*w*R) and goodness of fit (S) are based on F^2, conventional R-factors (R) are based on F, with F set to zero for negative F^2. The threshold expression of $F^2 > 2\sigma(F^2)$ is used only for calculating R-factors(gt) etc. and is not relevant to the choice of reflections for refinement. R-factors based on F^2 are statistically about twice as large as those based on F, and R-factors based on ALL data will be even larger. All esds (except the esd in the dihedral angle between two l.s. planes) are estimated using the full covariance matrix. The cell esds are taken into account individually in the estimation of esds in distances, angles and torsion angles; correlations between esds in cell parameters are only used when they are defined by crystal symmetry. An approximate (isotropic) treatment of cell esds is used for estimating esds involving l.s. planes.

Table 2. Atomic coordinates (x 10^4) and equivalent isotropic displacement parameters ($Å^2$x 10^3) for TA09 (CCDC 208195). U(eq) is defined as the trace of the orthogonalized U^{ij} tensor.

	x	y	z	U_{eq}
Y(1)	9453(1)	8894(1)	7521(1)	12(1)
Si(1)	7783(1)	8244(1)	6127(1)	16(1)
Si(2)	12752(1)	8425(1)	7380(1)	18(1)
O(1)	8637(1)	10312(1)	7098(1)	15(1)
O(2)	10070(1)	10077(1)	8242(1)	17(1)
O(3)	9432(1)	7895(1)	8131(1)	13(1)
N(1)	7750(1)	9491(1)	7951(1)	13(1)
C(1)	9232(2)	10964(2)	6807(1)	25(1)
C(2)	7617(2)	10737(1)	7269(1)	17(1)
C(3)	6956(2)	9992(1)	7517(1)	17(1)
C(4)	11292(2)	10323(2)	8441(1)	30(1)
C(5)	9390(2)	10002(1)	8667(1)	18(1)
C(6)	8089(2)	10104(1)	8425(1)	16(1)
C(7)	8879(2)	7669(1)	8538(1)	12(1)
C(8)	9384(2)	7051(1)	8949(1)	12(1)
C(9)	8738(2)	6878(1)	9357(1)	15(1)
C(10)	7640(2)	7284(1)	9390(1)	15(1)
C(11)	7172(2)	7887(1)	8977(1)	15(1)
C(12)	7748(2)	8068(1)	8554(1)	13(1)
C(13)	7104(2)	8632(1)	8089(1)	15(1)
C(14)	10606(2)	6592(1)	8951(1)	14(1)
C(15)	11576(2)	7348(1)	8985(1)	17(1)
C(16)	10564(2)	6007(1)	8443(1)	16(1)
C(17)	10991(2)	5942(1)	9426(1)	20(1)
C(18)	6950(2)	7094(1)	9843(1)	19(1)
C(19)	5698(2)	6725(2)	9614(1)	25(1)
C(20)	6832(2)	8007(2)	10147(1)	29(1)
C(21)	7566(2)	6368(2)	10239(1)	30(1)
C(22)	8313(2)	7920(1)	6822(1)	18(1)

C(23)	6545(2)	9120(1)	6063(1)	24(1)
C(24)	9006(2)	8759(2)	5821(1)	25(1)
C(25)	7188(2)	7232(1)	5670(1)	17(1)
C(26)	7975(2)	6561(1)	5535(1)	23(1)
C(27)	7585(2)	5808(1)	5206(1)	25(1)
C(28)	6387(2)	5714(1)	4994(1)	26(1)
C(29)	5582(2)	6370(1)	5115(1)	25(1)
C(30)	5985(2)	7114(1)	5451(1)	21(1)
C(31)	11341(2)	9065(1)	7189(1)	20(1)
C(32)	13766(2)	8387(2)	6877(1)	28(1)
C(33)	12471(2)	7176(1)	7535(1)	26(1)
C(34)	13601(2)	9000(1)	7999(1)	18(1)
C(35)	13745(2)	8581(1)	8502(1)	21(1)
C(36)	14195(2)	9057(1)	8967(1)	25(1)
C(37)	14551(2)	9980(1)	8943(1)	27(1)
C(38)	14472(2)	10408(1)	8450(1)	25(1)
C(39)	13997(2)	9933(1)	7988(1)	20(1)

Table 5. Anisotropic displacement parameters ($Å^2 x\ 10^4$) for TA09 (CCDC 208195). The anisotropic displacement factor exponent takes the form: $-2\pi^2$ [$h^2 a^{*2} U^{11}$ + ... + 2 h k a* b* U^{12}]

	U^{11}	U^{22}	U^{33}	U^{23}	U^{13}	U^{12}
Y(1)	122(1)	112(1)	124(1)	9(1)	22(1)	17(1)
Si(1)	185(3)	145(3)	135(3)	-10(2)	25(2)	23(2)
Si(2)	146(3)	154(3)	245(3)	9(2)	59(2)	-8(2)
O(1)	163(7)	116(6)	189(7)	35(5)	66(5)	23(5)
O(2)	143(7)	200(7)	169(7)	-31(5)	27(5)	-17(5)
O(3)	149(7)	135(6)	127(6)	13(5)	45(5)	28(5)
N(1)	149(8)	115(7)	128(8)	24(6)	28(6)	24(6)
C(1)	269(12)	215(12)	318(13)	116(10)	161(11)	51(10)
C(2)	183(11)	157(10)	186(11)	37(8)	52(9)	69(8)
C(3)	149(10)	174(10)	177(10)	32(8)	43(8)	56(8)
C(4)	196(12)	360(14)	335(14)	-119(12)	24(11)	-48(10)
C(5)	248(11)	157(10)	133(10)	-6(8)	20(9)	5(8)
C(6)	217(11)	133(10)	144(10)	-16(8)	74(8)	18(8)
C(7)	142(9)	100(9)	126(9)	-23(7)	18(8)	-30(7)
C(8)	137(9)	90(8)	123(9)	-29(7)	1(7)	-20(7)
C(9)	193(11)	110(9)	130(10)	20(7)	-1(8)	-10(8)
C(10)	189(10)	119(9)	134(9)	-18(7)	43(8)	-36(7)
C(11)	122(10)	132(9)	199(10)	-25(8)	49(8)	17(8)
C(12)	143(10)	95(9)	146(9)	3(7)	26(8)	-16(7)
C(13)	114(10)	154(10)	192(10)	5(8)	56(8)	3(7)
C(14)	145(10)	106(9)	159(9)	29(7)	29(8)	4(7)
C(15)	167(11)	166(10)	181(11)	2(9)	16(9)	-14(8)
C(16)	152(10)	133(10)	202(10)	4(8)	34(8)	9(9)
C(17)	182(11)	180(11)	216(11)	37(9)	15(9)	11(9)
C(18)	235(11)	184(10)	173(10)	24(8)	92(8)	20(8)
C(19)	269(13)	268(12)	238(12)	26(10)	117(10)	-33(10)
C(20)	379(15)	290(13)	235(12)	-36(10)	148(11)	-13(11)
C(21)	325(14)	376(14)	237(12)	123(10)	140(11)	49(11)
C(22)	180(11)	171(10)	192(11)	6(8)	37(9)	22(9)

C(23)	296(13)	228(12)	168(11)	-33(9)	-2(10)	92(9)
C(24)	320(13)	236(12)	189(11)	-17(9)	74(10)	-22(10)
C(25)	234(11)	146(9)	111(9)	29(7)	22(8)	12(8)
C(26)	234(12)	232(11)	199(11)	-14(9)	-37(9)	24(9)
C(27)	350(13)	163(10)	228(11)	-29(8)	13(10)	65(9)
C(28)	415(14)	171(10)	163(11)	2(8)	-19(10)	-75(10)
C(29)	258(12)	216(11)	235(11)	69(8)	-39(10)	-69(9)
C(30)	240(12)	191(10)	190(11)	38(8)	41(9)	7(9)
C(31)	171(10)	202(11)	218(11)	-2(9)	20(9)	0(8)
C(32)	251(13)	234(12)	382(14)	49(11)	137(11)	32(10)
C(33)	247(13)	222(11)	313(14)	2(10)	68(11)	-31(10)
C(34)	82(9)	168(10)	289(11)	24(8)	51(8)	27(8)
C(35)	120(10)	176(10)	340(12)	50(9)	35(9)	-9(8)
C(36)	182(11)	289(12)	270(12)	65(10)	22(9)	26(9)
C(37)	175(11)	294(12)	306(13)	-34(10)	-28(9)	-8(9)
C(38)	169(11)	179(11)	391(13)	10(10)	16(9)	-26(8)
C(39)	126(10)	206(10)	266(12)	50(9)	31(9)	-1(8)

Compound 7b (CCDC 292609)

Special Refinement Details

All four ethyl groups are disordered at the terminal methyl groups. The disorder adopts two conformations, with nearly equal populations (see Table 2 and Figures 1 & 2). Additionally, the crystal contains disordered solvent, presumably diethylether and/or petroleum ether. Solvent flattening (as implemented in SQUEEZE[1]) was used to model the electrons in the solvent region. Two voids (see Figures 3 & 4)p of 333Å^3 containing 92 electrons each were used to modify the observed intensities for final refinement. This fits well with expectations.

Refinement of F^2 against ALL reflections. The weighted R-factor (*w*R) and goodness of fit (S) are based on F^2, conventional R-factors (R) are based on F, with F set to zero for negative F^2. The threshold expression of $F^2 > 2\sigma(F^2)$ is used only for calculating R-factors(gt) etc. and is not relevant to the choice of reflections for refinement. R-factors based on F^2 are statistically about twice as large as those based on F, and R-factors based on ALL data will be even larger. All esds (except the esd in the dihedral angle between two l.s. planes) are estimated using the full covariance matrix. The cell esds are taken into account individually in the estimation of esds in distances, angles and torsion angles; correlations between esds in cell parameters are only used when they are defined by crystal symmetry. An approximate (isotropic) treatment of cell esds is used for estimating esds involving l.s. planes.

Table 2. Atomic coordinates (x 10^4) and equivalent isotropic displacement parameters (Å^{2}x 10^3) for SCM02 (CCDC 292609). U(eq) is defined as the trace of the orthogonalized U^{ij} tensor.

	x	y	z	U_{eq}	Occ
Y(1)	7455(1)	4441(1)	1450(1)	36(1)	1
Si(1)	8784(1)	2182(1)	2442(1)	33(1)	1
Si(2)	5854(1)	1936(2)	1068(1)	71(1)	1
O(1)	8125(2)	3600(3)	1026(1)	37(1)	1
N(1)	8391(2)	6240(4)	1400(2)	32(1)	1
N(2)	6942(3)	6185(5)	675(2)	52(2)	1
N(3)	7455(3)	6122(4)	2128(2)	46(1)	1
C(1)	9133(3)	5544(5)	1522(2)	34(1)	1
C(2)	9316(3)	4624(5)	1151(2)	26(1)	1
C(3)	10020(3)	4713(5)	1060(2)	29(1)	1
C(4)	10275(3)	3811(5)	772(2)	27(1)	1
C(5)	9782(3)	2787(5)	594(2)	32(2)	1
C(6)	9068(3)	2646(5)	673(2)	29(1)	1
C(7)	8808(3)	3615(5)	947(2)	27(1)	1
C(8)	11049(3)	3932(5)	677(2)	37(2)	1
C(9)	11148(3)	5298(5)	470(2)	63(2)	1
C(10)	11642(3)	3745(6)	1150(2)	74(2)	1
C(11)	11203(3)	2924(6)	321(2)	62(2)	1
C(12)	8562(3)	1479(5)	462(2)	41(2)	1
C(13)	8336(3)	721(5)	868(2)	49(2)	1
C(14)	8961(3)	493(5)	197(2)	53(2)	1
C(15)	7863(3)	1986(5)	104(2)	55(2)	1
C(16)	8278(3)	6845(5)	922(2)	44(2)	1
C(17)	7481(4)	7288(6)	720(2)	52(2)	1
C(18)	6965(5)	5384(8)	241(3)	99(3)	1

[1] Spek, A.L. (2003), J.Appl.Cryst. 36, 7-13

C(19A)	6681(10)	5810(18)	-184(6)	97(7)	0.448(6)
C(21A)	5824(19)	7170(20)	885(9)	222(19)	0.448(6)
C(25A)	6847(8)	8130(11)	2454(5)	69(6)	0.448(6)
C(27A)	6695(7)	4781(11)	2687(5)	48(4)	0.448(6)
C(19B)	6401(6)	4448(12)	35(4)	69(4)	0.552(6)
C(21B)	5917(6)	7745(10)	213(4)	66(4)	0.552(6)
C(25B)	6092(7)	6895(11)	1864(5)	81(5)	0.552(6)
C(27B)	7349(8)	6270(11)	2942(4)	76(5)	0.552(6)
C(20)	6193(5)	6734(9)	613(3)	89(3)	1
C(22)	8399(3)	7257(5)	1775(2)	48(2)	1
C(23)	8219(3)	6682(6)	2217(2)	52(2)	1
C(24)	6890(4)	7163(7)	1997(3)	90(3)	1
C(26)	7379(4)	5427(6)	2577(3)	85(3)	1
C(28)	7925(3)	2778(5)	2049(2)	42(2)	1
C(29)	8731(3)	375(4)	2588(2)	43(2)	1
C(30)	9630(3)	2362(5)	2188(2)	37(2)	1
C(31)	8946(3)	3103(5)	3023(2)	35(2)	1
C(32)	8533(3)	2817(5)	3357(2)	44(2)	1
C(33)	8558(4)	3560(5)	3765(2)	51(2)	1
C(34)	9050(4)	4606(6)	3857(2)	58(2)	1
C(35)	9481(4)	4919(6)	3546(2)	60(2)	1
C(36)	9436(3)	4162(5)	3134(2)	43(2)	1
C(37)	6191(3)	3550(5)	1279(2)	44(2)	1
C(38)	6355(4)	632(6)	1465(4)	214(7)	1
C(39)	5972(5)	1572(10)	448(4)	214(7)	1
C(40)	4837(4)	1636(7)	1032(2)	52(2)	1
C(41)	4463(4)	516(8)	836(3)	111(3)	1
C(42)	3711(5)	295(10)	805(3)	112(3)	1
C(43)	3292(5)	1197(11)	963(3)	98(3)	1
C(44)	3643(5)	2278(10)	1182(3)	108(3)	1
C(45)	4393(4)	2498(7)	1204(3)	71(2)	1

Table 5. Anisotropic displacement parameters ($Å^2 x\ 10^4$) for SCM02 (CCDC 292609). The anisotropic displacement factor exponent takes the form: $-2\pi^2$ [$h^2 a^{*2} U^{11}$ + ... + 2 h k a* b* U^{12}]

	U^{11}	U^{22}	U^{33}	U^{23}	U^{13}	U^{12}
Y(1)	324(4)	143(3)	550(4)	-40(3)	-8(3)	5(3)
Si(1)	472(12)	218(9)	286(11)	-31(8)	56(9)	37(8)
Si(2)	357(13)	421(13)	1330(20)	-287(13)	150(13)	-121(10)
O(1)	370(30)	170(20)	560(30)	-101(19)	70(20)	-101(19)
N(1)	440(30)	160(30)	330(30)	-50(20)	10(30)	50(20)
N(2)	480(40)	360(30)	660(40)	60(30)	10(30)	60(30)
N(3)	330(30)	220(30)	880(40)	-150(30)	230(30)	-50(30)
C(1)	330(40)	260(30)	430(40)	0(30)	50(30)	-80(30)
C(2)	390(40)	110(30)	260(40)	0(30)	10(30)	20(30)
C(3)	390(40)	140(30)	300(40)	0(30)	-10(30)	-90(30)
C(4)	360(40)	180(30)	230(40)	90(30)	10(30)	0(30)
C(5)	480(40)	190(30)	250(40)	100(30)	10(30)	60(30)
C(6)	390(40)	110(30)	320(40)	-20(30)	-20(30)	-40(30)
C(7)	370(40)	140(30)	270(40)	90(30)	30(30)	-30(30)
C(8)	420(40)	250(40)	390(40)	-10(30)	40(40)	40(30)

C(9)	700(50)	350(40)	880(60)	70(40)	280(40)	-100(40)
C(10)	430(50)	1080(60)	650(50)	40(40)	0(40)	240(40)
C(11)	640(50)	560(50)	740(50)	-70(40)	340(40)	-170(40)
C(12)	460(40)	340(40)	410(40)	-90(30)	90(40)	-30(30)
C(13)	660(50)	320(40)	520(40)	-80(30)	190(40)	-210(30)
C(14)	720(50)	300(40)	590(50)	-180(40)	200(40)	-230(40)
C(15)	590(50)	470(40)	510(50)	-210(30)	-20(40)	-170(40)
C(16)	580(50)	170(30)	540(50)	130(30)	60(40)	20(30)
C(17)	790(60)	350(40)	380(40)	90(30)	40(40)	50(40)
C(18)	1040(70)	820(60)	920(70)	-350(60)	-140(60)	-40(60)
C(19A)	1050(160)	1350(190)	370(120)	390(120)	-130(110)	280(130)
C(21A)	4200(500)	820(170)	1200(200)	-160(160)	-300(300)	1200(200)
C(25A)	770(120)	240(90)	1260(150)	-100(90)	660(110)	60(80)
C(27A)	510(100)	380(90)	660(110)	-230(70)	360(80)	-180(70)
C(19B)	580(90)	640(90)	700(100)	-30(90)	-140(70)	80(80)
C(21B)	790(100)	590(80)	560(90)	310(70)	70(70)	590(70)
C(25B)	810(120)	600(90)	1110(120)	-240(80)	400(100)	90(80)
C(27B)	1560(140)	590(90)	240(80)	-30(70)	390(80)	460(90)
C(20)	1240(80)	810(70)	610(70)	220(50)	210(60)	370(60)
C(22)	600(50)	210(40)	660(50)	-30(40)	190(40)	-60(30)
C(23)	440(50)	380(40)	730(50)	-230(40)	90(40)	-10(30)
C(24)	450(50)	640(50)	1420(80)	-400(50)	-150(50)	200(50)
C(26)	1120(70)	250(40)	1410(80)	-120(50)	760(60)	0(40)
C(28)	470(40)	260(30)	430(40)	-190(30)	-70(30)	70(30)
C(29)	610(40)	260(40)	360(40)	0(30)	-10(30)	70(30)
C(30)	420(40)	300(30)	360(40)	50(30)	30(30)	160(30)
C(31)	490(40)	240(40)	280(40)	60(30)	20(30)	40(30)
C(32)	850(50)	190(30)	320(40)	-20(30)	200(40)	-130(30)
C(33)	970(60)	270(40)	380(40)	-60(30)	330(40)	-40(40)
C(34)	1140(60)	340(40)	320(40)	-110(30)	290(40)	-160(40)
C(35)	970(60)	440(40)	410(50)	-230(40)	170(40)	-280(40)
C(36)	540(40)	420(40)	310(40)	-40(30)	50(30)	-120(40)
C(37)	410(40)	290(40)	620(50)	80(30)	100(30)	10(30)
C(38)	460(50)	260(50)	5200(200)	920(80)	-310(80)	-20(40)
C(39)	1680(100)	2770(130)	2480(130)	-2220(120)	1500(100)	-1630(100)
C(40)	350(50)	520(50)	570(50)	-10(40)	-110(40)	-20(40)
C(41)	420(50)	970(70)	1840(100)	-550(70)	70(60)	-240(50)
C(42)	560(70)	1100(90)	1540(90)	-240(70)	-70(60)	-460(60)
C(43)	440(60)	1190(90)	1220(90)	180(70)	0(60)	-200(60)
C(44)	470(60)	1220(80)	1580(90)	-200(70)	310(60)	10(60)
C(45)	380(50)	640(50)	1060(70)	50(50)	70(50)	-120(40)

Compound 8a (CCDC 268186)

Special Refinement Details

The ^{t}Bu group containing atoms C9, C10 and C11 is disordered by rotation around the C8-C4 bond. The disorder was modeled without restraints; the final refined ratio is 55:45.

Refinement of F^2 against ALL reflections. The weighted R-factor (*w*R) and goodness of fit (S) are based on F^2, conventional R-factors (R) are based on F, with F set to zero for negative F^2. The threshold expression of $F^2 > 2\sigma(F^2)$ is used only for calculating R-factors(gt) etc. and is not relevant to the choice of reflections for refinement. R-factors based on F^2 are statistically about twice as large as those based on F, and R-factors based on ALL data will be even larger. All esds (except the esd in the dihedral angle between two l.s. planes) are estimated using the full covariance matrix. The cell esds are taken into account individually in the estimation of esds in distances, angles and torsion angles; correlations between esds in cell parameters are only used when they are defined by crystal symmetry. An approximate (isotropic) treatment of cell esds is used for estimating esds involving l.s. planes.

Table 2. Atomic coordinates (x 10^4) and equivalent isotropic displacement parameters ($Å^2$x 10^3) for SCM01 (CCDC 268186). U(eq) is defined as the trace of the orthogonalized U^{ij} tensor.

	x	y	z	U_{eq}	Occ
Sc(1)	3794(1)	1667(1)	1515(1)	14(1)	1
Si(1)	3556(1)	111(1)	2203(1)	21(1)	1
Si(2)	2387(1)	613(1)	747(1)	21(1)	1
O(1)	5082(1)	1747(1)	1200(1)	16(1)	1
O(2)	3280(1)	2783(1)	1262(1)	20(1)	1
O(3)	2707(1)	2016(1)	2024(1)	19(1)	1
N(1)	4611(1)	2569(1)	1900(1)	14(1)	1
C(1)	5755(1)	2443(1)	1891(1)	16(1)	1
C(2)	6284(1)	2539(1)	1497(1)	16(1)	1
C(3)	7169(1)	2968(1)	1477(1)	18(1)	1
C(4)	7766(1)	3011(1)	1134(1)	18(1)	1
C(5)	7441(1)	2599(1)	812(1)	18(1)	1
C(6)	6560(1)	2159(1)	815(1)	15(1)	1
C(7)	5956(1)	2139(1)	1166(1)	15(1)	1
C(8)	8765(1)	3462(1)	1116(1)	23(1)	1
C(9A)	8688(3)	3980(2)	756(1)	36(1)	0.553(5)
C(10A)	8933(4)	3904(4)	1481(1)	65(2)	0.553(5)
C(11A)	9694(3)	2976(2)	1039(2)	60(2)	0.553(5)
C(9B)	9221(4)	3521(3)	707(1)	40(2)	0.447(5)
C(10B)	8562(4)	4199(3)	1287(2)	39(2)	0.447(5)
C(11B)	9593(3)	3090(3)	1387(2)	36(2)	0.447(5)
C(12)	6283(1)	1696(1)	455(1)	20(1)	1
C(13)	7042(1)	1799(1)	107(1)	29(1)	1
C(14)	5193(1)	1883(1)	304(1)	31(1)	1
C(15)	6329(1)	903(1)	576(1)	29(1)	1
C(16)	4347(1)	3301(1)	1762(1)	21(1)	1
C(17)	4063(1)	3319(1)	1331(1)	25(1)	1
C(18)	2826(1)	2874(1)	876(1)	29(1)	1
C(19)	4263(1)	2456(1)	2314(1)	18(1)	1
C(20)	3095(1)	2432(1)	2350(1)	22(1)	1
C(21)	1600(1)	1950(1)	2046(1)	35(1)	1

C(22)	4293(1)	687(1)	1864(1)	18(1)	1
C(23)	2234(1)	-144(1)	2016(1)	35(1)	1
C(24)	4219(2)	-764(1)	2319(1)	39(1)	1
C(25)	3367(1)	549(1)	2701(1)	18(1)	1
C(26)	4206(1)	863(1)	2899(1)	21(1)	1
C(27)	4101(1)	1181(1)	3268(1)	24(1)	1
C(28)	3145(1)	1188(1)	3456(1)	24(1)	1
C(29)	2300(1)	870(1)	3273(1)	22(1)	1
C(30)	2411(1)	562(1)	2901(1)	21(1)	1
C(31)	2423(1)	1181(1)	1190(1)	17(1)	1
C(32)	2415(2)	1146(1)	277(1)	37(1)	1
C(33)	3502(1)	-28(1)	748(1)	37(1)	1
C(34)	1162(1)	55(1)	709(1)	21(1)	1
C(35)	1008(1)	-415(1)	391(1)	27(1)	1
C(36)	106(2)	-816(1)	355(1)	34(1)	1
C(37)	-667(2)	-763(1)	636(1)	36(1)	1
C(38)	-547(1)	-302(1)	950(1)	34(1)	1
C(39)	358(1)	100(1)	985(1)	28(1)	1

Table 5. Anisotropic displacement parameters ($Å^2 x\ 10^4$) for SCM01 (CCDC 268186). The anisotropic displacement factor exponent takes the form: $-2\pi^2$ [$h^2 a^{*2} U^{11}$ + ... + 2 h k a* b* U^{12}]

	U^{11}	U^{22}	U^{33}	U^{23}	U^{13}	U^{12}
Sc(1)	148(2)	129(2)	154(2)	-8(1)	1(1)	-6(1)
Si(1)	290(3)	145(2)	198(3)	5(2)	29(2)	-26(2)
Si(2)	198(3)	214(3)	228(3)	-25(2)	-14(2)	-32(2)
O(1)	149(6)	154(6)	169(6)	-20(5)	21(5)	-38(5)
O(2)	229(7)	171(6)	202(7)	31(5)	-73(5)	-26(5)
O(3)	141(6)	231(7)	207(7)	-52(5)	11(5)	-18(5)
N(1)	160(7)	131(7)	138(8)	2(6)	-3(6)	19(6)
C(1)	156(9)	170(9)	159(9)	-20(7)	-20(7)	-12(7)
C(2)	162(9)	135(8)	170(9)	1(7)	4(8)	18(7)
C(3)	195(9)	155(9)	197(10)	-16(8)	-37(8)	-14(7)
C(4)	183(9)	145(9)	220(10)	40(8)	-9(8)	-4(7)
C(5)	180(9)	162(9)	182(10)	39(7)	38(7)	13(7)
C(6)	176(9)	122(8)	160(9)	8(7)	7(7)	16(7)
C(7)	161(9)	105(8)	182(10)	25(7)	-13(7)	9(7)
C(8)	186(9)	233(10)	266(11)	11(8)	0(8)	-71(8)
C(9A)	300(20)	300(20)	490(30)	140(20)	-20(20)	-167(19)
C(10A)	580(40)	970(50)	400(30)	-50(30)	10(30)	-600(40)
C(11A)	200(20)	440(30)	1160(60)	300(30)	-40(30)	-106(19)
C(9B)	340(30)	540(40)	330(30)	20(30)	0(20)	-260(30)
C(10B)	260(30)	230(30)	670(50)	-60(30)	80(30)	-150(20)
C(11B)	220(20)	360(30)	490(40)	90(30)	-70(20)	-120(20)
C(12)	231(9)	196(9)	174(9)	-28(8)	35(8)	-31(8)
C(13)	393(12)	261(11)	225(11)	-78(9)	86(9)	-99(9)
C(14)	320(11)	397(12)	226(11)	-44(9)	-20(9)	-37(9)
C(15)	386(12)	206(10)	274(11)	-59(8)	83(9)	-76(9)
C(16)	234(10)	116(9)	264(10)	-21(8)	-16(8)	0(8)
C(17)	297(10)	154(9)	286(11)	20(8)	-29(8)	-17(8)

C(18)	381(12)	238(10)	253(11)	43(9)	-131(9)	-5(9)
C(19)	202(9)	204(10)	138(9)	-33(7)	-1(7)	-6(8)
C(20)	223(10)	226(10)	196(10)	-60(8)	29(8)	-6(8)
C(21)	159(10)	522(13)	369(13)	-190(10)	52(9)	-56(9)
C(22)	190(9)	171(9)	188(10)	-24(8)	13(8)	8(7)
C(23)	451(13)	331(11)	253(11)	-27(9)	29(9)	-212(10)
C(24)	651(15)	204(11)	307(12)	30(9)	108(11)	81(10)
C(25)	218(9)	118(9)	196(10)	48(7)	2(8)	7(7)
C(26)	180(9)	219(10)	221(10)	26(8)	43(8)	-2(8)
C(27)	214(10)	249(10)	263(11)	-11(8)	-50(8)	-19(8)
C(28)	269(10)	234(10)	207(10)	-23(8)	6(8)	47(8)
C(29)	193(10)	230(10)	244(11)	24(8)	50(8)	28(8)
C(30)	199(10)	193(9)	236(10)	23(8)	-34(8)	-13(8)
C(31)	194(9)	150(9)	163(9)	16(7)	13(7)	-19(7)
C(32)	398(12)	461(13)	257(12)	10(10)	-31(9)	-225(10)
C(33)	252(11)	343(12)	509(14)	-175(10)	-24(10)	20(9)
C(34)	214(9)	159(9)	256(10)	18(8)	-50(8)	0(8)
C(35)	306(11)	218(10)	295(11)	4(9)	-44(9)	-36(8)
C(36)	386(12)	248(11)	373(13)	2(9)	-149(10)	-70(9)
C(37)	255(11)	278(12)	542(15)	90(10)	-128(11)	-108(9)
C(38)	211(11)	326(12)	484(14)	26(10)	15(10)	-32(9)
C(39)	242(11)	227(10)	379(12)	-21(9)	-17(9)	-17(8)